

I. Table of Contents

I.1. Abstract.....	ii
I.2. Acknowledgements.....	iv
Chapter 1.Introduction	1
1.1.....Introduction	1
1.2..... Motivation and Aims	2
1.2.1.....Development of the Volcanic Succession	2
1.2.2..... Volcanism and Mineralisation	3
1.2.3..... Aims	4
1.3..... Approach and Methodology	4
1.3.1..... Sample Selection	4
1.3.2..... Analytical Work	5
1.3.3..... Thesis Preparation	6
1.4..... Thesis Outline	6
Chapter 2. The North Island Volcanic Succession	8
2.1..... Geologic Setting of Northern New Zealand	8
2.1.1..... Basement	8
2.1.2..... The Southwest Pacific Region	8
2.2..... The North Island Volcanic Succession	10
2.2.1..... Northland Arc - Setting	10
2.2.2..... Northland Arc - Volcanism	11
2.2.3..... Coromandel Volcanic Zone - Setting	14
2.2.4..... Coromandel Volcanic Zone - Volcanism	14
2.2.5..... Taupo Volcanic Zone – Setting	17
2.2.6..... Taupo Volcanic Zone - Volcanism	18
2.3..... Hydrothermal Alteration of the Volcanic Succession	19
Chapter 3. Northland Arc Volcanism	22
3.1..... Summary	22
3.2..... Geochemistry of the Early Miocene Volcanic Succession of Northland, New Zealand, and Implications for the Evolution of Subduction in the Southwest Pacific.	23
3.2.0.0. Abstract	23
3.2.1..... Introduction	24
3.2.2..... Geologic Setting of the Northland Arc	25
3.2.3..... Volcanic Centres of the Northland Arc	27
3.2.4..... Sampling and Analytical Methods	28
3.2.5..... Geochemical Compositions	31
3.2.6..... REE Behaviour	36

3.2.7.....	Slab and Mantle Components	39
3.2.8.....	Isotope Properties	41
3.2.9.....	Summary of Petrogenetic Indicators	41
3.2.10.....	Discussion	43
3.2.10.1.....	<i>Polarity of Subduction</i>	43
3.2.10.2.....	<i>Comparison with Subsequent North Island Volcanism</i>	45
3.2.10.3.....	<i>Implications for SW Pacific Tectonic Development</i>	47
3.2.11.....	Conclusions	49
Chapter 4.....	Coromandel Volcanic Zone Volcanism	51
4.1.....	Summary	51
4.2....	The Transition from Intermediate to Silicic Volcanism in the North Island of New Zealand	53
4.2.0.0.....	<i>Abstract</i>	53
4.2.1.....	Introduction	54
4.2.2.....	Geologic Setting	54
4.2.3.....	Volcanic Stratigraphy	57
4.2.4.....	Sample Set and Analytical Methods	57
4.2.5.....	Petrography	60
4.2.6.....	Geochemistry	64
4.2.6.1.....	<i>Mercury Basalts</i>	64
4.2.6.2.....	<i>Coromandel Group</i>	68
4.2.6.3.....	<i>Whitianga Group</i>	71
4.2.7.....	Mixing Relationships	72
4.2.7.1.....	<i>Composition of the Primitive Component</i>	74
4.2.7.2.....	<i>Composition of the Evolved Component</i>	75
4.2.7.3.....	<i>Source of the Evolved Component</i>	76
4.2.8.....	Source of Whitianga Group Rhyolites	77
4.2.8.1.....	<i>Rhyolite Differentiation</i>	77
4.2.8.2.....	<i>Derivation of Least-Differentiated Rhyolites</i>	78
4.2.9.....	Discussion	79
4.2.9.1.....	<i>Mixed Origins</i>	79
4.2.9.2.....	<i>Preferred Model</i>	82
4.2.9.3.....	<i>Significance of the Initiation of Rhyolite Eruptions</i>	82
4.2.10.....	Conclusions	84
4.3.....	Volcanic development of the Coromandel Volcanic Zone	86
4.3.1.....	Coromandel Group Development	86
4.3.1.1.....	<i>Apparent Age Trend</i>	87
4.3.1.2.....	<i>Relation to Basaltic and Rhyolitic Volcanism</i>	90
4.3.2.....	Mantle Component in Mercury Basalts and Coromandel Group Rocks	90
4.3.2.1.....	<i>Conservative Element Distributions</i>	91
4.3.2.2.....	<i>Slab-Derived Fractions of Non-Conservative Elements</i>	92
4.3.3.....	Implications of Pb Isotope Data	93

4.3.3.1.....	<i>Motivation</i>	93
4.3.3.2.....	<i>Sample Selection and Methods</i>	96
4.3.3.3.....	<i>Results</i>	96
4.3.3.4.....	<i>Discussion</i>	97
Chapter 5.....	Kiwitahi Chain Volcanism	100
5.1.....	Summary	100
5.2.Evolving Volcanism at the Tip of a Propagating Arc: the Earliest High-Mg Andesites in Northern New Zealand.....		101
5.2.0.0.....	<i>Abstract</i>	101
5.2.1.....	Introduction	101
5.2.2.....	Geological Setting	102
5.2.3.....	The Kiwitahi Volcanic Chain	104
5.2.4.....	Sample Set and Analytical Methods	108
5.2.5.....	Geochemistry	111
5.2.5.1.....	<i>Crystal Fractionation</i>	113
5.2.5.2.....	<i>Mixing</i>	116
5.2.5.3.....	<i>Mantle vs. Crustal Contributions</i>	117
5.2.6.....	Discussion	120
5.2.6.1.....	<i>The Pre-6.7 Ma Kiwitahi Centers as an Extension of CVZ Volcanism</i>	120
5.2.6.2.....	<i>High-Mg Andesites in Northern New Zealand</i>	121
5.2.6.3.....	<i>What Does the Kiwitahi Chain Represent?</i>	123
5.2.7.....	Conclusions	125
Chapter 6.....	Application to Geochemical Exploration	126
6.1.....	Summary	126
6.2.Quantifying Metasomatism in Epithermal Au-Ag Deposits: a Case Study from the Waitekauri Area, New Zealand.....		127
6.2.0.0.....	<i>Abstract</i>	127
6.2.1.....	Introduction	127
6.2.2.....	The Hauraki Goldfield and Hauraki Volcanic Region	131
6.2.3.....	Geology of the Waitekauri Area	132
6.2.4.....	Sample Selection and Analytical Methods	139
6.2.5.....	Geochemistry of Unaltered Coromandel Group Rocks	141
6.2.5.1.....	<i>Zr and TiO₂ Concentrations in Unaltered Coromandel Group Rocks</i>	142
6.2.6.....	Estimation of Initial Rock Composition	144
6.2.6.1.....	<i>Effect of Metasomatic TiO₂ Loss</i>	145
6.2.6.2.....	<i>Apparent Mass Change Due to Natural Variation</i>	146
6.2.6.3.....	<i>Sodium and Magnesium Concentrations in Individual Formations</i>	147
6.2.7.....	Geochemistry of Altered Rocks	147
6.2.7.1.....	<i>Major Element Trends in Altered Rocks</i>	148
6.2.7.2.....	<i>Element Behavior During Metasomatism</i>	152
6.2.7.3.....	<i>Immobility of Th</i>	153

6.2.8.....	Geochemical Zonation in the Waitekauri Area	153
6.2.8.1.....	<i>Potassium and Rubidium</i>	160
6.2.8.2.....	<i>Barium</i>	160
6.2.8.3.....	<i>Silicon</i>	161
6.2.8.4.....	<i>Sodium and Calcium</i>	161
6.2.8.5.....	<i>Iron and Magnesium</i>	162
6.2.8.6.....	<i>Precious Metal and Pathfinder Element Concentrations</i>	162
6.2.8.7.....	<i>Other Geochemical Parameters</i>	163
6.2.8.8.....	<i>Summary of Alteration Geochemical Trends</i>	163
6.2.9.....	Discussion	164
6.2.9.1.....	<i>Vectors Towards Orebodies</i>	164
6.2.9.2.....	<i>Mass Transfer in the Waitekauri-Maratoto Area</i>	166
6.2.9.3.....	<i>Relationship Between Geochemistry and Alteration Mineralogy</i>	167
6.2.9.4.....	<i>Volume Change Associated with Alteration</i>	169
6.2.9.5.....	<i>Size of the Dataset and Application to Other Districts</i>	170
6.2.10.....	Conclusions	171
6.3.....	Determination of Protolith Composition in Whitianga Group Rhyolites	172
6.3.1.....	Introduction	172
6.3.2.....	Major Element Variation in Rhyolites	174
6.3.3.....	Trace Elements	174
6.3.4.....	Immobile Element Ratios and Bulk K ₂ O Concentration	176
6.3.5.....	Other Elements	177
6.3.6.....	Concluding Remarks	177
Chapter 7.....	Synthesis	179
7.1.....	Evolving Volcanic Style	179
7.1.1.....	Northland Arc Subduction System	182
7.1.2.....	Northland Arc to Colville Ridge Arc Transition	182
7.1.3.....	Evolving Tectonic Setting of the CVZ-TVZ Succession	186
7.1.3.1.....	<i>Hikurangi Plateau Collision</i>	186
7.1.3.2.....	<i>Hikurangi Margin Rotation</i>	187
7.1.3.3.....	<i>Age Trends in the CVZ</i>	187
7.1.3.4.....	<i>Inception of Rhyolitic Volcanism</i>	188
7.1.3.5.....	<i>Inception of Correlated Basaltic and Rhyolitic Volcanism</i>	190
7.1.3.6.....	<i>Inception of High-Magnesium Andesite Volcanism</i>	190
7.2.....	Volcanism and Mineralisation	191
7.2.1.....	Co-evolution of Volcanism and Mineralisation	191
7.2.1.1.....	<i>Andesitic Host Rocks</i>	191
7.2.1.2.....	<i>Rhyolitic Volcanism</i>	193
7.2.1.3.....	<i>Peak Mineralisation During Rhyolitic Quiescence</i>	193
7.2.2.....	Discussion	194
7.2.2.1.....	<i>Basaltic Gold Sources</i>	196
7.2.2.2.....	<i>Silicic Gold Sources</i>	196

7.3.....	Avenues for Future Research	198
7.3.1.....	Northland Arc Slab Provenance	199
7.3.2.....	Andesite Petrogenesis	199
7.3.3.....	Mantle vs. Slab Isotope Signature	200
7.3.4.....	Rhyolite Magma Chamber Development	201
7.4.....	Conclusions	202
Chapter 8.....	References	207
Appendices.....		219
Appendix A.....	Supplementary Dataset to Chapter 3	219
Appendix B.....	Appendix B. Supplementary bulk rock geochemistry dataset to Chapter 4	228
Appendix C.....	Supplementary crystal and groundmass geochemistry dataset to Chapter 4	246
C.1.....	AU45386 - Beeson's Island Volcanics, Kuaotunu Subgroup	246
C.2.....	AU45360 - Beeson's Island Volcanics, Kuaotunu Subgroup	246
C.3.....	R17872 - Kapukapu Andesite, Waiwawa Subgroup	246
C.4.....	R17869 - Kapukapu Andesite, Waiwawa Subgroup	246
C.5.....	R17831 - Kapukapu Andesite, Waiwawa Subgroup	247
C.6.....	R17861 - Waipupu Formation, Waiwawa Subgroup	247
C.7.....	R17880 - Waipupu Formation, Waiwawa Subgroup	247
C.8.....	AU45340 - Whangapoua Andesite, Kuaotunu Subgroup	247
C.9.....	R17874 - Whiritoa Andesite, Waiwawa Subgroup	248
C.10.....	R17866 - Whiritoa Andesite, Waiwawa Subgroup	248
C.11.....	R17856 - Whiritoa Andesite, Waiwawa Subgroup	248
C.12.....	AU60071 - Sugarloaf Basalt, Mercury Basalts	248
Appendix D.....	Supplementary Dataset to Chapter 6	254

II. List of Figures

Fig. 1.1	2
Fig. 2.1	11
Fig. 2.2	12
Fig. 2.3	13
Fig. 2.4	19
Fig. 3.1	25
Fig. 3.2	26
Fig. 3.3	32
Fig. 3.4	33

Fig. 3.5	34
Fig. 3.6	35
Fig. 3.7	37
Fig. 3.8	40
Fig. 4.1	55
Fig. 4.2	59
Fig. 4.3	64
Fig. 4.4	65
Fig. 4.5	66
Fig. 4.6	68
Fig. 4.7	69
Fig. 4.8	72
Fig. 4.10	74
Fig. 4.11	75
Fig. 4.12	80
Fig. 4.13	86
Fig. 4.14	88
Fig. 4.15	91
Fig. 4.16	92
Fig. 4.17	94
Fig. 4.18	95
Fig. 5.1	102
Fig. 5.2	103
Fig. 5.3	105
Fig. 5.4	109
Fig. 5.5	110
Fig. 5.6	111
Fig. 5.7	112
Fig. 5.8	112
Fig. 5.9	114
Fig. 5.10	115
Fig. 5.11	119
Fig. 5.12	120

Fig. 6.1	129
Fig. 6.2	141
Fig. 6.3	143
Fig. 6.4	146
Fig. 6.5	147
Fig. 6.6	148
Fig. 6.7	149
Fig. 6.8	150
Fig. 6.9	153
Fig. 6.10	165
Fig. 6.11	168
Fig. 6.12	172
Fig. 6.13	173
Fig. 6.14	175
Fig. 6.15	175
Fig. 7.1	180
Fig. 7.2	181
Fig. 7.3	182
Fig. 7.4	192
Fig. 7.5	194
Fig. 7.6	195

III. List of Tables

Table 1.1	5
Table 3.1	28
Table 3.2	39
Table 3.3	40
Table 4.1	60
Table 4.2	67
Table 4.3	95
Table 5.1	105
Table 6.1	133
Table 6.2	140

Table 6.3	143
Table 6.4	176
Appendix A.	219
Appendix B.	228
Appendix C.	246
Appendix D.	254

Chapter 1. Introduction

1.1. Introduction

New Zealand is a geologically young country where the most ancient rocks are no older than Late Paleozoic. Parts of the stratigraphic succession record volcanism and magmatism in a convergent plate boundary setting, the products of which are preserved in the pre-Cenozoic volcanoclastic and plutonic rocks of the basement terranes and in the volcanic rocks of the Cenozoic cover sequence. In the North Island, Cenozoic subduction-related volcanism began with the Late Oligocene eruptions in Northland, from where it migrated to its present locus in the central North Island. The gradual migration of the volcanic front means the older parts of the arc succession are comparatively well-preserved, providing an outstanding opportunity to study the development of the nascent arc.

From the Middle Miocene to the Quaternary, subduction-volcanism was concentrated in the Coromandel Volcanic Zone (CVZ), an area in the northwestern North Island comprising the Coromandel Peninsula, Great Barrier Island and surrounding islands. The CVZ was volcanically active between c. 18 and 1.95 Ma, a period spanning major tectonic reconfiguration of the SW Pacific region including the waning of volcanism in the Northland Arc (Herzer, 1995; Hayward et al., 2001), the cessation of backarc spreading in the South Fiji Basin (Mortimer et al., 2010) and the inception of backarc spreading in the Havre Trough (Ballance et al., 1999). Against this backdrop, volcanism in the CVZ developed from an initially andesitic suite to ultimately a wide spectrum of volcanic rock types including andesites, rhyolites, basalts and high-magnesium andesites, setting the stage for the volcanic rock types that comprise the modern Taupo Volcanic Zone (TVZ) in the central North Island.

Volcanism in the CVZ was accompanied by geothermal activity that produced extensive hydrothermal alteration of parts of the volcanic succession (Skinner, 1986), and which locally led to the formation of adularia-sericite epithermal gold-silver deposits hosted mainly by rocks of the volcanic succession. About 50 such deposits are known throughout the CVZ and form the Hauraki goldfield, a premier epithermal province in global terms where mining dates back to the late 19th century and is still ongoing. Although deposits occur in andesites and rhyolites, as well as metasedimentary basement rocks, over 95% of the gold has been produced from andesite-hosted deposits (Christie et al., 2007). Recent dating efforts have significantly refined the geochronology of epithermal mineralization in the Hauraki goldfield and show that, although mineralisation occurred over the course of c. 9 Myr, over 85% of gold has been produced

BESTPFE.COM
List of research project topics and materials

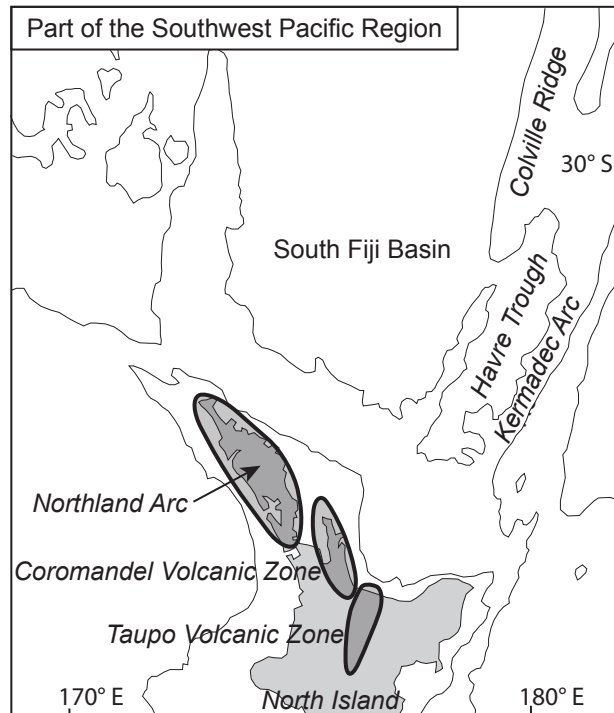


Fig. 1.1 Major tectonic features of the SW Pacific region and major volcanic zones of the North Island of New Zealand.

from deposits formed during a comparatively short interval between 7 and 6 Ma (Mauk and Hall, 2004; Mauk et al., in press).

1.2. Motivation and Aims

1.2.1. Development of the Volcanic Succession

The 2-0 Ma Taupo Volcanic Zone in the central North Island is a highly active, diverse volcanic system that has been used extensively as a natural laboratory for the study of arc magmatic processes (e.g. Ewart and Stipp, 1968; Reid, 1983; Gamble et al., 1993; McCulloch et al., 1994; Charlier et al., 2005; Price et al., 2005; Deering et al., 2008; Wilson and Charlier, 2009). By comparison, the Tertiary North Island volcanic succession has been the subject of fewer studies (e.g. Day et al., 1992; Blattner et al., 1996; Huang et al., 2000; Krippner, 2000; Nicholson et al., 2004). Nevertheless, the Tertiary succession dates back to at least the Late Oligocene and represents over 90% of the duration of Cenozoic subduction-related volcanism in New Zealand. Furthermore, the Tertiary succession records major modification of the erupted volcanic suite over time (Skinner, 1986; Smith et al., 1989; Herzer, 1995; Briggs et al., 2005), from initial cone-building andesitic volcanism to explosive, rhyolitic, caldera-forming eruptions (Briggs and Fulton, 1990; Krippner, 2000; Malengreau et al., 2000; Carter et al., 2003; Nicholson et al., 2004; Smith et al., 2006a) with subordinate basaltic volcanism (Skinner, 1976; Hollis, 1995; Hawthorn, 1996).

The evolution to more silicic volcanism suggests a general history of crustal modification by the ongoing intrusion of mantle-derived primitive magmas (e.g. Huppert and Sparks, 1988; Lipman, 2000; Annen et al., 2006). However, the first appearance of rhyolites in the North Island succession at 12 Ma (Carter et al., 2003; Nicholson et al., 2004) lags the onset of andesitic volcanism by more than 13 Myr, which is a substantially longer interval than the delay between precursor intermediate volcanism and silicic eruptions in e.g. the Kermadec Arc (c. 1 Myr; Smith et al., 2006b) or the Southern Rocky Mountains volcanic field (0-5 Myr; Lipman, 2007), suggesting that tectonic factors constrained the extent to which the early North Island magmatic system could develop. An improved understanding of the nature and development of the early arc magmatic system in New Zealand can help to elucidate the response of the arc magmatic system to regional tectonic reconfiguration.

1.2.2. Volcanism and Mineralisation

The occurrence of world-class gold deposits in parts of the North Island Tertiary volcanic succession makes understanding its volcanic development an economically significant endeavour. Better knowledge of the arc magmatic system that gave rise to the geothermal transport and deposition of precious metals in the epithermal environment can aid exploration programmes by helping to address the question why mineralisation was concentrated at particular intervals and in particular rock types. Additionally, establishing a high-quality major and trace element dataset helps to constrain the compositional range of host rocks to mineralisation in the Hauraki goldfield. Epithermal gold deposits essentially form in response to the percolation through the crust of hot hydrothermal fluids that preferentially dissolve certain elements and precipitate others, depending on temperature and fluid and rock composition (Giggenbach, 1984; Giggenbach, 1988). Hydrothermal alteration consequently modifies the mineralogical, chemical and isotopic composition of wall rocks in a geothermal system (Buchanan, 1981; Naito et al., 1993; Carlile et al., 1998; Leavitt and Arehart, 2005; Gemmell, 2007; Mauk and Simpson, 2007; Simpson and Mauk, in press). Geochemical exploration programmes routinely rely on analyses of the concentration of ‘epithermal suite’ trace elements (Au, Ag, and the pathfinder elements Se, Te, As, Sb, Hg, Tl) to identify areas of alteration (White and Hedenquist, 1995; Hedenquist et al., 2000). However, the epithermal suite elements mainly occur in minerals that are confined to epithermal veins. On a 100-1000m scale, major element mass changes can be a better tool for defining alteration because they reflect wall rock alteration mineralogy (MacLean, 1990; Madeisky, 1996; Sherlock, 1996; Warren et al., 2007; Urqueta et al., 2009). If the baseline geochemistry of the host rocks can be sufficiently constrained, a mass balance calculation

can be made to quantify the mass changes that occurred in altered rocks, providing an additional tool for geochemistry-based exploration programmes.

1.2.3. Aims

The principal aims of this study are as follows:

1) To collect, compile and interpret a high-quality baseline geochemical dataset on a suite of unaltered volcanic rocks that forms a representative section of the pre-TVZ arc volcanic succession, with an emphasis on the andesites of the Coromandel Volcanic Zone that predominantly host epithermal deposits in the Hauraki goldfield.

2) Use this dataset to study the magmatic processes that drove the volcanism in the CVZ, and document the evolution of the magmatic systems through time.

3) Interpret the dataset's implications for the relations between arc magmatism in the CVZ, mineralisation in the Hauraki goldfield and the Miocene-Pliocene tectonic reconfiguration of the SW Pacific region.

4) Collect, compile and interpret high-quality data geochemical data on altered volcanic rocks surrounding an epithermal gold deposit in the Hauraki goldfield. Test the applicability of whole-rock major and trace element geochemical in providing a vector towards mineralisation.

1.3. Approach and Methodology

1.3.1. Sample Selection

The samples analysed in this study are part of the rock collections at the University of Auckland, the University of Waikato and GNS Science, Ltd. The philosophy in sample selection was as follows. 1) Samples were chosen to obtain an approximately representative section through the volcanic stratigraphy of the Northland Arc and the Coromandel Volcanic Zone. 2) Samples were preferentially picked from radiometrically dated formations and volcanic centres. 3) More prominent formations, in terms of aerial extent or stratigraphic thickness, are represented by a relatively larger number of samples. 4) The selection of samples from a given formation is representative of the compositional range, determined based on petrographic descriptions and available major element analyses. 5) Samples were selected that were not or minimally altered by hydrothermal or chemical weathering processes. Where possible, samples were selected that had previously been used for radiometric dating or chemical analysis.

1.3.2. Analytical Work

The principal contribution of this project is a high-quality geochemical dataset for rocks of the volcanic succession in the Northland Arc and Coromandel Volcanic Zone. Additional datasets are presented of crystal and groundmass chemistry on a suite of CVZ andesites, and of radiogenic isotopes on a suite of CVZ basalts, andesites and rhyolites. Lastly, new geochemical data were obtained for this project on a suite of altered andesites of the Waitekauri area, representing an addition to an existing dataset of Waitekauri area altered andesite analyses. For the purpose of documenting the development of the North Island volcanic succession, the geochemical dataset must include analyses on trace elements of petrologic interest. These include the alkali elements (Rb, Cs), the alkali earth elements (Sr, Ba), transition metals (e.g. V, Sc, Cr, Ni), the high field strength elements (Zr, Nb, Hf, Ta), the rare earth elements (REE: La through to Lu) and the actinides (U, Th). Trace element concentrations were measured in two ways: by laser ablation ICP-MS on fused glass discs for the Northland Arc dataset, and by wet-chemistry dissolution ICP-MS for the CVZ dataset. The advantage of the laser ablation method is that analyses are performed rapidly at low cost on the same glass beads used for XRF analysis of major element composition. For the purpose of volcanic system studies this method yields a comprehensive dataset featuring all the required elements. However, the geochemical dataset on CVZ volcanic rocks is additionally intended

Table 1.1

CVZ	Coromandel Volcanic Zone
HAB	High-Alumina Basalt
HFSE	High Field Strength Element
HMA	High-Magnesium Andesite
HREE	Heavy Rare Earth Element
ICP-MS	Inductively Coupled Plasma Mass Spectrometry
IUGS	International Union of Geological Sciences
LA-ICP-MS	Laser Ablation ICP-MS
LCHZ	Lower Crustal Hot Zone
LILE	Large Ion Lithophile Elements
LREE	Light Rare Earth Element
MC-ICP-MS	Multicollector ICP-MS
MREE	Middle Rare Earth Element
NBFZ	Northland Boundary Fault Zone
OIB	Ocean Island Basalt
PER	Pearce Element Ratio
REE	Rare Earth Element
SFB	South Fiji Basin
TIMS	Thermal Ionisation Mass Spectrometry
TVZ	Taupo Volcanic Zone
VMFZ	Vening Meinesz Fracture Zone
XRF	X-Ray Fluorescence

Table 1.1 Acronyms used in this manuscript. Acronyms are also defined at the first instance in each chapter.

to serve as a baseline for the interpretation of altered rock data. For this purpose the dataset must include analyses on some minor and trace elements that are commonly applied in geochemical exploration for epithermal and porphyry deposits because they occur at elevated concentrations in and around such deposits. Such elements include the ‘epithermal suite’ of pathfinder elements (e.g. As, Sb, Hg, Se, Te, Tl), S, and potentially precious metals (Hedenquist et al., 2000; Leavitt and Arehart, 2005). Some elements that are of interest to geochemical exploration purposes are comparatively volatile (e.g. S, Hg), and are lost when sample is heated for the purpose of loss-on-ignition tests, or during the preparation of fused glass beads. For this reason, trace element analyses on CVZ volcanic rocks were obtained by ICP-MS following wet-chemistry acid dissolution sample preparation. A drawback of the dissolution approach is that some elements may not dissolve properly and are consequently measured at too low a concentration. This effect is evident at least for Zr and Hf. In this study, only XRF-based Zr concentration measurements on fused beads are used. The applied methods are described in Chapters 3-6.

1.3.3. Thesis Preparation

Data processing was performed in the proprietary Microsoft Excel spreadsheet formats (.xls and .xlsx) using Microsoft Excel 2008 for Mac. Diagrams and tables were prepared in Microsoft Excel. Maps were prepared using ArcGIS. All figures were drafted using Adobe Illustrator CS3. Photomicrographs were edited for contrast and sharpness using Adobe Photoshop CS3. The manuscript was prepared using Microsoft Word 2008 word processor and the Endnote X1 bibliographic referencing software. Adobe Indesign CS3 was used to format the layout, page, section and object numbering, and table of contents for the printed version. Spelling in this manuscript adheres to New Zealand English except where US English was used in manuscripts that have been submitted to journals. Acronyms that are in common use in the petrologic and/or New Zealand geologic literature have been used where appropriate and are defined at the first instance in each chapter. Additionally, Table 1.1 lists the used acronyms and their meanings. Units used are SI units.

1.4. Thesis Outline

The work done for this project is presented in the form of a series of papers that have been submitted for peer review with scientific journals of appropriate scope. Each paper is accompanied by an introduction that defines the scope of the paper and its relation to other elements of this thesis.

Chapter 2 describes the geologic setting of the North Island volcanic succession, and describes the

major components of the succession itself. It concludes with a description of the effects of hydrothermal alteration on various parts of the volcanic succession.

Chapter 3 presents whole-rock geochemical and isotope data on rocks representing the onland centres of the Northland Arc. The dataset is used to document the volcanic development of the Northland Arc and compare its distinct properties with those of the CVZ. This chapter represents work that has been accepted for publication in *Journal of Volcanology and Geothermal Research* (Booden et al., in press).

Chapter 4 presents whole-rock geochemical and isotope data and crystal chemical data on rocks representing the volcanic succession of the Coromandel Volcanic Zone. The dataset is used to document the volcanic development of the CVZ with particular emphasis on the relationship between basalts, andesites and rhyolites. This chapter represents work that has been submitted to *Lithos* as a research paper, and is currently in review.

Chapter 5 presents whole-rock geochemical and isotope data on rocks representing the Kiwitahi volcanic chain, a string of outlying volcanic centres associated with the CVZ. This dataset is used to document the development of the Kiwitahi chain in relation to the concurrent development of the much larger CVZ. This chapter represents work that has been published in *Journal of Volcanology and Geothermal Research* (Booden et al., 2010).

Chapter 6 presents whole-rock geochemical data on altered volcanic rocks of the Waitekauri area. Using the unaltered volcanic rock data presented in Chapter 4 as a baseline, the altered rock dataset is used to test the applicability of major element mass changes in geochemical exploration. This chapter represents work that has been accepted for publication in *Economic Geology* (Booden et al., in press).

Chapter 7 presents a synthesis of the data and interpretations in the papers and describes avenues for future study.

Chapter 2. The North Island Volcanic Succession

2.1. Geologic Setting of Northern New Zealand

2.1.1. Basement

New Zealand is the emergent part of a larger continental fragment that is about one third the area of Australia (Mortimer, 2004). The basement rocks of this 'Zealandia' (Luyendyk, 1995) are exposed on New Zealand and the surrounding islands. They form a series of terranes that comprise Paleozoic and pre-110 Ma Mesozoic, variably metamorphosed and deformed sedimentary, volcanic and plutonic rocks. The terranes generally strike N-S and are inferred to have formed at, or accreted to, the convergent margin of eastern Gondwana. The break-up of the supercontinent is recorded in Zealandia by the development of half-grabens and metamorphic core complexes between 110-85 Ma, representing the rifting of Zealandia from Gondwana (Spell et al., 2000; Laird and Bradshaw, 2003) and the subsequent opening of the Tasman Sea and Fairway-Aotea basins to the west and of the Southern Ocean to the south (Gaina et al., 1998; Close et al., 2009, and references therein; Collot et al., 2009). In the Gondwana jigsaw puzzle, Zealandia restores to a position SE of Tasmania, Australia (Sutherland, 1999), and N of Marie Byrd Land, Antarctica (Stock and Candle, 2002).

2.1.2. The Southwest Pacific Region

Zealandia straddles the N- to NNE-striking Australian-Pacific convergent plate boundary, where the Cretaceous Pacific plate (e.g. Watts et al., 1988) subducts in western direction underneath the Australasian plate, giving rise to subduction-related volcanism on the Australasian plate that forms the c. 2500 km long Tonga-Kermadec arc (Smith and Price, 2006). This arc is contiguous with the Taupo Volcanic Zone in the central North Island. North and northeast of Zealandia, behind-arc from the convergent plate boundary, lies the SW Pacific region, which is characterised by a complex of generally N-trending continental ribbons, spreading centres and volcanic arcs, the origin and evolution of which has been the subject of recent debate (Herzer et al., 2000; Crawford et al., 2003; Schellart et al., 2006; Whattam et al., 2006; Mortimer et al., 2007; Schellart, 2007; Whattam et al., 2008; Herzer et al., 2009; Mortimer et al., 2010). The spreading centres generally become older farther west from the present plate boundary. Directly behind, i.e. to the west of, the Kermadec Arc lies the Havre Trough backarc basin, a region of

nascent, disorganised seafloor spreading since approximately 5.5 Ma (Ballance et al., 1999; Wysoczanski et al., 2010). To the north, the Havre Trough is contiguous with the Lau backarc basin. The rates of convergence along the plate boundary, as well as the rates of extension in the back-arc basins, increase in a northward direction, from 42 and 8 mm yr⁻¹ (Darby et al., 2000), respectively, at the North Island segment, to 53 and 15 mm yr⁻¹ at 35°S, to 85 and 159 mm yr⁻¹ at 16°S near the northern termination of the arc (DeMets et al., 1994). To the west, the Havre Trough backarc basin is bounded by the NNE-striking Colville Ridge. This is essentially the extinct western part of what is now the Kermadec Arc (Ballance et al., 1999). ⁴⁰Ar/³⁹Ar dating of dredged basalt from the Colville Ridge indicates that it was an active volcanic arc at least as early as 16.7 Ma (Mortimer et al., 2010). The Colville Ridge and the Kermadec each have sharply defined boundaries with the intervening Havre Trough backarc basin, characterised by c. 2.5 km scarp faces on both sides. Within the Havre Trough basin, the thickest sediment accumulation occurs on the western side (Ballance et al., 1999). Volcanic edifices occur within the basin along lineaments that strike perpendicular to the arc and are aligned with some Kermadec Arc volcanoes. These trails have been interpreted as recording migrating arc volcanism in response to trenchward retreat of the volcanic front (Wright et al., 1996).

To the west of the Colville Ridge consecutively occur the 1200 km wide South Fiji Basin spreading center, the Three Kings Ridge, the Norfolk basin and the Norfolk Ridge. South Fiji and Norfolk basin MORB and back-arc basin basalts have been dated by ⁴⁰Ar/³⁹Ar method at Late Oligocene to Early Miocene (26-18 Ma) (Mortimer et al., 1998; Mortimer et al., 2007) although magnetic anomaly data also suggest that parts of the Norfolk Basin may be Cretaceous (Davey, 1982; Malahoff et al., 1982). The Norfolk basin experienced extensional tectonics from c. 34 Ma (DiCaprio et al., 2009). The Norfolk Ridge is a continental ribbon that comprises Mesozoic basement crust (Mortimer et al., 1998). The Norfolk and Three Kings ridges were each the site of Early Miocene (32-26 Ma) subduction- and rift-related volcanism (Mortimer et al., 2007). The SW Pacific volcanic ridges and backarc basins are separated from the Mesozoic crust of Zealandia by the NW-striking Vening Meinesz Fracture Zone (VMFZ). Between the South Fiji Basin and Zealandia, the Northland Plateau additionally occurs north of the VMFZ. It comprises c. 12-16 km thick crust and is divided into a sedimentary inner plateau on the continental side and a volcanic outer plateau, which is geophysically contiguous with the Three Kings ridge (Herzer et al., 2000; Herzer et al., 2009).

2.2. The North Island Volcanic Succession

Cenozoic subduction-related volcanic rocks in northern New Zealand principally occur in a belt stretching from Northland, via the Coromandel region to the central North Island (Fig. 2.1). Submerged and buried subduction-related volcanic rocks further occur offshore west of the Northland, Waikato and Taranaki regions, and several volcanic centres formed in a behind-arc setting in the western North Island. The succession has been geographically divided into three major volcanic zones: the Northland Arc, which comprises Late Oligocene to Middle Miocene volcanic centres in Northland and the offshore Northland Basin; the Coromandel Volcanic Zone, which comprises Middle Miocene to Pleistocene volcanic centres in the Coromandel peninsula, on Great Barrier Island and in the wider Hauraki region; and the Taupo Volcanic Zone, which comprises Pleistocene-Recent volcanic centres in the central North Island and the Bay of Plenty.

2.2.1. Northland Arc - Setting

The remnants of Late Oligocene to Middle Miocene subduction-related volcanism are preserved on the NW-trending Northland Peninsula, which extends from the North Island and is contiguous with the submerged Reinga Ridge (Fig. 2.1). It is bounded in the west by the Cretaceous-Paleogene Northland Graben (Uruski et al., 2004). To the north, the continental shelf extends to the Vening Meinesz Fracture Zone. The basement comprises deformed Permian to Jurassic metasedimentary and igneous rocks of the Murihiku, Maitai and Waipapa basement terranes (Ballance and Campbell, 1993; Black, 1994; Sivell and McCulloch, 2000; Kear and Mortimer, 2003; Adams and Maas, 2004; Mortimer, 2004). The smaller Mt. Camel Terrane comprises a distinct Late Cretaceous sequence of clastic sediments and keratophyric volcanic rocks (Isaac et al., 1988; Nicholson and Black, 2004). Early Tertiary sedimentary rocks locally unconformably overlie the basement rocks. Nappes of the Northland Allochthon comprising allochthonous Cretaceous to Paleogene igneous and sedimentary rocks in turn overlie the basement and its autochthonous cover. These nappes were thrust onto Northland in southeastern and southwestern direction during the Oligocene and Miocene and have total stratigraphic thickness of c. 7 km (Ballance and Spörli, 1979). Rootless ophiolite massifs occur in the uppermost nappe (Sharp et al., 1989; Malpas et al., 1992). They comprise minor Cretaceous oceanic crust, but mostly Oligocene oceanic crust with a subduced arc-type trace element signature, which has been inferred to represent oceanic lithosphere formed in a fore-arc spreading center over a NE-dipping subduction zone north of New Zealand. Additionally, minor 25-15 Ma boninitic, alkalic and calc-alkaline rocks occur that possibly represent fore-arc correlatives to the

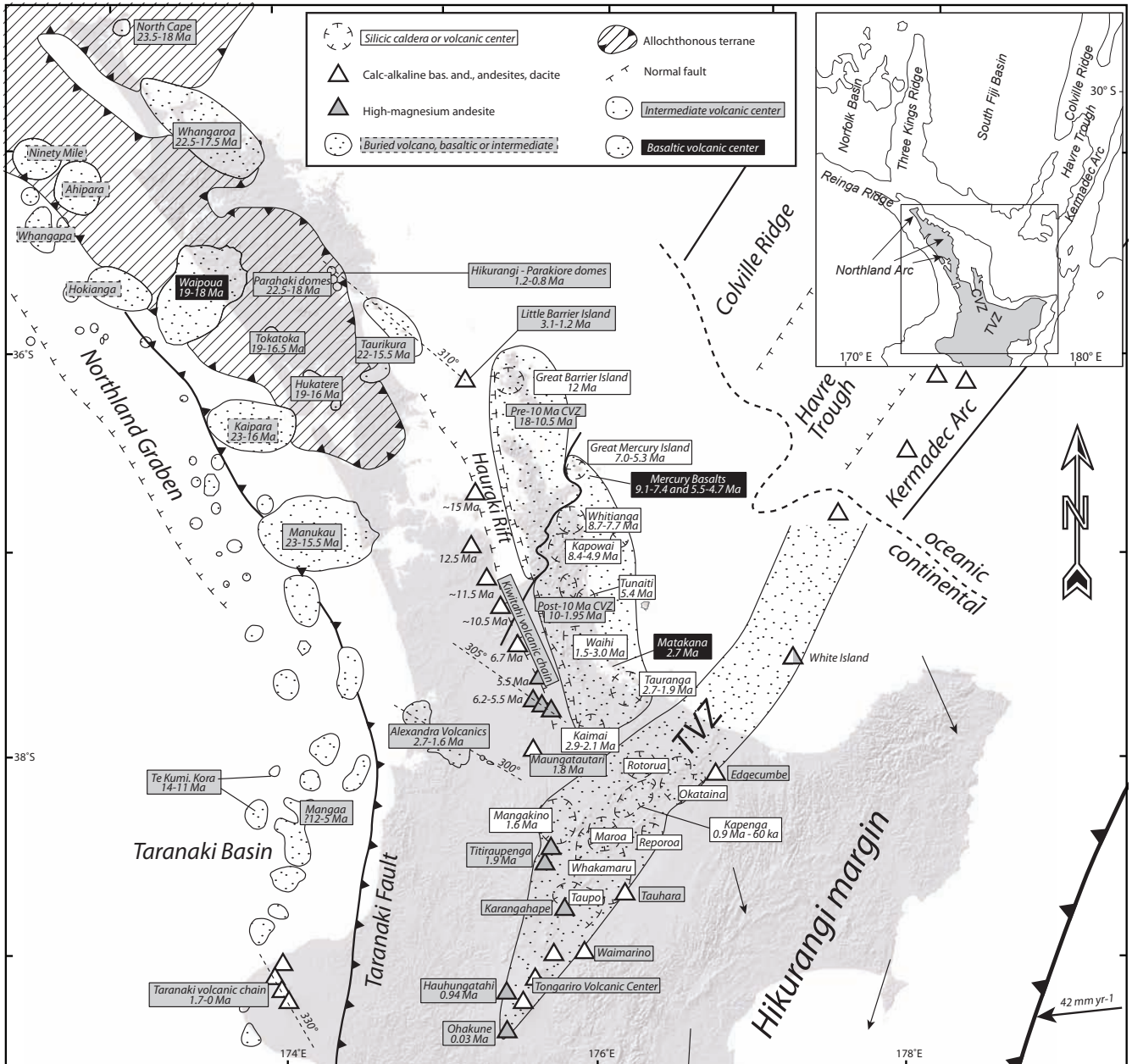


Fig. 2.1 Distribution of subduction-related Cenozoic volcanic rocks in the North Island. Compiled from Skinner (1986), Black et al. (1992), Herzer (1995), Houghton et al. (1995), Wilson et al. (1995), Price et al. (1999) and Hayward et al. (2001).

developing Northland Arc (Whattam et al., 2004; Whattam et al., 2006).

2.2.2. Northland Arc - Volcanism

From the Late Oligocene to the early Middle Miocene, two parallel volcanic belts separated by 30-60 km formed in Northland (Ballance, 1976; Kear, 1994). The belts were simultaneously active and do not show an unequivocal trend in the distribution of individual centers' ages, other than that the oldest rocks are preserved in the northernmost center (~25.5 Ma, North Cape) and that volcanism persisted longest in the south (~15.5 Ma, Manukau/Waitakere center; Fig. 2.2) (Hayward et al., 2001). The known

BEST PRACTICE
List of research project topics and materials

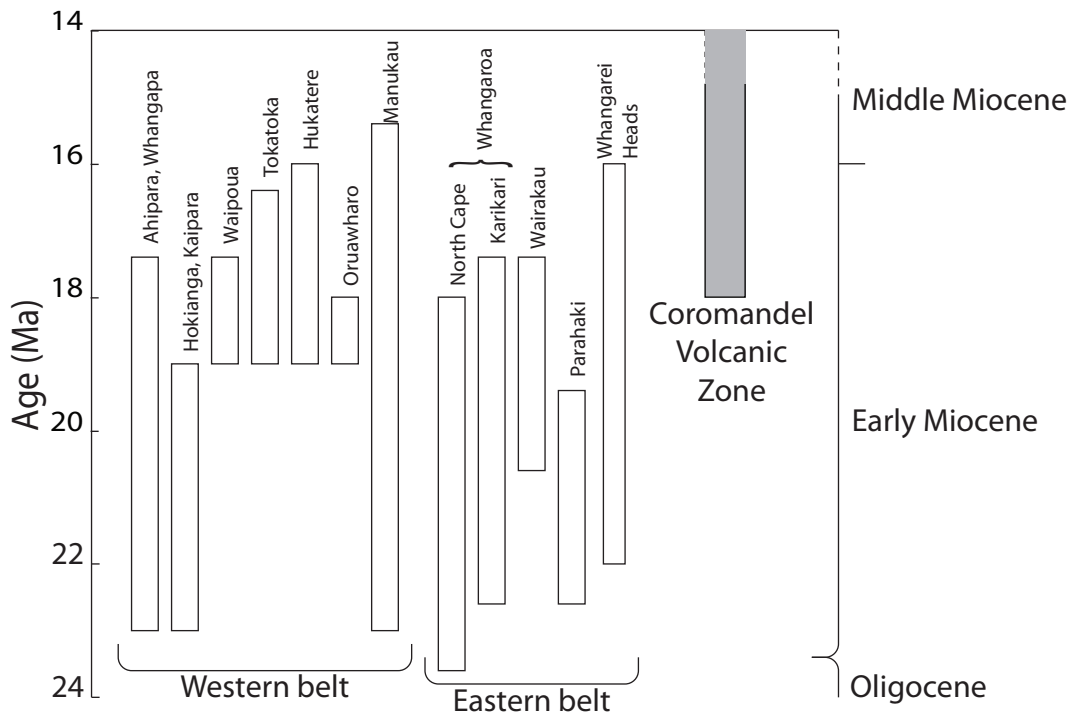


Fig. 2.2 Age ranges of the major volcanic centres of the Northland Arc. Based on the compilation of Hayward et al. (2001).

Northland Arc is unusually non-linear, being approximately 200 km wide (NE to SW) and 350 km long, striking NW. However, a dredged basaltic andesite from the Reinga Ridge, $^{40}\text{Ar}/^{39}\text{Ar}$ dated at 21.0 Ma, could represent the northwesternmost known Northland Arc activity, and if so the total length of the arc is at least 500 km (Mortimer et al., 2010). Northland Arc rocks generally have an arc-type trace element composition. Additionally, a distinct style of volcanism is recorded by polymict, partly volcanoclastic conglomerates in the Waitemata Basin containing 20 Ma basaltic pebbles with an ocean island basalt (OIB)-like trace element distribution. They have been interpreted to represent asthenosphere-derived magmas that erupted where mantle upwelling occurred around the slab edge (Shane et al., 2010, and references therein).

Four western belt volcanic centers are preserved onshore. The Waipoua center is the remnant of a basaltic shield volcano, and the Manukau/Waitakere center is the remnant of a basaltic andesitic cone complex (Smith et al., 1989). The remains of both of these centers still form topographic highs onshore and can be traced on seismic sections up to 30-50 km west of the present coastline (Herzer, 1995). The Hukatere and Tokatoka centers have a much smaller aerial extent, occur entirely on-land, and comprise dispersed plugs, dykes, flows and pyroclastic sequences (Smith et al., 1989). Additionally, six larger, and numerous smaller volcanic centers have been identified on seismic sections off the west coast of Northland. The maximum ascertainable ages of the oldest centers are around 22 Ma, although the remains of earlier volcanism may be masked by younger rocks. Volcanism in the offshore western belt declined

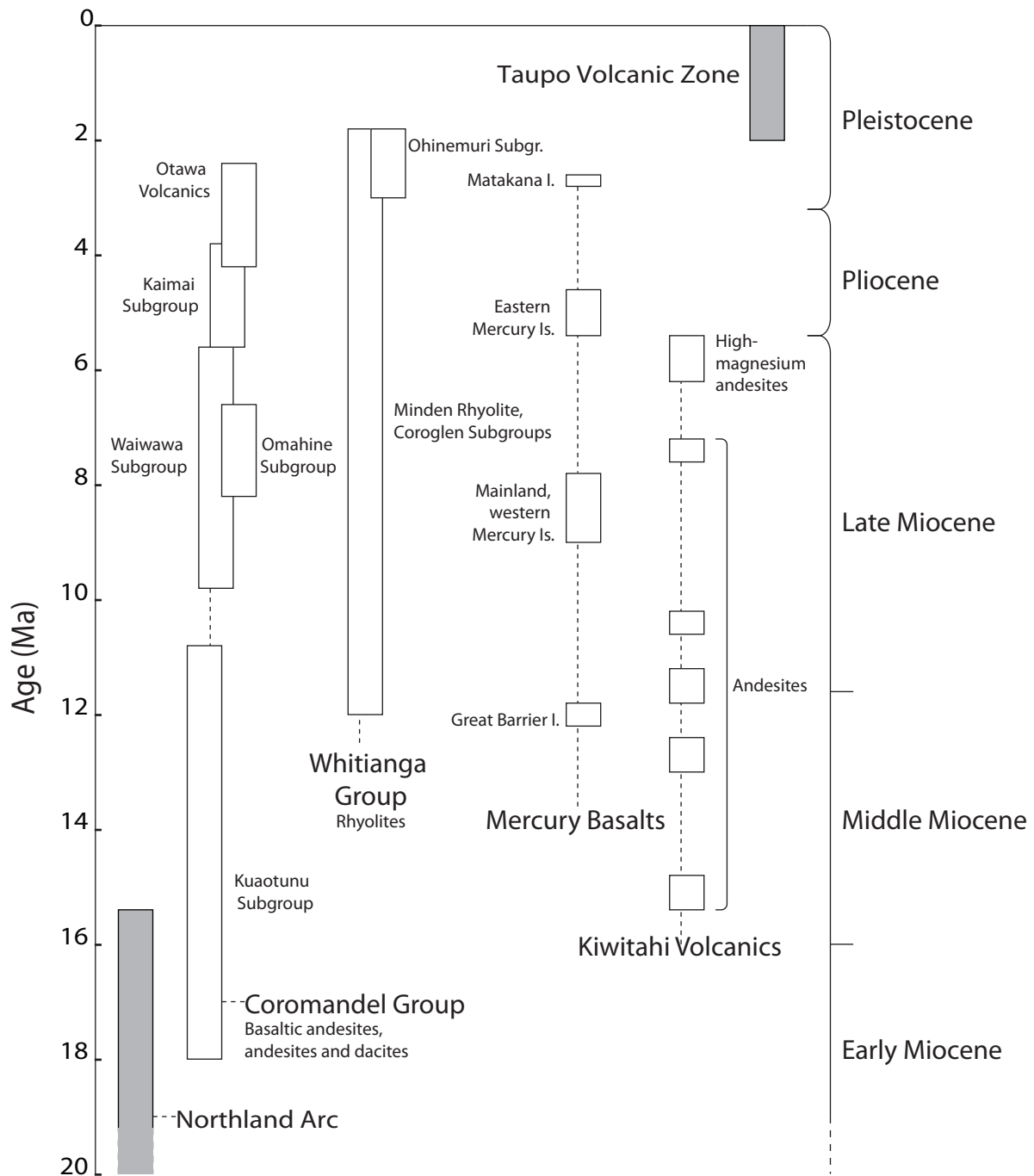


Fig. 2.3 Volcanic stratigraphy of the Coromandel Volcanic Zone at the Subgroup level. Compiled from data in Skinner (1986), Adams et al. (1994), Brathwaite and Christie (1996), Nicholson et al. (2004) and Briggs et al. (2005).

from ~19 Ma and had ceased entirely by 16 Ma (Herzer, 1995). Western belt rocks are typically strongly porphyritic plagioclase + pyroxene ± olivine phyric basalts, basaltic andesites and andesites; dacites and rhyolites are rare (Smith et al., 1989).

The eastern belt comprises three major volcanic and sub-volcanic centers that are preserved partly on-shore along the east coast of Northland. The predominant rock types in this eastern belt are two-pyroxene andesites, hornblende andesite and hornblende dacites, with subordinate rhyolite and basaltic andesite (Smith et al., 1989). Some andesite lavas at the Taurikura center contain grossular-rich garnet (Day et al.,

1992). In contrast to the western belt, basalts are nearly absent (Smith et al., 1989).

2.2.3. Coromandel Volcanic Zone - Setting

The Coromandel Volcanic Zone (CVZ) comprises volcanic rocks on Great Barrier Island, the Coromandel Peninsula and surrounding islands. The wider 'Hauraki Volcanic Region' further includes small volcanic centers of the Kiwitahi volcanic chain (Skinner, 1986). The Miocene-Pliocene CVZ succession erupted to the SE of the older Northland Arc eastern belt, and is overlapped in its southeastern segment by deposits of the younger Taupo Volcanic Zone (TVZ).

Mesozoic metasedimentary basement rocks of the Waipapa Terrane are exposed in the northern Coromandel peninsula and on Great Barrier Island (Skinner, 1972). At localities in the northern Coromandel peninsula and on Great Barrier Island, Waipapa Terrane rocks have whole-rock K-Ar ages between 142.7 ± 2.8 and 101.4 ± 2.0 Ma (Adams and Maas, 2004). The basement is locally unconformably overlain by Early Cenozoic sediments (Skinner, 1986). The NNW-trending Coromandel peninsula is a horst that follows basement fault trends, and is flanked by the Hauraki Rift, a half-graben that is downthrown to the east (Hochstein et al., 1986; Hochstein and Ballance, 1993). The timing of the initiation of subsidence in the Hauraki Rift is ambiguous. Hochstein and Ballance (1993) suggested a possible Late Miocene inception at c. 7 Ma. Hayward et al. (2006) proposed possible initiation in the early Pleistocene, based on the occurrence of quartz vein and altered andesite pebbles with a likely provenance in the Coromandel peninsula in Pleistocene conglomerates west of the Hauraki Rift. Briggs et al. (2005) demonstrated that in its southern segment, at least 40% of throw on the Hauraki Fault occurred between 2.09 and 1.21 Ma. Each of these interpretations has subsidence post-dating most CVZ volcanism.

2.2.4. Coromandel Volcanic Zone - Volcanism

The CVZ volcanic succession covers much of Great Barrier Island, the Coromandel Peninsula and the wider Hauraki region. As well, submerged igneous rocks form a plateau that extends towards the Colville Ridge (Skinner, 1986). The oldest, 18 Ma volcanic rocks occur in the northern Coromandel Peninsula, the youngest c. 2 Ma rocks occur in the southernmost CVZ (Fig. 2.3; Adams et al., 1994a; Brathwaite and Christie, 1996; Briggs et al., 2005). The same age trend occurs in the SSE-striking Kiwitahi chain, a series of small volcanic centres that formed along the western boundary of the Hauraki Rift (Black et al., 1992). Volcanic rocks in the CVZ form four main rock types: basalts, high-magnesium andesites, calc-alkaline andesites and rhyolites. Calc-alkaline andesites and rhyolites form approximately 60% and 40%

of the volcanic cover, respectively (Christie et al., 2007), whereas high-magnesium andesites and basalts erupted in subordinate volumes at the continental and oceanic margins of the CVZ.

Coromandel Group Early volcanism in the CVZ, between 18-12 Ma, consisted only of basaltic andesitic, andesitic and dacitic cone-building eruptions in the northern Coromandel peninsula, on Great Barrier Island and in the northern Kiwitahi chain (Black et al., 1992; Adams et al., 1994a). Between 12 and 2.5 Ma, the same style of andesitic volcanism persisted in addition to the progressive appearance of rhyolites and basalts (c. 12 Ma) and high-magnesium andesites (c. 6.2 Ma). This andesitic succession forms the Coromandel Group and occurs as massive flows, autoclastic breccias, lahars, tuffs and dykes (Skinner, 1986). As well, uplifted basement rocks host shallowly intruded, subvolcanic plutons at Paritu in the northern Coromandel peninsula, at Miner's Head on Great Barrier Island and on Cuvier Island in the northern CVZ (Black, 1967; Skinner, 1972). The plutons comprise gabbro, diorite, granodiorite and tonalite with ages in the range 17.6-16.4 Ma (Richards et al., 1966; Adams et al., 1994a; Adams et al., 1994b). The Coromandel Group succession is subdivided into four subgroups, each comprising a number of formations distinguished on the basis of petrographic properties and field relations (Skinner, 1986). The volcanic and subvolcanic Coromandel Group rocks in the northern CVZ form the Kuaotunu Subgroup. Coromandel Group rocks in the central CVZ with ages between 10 and 5.5 Ma form the Waiwawa and Omahine Subgroups, which are distinguished on a stratigraphic basis: Waiwawa Subgroup andesites occur at a lower stratigraphic level than Whitianga Group rhyolites, whereas the Omahine Subgroup comprises andesites that overlie the rhyolitic succession of the Whitianga Group. The Kaimai Subgroup comprises the andesitic rocks in the southern CVZ. The relative chronology was validated by radiometric dating (Adams et al., 1994a; Brathwaite and Christie, 1996; Briggs et al., 2005): Kuaotunu Subgroup rocks erupted prior to 10.5 Ma; the Waiwawa and Omahine Subgroups have mostly overlapping ages between c. 10-5.5 Ma, although locally Omahine Subgroup rocks postdate Waiwawa Subgroup rocks; and Kaimai Subgroup rocks, including the andesitic rocks of the southernmost CVZ, have ages younger than 6 Ma.

Whitianga Group Rhyolites in the CVZ form the Whitianga Group and occur on Great Barrier Island, on Great Mercury Island and the Aldermen Islands east of the Coromandel Peninsula, and on the eastern half of the peninsula itself. Whitianga Group includes the eruptive silicic rocks that are preserved on the Coromandel Peninsula, Great Barrier Island, and the Aldermen and Mercury Islands. Whitianga Group rhyolites principally occur as lavas and as ignimbrite sheets, related to c. 12 volcanic centres, of which at least some were calderas (Briggs and Fulton, 1990; Skinner, 1993; Skinner, 1995; Brathwaite

and Christie, 1996; Briggs et al., 1996; Malengreau et al., 2000; Smith et al., 2006a). The earliest silicic activity is recorded on Great Barrier Island and nearby Rakitu Island, dated at c. 11.5 Ma (Nicholson et al., 2004). Silicic activity continued in offshore centers and recommenced on Great Barrier Island between c. 8.8-8.1 Ma (Nicholson et al., 2004). On the Coromandel Peninsula, the oldest recorded silicic eruption formed the Carina Rock Ignimbrite (c. 10 Ma); major silicic activity associated with caldera formation on the Coromandel Peninsula is recorded from c. 8.1 Ma (Adams et al., 1994a). Rhyolitic eruptions in the CVZ continued at least until 1.95 Ma in the Tauranga area (Adams et al., 1994a,b; Briggs et al., 2005). Although the onshore record shows hiatuses, fission-track ages of silicic tephras recovered by ocean drilling in the Pacific east of the CVZ show a mostly continuous record of eruptions from c. 12 Ma to the end of CVZ activity. However, a significant, c. 700 kyr hiatus with no recorded silicic eruptions occurred between 7.0 and 6.3 Ma (Carter et al., 2003).

Three subgroups of the Whitianga Group are identified by Skinner (1986) and Brathwaite and Christie (1996), each comprising a number of formations. The Coroglen and Ohinemuri subgroups comprise ignimbrites, some of which record caldera-forming eruptions, as well as diverse intercalated rocks. The Minden Rhyolite Subgroup includes rhyolitic lavas that occur mainly as domes. About eight calderas have been identified, with diameters in the order of 15 to 20 km based on field mapping and geophysical data (Skinner, 1986; Briggs and Fulton, 1990; Malengreau et al., 2000; Smith et al., 2006a). The calderas are characterised by regional gravity field lows, contrasting with the neutral or positive anomalies associated with intermediate volcanics of Coromandel Group. Gravity data modelling indicates the Kapowai, Whitianga and Wharekawa calderas in the northern and central CVZ are filled with rhyolitic material to depths of 1.5-1.8 km below sea level (Malengreau et al., 2000). The Waihi Caldera in the southern CVZ comprises silicic material to a depth of close to 3 km, and has been identified as a trapdoor caldera that follows pre-existing fault patterns (Smith et al., 2006a).

Mercury Basalts Basaltic and basaltic andesitic rocks that erupted in the Mercury Islands, Aldermen Islands and on the eastern sides of Great Barrier Island and the Coromandel Peninsula form the Mercury Basalts. They are preserved as the remnants of small volcanoes, some of which formed through strombolian type eruptions producing ash and bombs, but more commonly most centres formed through Hawaiian-type sheet flows with a central spatter cone. Mercury Basalts are also preserved as dikes, commonly intruding rhyolite (Skinner, 1976; Skinner, 1986). The oldest preserved Mercury Basalts occur on Rakitu Island near Great Barrier Island and have been dated at c. 12.1 Ma, penecontemporaneous with rhyolitic volcanism in the same location (Nicholson et al., 2004). Subsequent basalt eruptions occurred

on the Coromandel Peninsula between 9.1 and 7.8 Ma, on the Mercury Islands and at Woody Hill on the peninsula between 6.0-4.6 Ma, and on Matakana Island at 2.7 Ma (Adams et al., 1994a; Briggs et al., 2005). Basaltic rocks that form the Sugarloaf rocks north of the Aldermen Islands are undated. Otherwise, the rocks on Kuaotunu Peninsula are generally more primitive than those of the Mercury Islands (Adams et al., 1994a), indicating a trend to more evolved compositions with time.

Kiwitahi Volcanics A chain of volcanic centres, the Kiwitahi Volcanics, occurs along the western boundary of the Hauraki Rift. They are included in the Coromandel Group (Skinner, 1986). The centres are typically very small and poorly preserved, commonly only as fields of massive boulders that probably represent remnants of lava flows. Only the southernmost, youngest centres preserve a volcanic cone morphology. The Kiwitahi centres generally become younger to the south. The four oldest centres erupted between between c. 15 Ma and 10.5 Ma (Black et al., 1992) and comprise hornblende-phyric andesite comparable to the andesites of the Kuaotunu Subgroup. The younger Tahuna centre erupted at 6.7 Ma (Black et al., 1992) and comprises hornblende-absent andesite, comparable to the andesite of roughly contemporaneous formations of the Waiwawa Subgroup (Brathwaite and Christie, 1996). Between 6.2-5.5 Ma, clinopyroxene-dominated basaltic andesites erupted in four centres at the southern end of the chain. These rocks do not directly resemble coeval andesites in the CVZ. Additionally, olivine-phyric basaltic andesite erupted at c. 8 Ma from a vent in close geographic association with the oldest, c. 15 Ma centre at Stony Batter on Waiheke Island (Black et al., 1992). The Stony Batter basaltic andesites compositionally resemble slightly older rocks that erupted at Ti Point in Northland, and have been interpreted as part of a backarc volcanic suite (Black et al., 1992; Smith et al., 1993; Smith et al., 1995; Huang et al., 2000)

2.2.5. Taupo Volcanic Zone – Setting

The Taupo Volcanic Zone (TVZ) is a rifted arc at the continental tip of the oceanic Kermadec-Havre Trough arc-backarc system, extending c. 250 km from Ruapehu to White Island (Fig. 2.1). The TVZ is an area of NW-SE-directed backarc extension at a rate of c. 8 mm yr⁻¹ characterised by basement subsidence along normal faults (Darby et al., 2000), contiguous along strike with the Havre Trough backarc basin and the Kermadec Arc. Volcanic sediments occur to 3 km depth, overlying a felsic crust that extends to 16 km depth, compared to 25-30 km elsewhere in the North Island; denser rocks, possibly mantle-derived basaltic intrusives and cumulates, extend to 30 km depth (Harrison and White, 2006; Stern et al., 2010). Extension in the TVZ is maintained by the clockwise rotation of the Hikurangi margin, which leads to compression in the southern North Island (Stern et al., 2006). The basement comprises metasedimentary

rocks of the Waipapa and Torlesse terranes, which have detrital zircon age spectra that indicate continuous deposition between 260 and 120 Ma (Adams et al., 2009).

2.2.6. Taupo Volcanic Zone - Volcanism

The Taupo Volcanic Zone erupted a comparable suite of rocks to the Coromandel Volcanic Zone: calc-alkaline andesites, high-magnesium andesites, rhyolites and basalts. Compared to the CVZ, however, the TVZ erupted a greater proportion of rhyolite relative to andesite (Wilson et al., 1995). Andesitic eruptions since 2 Ma formed cone volcanoes that presently predominate at the northern and southern tips of the TVZ and also occur along the eastern, trenchward rim. Additionally, buried andesitic volcanoes occur within the central, rhyolite-dominated TVZ (Wilson et al., 1995). Regular TVZ andesites are predominantly plagioclase + clinopyroxene-phyric calc-alkaline rocks. Olivine occurs in some basaltic andesites and orthopyroxene in SiO₂-rich andesites and dacites, whereas hornblende is a rare component (Cole, 1978; Graham and Hackett, 1987; Price et al., 2005). Additionally, clinopyroxene-phyric HMAs erupted from volcanoes along the western margin of the TVZ, where they locally pre-date calc-alkaline andesitic activity (Cole and Teoh, 1975; Houghton and Hackett, 1984; Froude and Cole, 1985; Graham and Hackett, 1987; Cameron et al., 2010). Additionally, subordinate high-magnesium andesites have erupted from the calc-alkaline White Island volcano since the 1970s (Cole et al., 2000).

Rhyolitic eruptions formed 8 major calderas in the central TVZ from 1.6 Ma, six of which have formed since 0.34 Ma (Houghton and Wilson, 1995). The dormant Taupo and Okataina volcanoes are the most productive volcanoes globally (Crisp, 1984; Wilson et al., 1984b; Wilson, 1993) and rhyolitic eruptions account for approximately 95% of TVZ volcanism (Healy, 1962; Wilson et al., 1995; Wilson et al., 2009). Rhyolite lavas generally have <30 vol% crystals comprising plagioclase, quartz and Fe/Ti oxides in addition to variably pyroxene, biotite and hornblende (Sutton et al., 1995; Deering et al., 2008). Basalts in the TVZ erupted in association with some calderas and with andesitic vents. They also acted as a mafic end-member component to magma mixing processes, such as in the formation of dacite from rhyolite, and triggering of rhyolitic eruptions (Wilson et al., 1984a; Leonard et al., 2002; Shane et al., 2007). The erupted TVZ basalts are porphyritic with principally olivine, plagioclase and clinopyroxene, and orthopyroxene in more silicic basalts. Crystallinity ranges from ~5 vol% in the most mafic basalts (e.g. Kakuki) to 20-50 vol% in more silicic basalts (e.g. at Ruapehu, Tongariro). Some TVZ basalts are high-alumina basalts (HAB, definition of Crawford et al., 1987).



Fig. 2.4 Epithermal deposits of the Hauraki goldfield. Modified from Christie et al. (2007). NA: Northland Arc; CVZ; Coromandel Volcanic Zone; TVZ; Taupo Volcanic Zone; CR: Colville Ridge; KA: Kermadec Arc.

2.3. Hydrothermal Alteration of the Volcanic Succession

Hydrothermal alteration has affected significant parts of the North Island arc volcanic succession. Current geothermal activity occurs mainly in the Taupo Volcanic Zone, where the upwelling of hydrothermal waters in 23 major active geothermal accounts for c. 70% of the total heat flow (Bibby et al., 1995; Hochstein, 1995). TVZ geothermal systems are driven by the deep (>5 km) circulation of meteoric water heated by intrusive rocks or magma. The composition of magmatic components in upwelling hy-

hydrothermal waters varies across the TVZ, possibly correlated with magmatic source type. Hydrothermal waters in systems in the eastern TVZ have high gas contents and contain up to 15% magmatic-derived water, and have been linked to andesitic sources, whereas waters in western geothermal systems have lower gas and magmatic water contents and have been linked to basaltic sources (Giggenbach, 1995). Extensive mineralogical, chemical and isotopic alteration of wall rocks accompanies the upwelling of hot hydrothermal waters in the TVZ. In the shallow geothermal environment, hot (>250° C) waters with high dissolved gas (CO₂, H₂S, Cl, etc.) concentrations interact with wall rocks in the central upwelling column to form the propylitic alteration mineral assemblage of quartz, K-feldspar (adularia), albite, illite, chlorite, pyrite, calcite and epidote (Giggenbach, 1984; Simmons and Browne, 2000). In permeable settings where fluid/rock ratios are high, potassic alteration forms K-feldspar and silica, and precious metals can be deposited. In the system periphery, an argillic assemblage of illite, smectite, kaolinite, calcite and silica is formed (Simmons and Browne, 2000).

Small-scale geothermal occurrences are also spread throughout older parts of the volcanic succession in the Coromandel Volcanic Zone (e.g. Hot Water Beach geothermal area; Ovens, 1976) and in Northland (e.g. Ngawha geothermal area; Browne et al., 1981). More importantly, the CVZ and Northland Arc successions show evidence in numerous locations for extinct geothermal activity in the form of hydrothermal alteration of volcanic and basement rocks. The paleosystems are defined by zones of altered rocks typically 5-50 km² in area, comparable to the size of active geothermal systems in the TVZ (Simpson and Mauk, 2004). They also show comparable styles of wall rock alteration, characterised by predominantly low-sulphidation quartz ± adularia ± calcite ± illite type assemblages and minor argillic alteration. Differential erosion has exposed varying levels of such extinct hydrothermal systems, from near-paleosurface to c. 1300 m depth. Associated mineral deposits range from relatively shallow epithermal precious metal (Au-Ag) deposits, to deeper porphyry type Au + base metal deposits (Christie et al., 2007). Epithermal-level deposits are the most commonly exposed.

Although geothermal activity affected rocks throughout the North Island arc volcanic succession, economic precious and base metal mineralizations has effectively been confined to the Coromandel Volcanic Zone. There are no known epithermal gold deposits associated with Northland volcanic rocks, despite the occurrence of hot springs-type Au-Ag prospects that could grade into epithermal deposits at depth (Christie and Barker, 2007). In the TVZ, hydrothermal fluids precipitate Au-rich scales on back-pressure plates in geothermal power stations (Brown, 1986), and the measured gold flux in some TVZ geothermal systems is sufficient to create a world-class deposit within ca. 50 kyr (Simmons and Brown, 2007).

Nevertheless, no economic deposits are known in the TVZ. In contrast, the Hauraki goldfield in the CVZ comprises c. 50 low-sulphidation epithermal gold deposits. About 320,000 kg gold and 1.5 million kg silver were produced in the Hauraki goldfield between 1862 and 2006, with andesite-hosted deposits yielding 97% of historic production (Christie et al., 2007). Mineralisation occurs in steeply dipping NNW to NNE-NE-striking quartz veins that follow basement structural trends (Spörli et al., 2006), with most gold production from veins that strike 000°-030° and 040°-070° (Christie et al., 2007).

Of the Hauraki goldfield deposits, 18 have been dated using $^{40}\text{Ar}/^{39}\text{Ar}$, K/Ar and Re-Os methods on vein- and wall-rock-hosted alteration minerals (Skinner, 1986; Mauk and Hall, 2004; Mauk et al., in press). Of the 18 dated deposits, 10 formed between 7.1 and 5.7 Ma. Seven other deposits formed between 17 and 10 Ma, at an average rate of 1 deposit Myr^{-1} . No known deposits formed between the 10.8 Ma Waiomu deposit and the 8.3 Ma Ohui deposit. The deposits of the 7.1-5.7 Ma interval produced 85% percent of total gold (data compiled by Christie et al., 2007) so the production of economic gold deposits was highly punctuated in time. Furthermore, gold endowment in this interval is strongly skewed towards three highly productive deposits, dominated by the Martha deposit (63.1% of total gold), Karangahake (8.9% of total gold) and Golden Cross (7.1% of total gold) deposits. The 11 Ma northern province Thames deposit further produced 13.6% of total gold, whereas the remaining 90% of known deposits each yielded around 1% or less of the total gold production.

Chapter 3. Northland Arc Volcanism

3.1. Summary

The Northland Arc represents the earliest stage of Cenozoic arc volcanism in northern New Zealand. Its waning overlapped in time with the onset of volcanism in the Coromandel Volcanic Zone, and the Northland Arc's eastern belt is contiguous with the Coromandel Volcanic Zone. An open question is whether the earliest CVZ volcanism occurred as the last manifestation of the Northland Arc tectonic configuration, or the first manifestation of the modern configuration associated with the young CVZ and the TVZ. As well, competing hypotheses exist regarding the nature of the subduction system(s) that drove Northland Arc volcanism. This chapter presents new geochemical and isotope data on a suite of rocks representing the major onland centres of the Northland Arc, in the form of a paper that has been accepted for publication in *Journal of Volcanology and Geothermal Research*. These data are used to assess the petrogenesis of rocks in the various Northland Arc centers, with particular emphasis on differences between centres of the eastern and western belts. Western belt rocks are generally more mafic (basaltic and basaltic andesitic), have unfractionated REE ratios, and relatively unradiogenic isotope compositions. Eastern belt rocks generally have more silicic compositions (andesitic and dacitic), have increasingly fractionated REE ratios with increasing SiO₂, and have relatively radiogenic isotope compositions. The different REE behaviour correlates with the general presence in eastern belt rocks of REE-fractionating minerals hornblende and, subordinately, garnet. In contrast, the western belt rocks characteristically lack hornblende and garnet. Their plagioclase + pyroxene-dominated crystal assemblages comprise phases that readily crystallize at shallow depth. The difference in isotope properties suggests the western belt magmas developed in closed magmatic systems, relative to the crust. These features can be interpreted to indicate that eastern belt magmas developed in the deep and middle crust in a 'hot zone'-like setting, whereas western belt magmas experienced relatively little crustal differentiation. Nevertheless, rocks in both belts have comparable arc-type trace element signatures and the contrasting natures of the belts do not appear to pertain to subduction polarity. Instead, variation in crustal thickness or composition across the arc may be critical, with potentially thin crust in the west allowing ponding at shallow depth of mafic magmas, and thicker crust in the east leading to ponding and differentiation in the deep crust.

3.2. Geochemistry of the Early Miocene Volcanic Succession of Northland, New Zealand, and Implications for the Evolution of Subduction in the Southwest Pacific.

Mathijs A. Booden^{1*}, Ian E.M. Smith, Philippa M. Black, Jeffrey L. Mauk

School of Geography, Geology and Environmental Science, The University of Auckland, PB92019 Auckland, New Zealand

3.2.0.0. Abstract

Latest Oligocene and Early Miocene volcanic rocks occur on the Northland Peninsula, New Zealand, and record the inception of Cenozoic subduction-related volcanism in the North Island that eventually evolved to its present manifestation in the Taupo Volcanic Zone. This NW-striking Northland Arc is continuous with the Reinga Ridge and comprises two parallel belts of volcanic centres c. 60 km apart. A plethora of tectonic models have been proposed for its origins. We acquired new trace element and Sr-Nd isotope data to better constrain such models. All Northland Arc rocks carry an arc-type trace element signature, however distinct differences exist between rocks of the eastern and western belt. Eastern belt rocks are typically andesites and dacites and have relatively evolved isotope ratios indicating assimilated crustal material, and commonly contain hornblende. Additionally some eastern belt rocks with highly evolved isotope compositions show fractionated REE compositions consistent with residual garnet, and some contain garnetiferous inclusions in addition to schistose crustal fragments. In contrast, western belt rocks are mostly basalts or basaltic andesites with relatively primitive Sr-Nd isotope compositions, do not contain hornblende and show no rare earth element evidence for cryptic amphibole fractionation. Eastern and western belt rocks contain comparable slab-derived fractions of fluid-mobile trace elements and invariably possess an arc signature. Therefore the difference between the belts may be best explained as due to variation in crustal thickness across the Northland Peninsula, where western belt centres erupted onto a thinner crustal section than eastern belt rocks.

The consistent arc signature throughout the Northland Arc favours an origin in response to an actual, if short-lived subduction event, rather than slab detachment as proposed in some models. No Northland Arc rocks possess a convincing adakite-like composition that might reflect the subduction of very young oceanic lithosphere such as that of the Oligocene South Fiji Basin. Therefore we favour a model in which subduction of old (Cretaceous) lithosphere drove subduction.

Keywords: Northland; SW Pacific; subduction; continental arc; geochemistry.

3.2.1. Introduction

The tectonic and associated volcanic evolution of the SW Pacific region is a matter of ongoing debate (Crawford et al., 2003; Mortimer et al., 2007; Schellart, 2007; Whattam et al., 2008; Herzer et al., 2009). This dynamically evolving boundary separating the Pacific and Australian plates is defined by a legacy of Cenozoic volcanic rock associations that have characterised the nature of the plate boundary in time and space. A key part of this plate boundary system lies in northern New Zealand where the circum-Pacific ‘ring of fire’ reaches its southwestern termination and where there has been a complex sequence of temporally and spatially discrete volcanic systems that trace the inception of subduction and its subsequent spatial evolution as a convergent plate boundary. In this paper we describe the rocks that represent the beginnings of Cenozoic plate convergence in the northern New Zealand region; these are the rocks of the Northland Arc. An overview of the tectonic elements that comprise the wider SW Pacific region is beyond the scope of this paper. Useful discussions on this subject are provided by Crawford et al (2003) and Mortimer et al. (2010). We summarise the present-day location of ridges and basins in the immediate area in Figure 3.1 (inset).

Northland Arc rocks are the oldest Cenozoic arc-type volcanic rocks that occur above sea level on New Zealand’s North Island (Fig. 3.1). Some are dated to the earliest Miocene but volcanic activity in Northland became continuous between c. 23 Ma and 16 Ma (Fig. 3.2), forming numerous volcanic centres that collectively comprise the Northland Arc (Smith et al., 1989 and references therein; Herzer, 1995; Hayward et al., 2001). The Northland Arc was a precursor to later subduction-related volcanism in the Coromandel and Taranaki Basin areas. Ultimately this volcanism developed into the currently active Taupo Volcanic Zone.

Hitherto analytical data for Northland Arc rocks have been contained in unpublished theses and in short published summaries (Smith et al., 1989; 1995). Here we present the first high-quality data set of new whole-rock major and trace element analyses for a suite of volcanic rocks that represent the major on-land volcanic and sub-volcanic centers of the Northland Arc, together with whole-rock Sr-Nd isotope data for selected rocks. The aim of the paper is to examine the nature and tectonic implications of the arc and we specifically address the question of whether across-arc variation in geochemical parameters can define the polarity of the extinct subduction system and discuss implications for the development of volcanism in the SW Pacific region.

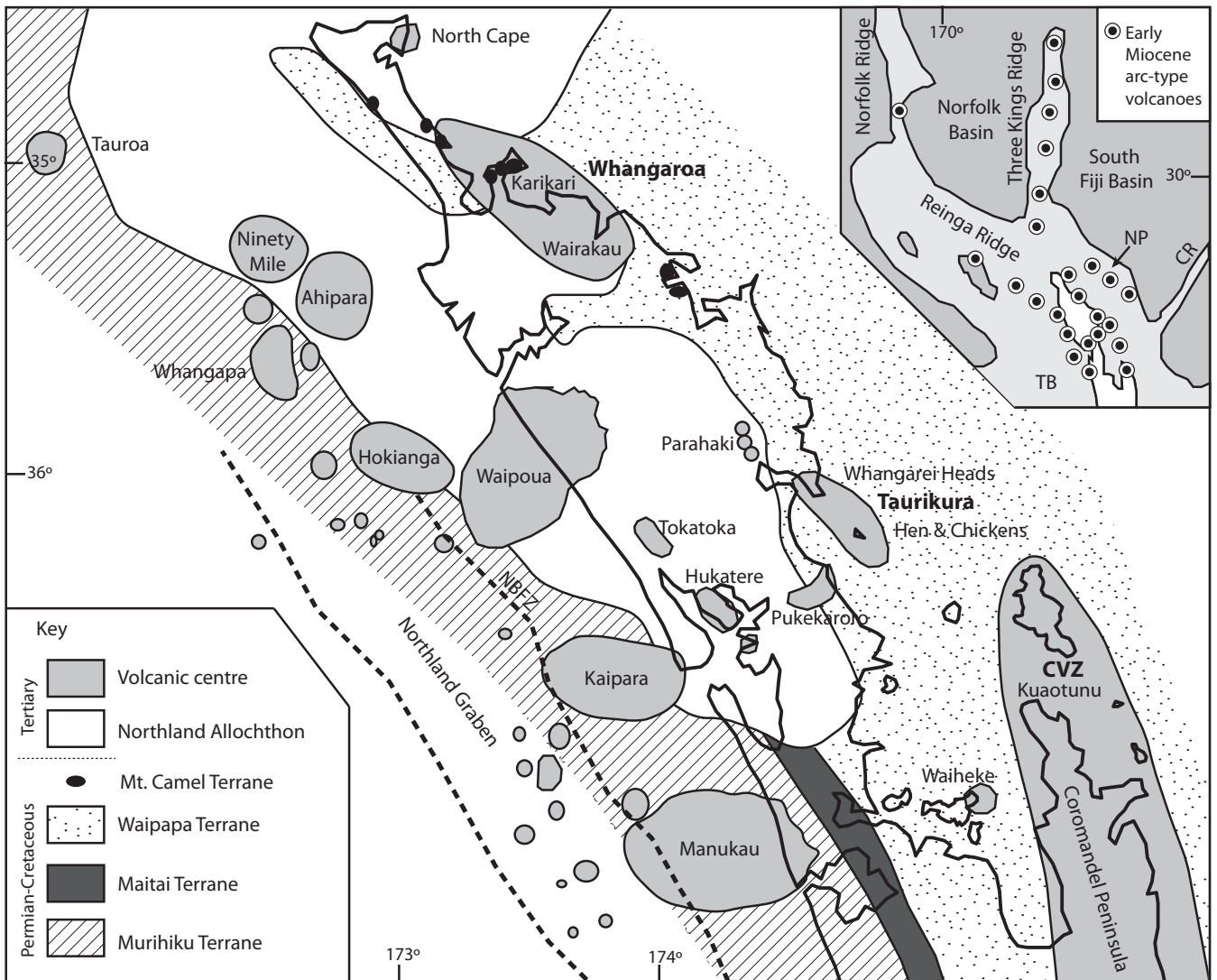


Fig. 3.1 Simple geologic map of the Northland Peninsula. Extent of basement terranes and the Northland Allochthon after Mortimer (2004), Neogene volcanic centres after Herzer (1995; 2009) and Hayward et al. (2001). NBFZ – Northland Boundary Fault Zone. Inset shows the locations of the main ridges, basins and Early Miocene arc-type volcanoes in the immediate area after Hayward et al. (2001). CR – Colville Ridge; NP – Northland Plateau; TB – Taranaki Basin.

3.2.2. Geologic Setting of the Northland Arc

The volcanic centres of the Northland Arc occur on the Northland Peninsula, which is the subaerial north-western extension of the New Zealand microcontinent. The basement of the Northland Peninsula consists of Permian to Jurassic metasedimentary rocks that are described as western (Murihiku) and eastern (Waipapa) Terranes, separated along the peninsula axis by the Maitai Terrane (Fig. 3.1). Murihiku Terrane represents a Late Permian to Late Jurassic fore- or back-arc basin; the Maitai Terrane comprises a Permian ophiolite complex with overlying Permian to Triassic volcanoclastic sequence; the Waipapa Terrane comprises Triassic to Early Jurassic basalt, chert and limestone with tectonically associated clastic trench deposits (Ballance and Campbell, 1993; Black, 1994; Sivell and McCulloch, 2000). The Mt.

Camel Terrane occurs in the far north and is a distinct Late Cretaceous sequence of clastic sediments and keratophytic volcanic rocks (Isaac et al., 1988; Nicholson and Black, 2004). These basement rocks are unconformably overlain by autochthonous Tertiary sedimentary rocks and by the complexly folded, fractured and sheared thrust sheets of the Northland Allochthon. The Allochthon comprises Cretaceous to Oligocene sedimentary sequences that have a total stratigraphic thickness of c. 7 km (Ballance and Spörli, 1979). The topmost section of the allochthon comprises a number of isolated, rootless massifs covering c. $2.6 \cdot 10^3$ km² (Sharp et al., 1989; Malpas et al., 1992). Many of the massifs have an oceanic crust-like architecture, but comprise rocks with a subduced arc-type trace element signature. Their interpretation has in the past been tempered by uncertainties as to the age of the rocks as well as their geochemical nature. Recently it has been recognised that they represent at least two discrete rock associations with distinct temporal ranges and tectonic significance (Whattam et al., 2004). However, the bulk of these rocks are now generally interpreted (Whattam et al., 2004) to represent oceanic lithosphere formed over a NE-dipping subduction zone north of the Northland Peninsula between 26-29 Ma, and obducted in the Late Oligocene just prior to or coeval with the earliest Northland Arc volcanic activity.

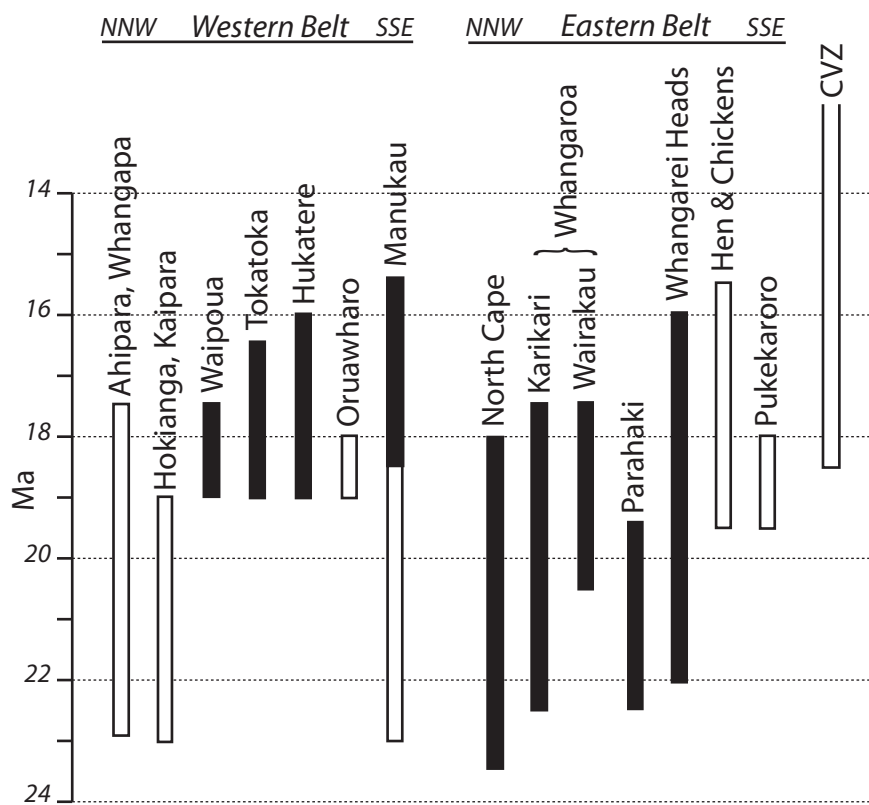


Fig. 3.2 Age ranges for the Neogene volcanic centres of the Northland Arc and Coromandel. Black bars indicate centres from which samples are included in this study. Modified after Hayward et al. (2001).

3.2.3. Volcanic Centres of the Northland Arc

The on-land volcanic centres that form the Northland Arc extend from North Cape to the Auckland region, and to the northern Coromandel Peninsula (Fig. 3.1). The centres are sited along the eastern and western sides of the Northland peninsula, separated by a 30-60 km wide non-volcanic belt and for this reason the arc has often been regarded as two discrete volcanic arcs (e.g. Waitakare and Coromandel arcs of Ballance, 1976; Marshall and Searle belts of Kear, 1994). Here we follow the ‘eastern’ and ‘western’ belt terminology of Thompson (1965). Rocks from each of these belts erupted contemporaneously, and this led Hayward et al. (2001) to conclude that the belts comprise a single arc with a width of c. 200 km. The Northland Arc has a length of c. 350 km on land, but extends to the NW as the submerged Reinga Ridge. A dredged basaltic andesite from the Reinga Ridge with a $^{40}\text{Ar}/^{39}\text{Ar}$ age of 21.0 Ma is the most north-western Northland Arc rock known and makes for a total known arc length of c. 500 km (Mortimer et al., 2010). However, the Reinga Ridge extends even further west and volcanic activity possibly extended to the present Norfolk Ridge, for a maximum arc length of c. 850 km (Fig. 3.1, inset; Mortimer et al., 1998).

The eruptive centres of the western belt are only partly exposed on land; they are mostly submerged and buried in post-volcanic offshore sedimentary basins. Rocks in the western belt centres are predominantly basalts, basaltic andesites and two-pyroxene andesites. They are typically strongly porphyritic rocks, dominated by plagioclase and pyroxene. Hornblende is absent except in the andesites of the Tokatoka centre (Smith et al., 1989). Dacite and rhyolite are rare, although they occur commonly as clasts in associated volcanoclastic sediments. The major on-land centres represented in this study are the Waipoua basaltic shield volcano including Omapere conglomerate, the Manukau andesitic stratovolcano complex, and the smaller Tokatoka and Hukatere complexes comprising dispersed outcrops of plugs, dykes and lava flows together with pyroclastic sequences. The western belt is also thought to include six major buried off-shore centres: the Kaipara Volcanic Complex, and the relatively smaller Hokianga, Whangape, Ahipara, Ninety Mile and Tauroa centres. All of these are presumably stratovolcanic complexes but none have been sampled by dredging or drilling (Herzer, 1995). Shane et al. (2010) have raised the possibility that some of these may represent an earlier distinct episode of intraplate basaltic volcanism. The long apparent duration of activity of the Manukau centre is principally based on seismic stratigraphy (c. 22-15 Ma; Herzer, 1995), however only two breccia clasts from on-land exposures yield ages older than 18.4 Ma (Hayward, 1993; Hayward et al., 2001). It is possible that the older Manukau centre rocks could also represent intraplate activity, and this could place the onset of arc volcanism proper in the southern North-

land Arc at a younger date (i.e. post-19 Ma). If a younger age for the Manukau centre is accepted the western belt centre ages show a north-south younging similar to that of the eastern belt centres. Seismic age constraints on the offshore volcanic centres indicate eruption within the timeframe defined by on-land centres (Herzer, 1995). Figure 3.2 summarises age ranges for Northland Arc volcanic centres.

The centres that comprise the eastern belt are all exposed partly or wholly on land. The major eastern belt centres are the North Cape, Karikari & Wairakau (together referred to as Whangaroa by Hayward et al. (2001)) and Whangarei Heads-Hen and Chickens (together referred to as Taurikura) centres, all of which are predominantly andesitic, as well as the Parahaki dacites. Rocks are typically porphyritic two-pyroxene andesites, hornblende andesites and hornblende dacites. Basaltic andesites are rare and basalts are virtually absent in eastern belt centres (Smith et al., 1989). Radiometric and biostratigraphic dates indicate that the earliest eruptions occurred near North Cape in the latest Oligocene (c. 23.5 Ma) followed within 1.5 Myr by the onset of activity at the Karikari and Whangarei Heads centres. Activity lasted to c. 16-15.5 Ma with the youngest rocks occurring in the Taurikura centre. Volcanic rocks of the Kuaotunu centre, in northern Coromandel Peninsula, are not included in this study but have been considered to be a part of the eastern belt of the Northland Arc by some workers (e.g. Hayward et al., 2001).

Garnet-bearing andesite lavas occur at Whangarei Heads (Day et al., 1992). Garnet in these lavas occurs as xenocrysts and in xenolithic fragments. Further, Whangarei Heads lavas contain amphibole-rich inclusions that could represent cumulates, and schistose mafic inclusions that are clearly not magmatic but possibly represent parts of the crust that underlies the greywacke basement. Although a detailed description of these lavas and their inclusions is outside the scope of this study, we include geochemical and isotope data for some inclusions because they provide a unique perspective on the crustal architecture beneath the eastern belt volcanoes (Table 3.3).

3.2.4. Sampling and Analytical Methods

Rock fragments from which weathered surfaces had been removed were soaked in distilled water, dried and then crushed between tungsten carbide plates and 100 g aliquots ground to <200 mesh in a tungsten carbide ring grinder. Major and some trace element data were determined by X-ray fluorescence (Table 3.1 (following pages)) Whole-rock geochemistry of representative Northland Arc volcanic rocks. All concentrations measured by XRF at the University of Auckland except italicized elements by LA-ICP-MS at the Australian National University. LOI – Loss on Ignition. Major element oxide compositions have been normalised to 100% and are reported in weight percent. Trace elements are reported in parts per million.

Sample	38649	38651	38650	41244	41386	41294	34917	34930	39762	33115	19901	32942	32953	33095	33005
Locality	North Cape		~	Karikari		~	Wairakau		~	Whangarei		~	Parahaki		~
Rock type	Bas. and.	And.	Dac.	Basalt	Bas. and.	Trach. dac.	Bas. and.	An-desite	An-desite	Bas. and.	And.	And.	Rhyo-lite	Trach. dac.	Rhyo-lite
SiO ₂	54.8	59.7	63.3	49.0	56.5	67.9	56.0	58.1	62.4	55.6	59.1	60.6	71.4	66.7	69.5
TiO ₂	1.2	0.7	0.6	1.4	0.7	0.4	0.8	0.8	0.8	0.7	1.0	0.9	0.2	0.6	0.3
Al ₂ O ₃	14.8	17.1	17.5	13.2	15.7	16.6	13.9	14.7	17.5	16.0	17.8	18.6	17.2	17.6	17.4
FeO	9.60	4.55	3.38	11.95	7.24	1.85	6.43	5.48	3.45	5.86	5.52	4.31	1.20	2.38	1.73
Fe ₂ O ₃	2.88	1.59	1.35	2.39	2.17	0.74	1.93	1.92	1.21	1.76	1.93	1.51	0.60	0.95	0.69
MnO	0.2	0.1	0.1	0.2	0.2	0.0	0.1	0.1	0.1	0.1	0.2	0.1	0.0	0.0	0.0
MgO	3.8	4.4	2.7	10.6	6.8	0.9	8.5	6.3	2.8	8.1	3.2	2.2	0.4	1.2	0.6
CaO	8.3	6.8	5.3	9.3	6.6	3.4	7.8	7.5	5.3	7.9	6.7	6.0	2.2	3.3	3.0
Na ₂ O	3.5	3.8	4.4	1.6	2.6	4.1	2.5	2.7	3.6	2.7	2.7	4.2	4.0	4.3	4.5
K ₂ O	0.8	1.1	1.3	0.3	1.4	4.0	1.9	2.1	2.7	1.1	1.6	1.4	2.8	2.9	2.1
P ₂ O ₅	0.2	0.2	0.1	0.1	0.1	0.1	0.2	0.2	0.2	0.1	0.2	0.2	0.1	0.1	0.1
LOI	1.03	1.17	1.35	0.17	2.71	0.36	0.92	1.06	1.44	0.85	2.29	1.15	1.74	1.09	1.10
Sc	39.4	22.8	11.6	49.8	28.9	9.0	28.8	27.3	18.6	29.5	25.7	8.8	2.6	6.6	3.1
V	444.1	152.0	92.3	507.7	193.4	72.5	211.1	202.8	156.4	177.5	165.3	71.0	39.7	55.6	40.6
Cr	18.6	174.4	62.4	289.8	388.5	18.5	505.9	328.2	113.0	598.7	16.5	21.7	5.7	18.8	7.3
Co	57.3	37.3	30.7	53.3	34.0	38.3	45.2	38.4	26.5	40.9	91.0	20.6	7.0	22.9	19.5
Ni	14.5	35.6	21.9	60.9	96.7	6.7	114.3	61.6	29.4	140.6	7.1	11.9	3.8	15.0	4.1
Cu	165.8	31.6	24.1	30.0	74.2	11.0	48.3	41.7	38.7	44.4	29.8	17.7	10.5	12.1	9.0
Zn	89.2	52.3	53.3	93.4	77.2	18.0	54.5	53.7	53.3	52.8	672.8	53.1	48.9	53.2	53.2
Ga	16.4	17.0	17.5	13.1	14.2	17.0	14.4	15.2	18.5	14.1	16.5	19.1	19.0	18.4	19.3
Rb	16.7	64.4	66.2	8.2	39.4	111.4	50.8	58.0	90.2	38.9	48.8	43.0	107.4	97.0	76.7
Sr	261	295	322	204	211	243	338	348	357	178	272	323	226	266	269
Y	27.05	14.01	12.21	10.82	16.81	23.48	17.77	18.18	19.62	18.28	22.16	12.75	1.65	11.24	4.08
Zr	85	105	126	25	84	234	113	123	168	79	82	266	143	142	179
Nb	2.6	5.2	5.8	1.5	3.8	7.7	4.6	5.2	6.9	3.7	6.4	7.9	8.8	7.4	9.0
Cs	2.4	5.0	4.3	0.4	4.8	1.5	2.5	2.9	6.2	1.5	0.5	3.9	4.4	1.8	4.0
Ba	345	423	570	83	261	653	356	412	483	225	255	300	583	563	510
La	11.3	13.6	14.6	3.4	10.6	25.6	15.8	17.1	20.8	10.1	25.0	42.6	20.0	21.9	29.7
Ce	25.2	29.6	30.1	7.9	23.9	52.9	33.3	35.5	43.5	21.4	31.9	88.8	39.2	47.0	57.5
Pr	3.3	3.4	3.3	1.1	3.0	5.9	4.1	4.4	5.1	2.7	3.7	9.9	4.0	5.2	6.0
Nd	15.8	14.3	13.3	5.4	13.4	23.4	17.4	18.2	21.4	11.5	15.9	39.2	14.7	21.0	22.4
Sm	4.2	3.0	2.7	1.6	3.3	4.7	3.9	4.0	4.6	2.7	3.8	7.0	2.4	4.2	3.8
Eu	1.32	0.92	0.74	0.64	0.85	0.94	1.06	1.09	1.17	0.83	0.98	1.67	0.60	1.02	0.92
Gd	4.6	2.8	2.4	1.9	3.5	4.3	3.6	3.8	4.2	2.9	4.0	5.4	1.4	3.7	2.4
Tb	0.72	0.43	0.33	0.31	0.51	0.65	0.52	0.53	0.59	0.48	0.65	0.64	0.13	0.46	0.24
Dy	5.0	2.8	2.1	2.2	3.4	4.4	3.5	3.5	3.8	3.2	4.3	3.1	0.4	2.5	1.1
Ho	1.06	0.55	0.41	0.44	0.67	0.87	0.68	0.69	0.73	0.68	0.86	0.46	0.05	0.39	0.14
Er	3.2	1.6	1.2	1.3	1.9	2.6	1.9	2.0	2.1	2.1	2.5	1.1	0.1	1.0	0.3
Tm	0.48	0.25	0.19	0.20	0.30	0.38	0.30	0.31	0.33	0.33	0.37	0.15	0.03	0.13	0.05
Yb	3.2	1.6	1.2	1.3	2.1	2.7	1.96	1.97	2.19	2.0	2.38	1.00	0.08	0.7	0.3
Lu	0.48	0.24	0.18	0.20	0.30	0.40	0.28	0.28	0.30	0.34	0.34	0.13	0.01	0.12	0.04
Hf	2.71	3.04	3.74	0.82	2.45	6.46	3.2	3.5	4.5	2.19	2.7	6.4	4.3	4.08	4.95
Ta	0.38	0.97	0.90	0.30	0.39	1.53	0.69	0.92	0.85	0.31	0.97	0.80	0.69	0.73	1.03
Pb	7.05	13.48	13.97	2.69	5.02	5.45	7.87	9.04	12.06	8.90	34.52	10.18	17.56	17.54	17.20
Th	3.55	5.97	6.03	0.94	3.71	14.00	6.11	6.77	9.25	4.11	9.78	17.86	10.45	9.07	12.93
U	0.89	1.64	1.54	0.26	1.14	3.19	1.41	1.57	2.27	1.09	2.36	2.51	2.68	2.84	2.65

	32985	5715	5716b	5716a	26720	23223	23222	36210	38515	38496	7841	7305	7306	24275	24175	38485	
Loc.	~	Omapere			~	Waipoua		~	Hukatere		~	Tokatoka		~	Manukau		~
Rock type	Rhyolite	Bas. and.	Trachyte	Trachyte	Basalt	Basalt	Basalt	Basalt	And.	Trach. dac.	Basalt	And.	Rhyolite	Basalt	And.	Trach. dac.	
SiO ₂	70.8	56.3	62.3	62.4	48.5	50.1	50.9	48.1	58.7	65.8	48.7	58.7	72.2	46.6	63.4	66.7	
TiO ₂	0.2	0.7	0.3	0.2	1.0	1.2	1.4	1.0	0.9	0.7	1.1	0.6	0.3	0.9	0.9	0.9	
Al ₂ O ₃	16.7	17.0	21.0	20.8	17.7	17.9	15.3	15.3	18.1	16.0	16.5	16.5	16.9	20.7	16.0	16.6	
FeO	1.13	5.90	1.39	1.30	8.69	9.65	11.86	9.03	5.48	3.70	9.24	4.71	0.37	9.18	4.87	2.90	
Fe ₂ O ₃	0.57	1.77	0.49	0.45	1.74	1.93	2.37	1.81	1.92	1.48	1.85	1.65	0.19	1.84	1.95	1.16	
MnO	0.0	0.1	0.0	0.0	0.2	0.2	0.2	0.2	0.2	0.1	0.2	0.1	0.0	0.2	0.1	0.0	
MgO	0.4	6.1	0.3	0.7	6.2	4.3	4.4	10.9	2.4	0.9	7.5	6.3	0.1	6.1	1.2	0.2	
CaO	3.0	8.2	3.2	3.3	12.5	10.6	9.2	10.0	6.1	2.9	11.2	7.0	2.8	12.7	4.2	3.5	
Na ₂ O	4.6	3.0	5.7	5.9	2.5	3.1	3.3	2.3	3.9	5.0	2.9	3.2	4.5	1.8	4.4	5.4	
K ₂ O	2.5	0.8	5.3	4.8	0.7	0.8	0.8	1.2	2.1	3.2	0.9	1.1	2.6	0.1	2.6	2.3	
P ₂ O ₅	0.1	0.1	0.1	0.1	0.2	0.2	0.2	0.2	0.2	0.2	0.1	0.1	0.1	0.0	0.3	0.3	
LOI	0.72	1.17	0.33	0.19	0.48	-0.06	-0.26	1.34	0.27	1.45	2.67	0.60	0.89	-0.24	0.27	0.22	
Sc	2.3	28.6	2.7	2.4	36.5	32.7	39.1	38.0	21.5	13.6	54.4	24.1	3.5	37.2	22.3	19.6	
V	39.8	197.7	42.3	57.4	306.7	370.2	457.2	282.4	169.9	66.4	408.5	164.9	44.2	423.3	66.0	59.9	
Cr	6.5	248.4	6.7	6.6	136.7	32.0	7.6	667.3	11.3	6.6	183.7	358.2	6.5	29.5	6.9	6.3	
Co	18.7	31.9	9.0	5.1	38.9	38.0	47.8	46.8	33.6	23.9	41.9	31.4	6.6	46.8	20.3	11.7	
Ni	3.9	49.4	3.9	6.9	56.0	23.2	15.0	199.1	10.5	6.1	42.3	97.1	4.3	14.6	4.4	4.1	
Cu	7.5	29.4	9.5	18.5	148.4	115.0	138.5	63.3	16.2	27.2	61.2	48.6	11.3	36.9	17.0	181.6	
Zn	56.1	54.5	60.1	65.3	53.8	69.0	89.7	58.2	175.7	99.2	56.7	62.8	30.0	56.7	73.1	81.6	
Ga	19.1	15.6	20.2	21.6	15.5	17.5	17.1	14.2	19.5	17.5	15.9	16.0	18.3	15.8	17.7	19.6	
Rb	90.6	34.9	129.4	136.3	15.7	14.5	14.0	34.2	56.7	98.2	20.0	40.1	104.5	0.8	78.5	48.7	
Sr	263	243	365	333	397	330	293	294	281	146	292	205	294	292	199	188	
Y	2.23	16.43	1.79	1.38	17.3	22.8	26.8	18.74	57.54	44.14	17.5	65.6	13.6	6.6	41.9	47.8	
Zr	152	102	135	106	65	84	85	82	153	281	70	91	196	9	239	189	
Nb	8.5	4.6	5.5	3.2	4.9	4.6	3.9	4.8	7.7	14.6	2.5	3.0	9.9	0.3	7.2	4.6	
Cs	3.3	2.4	1.5	2.8	0.2	0.5	0.2	1.5	2.7	5.7	0.9	2.7	3.0	0.0	3.2	1.3	
Ba	559	313	1528	1114	249	322	305	325	425	766	320	293	1349	35	442	450	
La	26.2	11.3	10.8	6.5	10.3	11.7	10.5	12.7	57.9	32.1	9.3	36.0	30.4	1.8	24.2	25.0	
Ce	51.0	24.9	21.2	13.3	21.8	25.0	22.9	27.2	109.5	66.4	20.6	69.9	58.7	3.9	53.5	44.5	
Pr	5.3	3.0	2.1	1.5	2.8	3.3	3.2	3.5	12.9	8.0	2.9	9.5	5.9	0.6	6.8	8.0	
Nd	19.5	12.9	7.8	6.0	13.5	16.2	15.1	15.5	56.9	34.1	13.7	45.0	20.7	2.9	30.1	37.3	
Sm	3.2	2.9	1.3	1.1	3.3	3.9	4.2	3.7	12.3	7.5	3.5	10.9	3.2	0.9	7.0	9.1	
Eu	0.85	0.93	0.39	0.39	1.04	1.31	1.35	1.17	3.51	1.72	1.08	2.96	0.97	0.64	1.64	2.38	
Gd	1.7	3.0	0.9	0.8	3.32	4.25	4.70	3.7	13.9	8.0	3.72	12.71	2.72	1.11	7.25	9.85	
Tb	0.16	0.48	0.10	0.09	0.51	0.69	0.72	0.59	2.08	1.26	0.54	1.78	0.37	0.18	1.13	1.50	
Dy	0.6	3.2	0.5	0.3	3.4	4.4	5.1	3.7	13.2	8.3	3.6	11.7	2.3	1.3	7.6	9.9	
Ho	0.09	0.67	0.08	0.05	0.70	0.89	1.05	0.73	2.55	1.66	0.69	2.43	0.48	0.28	1.62	1.94	
Er	0.2	1.9	0.2	0.1	1.9	2.6	3.1	2.0	7.0	5.0	2.0	7.0	1.4	0.8	4.6	5.5	
Tm	0.03	0.29	0.04	0.03	0.29	0.41	0.48	0.31	1.03	0.74	0.31	0.97	0.24	0.12	0.72	0.81	
Yb	0.1	2.0	0.2	0.1	1.90	2.69	3.14	2.01	7.05	5.05	1.86	6.75	1.84	0.86	4.89	5.13	
Lu	0.01	0.30	0.02	0.02	0.27	0.40	0.45	0.31	0.97	0.73	0.26	1.02	0.31	0.13	0.72	0.73	
Hf	4.49	2.81	4.09	3.74	1.9	2.5	2.5	2.3	4.1	7.7	2.8	2.5	4.9	0.3	6.6	5.5	
Ta	0.77	0.63	0.68	0.33	0.34	0.33	0.31	0.39	0.87	1.35	0.33	0.55	0.98	0.57	0.62	0.69	
Pb	18.80	9.06	23.22	23.34	4.8	6.3	9.0	6.02	11.47	20.91	3.5	10.1	20.0	1.3	11.6	7.1	
Th	12.00	4.63	4.08	2.81	2.4	3.1	2.6	3.75	7.08	13.34	3.1	4.0	13.4	0.1	10.0	6.9	
U	2.71	1.24	0.96	1.57	0.6	0.8	0.7	0.82	1.63	3.31	0.6	1.2	3.7	0.0	2.2	8.8	

spectrometry (XRF) on fused glass discs prepared with SPECTRACHEM 12-22 flux. For the trace elements a suite of 36 international standards were used for calibration and Siemens SPECTRA 3000 software was used for data reduction. The Compton scatter of X-ray tube line RhK β 1 was used to correct for mass attenuation and appropriate corrections were used for those elements analyzed at energies below the Fe absorption edge. For XRF major oxide analyses precision is generally better than 1% (at 2 σ) and for trace elements it is 1% for Sr and Zr, 1-3% for V, Cr, Zn and Y, 3-5% for Ba, 5-10% for Rb and Nb, Detection limits are <2 ppm for Rb, Sr, Y, Zr and Nb, 2-5ppm for V, Cr, and Zn, and 5-10 ppm for Ba.

Additional trace element data were obtained by laser ablation inductively coupled plasma source mass spectrometry (LA-ICP-MS) at the Australian National University using fused glass discs and an EXCI-MER laser system, operating in the ultra-violet spectrum at a wavelength of 193nm (Eggins et al., 1998). A standard of NIST 612 was run after every 15 analyses. Si concentrations obtained by XRF were used as the internal standard to account for any variation in ablation yield between samples and calibration standards and the 'matrix effect' of variations between counts per second and ppm of different elements. During the course of the analyses, BCR-2 glass standard was also analysed (every 30 analyses) to provide an independent assessment of accuracy and precision.

For isotope analyses, rock samples were crushed to coarse chips (<0.5 cm³) and fresh pieces were hand-picked. To avoid surface contamination the rock chips were then leached with 4M HCl at a temperature less than 100°C for 1 hour. The chips were ground to less than 200 mesh by using a silicon nitride mortar. The samples were leached further with 2 ml of 4 M HCl, at a temperature of 100° C for 1 hour, prior to sample dissolution. The analytical procedure for chemical separation and mass spectrometry followed Yoshikawa and Nakamura (1993) and Shibata et al. (1989) for Sr and Nd isotopes respectively. Mass spectrometry was carried out on a Finnigan MAT 261 equipped with five Faraday cups and using static multicollection mode at the Pheasant Memorial Laboratory, Okayama University, Misasa. Normalizing factors to correct isotopic fractionation in the mass spectrometer for Sr, Nd, and Pb isotope analyses are ⁸⁶Sr/⁸⁸Sr = 0.1194, ¹⁴⁶Nd/¹⁴⁴Nd = 0.7219, and 0.129% per atomic mass unit, respectively. Measured ratios for standard materials were ⁸⁷Sr/⁸⁶Sr = 0.710239 ± 11 (2sm) for NBS987 (n=5), ¹⁴³Nd/¹⁴⁴Nd = 0.511839 ± 05 (2sm) for La Jolla (n = 50), and ²⁰⁶Pb/²⁰⁴Pb = 16.9394 ± 0.0030 (2sm), ²⁰⁷Pb/²⁰⁴Pb = 15.4964 ± 0.0030 (2sm), and ²⁰⁸Pb/²⁰⁴Pb = 37.7174 ± 0.0100 (2sm) for NBS981 (n = 13).

3.2.5. Geochemical Compositions

Geochemical and isotope compositions of Northland Arc volcanic rocks and some lithic inclusions



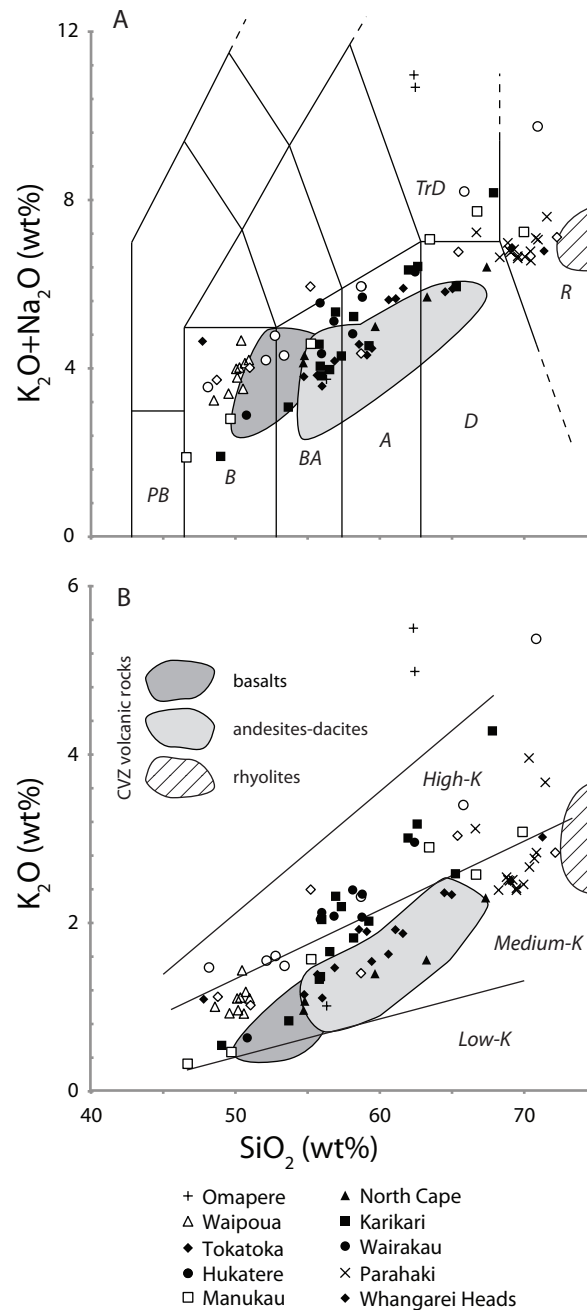


Fig. 3.3 Major element classification diagrams. A: (Na_2O+K_2O) - SiO_2 IUGS volcanic rock classification of Le Bas et al. (1986). PB – Picritic basalt; B – Basalt; BA – Basaltic andesite; A – Andesite; D – Dacite; TrD – Trachydacite. B: K_2O - SiO_2 classification of Gill (1981). Shaded fields in this and following diagrams indicate the composition of Coromandel Volcanic Zone volcanic rocks (unpublished dataset).

are presented in Tables 3.1-3.3 and Figures 3.3-3.9. Because this is an overview study of a large number of volcanoes, and because these are relatively old volcanoes with relatively poorly exposed stratigraphy, the number of rock samples per volcano is small. The samples from any single centre are not necessarily all cogenetic and may not capture the total range in compositional variation. Nevertheless we describe rocks of each centre on the assumption that they formed through similar processes and merely represent different aliquots of the range of compositions that existed in the magmatic system of each volcano.

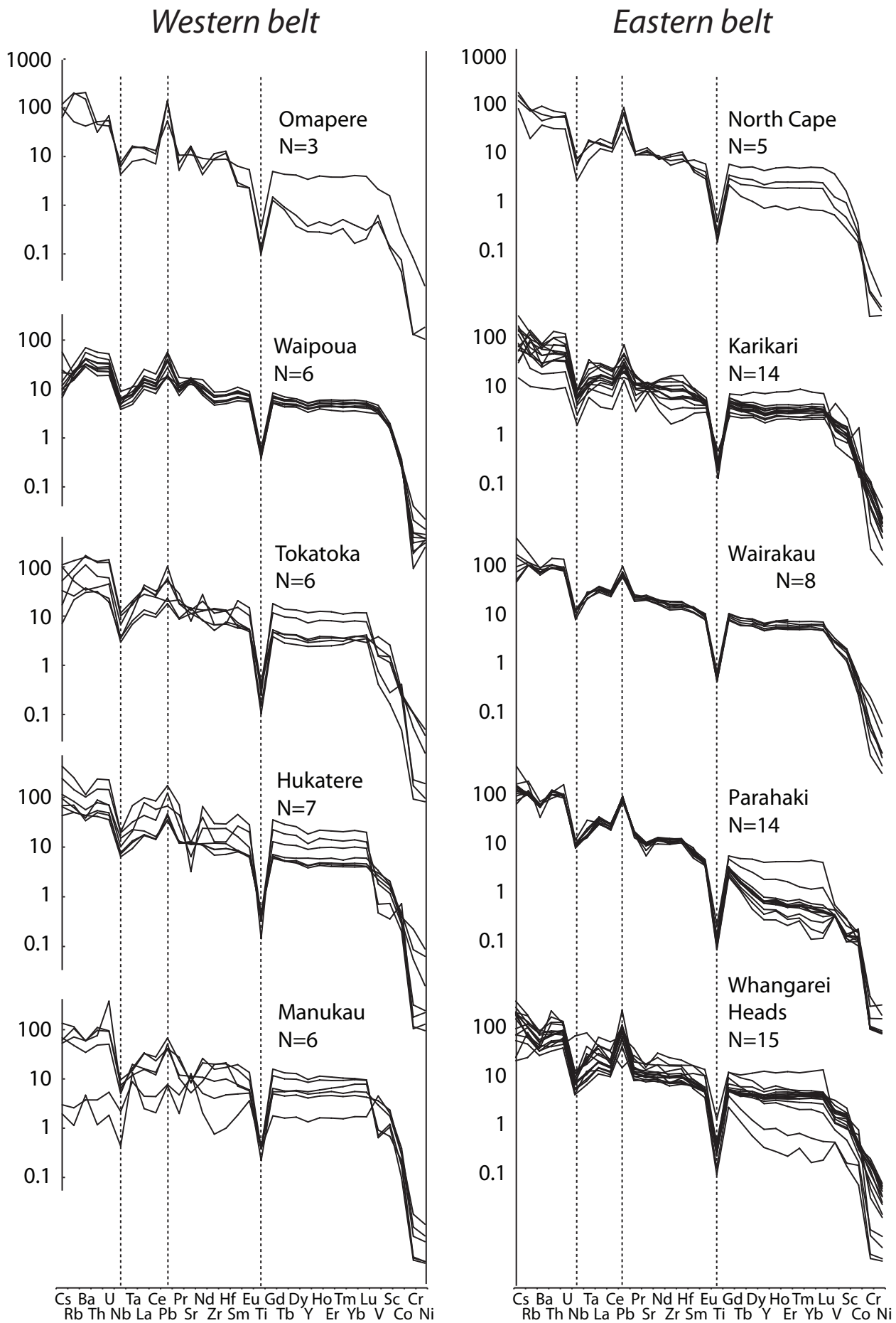


Fig. 3.4 Extended trace element distribution diagrams normalised to the bulk silicate Earth (BSE) model composition of McDonough and Sun (1995).

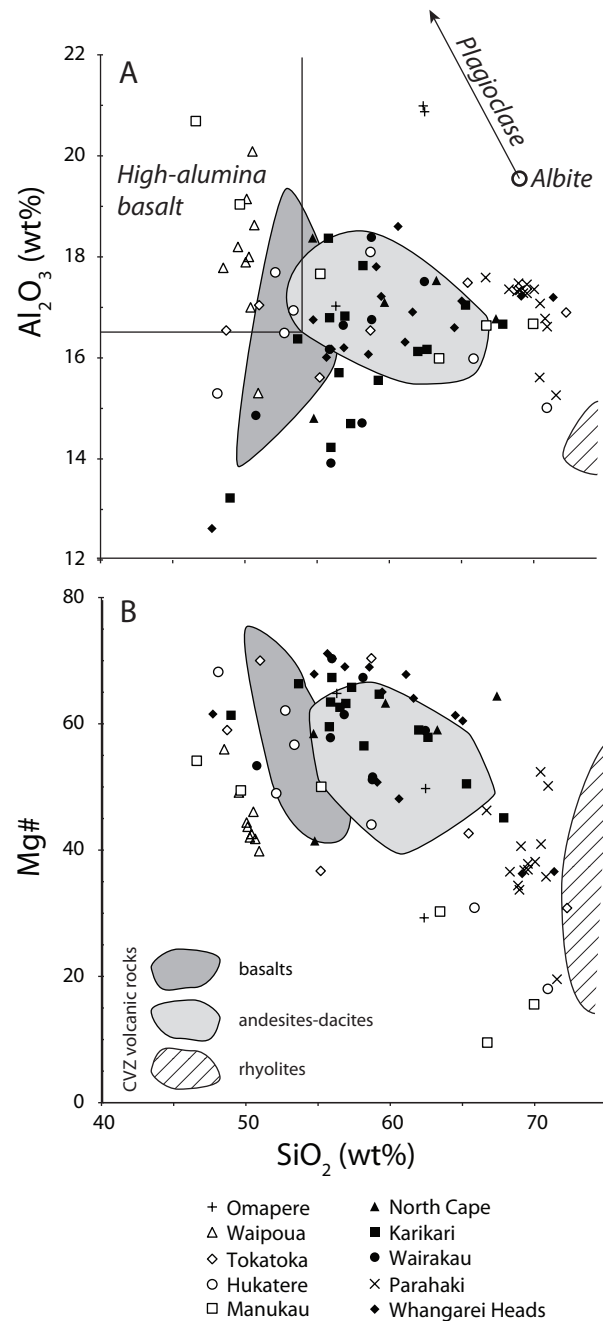


Fig. 3.5 Major element diagrams. A: Al_2O_3 - SiO_2 . HAB = high-alumina basalt following Crawford et al. (1987). Ab = ideal composition of albite. Plag. = compositional range of plagioclase solid solution series. B: Mg#- SiO_2 for western and eastern belt rocks, respectively. Mg# = molar $Mg/(Mg+Fe^{2+})$.

The volcanic rocks of the Northland Arc are basalts, silica-oversaturated basaltic andesites, andesites and dacites, and low-silica rhyolites as well as rare trachybasalt and trachyte following the IUGS total alkali-silica classification (Fig. 3.3A; c.f. Le Bas et al., 1986). Total alkali contents are slightly higher at given SiO_2 in the western belt relative to the eastern belt, but rocks from both belts are predominantly of medium- to high-K composition following the classification of Gill (1981; Fig. 3.3B). Rocks range in SiO_2 concentration between 45% and 73% without a significant compositional gap. Rocks of some volcanic centres form arrays in Figures 3.3A and 3.3B that show consistent differences in total alkali or

K_2O contents at given SiO_2 (compare e.g. Wairakau, Whangarei Heads and North Cape samples in Fig. 3.3A). The differences in alkali content at given SiO_2 are comparable in magnitude to similar differences between data arrays formed by rocks of the active Mt Ruapehu and Mt Taranaki volcanoes (Price et al., 1999; Price et al., 2005). All Northland Arc volcanic rocks share an arc-type minor and trace element signature with large ion lithophile element (LILE) enrichments of 50-100 times relative to bulk silicate Earth (BSE), a positive Pb anomaly, distinct negative anomalies for Nb, Ta and Ti, and enrichment of light rare earth elements (LREE) relative to heavy REE (HREE) (Fig. 3.4). In addition, rocks at some centres exhibit relatively depleted HREE abundances that can indicate garnet fractionation (discussed below).

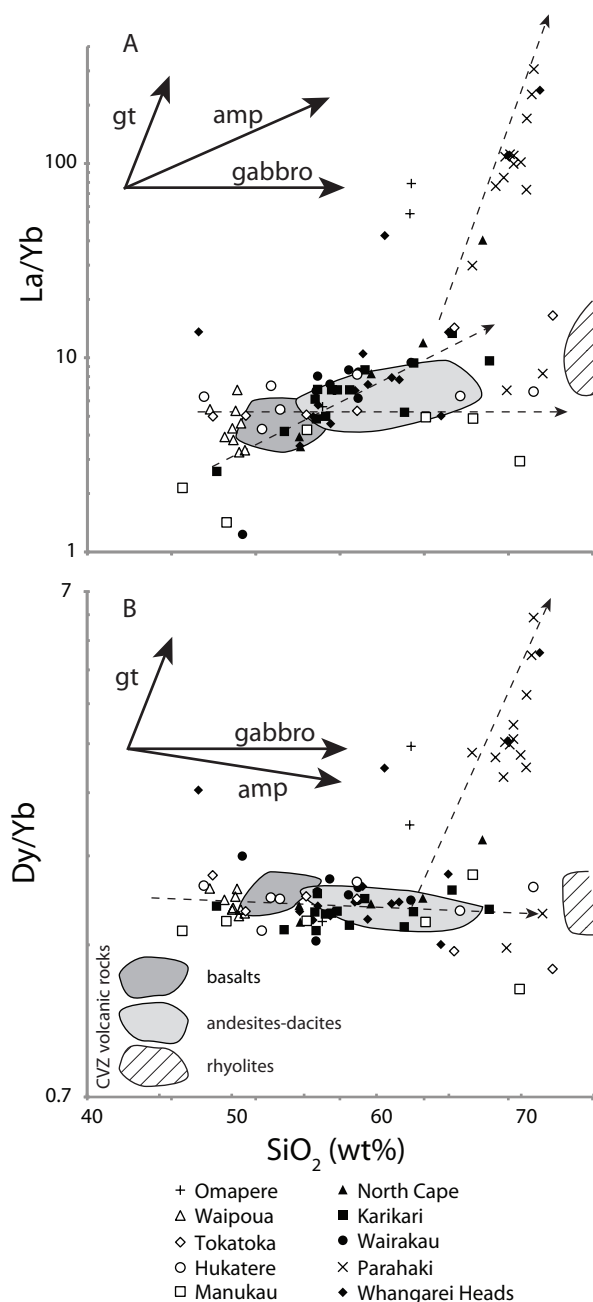


Fig. 3.6 REE diagrams. A: La/Yb- SiO_2 . B: Dy/Yb- SiO_2 . Arrows indicate expected differentiation trends for particular residual minerals or assemblages, after Davidson et al. (2007).

Plagioclase dominates the phenocryst assemblage in basaltic to dacitic Northland Arc rocks and sorting of plagioclase in the magmatic system or during eruption exerts the principal control on Al_2O_3 concentrations in the erupted volcanic rocks. Western belt rocks with SiO_2 contents up to c. 52% have Al_2O_3 concentrations up to c. 21% (Fig. 3.5A). Most but not all are high-alumina basalts (HABs) following the definition of Crawford et al. (1987). Rocks of the Waipoua and Manukau centres have the strongest affinity with HAB field. However, such trends do not necessarily reflect processes in the deeper magmatic system. Pearce element ratio (PER) diagrams can be used to determine whether the sorting of particular phases control major element rock composition (Pearce, 1968). On a PER diagram that controls for olivine + clinopyroxene + plagioclase sorting (e.g. molar Si/Th vs. molar $(\text{Al}/4 + (\text{Fe}^{2+} + \text{Mg})/2 + 3\text{Ca}/2 + 11\text{Na}/4)/\text{Th}$), Waipoua basalts (N=7) form a strongly correlated array ($r=1.00$) with slope 0.86. Other plausible mineral assemblages yield poorer correlations and/or slopes further from 1, so it appears that sorting of an olivine + clinopyroxene + plagioclase mineral assemblage, relative to an entraining melt, could be the dominant source of the major element trend. Waipoua and Manukau rocks have molar $\text{Mg}/(\text{Mg} + \text{Fe}^{2+})$ (Mg#) values of less than 55 and <7% MgO. Rocks of the Hukatere and Tokatoka centres, in contrast, have up to 11% MgO, Mg# values up to 70 and no particular affinity with the HAB field. Rocks of each western belt centre show gradually decreasing Mg# and MgO with increasing SiO_2 (Fig. 3.5B).

Eastern belt rocks have Al_2O_3 concentrations between 12.5 and 18.5% and have no affinity with the HAB field (Fig. 3.5A). Rocks of eastern belt centres other than Parahaki dacites have Mg# between 50 and 70. Parahaki dacites trend to lower Mg# with increasing SiO_2 (Fig. 3.5B).

3.2.6. REE Behaviour

Western belt centres are characteristically strongly porphyritic containing plagioclase and a mafic assemblage of olivine + clinopyroxene in basalts and basaltic andesites to clinopyroxene + orthopyroxene + titanomagnetite in andesites and dacites; hornblende only occurs in rocks at Tokatoka (Smith et al., 1989). Hornblende (amphibole) is not stable at shallow depth and can be resorbed before eruption, but its presence or absence in a magmatic system can be assessed based on the fractionation of REE ratios in erupted rocks (Davidson et al., 2007). Constant La/Yb and Dy/Yb with increasing SiO_2 are consistent with the sorting (through fractional crystallisation or crystal-liquid mixing) of a gabbroic olivine \pm plagioclase \pm pyroxene mineral assemblage, as REE do not partition strongly into either olivine, pyroxene or plagioclase. Increasing La/Yb and decreasing Dy/Yb with SiO_2 can indicate amphibole fractionation as the MREE (e.g. Dy) partition into amphibole whereas HREE are less compatible and LREE are incom-

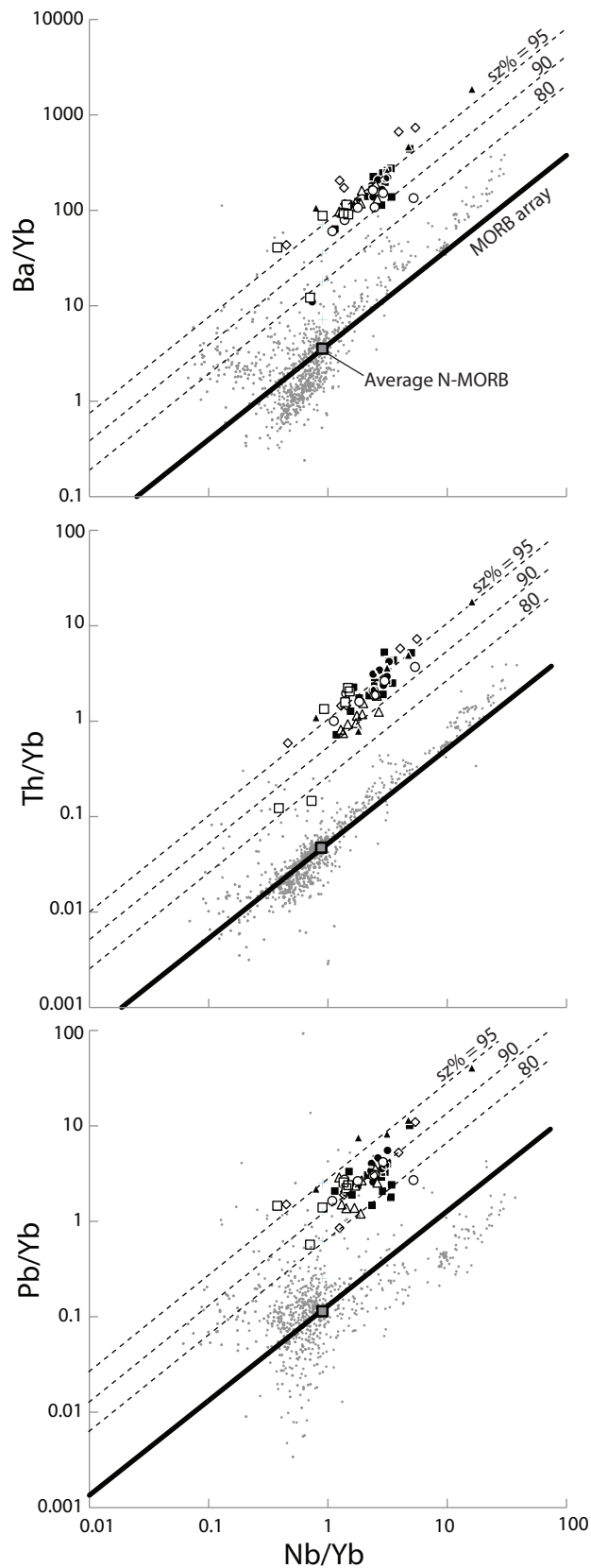


Fig. 3.7 Incompatible element diagrams. Grey box and black line represent average MORB composition (Hofmann, 1988) and the associated MORB array. Dashed lines represent compositions with equal subduction zone-derived component (sz%) of the non-conservative element (Ba, Th, Pb) relative to the MORB array. Grey dots represent spreading centre rock compositions from the PETDB database.

patible in amphibole (Bottazzi et al., 1999). Increasing Dy/Yb with SiO₂ can indicate garnet fractionation as the heavier REE are progressively more compatible in garnet (Johnson, 1994). Western belt rocks of all centres show relatively constant La/Yb and constant or slightly decreasing Dy/Yb with increasing SiO₂ (Figs. 3.6A-B). The hornblende-bearing rocks of the Tokatoka centre form the exception, having higher La/Yb and lower Dy/Yb at comparatively high SiO₂. This trend is consistent with fractionation of hornblende. In contrast, La/Yb- and Dy/Yb values are apparently not fractionated in Waipoua, Manukau and Hukatere rocks even at higher SiO₂ contents, suggesting that amphibole did not play a significant role in the formation of western belt volcanic rocks other than those at Tokatoka. Two andesitic clasts from the Omapere conglomerate have both high La/Yb and Dy/Yb (Figs. 3.6A-B) and relatively depleted HREE concentrations (Fig. 3.4) suggesting that fractionation of garnet at some stage may have played a role in their origin.

The porphyritic volcanic rocks of the eastern belt typically comprise complexly zoned plagioclase with a mafic assemblage consisting of rare olivine, ortho- and clinopyroxene, clinopyroxene + hornblende, hornblende + biotite, and biotite. Garnet occurs locally, particularly at Whangarei Heads (Smith et al., 1989). Rocks of eastern belt centres show increasing La/Yb and decreasing Dy/Yb with SiO₂ (Fig. 3.6). This suggests that amphibole was present at some stage in the magmatic systems of the eastern belt and was residual to crystal fractionation, partial melting and/or mixing processes. This is consistent with the common presence of hornblende as a phenocryst phase in eastern belt rocks. Furthermore, amphibolitic inclusions occur in andesitic Whangarei Heads lavas and could represent residues to magmatic differentiation processes in the middle or deep crust.

In Parahaki dacites and some Whangarei Heads samples, La/Yb and Dy/Yb are strongly fractionated to greater values. This plausibly reflects the fractionation of garnet at some stage of development (Figs. 3.6A-B), consistent with the presence of garnet in some Whangarei Heads andesites. Apparently garnet was a residual phase in the petrogenesis of dacites of the Parahaki centre, but was removed efficiently from the erupted magma. In contrast, garnet and garnet-bearing xenoliths became entrained in the Whangarei Heads andesites and for this reason bulk rock REE ratios in these andesites do not necessarily bear a residual-garnet signature. The presence of a residual garnet signature in the Parahaki dacites is intriguing as it indicates that these silicic magmas erupted from the deep crust (discussed below), in contrast to younger silicic rocks in the North Island for which a comparatively shallow (<16 km) source is generally inferred (Charlier et al., 2005; Wilson and Charlier, 2009).

Table 3.2

Sample	Centre	Type	$^{87}\text{Sr}/^{86}\text{Sr}$	$^{143}\text{Nd}/^{144}\text{Nd}$
37985	Karikari	Lava	0.705258	0.512770
41347	Karikari	Lava	0.705042	0.512764
34917	Wairakau	Lava	0.704334	0.512819
34924	Wairakau	Lava	0.704738	0.512755
NB20	Whangarei Hds	Cognate incl.	0.70565	0.512803
NB26	Whangarei Hds	Cognate incl.	0.70665	0.512676
NB28	Whangarei Hds	Cognate incl.	0.70649	0.512761
NB33	Whangarei Hds	Cognate incl.	0.70765	0.512710
NB39	Whangarei Hds	Cognate incl.	0.70637	0.512681
NB24	Whangarei Hds	Xenolithic incl.	0.70369	0.513123
NB25	Whangarei Hds	Xenolithic incl.	0.70456	0.513069
NB29	Whangarei Hds	Xenolithic incl.	0.70517	0.513001
32967	Whangarei Hds	Lava	0.70703	0.512613
32995	Whangarei Hds	Lava	0.70696	0.512611
33033	Whangarei Hds	Lava	0.70685	0.512645
33058	Whangarei Hds	Lava	0.70642	0.512729
33095	Whangarei Hds	Lava	0.70718	0.512587
33101	Whangarei Hds	Lava	0.70642	0.512700
33129	Whangarei Hds	Lava	0.70684	0.512615
33172	Whangarei Hds	Lava	0.70739	0.512616
3/23	Parahaki Dacite	Lava	0.707516	0.512457
26410	Waipoua	Lava	0.703708	0.512952
26411	Waipoua	Lava	0.703790	0.512908
890	Hukatere	Lava	0.703610	0.512889
10320	Hukatere	Lava	0.703925	0.512883
10323	Hukatere	Lava	0.704077	0.512880
7304	Tokatoka	Lava	0.704572	0.512892

Table 3.2 Whole-rock Sr-Nd isotope compositions.

3.2.7. Slab and Mantle Components

The trace element composition of arc magmas prior to modification by crustal differentiation processes reflects the composition of mantle wedge peridotite, metasomatisation by slab-derived fluids and partial melting. Some elements are readily transported from slab to mantle wedge (non-conservative elements, e.g. Ba, Th) whereas some other elements are essentially immobile and are not added by slab-fluids (conservative elements, e.g. Nb, Yb). The fraction of a non-conservative element in an arc magma that is slab-derived can be estimated using a diagram that plots incompatible element ratios $X/Y-Z/Y$, where X is the non-conservative element and Z and Y are conservative elements (Pearce, 1982; Pearce, 1983). We use Yb and Nb as conservative incompatible elements to assess the subduction component

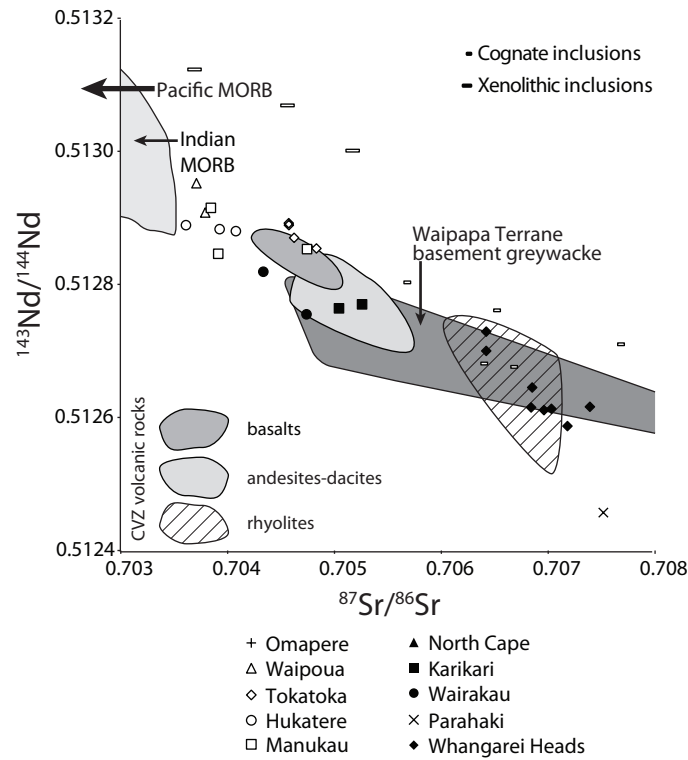


Fig. 3.8 $^{143}\text{Nd}/^{144}\text{Nd}$ - $^{87}\text{Sr}/^{86}\text{Sr}$ diagram. Cognate and xenolithic inclusions occur in Whangarei Heads lavas as described in the text. MORB and basement reference fields based on Zindler and Hart (1986) and McCulloch et al. (1994).

of the non-conservative elements Ba, Th and Pb in Northland Arc volcanic rocks (Fig. 3.7). Subduction components for Th, Ba and Pb are in the order of 80 to 95% relative to average N-MORB (Hofmann, 1988). Comparable subduction-derived fractions occur in continental and oceanic arc rocks elsewhere (e.g. Pearce et al., 1995; Green, 2006; Smith et al., 2009). A key feature of these diagrams is that there is apparently no significant difference between eastern and western belt rocks in the subduction-derived fraction of non-conservative elements. Therefore, the source mantle segments underneath both the eastern and western belt were metasomatised to a similar extent by slab-derived fluids, as also suggested by the comparable incompatible element enrichments in eastern and western belt rocks (Fig. 3.4). Because

Table 3.3

Sample	Type	SiO ₂	TiO ₂	Al ₂ O ₃	Fe ₂ O _{3t}	MnO	MgO	CaO	Na ₂ O	K ₂ O	P ₂ O ₅	Sum	LOI
NB20	Cognate	42.3	1.38	22.2	12.0	0.23	5.6	12.4	1.8	0.26	1.04	99.1	0.54
NB26	Cognate	43.2	1.56	15.9	11.9	0.16	12.5	11.2	2.0	0.47	0.55	99.3	0.02
NB28	Cognate	41.6	1.17	20.8	11.7	0.2	7.6	8.9	1.8	0.4	2.37	96.5	0.21
NB33	Cognate	40.0	1.22	20.4	9.5	0.14	9.3	7.2	1.5	0.37	4.19	93.8	0.06
NB39	Cognate	49.3	0.54	28.1	2.1	0.05	1.7	9.9	3.6	0.25	1.87	97.5	0.14
NB24	Xenolithic	49.6	1.62	15.3	11.7	0.19	6.8	9.7	2.9	0.35	0.84	99.0	0.18
NB25	Xenolithic	46.8	1.84	16.1	11.8	0.18	5.3	11.1	2.3	0.45	2.1	98.0	0.23
NB29	Xenolithic	43.9	1.42	15.0	14.3	0.25	8.3	11.8	2.2	0.39	0.96	98.5	0.22

Table 3.3 Whole-rock major element oxide geochemistry of inclusions in Whangarei Heads lavas. All concentrations measured by XRF at the University of Auckland and reported in weight percent. LOI: loss on ignition.

the mantle-derived component is apparently similar in eastern and western belt volcanic rocks, the geochemical and isotopic differences between the belts (as discussed above and in Sections 3.3.6, 3.3.8) may principally reflect a different crustal differentiation history.

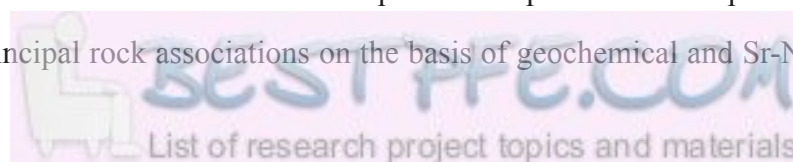
3.2.8. Isotope Properties

Western and eastern belt rocks have distinct, non-overlapping Sr-Nd isotope compositions (Fig. 3.8, Table 3.2). Rocks of the western belt centres all have $^{87}\text{Sr}/^{86}\text{Sr} < 0.705$ and $^{143}\text{Nd}/^{144}\text{Nd} > 0.5128$, whereas rocks from the Karikari and Wairakau centres have lower $^{143}\text{Nd}/^{144}\text{Nd}$ values between 0.5128 and 0.5130 and $^{87}\text{Sr}/^{86}\text{Sr}$ values between 0.7044 and 0.7054. Western and eastern belt volcanic centres overlie basement rocks of the Murihiku and Bay of Islands or Waipapa terranes, respectively, which have similar Permian-Jurassic ages (Adams and Maas, 2004; Mortimer, 2004). We tentatively interpret the difference to indicate that a significant crustal contaminant component may be present in Karikari-Wairakau centre rocks, but that no significant crustal component is present in western belt rocks.

Rocks of the Whangarei Heads and Parahaki centres have more evolved isotope ratios than Karikari-Wairakau centre rocks, with $^{87}\text{Sr}/^{86}\text{Sr}$ typically >0.706 . These rocks must therefore contain a substantial or dominant crustal component. Inclusions in Whangarei Heads lavas have much more variable Sr-Nd isotope compositions. Amphibolite and gabbroic inclusions have evolved isotope compositions comparable to that of their the host lavas, indicating a cognate origin. These inclusions possibly represent cumulates from high pressure crystallisation, consistent with the correlation between La/Yb and SiO_2 in Whangarei Heads lavas (Fig. 3.6). In contrast, schistose mafic inclusions in these lavas have relatively primitive Sr-Nd isotope compositions. These inclusions appear to represent metamorphic crustal rocks that are not associated with Tertiary magmatism other than as a potential contaminant. Because they are not a part of the Mesozoic greywacke basement as it occurs at the surface, we postulate that they represent deeper crustal rocks that occur between the greywacke terranes and the deep (35-45 km) crustal source of the Whangarei Heads andesites and the Parahaki dacites.

3.2.9. Summary of Petrogenetic Indicators

The volcanic centres of the Northland Arc comprise a heterogeneous suite of rocks that were erupted over a significant time period and which can be interpreted to represent several petrogenetic pathways. We distinguish three principal rock associations on the basis of geochemical and Sr-Nd isotope characteristics.



Centres of the western belt comprise basalts and andesites that evolved in amphibole-absent magmatic systems. These rocks apparently differentiated through the sorting of a gabbroic (plagioclase + clinopyroxene ± orthopyroxene ± olivine) mineral assemblage. These minerals have SiO₂ contents comparable to or greater than those of basalts or basaltic andesites, therefore fractionation of a gabbroic assemblage provided little leverage to alter bulk rock SiO₂ contents. Consequently, western belt rocks retained basaltic or basaltic andesitic SiO₂ concentrations. Incompatible trace element ratios indicate limited assimilation of evolved crustal material, and low ⁸⁷Sr/⁸⁶Sr and high ¹⁴³Nd/¹⁴⁴Nd suggest that western belt rocks contain a very minor, if any, crustal component. Rocks of this type comprise the Waipoua basaltic shield volcano, the Hukatere centre and the Manukau andesitic complex cone volcano. No equivalent amphibole-absent systems exist in the Northland Arc eastern belt or in the successor Coromandel Volcanic Zone (Booden et al., 2009).

Second, andesites and dacites that evolved in amphibole-present magmatic systems through the sorting of an amphibole + gabbro mineral assemblage and the assimilation of possibly crust-derived material with evolved Sr-Nd isotope compositions. The fractionation of amphibole allowed these rocks to acquire andesitic to dacitic SiO₂ concentrations. Andesites and dacites of this type comprise the western Tokatoka centre, and the eastern belt North Cape and Karikari-Wairakau centres. They are the most directly comparable in terms of geochemistry and mineralogy to the andesites and dacites of the successor Coromandel Volcanic Zone, and to the products of the current volcanism in the central North Island.

Finally, andesites, dacites and (*sensu stricto*) rhyolites of the Whangarei Heads and Parahaki centres. Whangarei Heads lavas show REE evidence for cryptic amphibole fractionation and contain amphibolitic inclusions. However, the key features that distinguish Whangarei Heads andesites and Parahaki dacites from any other rocks in the North Island volcanic record are 1) the role of garnet in their development as indicated by high whole-rock La/Yb and Dy/Yb ratios in many samples, and by the presence of garnet xenoliths and xenocrysts in Whangarei Heads lavas, and 2) highly evolved Sr-Nd isotope compositions that imply strong crustal involvement in their petrogenesis. Day et al. (1992) estimated formational depths for garnet in Whangarei Heads andesites at between 35 and 45 km. The presence of garnet, combined with evolved isotope signatures, suggests interaction with old crust at depths between 35 and 45 km in the presence of residual garnet. This could reflect crustal thickening by the obduction of the Northland ophiolite several millions of years earlier, although Whangarei Heads andesites did not erupt onto allochthonous rocks but onto Bay of Islands Terrane basement. In any case, the anomalous nature of the Whangarei Heads-Parahaki volcanic rocks in the North Island record suggest a thicker crust in eastern

Northland than elsewhere in the North Island (discussed below).

3.2.10. Discussion

Here we discuss the geochemical evidence that could constrain the polarity of subduction underneath the Northland Arc, the similarities and differences between Northland Arc volcanism and subsequent subduction-related North Island volcanism, and implications of Northland Arc development for regional SW Pacific tectonic development.

3.2.10.1. *Polarity of Subduction*

All volcanic rocks of the Northland Arc have an arc-type minor and trace element signature and logically volcanism of the Northland Arc developed in response to subduction. The contemporaneity of volcanism in the eastern and western belts and the close spatial association of these belts suggest that volcanism was driven by magmas derived from the same mantle wedge, over the same subducted slab. The polarity of subduction underneath the Northland Arc is potentially reflected in geochemical characteristics of the most primitive rocks (for the purpose of this discussion, those with MgO >6%) of the western and eastern belt. The principal geochemical difference between eastern and western belt volcanic rocks is the amphibole-absent nature of the magmas that drove volcanism in the Waipoua and Manukau centres. Nevertheless all Northland Arc rocks possess a convincing arc signature (Fig. 3.4) and have similar fractions of slab-derived incompatible elements (Fig. 3.7). This suggests similar slab-fluid input in the mantle beneath the two belts. We infer that primitive magmas in the eastern and western belts were the products of a mantle wedge that had been metasomatised by similar slab-derived fluids.

Higher incompatible trace element concentrations in rocks further from the volcanic front have been ascribed to decreasing degrees of partial melting in the underlying portion of the mantle wedge (e.g. Tatsumi, 1989). Incompatible alkali element (K_2O , Rb, Cs) concentrations in rocks with MgO >6% are slightly lower in western belt rocks compared to eastern belt rocks. For example, Cs is <2 ppm in western belt rocks with >6% MgO, but <5 ppm in comparable eastern belt rocks. Rb in the same rocks is <43 ppm in western belt rocks but <72 ppm in eastern belt rocks. These numbers could tentatively support eastward-dipping subduction where the western belt represents the volcanic front and the eastern belt more distal volcanism. A higher degree of partial melting in the mantle underneath the western belt could be consistent with the apparently more voluminous volcanism there (e.g. Herzer, 1995) compared to the eastern belt. However, the differences in minimum incompatible element concentrations are small and

could also be explained by the more pronounced crustal modification of eastern belt rocks.

Ultimately, the mantle-derived magmas that drove volcanism in the eastern and western belt appear to have been of comparable composition (as discussed in Section 3.3.7). Therefore, crustal modification of the mantle-derived magmas may have primarily constrained the compositions of the volcanic end products. The principal geochemical differences between eastern and western belt magmas are: 1) the geochemical evidence of amphibole fractionation, and the common presence of amphibole, in eastern belt rocks, and the absence of these in western belt rocks other than at Tokatoka; 2) more pronounced evidence for crustal interaction (assimilation) in eastern belt rocks, in the form of more evolved Sr-Nd isotope compositions and the presence of schistose inclusions of unknown, but clearly crustal, provenance in some lavas; and 3) evidence for the involvement of garnet, in the form of fractionated REE ratios and of garnet crystal inclusions in some lavas. These features can all support a thicker crustal section underlying the eastern belt, relative to the western belt. The crust-mantle boundary beneath Northland as determined from seismic refraction studies (Stern et al., 1987) is ~30km. Igneous xenoliths in lavas of the Taurikura Complex on the eastern side of Northland contain mineral assemblages that crystallised at greater depths than this (>35 km; Day et al., 1992). This observation has been interpreted to indicate either localised thicker crust beneath eastern Northland or a sub-crustal zone of mantle-crust interaction (Day et al., 1992). A thicker crustal section beneath eastern Northland can also help in establishing a complex magmatic system in the middle and deep crust in which differentiated (basaltic andesitic, andesitic and dacitic) magmas exist at depth and can evolve in the presence of residual amphibole. A complex magmatic system, with potentially longer magmatic residence times and repeated episodes of magma freezing, partial melting and magma mixing, would in turn favour more extensive crustal assimilation leading to more evolved isotope compositions. A significant difference in crustal thickness across the Northland Peninsula could therefore help explain the differences between eastern and western belt volcanism.

Horspool et al. (2006) estimate a Moho depth of 29 ± 1 km underneath the southern end of Northland, shallowing to 26 ± 1 km in the North Cape area, however their study was based on an array parallel to the Northland Arc belts, and did not resolve if and how Moho depth varies across the Northland Peninsula. Other geophysical studies have imaged shallower crustal features along arrays that cross the west coast (Uruski et al., 2004; Lin et al., 2007). There, the Northland Peninsula is bounded by the west-verging, reverse Northland Boundary Fault Zone (NBFZ) that separates the peninsula from the greater Taranaki Basin. The Northland Graben west of the NBFZ is a Cretaceous-Paleogene depocentre (Uruski et al.,

2004), and extends to the west as the Late Cretaceous Fairway-Aotea continental basin (Collot et al., 2009). Western belt volcanoes are closely aligned with the Northland Graben and the NBFZ. Therefore, the western belt centres appear to have formed on crust along the western margin of Northland that had been thinned by Cretaceous to Paleogene extension. In contrast, eastern belt centres erupted onto topographically higher terrain in the central part of the Northland Peninsula continental platform.

3.2.10.2. *Comparison with Subsequent North Island Volcanism*

The volcanic activity along the eastern belt of the Northland Arc is contiguous in space and time with Mid-Miocene to Pliocene activity on what are now Great Barrier Island and the Coromandel Peninsula (the Coromandel Volcanic Zone, CVZ). Volcanism in the CVZ initially manifested as andesitic-dacitic stratovolcano-building activity from c. 18 Ma (Kuaotunu centre). From c. 12 Ma, rhyolitic caldera-forming eruptions and minor basaltic eruptions also occurred alongside continuing andesitic volcanism (Skinner, 1986; Adams et al., 1994; Brathwaite and Christie, 1996; Nicholson et al., 2004; Briggs et al., 2005). In models of SW Pacific tectonic development, subduction volcanism in the CVZ has commonly been ascribed to west-directed subduction of Pacific plate lithosphere along the Colville-Lau arc, with the CVZ as the continental edge of this arc (e.g. Herzer, 1995; Brathwaite and Skinner, 1997; Mortimer et al., 2007). Given the comparatively certain tectonic setting of CVZ subduction-related volcanism, it is informative to compare the products of volcanism in the CVZ and the Northland Arc. New CVZ volcanic rock data acquired by us are plotted as fields in Figures 3.3, 3.5, 3.6 and 3.8 for comparison with Northland Arc compositions. CVZ andesites and dacites are porphyritic arc volcanic rocks with a mineral assemblage dominated by plagioclase with additional clino- and/or orthopyroxene, olivine in some basaltic andesites, and hornblende or relic resorbed hornblende common in many rocks (Skinner, 1972; Skinner, 1976; Skinner, 1986; Houghton and Cuthbertson, 1988; Skinner, 1993; Skinner, 1995; Brathwaite and Christie, 1996; Briggs et al., 1996). They are therefore similar to Karikari-Wairakau centre rocks of the Northland Arc eastern belt. Compared to Northland Arc rocks, CVZ volcanic rocks have a relatively narrow compositional range. All are medium-K calc-alkaline rocks with an arc-type trace and minor element distribution (Figs. 3-4). CVZ basalts, andesites and dacites have increasing La/Yb and decreasing Dy/Yb with SiO₂, indicating the presence of amphibole in the magmatic system, even though CVZ rocks that formed post-10 Ma only contain rare resorbed amphibole (Fig. 3.6). A key difference between the CVZ and Northland Arc therefore is that in the CVZ, post-10 Ma rocks display evidence for cryptic amphibole fractionation. It is possible that this reflects a relatively hot magmatic system or a system with

longer residence times at shallow levels, wherein amphibole was more efficiently resorbed (c.f. Rutherford and Hill, 1993). The amphibole-present nature of pre-10 Ma CVZ andesites and dacites makes them mineralogically similar to eastern belt Northland Arc rocks, in addition to the geochemical similarity. CVZ andesites and dacites also have $^{87}\text{Sr}/^{86}\text{Sr}$ and $^{143}\text{Nd}/^{144}\text{Nd}$ ratios similar to those in equivalent rocks of the Karikari-Wairakau centre, suggesting a comparable degree of crustal interaction (Fig. 3.8). Thus, CVZ and Karikari-Wairakau centre volcanism appear to be products of comparable magmatic systems. This contrasts with volcanism in the Northland Arc western belt in which a gabbroic mineral assemblage appears to control magmatic differentiation, and for which Sr-Nd isotope data suggest the presence of a much smaller, if any, assimilated crustal component.

A principal difference in volcanic style between the younger CVZ and the Northland Arc eastern belt (specifically the Karikari-Wairakau centre) lies in the fact that in the CVZ, volcanism developed towards a broad spectrum of andesitic-dacitic stratovolcano-building, rhyolitic caldera-forming eruptions and small-scale basaltic eruptions. Although some dacites and rhyolites occur throughout the Northland Arc, silicic rocks are not nearly as volumetrically significant as in the CVZ. Oceanic tephra records also indicate that explosive silicic volcanism was insignificant in the North Island before c. 12 Ma (Carter et al., 2003), well after the cessation of significant subduction in the Northland Arc (Hayward et al., 2001) but coeval with the appearance of the first rhyolitic centres on Great Barrier Island (Nicholson et al., 2004).

In both the Northland Arc eastern belt centres and in the CVZ, the preconditions for dehydration melting of stalled parts of the magmatic system were met in the sense that amphibole-bearing rocks presumably existed, as residues to magmatic differentiation involving amphibole fractionation, in the respective systems (c.f. Fig. 3.6). Maturation of a magmatic system to one capable of producing and erupting silicic magmas may only take in the order of 1 Myr (Smith et al., 2003; e.g. in the Kermadec Arc oceanic setting: Price et al., 2005; southern Rocky Mountains volcanic field: Lipman, 2007). Therefore, the relatively insignificant volume of silicic eruptive rocks in the Northland Arc despite ongoing basaltic-andesitic volcanism over a 5-8 Myr period of activity suggests that tectonic factors limited the development to a 'mature' magmatic system. Possibly, the rate of crustal extension may have been too slow until c. 10 Ma (Nicol et al., 2007) to increase the temperature in the deep or middle crust sufficiently, by passively raising the geotherm and/or enabling intrusion from the mantle, to enable crustal anatexis or remelting of parts of the magmatic system to produce silicic magmas. Otherwise, the style and geochemistry of andesitic volcanism were comparable in the CVZ and the Karikari-Wairakau centre. An implication of this is that models involving very rapid slab rollback of the Colville-Lau Ridge during the Late Oligocene

must assume that this did not lead to significant extensional stress in the Northland Peninsula crust. It is possible that actual extension was entirely confined to the domain north of the Vening Meinesz Fracture Zone, however we suggest that models that do not require rapid rollback of the Colville-Lau Ridge in the late Oligocene, such as the arc collision model of Herzer et al. (2009) or the South Fiji Basin subduction model of Whattam et al. (2006) may better fit this loose constraint.

3.2.10.3. *Implications for SW Pacific Tectonic Development*

A plethora of models have been proposed for the Cenozoic tectonic history of the SW Pacific region. The relative dearth of geochronological and compositional data for the rocks that make up the ridges and basins in the SW Pacific continues to hinder proper testing of many of the predictions of these models. The geochemical dataset for the on-shore Northland Arc volcanic rocks now allows us to address some of the potential implications of the proposed causes of volcanism in the Northland Arc.

In some models for Northland Arc evolution, volcanism is partly or entirely ascribed to W or WNW-directed subduction of Pacific lithosphere (Mortimer et al., 2007; Herzer et al., 2009). The Pacific lithosphere that is currently subducting at the Kermadec trench is of Cretaceous age (Lonsdale, 1997; Castillo et al., 2009). It can be assumed that the Pacific lithosphere that would have subducted in the Late Oligocene or Early Miocene was likewise old, i.e. certainly >60 Myr, and readily subductible. In both the ‘arc unzipping’ model of Mortimer et al. (2007) and the ‘arc collision’ model of Herzer et al. (2009), the Colville Ridge (then the active Colville Arc) is present in some form or other at 23-20 Ma with the Northland Arc some distance along strike off its southern end. West- or WNW-dipping subduction underneath the NW-trending Northland Arc itself would necessarily have been oblique. Northland Arc volcanism driven by Pacific Plate subduction is an attractive possibility; not only did the same mechanism probably account for Miocene volcanism in the successor Coromandel Volcanic Zone (and presently drives volcanism in the central North Island), it also fits well with the strong similarity between eastern belt (particularly Karikari-Wairakau centre) volcanic rocks and those of the Coromandel Volcanic Zone (as discussed in Section 3.2.10.2). The age of activity along the Colville Arc has long been constrained by a single 5.4 ± 0.1 Ma whole-rock K-Ar date on a dredged basalt (Adams et al., 1994). Recently a plagioclase separate from an identical rock from the same dredge sample yielded a $^{40}\text{Ar}/^{39}\text{Ar}$ age of 16.68 ± 0.20 Ma that supersedes the younger date as the formation age of the rock. The younger date may represent a hydrothermal event (Mortimer et al., 2010). The new, older date extends the known period of activity in the Colville Arc to a period that overlaps with the latest activity in the Northland Arc (e.g. the Whan-

Whangarei Heads, Hen and Chickens and Manukau centres; Hayward et al. (2001)) and the earliest activity in the Coromandel Volcanic Zone (Adams et al., 1994). It is plausible that older rocks exist deeper in the Colville Ridge volcanic pile that have not been sampled by the dredge. If Colville Arc activity started a few million years before 16.7 Ma, it overlapped in time with most or all Northland Arc volcanism. Thus, Pacific plate subduction could have driven the volcanism in Northland.

In models of west- or southwest-dipping subduction, the subduction of South Fiji Basin (SFB) lithosphere from its position north of Northland is the only viable alternative to Pacific plate subduction. SFB subduction is predicted by the models of Crawford et al. (2003) and Whattam et al. (2006). South Fiji Basin oceanic lithosphere is of Oligocene and/or Early Miocene age (Herzer and Mortimer, 1998; Herzer et al., 2000; Mortimer et al., 2007), hence these models require the subduction of young (probably <10 Myr) and by implication buoyant (Cloos, 1993) oceanic lithosphere. The subduction of young, hot lithosphere potentially gives rise to a shallow-dipping slab and to slab melting. A shallow-dipping slab could help to explain the large width of the Northland Arc (c. 200 km). Subduction of young, hot oceanic crust can generate magmas with an adakitic trace element signature by slab melting. Key to this signature is an extreme depletion in Y and HREE due to the presence of residual garnet in the slab, and high Sr concentrations (typically > 400 ppm) reflecting ubiquitous plagioclase (Defant and Drummond, 1990; Martin et al., 2005). Low Y and HREE concentrations and high Sr/Y (up to 150) occur in some Whangarei Heads and most Parahaki samples and clearly reflect residual garnet, as do strongly fractionated La/Yb and Dy/Yb ratios in Parahaki dacites and some Whangarei Heads rocks. However, garnet occurs in Whangarei Heads lavas as inclusions and entrained crystals, together with schistose inclusions of crustal origin. Furthermore, the strongly evolved isotope compositions of Whangarei Heads and Parahaki rocks do not argue for an origin as melts derived from young oceanic lithosphere. Rather, we infer an origin in deep, anomalously thick crust (as discussed in Section 3.2.9). Therefore the occurrence of these rocks does not imply slab melting. Rocks of the Karikari-Wairakau centre and of the western belt centres have lower $^{87}\text{Sr}/^{86}\text{Sr}$ ratios than Whangarei Heads and Parahaki centre rocks, but in turn do not show any particular adakitic affinity in terms of Sr, Y and HREE concentrations. Although we do not reject the hypothesis of South Fiji Basin subduction, the current geochemical dataset does not specifically support the subduction of young oceanic lithosphere as a driver of Northland Arc volcanism. Resolution of the question whether old or young lithosphere subducted may ultimately require detailed Pb isotope data on the premise that the young South Fiji Basin lithosphere must have had a less evolved Pb isotope composition than old Pacific lithosphere. Pb in subduction basalts may be up to 95% slab-derived and carry a recognizable

slab signature (Green, 2006; Hoernle et al., 2008; Schuth et al., 2009). C. 80-95% of Pb in Northland Arc rocks appears to be derived from the subducting slab (Fig. 3.8). Therefore the isotopic signature of the subducted slab can potentially be identified in mafic Northland Arc volcanic rocks.

Whattam et al. (2008) speculate that west-dipping subduction only gave rise to eastern belt volcanism, which is contiguous with volcanism in the Three Kings Ridge, but that western belt volcanism developed over a detached fragment of the subducted South Loyalty Basin slab. This interpretation is attractive because it predicts that volcanism in the western belt would largely be driven by dry magmas formed by partial melting of upwelling hot asthenosphere. Dry magmas would not crystallise amphibole, therefore an anhydrous gabbroic assemblage would dominate differentiation processes. As another alternative, Schellart (2007) sought the source of Northland Arc volcanism in the detachment of a previously NE-dipping slab of oceanic lithosphere attached to the northern passive margin of the New Zealand microcontinent. Detachment of this slab would have been initiated by the arrival of Northland continental lithosphere at the subduction hinge. Schellart's (2007) model does not distinguish between western and eastern belt volcanism and does not readily provide an explanation for their amphibole-absent vs. amphibole-present nature, respectively.

A difficulty with models that invoke slab detachment as a source of magmatism is that this predicts melting as a result of upwelling of hot mantle. The magmatic products of such melting would not be expected to carry an arc trace element signature per se. Even if parts of the upwelling mantle had previously been metasomatised by subduction-related processes, some intraplate-type trace element characteristics might be expected in at least some volcanic centres. In Northland, only displaced 20.0 Ma volcanic clasts in the Waitemata Basin carry an intraplate signature; the occurrence of these rocks may be best explained as reflecting localised mantle upwelling around the edge of a subducted slab (Shane et al., 2010). In contrast, the volcanic rocks of the Northland Arc proper uniformly carry an arc trace element signature. Consequently, we prefer an interpretation where all Northland Arc volcanism occurs over a subducting slab. The absence of a clear adakitic signature in any of the centres suggests that the subducted slab comprised old (Cretaceous, Pacific) lithosphere rather than young (Oligocene, South Fiji Basin lithosphere).

3.2.11. Conclusions

New geochemical and Sr-Nd isotope data for the Early Miocene volcanic rocks of the Northland Arc show subtle but distinct differences between western and eastern belt volcanism, even though rocks in both belts carry a clear arc-type trace element signature. Eastern belt rocks are the products of amphibole-

present magmatic systems and show trace element and isotopic evidence for relatively extensive crustal interaction in their petrogenesis. This style of volcanism contrasts with the amphibole-absent magmatic systems that are prevalent in the western belt. Western belt rocks, specifically at the Waipoua, Hukatere and Manukau centres, do not contain phenocrystic hornblende and do not show REE fractionation characteristic of cryptic amphibole fractionation. The absence of amphibole and the dominance of 'gabbroic' minerals suggests that the mineral assemblage did not provide much leverage to increase SiO₂ contents with ongoing differentiation and consequently the magmas largely remained basaltic or basaltic andesitic. Anorthitic plagioclase accumulation drove compositions towards the high-alumina basalt field, possibly at late stages of magmatic development. Western belt rocks have relatively primitive Sr-Nd isotope compositions suggesting that crustal involvement in magmatic differentiation processes was minimal. Nevertheless, eastern and western belt rocks carry a similar arc-type trace element signature, and contain similar slab-derived fractions of non-conservative elements (Ba, Th, Pb). We conclude that primary magmas in both belts originated in a mantle that was metasomatised by slab fluids.

Because the geochemical differences between eastern and western belt rocks do not appear to be due to a contrast in mantle origin, we propose that a heterogeneous crustal section across the Northland Peninsula gave rise to the differences in magmatic development. The eastern belt centres erupted over the centre of the Northland extension of the New Zealand microcontinent, on topographically higher terrain, whereas western belt centres largely erupted onto topographically lower (presently submerged) terrain along the boundary between the Northland High and the greater Taranaki Basin, which was an area of extension in Cretaceous-Paleogene times. A thicker crustal section underlying the eastern belt can help to explain the development of amphibole-bearing magmatic systems in the deep and middle crust and more extensive crustal involvement. Anomalously thick crust underlying the Whangarei Heads and Parahaki centres could help to explain the formation of magmas with evolved Sr-Nd isotope compositions in the presence of residual garnet.

The subducting slab that drove volcanism could have been either west-dipping Pacific or South Fiji Basin lithosphere. Given that none of the studied Northland Arc rocks possess a convincing adakite-type signature, we favour the subduction of old (Cretaceous) Pacific lithosphere rather than young (Oligocene) South Fiji Basin lithosphere.

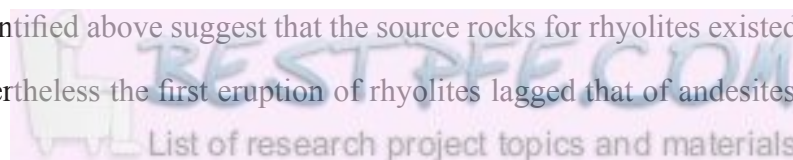
Chapter 4. Coromandel Volcanic Zone Volcanism

4.1. Summary

Volcanism in the Coromandel Volcanic Zone (CVZ) spanned c. 16 Myr and encompassed a wide range of volcanic rock types. One of the principal aims of this study is to document the development of the erupted rock suite through time and examine the relations between the basalts, andesites and rhyolites that form the volcanic succession. This chapter presents new geochemical and isotope data on rocks representing the entire CVZ volcanic stratigraphy, in the form of a paper that is in review for publication in *Lithos*. The bulk compositions of the relatively low-phyric Mercury Basalts and Whitianga Group rhyolites approximate melt compositions. The compositional variation within these groups can be explained by fractionation of phenocryst assemblages. The more crystal-rich Coromandel Group andesites have bulk compositions that are not readily explained by crystal fractionation of the observed phenocryst minerals. The crystals in andesites have compositions that correlate weakly or not at all with bulk rock chemistry, whereas groundmass compositions correlate with bulk composition. Coromandel Group andesites therefore do not represent melts but mixtures of crystals and melts, where the silicic melt component has high-silica andesitic, dacitic to rhyolitic composition. The mafic component in Coromandel Group andesites appears to have a comparable composition to Mercury Basalts; the silicic component is similar in some respects to Whitianga Group rhyolites, although it may be less silicic and less alkaline than typical Whitianga Group rhyolite. Isotope properties indicate the presence in Coromandel Group rocks of a substantial crust-derived Sr component, indicating that some or all components of the andesites formed in an open system characterised by assimilation of crustal rocks.

The least-differentiated Whitianga Group rhyolites have bulk compositions that are comparable to those of experimental partial melts derived under crustal conditions from hornblende gabbro starting materials with compositions identical to those of Mercury Basalts. More differentiated rhyolite compositions can be derived by feldspar fractionation from least-differentiated rhyolites. The implied genetic link between rhyolites and Mercury Basalt-like source rocks suggests that rhyolites formed by remelting of previously stalled parts of the CVZ magmatic system, plausibly in response to ongoing heating of the arc crust.

The genetic links identified above suggest that the source rocks for rhyolites existed at all times in the magmatic system. Nevertheless the first eruption of rhyolites lagged that of andesites in the CVZ by c.



6 Myr, and in the wider North Island volcanic succession by c. 13 Myr. These long delay times contrast with the much shorter delay between andesitic and rhyolitic volcanism in younger parts of the North Island volcanic succession and elsewhere, suggesting that tectonic factors initially inhibited the inception of silicic volcanism.

This chapter concludes with a section specifically detailing aspects of the development through time of the CVZ succession. Coromandel Group andesites throughout the succession plot along the same compositional arrays, indicating that they formed by similar processes. However, within the Kuaotunu Subgroup (18-10.5 Ma) the maximum degree of differentiation increases with time. A similar trend exists in younger Waiwawa Subgroup rocks. These trends could reflect the greater availability over time of silicic melts, to be incorporated as the silicic component in Coromandel Group andesites. Additionally, Pb isotope data are presented that have been collected to assess whether the oldest CVZ rocks show evidence for the involvement of young South Fiji Basin lithosphere subduction. Although the Pb isotope dataset is small, it does not provide any indication for involvement of young lithosphere and instead suggests that older and/or more differentiated material was subducted during early CVZ activity.

4.2. The Transition from Intermediate to Silicic Volcanism in the North Island of New Zealand

Mathijs A. Booden, Ian E.M. Smith, Jeffrey L. Mauk, Philippa M. Black

School of Environment, The University of Auckland, Private Bag 92019, Auckland 1142, New Zealand

4.2.0.0. Abstract

The volcanic succession in the North Island of New Zealand documents evolving volcanism from the Late Oligocene (c. 25.5 Ma) to the present at the dynamic Australasian-Pacific plate boundary. Between c. 18 Ma and 1.95 Ma, the locus of activity was in the Coromandel Volcanic Zone. Initial intermediate volcanism, recorded by basaltic andesites, andesites and dacites that are compositionally comparable to those of the predecessor Northland Arc, was joined from 12 Ma by rhyolitic and basaltic volcanism. The andesitic volcanic rocks of the CVZ define a calc-alkaline differentiation trend and show variable initial $^{87}\text{Sr}/^{86}\text{Sr}$ values that indicate open-system interaction with the Mesozoic basement. They are typically strongly porphyritic with phenocryst assemblages dominated by plagioclase and pyroxene. Seriate porphyritic textures are common, where smaller crystals may be fragments of larger phenocrysts or glomeroporphyritic crystal aggregates. Plagioclase and pyroxene compositions do not correlate with bulk rock compositions, whereas groundmass compositions do correlate with bulk rock composition, and are invariably more silicic than the bulk rock. The porphyritic CVZ andesites can be described as mixtures of a mafic component, mainly represented by a crystal assemblage and a silicic component mainly represented by the groundmass. The mafic component in the andesites apparently has a basaltic composition, comparable to that of the calc-alkaline basalts that erupted in the CVZ from 12 Ma. The silicic component in the andesites is comparable in some respects to the bulk compositions of rhyolites that erupted in the CVZ from 12 Ma, but appears to have been less alkaline and less silicic than the erupted rhyolites. Experimental partial melts with compositions corresponding to the inferred silicic component in CVZ andesites have been derived from relatively low-potassic, more tholeiitic basalts. Partial melt compositions matching CVZ rhyolites have been derived from basalts with comparable compositions to calc-alkaline CVZ basalts. The appearance of rhyolites at 12 Ma may record the first instance of significant re-melting of stalled basaltic to intermediate calc-alkaline rocks in the North Island volcanic succession. Nevertheless, the calc-alkaline source rocks for rhyolites appear to have been common prior to 12 Ma. It is possible that their initial failure to evolve into a silicic magmatic system relates to tectonic constraints imposed on the arc crust by the evolving Australasian-Pacific plate boundary.

Keywords: Andesite; rhyolite; basalt; subduction; Coromandel; North Island.

4.2.1. Introduction

Volcanic arc systems are known to persist in a relatively steady state over geologically long periods of time in some tectonic situations (e.g., the active margin of South America; Willner et al., 2004; Glodny et al., 2006), but in some cases arcs evolve rapidly in response to changes in the nature of plate boundaries. The Late Cenozoic volcanic succession in the North Island of New Zealand preserves a 25 million year record of evolving arc volcanism in a dynamic plate tectonic setting that shows a trend over time from basalt- and andesite-dominated shield and cone volcanism with limited silicic activity (Smith et al., 1989), to andesite- and rhyolite-dominated activity (Skinner, 1986), to overwhelmingly silicic volcanism in the Taupo Volcanic Zone (TVZ; Wilson et al., 1995). Because the locus of volcanism shifted continuously over time, older parts of the succession are relatively well preserved, providing an outstanding opportunity to examine the nascent development of a continental volcanic arc. The Middle Miocene to Pliocene part of this succession is preserved on the Coromandel Peninsula and surrounding islands as the Coromandel Volcanic Zone (CVZ; Fig. 4.1). Andesitic volcanism, which had occurred more or less continuously in northern New Zealand since the Early Miocene, was here joined by the first rhyolitic eruptions and by sporadic basaltic volcanism from 12 Ma (Skinner, 1986; Adams et al., 1994; Nicholson et al., 2004). Andesites, basalts and rhyolites provide snapshots of magma compositions that existed in the CVZ magmatic system. In this paper, we present new major and trace element and isotopic data for rocks that span the CVZ compositional spectrum, and use these to document the development of the magmatic system.

4.2.2. Geologic Setting

Current arc volcanism in northern New Zealand occurs at the continental tip of the largely oceanic Kermadec-Tonga arc system, and has since 2 Ma been concentrated in the central North Island (Taupo Volcanic Zone, TVZ; Fig. 4.1). The TVZ-Kermadec-Tonga system is developed on the Australasian plate over the west-dipping Cretaceous Pacific plate, which at the latitude of New Zealand comprises 17 km thick oceanic crust of the Hikurangi Plateau but gives way to the north to similarly aged 9 km thick oceanic crust. The rate of convergence is inversely correlated with the thickness of the subducted plate, increasing from c. 42 mm yr⁻¹ in the New Zealand segment to 53 mm yr⁻¹ at 35°S (DeMets et al., 1994). The rate of backarc opening shows a concomitant increase, from nil at the southern tip of the TVZ (Stern

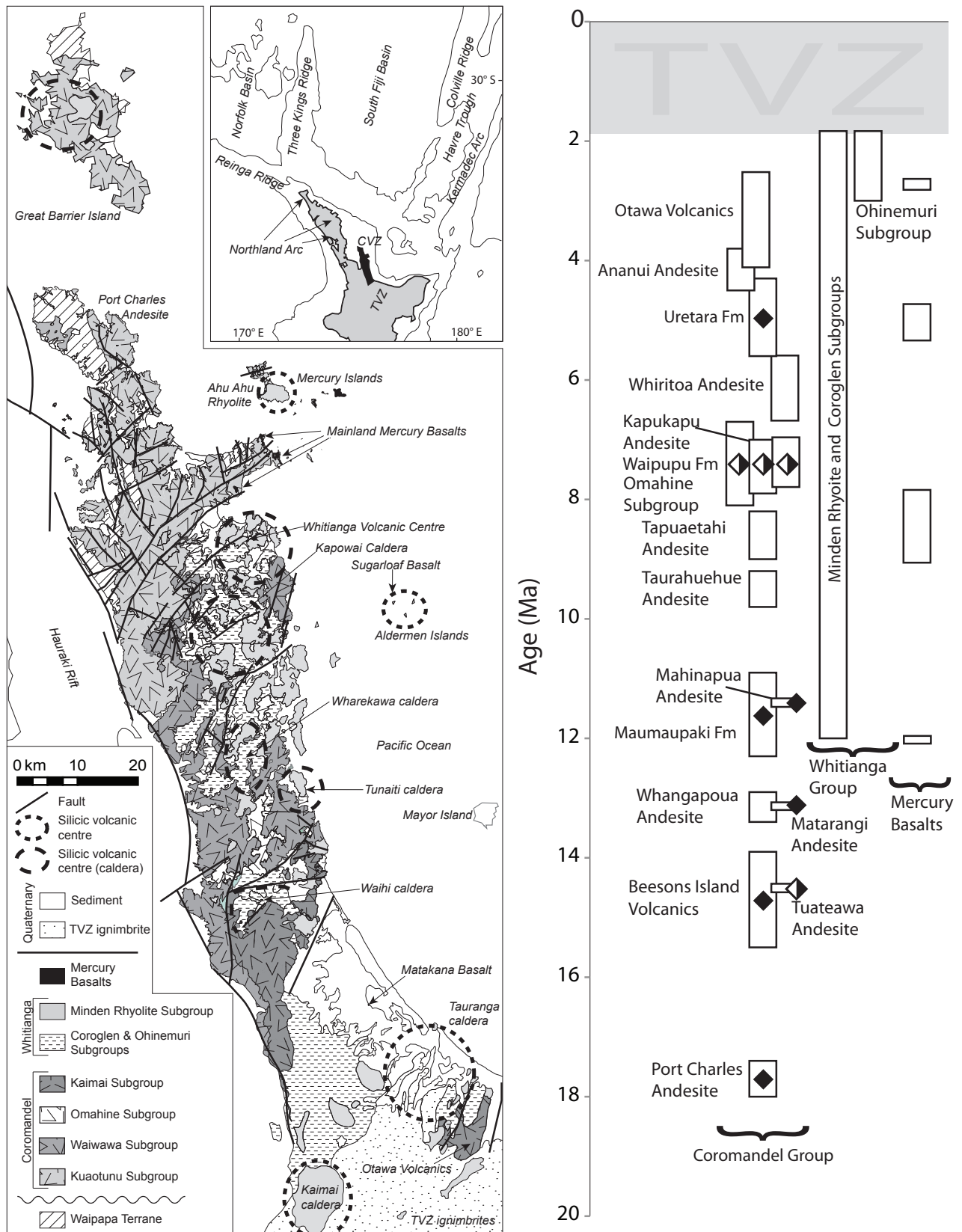


Fig. 4.1 Geologic map of the Coromandel Volcanic Zone compiled from Edbrooke (2001), Brathwaite and Christie (1996), Briggs et al. (1996), Houghton and Cuthbertson (1988) and Skinner (1976, 1993, 1995). Inset shows the location of the major tectonic features in the region. Simple stratigraphic column of the regional volcanic stratigraphy compiled from references above. Filled and half-filled diamonds indicate the presence in Coromandel Group rocks of amphibole and resorbed amphibole, respectively, in addition to the common plagioclase + pyroxene assemblage.

et al., 2006) to c. 8 mm yr⁻¹ in the central TVZ (Darby et al., 2000). The rifting segment of the TVZ is contiguous towards the north with the Havre Trough backarc basin, a nascent spreading center since 5.5 Ma (Wysoczanski et al., 2010) that is extending at a rate of 15 mm yr⁻¹ at 35°S (DeMets et al., 1994). Calc-alkaline and high-magnesian andesites erupt at the southern and northern segments of the TVZ. Highly productive caldera-forming rhyolitic volcanism dominates the central segment, and basalts occur sporadically throughout the TVZ (Houghton and Wilson, 1995; Wilson et al., 1995).

From the Middle Miocene to the earliest Pleistocene, arc volcanism occurred northwest of the current TVZ where volcanic rocks cover parts of the Coromandel Peninsula, Great Barrier Island, the Mercury Islands and surrounding smaller islands (Fig. 4.1) (Skinner, 1986). There, the volcanic succession records more or less continuous volcanism (Adams et al., 1994) and includes all of the rock types that also occur in the TVZ. However, in the CVZ only andesites erupted through the entire duration of the zone, starting with the oldest preserved, 18 Ma Port Charles Andesite (Adams et al., 1994) and terminating with the 2.54 Ma Ottawa Volcanics (Briggs et al., 2005). Rhyolites and basalts are preserved from 12 Ma. Approximately 12 major silicic volcanic centers have been identified, some of which were calderas (Adams et al., 1994; Brathwaite and Christie, 1996; Nicholson et al., 2004; Briggs et al., 2005). Basalts erupted episodically, principally along the eastern margin of the CVZ (Adams et al., 1994; Briggs et al., 2005) and high-magnesian andesites erupted between 6.2 and 5.5 Ma at its southwestern margin (Black et al., 1992).

The NNW-trending Coromandel Peninsula is a horst structure bounded in the west by the parallel Hauraki Rift, a half-graben that is down-thrown to the east (Hochstein et al., 1986). Basement structures predominantly strike NNW and NE-NNE and influence the orientation of faults, hydrothermal veins and caldera boundaries developed in the volcanic cover (Smith et al., 2006a). The NNW-trending Coromandel peninsula also reflects basement trends, and the strike of the elongate CVZ does not necessarily reflect the orientation of the associated subduction system. Rather, on a regional scale the CVZ appears to be at the continental tip of an extinct NNE-trending volcanic arc, the Colville Ridge (Fig. 4.1), which was volcanically active at least as early as 16.7 Ma (Mortimer et al., 2010). Prior to rifting of the Havre Trough backarc basin, the Colville Ridge formed a single volcanic arc with the still-active Kermadec Ridge arc (Ballance et al., 1999). SSW of the CVZ, cone volcanoes formed between 14-8 Ma in the Taranaki Basin (King and Thrasher, 1996). Further north, volcanic activity occurred along the Lau Ridge between 14 and 5 Ma (Whelan et al., 1985). Based on the coeval arc volcanism in these segments, Herzer (1995) proposed the existence of a single NNE-trending Miocene Taranaki-Colville-Lau arc with a total

length of c. 2500 km.

4.2.3. Volcanic Stratigraphy

The CVZ volcanic succession erupted onto metasedimentary, Mesozoic basement graywackes of the Waipapa Terrane that are exposed in the northern Coromandel Peninsula and on Great Barrier Island, but are completely covered by volcanic rocks to the south (Fig. 4.1; Skinner, 1972). The current volcano-stratigraphic subdivision of Skinner (1986) distinguishes three groups on the basis of dominant rock type: the Mercury Basalts (mafic rocks), the Coromandel Group (intermediate rocks) and the Whitianga Group (felsic rocks).

The Coromandel Group includes cone-related basaltic andesites, andesites and minor dacites (collectively termed andesites hereafter) that primarily occur as lava flows, autoclastic breccias, lahars and tuffs, and in the northern CVZ shallow sub-volcanic intrusions. Within each formation, rocks commonly show a progression from less silicic basal rocks to more silicic rocks near the formation top (Skinner, 1986). The oldest dated Coromandel Group rocks form the 17.7 Ma Port Charles Andesite in the northern CVZ (Adams et al., 1994), whereas the youngest form the 2.5 Ma Ottawa Volcanics which occur in the south (Briggs et al., 2005). The Whitianga Group includes rhyolites that occur as ignimbrites, lava flows and domes, predominantly in the eastern half of the CVZ (Skinner, 1986). The oldest, 12 Ma rhyolites occur in the northern CVZ and the youngest, 1.95 Ma rhyolite dome in the southernmost CVZ (Adams et al., 1994; Brathwaite and Christie, 1996; Nicholson et al., 2004; Briggs et al., 2005). Rhyolites are associated with about 12 silicic volcanic centers, many of which have been identified as calderas (Briggs and Fulton, 1990; Krippner, 2000; Malengreau et al., 2000; Smith et al., 2006a). The Mercury Basalts comprise small volcanoes along the eastern Coromandel Peninsula, on Great Barrier Island and on islands east of the mainland. The oldest preserved, 12 Ma basalt occurs near Great Barrier Island (Nicholson et al., 2004). Further basalts erupted episodically between 9.1-7.8 Ma and between 5.5-4.7 Ma in the northern CVZ (Adams et al., 1994) and at 2.7 Ma in the southernmost CVZ (Hollis, 1995; Briggs et al., 2005). The minimum ages of formations through the CVZ decrease towards the south (Adams et al., 1994).

4.2.4. Sample Set and Analytical Methods

This study is based on a sample set of ~140 fresh, unaltered volcanic rocks from collections at University of Auckland, University of Waikato and GNS Science that were originally collected and described for mapping and research. Most were previously analyzed by XRF and some were used in K-Ar and

$^{40}\text{Ar}/^{39}\text{Ar}$ dating studies. The dataset presented here consists of new XRF and ICP-MS major and trace element data together with new Sr-Nd isotope data for a subset of samples. We used samples of lavas because these are the freshest, best-preserved rocks. Samples represent massive flows, autoclastic breccias, dykes intruded into volcanic rocks and massive boulders in reworked deposits where the rocks are part of an identifiable formation. Aliquots (100-200 g) of fresh rock samples were crushed between tungsten-carbide plates and any weathered fragments removed before grinding in a tungsten-carbide ring mill to <200 mesh. Major and some trace element concentrations were measured at the University of Auckland by X-ray fluorescence spectrometry (XRF) on fused glass discs prepared with SPECTRACHEM 12-22 flux. For the trace elements a suite of 36 international standards were used for calibration and Siemens SPECTRA 3000 software was used for data reduction. The Compton scatter of X-ray tube line RhK β 1 was used to correct for mass attenuation and appropriate corrections were used for those elements analyzed at energies below the Fe absorption edge. For XRF major oxide analyses precision is generally better than 1% (at 2σ) and for trace elements it is 1% for Sr and Zr, 1-3% for V, Cr, Zn and Y, 3-5% for Ba, 5-10% for Rb and Nb, Detection limits are <2ppm for Rb, Sr, Y, Zr and Nb, 2-5ppm for V, Cr, and Zn, and 5-10ppm for Ba. We report major elements (Na, Mg, Al, Si, P, K, Ca, Ti, Mn, Fe) as their respective oxides (Na_2O , MgO , Al_2O_3 , SiO_2 , P_2O_5 , K_2O , CaO , TiO_2 , MnO , FeO , Fe_2O_3) normalized to 100% on a volatile-free basis, using the $\text{FeO}/\text{Fe}_2\text{O}_3$ ratios recommended by Middlemost (1989). Additional trace element concentrations were measured by ICP-MS at ALS Chemex Vancouver following a four-acid (nitric, hydrochloric, perchloric and hydrofluoric acids) digest procedure. Reproducibility, including sample splitting, is better than 10% for the relevant trace elements. Table 4.1 lists representative geochemical analyses. The full dataset is available as Online Supplement 1 [presented in Appendix B].

Electron microprobe analyses were performed using a Jeol JXA-840 probe fitted with a PGT Prism 2000 EDS detector at University of Auckland. An absorbed current of 1.5 nA at 15 kV and a $\sim 2\ \mu\text{m}$ beam was used for mineral analyses and was defocused to $20\ \mu\text{m}$ for groundmass analyses. Reproducibility is better than 6% 2σ for the major elements reported here. Table 4.2 lists representative crystal and groundmass geochemical analyses. The full crystal and groundmass chemistry dataset is available as Online Supplement 2 [presented in Appendix C].

Whole-rock Sr isotope compositions were determined on aliquots of the same samples used for ICP analysis, at VU University, Amsterdam. Strontium was extracted using standard resin column techniques and analyzed on a Finnigan Mat 262 TIMS (Heumann and Davies, 2002). Analyses were performed on 200 ng sample aliquots, whereas blanks were three orders of magnitude smaller and therefore negligible.

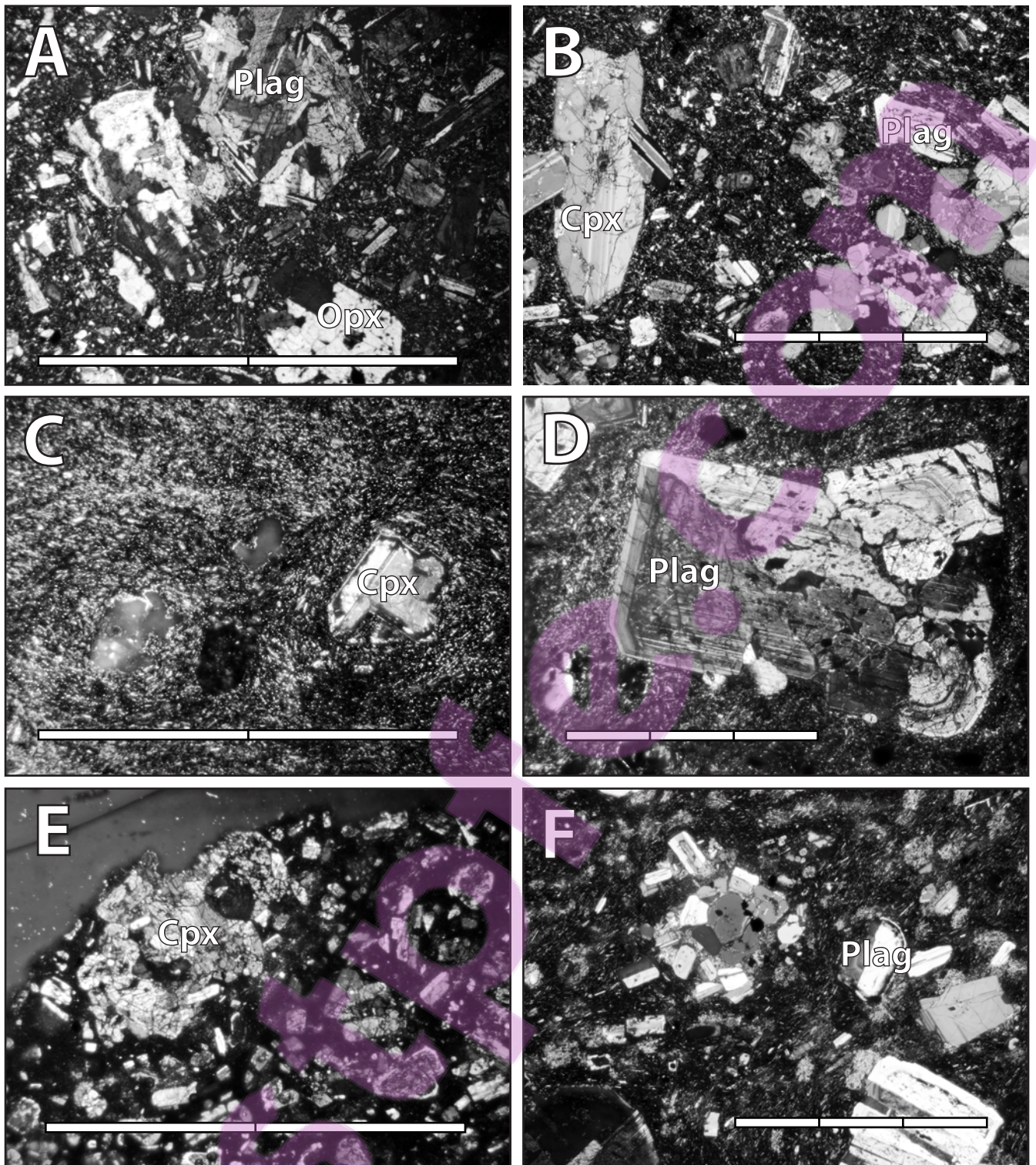


Fig. 4.2 Thin-section photomicrographs. Scale bar segments indicate 1 mm increments. A. AU45386. Pyroxene andesite, Beeson's Island Volcanics. B. R17876. Pyroxene andesite, Waipupu Formation. C. R17831. Pyroxene andesite, Kapukapu Andesite. D. R17880. Pyroxene andesite, Waipupu Formation. E. AU45340. Pyroxene andesite, Whangapoua Andesite. F. R17856. Pyroxene andesite, Whiritoa Andesite.

Within-run analytical errors are negligible compared to the geologic variation in isotope ratios. Table 4.1 lists isotope data, as well as calculated initial isotope ratios based on available K-Ar and ^{40}Ar - ^{39}Ar dates and measured Rb/Sr ratios.

4.2.5. Petrography

Coromandel Group andesites are typically 20-60% crystalline, porphyritic plagioclase + pyroxene + Fe-Ti-oxide phenocrysts with a granular groundmass rich in plagioclase laths and pyroxene microcrystals. Orthopyroxene and clinopyroxene are both common. Olivine occurs in some basaltic andesites, and quartz and biotite in some dacites. Additionally, amphibole is a common phenocryst in pre-10 Ma formations, but it only occurs as resorbed crystals, commonly with opaque reaction rims, in younger formations.

Plagioclase is the dominant mineral in most samples and occurs as euhedral or subhedral crystals up to 2-3 mm in size, some of which show complex internal structure (Fig. 4.2). Oscillatory zoning, internal resorption surfaces and growth rims that are either rich or lacking in inclusions occur. Some samples contain crystals with turbid cores that are surrounded by clear rims, or turbid rims overgrown by a clear outer rim. Some large crystals have internal fracture planes along which glassy patches occur. We interpret these features to indicate that plagioclase crystals in many andesite samples experienced disequilibrium conditions resulting in small amounts of resorption by the surrounding melt.

Some seriate porphyritic andesites contain ubiquitous angular plagioclase crystals that occasionally show optical zoning crossing the crystal margins. As well, plagioclase and pyroxene crystals commonly occur in glomeroporphyritic crystal aggregates. Where this is the case, the glomeroporphyritic crystals are petrographically similar to single crystals in the same rock. Some glomeroporphyritic aggregates are surrounded by a zone in which the matrix contains a high concentration of single crystals, which appear similar to the crystals that comprise the aggregate. We interpret these features to indicate that the crystals in many andesite samples are fragments derived from larger crystals and/or from disaggregated glomeroporphyritic crystal aggregates, suggesting that they are part of a remobilized crystal fraction. Where this is the case, the crystals and the melt that entrains them are not necessarily genetically related and the bulk rock composition may not represent a melt composition. However, because the petrographic features described above occur in samples of lavas, it is possible that they pertain solely to eruptive processes, e.g. the disaggregation of partly solidified magma prior to or during an eruption.

Table 4.1 (following pages) Representative whole-rock geochemical analyses of fresh unaltered volcanic rocks. The complete dataset is presented in Online Supplement 1 [Appendix B]. Major element oxide concentrations in weight percent measured by XRF and normalized to 100% volatile-free. Minor and trace element concentrations in parts per million determined by XRF, and by wet-chemistry ICP-MS (italicized). Sr isotope ratios measured by thermal ionization mass spectrometry, as described in text. Initial isotope values calculated using the ages listed here and decay constant ^{87}Rb : $1.398 \cdot 10^{-11} \text{ yr}^{-1}$ (Nebel et al., 2006).

Table 4.1

	Mercury Basalts				Kuaotunu Subgroup						Waiwawa Subgroup				
Sample	AU 60071	BH76	SP099	BH35	R 12392	R 12391	R 12404	R 12397	R 10432	R 12399	R 12415	R 12767	R 12382	R 17862	R 17864
Unit	Sugar- loaf	Toka- rahu	Motu- roa	Opito Point	Port Char.	Port Char.	Bees. Island	Bees. Island	Wha- ngap.	Wha- ngap.	Mau- mau.	Taura- hue.	Ta- puae.	Kapu- kapu	Kapu- kapu
	Ol	Ol px pl	Pl ol px	Aphy- ric	Hbl px pl	Hbl px pl	Hbl px pl	Hbl px pl	Px pl	Px pl	Hbl px pl	Px pl	Px pl	Px pl	Px pl
SiO ₂	50.82	51.67	56.05	54.03	56.15	55.44	57.40	60.75	59.11	56.37	61.18	56.10	60.12	57.88	60.41
TiO ₂	0.73	1.06	1.04	1.14	1.02	1.12	0.97	0.82	0.73	0.90	0.71	1.05	0.71	0.77	0.62
Al ₂ O ₃	14.10	15.71	16.78	17.27	17.68	19.04	17.63	17.13	17.59	18.35	17.35	18.03	17.01	17.80	16.39
FeO	7.76	7.40	6.72	7.82	6.18	6.31	5.87	5.02	5.29	6.37	5.27	6.53	5.13	5.37	4.89
Fe ₂ O ₃	1.55	1.48	2.02	2.34	1.85	1.89	2.05	1.76	1.85	1.91	1.85	1.96	1.79	1.88	1.71
MnO	0.16	0.15	0.17	0.18	0.14	0.15	0.16	0.15	0.11	0.14	0.14	0.18	0.15	0.11	0.13
MgO	12.40	9.29	4.92	4.68	4.35	3.43	3.70	3.00	3.75	3.78	1.99	3.68	3.69	3.82	4.04
CaO	9.78	9.38	7.7	8.74	8.06	7.82	7.29	6.45	6.68	7.75	6.17	7.66	6.62	8.31	7.14
Na ₂ O	2.11	3.08	3.18	3.12	3.46	3.62	3.17	3.16	3.14	3.00	3.25	3.14	3.05	2.64	3.01
K ₂ O	0.48	0.60	1.26	0.54	0.87	0.91	1.46	1.50	1.52	1.16	1.82	1.36	1.50	1.14	1.40
P ₂ O ₅	0.11	0.18	0.16	0.14	0.14	0.17	0.18	0.14	0.12	0.13	0.14	0.18	0.11	0.15	0.12
Sc	35.8	31.7	27.8	35.0	32.5	24.3	24.6	26.7	24.5	29.4	21.5	27.2	24.4	27.7	21.0
V	235	227	192	317	244	217	184	184	164	220	156	216	176	190	140
Cr	906	462	167	16	57	19	23	19	51	50	26	7	50	42	167
Co	58.2	44.4	41.2	31.8	55.9	37.4	34.6	28.3	31.2	27.1	21.4	75.2	44.5	51	31.2
Ni	264.0	192.5	98.2	3.5	14.1	8.0	13.1	6.8	14.3	10.9	6.3	3.3	16.9	76.5	43.5
Cu	63.5	31.3	40.9	32.7	19.7	27.3	54.0	27.4	31.2	19.1	25.8	13.0	24.5	39.0	43.9
Zn	75	82	80	102	85	83	79	75	79	70	59	78	66	94	69
Ga	15	17	20	19	23	24	23	23	23	22	21	23	21	23	21
Rb	5	16	48	15	23	26	48	72	53	38	61	43	51	28	49
Sr	307	294	272	303	211	233	219	300	195	266	266	310	215	271	219
Y	19.0	26.3	24.6	25.4	22.6	22.7	27.0	23.1	22.9	28.0	20.7	25.2	33.3	19.9	19.9
Zr	67	110	134	86	106	115	130	125	112	103	124	136	121	111	113
Nb	2.2	4.8	5.2	3.9	3.8	4.0	5.3	6.1	5.4	5.1	5.6	8.2	4.3	4.2	4.4
Cs	0.35	0.69	9.88	0.94	0.64	0.93	2.43	3.88	1.57	3.64	1.97	1.42	1.92	4.24	1.24
Ba	132	207	254	219	135	170	276	263	269	196	298	263	287	293	332
La	6.9	13.2	12.6	8.8	10.8	9.1	14.3	17.6	16.9	14.5	16.5	16.3	15.5	11.4	14.1
Ce	18.6	31.0	28.7	21.9	24.1	21.3	31.6	35.7	32.6	29.0	35.2	37.1	30.6	23.9	24.1
Pr	2.43	4.24	3.84	3.14	3.00	2.70	4.00	4.20	3.70	3.70	4.10	4.60	4.10	3.10	3.10
Nd	9.90	16.90	16.6	12.90	13.00	12.10	16.90	16.30	15.70	15.70	15.80	18.90	16.90	13.20	12.70
Sm	2.45	3.99	3.97	3.38	3.30	3.20	4.00	3.70	3.60	3.70	3.40	4.30	4.20	3.10	3.00
Eu	0.92	1.39	1.23	1.30	1.10	1.10	1.20	1.20	1.00	1.20	1.10	1.40	1.10	0.80	0.70
Gd	2.86	4.43	4.33	3.96	3.80	3.50	4.50	4.20	3.80	4.30	3.80	4.90	4.40	2.90	2.80
Tb	0.51	0.75	0.72	0.71	0.70	0.60	0.80	0.70	0.60	0.70	0.60	0.80	0.90	0.50	0.50
Dy	2.89	4.12	4.36	4.08	4.00	4.00	4.80	4.10	3.90	4.40	3.60	4.60	5.10	3.70	3.60
Ho	0.68	0.93	0.95	0.97	0.80	0.80	1.00	0.80	0.80	0.90	0.70	0.90	1.10	0.70	0.70
Er	1.93	2.56	2.70	2.61	2.50	2.50	3.00	2.50	2.60	2.70	2.30	2.80	3.40	2.30	2.40
Tm	0.28	0.38	0.40	0.40	0.30	0.30	0.40	0.30	0.40	0.30	0.30	0.30	0.50	0.30	0.30
Yb	1.75	2.33	2.49	2.43	2.20	2.30	2.90	2.40	2.60	2.50	2.10	2.60	3.30	2.20	2.30
Lu	0.29	0.38	0.39	0.41	0.30	0.30	0.40	0.30	0.30	0.30	0.30	0.30	0.60	0.30	0.30
Hf	1.8	2.7	3.3	2.2	2.8	3.0	3.3	3.1	3.6	2.7	2.4	3.8	3.0	3.3	3.5
Ta	0.18	0.34	0.43	0.27	0.78	0.65	0.81	0.57	0.42	0.64	0.59	1.44	0.87	0.34	0.36
Pb	2.7	4.7	8.0	3.0	4.0	4.1	7.2	9.6	16.0	7.8	7.4	6.2	5.7	6.6	5.7
Th	1.5	2.3	4.1	1.2	3.0	2.9	4.1	5.6	5.1	3.5	6.4	4.3	4.2	3.5	3.7
U	0.2	0.3	1.1	0.1	0.8	0.7	1.0	1.6	1.2	0.8	1.4	1.0	1.0	0.8	1.0

Table 4.1 (ct'd)		Omahine Subgroup			Kaimai Subgroup		Whitianga Group					
Sample	R 17866	R12413	R17878	R17868	R17860	R17847	SK995	SK600	SK1005	BF67	SA1279	JR14
Unit	Whi- ritoa Px pl	Tau- raukau Px pl	Whaka- moehau Px pl	Whaka- moehau Px pl	Uretara Px pl	Ananui Px pl	Pinna- cles Pl opx	Rangi- hau Pl opx	Ruahine Bi pl	Tunaiti Bi pl	One- mana Bi pl	Lillie's Bi pl
SiO ₂	58.37	59.66	64.63	68.48	60.49	58.56	74.02	75.41	75.75	76.28	77.64	76.38
TiO ₂	0.67	0.61	0.57	0.46	0.62	0.68	0.48	0.36	0.22	0.14	0.09	0.14
Al ₂ O ₃	15.91	16.12	15.99	15.32	16.30	18.32	13.98	13.89	13.62	13.03	13.06	13.33
FeO	5.53	4.87	3.63	2.85	5.03	4.75	1.00	0.44	0.64	0.54	0.39	0.42
Fe ₂ O ₃	1.94	1.70	1.45	1.14	1.76	1.66	1.99	0.87	1.27	1.08	0.77	0.83
MnO	0.14	0.11	0.07	0.06	0.10	0.11	0.03	0.02	0.02	0.01	0.02	0.02
MgO	5.51	4.61	2.79	1.79	4.13	3.84	0.11	0.06	0.11	0.23	0.32	0.20
CaO	7.58	7.60	5.70	3.97	6.92	7.63	1.35	1.42	1.38	1.04	1.13	0.87
Na ₂ O	2.75	2.99	3.00	3.27	2.99	2.82	4.50	4.83	3.32	3.61	2.18	3.12
K ₂ O	1.37	1.48	1.96	2.44	1.44	1.40	2.51	2.66	3.63	3.85	4.40	4.68
P ₂ O ₅	0.11	0.12	0.11	0.10	0.11	0.12	0.04	0.04	0.03	0.02	0.01	0.01
Sc	25.2	23.6	17.7	11.0	20.8	20.5	12.4	11.9	3.1	5.5	4.9	3.4
V	164	144	112	75	135	144	14	7	20	8	1	9
Cr	194	124	84	25	147	30	3	3	3	0	2	3
Co	33.3	32.9	16.3	15.3	28	30.6	9.2	14.5	8.3	39.5	28.6	8.9
Ni	51.7	40.5	13.8	10.1	42.0	12.1	0.2	0.2	0.7	0.8	0.7	0.8
Cu	27.1	30.8	15.0	11.0	23.6	18	2.4	0.9	1.1	13.3	0.9	1.7
Zn	70	56	60	52	67	69	63	36	28	48	33	22
Ga	21	20	20	20	19	21	16	16	12	13	15	15
Rb	48	43	68	86	55	39	70	77	128	140	183	188
Sr	232	285	235	193	245	275	108	110	75	81	113	58
Y	17.2	26.0	14.3	15.0	16.1	17.2	28.9	39.8	6.3	44.8	33.2	17.8
Zr	106	123	113	130	101	91	286	283	111	125	90	93
Nb	4.7	4.4	4.7	5.5	4.2	4.8	9.9	10.0	6.0	6.7	6.4	9.1
Cs	1.97	1.54	2.01	2.20	3.29	2.97	1.48	0.89	3.46	8.14	27.90	10.00
Ba	278	278	356	487	295	229	652	674	814	676	761	600
La	11.7	19.0	15.6	17.5	11.0	10.8	59.8	30.4	20.5	33.8	36.4	28.6
Ce	24.6	39.6	28.5	33.9	22.8	20.9	54.8	62.4	32.1	52.8	58.4	53.0
Pr	3.00	4.80	3.40	3.80	2.90	2.9	7.07	7.73	3.29	7.90	8.40	6.04
Nd	12.20	19.50	12.80	14.00	11.80	12.1	28.80	31.40	10.70	28.70	27.70	18.00
Sm	2.80	4.20	2.60	2.70	2.60	2.80	6.09	6.90	1.71	5.78	5.53	3.09
Eu	0.70	1.10	0.60	0.60	0.60	0.70	1.70	1.61	0.35	1.16	0.81	0.59
Gd	2.60	4.60	2.40	2.30	2.40	2.70	6.29	7.01	1.74	7.37	6.12	3.33
Tb	0.40	0.80	0.40	0.40	0.40	0.50	0.94	1.09	0.21	1.29	0.99	0.50
Dy	3.20	4.40	2.70	2.80	3.00	3.30	6.06	7.21	1.29	7.67	5.27	2.57
Ho	0.60	0.90	0.50	0.50	0.60	0.60	1.24	1.46	0.25	1.71	1.18	0.56
Er	2.00	2.80	1.70	1.70	1.90	2.00	3.96	4.46	0.93	5.33	3.16	1.62
Tm	0.30	0.30	0.20	0.30	0.20	0.30	0.56	0.67	0.12	0.75	0.46	0.24
Yb	2.00	2.50	1.70	1.90	1.90	1.90	4.01	4.37	1.01	4.08	2.77	1.59
Lu	0.20	0.30	0.20	0.20	0.20	0.30	0.56	0.68	0.14	0.67	0.45	0.25
Hf	3.0	3.5	2.2	2.1	2.8	2.80	7.6	7.6	2.0	2.1	2.9	2.4
Ta	0.36	0.64	0.37	0.51	0.34	0.38	0.74	0.77	0.70	0.83	0.75	1.09
Pb	6.3	9.8	7.0	9.0	6.0	6.9	13.2	13.9	11.3	22.4	15.1	19.7
Th	4.2	5.2	4.9	7.3	4.2	3.0	8.7	8.8	12.4	13.8	14.0	20.7
U	1.0	1.2	1.1	1.6	1.0	0.8	1.9	2.0	2.2	2.4	2.9	4.4

Table 4.1 (ct'd)

Sample	Age (Ma)	$^{87}\text{Sr}/^{86}\text{Sr}$	$(^{87}\text{Sr}/^{86}\text{Sr})_i$
AU60071	83	0.704389	0.704383
BH76	7.81	0.704351	0.704334
SP099	53	0.705015	0.70498
BH35	8.71	0.70482	0.704803
R12392	17.71	0.704598	0.704521
R12391	17.71	0.704617	0.704538
R12404	14.71	0.70544	0.705312
R12397	14.71	0.704776	0.704636
R10432	13.11	0.706016	0.705874
R12399	13.11	0.705242	0.705168
R12415	11.61	0.705238	0.705132
R12767	9.51	0.705356	0.705303
R12382	8.61	0.705164	0.705083
R17862	7.32	0.705223	0.705193
R17864	7.32	0.705031	0.704966
R17866	6.12	0.705488	0.705437
R12413	7.41	0.704651	0.704606
R17878	6.52	0.705117	0.705042
R17868	6.52	0.705498	0.705383
R17860	52	0.705567	0.705523
R17847	4.22	0.705683	0.705659
SK995	83	0.705219	0.705013
SK600	83	0.705109	0.704887
SK1005	83	0.705806	0.705376
BF67	53	0.707042	0.706699
SA1279	83	0.707004	0.70649
JR14	7.71	0.706127	0.705141

Rhyolitic lavas of the Whitianga Group form the Minden Rhyolite Subgroup. Compared to andesites they are weakly porphyritic with 5-20% crystals, generally in glassy, although devitrified, groundmass. Quartz and plagioclase are the dominant minerals. Plagioclase occurs as single crystals, as well as in glomeroporphyritic aggregates and as angular fragments. Additionally, orthopyroxene (and subordinate clinopyroxene), biotite, hornblende and alkali feldspar variously occur. In mapping rhyolite formations, a distinction has been made between pyroxene-phyric rhyolites and rhyolites with hydrous mafic minerals and/or alkali feldspar (Skinner, 1986; Brathwaite and Christie, 1996; Krippner, 2000; Nicholson et al., 2004; Briggs et al., 2005). In addition to lavas, welded and non-welded rhyolitic ignimbrites occur and form the Coroglen Subgroup of the Whitianga Group.

Mercury Basalts are aphyric to porphyritic high-silica basalts and basaltic andesites containing the mineral assemblages olivine, olivine + plagioclase, plagioclase + pyroxene + olivine or plagioclase + clinopyroxene + Fe-Ti-oxide; they typically have a plagioclase + pyroxene \pm Fe-Ti-oxide groundmass (Skinner, 1986; Hawthorn, 1996). Resorbed hornblende is rare.

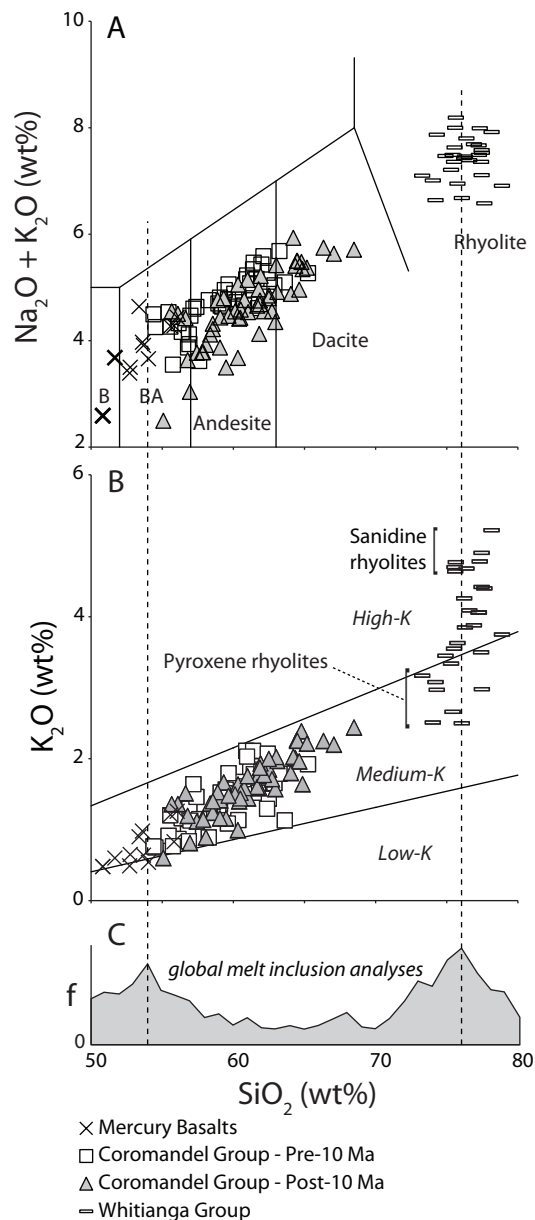


Fig. 4.3 Major element characterization of CVZ volcanic rocks. A. Total alkali-silica classification of Le Bas et al. (1986). B – basalt; BA – basaltic andesite. B. K_2O - SiO_2 classification of Gill (1981). C. Histogram of the bimodal melt inclusion SiO_2 concentration distribution in andesite-hosted minerals worldwide, based on the compilation of Reubi and Blundy (2009). Dashed lines extend the low-silica (54% SiO_2) and high-silica (76% SiO_2) frequency peaks to preceding diagrams.

4.2.6. Geochemistry

The volcanic rocks of the CVZ are basalts, andesites, dacites and rhyolites based on the IUGS total alkali-silica classification (Fig. 4.3A). Basalts to dacites are medium-potassic rocks that form an apparently continuous calc-alkaline differentiation trend (Fig. 4.3B).

4.2.6.1. Mercury Basalts

The Mercury Basalts have variable Al_2O_3 concentrations of 12-20% that correlate positively with

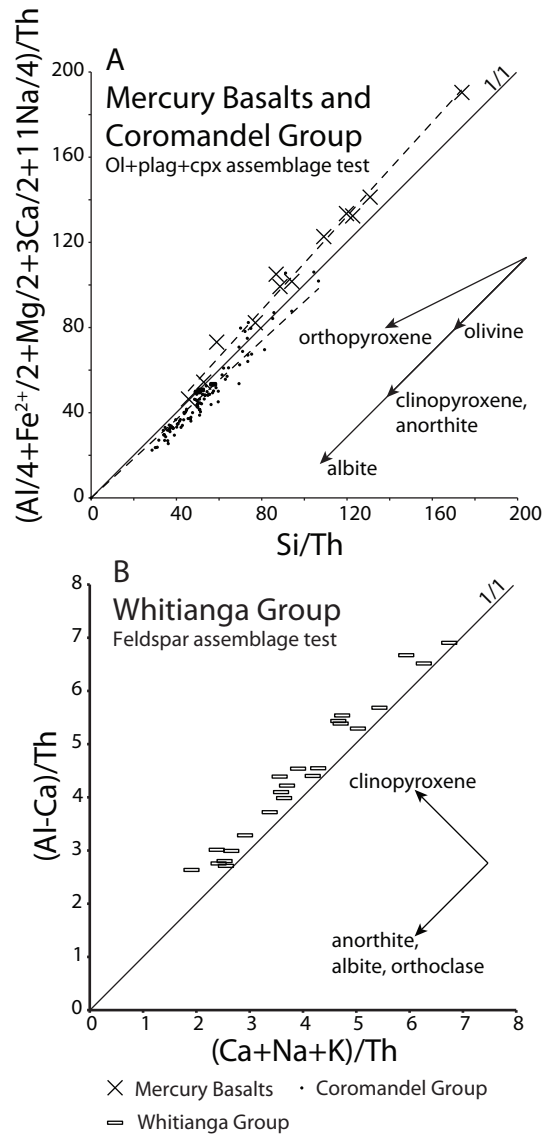


Fig. 4.4 . Pearce element ratio assemblage test diagrams. A. Assemblage test for olivine + plagioclase + clinopyroxene. B. Assemblage test for feldspar species. The axial ratios were derived using the Axis program (<http://ees.acadiau.ca/~cstanley/software.html>). Magnesium and ferrous iron are assumed to be interchangeable with respect to partitioning into minerals, and Th is assumed to be excluded from the fractionating mineral assemblage.

SiO₂; some can be defined as high-alumina basalts (HAB, following Crawford et al., 1987). The major element trends in Mercury Basalts could represent deep processes and/or sub-volcanic or syn-eruptive fractionation of entrained crystal content. Pearce element ratio (PER) diagrams can be used to test the hypothesis that fractionation of a particular mineral assemblage is responsible for major element trends, provided that at least one element is wholly partitioned into the melt and excluded from the mineral assemblage (Pearce, 1968). We use Th as the conserved element. On a plagioclase + clinopyroxene + olivine assemblage test diagram (molar $(Al/4 + (Fe+Mg)/2 + 3Ca/2 + 11Na/4)/Th$ vs. Si/Th ; Fig. 4.4A), Mercury Basalts form an array with correlation coefficient 0.99 along a line with slope 1. Assemblage

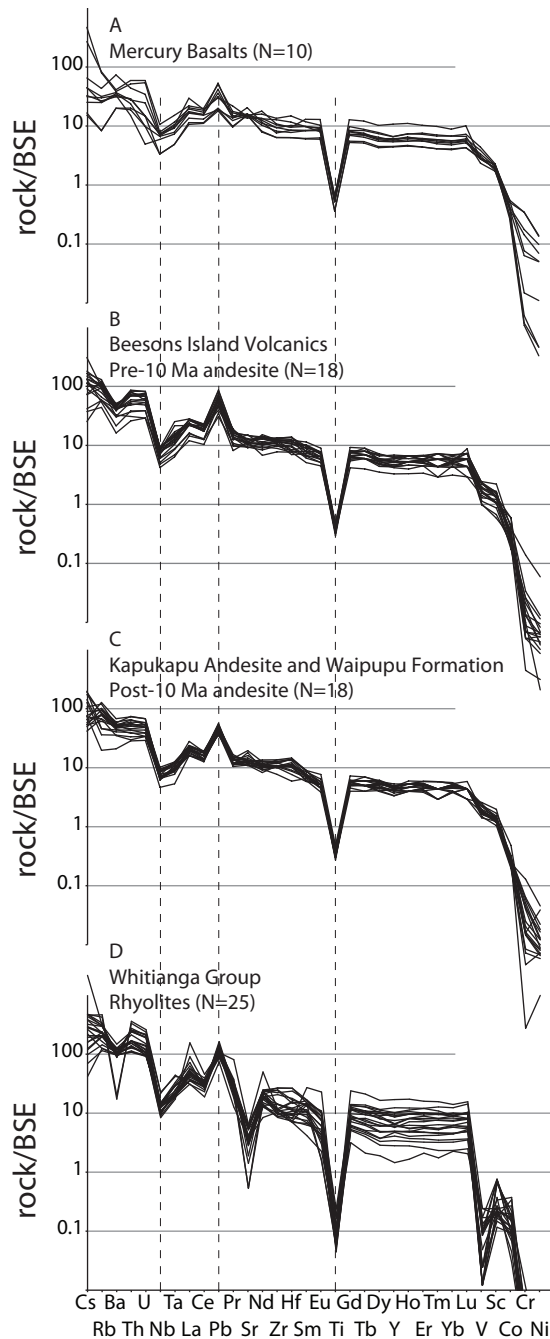


Fig. 4.5 Extended trace element distribution diagrams for rocks from selected stratigraphic units. Normalized to the model bulk silicate Earth (BSE) composition of McDonough and Sun (1988). A. Mercury Basalts. B. Beesons Island Volcanics (pre-10 Ma Coromandel Group). C. Kapukapu Andesite and Waipupu Formation (post-10 Ma Coromandel Group). D. Whitianga Group rhyolites.

tests for two-phase combinations of plagioclase, clinopyroxene and olivine yield unsatisfactory results. Hence, fractionation of the three major phenocryst minerals can account for the observed major element variation in Mercury Basalts.

All Mercury Basalts have a general arc-type trace element signature, but show considerable variation in the magnitude of highly incompatible element enrichment (Fig. 4.5A). The Sugarloaf Basalt has

Table 4.2

	SiO ₂	TiO ₂	Al ₂ O ₃	FeO	MnO	MgO	CaO	Na ₂ O	K ₂ O	P ₂ O ₅	SO ₃	Cl	Cr ₂ O ₃	NiO	Sum
AU45386	Beeson's Island Volcanics, Kuaotunu Subgroup, Coromandel Group														
Groundmass	63.0	0.4	19.6	1.5	0.1	0.3	5.6	4.9	2.1	0.1	0.0	0.0	0.1	0.2	97.8
Glomeroporphyritic orthopyroxene	53.3	0.4	1.5	18.8	0.5	24.0	1.5	0.0	0.1	0.0	0.0	0.1	0.0	0.0	100.0
Opx, single, adjacent to glomerocryst	53.6	0.3	1.6	19.8	0.4	23.6	1.6	0.0	0.1	0.0	0.0	0.0	0.0	0.0	100.9
Glomeroporphyritic plagioclase	49.4	0.1	31.0	0.7	0.0	0.0	14.9	2.9	0.2	0.1	0.0	0.0	0.1	0.0	99.5
Plag, single, adjacent to glomerocryst	51.4	0.1	29.8	0.6	0.1	0.0	13.6	3.5	0.3	0.0	0.0	0.0	0.0	0.0	99.4
R17831	Kapukapu Andesite, Waiwawa Subgroup, Coromandel Group														
Groundmass	61.5	0.4	18.7	2.9	0.2	1.1	6.5	3.7	2.3	0.2	0.0	0.1	-0.0	0.0	97.6
Orthopyroxene in glomerocryst	53.3	0.3	1.5	16.4	0.4	25.7	1.2	0.1	0.0	-0.1	0.1	0.1	0.1	-0.1	98.9
Orthopyroxene; single, rim	53.3	0.3	1.9	16.9	0.4	25.7	1.4	0.1	0.1	-0.1	0.1	0.1	0.0	-0.2	99.9
Plagioclase; single, core	46.7	-0.0	32.9	0.3	0.0	0.2	17.0	1.6	0.1	-0.1	-0.0	0.0	0.1	-0.1	98.7
Plagioclase; single, rim	45.7	0.1	33.7	0.5	-0.0	0.2	17.6	1.3	0.1	-0.1	0.1	-0.0	-0.0	0.2	99.3
R17866	Whiritoa Andesite, Waiwawa Subgroup, Coromandel Group														
Plagioclase; single, core	56.8	0.0	26.1	0.3	-0.0	0.0	9.1	5.8	0.5	0.1	-0.0	-0.0	0.0	-0.0	98.8
Plagioclase; single, rim	50.0	-0.0	30.3	0.1	-0.0	-0.1	13.7	3.3	0.3	0.0	-0.0	-0.0	-0.0	0.1	97.8
R17861	Waipupu Formation, Waiwawa Subgroup, Coromandel Group														
Plag; core	46.5	0.1	32.9	0.5	0.1	-0.1	17.1	1.6	0.1	-0.1	-0.1	0.1	0.0	-0.0	98.7
Plag; outer rim	50.2	0.0	30.7	0.9	-0.1	0.0	14.9	3.0	0.3	0.0	-0.0	-0.1	0.3	0.0	99.9
AU60071	Sugarloaf Basalt, Mercury Basalts														
Olivine	40.3	-0.1	0.1	15.5	0.3	43.7	0.2	-0.2	0.0	-0.1	0.2	0.0	0.0	0.1	100.1
Orthopyroxene	51.8	0.7	1.4	16.2	0.4	27.8	1.4	-0.1	0.1	0.1	0.1	0.0	0.1	0.1	99.8
Groundmass	52.2	0.5	10.3	12.3	0.3	18.0	4.8	1.4	0.2	0.2	0.1	0.1	0.0	0.1	100.4

Table 4.2 Representative crystal and groundmass composition data. The complete dataset is presented in Online Supplement 2 [Appendic C].

the lowest incompatible element concentrations (e.g. 5 ppm Rb, 67 ppm Zr) among the samples in our dataset. With 12% MgO at Mg# 72 (Mg# = molar Mg/(Mg+Fe²⁺)) it is geochemically comparable to the primitive basalts in the TVZ and the Kermadec Arc (Gamble et al., 1990). It is a porphyritic basalt with c. 20 vol% mm-sized euhedral olivine phenocrysts in a fine-grained to aphanitic groundmass of pyroxene and plagioclase microcrystals. In contrast, low MgO, Ni and Cr concentrations occur in aphyric Mercury Basalts, which may represent melt fractions that were separated from a mafic crystal fraction. Although these aphyric rocks also have variably elevated incompatible element enrichments compared to the Sugarloaf Basalt, there is no unambiguous inverse correlation between incompatible element enrichment and compatible element depletion. This suggests that incompatible element enrichment is not solely a result of the fractionation of a plagioclase + olivine + clinopyroxene assemblage and that open system addition of incompatible elements has also occurred in Mercury Basalts magmas. Consequently, we view the low incompatible trace element concentrations in the Sugarloaf Basalt as the best approximation in the CVZ

of corresponding values in primitive mantle magmas.

4.2.6.2. Coromandel Group

Rocks of the andesitic Coromandel Group suite have Al_2O_3 concentrations between 15 and 19 wt%

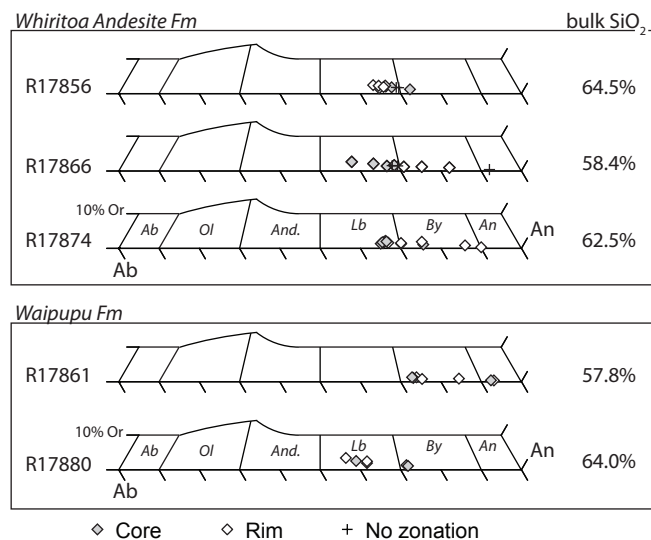


Fig. 4.6 Plagioclase compositions, expressed in terms of the anorthite-albite-orthoclase ternary system, in samples from the Whiritoa Andesite and Waipupu Formation.

that generally decrease with increasing SiO_2 . They typically have <5 wt% MgO, comparable to differentiated Mercury Basalts. They are crystal-rich rocks in which some component of compositional variation must also reflect the fractionation of phenocrysts within lava flows or volcanic conduits. On the plagioclase + clinopyroxene + olivine assemblage test diagram, Coromandel Group rocks define a strongly correlated array ($r = 0.96$) with a slope close to 1, indicating that fractionation of these minerals can largely explain compositional trends (Fig. 4.4A). However, the slope of the array is less than 1 which is consistent with additional fractionation of commonly occurring orthopyroxene. All Coromandel Group rocks have a consistent arc-type trace element distribution (Figs. 4.5B-C). A key feature is that rocks of all formations in this sample set, spanning 13 million years, essentially plot along the same major and trace element array.

Recent studies on the petrogenesis of intermediate arc-type volcanic rocks show that such rocks commonly represent magmatic mixtures of a melt and an entrained crystal cargo composed partly or wholly of remobilized older crystals that did not form from the entraining melt (e.g. Turner et al., 2003; Price et al., 2005). Melt inclusions in andesite-hosted minerals worldwide have a bimodal distribution with peaks at 54% SiO_2 (principally olivine-hosted inclusions) and 76% SiO_2 (principally plagioclase- and

amphibole-hosted inclusions; Reubi and Blundy, 2009). Consequently, the common CVZ andesite compositions correspond to uncommon melt compositions. Coromandel Group andesite mineral associations have features suggesting that at least part of the crystal populations did not form exclusively from the associated melt (Section 4.2.5). Major element analyses of crystal cores and rims also indicate genetic dissociation between parts of crystals and devitrified groundmass composition. Within some Coromandel

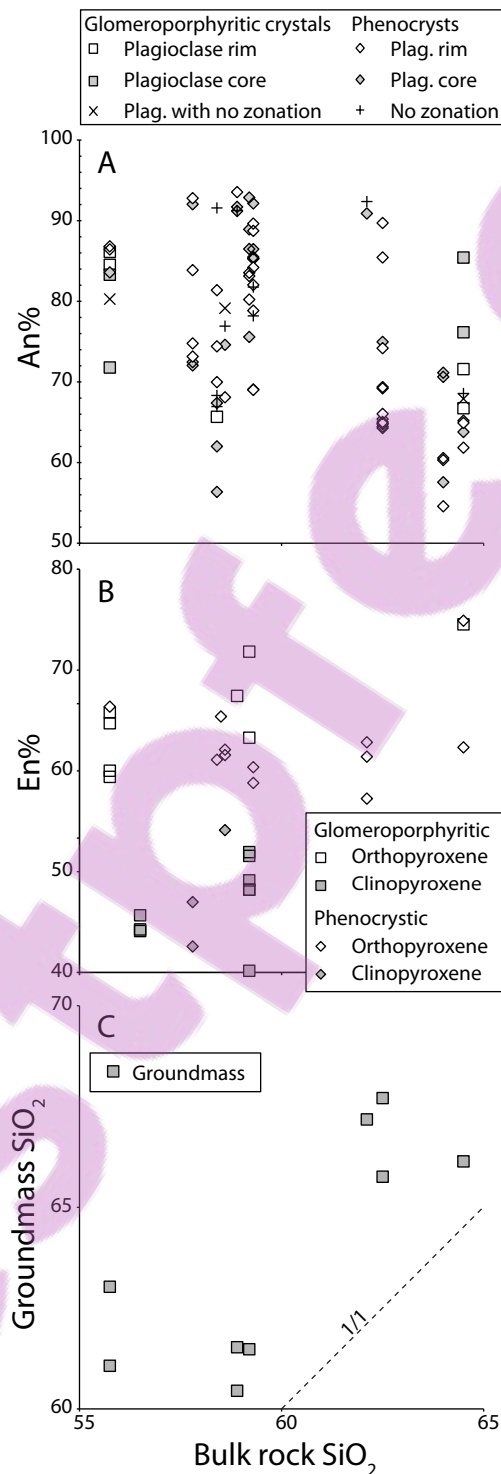


Fig. 4.7 Component compositions vs. bulk rock SiO_2 in Coromandel Group rocks. A. Anorthite concentration in plagioclase. B. Enstatite concentration in pyroxene. C. Groundmass SiO_2 concentration.

Group formations, plagioclase crystals have comparable core compositions in different samples, whereas the compositions of crystal rims differ between samples. For example, plagioclase core compositions in three Whiritoa Andesite samples have comparable, predominantly anorthitic labradorite compositions. The associated rims are slightly more sodic than the cores in one of the samples, which has a dacitic bulk composition (Fig. 4.6). In contrast, they are more calcic (bytownite to anorthite) in two other samples with andesitic bulk compositions. These rocks may contain crystals with cores derived from a common source, but rims formed in equilibrium with different compositions of entraining melt. Secondly, an andesite and dacite of the Waipupu Formation both have some plagioclase crystals with cores of comparable sodic bytownite compositions, but additionally contain plagioclase crystals with different composition cores (Fig. 4.6). The andesite additionally contains plagioclase with anorthitic cores, and the dacite a plagioclase with labradoritic core. The associated rims mostly have similar compositions to the more differentiated crystal cores. We interpret this as a possible example of juxtaposition of crystal cores from different sources entrained in a melt that is unrelated to some or all of the crystal cores.

Crystal compositions in Coromandel Group andesites correlate marginally with bulk rock composition (Fig. 4.7A). Analyzed plagioclase compositions in all rocks range between An_{55} and An_{94} , where andesites as well as dacites contain crystals with compositions that span much or all of the total range. Analyzed orthopyroxene and clinopyroxene compositions do not correlate significantly with bulk rock compositions (Fig. 4.7B). In other words, plagioclase and pyroxene crystals of any composition can occur in Coromandel Group rocks of any composition, consistent with the hypothesis that the crystal content of such rocks is not necessarily related to the entraining melt and can comprise crystals from various sources.

Analysis of groundmass compositions as a proxy for melt composition is commonly hindered in Coromandel Group andesites by a seriate porphyritic texture where angular clastic fragments, possibly derived from larger crystals, litter the groundmass. Where reliable analyses could be obtained, groundmass compositions correlate with bulk rock composition in terms of SiO_2 content (Fig. 4.7C) and other geochemical parameters. This contrasts with the results for crystal compositions and suggests that groundmass/melt compositions more directly control the bulk composition of Coromandel Group rocks. Groundmass compositions range from high-silica andesite to low-silica-rhyolite. Significantly, all analyzed groundmasses have greater SiO_2 concentrations than the associated bulk rock.

The regional scale of this study, and the comparatively poorly constrained internal stratigraphy of the volcanic formations of the CVZ, do not permit a detailed investigation of crystal and melt populations in

terms of a singular magmatic system. Nevertheless, these results suggest that distinct crystal populations existed and were entrained by melts of variable compositions to form the Coromandel Group magmatic suite.

4.2.6.3. *Whitianga Group*

Whitianga Group rhyolites are medium- to high-potassic with 73-79% SiO₂ (Fig. 4.3B) and are mostly peraluminous. The analyzed samples form an array in some major and trace element diagrams. Along this array, Na₂O and K₂O correlate negatively, and SiO₂ concentration and ASI values correlate weakly with K₂O. Trace elements correlate with either K₂O (e.g. Rb, Th, Nb) or Na₂O (e.g. Zr). Major element compositional variation appears to be strongly controlled by feldspar fractionation. On a PER assemblage test diagram for the feldspar species anorthite, albite and orthoclase ((Al-Ca)/Th vs. (Ca+Na+K)/Th, where Th is assumed to be excluded from the mineral assemblage), Whitianga Group rhyolites form an array with slope 1 and correlation coefficient 0.98 (Fig. 4.4B). Assemblage tests featuring combinations of albite + anorthite or albite + orthoclase yield unsatisfactory results, which indicates that fractionation of all three feldspar end member species contributed to rhyolite major element variation. Although orthopyroxene, biotite and hornblende occur in addition to feldspar, fractionation of these minerals may not have significantly affected rhyolite major element variation.

The compositional variation along the rhyolite array correlates with phenocryst mineralogy. We distinguish two end-member rhyolite types: (1) 'pyroxene rhyolites' have an anhydrous plagioclase ± orthopyroxene phenocryst mineral assemblage. These have c. 2.5% K₂O, 73-75% SiO₂, >100 ppm Sr, no significant Eu anomaly ((Eu/Eu*)_N ≈ 1) and ASI values generally between 1 and 1.2. Pyroxene rhyolites form the Rangihau Rhyolite formation (Skinner, 1995) and the Bowentown Rhyolite dome, and correlate with Group I and III rhyolites of Krippner (2000). (2) 'Sanidine rhyolites' have a hydrous sanidine + hornblende + biotite phenocryst assemblage. These have c. 5% K₂O, >77% SiO₂, c. 11 ppm Sr, a pronounced Eu anomaly ((Eu/Eu*)_N << 1) and ASI > 1.1. Sanidine rhyolites form the Ahu Ahu Rhyolite (Skinner, 1976). Geochemically intermediate rhyolites have mixed phenocryst assemblages comprising plagioclase + biotite ± hornblende ± orthopyroxene (+ quartz). Such rhyolites occur as the Ruahine, Purangi and Whenuakite Rhyolites of Skinner (1995), Group II and IV rhyolites of Krippner (2000), and occur in the southern CVZ (Brathwaite and Christie, 1996; Briggs et al., 2005), so have a wider geographic distribution than the end-member types (Fig. 4.1). A comparable compositional spectrum has been identified for TVZ rhyolites (Deering et al., 2008; Deering et al., 2010).

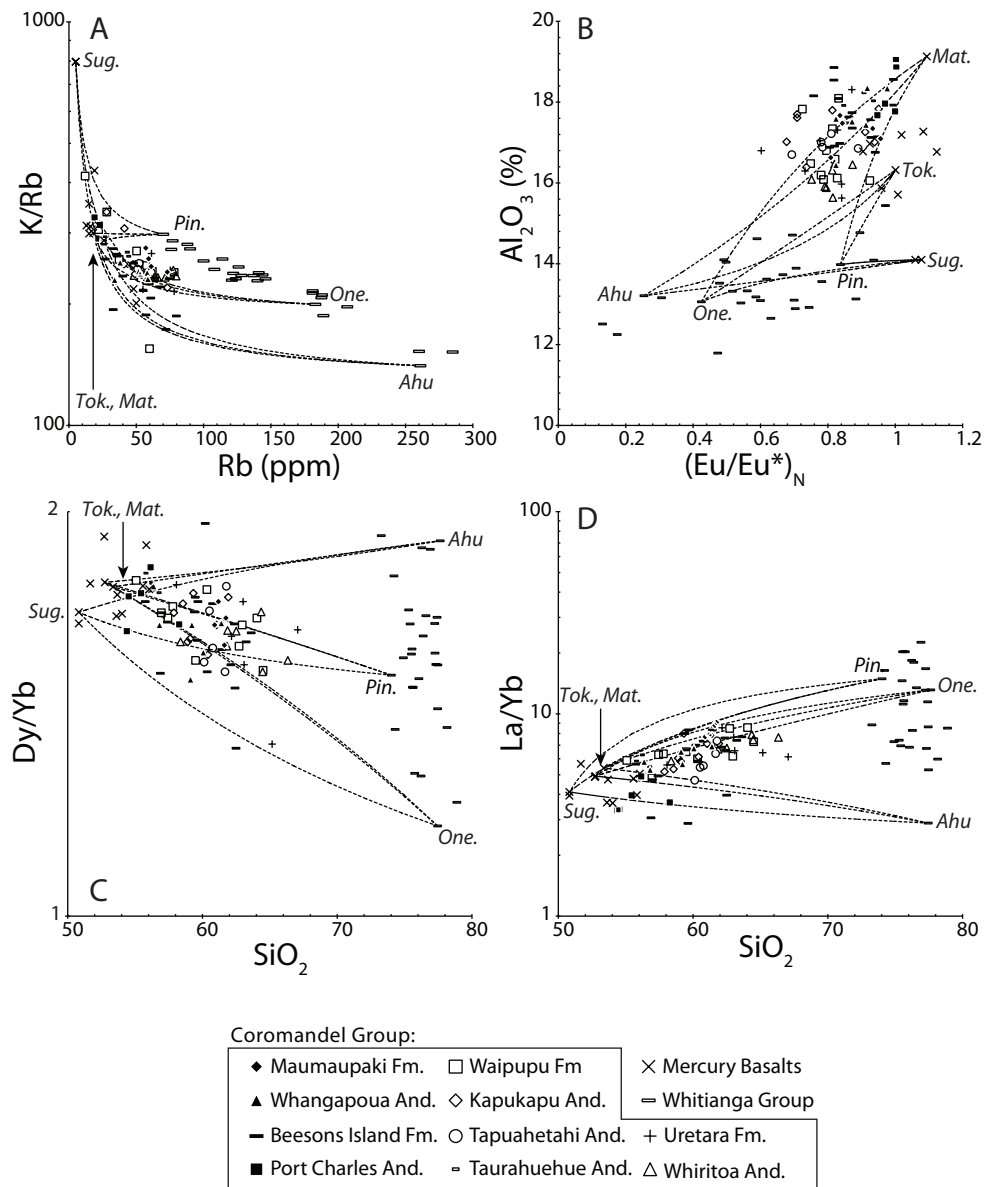


Fig. 4.8 Major and trace element variation diagrams. Dotted lines represent binary mixing curves between Mercury Basalt and Whitianga Group rhyolite compositions. Sug. – Sugarloaf basalt; Tok. – Tokarahu basalt; Mat. – Matakana basalt; Pin. – Pinnacles dome rhyolite representing a least-differentiated, pyroxene rhyolite composition; One. – Onemana dome rhyolite representing an intermediate rhyolite composition; Ahu – Ahu Ahu Rhyolite, representing a differentiated, sanidine rhyolite composition. Value of $(Eu/Eu^*)_N$ represents the magnitude of the europium anomaly in the chondrite-normalized REE distribution, where $Eu^* = \sqrt{(Sm_N \cdot Gd_N)}$. Normalization to the chondrite composition of McDonough and Sun (1995).

4.2.7. Mixing Relationships

The petrographic and crystal-chemical properties of Coromandel Group andesites suggest that these intermediate rocks are mixtures of one or more silicic and mafic components. The evolved component in each sample is presumably primarily represented by the groundmass/melt, which may itself be a mixture. The more primitive component is represented at least in part by the plagioclase + pyroxene ± hornblende crystal cargo, but may also be a component of the groundmass/melt. In the CVZ, primitive (51-56%

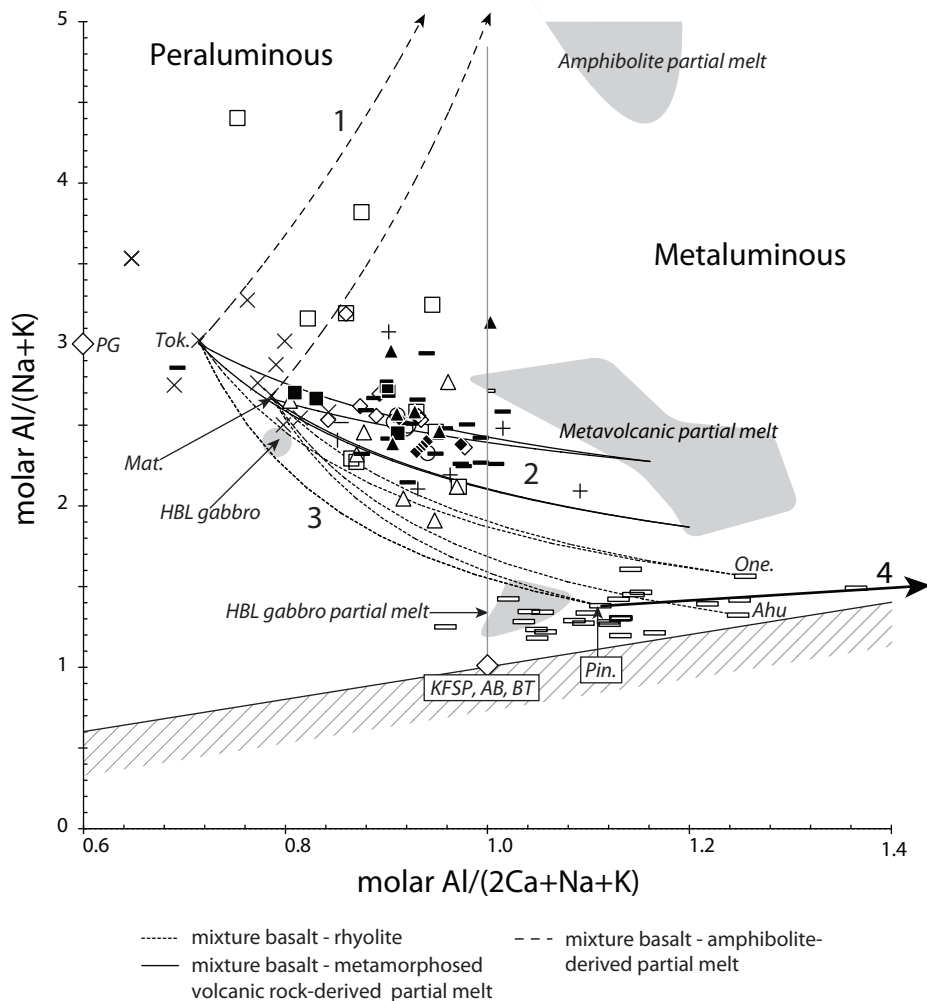


Fig. 4.9 Molar $\text{Al}/(2\text{Ca}+\text{Na}+\text{K})$ vs. $\text{Al}/(\text{Na}+\text{K})$. Shaded fields: experimental and measured compositions as indicated. Hornblende gabbro partial melt derived at 7 kbar and at $f\text{O}_2$ between $\text{NNO}+1$ to $+4$ (Sisson et al., 2005). Metamorphosed volcanic rock partial melts derived at 6.9 kbar and at $f\text{O}_2$ between $\text{NNO}+1$ to $+2$ (Beard and Lofgren, 1991). Amphibolite partial melt derived at 10 kbar and at $f\text{O}_2$ between $\text{NNO}+0.5$ to $+1$ (Wolf and Wyllie, 1994). Diamonds represent ideal mineral compositions: AB – albite; KFSP – orthoclase; BT – biotite; PG – pargasite; HBL – hornblende. Pin. – Pinnacles rhyolite; One. – One-mana dome rhyolite; Ahu – Ahu Ahu rhyolite. Lines: 1 (dashed) – binary mixing between Mercury Basalts and amphibolite partial melts of Wolf and Wyllie (1994); 2 (solid) – binary mixing between Mercury Basalts and metamorphosed volcanic rock partial melts of Beard and Lofgren (1991); 3 (dotted) – binary mixing between Mercury Basalts and Whitianga Group rhyolites; 4 (solid bold arrow) – modeled effect of plagioclase fractionation from a Pinnacles rhyolite composition magma.

SiO_2) and silicic (73-79% SiO_2) magmas erupted in addition to the Coromandel Group andesitic suite. These resemble the most common compositions of melt inclusions in andesite-hosted minerals worldwide (Fig. 4.3; 54% and 76% SiO_2 , respectively; Reubi and Blundy, 2009). It is relevant to investigate whether simple binary mixing of some of the erupted basalts and rhyolites can account for the compositional trends in Coromandel Group andesites. To this end, we derived binary mixing trends between

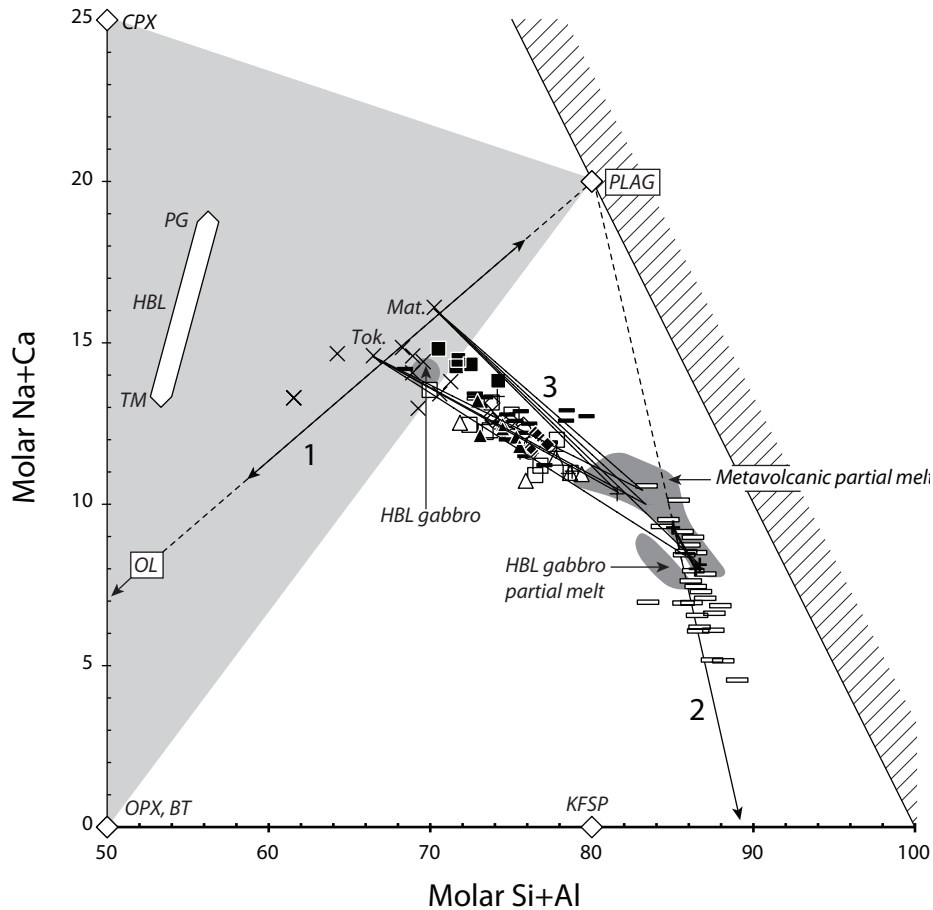


Fig. 4.10 Al+Si vs. Na+Ca expressed as molar percentages of total major element cations. Shaded field: potential compositional range of a plagioclase + pyroxene ± hornblende crystal assemblage. Diamonds represent ideal mineral compositions: BT – biotite; CPX – clinopyroxene; KFSP – K-feldspar; OL – olivine; OPX – orthopyroxene; PLAG – plagioclase; PG – pargasite; TM – tremolite; HBL – hornblende. Lines: 1 – fractionation/accumulation of olivine and plagioclase along their mutual tie line; 2 – modeled effect of plagioclase fractionation from a Pinnacles pyroxene rhyolite composition magma; 3 – binary mixing between Mercury Basalts and metamorphosed volcanic rock partial melts of Beard and Lofgren (1991). Key as in Figure 4.8.

three different Mercury Basalts compositions and three different Whitianga Group rhyolite compositions, chosen to represent the compositional range in basalts and rhyolites in some geochemical variation diagrams (Fig. 4.8).

4.2.7.1. Composition of the Primitive Component

Among the analyzed Mercury Basalts, the sample that most consistently yields mixing lines with rhyolite compositions that overlap with Coromandel Group bulk compositions is the Matakana basalt (Fig. 4.8). This is the most alumina-rich Mercury Basalt analyzed. Less alumina-rich basalts yield mixing lines with rhyolite compositions that overlap marginally or not at all with andesite bulk compositions in

some diagrams. Two possible interpretations for this are: (1) the hypothetical primitive end member component in Coromandel Group andesites represents a plagioclase-accumulative magma like the Matakana basalt. It is possible that such a component is admixed in the groundmass/melt of some Coromandel Group andesites and/or contributed a plagioclase crystal fraction to some andesites; (2) the mafic end member is simply dominated by the plagioclase (+ clinopyroxene + orthopyroxene ± hornblende) crystal assemblage that forms 20-60 vol% of typical Coromandel Group andesites, and the bulk composition of this assemblage broadly resembles the bulk composition of the Matakana basalt.

4.2.7.2. *Composition of the Evolved Component*

There is no clear match with any one specific rhyolite composition as the silicic end member component to mixing. Apparently, no one erupted rhyolite composition is entirely representative of the major and trace element composition of a possible silicic end member component present in the Coromandel Group andesites. This is not surprising given that the erupted rhyolites likely represent snapshot compositions of magmas in shallow chambers (e.g. Lipman, 2007). Additionally, mixtures between any of the analyzed basalts and rhyolites fail to overlap with andesite bulk compositions in a diagram of aluminosity vs. alkalinity (molar Al/(2Ca+Na+K) vs. Al/(Na+K), Fig. 4.9). The trends in Figs. 4.8-4.9 nevertheless suggest some properties of the hypothetical silicic end member to Coromandel Group andesites: (1) It has

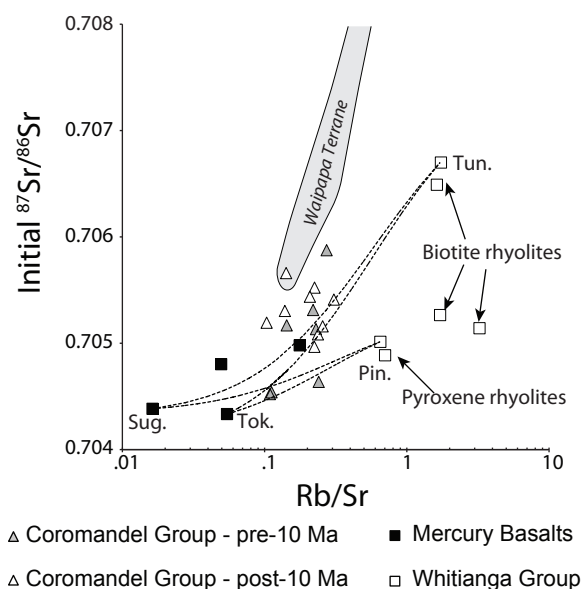


Fig. 4.11 Initial ⁸⁷Sr/⁸⁶Sr vs. Rb/Sr. Data on Waipapa Terrane metasediments from the Motutapu, Hunua and Pokeno localities of Adams and Maas (2004). The Waipapa Terrane ⁸⁷Sr/⁸⁶Sr values have been corrected to the respective values at 10 Ma, using the Rb/Sr ratios in Adams and Maas (2004). Dashed lines: binary mixing line between Mercury Basalt and Whitianga Group rhyolite compositions.

low Al_2O_3 concentration compared to the mafic end member, and $(\text{Eu}^*/\text{Eu})_N$ values smaller than 1; (2) despite its comparatively low Al_2O_3 concentration, it must have a greater molar $\text{Al}/(\text{Na}+\text{K})$ value than any erupted rhyolite; (3) it has fractionated rare earth element ratios (greater La/Yb and lower Dy/Yb) relative to the mafic end member. The fractionated REE ratios (La/Yb , Dy/Yb) suggest the presence of residual amphibole in the source of the silicic component (c.f. Davidson et al., 2007) and fractionated $(\text{Eu}^*/\text{Eu})_N$ values indicate residual plagioclase.

4.2.7.3. *Source of the Evolved Component*

Mineral compositions in a diagram plotting molar $(\text{Al}+\text{Si})/\text{cations}$ vs. $(\text{Ca}+\text{Na})/\text{cations}$ values (Fig. 4.10) show the range in possible bulk compositions for the plagioclase + clinopyroxene + orthopyroxene \pm hornblende crystal assemblages in Coromandel Group andesites. Mercury Basalts bulk compositions plot within this field of possible crystal assemblage compositions, so their bulk compositions can be described in terms of a mixture of the minerals that form the crystal assemblage in Coromandel Group andesites. Bulk andesite compositions, in contrast, predominantly plot outside the field of crystal assemblage composition. They form an array that trends between the bulk compositions of Mercury Basalts and of the least differentiated rhyolites. Of the phenocryst minerals in andesites, pargasitic hornblende plots along the extrapolation of the andesite array to more primitive compositions. Consistent with the inference that the silicic component has fractionated REE ratios, this suggests that amphibole fractionation was a vital process in the generation of the silicic end member composition in Coromandel Group andesites. Experimental partial melt compositions derived in dehydration melting experiments under crustal conditions (7-10 kbar, $f\text{O}_2$ approximately $\text{NNO}+0.5$ to $+4$) on amphibole-phyric source rocks are plotted in Fig. 4.9 and show a wide range in molar $\text{Al}/(\text{Na}+\text{K})$ values. Binary mixing between experimental melts and Mercury Basalts compositions overlap with bulk Coromandel Group andesite compositions for some partial melts derived from greenschist-facies metamorphosed basalts and basaltic andesites (Beard and Lofgren, 1991). The source rocks in that study are compositionally comparable to Mercury Basalts, except that they have low K_2O contents and a more tholeiitic affinity (Beard and Lofgren, 1991). The K_2O content of the partial melt is sensitive to that in the source rock due to its incompatibility in the dominant plagioclase + pyroxene \pm hornblende \pm olivine mineral assemblage. These particular partial melts are not a convincing match with the expected silicic component in Coromandel Group andesites because their K_2O concentrations are too low to explain the medium-K differentiation trend in andesites. However, this comparison shows that partial melts with greater $\text{Al}/(\text{Na}+\text{K})$ values can be derived by dehydration melting

under crustal conditions from rocks with comparable compositions to Mercury Basalts.

Radiogenic isotope ratios of Coromandel Group andesites provide an additional constraint on the origin of the evolved component. Initial values for $^{87}\text{Sr}/^{86}\text{Sr}$ in the analyzed andesites range between 0.7045 and 0.7059, compared to initial $^{87}\text{Sr}/^{86}\text{Sr}$ values between 0.7043 and 0.7050 in Mercury Basalts. The larger values in some andesites are consistent with the presence of some fraction of crustal material in Coromandel Group andesites. At localities close to the CVZ, Adams and Maas (2004) reported whole-rock $^{87}\text{Sr}/^{86}\text{Sr}$ values of 0.7055-0.7077 in Waipapa Terrane metapelite, metasilstone and metagraywacke samples (N=18). Thus, in general the silicic component in Coromandel Group andesites appears to have evolved in an open system with variable input of crust-derived Sr.

4.2.8. Source of Whitianga Group Rhyolites

Whitianga Group rhyolite bulk compositions form an array in many variation diagrams. The mixing relationships with least-differentiated magmas indicate that Whitianga Group rhyolites along this array are distinct from the evolved component in the Coromandel Group andesites. What then is the source of rhyolites in the CVZ, and how do they form the observed compositional spectrum?

4.2.8.1. Rhyolite Differentiation

As noted, major element variation along the rhyolite compositional array appears to be controlled principally by plagioclase feldspar fractionation or accumulation (Figs. 4.4B, 4.10). Additionally, Sr and $(\text{Eu}/\text{Eu}^*)_N$ decrease along the rhyolite compositional array whereas incompatible element concentrations (Rb, Th) increase, consistent with plagioclase fractionation. Plagioclase could exert its control on rhyolite composition either as a residual phase, or as a fractionating phase in rhyolite magmas. Plagioclase commonly occurs as a phenocryst in Whitianga Group rhyolite magmas, where it can have more albitic compositions (Skinner, 1995) than plagioclase in Coromandel Group andesites. Fractionating plagioclase feldspar from a least-differentiated rhyolite composition (Pinnacles pyroxene rhyolite) yields differentiated magmas whose compositions overlap with those of more differentiated rhyolites (Fig. 4.9). Other minerals than plagioclase do not appear to significantly influence major element variation along the rhyolite compositional spectrum either by fractionation or accumulation (Fig. 4.10). In particular, fractionated La/Yb and Dy/Yb values occur in many analyzed rhyolites. The fact that Dy/Yb values are greater in Whitianga Group rhyolites than in less-differentiated rocks of the CVZ suggests a role for amphibole (c.f. Davidson et al., 2007) or another mineral (e.g. apatite) that preferentially incorporates the middle REE.

However, the rhyolite REE ratio values do not correlate significantly with major element variation along the rhyolite array, in contrast to plagioclase-sensitive parameters such as Sr and $(\text{Eu}/\text{Eu}^*)_N$. We interpret this to indicate that these fractionated REE ratios do not reflect the fractionation of minerals from the rhyolite magma. It is possible that they reflect REE fractionation by residual minerals in the source of the rhyolites or that they are inherited from the source rocks. In summary, it appears plausible that the differentiated Whitianga Group rhyolites are derived from least-differentiated rhyolites principally by plagioclase fractionation.

4.2.8.2. *Derivation of Least-Differentiated Rhyolites*

The least-differentiated rhyolites are not compositionally contiguous with the most differentiated dacites of the Coromandel Group. For example, least-differentiated rhyolites have considerably greater SiO_2 contents (~73%) than dacites (<64%), and have molar $\text{Al}/(\text{K}+\text{Na}+\text{Ca})$ values that approximate $\text{Al}/(\text{K}+\text{Na})$, whereas in Coromandel Group dacites $\text{Al}/(\text{K}+\text{Na}) > \text{Al}/(\text{K}+\text{Na}+\text{Ca})$ (Fig. 4.9). Further, the least-differentiated Whitianga Group rhyolites have lower incompatible element concentrations (e.g. Rb) and less-fractionated K/Rb values (Fig. 4.8A) than most-differentiated dacites. The compositional trends in the Coromandel Group suite therefore argue against the formation of Whitianga Group rhyolites by extreme differentiation from Coromandel Group magmas.

Because Whitianga Group rhyolites have low crystal contents (Skinner, 1995; Krippner, 2000), their bulk compositions approximate melt compositions. An excellent compositional match exists between least-differentiated Whitianga Group rhyolites and partial melts derived from hornblende gabbro and hornblende-phyric basaltic andesite in experiments by Sisson et al. (2005). Geochemically, the studied source rocks are sodic high-alumina basalts. They have entirely comparable major element compositions to Mercury Basalts, including c. 1% K_2O . Melt fractions were in the order of 10-25%. Given the similar major element compositions, it is possible that these starting materials are representative of the plutonic equivalent to Mercury Basalts or some Coromandel Group basaltic andesites, which can be assumed to have been hornblende-phyric at pressures within the amphibole stability field (i.e. greater than c. 200 Mpa).

As for Coromandel Group andesites, radiogenic isotope values in Whitianga Group rhyolites can help to constrain the presence or absence of a crustal component. The analyzed rhyolites have initial $^{87}\text{Sr}/^{86}\text{Sr}$ values between 0.7049 and 0.7067. Some samples have initial $^{87}\text{Sr}/^{86}\text{Sr}$ values less than 0.7054, overlapping with initial values in Coromandel Group andesites and some Mercury Basalts. Such comparatively

low values can be inherited from potential igneous, basaltic andesitic or andesitic source rocks to the rhyolites, and require no direct crustal involvement in their formation. Samples in this group include the two analyzed pyroxene rhyolites, as well as two rhyolites with intermediate geochemical compositions. Two other intermediate rhyolite samples have initial $^{87}\text{Sr}/^{86}\text{Sr}$ values greater than 0.7064. These values exceed the greatest observed initial $^{87}\text{Sr}/^{86}\text{Sr}$ values in Coromandel Group andesites and overlap with $^{87}\text{Sr}/^{86}\text{Sr}$ values in Waipapa Terrane metasediments. Such values cannot have been inherited from a purely mantle-derived igneous source and require some crustal involvement, or an entirely crustal source, during rhyolite formation. These results suggest a mixed origin for Whitianga Group rhyolites, where some contain a substantial crustal Sr component and some a much smaller crustal Sr component.

4.2.9. Discussion

4.2.9.1. *Mixed Origins*

The Late Cenozoic volcanic succession in northern New Zealand preserves the record of a constantly evolving continental arc. In this dynamic setting, the eruption of calc-alkaline andesites was a more or less constant factor against the backdrop of a general shift towards a greater proportion of silicic volcanism over time. In the Late Oligocene to Middle Miocene Northland arc, andesitic volcanism co-existed with voluminous basaltic shield volcanism (Smith et al., 1989; Herzer, 1995). In the Middle Miocene to Pleistocene CVZ, early andesitic volcanism was joined from 12 Ma by rhyolitic volcanism and the sporadic small-scale eruption of basalts (Adams et al., 1994; Nicholson et al., 2004). In the Pleistocene to present TVZ, andesitic volcanism at the edges of the zone is subordinate to rhyolitic volcanism in the central TVZ in terms of eruption volume, but extinct, buried andesitic volcanoes nevertheless occur in the entire TVZ (Wilson et al., 1995). Andesite major element compositions in the Northland Arc, the CVZ and the TVZ nevertheless define comparable medium-K differentiation trends (Smith et al., 1989; Graham et al., 1995).

The medium-K andesites of the CVZ have comparable mineralogical and chemical compositions to intermediate volcanic rocks (c. 53-66% SiO_2) globally. A growing body of evidence indicates that such intermediate arc volcanic rocks have bulk compositions that do not represent melts because the crystal content is not directly related to the entraining melt (e.g. Turner et al., 2003; Price et al., 2005). The andesites of the CVZ also show textural and crystal chemical signs of comprising juxtaposed components that represent distinct crystal populations and melt batches. Consequently, we interpret the consistent

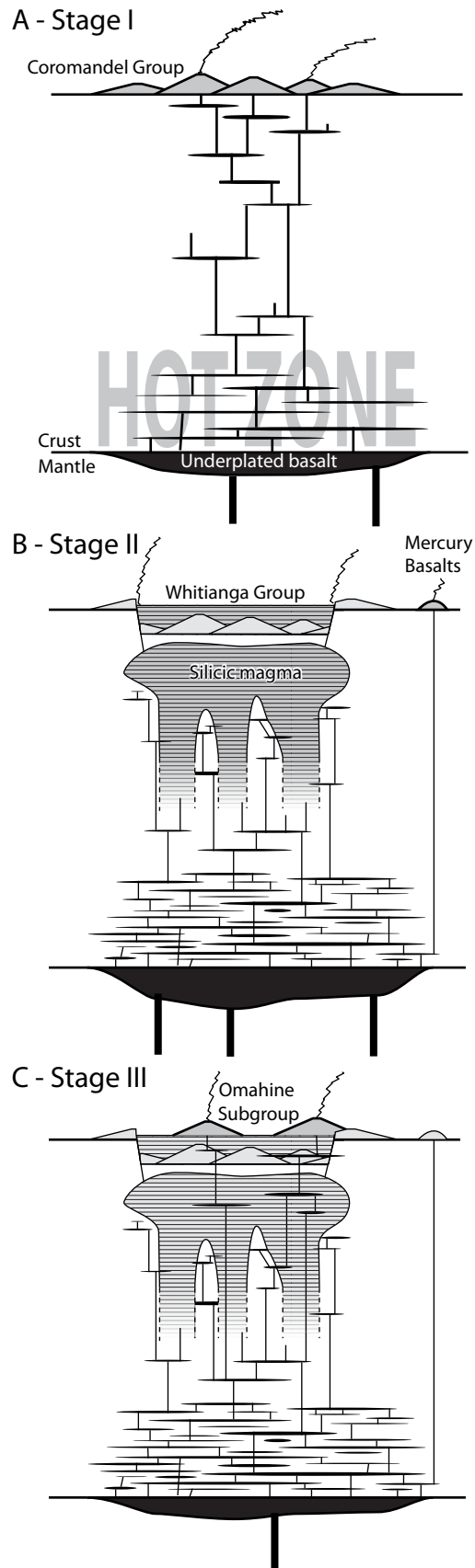


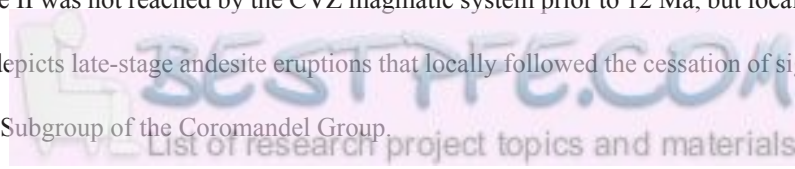
Fig. 4.12 Cartoon model of the CVZ magmatic system. Stage I depicts an andesite-producing magmatic system. A lower crustal hot zone has developed under the influence of mantle-derived basaltic magmas. Partial melting of basement rocks and/or igneous forerunners produces silicic material. Mixing of basaltic magmas, silicic magmas and predominantly basaltic crystal assemblages produces intermediate magmas that can ascend to shallow depth. Eruption of these intermediate magmas

compositions of andesites in the CVZ and the wider North Island succession to represent the leveling effect of mixing processes on the bulk composition of potentially variable magma batches.

Given that they are mixtures, the andesites must comprise one or more mafic and silicic end member compositions. Their porphyritic nature suggests a major role for the entrained crystal assemblage as a mafic end member. As noted in Section 4.2.7.1, the overall crystal assemblage composition in Coromandel Group andesites appears to be effectively constrained to the bulk compositions of the mafic magmas in the system. Based on the differentiation trends in Coromandel Group andesites, the silicic component in the andesites appears to resemble Whitianga Group rhyolite compositions in many respects (Fig. 4.8), however, the silicic component appears to differ from Whitianga Group rhyolites in some ways: (1) it appears to be less silicic, given that the most evolved bulk compositions (c. 68% SiO₂ in one extreme sample) and the most evolved groundmass compositions (66-68% SiO₂) are all significantly less silicic than the least evolved Whitianga Group rhyolite compositions (Fig. 4.3); (2) it is less alkaline, given that Coromandel Group andesite bulk compositions have greater Al/(Na+K) values than projected mixtures between Mercury Basalts and Whitianga Group rhyolites (Fig. 4.9). The silicic component to Coromandel Group andesites therefore does not correspond to any erupted magma. A comparison with experimental partial melts shows that a possibly corresponding silicic melt could be derived by partial melting of amphibole-phyric source rocks similar to, but less silicic than Mercury Basalts and with a more tholeiitic affinity. Such magmas did not erupt in the CVZ but it is tentatively possible that they existed at depth and could not ascend the magmatic system without acquiring calc-alkaline characteristics (e.g. Hora et al., 2009), which would have changed them to Mercury Basalts-like, or more evolved, calc-alkaline compositions.

The least-differentiated Whitianga Group rhyolites are low-phyric and therefore approximate melt compositions. Their bulk compositions overlap with those of experimental partial melts derived from hornblende gabbro, where the source rock is geochemically entirely comparable to Mercury Basalts bulk compositions. The Whitianga Group rhyolites therefore could have formed from rocks that were presum-

formed most of the Coromandel Group. Stage II depicts an evolved magmatic system where ongoing magmatism or increased mafic intrusion into the lower crustal hot zone has induced significant production of silicic material, ultimately leading to silicic volcanic activity. Stage II was not reached by the CVZ magmatic system prior to 12 Ma, but locally Stage I in all cases preceded Stage II. Stage III depicts late-stage andesite eruptions that locally followed the cessation of significant silicic activity and formed the Omahine Subgroup of the Coromandel Group.



ably abundant in the andesitic CVZ magmatic system. Plagioclase fractionation from least-differentiated rhyolites can account for the major element compositions and trace element properties of differentiated rhyolites.

4.2.9.2. *Preferred Model*

The CVZ volcanic system involves a progression from an initial stage of andesitic volcanism to an evolved stage with rhyolitic volcanism. This progression occurred repeatedly in locations progressively farther to the south and east (Adams et al., 1994; Briggs et al., 2005). We propose that the first stage of volcanism occurred over a magmatic system where a lower crustal hot zone had developed, in which andesitic magmas formed by the mixing of evolved, silicic melts or magmas, partly comprising crustal material, and mafic magmas or crystal assemblages with an overall mafic composition (Fig. 4.12). Prior to 12 Ma, magmatic systems in the North Island did not evolve beyond this stage. In a second stage, rhyolitic volcanism occurred and locally overwhelmed andesitic volcanism. It is possible that rhyolite magmas originated by the partial remelting of stalled, basaltic to andesitic precursor magmas, as well as of crustal rocks. This second stage was developed locally after 12 Ma. Late-stage Coromandel Group andesites of the Omahine Subgroup erupted after the cessation of significant rhyolitic volcanism. It is possible that they represent a waning stage of magmatic activity, where significant amounts of rhyolitic magma were no longer produced and magmatism reverted to being dominated by mixed mafic-silicic, i.e. andesitic magmas.

4.2.9.3. *Significance of the Initiation of Rhyolite Eruptions*

Andesitic subduction-related volcanism occurred more or less continuously from the earliest 25.5 Ma eruptions in northern Northland (Hayward et al., 2001) to the present activity in the central North Island. Rhyolitic eruptions, in contrast, occurred from 12 Ma (Carter et al., 2003; Nicholson et al., 2004). It is possible that the 13.5 Myr delay between the first andesitic activity and the inception of silicic eruptions reflects the time required for maturation of the magmatic system to one capable of producing significant volumes of silicic melt. However, the delay is apparently considerably longer than that required in the current SW Pacific setting. For example, volcanoes in the oceanic Kermadec Arc can evolve to erupt silicic magmas within the span of c. 1 Myr (Smith et al., 2006b). In the TVZ, andesitic volcanism locally preceded rhyolitic volcanism in a system that evolved within 2 Myr (Houghton and Wilson, 1995; Wilson et al., 1995). In the southern Rocky Mountains volcanic field, delay times between initial andesitic

volcanism and rhyolitic volcanism were at most 5 Myr, and generally <1 Myr (Lipman, 2007).

As discussed, the least-evolved Whitianga Group rhyolites may represent the partial melting products of the plutonic equivalents to Mercury Basalts. Mercury Basalts appear to also have comparable compositions to the mafic end member to mixing processes that produced Coromandel Group andesites. Given that comparable andesites erupted throughout the North Island succession, the Northland Arc, CVZ and TVZ appear at depth to have been comparable magmatic systems, suggesting that potential source rocks to produce rhyolitic melts occurred in each system. Nevertheless, the pre-12 Ma magmatic systems did not evolve to produce rhyolites. The delayed appearance of rhyolites could be related to factors that inhibited sufficient heating of the early magmatic systems, such that dehydration melting of precursor plutonic rocks could not occur. Possible causes are an insufficient rate of extension imposed on the arc crust prior to 12 Ma, an insufficient rate of magma flux from the mantle prior to 12 Ma, or influence of potential pre-existing regional variation in crustal thickness or composition. We cannot quantify the magma flux rate based on our data. Crustal thickness variation in northern New Zealand appears to be comparatively minor, e.g. varying from 26 km in northern Northland to 29-30 km in the western North Island and CVZ (Horspool et al., 2006; Davey, 2010). On the other hand, in the TVZ a clear relationship exists between extensional tectonics and rhyolitic volcanism. Rhyolitic volcanism is confined to the central TVZ, which is actively rifting (Darby et al., 2000), whereas andesites at the southern tip of the TVZ erupt near the transition to a compressional regime (Stern et al., 2006). By inference, we suggest a role for extension imposed on the arc crust in enabling the advent of silicic volcanism from 12 Ma on. An additional indication for the influence of extension on arc volcanism is the sporadic appearance, also from 12 Ma, of basalts, typically associated with rhyolitic volcanism (Nicholson et al., 2004).

On a regional scale, the 12 Ma instant corresponds to an increase in the displacement rate of the Pacific plate (Atwater and Stock, 1998) suggesting that a global perturbation in plate tectonic movement affected the SW Pacific system. Within the regional SW Pacific setting, extension in response to inferred Pacific plate slab rollback has sequentially produced backarc basins with N-NNE trending spreading axes parallel to the Pacific subduction system (Mortimer et al., 2007; Herzer et al., 2009). Backarc spreading ceased between 15 and 6 Ma (Mortimer et al., 2010) bracketing the inception of rhyolitic volcanism in the CVZ. One tentative possibility is that the cessation of backarc spreading led to the transfer of extensional stress from the backarc to the arc crust, and that this led to the development of rhyolitic volcanism within several Myr.

4.2.10. Conclusions

The volcanic succession of the Coromandel Volcanic Zone records the eruption of a spectrum of arc volcanic rock types. Basalts, andesites and rhyolites are related to each other through partial melting of igneous precursors and crustal rocks, mixing of melts and crystal assemblages, and crystal fractionation processes. We suggest the following broad petrogenetic relationships on the regional scale of the CVZ.

(1) The Mercury Basalts have major element compositions controlled by fractionation and/or accumulation of plagioclase + clinopyroxene + olivine. Their bulk compositions overlap with those of the most frequently occurring mafic melt inclusions in andesite-hosted olivine worldwide. This suggests that Mercury Basalts compositionally resemble actual melt compositions in the CVZ magmatic system.

(2) The porphyritic basaltic andesites, andesites and dacites of the Coromandel Group have bulk compositions that do not correspond to frequently occurring melt inclusion compositions, and have textural and crystal chemical properties that suggest that they comprise mixtures of melts and entrained crystal assemblages. Their bulk compositions define a medium-K differentiation trend that we infer to represent varying degrees of mixing between a mafic and a silicic component. The mafic component in andesites is represented principally by the entrained crystal assemblage and partly by the groundmass/melt. It appears to have a comparable composition to Mercury Basalts. The silicic component in andesites is mainly represented by the groundmass/melt. It is comparable in many respects to Whitianga Group rhyolites but is less alkaline and less silicic than the erupted rhyolites. This component appears to resemble partial melts derived under crustal conditions from amphibole-phyric basaltic or basaltic andesitic rocks with slightly lower K_2O contents than Mercury Basalts. Radiogenic isotope properties suggest that the silicic component at least partly comprises crust-derived Sr.

(3) The Whitianga Group rhyolites have low crystal contents, so their bulk compositions are an approximation of melt compositions. They define a compositional array that reflects fractionation and/or accumulation of plagioclase. The least-differentiated end of this array overlaps in major element composition with experimental partial melts derived from basaltic andesite and hornblende gabbro under crustal conditions. These source rocks have entirely comparable major element compositions to Mercury Basalts, therefore the least-differentiated Whitianga Group rhyolites were plausibly derived by partial remelting of stalled, basaltic or basaltic andesitic precursor rocks. Some Whitianga Group rhyolites have comparable $^{87}Sr/^{86}Sr$ values to Coromandel Group basaltic andesites and andesites and could be derived by remelting of plutonic equivalents. Other rhyolites have more evolved $^{87}Sr/^{86}Sr$ values than Coromandel Group rocks and must additionally comprise a substantial crustal component.

The inception of rhyolitic volcanism and associated sporadic basaltic eruptions at 12 Ma marks a distinct evolution of the North Island arc magmatic system following at least 13.5 Myr of andesitic activity. Given that the potential source rock for rhyolitic partial melts, basaltic andesitic hornblende gabbro, appears to be a common product of an andesite-forming magmatic system, we relate the initial failure to evolve to a rhyolite-producing system to insufficient heating of the arc crust prior to 12 Ma. The combined appearance of rhyolites and dense basalts from 12 Ma suggests that increased extension was a factor in sufficiently heating the arc crust for rhyolite production.

4.3. Volcanic development of the Coromandel Volcanic Zone

Activity of the Coromandel Volcanic Zone spanned ca. 16 Myr. Its lifetime witnessed the cessation of backarc spreading in the South Fiji Basin (Mortimer et al., 2010), the inception of silicic volcanism in the North Island (Carter et al., 2003; Nicholson et al., 2004), and the advent of backarc spreading in the Havre Trough (Ballance et al., 1999; Wysoczanski et al., 2010). One of the principal aims of this project is to document the evolution of the CVZ through time. The preceding sections of this chapter describe the geochemical properties and interrelation of the basalts, andesites and rhyolites of the CVZ. This section specifically describes compositional changes in time.

4.3.1. Coromandel Group Development

Coromandel Group andesites have bulk rock compositions that describe a general calc-alkaline differentiation trend. The dataset obtained in this study is the first comprehensive dataset featuring high-quality trace element data that represents a section through the whole Coromandel Group. A key outcome is that

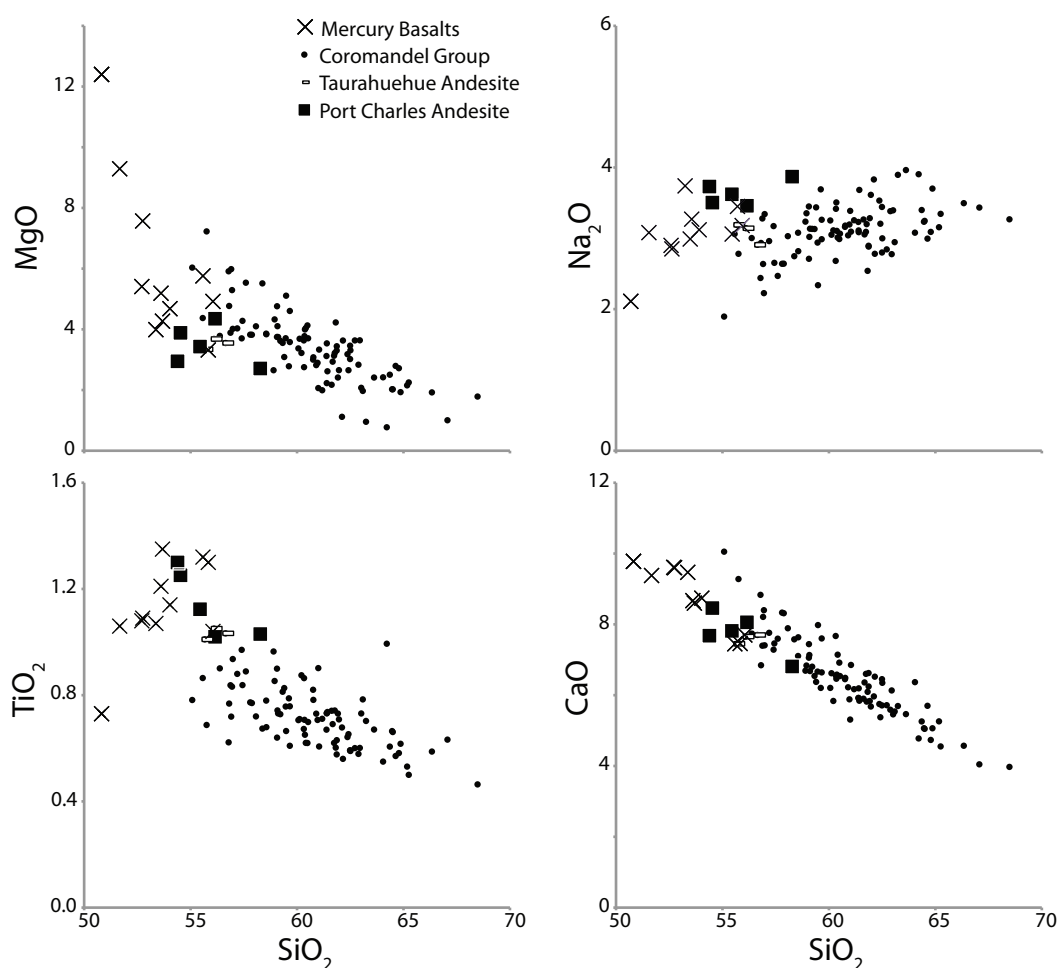


Fig. 4.13 Major element variation diagrams of Coromandel Group and Mercury Basalts rocks. Port Charles Andesite and Taurahuehue Andesite are formations of the Coromandel Group. Based on the dataset presented in Section 4.2.

there are virtually no substantial differences from the calc-alkaline differentiation trend in terms of major and trace element composition between formations of any age (Figs. 4.5, 4.7). This is despite the fact that some formations formed prior to local rhyolitic volcanism and others post-date local rhyolitic volcanism. As well, some andesites erupted with phenocrystic amphibole, particularly pre-10 Ma, and others with only resorbed or absent hornblende. These features largely do not translate into discernible geochemical differences between formations.

Although rocks of most Coromandel Group formations adhere to the same calc-alkaline differentiation trends, rocks of the Port Charles Andesite and of the Taurahuehue Andesite have slightly deviating geochemical properties. Rocks of the Port Charles Andesite and the Taurahuehue Formation show similar geochemical differences from other Coromandel Group andesites (Fig. 4.13). 1) They are characterised by comparatively mafic, basaltic andesitic compositions; 2) they have comparatively high Na₂O and TiO₂ concentrations, and slightly low MgO concentrations, relative to other Coromandel Group andesites. Mercury Basalts likewise have comparatively high Na₂O and TiO₂ compared to Coromandel Group rocks, and although some Mercury Basalts have greater MgO concentrations than Coromandel Group rocks, most have similar MgO values at lower SiO₂. The Port Charles Andesite and Taurahuehue Andesite rocks consequently overlap with, or appear to plot along, the extended Mercury Basalts trend in the MgO-SiO₂ diagram and other major element variation diagrams and have comparable bulk compositions to the more differentiated Mercury Basalts. In the preceding sections, Coromandel Group rocks have been interpreted to comprise a mafic and a silicic component. The mafic component appears to be comparable to the bulk composition of the more differentiated Mercury Basalts. The silicic component generally appears to resemble Whitianga Group rhyolite bulk compositions, but is less alkaline and less silicic. The low SiO₂ contents of the Port Charles Andesite and Taurahuehue Andesite suggest that they contain a relatively small silicic component.

4.3.1.1. *Apparent Age Trend*

The Port Charles and Taurahuehue Andesites occur at the base of the Kuaotunu Subgroup and the Waiwawa Subgroup, respectively (Adams et al., 1994). They may represent the earliest erupted products of the respective magmatic systems. The Port Charles Andesite contains relatively mafic rocks, and was followed by other formations of the Kuaotunu Subgroup that contain rocks with considerably greater SiO₂ contents (Fig. 4.14). As well, rocks of subsequent formations have MgO, TiO₂, Na₂O and CaO concentrations that conform to the differentiation trend defined by the majority of Coromandel Group rocks.

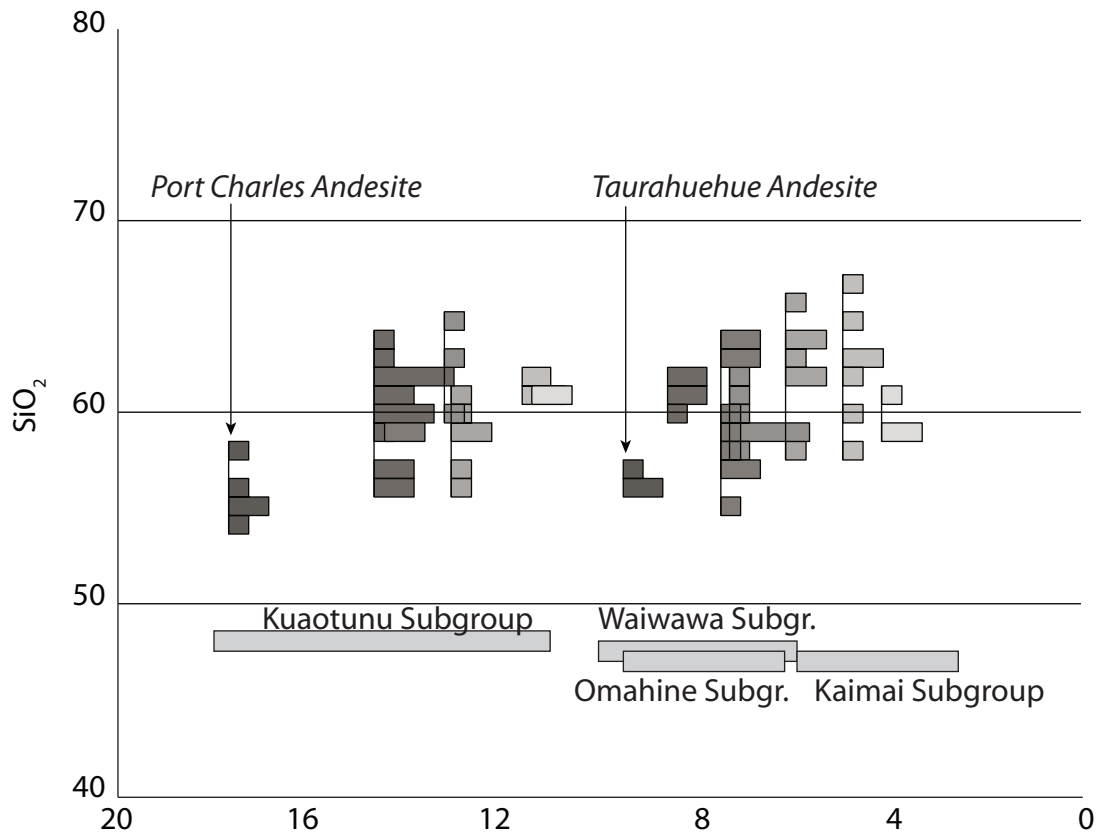


Fig. 4.14 Time vs. bulk rock SiO_2 content in Coromandel Group rocks. Histograms indicate number of samples, in each formation, with given SiO_2 content. Based on the dataset presented in Section 4.2.

Likewise, the Taurahuehue Andesite contains rocks that are relatively mafic, whereas rocks of subsequent formations of the Waiwawa, Omahine and Kaimai subgroups generally have greater SiO_2 contents (Fig. 4.14). The maximum SiO_2 values in rocks of each formation appear to increase with time in the Kuaotunu Subgroup. The same trend appears again in rocks of the younger subgroups.

The number of samples representing each formation is relatively low (generally $N < 10$) and as such the dataset may not be representative of the range in compositions erupted at each center/formation. Nevertheless, the general trend of increasing maximum SiO_2 content with time with the Kuaotunu and younger subgroups is comparable to the trend, commonly observed within Coromandel Group formations, of increasingly silicic erupted rocks from the base to the top of the formation (Skinner, 1986). The trend to greater maximum SiO_2 contents reflects a greater fraction of silicic component. Within each formation, this trend may reflect subvolcanic differentiation processes including fractionation of a gabbroic mineral assemblage from an andesitic magma. On the multi-million year scale of the Coromandel Group subgroups, however, many magmatic systems must have existed to feed individual volcanoes and form the various formations. Apparently, the early magmatic systems within both the Kuaotunu and Waiwawa Subgroups were limited in the extent to which they could produce andesitic magmas, as opposed to ba-

saltic andesitic magmas. The magmatic systems that subsequently developed erupted magmas with andesitic to dacitic compositions. Thus, on the subgroup scale the trend to greater maximum SiO₂ contents may reflect the increasing availability, with time, of silicic melt/magma to interact with mafic magmas or crystal assemblages and form andesitic mixtures. This is plausibly a consequence of thermal maturation of the magmatic system. In a lower crustal 'hot zone' environment, incremental heating by continuing intrusion of and underplating by hot basaltic magma from the mantle increases the availability of silicic partial melts derived from crustal and igneous rocks (Annen et al., 2006).

The eruption of the Taurahuehue Andesite followed a c. 500 kyr hiatus in andesitic activity in the CVZ, at least as recorded by the onland volcanic record (Adams et al., 1994). The renewed activity marked an apparent shift in the locus of volcanism. Kuaotunu Subgroup rocks are mainly preserved NW of a NNE-striking line from Thames to Whitianga, whereas rocks of the Waiwawa and Omahine subgroups occur SE of this line (Fig. 4.1). Given that volcanic rocks in the CVZ are downfaulted towards the south and east along basement-controlled NNE-striking normal faults (Skinner, 1986), it is possible that the apparent age trend reflects differential erosion, where deeper erosion towards the NW has exposed older rocks. However, if substantial post-10 Ma volcanism occurred NW of the Thames-Whitianga line, intrusive rocks of appropriate age might be expected within the older volcanic rocks, yet no such rocks are known (Adams et al., 1994). As well, the ages of alteration minerals in mineral deposits hosted by Kuaotunu Subgroup rocks exceed 10 Ma (Mauk et al., in press), suggesting that no significant hydrothermal activity occurred in Kuaotunu Subgroup rocks following the cessation of Kuaotunu Subgroup volcanism. These features argue against continued magmatism in the area where the Kuaotunu Subgroup formed.

It is less clear whether Kuaotunu Subgroup volcanism also occurred in the area where the Waiwawa Subgroup formed. It is possible that there was significant spatial overlap and that Kuaotunu Subgroup rocks occur at the base of the volcanic stack in the eastern central, and possibly the southern Coromandel. However, they are not known to occur at the surface (Skinner, 1995; Brathwaite and Christie, 1996). If no significant magmatism occurred in the area of post-Kuaotunu Subgroup activity, then the earliest erupted products in this area should hypothetically be relatively mafic. The Mercury Basalt-like compositions of rocks of the Taurahuehue Andesite are in agreement with this. Thus, the inception of Waiwawa Subgroup volcanism can be interpreted as a reset of the development of the CVZ magmatic system, associated with a shift in the locus of magmatism towards the south and east.

4.3.1.2. *Relation to Basaltic and Rhyolitic Volcanism*

The earliest preserved rhyolites and basalts in the CVZ have been dated at 12 Ma (Carter et al., 2003; Nicholson et al., 2004). They occur on Great Barrier Island in spatial association with volcanic and shallow plutonic intermediate rocks of the Coromandel Group (Skinner, 1986). The intrusive rocks, occurring as andesite and quartz-porphyry dikes, have K-Ar ages between 16.3 ± 0.3 and 18.5 ± 0.4 Ma, whereas basaltic andesite flows have K-Ar ages of 12.3 ± 0.4 and 13.8 ± 0.4 Ma (Adams et al., 1994). On Great Barrier Island, the earliest recorded eruption of rhyolites-basalts therefore post-dates the earliest recorded andesitic magmatism by c. 4-6 Ma.

Apart from the Great Barrier occurrence, no record of rhyolitic activity exists in the CVZ from the time of Kuaotunu Subgroup activity. A renewed and widespread pulse of rhyolitic volcanism started about 10 Ma, as recorded by the c. 10 Ma Carina Rock Ignimbrite on the Coromandel Peninsula (Adams et al., 1994) and by a number of rhyolites on Great Barrier Island and on islands to the NW dated at c. 10-8 Ma (Nicholson et al., 2004). Carina Rock Ignimbrite eruption preceded Taurahuehue Andesite eruption. Rhyolitic volcanism on the Coromandel Peninsula developed to form the Whitianga and Kapowai calderas, where rhyolite ignimbrites formed from c. 9 Ma and domes formed from c. 8 Ma (Adams et al., 1994). The accumulation of rhyolite tephra in oceanic drill core occurred at an increasing rate from about 8 Ma (Carter et al., 2003). Basalts erupted from c. 9 Ma in the Coromandel Peninsula (Adams et al., 1994). The proposed reset of the Coromandel Group magmatic system therefore does not unambiguously correlate with rhyolitic volcanism. However, it does precede the increased rate of explosive rhyolitic tephra production, and caldera-forming eruptions Great Barrier Island and the Coromandel Peninsula, by 1-2 Myr. Thus, it appears that a principal difference between Kuaotunu Subgroup volcanism and later Coromandel Group volcanism was that the aggregated magmatic systems that formed the Kuaotunu Subgroup only sporadically evolved to systems capable of erupting silicic magmas. Further, they only did so during the final 2 Myr of Kuaotunu Subgroup activity. In contrast, the aggregate magmatic systems that formed the Waiwawa Subgroup appear to have rapidly (1-2 Myr) evolved to systems capable of erupting rhyolites.

4.3.2. **Mantle Component in Mercury Basalts and Coromandel Group Rocks**

All CVZ volcanic rocks have an arc-type trace element signature (Fig. 4.5) that reflects the subduction-related origin of the mantle magmas that drove volcanism. It is relevant to assess the geochemical features of the least differentiated Mercury Basalts and Coromandel Group rocks that may constrain their mantle heritage. The approach in this section is identical to that applied in Chapter 3 for the least-

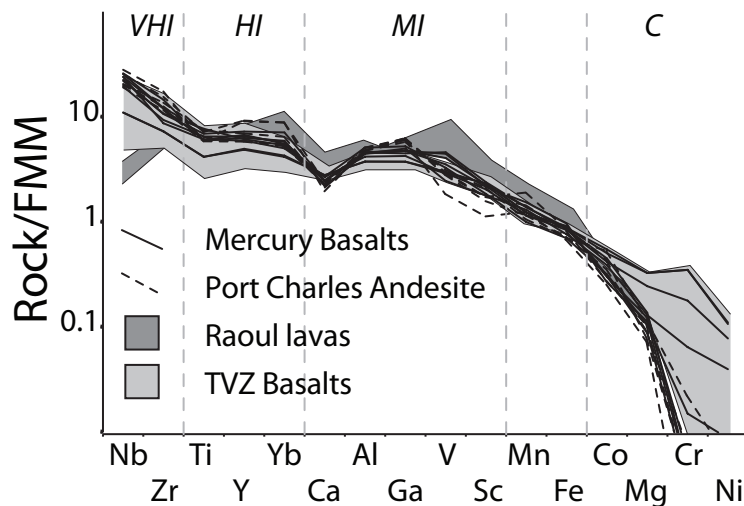


Fig. 4.15 Conservative element distribution in Port Charles Andesite and Mercury Basalts normalised to the fertile MORB mantle (FMM) composition of Pearce and Parkinson (1993). Raoul field from Smith et al. (2009), TVZ basalts from Gamble et al. (1990). VHI – very highly incompatible; HI – highly incompatible; MI – moderately incompatible; C – compatible.

differentiated rocks of the Northland Arc, based on the distribution of elements that are not added to the mantle wedge from the subducted slab (i.e. conservative elements). Additionally, Pb isotope data for some Mercury Basalts and Coromandel Group rocks may also provide a window into the earlier enrichment/depletion history of the mantle.

4.3.2.1. Conservative Element Distributions

The Port Charles Andesite and the Mercury Basalts, representing the least-differentiated rocks that erupted prior to and after the inception of silicic volcanism, respectively, have essentially identical conservative element distributions. These rocks show increasing enrichments with increasing element incompatibility relative to a fertile MORB mantle (4.15). Very highly incompatible elements are enriched relative to highly and moderately incompatible elements, a distribution that is consistent with ca. 25% partial melting of fertile MORB mantle, with no particular indication for previous depletion (Pearce and Parkinson, 1993). Taupo Volcanic Zone basalts (Gamble et al., 1990) have an identical distribution to the least-differentiated CVZ rocks. In contrast, Raoul Island lavas, representative of the oceanic Kermadec Arc, have relatively depleted Nb suggesting that the source mantle experienced low-degree (ca. 2%) partial melt extraction prior to the extraction of arc magmas (Smith et al., 2009; Fig. 4.15). For Raoul this relates to the Havre Trough back-arc basin, where nascent seafloor spreading actively occurs (Wysoczanski et al., 2010). A possible implication is that the CVZ arc segment did not include such a

BEST PAPER.COM
List of research project topics and materials

spreading back-arc basin, consistent with a suggested regional lull in back-arc spreading between 15 and 6 Ma (Mortimer et al., 2010). The similarity to the conservative element signature of TVZ basalts suggests that this is more generally a feature of North Island arc volcanism.

4.3.2.2. Slab-Derived Fractions of Non-Conservative Elements

Slab-fluid mobile (i.e. non-conservative) elements enter the mantle wedge from the subducted slab. The extent to which a non-conservative element in an arc magma is slab-derived can be assessed in a diagram that plots incompatible element ratios X/Z vs. Y/Z , where X is the non-conservative element and Y and Z are conservative elements (Pearce et al., 1995). Nb/Yb is sensitive to fractional melting, melt pooling and mantle enrichment or depletion events, so plotting X/Yb vs. Nb/Yb normalises for these effects. Here, the element ratios La/Yb , Ba/Yb , Pb/Yb and Th/Yb are plotted against Nb/Yb (4.16). Mercury Basalts and Coromandel Group andesites form arrays that are displaced from the MORB array (based on the average MORB composition of Hofmann (1988), indicating the presence of a significant slab-derived component for La, Ba, Pb and Th. Values of Nb/Yb broadly correlate with SiO_2 concentration along these arrays, which is as expected because the bulk partition coefficient for Nb is much smaller than for Yb during differentiation in the crust. Thus, greater Nb/Yb values occur in more differentiated rocks.

For La/Yb , the CVZ rock array trends parallel to the MORB array. The displacement from the

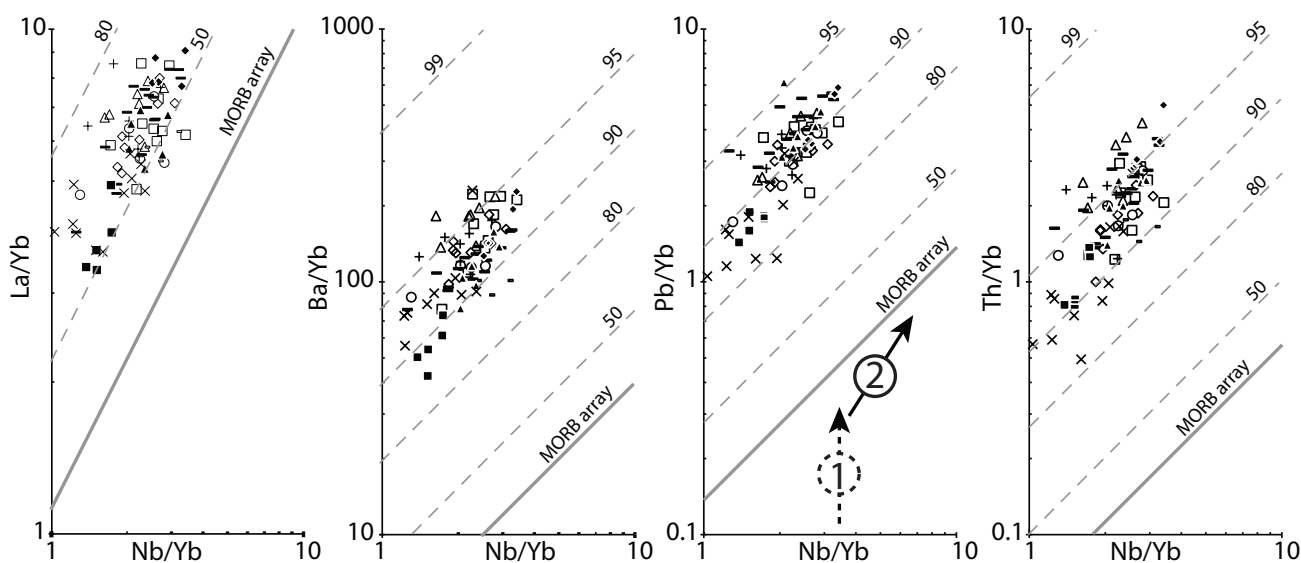


Fig. 4.16 Incompatible element diagrams. Nb and Yb are assumed to be immobile in slab-derived fluids. Slab-derived fractions calculated relative to the average N-MORB composition given by Hofmann (1988). Arrows indicate (1) the addition of slab-derived fraction to the mantle source, and (2) crustal differentiation of the arc magmas. Key as in Fig. 4.8.

MORB array indicates that c. 50% of La in basaltic and andesitic CVZ rocks is slab-derived. The Ba/Yb, Pb/Yb and Th/Yb arrays all trend away from the MORB array with increasing Nb/Yb. This behaviour contrasts with the MORB-parallel trends that are observed in oceanic arc rocks (Pearce et al., 1995). The divergent trends in the CVZ rocks are best explained as a crustal modification feature, due to the greater incompatibility of Ba, Pb and Th relative to Nb during crustal differentiation processes. It follows that only rocks with the lowest Nb/Yb ratios can preserve Ba/Yb, Pb/Yb and Th/Yb values that are indicative of the values in mantle-derived magmas. The displacement upwards from the MORB array, of the rocks with the least enrichment of non-conservative elements, provides a maximum estimate of the non-conservative element's slab-derived fraction.

The smallest Pb/Yb and Th/Yb ratios occur in Mercury Basalts, and suggest that at least c. 80% of Pb and Th in Mercury Basalts is slab-derived. This value for Th is comparable to the slab-derived Th fraction in volcanic rocks in arc rocks globally (Pearce et al., 1995; Green, 2006; Smith et al., 2009). The smallest Ba/Yb ratios occur in Port Charles Andesite, and suggest that approximately 90% of Ba in Port Charles Andesites is slab-derived, whereas Mercury Basalts appear to contain more than 90% slab-derived Ba. As for Th, the apparent minimum slab-derived Ba fraction in CVZ rocks is comparable to that determined for arc rocks worldwide.

For Pb, slab-derived fractions of 95% and greater have been determined in oceanic and continental arc settings worldwide (Pearce et al., 1995; Green, 2006; Smith et al., 2009). The slab-derived Pb fraction in CVZ rocks, at 80-95%, therefore appears to be relatively small relative to that in otherwise comparable arc rocks elsewhere. It is not immediately clear what the significance, if any, is of this variation.

4.3.3. Implications of Pb Isotope Data

4.3.3.1. Motivation

Although slab-derived Pb fractions in CVZ volcanic rocks appear to be lower than in comparable arc rocks elsewhere, most Pb in CVZ rocks nonetheless represents Pb extracted from the subducted slab. As such, the isotopic composition of Pb in CVZ volcanic rocks could potentially distinguish between the subduction of slabs with different ages, specifically, between subduction of Cretaceous Pacific lithosphere and Oligocene South Fiji Basin lithosphere. Age-related features that may affect the Pb isotope composition of the subducted slab are 1) production of radiogenic Pb, and 2) accumulation of continent-derived sediment.

The parent elements Th and U generally act more incompatibly than the daughter element Pb during mantle partial melting. As a consequence, mantle-derived melts will tend to be enriched to some extent in Th and U relative to Pb, compared to the source, and will over time acquire a greater fraction of radiogenic Pb. Due to the same principle, continent-derived sediments can be expected to have a relatively high fraction of radiogenic Pb. Older oceanic crust will generally have acquired a greater amount of sediment, which, if subducted with the rest of the slab, would contribute its Pb to the slab-derived Pb fraction in arc volcanic rocks. It follows that a relatively old, Cretaceous subducted slab (e.g. Pacific plate lithosphere) is expected to lead to relatively large $^{206}\text{Pb}/^{204}\text{Pb}$, $^{207}\text{Pb}/^{204}\text{Pb}$ and $^{208}\text{Pb}/^{204}\text{Pb}$ values in arc volcanic rocks of the North Island succession, whereas a relatively young slab (e.g. Oligocene South Fiji Basin lithosphere) is expected to lead to relatively lower values.

As discussed in Chapter 3, subduction of either Pacific or South Fiji Basin lithosphere has variably

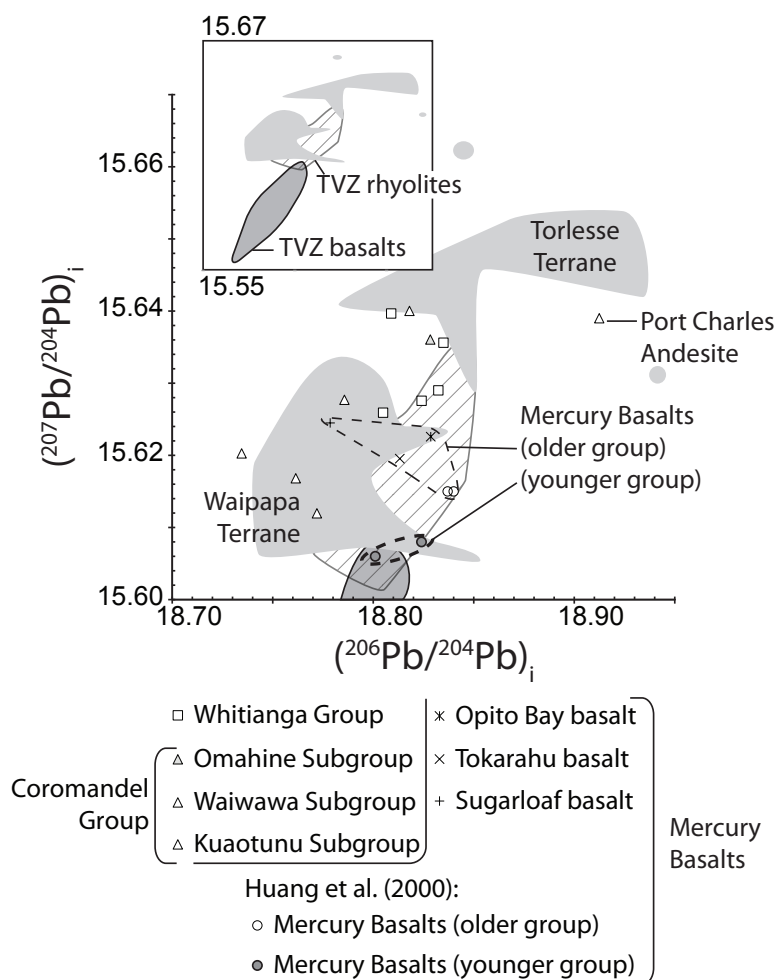


Fig. 4.17 Initial $^{206}\text{Pb}/^{204}\text{Pb}$ vs. $^{207}\text{Pb}/^{204}\text{Pb}$. Initial values were calculated based on published K-Ar ages and measured U/Pb values (Table 4.3). Non-age corrected values for Quaternary TVZ rhyolites and basalts from Graham et al. (1992). Inset: The same diagram, extended down to $^{207}\text{Pb}/^{204}\text{Pb} = 15.55$ to show the full range of Pb isotope values in TVZ basalts. The minimal $^{207}\text{Pb}/^{204}\text{Pb}$ value in TVZ basalts is 15.551 in the Kakuki basalt.

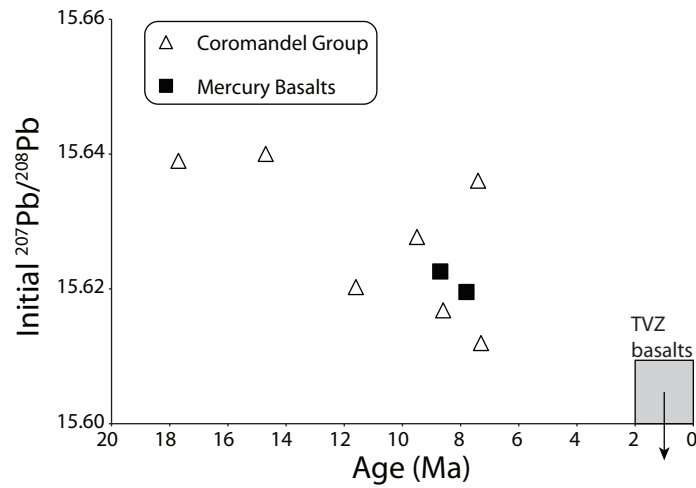


Fig. 4.18 Initial whole-rock Pb isotope compositions vs. age for Coromandel Group and Mercury Basalts rocks. TVZ basalts range from Graham et al. (1992).

been proposed to have been responsible for Northland Arc volcanism (e.g. Herzer, 1995; Whattam et al., 2006). This question is particularly relevant for the history of the CVZ as some classifications (e.g. Hayward et al., 2001) have included the pre-10 Ma volcanism in the CVZ as part of the Northland Arc. The earliest CVZ volcanism overlapped significantly with that in the Northland Arc, where volcanism lasted to c. 15.5 Ma (Hayward et al., 2001), and the CVZ occurs along strike from the centres of the Northland Arc eastern belt (Fig. 3.1). It is therefore possible that a potential Pb isotope signature for subducted South Fiji Basin lithosphere is present in the mafic rocks of the CVZ.

Table 4.3

Sample	Age (Ma)	$^{206}\text{Pb}/^{204}\text{Pb}$		$^{207}\text{Pb}/^{204}\text{Pb}$		$^{208}\text{Pb}/^{204}\text{Pb}$		Initial values	
		2σ	2σ	2σ	2σ	$^{206}\text{Pb}/^{204}\text{Pb}$	$^{207}\text{Pb}/^{204}\text{Pb}$		
R12404 (Beesons Island Volcanics)	14.7	18.841	0.001	15.641	0.001	38.741	0.002	18.818	15.640
R12391 (Port Charles Andesite)	17.7	18.946	0.001	15.641	0.001	38.794	0.002	18.912	15.639
R12415 (Maunaupaki Formation)	11.6	18.759	0.001	15.621	0.001	38.679	0.002	18.735	15.620
R17868 (Whakamoehau Andesite)	6.5	18.841	0.001	15.637	0.001	38.747	0.002	18.828	15.636
R12382 (Tapuaetahi Andesite)	8.6	18.778	0.002	15.618	0.002	38.661	0.004	18.761	15.617
R17864 (Kapukapu Andesite)	7.3	18.786	0.002	15.613	0.002	38.664	0.005	18.772	15.612
R12767 (Taurahuehue Andesite)	9.5	18.803	0.001	15.628	0.001	38.706	0.002	18.786	15.628
NZ6C (Sugarloaf basalt)	8.0	18.785	0.002	15.625	0.002	38.662	0.003	18.779	15.624
BH76 (Tokarahu basalt)	7.8	18.819	0.001	15.620	0.002	38.685	0.003	18.813	15.620
BH35 (Opito Bay basalt)	8.7	18.832	0.001	15.623	0.002	38.719	0.002	18.829	15.623
SP079 (Ahu Ahu rhyolite)	5.3	18.834	0.002	15.636	0.002	38.734	0.005	18.821	15.635
SK1005 (Kapowai rhyolite)	8.0	18.826	0.002	15.640	0.002	38.739	0.004	18.809	15.640
SK995 (Kapowai rhyolite)	8.0	18.848	0.001	15.636	0.002	38.750	0.002	18.835	15.636
SK600 (Kapowai rhyolite)	8.0	18.818	0.001	15.626	0.002	38.703	0.002	18.805	15.626
BF67 (Tunaiti rhyolite)	5.0	18.830	0.002	15.628	0.002	38.706	0.004	18.824	15.628
JR14 (Whitianga rhyolite)	7.7	18.851	0.001	15.630	0.002	38.730	0.002	18.832	15.629

Table 4.3 Pb isotope data.

4.3.3.2. *Sample Selection and Methods*

A 20 sample subset was selected for Pb isotope analyses from the samples that had been used for Sr isotope analysis. Samples were selected to provide an optimal representation of the known geochemical and isotopic variation in the dataset. Lead isotope compositions were measured on a Neptune MC-ICP-MS following techniques described in Elburg et al. (2005) at the mass spectrometry lab of VU University, Amsterdam. Analyses were performed on sample aliquots prepared as described in Section 4.2.4. Each aliquot was weighted to contain c. 100 ng Pb, whereas blank Pb concentrations were in the order of 100 pg and therefore negligible. Within-run analytical errors were negligible compared to the geologic variation in isotope ratios. Initial Pb isotope compositions have been calculated on the basis the elemental U/Pb ratios as determined by ICP-MS, and formation ages from literature, using the following decay constants: ^{235}U : $9.8486 \cdot 10^{-10} \text{ yr}^{-1}$, ^{238}U : $1.55125 \cdot 10^{-10} \text{ yr}^{-1}$ (Jaffey et al., 1971). Results are listed in Table 4.3.

4.3.3.3. *Results*

Lead isotope ratios in the Port Charles Andesite and the Mercury Basalts are comparatively large ($^{207}\text{Pb}/^{204}\text{Pb}$ values of 15.62-3), relative to the values in comparable basalts from the TVZ (Fig. 4.17). The Pb isotope compositions in Port Charles Andesite and Mercury Basalts are, however, comparable to the values in more differentiated Coromandel Group andesites, and in Whitianga Group rhyolites. Additionally, the Pb isotope compositions that were measured for Mercury Basalts by Huang et al. (2000) are likewise large compared to values in TVZ basalts (Fig. 4.17).

Basement rocks of the Waipapa and Torlesse terranes have contrasting Pb isotope compositions, with greater $^{206}\text{Pb}/^{204}\text{Pb}$ and $^{207}\text{Pb}/^{204}\text{Pb}$ values in Torlesse terrane rocks. The Pb isotope compositions of CVZ volcanic rocks partly overlap with those of Waipapa terrane basement rocks. Additionally, some CVZ volcanic rocks have Pb isotope compositions that are intermediate between the fields defined by Waipapa and Torlesse terrane rocks. Coromandel Group andesites and Whitianga Group rhyolites have a larger compositional range than the Mercury Basalts, both to greater and smaller values of $^{206}\text{Pb}/^{204}\text{Pb}$ and $^{207}\text{Pb}/^{204}\text{Pb}$.

The limited Pb data presented here do not point to an unequivocal trend in Pb isotope compositions over time. Nonetheless, the greatest initial $^{206}\text{Pb}/^{204}\text{Pb}$ and $^{207}\text{Pb}/^{204}\text{Pb}$ values, e.g. at c. 15.64 for $^{207}\text{Pb}/^{204}\text{Pb}$, occur in the two oldest analysed CVZ volcanic rock samples, of the Port Charles Andesite and Beesons Island Volcanics formations. Subsequently formed rocks of the Coromandel Group and the

Mercury Basalts have smaller initial $^{206}\text{Pb}/^{204}\text{Pb}$ and $^{207}\text{Pb}/^{204}\text{Pb}$ values that range between c. 15.64 and 15.61 for $^{207}\text{Pb}/^{204}\text{Pb}$. The younger group includes samples from 12 Ma. There is no discernable trend over time within the younger group, however the dataset as a whole, limited as it is, suggests a decrease over time in the average initial $^{206}\text{Pb}/^{204}\text{Pb}$ and $^{207}\text{Pb}/^{204}\text{Pb}$ values in basaltic to andesitic volcanic rocks of the CVZ. Analysed basalts of the TVZ (dataset of Graham et al., 1992)) have lower initial Pb isotope values than any of the analysed CVZ rocks. As such they appear to continue the trend in CVZ volcanic rocks to lower initial Pb isotope values over time.

4.3.3.4. *Discussion*

Ratios of non-conservative to conservative elements in the least differentiated Coromandel Group rocks and in Mercury Basalts indicate that at least c. 80% of the Pb content in these rocks was derived from the subducted slab (Section 4.3.2.2). It follows that the initial whole-rock Pb isotope compositions of those least differentiated rocks approximate the isotope composition of the slab-derived Pb component.

As discussed in Section 4.3.3.1, some workers have raised the possibility that subduction of Oligocene South Fiji Basin lithosphere drove the Early to Middle Miocene volcanism in the Northland Arc, and therefore possibly in the early CVZ. The principal alternative is subduction of Cretaceous Pacific plate lithosphere. Provided that these contrasting options affect the Pb isotope composition of the resulting volcanism, the expected effect is that subduction of young South Fiji Basin lithosphere would be correlated with lower $^{206}\text{Pb}/^{204}\text{Pb}$ and $^{207}\text{Pb}/^{204}\text{Pb}$ values than subduction of old Pacific lithosphere.

The basalts of the TVZ, which unequivocally record magmatism in response to steady subduction of the Pacific plate, provide a baseline for the Pb isotope compositions that correlate with subduction of the Pacific plate. The Pb isotope values in analysed TVZ basalts are significantly smaller than those in the least-differentiated CVZ basalts and andesites (Fig. 4.17). Additionally, the oldest CVZ volcanic rocks have the greatest $^{206}\text{Pb}/^{204}\text{Pb}$ and $^{207}\text{Pb}/^{204}\text{Pb}$ values in the dataset (Fig. 4.18). This is the opposite of what would be expected if the subduction of young South Fiji Basin crust was responsible for the earliest CVZ volcanism. Consequently, it appears more probable that the earliest magmatism in the CVZ occurred in response to the subduction of old Pacific crust.

The above inference does not rule out the involvement of South Fiji Basin lithosphere in Northland Arc volcanism. It is possible that the early volcanism in the CVZ (i.e. 10-18 Ma) occurred entirely in response to a newly established subduction system involving the Pacific plate, but that earlier and partly

contemporaneous volcanism in the Northland Arc occurred over a different subduction system involving South Fiji Basin lithosphere. As discussed in Chapter 3, trace element distributions of Northland Arc volcanic rocks point to a definite subduction-related origin, but do not specifically suggest the subduction of very young crust. Lead isotope data on Northland Arc rocks have not yet been acquired in the course of this study. Collection of Pb isotope data for a suite of least-differentiated Northland Arc volcanic rocks could be a useful tool in determining whether South Fiji Basin lithosphere was or was not involved in Northland Arc volcanism.

If subducted South Fiji Basin lithosphere was not involved in the early CVZ volcanism, the principal alternative is subduction of Pacific plate lithosphere, as is the case in the modern subduction system. This does not imply that all CVZ and TVZ volcanism occurred over the same subduction system; it is possible, for instance, that early volcanism occurred over a SW-oriented subduction system as proposed by Herzer et al. (2009). Given that at least 80% of Pb in the least differentiated CVZ volcanic rocks was derived from the subducted slab (Section 4.3.2.2), it is relevant to consider why the Pb isotope compositions in CVZ volcanic rocks are consistently greater than those in the younger TVZ basalts, if all CVZ and TVZ volcanism occurred in response to subduction of Pacific plate lithosphere. Possible factors include 1) spatial variation in slab Pb isotope composition, 2) variation in the Pb isotope composition of any subducted sediment, 3) variation in the amount of subducted sediment, where the sediment has a contrasting Pb isotope composition to the associated oceanic lithosphere.

The data collected for this study do not resolve between the three options given above. Evidently, it cannot be excluded that spatial variation in Pb isotope signature within the Pacific plate was a factor. However, if subducted sediment played a role, it seems plausible that its Pb isotope signature would have resembled the Pb isotope compositions of the New Zealand basement terranes, these being the probable sources for sedimentary material in the subductions zone(s). Indeed, the Pb isotope compositional ranges for two major basement terranes in the North Island, Waipapa and Torlesse, overlap with and bound the compositional range for the CVZ volcanic rocks. For differentiated rocks, such as Whitianga Group rhyolites, this could reflect the presence of a substantial component of crustal Pb. Rocks of the Waipapa Terrane underlie the CVZ volcanic succession (Black, 1994), and additionally, rocks of other terranes may occur as the boundaries of basement terranes may be complex at depth (Charlier et al., 2010). For least differentiated rocks, however, Pb appears to be predominantly derived from the subducted slab and therefore its isotopic composition must reflect that of the slab. Thus the overlap in Pb isotope compositions between least differentiated CVZ volcanic rocks and North Island basement terrane rocks can be

interpreted to indicate that the volcanic rocks' Pb isotope signature was largely determined by Pb derived from subducted sediments.

Bestpfe.com

Chapter 5. Kiwitahi Chain Volcanism

5.1. Summary

The minimum ages of volcanic rocks in Coromandel Volcanic Zone decrease towards the south and west. A trend of generally decreasing ages towards the SSE also occurs in the Kiwitahi chain of volcanic centres, on the western, continental edge of the CVZ. Unlike the complex volcanic stratigraphy in the CVZ, the Kiwitahi centres erupted in spatial isolation and separated by intervals of 1 Myr or more. Nevertheless, the erupted basaltic andesites and andesites are in part comparable to equivalent rocks in the CVZ. This chapter presents new bulk rock geochemical and isotope data for Kiwitahi volcanic rocks in the form of a paper that has been published in *Journal of Volcanology and Geothermal Research*. The paper documents the development of the Kiwitahi centres, which for the first c. 9 Myr of intermittent eruption had generally comparable compositions to andesites in the CVZ. A notable difference with CVZ andesites, however, is the consistently low enrichment in the highly incompatible elements in Kiwitahi andesites. The youngest Kiwitahi rocks, basaltic andesites erupted between 6.2-5.5 Ma, have markedly different compositions to CVZ andesites and older Kiwitahi andesites, and can be classified as high-Mg andesites. Their trace element distribution is comparable to that of high-Mg andesites in the TVZ. The Kiwitahi chain, and the chain of high-Mg andesite centres in the western TVZ, are interpreted as recording volcanism over the continental edge of the migrating arc magmatic system, the bulk of which at any time was located to the north and east.

5.2. Evolving Volcanism at the Tip of a Propagating Arc: the Earliest High-Mg Andesites in Northern New Zealand

Mathijs A. Booden, Ian E.M. Smith, Jeffrey L. Mauk, Philippa M. Black

Published in *Journal of Volcanology and Geothermal Research* vol. 195, pp. 83-96.

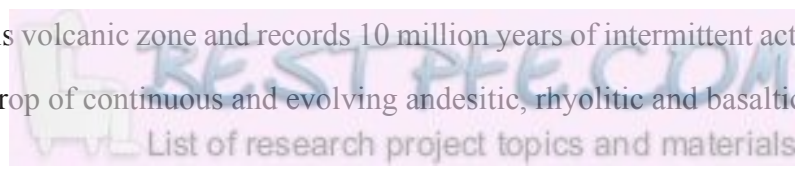
5.2.0.0. Abstract

A NNW-striking string of isolated volcanic centers, the Kiwitahi chain, erupted between 15 and 5.5 Ma in northern New Zealand. Prior to 6.2 Ma, the erupted rocks were plagioclase- and hornblende-dominated andesites, which are geochemically comparable to coeval andesites erupted in the nearby, much larger Coromandel Volcanic Zone (CVZ). Compared to CVZ andesites, however, the Kiwitahi andesites show more subdued incompatible element enrichments, and they generally have relatively unradiogenic Sr isotope compositions. These features, and the small eruption volumes involved, suggest that the Kiwitahi centers formed over the edge of a magmatic system that was centered on the CVZ. The Kiwitahi centers progressively become younger towards the SSE representing the migration over the time of the edge of this magmatic system. Between 6.2 and 5.5 Ma, four centers at the southern end of the chain erupted pyroxene-dominated, high-magnesium andesites that are geochemically unlike coeval andesites in the CVZ, but similar to Quaternary high-Mg andesites erupted along the western edge of the Taupo Volcanic Zone. These are the earliest known high-Mg andesites in northern New Zealand; their appearance may mark the inception of the current configuration where high-Mg andesite eruptions precede regular andesitic volcanism at the leading edge of the arc.

Keywords High-Mg andesite; subduction; volcanism; petrogenesis.

5.2.1. Introduction

The SW Pacific region has had a tumultuous Tertiary tectonic history where the convergence of the Pacific and Australasian plates has given rise to multiple episodes of subduction and back-arc spreading (e.g. Crawford et al., 2003; Schellart et al., 2006; Mortimer et al., 2007; Whattam et al., 2008; Herzer et al., 2009). Tertiary subduction-related volcanism in northern New Zealand has developed in response to dynamic plate configuration readjustments, gradually shifting from Northland to the Taupo Volcanic Zone over the course of 25 million years (Adams et al., 1994; Hayward et al., 2001 and references therein; Briggs et al., 2005). From the Middle Miocene to the Early Pleistocene, the Coromandel Peninsula was the locus of activity (Skinner, 1986), representing what may have been the continental edge of the primarily oceanic Colville Arc (Ballance et al., 1999). A chain of small volcanic centers, the Kiwitahi chain, formed at the edge of this volcanic zone and records 10 million years of intermittent activity (Black et al., 1992) against the backdrop of continuous and evolving andesitic, rhyolitic and basaltic volcanism in the



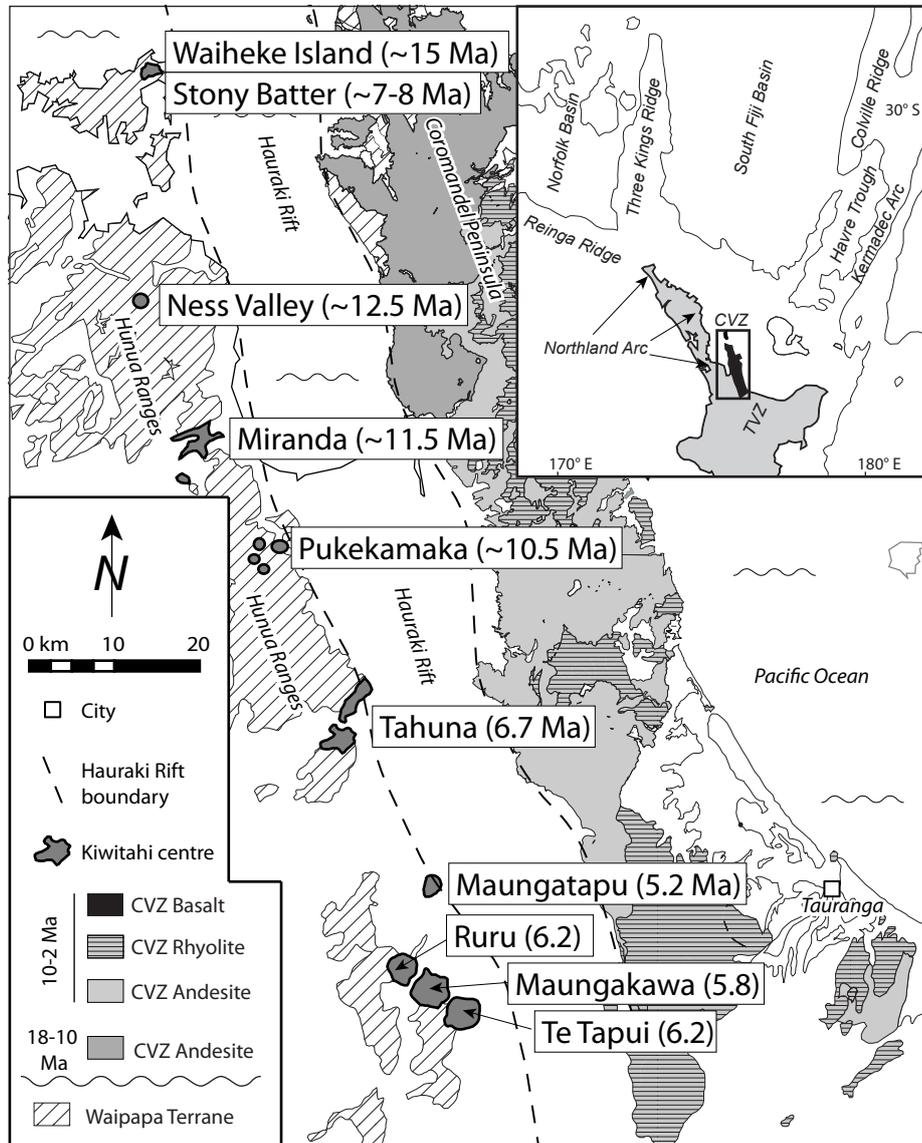


Fig. 5.1 Geologic map of the Hauraki Volcanic Region based on Skinner (1986). CVZ: Coromandel Volcanic Zone. Ages in Ma from Black et al. (1992).

Coromandel Volcanic Zone. The Kiwitahi chain's eruptive products evolved from plagioclase-dominant andesites to clinopyroxene-dominant high-Mg andesites during this time. This paper presents new geochemical and isotope data that document this evolution and we discuss the relationship of the Kiwitahi volcanic chain to coeval volcanism in the Coromandel Volcanic Zone and to the subsequent eruption of high-Mg andesites in the Taupo Volcanic Zone.

5.2.2. Geological Setting

The NNW-striking Kiwitahi Volcanic chain comprises nine volcanic centers that erupted from 15 to 5 Ma (Black et al., 1992). The centers generally become younger towards the SSE. The Kiwitahi chain flanks the western boundary of the NNW-striking, 300 by 20-40 km Hauraki Rift. This is a double half-

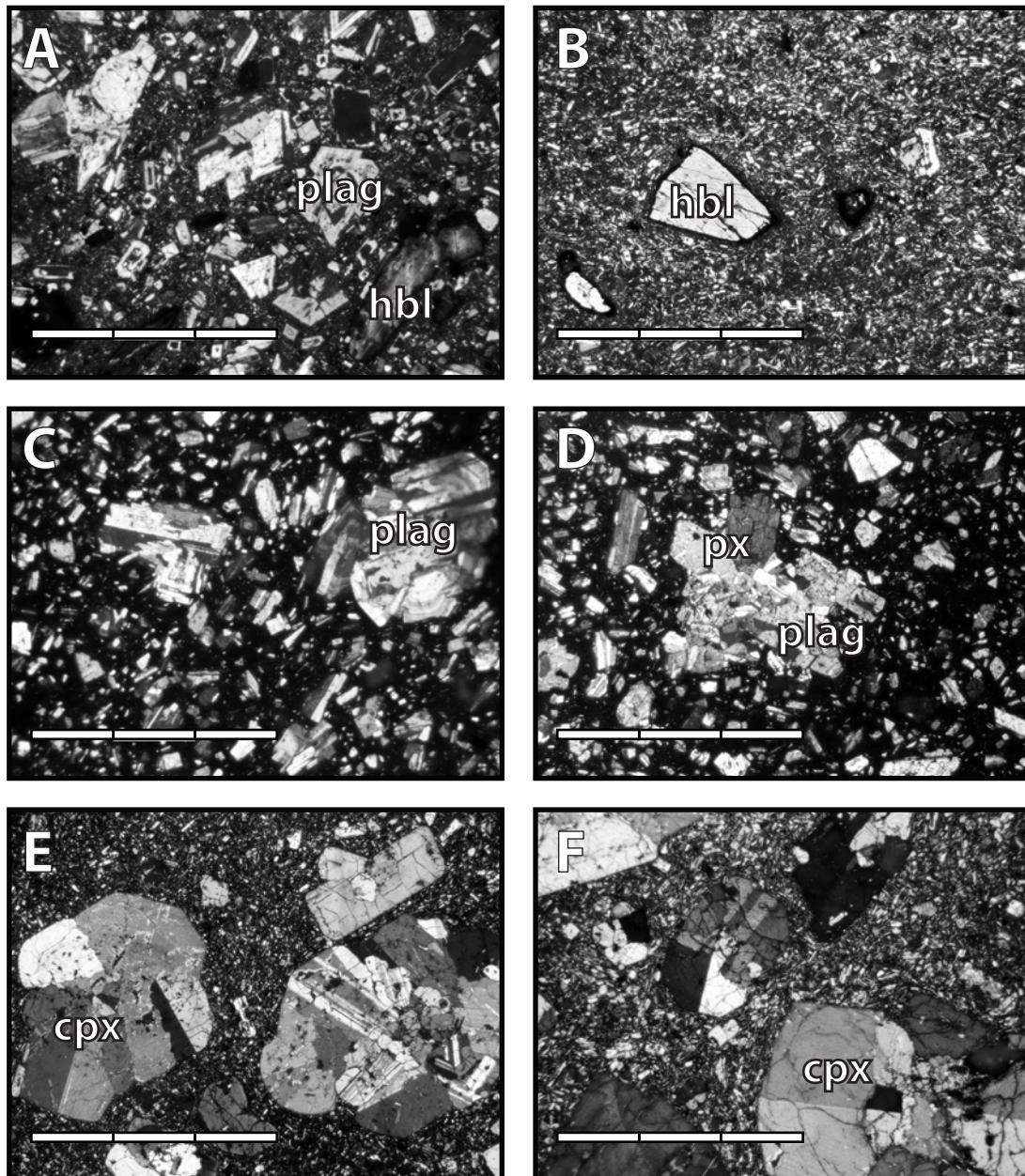


Fig. 5.2 Thin section photomicrographs of representative Kiwitahi volcanic rocks. Scale bars 3 mm. A. AU43909. NE Waiheke Island plagioclase + pyroxene + hornblende andesite. B. AU40682. Pukekamaka hornblende andesite. C. AU40684 Tahuna plagioclase + pyroxene andesite. D. AU40706. Ruru plagioclase + pyroxene basaltic andesite. E. AU42562. Te Tapui clinopyroxene basaltic andesite. F. AU40692. Maungatapu clinopyroxene basaltic andesite.

graben that comprises a western half-graben, which is downthrown 2-3.5 km along the median, normal, west-dipping Kerepehi Fault; a buried median horst; and an eastern fault angle depression along the normal, west-dipping Hauraki Fault. The Hauraki Rift boundary is locally offset along NE-striking faults (Hochstein and Nixon, 1979; Hochstein et al., 1986; de Lange and Lowe, 1990). The Hauraki Rift is probably no older than 7 Ma (Hochstein and Ballance, 1993) and therefore post-dates all but the youngest Kiwitahi centers. Voluminous subduction-related volcanic rocks occur to the east of the Hauraki Rift

as the Coromandel Volcanic Zone (CVZ) and include basalts, andesites and rhyolites (Fig. 5.1; Skinner, 1986). The CVZ was initially (18-12 Ma) dominated by andesitic volcanism. From 12 Ma, silicic eruptions occurred (Carter et al., 2003; Nicholson et al., 2004) that were joined from 9 Ma by sporadic basaltic eruptions (Adams et al., 1994). Locally in the CVZ, the inception of andesitic volcanism preceded the inception of silicic volcanism, and andesitic volcanism generally continued until after the cessation of significant silicic volcanism (Skinner, 1986). An extinct NNE-striking volcanic arc, the Colville Ridge, impinges on New Zealand at the CVZ. The Colville arc was active at least as early as 16.7 Ma (Mortimer et al., 2010) and it is likely that at least part of the CVZ represented the continental tip of this largely oceanic arc, in a similar tectonic configuration to the current Taupo Volcanic Zone-Kermadec Arc system.

5.2.3. The Kiwitahi Volcanic Chain

The Kiwitahi centers erupted through and onto Jurassic greywacke basement rocks of the Waipapa Terrane (Skinner, 1972; Edbrooke, 2001). Lavas, breccias, agglomerates and dykes occur and likely represent the remains of small cone volcanoes or monoeruptive centers. The Kiwitahi centers generally become younger towards the SSE (Black et al., 1992). We view this as analogous to the general SSE migration of the volcanic front in the CVZ (Skinner, 1986). Only the youngest, southernmost centers show preserved volcanic landforms. Because the Kiwitahi eruptions were widely separated in time, it appears likely that the magmas from the different centers were not directly genetically related to each other. We distinguish the following petrologic groups. (1) The four oldest centers (NE Waiheke Island, Ness Valley, Miranda and Pukekamaka (Waiheke-Pukekamaka)) formed between 15 and 10 Ma (following K-Ar ages of Black et al., 1992) characteristically have hornblende. They comprise porphyritic, plagioclase- or hornblende-dominant (+ pyroxene) basaltic andesite, andesite and minor dacite with 15-50 vol% crystal content (Fig. 5.2A-B). Hornblende crystals are typically subhedral rounded and opaque-rimmed, suggesting resorption by the melt, whereas plagioclase and pyroxene typically form euhedral to subhedral, commonly angular crystals. The least-porphyritic rocks (15-20 vol% crystals, Pukekamaka center) have hornblende phenocrysts with only subordinate plagioclase and pyroxene.

(2) The 6.7 Ma Tahuna center erupted plagioclase + pyroxene andesites. Tahuna rocks are petrographically comparable to the andesites of the older centers, but lack hornblende (Fig. 5.2C).

(3) The four youngest centers (Ruru, Te Tapui, Maungakawa and Maungatapu (Ruru-Maungatapu)) erupted between 6.2 and 5.5 Ma at the southern end of the Kiwitahi chain. Ruru, Te Tapui and Maungakawa are small eroded cones aligned along a 305° trend; Maungatapu is another cone located ~10

km further north. The Ruru-Maungatapu centers comprise porphyritic basaltic andesites with typically less than 30% crystals (Fig. 5.2D-F). Plagioclase occurs as a minor phenocryst phase at Ruru, the oldest center, but not in the subsequently formed centers. Angular to sub-rounded, typically eu- to subhedral clinopyroxene is the dominant phenocryst in rocks at each center. Petrographically similar clinopyroxene

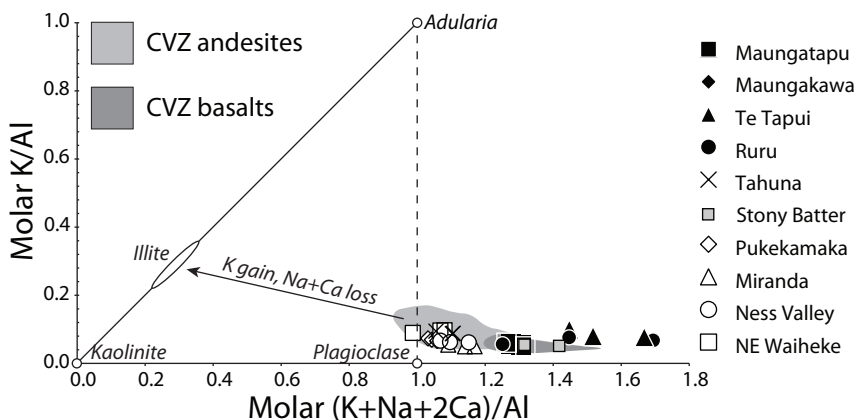


Fig. 5.3 Molar K/Al vs. molar (K+Na+2Ca)/Al (Madeisky, 1996). In this diagram, the alteration minerals kaolinite, illite and adularia plot on a line of slope 1. Unaltered basaltic to andesitic volcanic rocks typically have molar (K+Na+2Ca)/Al values > 1. Potassium metasomatism leads to decreasing molar (K+Na+2Ca)/Al and increasing molar K/Al values, which is not observed for any of the Kiwitahi rocks.

crystals also occur with Fe-Ti oxides in glomeroporphyritic aggregates, usually without plagioclase. Subordinate olivine occurs in some samples. Groundmasses comprise fine-grained plagioclase + pyroxene + Fe-Ti oxides. The dominance of pyroxene and the near-absence of phenocrystic plagioclase sets these rocks apart from the plagioclase-dominant andesites that erupted in the same timeframe to the NNE in the CVZ, and from the Waiheke-Pukekamaka and Tahuna centers.

In addition to the centers described above, basaltic andesites of the Stony Batter center erupted between 6.9-8.3 Ma on Waiheke Island in close spatial association with the much older NE Waiheke center (Kuschel, 1988; Black et al., 1992). The Stony Batter rocks are porphyritic olivine ± clinopyroxene basaltic andesites with plagioclase in the groundmass (Smith et al., 1993). Their eruption at the northern end of the Kiwitahi chain does not conform to the south-directed younging trend defined by the other centers. Petrographically and chemically they are similar to 8.4-10 Ma basaltic andesites of the Ti Point center in Northland, and with those have been interpreted as the product of backarc magmatism associated with the CVZ (Smith et al., 1993; Smith et al., 1995).

Table 5.1 (following pages). Major (wt%) and trace (ppm) element geochemistry and Sr-Pb isotope properties of Kiwitahi volcanic rocks. Initial isotope values calculated as described in Figure 5.10 caption.

Table 5.1	NE Waiheke			Ness Valley			Miranda			Pukekamaka				Tahuna	
AU#	43909	43906	43904	40672	40674	40673	40676	40703	40702	40681	40682	40680	40683	40685	40684
SiO ₂	60.93	61.17	61.19	55.81	58.51	58.60	55.98	56.26	57.81	59.89	60.15	60.32	60.57	58.98	59.14
TiO ₂	0.79	0.71	0.71	0.97	0.77	0.84	0.77	0.77	0.73	0.57	0.59	0.57	0.58	0.77	0.77
Al ₂ O ₃	18.09	17.32	17.40	17.95	17.76	16.89	17.81	18.06	18.32	18.87	18.41	18.80	18.20	17.71	17.78
FeO	4.79	4.62	4.61	6.83	6.01	6.50	6.52	6.33	5.49	4.75	4.74	4.73	4.64	5.22	5.05
Fe ₂ O ₃	1.68	1.62	1.61	2.05	2.10	2.27	1.95	1.90	1.92	1.66	1.66	1.65	1.62	1.83	1.77
MnO	0.09	0.08	0.08	0.17	0.13	0.16	0.18	0.14	0.13	0.14	0.12	0.14	0.12	0.12	0.12
MgO	2.48	2.84	2.83	3.89	3.03	3.82	4.49	4.36	3.72	2.07	2.40	1.92	2.87	3.48	3.44
CaO	5.67	6.09	6.07	7.88	6.93	6.52	8.14	8.00	7.57	7.30	6.90	7.08	6.66	7.16	7.15
Na ₂ O	3.61	3.62	3.57	3.18	3.51	3.08	3.11	3.12	3.17	3.31	3.39	3.30	3.25	3.04	3.09
K ₂ O	1.50	1.56	1.55	1.02	1.02	1.04	0.83	0.84	0.93	1.15	1.35	1.20	1.24	1.45	1.43
P ₂ O ₅	0.23	0.23	0.22	0.15	0.13	0.15	0.13	0.13	0.12	0.17	0.16	0.17	0.15	0.14	0.14
Phenocryst minerals	Pl px hbl	Pl px hbl	Pl px hbl	Pl px	Pl px hbl	Pl px hbl	Pl px	Pl px hbl	Pl px hbl	Hbl	Hbl	Hbl	Hbl pl	Pl px	Pl px
Sc	17	15.1	23.2	27.3	20.4	24.1	22.2	26.4	23	10.2	14.3	10.8	14.6	24.6	24.2
V	135	116	173	211	167	175	180	176	179	124	142	124	139	167	166
Cr	10	16	17	17	13	33	88	85	6	b.d.	6	b.d.	12	26	24
Co	22.6	28.9	38.2	41.6	28.2	26.6	29.2	24.3	32.4	20.6	22.2	27.6	19.3	32	29.5
Ni	15.1	13.2	13.5	6.4	17.7	12.4	25.2	21.6	7.1	2.2	5	2.4	5.7	11.5	11.1
Cu	16.7	18.9	37	26.7	50.1	40.6	32.1	42.7	28.8	30.4	35.5	32.5	28.4	15.6	16
Zn	105	72	98	91	112	81	76	76	75	74	76	74	68	81	82
Ga	24	21	21	23	23	23	21	23	22	25	25	24	25	21	22
Rb	44	53	51	31	33	34	24	26	30	39	40	37	34	48	47
Sr	334	395	251	228	218	244	228	232	209	466	413	453	365	256	257
Y	32.7	17.6	39.3	25.3	22.3	25.1	20.4	18.8	18.7	17.8	23.9	13.3	14.2	17.8	25.6
Zr	138	137	135	109	108	111	90	89	94	113	108	110	101	116	117
Nb	12	11.6	6.4	4	3.4	4.4	4.1	4.1	4	3.6	3.5	3.5	3.3	5.6	5.5
Cs	0.89	2.72	1.61	0.49	0.59	0.83	0.51	0.71	0.6	1.61	0.69	1.89	1.08	2.25	2.1
Ba	474	543	555	191	173	208	154	151	140	257	291	272	245	287	321
La	34.8	33.2	35.5	11.1	11.1	12.9	8.5	8	9.3	15.1	15.3	11	11.3	12.5	13.6
Ce	58	52.1	73.9	24.5	23.5	27.3	18.3	17.1	17.9	28.2	26.4	21.7	22.2	26.4	27.1
Pr	6.9	6	9.2	3.3	3.1	3.6	2.5	2	2	3.9	3.9	2.9	2.5	2.9	3.1
Nd	28.2	23.1	39.3	14.8	13.4	15.4	11.2	9.6	9.5	15.8	15.6	11.7	10.9	12.8	13.6
Sm	5.3	4.3	8.8	3.6	3.1	3.6	2.8	2.3	2.3	3.2	3.3	2.4	2.3	2.9	3.1
Eu	1.8	1.2	2.6	1	0.8	0.9	0.8	0.9	0.8	0.8	0.8	0.6	0.7	0.9	0.9
Gd	7	4.6	9.8	3.4	2.9	3.4	2.8	3.1	3.1	3	3.2	2	2.6	3.2	3.6
Tb	1.1	0.7	1.6	0.6	0.6	0.6	0.5	0.6	0.6	0.5	0.5	0.3	0.4	0.6	0.6
Dy	6.1	3.5	9	4.8	4.1	4.4	3.8	3.4	3.5	3.3	4	2.5	2.5	3.3	3.9
Ho	1.4	0.7	1.9	1	0.8	0.9	0.8	0.8	0.8	0.7	0.8	0.5	0.6	0.7	0.9
Er	3.7	2	5.1	3	2.6	2.8	2.4	2.1	2.2	2.1	2.6	1.6	1.6	2.1	2.5
Tm	0.5	0.3	0.7	0.4	0.3	0.4	0.3	0.3	0.3	0.3	0.4	0.2	0.2	0.3	0.4
Yb	3.2	1.8	5.3	2.8	2.4	2.7	2.3	2	2.2	2	2.7	1.6	1.6	2	2.3
Lu	0.5	0.3	0.8	0.4	0.3	0.3	0.3	0.3	0.3	0.3	0.3	0.2	0.3	0.3	0.4
Hf	3.6	3.3	4.4	3.4	3	3.4	2.6	2.6	2.5	3.4	2.9	3.2	2.6	3.7	3.7
Ta	0.65	0.67	0.48	0.47	0.31	0.37	0.39	0.26	0.3	0.39	0.37	0.42	0.31	0.77	0.71
Pb	9.9	12	10.5	3.8	4.9	5.8	3.9	3.2	4.6	7.1	7	7.7	5.9	8.1	8.1
Th	7.1	7.7	5.4	2.6	2	3.3	1.4	1.8	1.5	2.8	2.9	3.1	2.6	3.7	3.3
U	1.9	1.7	1.4	0.6	0.6	0.9	0.4	0.5	0.4	0.7	0.7	0.8	0.6	0.8	0.8

Table 5.1 (ct'd)	Tahuna	Ruru			Te Tapui			Maungakawa			Maungatapu		Stony Batter	
AU#	40704	40706	40707	40708	42562	40712	40713	40692	40711	40710	42559	40686	42563	42564
SiO ₂	60.03	53.50	53.82	56.50	55.69	56.34	57.19	55.54	55.54	57.51	55.13	55.42	52.83	53.98
TiO ₂	0.75	0.68	0.79	0.65	0.56	0.57	0.61	0.62	0.62	0.59	0.72	0.72	1.08	1.24
Al ₂ O ₃	17.59	13.92	17.12	15.71	13.16	13.56	14.24	14.18	14.28	14.47	16.38	16.34	15.73	17.32
FeO	5.14	7.17	7.56	6.35	6.95	6.82	6.71	7.17	7.12	6.54	6.90	6.94	6.77	6.54
Fe ₂ O ₃	1.80	2.15	2.27	1.90	2.09	2.05	2.35	2.15	2.14	2.29	2.07	2.08	2.03	1.96
MnO	0.11	0.15	0.17	0.12	0.15	0.14	0.13	0.15	0.13	0.13	0.14	0.17	0.15	0.14
MgO	3.21	8.67	5.65	5.32	8.48	8.34	6.42	7.22	7.15	6.12	6.11	6.02	8.25	5.30
CaO	6.66	10.53	8.93	9.52	9.61	8.76	8.43	9.36	9.48	8.26	9.00	8.69	9.35	9.12
Na ₂ O	2.91	2.13	2.56	2.57	2.11	2.16	2.35	2.36	2.31	2.49	2.51	2.49	2.73	3.20
K ₂ O	1.54	0.87	0.89	1.11	0.94	1.00	1.31	1.00	0.96	1.32	0.80	0.88	0.75	0.87
P ₂ O ₅	0.13	0.09	0.11	0.11	0.09	0.09	0.10	0.09	0.08	0.10	0.11	0.11	0.17	0.21
Phenocryst minerals	Pl px	Pl px ol	Plag px	Plag px	Px	Px	Px	Px	Px	Px	Px	Px	Ol+px	Ol+px
Sc	23.2	46	32.7	30.9	39.4	40.2	37.2	37.2	40.7	37.2	33.3	34	33	31
V	154	236	237	190	206	206	217	204	218	213	209	210	218	239
Cr	24	344	67	124	361	365	148	221	212	138	90	83	391	67
Co	34.9	53	40.4	27.8	47.1	50.2	39.5	50.4	44.7	35.2	42.9	44.2	47.2	45.4
Ni	13.7	62.8	19.7	17.7	67.3	66.4	28	40.6	29.9	24.5	26.9	26.9	100.5	20.2
Cu	17	78.4	89.3	24.7	261	189.5	76.5	128	47.1	44.6	68.7	67.4	73.4	52.7
Zn	78	72	60	47	87	68	67	73	79	63	73	237	82	78
Ga	22	21	22	23	19	20	22	20	20	21	23	20	21	26
Rb	52	13	11	13	18	24	18	14	13	20	16	20	15	18
Sr	246	372	376	449	378	399	532	497	483	562	372	370	308	376
Y	17.8	22	84	30.7	151	29	53.8	26.9	97	177	106.5	115	68	23
Zr	121	75	84	79	71	73	76	72	72	84	76	79	110	130
Nb	5.5	2	2.1	2.1	2.1	2.4	1.6	1.7	1.6	2	2.4	2.5	5.0	5.9
Cs	2.37	0.81	0.21	0.4	0.93	1.38	0.72	0.38	0.98	0.66	0.39	0.53	0.30	0.29
Ba	303	142	195	170	168	237	271	159	135	229	162	191	183	203
La	13.3	11.3	16.5	12.8	95.7	28.2	45.1	17.3	154	94.4	56.2	50.4	19.4	12.9
Ce	28.2	19.4	20.8	17.6	57.9	25.9	38.6	19.7	27.3	40.9	25	62	24	28
Pr	3.1	2.3	3	2.3	27.3	6.1	10.4	3.7	42.3	18.1	9.4	15.3	3.8	3.4
Nd	13.4	10.7	14.6	10.4	133	25.5	46.3	16.6	158.5	82.5	40.3	83.5	17.7	15.4
Sm	2.9	2.4	3.2	2.3	35.6	5.3	10.2	3.5	31.3	18.4	8	24.7	4.0	3.6
Eu	0.9	0.9	1.4	0.8	10	1.6	3.2	1.2	7.6	7.2	2.6	9.4	1.6	1.2
Gd	3.3	3.2	6	2.9	37.8	6.2	10.9	4.3	30.4	26.2	11.8	28.1	6.1	4.3
Tb	0.6	0.6	0.9	0.5	6.2	1	1.7	0.7	4.3	4	1.9	4.6	1.1	0.7
Dy	3.4	3.5	6	3	38.2	5.6	9.5	4.4	22.8	26.3	12.9	28.3	8.0	4.5
Ho	0.7	0.8	1.6	0.7	8.6	1.2	2.1	1	4.7	6.6	3.3	6.3	2.1	1.0
Er	2.1	2.3	4.5	2	22.4	3.3	5.5	2.9	12.7	17.8	9.2	15.7	6.1	2.7
Tm	0.3	0.3	0.5	0.3	3.3	0.4	0.7	0.4	1.7	2.4	1.3	2.3	0.8	0.4
Yb	2	2.2	2.8	1.8	25.2	3	4.9	2.9	11.7	15	7.9	16.3	4.6	2.4
Lu	0.3	0.3	0.4	0.3	3.9	0.4	0.7	0.5	1.7	2.3	1.2	2.6	0.7	0.4
Hf	3.6	2.2	2.3	1.4	2.3	2.1	2	2.1	2.1	2.4	2	2.4	2.9	3.5
Ta	0.4	0.22	0.21	0.18	0.39	0.22	0.16	0.29	0.2	0.24	0.46	0.3	0.6	0.6
Pb	8.3	3.3	3.2	1.9	5.5	4.7	5.9	2.4	4.3	4.2	4.2	4.9	2.8	3.8
Th	3.6	4.1	3.2	2.3	3.4	4.2	5.9	2.7	3	5.1	2.1	2.7	2.0	2.1
U	0.9	0.7	0.7	0.5	0.7	0.9	1.1	0.6	0.7	1.1	0.5	0.7	0.4	0.4

Table 5.1 (ct'd)

	43906	40672	40703	40683	40685	40706	40708	40712
$^{87}\text{Sr}/^{86}\text{Sr}$	0.70493	0.70494	0.70480	0.70436	0.70586	0.704	0.704	0.704
$(^{87}\text{Sr}/^{86}\text{Sr})_i$	0.70485	0.70487	0.70475	0.70432	0.70581	0.704	0.704	0.704
$^{206}\text{Pb}/^{204}\text{Pb}$		18.802	18.823		18.832		18.667	
$(^{206}\text{Pb}/^{204}\text{Pb})_i$		18.780	18.803		18.825		18.649	
$^{207}\text{Pb}/^{204}\text{Pb}$		15.623	15.621		15.637		15.552	
$(^{207}\text{Pb}/^{204}\text{Pb})_i$		15.622	15.620		15.637		15.551	
$^{208}\text{Pb}/^{204}\text{Pb}$		38.497	38.723		38.740		38.497	

5.2.4. Sample Set and Analytical Methods

The sample set on which this paper is based consists of 29 fresh, unaltered volcanic rocks from the collection at the University of Auckland that were originally collected and described for major and trace element analysis (Kuschel, 1988) and K-Ar dating (Black et al., 1992). The dataset presented in this study consists of new XRF and ICP-MS major and trace element data as well as new Sr-Pb isotope data for several samples. Samples represent lavas, breccias and small intrusive bodies. Rocks in several centers, especially the NE Waiheke, Miranda and Ruru-Maungatapu centers, have been affected by a hydrothermal process that precipitated rare earth element (REE-) rich minerals in microscopic veinlets and patches (Kuschel and Smith, 1992). The alteration in these rocks is non-pervasive, being confined to precipitation in the veinlets and patches, which contain 60 to 90% $(\text{REE})_2\text{O}_3 + \text{Y}_2\text{O}_3$, as well as SiO_2 , Al_2O_3 , CaO , Pb , Th and U . Patches are filled with a mineral that resembles kimuraite ($\text{CaY}_2(\text{CO}_3)_4 \cdot 6\text{H}_2\text{O}$); the veinlet-filling material could not be identified (Kuschel and Smith, 1992). REE abundances in affected rocks are considerably increased, e.g. La up to 154 ppm, from what we consider average values in unaffected Kiritahi chain rocks, e.g. c. 8-20 ppm La (Table 5.1). Where possible, we selected samples for our analyses that appeared unaffected based on existing XRF measurements of REE concentrations. Analysed rocks that do show secondary REE enrichment nevertheless do not show significant major element mobility (Fig. 5.3).

We crushed 100-200 g aliquots of fresh rock samples between tungsten-carbide plates and removed any weathered fragments before grinding in a tungsten-carbide ring mill to <200 mesh. Major and some trace element concentrations were measured at the University of Auckland by X-ray fluorescence spectrometry (XRF) on fused glass discs prepared with SPECTRACHEM 12-22 flux. For the trace elements a suite of 36 international standards were used for calibration and Siemens SPECTRA 3000 software was used for data reduction. The Compton scatter of X-ray tube line $\text{RhK}\beta_1$ was used to correct for mass attenuation and appropriate corrections were used for those elements analyzed at energies below the Fe

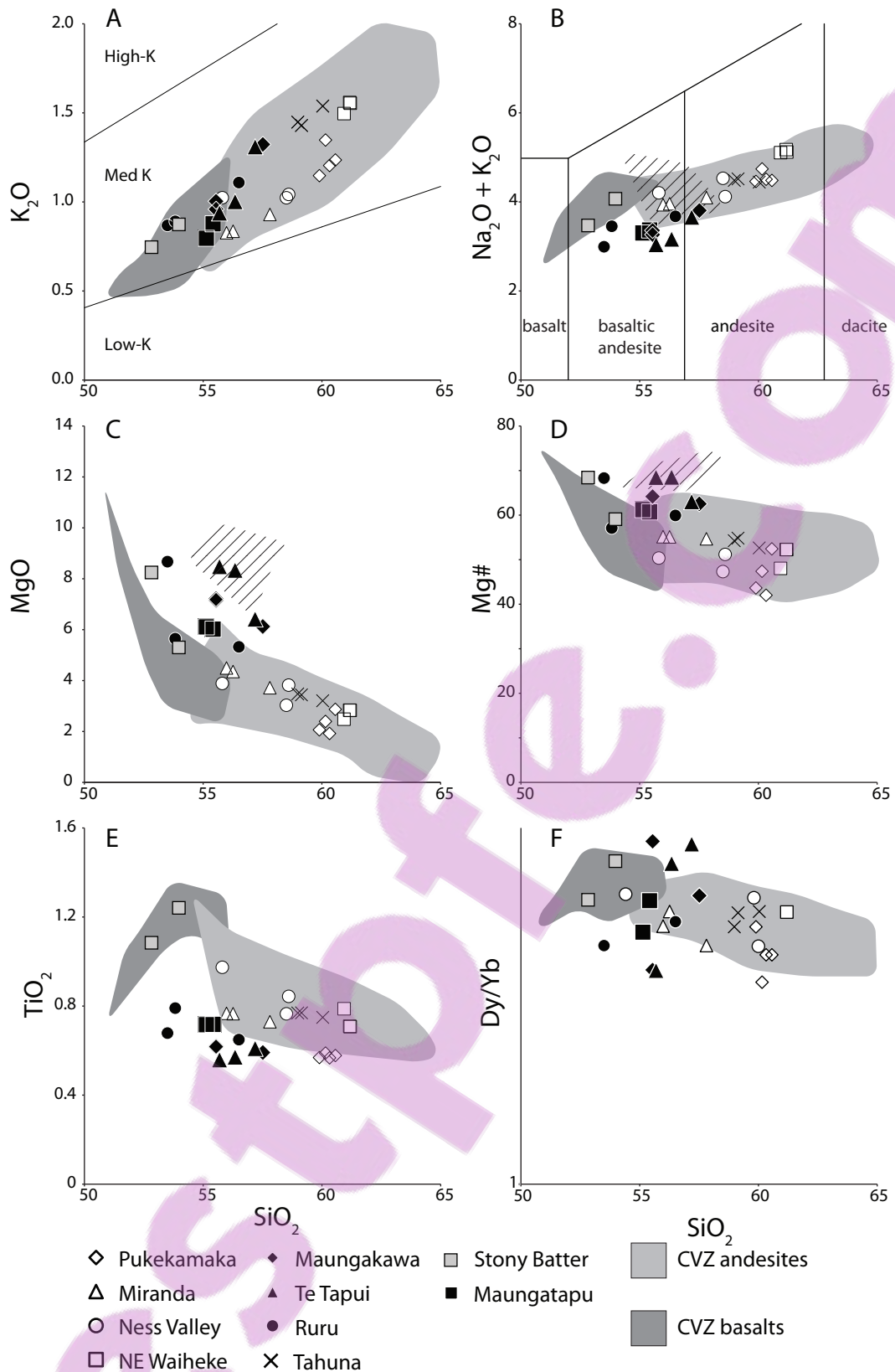


Fig. 5.4 Major and trace element variation diagrams. Coromandel Volcanic Zone andesite and basalt fields based on the dataset presented in Booden et al. (2009). Diagonal stripes: high-Mg andesite compositions from the compilation of Wood and Turner (2009).

absorption edge. For XRF major oxide analyses precision is generally better than 1% (at 2s) and for trace elements it is 1% for Sr and Zr, 1-3% for V, Cr, Zn and Y, 3-5% for Ba, 5-10% for Rb and Nb, Detection

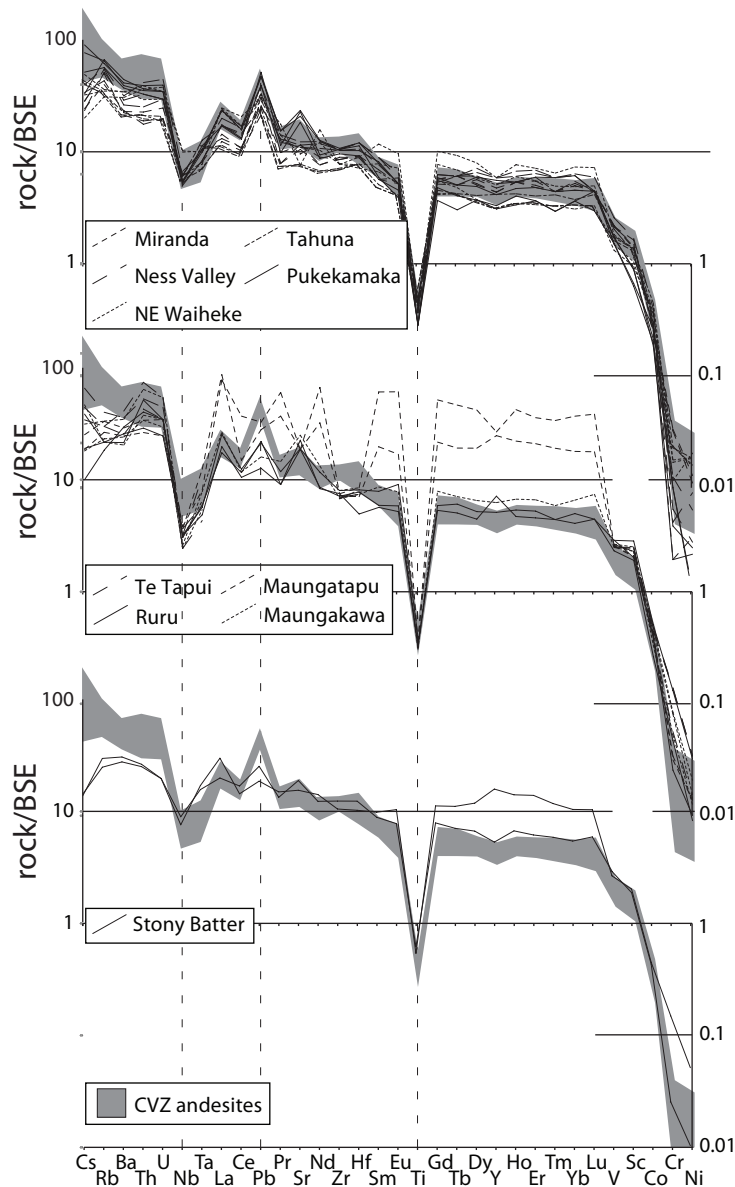


Fig. 5.5 Trace element distribution diagrams normalized relative to the bulk silicate earth (BSE) composition of McDonough and Sun (1995). Coromandel Volcanic Zone andesite and basalt fields based on the dataset presented in Booden et al. (2009).

limits are <2ppm for Rb, Sr, Y, Zr and Nb, 2-5ppm for V, Cr, and Zn, and 5-10ppm for Ba. We report major elements (Na, Mg, Al, Si, P, K, Ca, Ti, Mn, Fe) as their respective oxides (Na_2O , MgO , Al_2O_3 , SiO_2 , P_2O_5 , K_2O , CaO , TiO_2 , MnO , FeO , Fe_2O_3) normalized to 100% on a volatile-free basis, using the $\text{FeO}/\text{Fe}_2\text{O}_3$ ratios recommended by Middlemost (1989). Additional trace element concentrations were measured by ICP-MS at ALS Chemex Vancouver following a four-acid digest procedure. Reproducibility including sample splitting is better than 10% for the relevant trace elements. Whole-rock geochemical results are presented in Table 5.1.

Whole-rock Sr and Pb isotope compositions were determined on aliquots of the same samples used for ICP analysis, at VU University, Amsterdam. Strontium was extracted using standard resin column

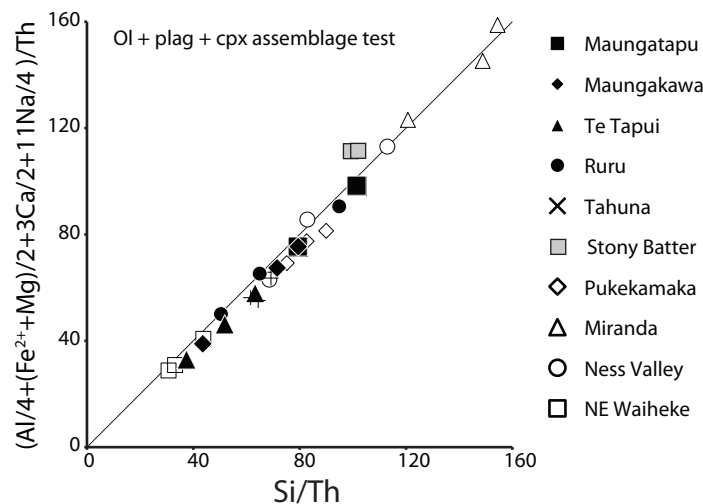
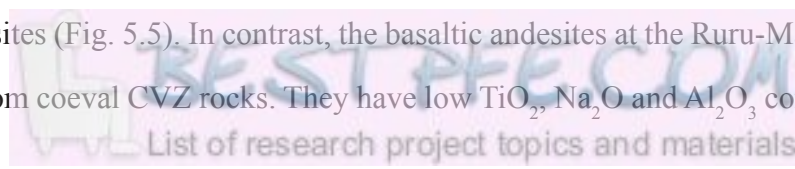


Fig. 5.6 Pearce element ratio assemblage test diagram for the assemblage olivine + plagioclase + clinopyroxene. The axial ratios were derived using the Axis program (<http://ees.acadiau.ca/~cstanley/software.html>) using the major elements Si, Al, Ca, Na, Mg and Fe. Mg and ferrous iron are assumed to be interchangeable with respect to partitioning into minerals, and Th is assumed to be excluded from the fractionating mineral assemblage.

techniques and analyzed on a Finnigan Mat 262 TIMS following techniques described in Heumann and Davies (2002). Lead was separated and Pb isotope compositions were measured on a Neptune MC-ICP-MS following techniques described in Elburg et al. (2005). Analyses were performed on 200 ng Sr and 100 ng Pb sample aliquots, whereas blanks were three orders of magnitude smaller and therefore negligible. Errors reported here are within-run analytical errors and are negligible compared to the geologic variation in isotope ratios. Whole-rock isotope results are presented in Table 5.1.

5.2.5. Geochemistry

Kiwitahi volcanic rocks from all centers are medium-potassic rocks (Gill, 1981) with bulk rock compositions predominantly in the basaltic andesite and andesite fields (Fig. 5.3A-B; Le Bas et al., 1986). Minor dacites additionally occur at Miranda (Black et al., 1992) but were not analyzed for this study. All rocks in the Kiwitahi volcanic chain have an arc-type trace element distribution characterized by enrichment in the incompatible elements and negative anomalies for the high field strength elements including Nb and Ti (Fig. 5.5). The basaltic andesites and andesites at the Waiheke-Pukekamaka and Tahuna centers in all respects have a comparable major element composition to coeval CVZ andesites (Fig. 5.4), although they show relatively low enrichment in incompatible trace elements (Cs, Rb, Ba, U, Th) compared to CVZ andesites (Fig. 5.5). In contrast, the basaltic andesites at the Ruru-Maungatapu centers differ in key respects from coeval CVZ rocks. They have low TiO_2 , Na_2O and Al_2O_3 concentrations, high



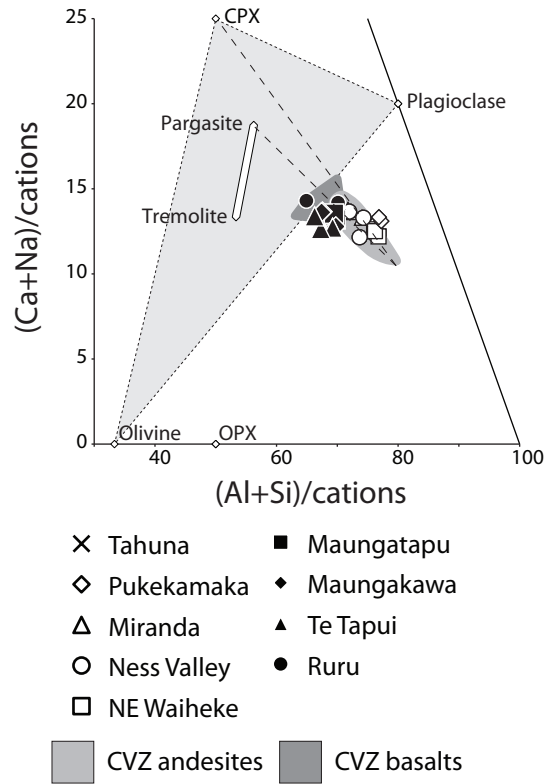


Fig. 5.7 Al+Si vs. Ca+Na, expressed as molar percentage of major element cations. Coromandel Volcanic Zone andesite and basalt fields based on the dataset presented in Booden et al. (2009).

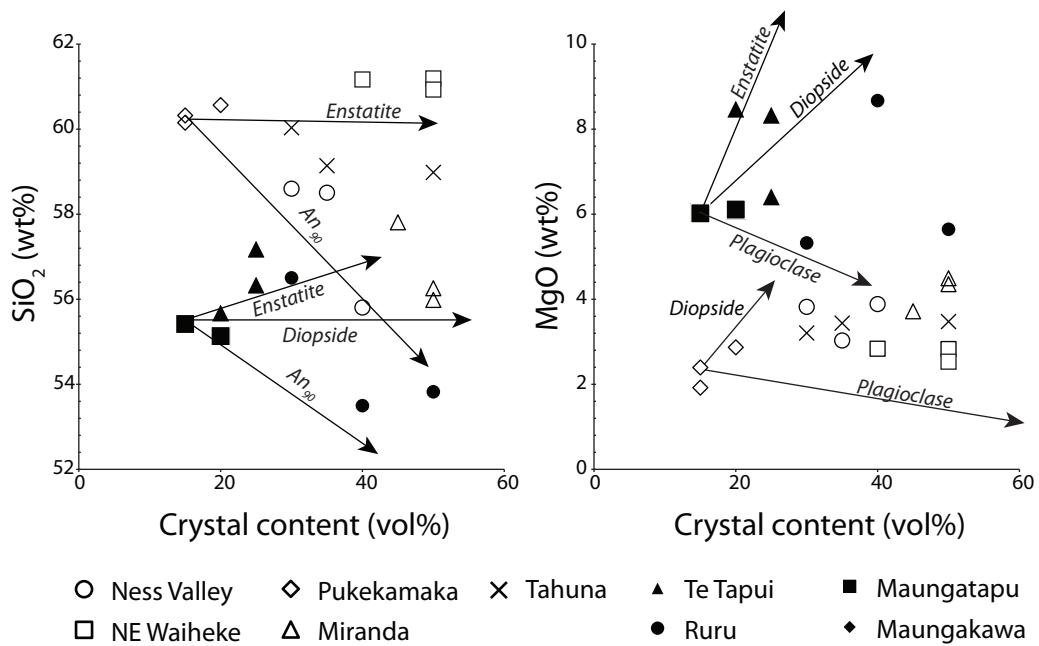


Fig. 5.8 Bulk rock composition data (wt%) vs. crystal content (vol%), estimated in thin section. Arrows indicate expected effect of bulk composition of accumulation of diopside, enstatite and calcic plagioclase (An₉₀) in the most aphyric rocks.

MgO concentrations and high Mg# values (Mg# = molar (Mg/(Mg+Fe²⁺))), relative to CVZ andesites (Fig. 5.4). The Ruru-Maungatapu center rocks also have high Sr and Cr, and low Al, Cs, Rb, Ba, Nb, Zr and Hf relative to coeval CVZ andesites (Fig. 5.5). The Stony Batter basaltic andesites have comparable major element compositions to CVZ basalts (Fig. 5.4). Their trace element distribution (Fig. 5.5) is also comparable to that of CVZ basalts (not shown). Thus, Stony Batter rocks do not have the high MgO contents and low TiO₂ and Nb contents that are characteristic of the Ruru-Maungatapu basaltic andesites. Given their eruption location behind the main arc, their compositional affinity with coeval basalts erupted in the main arc is generally consistent with an origin in a backarc setting (c.f. Smith et al., 1993; Huang et al., 2000). The scope of the rest of this paper is on the other Kiwitahi centers, which we view as part of the main arc.

5.2.5.1. *Crystal Fractionation*

Samples of some centers show limited compositional trends, which may reflect sub-volcanic or syn-eruptive crystal sorting of the phenocryst assemblage. All samples plot along a line with slope 1 through the origin in a Pearce element ratio (PER) assemblage test diagram for the effect of fractionation or accumulation of olivine ± plagioclase ± clinopyroxene on bulk rock chemistry (Fig. 5.6). This indicates that fractionation of the principal phenocryst minerals can essentially explain compositional variation for the Kiwitahi volcanic rocks.

In addition to the role of the gabbroic olivine ± plagioclase ± clinopyroxene assemblage, the presence of hornblende in rocks of the Waiheke-Pukekamaka centers suggests a role for amphibole fractionation during magmatic differentiation. Amphibole is common in cognate xenoliths in arc volcanic rocks (e.g. at Taranaki volcano; Gruender et al., 2010) as well as in cumulates in arc crustal sections (Jagoutz et al., 2009; Larocque and Canil, 2010). Amphibole fractionation preferentially depletes a magma in the middle REE (e.g. Dy), which leads to decreasing values for the Dy/Yb ratio with increasing differentiation. On this basis, amphibole fractionation has been inferred to have affected the magmatic differentiation even of volcanic rock suites that lack amphibole (Davidson et al., 2007). The compositional range of the rocks of the Waiheke-Pukekamaka centers is too small to identify whether REE ratios consistently correlate with differentiation indices such as SiO₂. However, Waiheke-Pukekamaka rocks compositionally overlap with the CVZ andesite suite, which has a wider compositional range and shows a trend to smaller Dy/Yb values with increasing SiO₂ (Fig. 5.4F). Tahuna andesites also overlap with CVZ andesites. The effect of amphibole fractionation is further illustrated on an Al+Si vs. Na+Ca diagram (Fig. 5.7), where the

Waiheke-Pukekamaka and Tahuna Kiwitahi centers also do not define a discernible trend but plot within the field defined by CVZ andesites. The CVZ andesite field is elongate and aligned with the compositions of parasitic amphibole and of clinopyroxene. We infer that amphibole fractionation directly or indirectly affected the differentiation of the magmas that erupted at the Waiheke-Pukekamaka and Tahuna centers. This process was cryptic at Tahuna where hornblende is absent, which corresponds to the general rarity of amphibole in CVZ andesites younger than 10 Ma (Skinner, 1986). The absence of amphibole in Tahuna center rocks presumably reflects its resorption at low pressure (c.f. Rutherford and Hill, 1993) but not its absence in the deeper magmatic system.

Rocks of the Ruru-Maungatapu centers do not entirely overlap with the CVZ array in Figure 5.7, but cluster near the olivine-plagioclase tie line. They therefore show no particular indication for the effects of amphibole fractionation or clinopyroxene fractionation. Together with the absence of any resorbed amphibole in these rocks, we interpret this to suggest that amphibole was also absent in the deeper magmatic system.

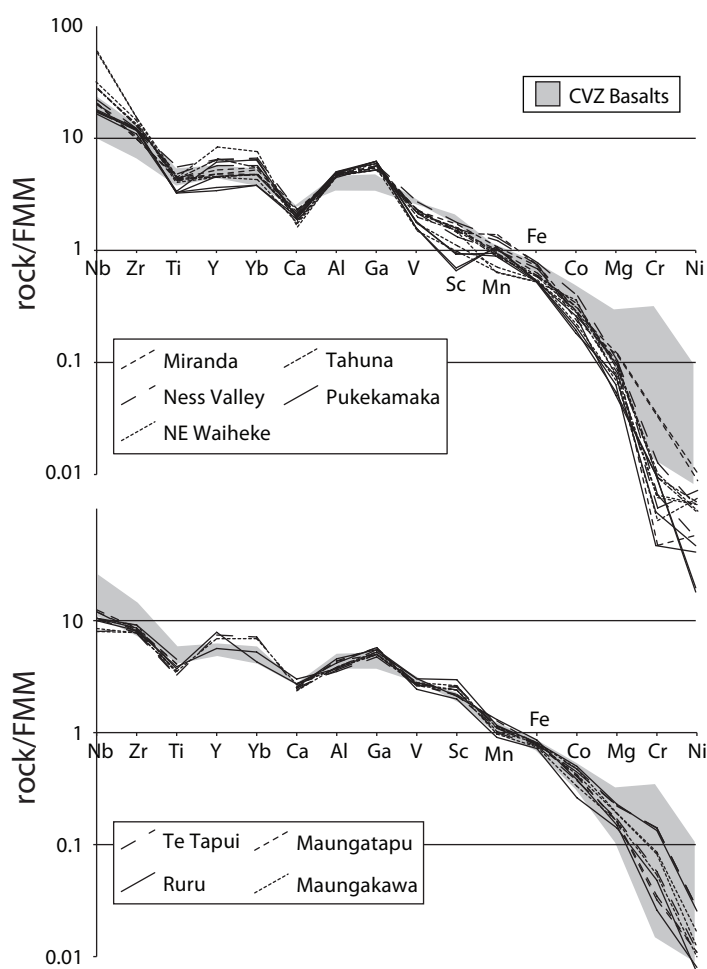


Fig. 5.9 Conservative element distribution normalized to fertile MORB mantle (Pearce and Parkinson, 1993). Coromandel Volcanic Zone basalt field based on our unpublished data.

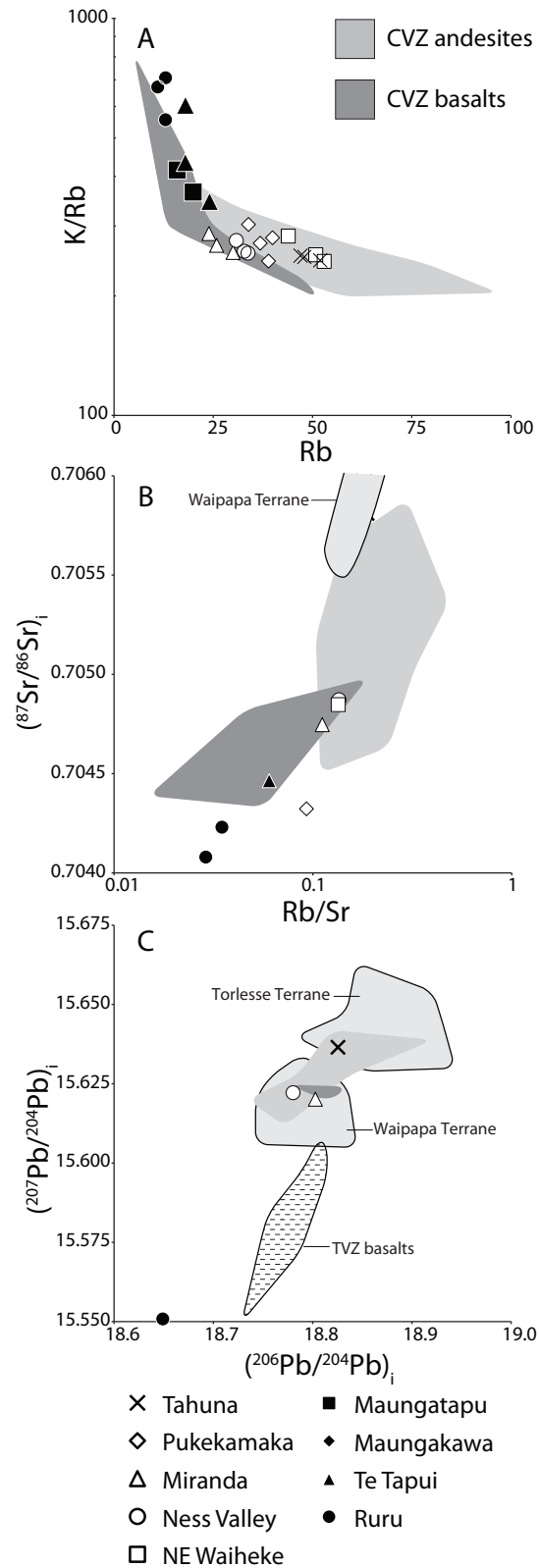


Fig. 5.10 A. K/Rb vs. Rb. B. Initial $^{87}\text{Sr}/^{86}\text{Sr}$ values vs. Rb/Sr. Initial values calculated using a ^{87}Rb decay constant of $1.398 \cdot 10^{-11}$ (Nebel et al., 2006) using the ages listed in Fig. 5.1. Waipapa Terrane data from Adams and Maas (2004), not corrected for age which makes no significant difference. Coromandel Volcanic Zone andesite and basalt fields based on the dataset presented in Booden et al. (2009). C. Initial $^{206}\text{Pb}/^{204}\text{Pb}$ vs. $^{207}\text{Pb}/^{204}\text{Pb}$. Initial values calculated using decay constants of $1.5514 \cdot 10^{-10}$ and $9.8486 \cdot 10^{-10}$ for ^{238}U and ^{235}U , respectively. Taupo Volcanic Zone basalt field based on data from McCulloch et al. (1994). Waipapa and Torlesse Terrane fields based on data from Graham et al. (1992) and McCulloch et al. (1994).

5.2.5.2. *Mixing*

At Tahuna and the older centers, plagioclase and pyroxene commonly occur in the form of glomeroporphyritic aggregates of multiple crystals as well as in the form of single phenocrysts. Bulk rock chemistry indicates that the accumulation or fractionation of this crystal cargo controls magma compositions. Consequently, bulk rock compositions tentatively correlate with crystal content (Fig. 5.8). The minimum bulk SiO₂ concentrations of rocks of the Ness Valley, Miranda, Pukekamaka and Tahuna centers generally become less silicic with increasing crystal content and broadly fall along an expected trend for anorthitic plagioclase (90% anorthite, An₉₀) accumulation (Fig. 5.8). Considerable scatter occurs, which can be attributed to accumulation of pyroxene and/or more albitic plagioclase, as well as variations in groundmass composition. As well, bulk rock compositions become more MgO-rich with crystal content consistent with pyroxene accumulation. We interpret this to indicate that the rocks comprise a relatively silicic melt component, at least partly represented by the groundmass, in which plagioclase + pyroxene crystals accumulated. The best approximation to a melt composition may be represented by the low-phyric Pukekamaka andesites, which contain no feldspar or pyroxene phenocrysts and only comprise 15-20 vol% hornblende crystals.

In the Ruru-Maungatapu centers, only the plagioclase-phyric rocks of the Ruru center show decreasing SiO₂ with increasing crystal content, consistent with anorthitic plagioclase accumulation in addition to pyroxene (Fig. 5.8). In contrast, rocks of the Te Tapui, Maungakawa and Maungatapu centers have slightly increasing SiO₂ with crystal content, consistent with accumulation of pyroxene only. As in the case of the older center rocks, we interpret the broad correlation between crystal content and bulk rock composition to indicate that the phenocrysts and glomeroporphyritic aggregates are entrained components that are accumulative in the magmas, and not necessarily the products of crystallization from the entraining melt.

The most aphyric rocks in both the older Waiheke-Pukekamaka + Tahuna suite and the younger Ruru-Maungatapu suite each comprise c. 20% crystals, so their bulk compositions are an approximation of groundmass compositions. Rocks of the older suite appear to have andesitic groundmass compositions (c. 60% SiO₂) with c. 2-3% MgO. Pukekamaka rocks also have relatively fractionated Dy/Yb values and low TiO₂ concentrations (Fig. 5.4F) consistent with amphibole fractionation. We consequently interpret the Waiheke-Pukekamaka and Tahuna basaltic andesites and andesites as comprising mixtures of crystals (hornblende ± plagioclase ± pyroxene) and an andesitic melt component, generated at least in part by amphibole fractionation. In contrast, rocks of the Ruru-Maungatapu suite apparently have basaltic

andesitic groundmass compositions (55-56% SiO₂) with c. 6-8% MgO, representing a non-differentiated component.

5.2.5.3. *Mantle vs. Crustal Contributions*

The distribution in arc volcanic rocks of elements that are not significantly transferred from the subducted slab to the mantle wedge serves as a window into the history of the mantle prior to partial melting. Normalizing the distribution of such conserved elements to a hypothetical fertile MORB mantle composition shows that all Kiwitahi rocks have comparable distributions (Fig. 5.9; Pearce and Parkinson, 1993). Relative to CVZ basalts, the conserved element distributions of Waiheke-Pukekamaka and Tahuna rocks appear to have been modified by differentiation in the crust: these rocks are relatively enriched in Nb and Zr, and have relatively low V, Sc and compatible elements. In contrast, the pattern in the Ruru-Maungatapu center basaltic andesites is broadly comparable to that in CVZ basalts, although Ruru-Maungatapu center rocks have comparatively low Nb, Zr and Ti enrichments. Consequently, the highly incompatible elements Nb and Zr show comparable enrichment to less incompatible elements. This is not evidence for a previous depletion episode, as that could yield considerably depleted Nb even at only c. 2% partial melt extraction (Smith et al., 2009). Instead, we interpret the somewhat lower concentrations of Nb and Zr as an indication for a higher degree of mantle partial melting (c.f. Pearce and Parkinson, 1993) compared to CVZ basalts, of an essentially similar mantle source (i.e. unmodified fertile MORB-type mantle).

The assimilation of crust-derived partial melts can influence magmatic differentiation, particularly where differentiation occurs in a 'hot zone' near the crust-mantle interface where abundant energy is available to promote anatexis of the crust or of predecessor intrusions (Annen et al., 2006). Assimilation can affect incompatible element ratios, such as K/Rb, that should remain constant if magmatic differentiation occurs only through crystal fractionation. In Ruru-Maungatapu center rocks, which mainly comprise clinopyroxene in which K and Rb are highly incompatible, the K/Rb ratio shows sharply decreasing values over a small increase in Rb concentration. We interpret this to reflect assimilation of partial melt with a low K/Rb ratio (Fig. 5.10A). The K/Rb ratios in Ruru-Maungatapu rocks are comparable to those in CVZ basalts. The Waiheke-Pukekamaka and Tahuna rocks, in contrast, have smaller K/Rb ratios and overlap in composition with CVZ andesites, suggesting more extensive assimilation occurred in these magmas.

Because the Kiwitahi centers erupted through Jurassic basement rocks, initial radiogenic isotope ratios can potentially distinguish between the contributions of old crust and young syn-magmatic rocks to

the assimilation process, and we acquired Sr and Pb isotope data on several bulk rock samples to assess this. Initial $^{87}\text{Sr}/^{86}\text{Sr}$ ratios are smallest in two Ruru rocks (Fig. 5.10B), where they correlate with large K/Rb ratios and therefore suggest little or no assimilated component in these rocks. It is possible that the initial $^{87}\text{Sr}/^{86}\text{Sr}$ ratio in Ruru rocks (0.7041-2), which is smaller than in CVZ basalts approximates the corresponding value in primary mantle magma. In contrast, basaltic andesites and andesites of the Waiheke-Pukekamaka and Tahuna centers have initial $^{87}\text{Sr}/^{86}\text{Sr}$ ratios greater than 0.7043. These values generally overlap with the range of values in CVZ basalts and the least-radiogenic CVZ andesites, although the Tahuna sample has a greater initial $^{87}\text{Sr}/^{86}\text{Sr}$ ratio value of 0.7058. We infer that the Waiheke-Pukekamaka and Tahuna center rocks generally contain a larger crustal Sr component than Ruru-Maungatapu center rocks. The initial $^{87}\text{Sr}/^{86}\text{Sr}$ ratio of 0.7043 in the Pukekamaka sample is identical to that in the least-radiogenic CVZ basalts. This value could represent the Sr isotope composition of primary mantle magma at the time, prior to the eruption of the Ruru-Maungatapu centers. Although the number of data points in Figure 5.10B is small, we speculate that the Sr isotopic composition of primary mantle magmas may have become less radiogenic at the time of the Ruru-Maungatapu eruptions.

Pb isotope data potentially help constrain possible assimilation of crustal material (Fig. 5.10C). In terms of initial $^{207}\text{Pb}/^{204}\text{Pb}$ - $^{206}\text{Pb}/^{204}\text{Pb}$ values, the Waiheke-Pukekamaka and Tahuna center rocks plot within the field of CVZ andesites. With the exception of the Tahuna sample, they have a comparable Pb isotope composition to CVZ basalts. In contrast, one Ruru sample has distinctly unradiogenic initial Pb isotope ratios, with an initial $^{207}\text{Pb}/^{204}\text{Pb}$ ratio comparable to the least radiogenic ratios found in TVZ basalts (Fig. 5.10C). Lead in arc basalts and in andesites has been demonstrated to be predominantly derived from the subducted slab (Pearce et al., 1995; Green, 2006; Smith et al., 2009). The slab-derived fraction of an incompatible element M can be estimated in a plot of M/Yb vs. Nb/Yb (Pearce et al., 1995), on the assumption that Nb and Yb are not transferred significantly from slab to mantle wedge. On this basis, we estimate that at least 85% of Pb in all Kiwitahi rocks is slab-derived. The initial $^{207}\text{Pb}/^{204}\text{Pb}$ - $^{206}\text{Pb}/^{204}\text{Pb}$ values in Waiheke-Pukekamaka rocks and CVZ basalts are intermediate between those of the major Waipapa and Torlesse basement terranes on the North Island, so it is possible that the Pb isotope values in Waiheke-Pukekamaka rocks reflect the presence in the subducted slab of sediments derived from these basement terranes. Further, the drop in initial $^{207}\text{Pb}/^{204}\text{Pb}$ values between the eruption of the Tahuna center (6.7 Ma) and the Ruru-Maungatapu centers (post-6.2 Ma) likely reflects a change in the isotopic composition of Pb in the subducted slab.

Correlated with the decrease in $^{207}\text{Pb}/^{204}\text{Pb}$ values is the somewhat lower initial $^{87}\text{Sr}/^{86}\text{Sr}$ ratio value in

Ruru-Maungatapu centers rocks, relative to the lowest initial $^{87}\text{Sr}/^{86}\text{Sr}$ values in the older centers, noted above. Per the method outlined above, we estimate Sr in the Kiwitahi rocks to be at least 50% slab-derived. Consequently, a smaller response to slab-derived Sr isotope composition is expected relative to slab-derived Pb isotope composition. Although the number of data points is very limited, the drop in initial $^{207}\text{Pb}/^{204}\text{Pb}$ values is consistent with the drop seen between the values in 9-7 Ma CVZ basalts, and

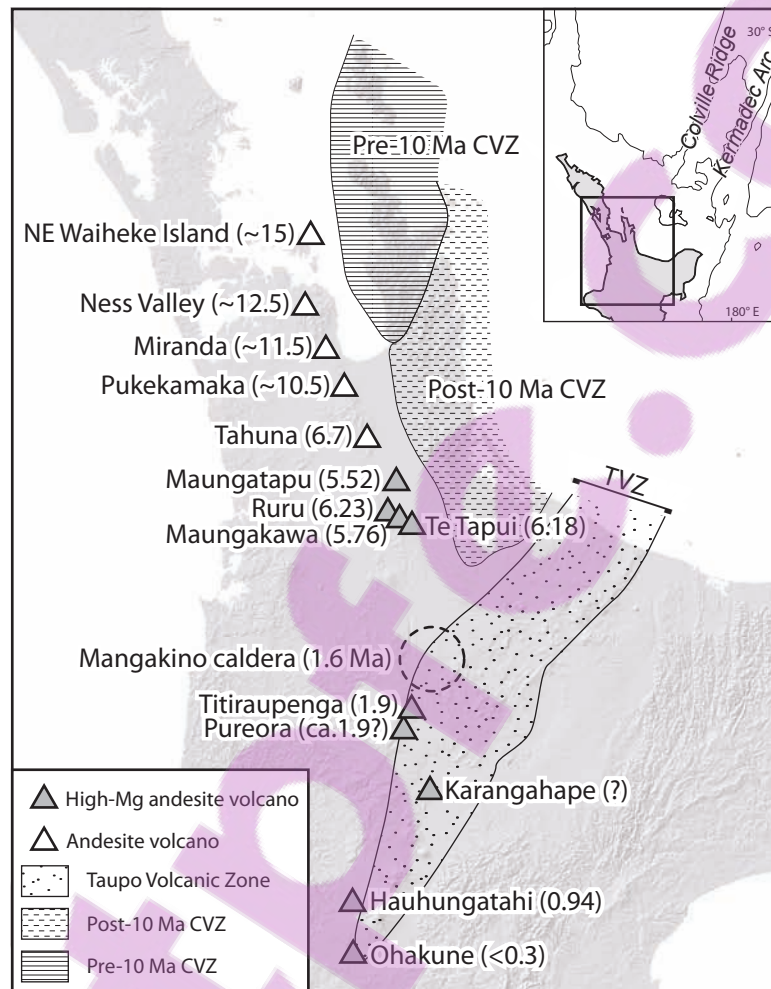


Fig. 5.11 The Kiwitahi chain and high-Mg andesite volcanoes in the North Island, compiled Ages in Ma between parentheses, from Black et al. (1992), Cameron et al. (2010) and from compiled data in Wilson et al. (1995). White triangles: pre-6.7 Kiwitahi centers. Grey triangles: high-Mg andesite volcanoes. CVZ: Coromandel Volcanic Zone; TVZ: Taupo Volcanic Zone.

Quaternary TVZ basalts (Fig. 5.10C). It is possible that the eruptions of the Tahuna (6.7 Ma) and Ruru (6.2 Ma) centers bracket the change in slab isotopic composition.

Kiwitahi rocks (except Tahuna; Fig. 5.10B), this feature is best explained as reflecting lesser interaction with differentiated crustal partial melts in the petrogenesis of the Kiwitahi magmas. We envisage the generation of Kiwitahi magmas as occurring on the edge of a 'hot zone' near the crust-mantle interface (c.f. Annen et al., 2006), the central and most energetic part of which was located at any given instant in time underneath the CVZ. The hot zone underlying the CVZ produced intermediate and eventually silicic magmas from basaltic mantle magmas through amphibole \pm clinopyroxene fractionation and assimilation, where the assimilant was variably derived from the crust and from earlier intrusions (Booden et al., 2009). We surmise that, on the edge of the hot zone, a less energetic environment existed where crustal anatexis was suppressed and magmas did not readily absorb a substantial crustal component. The smaller magma volumes that were presumably involved are consistent with less frequent eruptions and more mafic magma compositions (typically $<60\%$ SiO₂), relative to the CVZ. This regime gave rise to the eruptions at the Waiheke-Pukekamaka and Tahuna centers.

5.2.6.2. *High-Mg Andesites in Northern New Zealand*

The post-6 Ma Kiwitahi centers erupted high-Mg andesites that have no equivalent in the CVZ. High-Mg andesites form a small fraction of arc volcanic rocks globally, but are petrologically important because their geochemical compositions closely resemble the estimated composition of the bulk continental crust (Kelemen, 1995). High-Mg andesite formation has been variously ascribed to interaction between ascending basaltic melts and peridotite (e.g. Kelemen, 1995), partial melting of pyroxenite formed by reaction of slab fluids with peridotite (Straub et al., 2008) and anhydrous partial melting of peridotite at relatively low pressure (0.5 GPa; Mashima, 2009). Recent experimental results indicate that high-Mg andesites can form in equilibrium with a harzburgite residue, but not a fertile lherzolite residue (Wood and Turner, 2009). Formation of a harzburgite residue requires a relatively large degree of partial melting. As noted above, the trace element composition of the Ruru-Maungatapu high-Mg andesites suggests a relatively high degree of partial melting of their mantle source relative to older Kiwitahi rocks (Fig. 5.9). Hence, it appears that a prolonged (c. 700 kyr duration) pulse of high-degree partial melting occurred in the mantle at the tip of the Colville-Coromandel arc system from 6.2 Ma.

The start of this hypothetical event correlates in time with the proposed inception of subsidence in the Hauraki Rift, at least in its southern segment, sometime between 7 and 6 Ma (Hochstein and Ballance, 1993). The 6.2 Ma eruption of the Ruru center correlates with renewed rhyolitic volcanism in the CVZ, following a c. 700 kyr period of quiescence (Carter et al., 2003). The 5.5 Ma eruption of the Maungatapu



center correlates with the onset of a renewed pulse of basaltic volcanism in the northern CVZ (Adams et al., 1994). The final Kiwitahi high-Mg andesite eruptions at 5.5 Ma coincide with the initiation of rifting of the Colville Arc to form the Havre Trough backarc basin (Wysoczanski et al., 2010). Each of these features can be interpreted as reflecting an extensional tectonic regime, so the Ruru-Maungatapu high-Mg andesites appear to have erupted during a pronounced phase of extension in northern New Zealand.

The Kiwitahi high-Mg andesites are the oldest known such rocks in the Tertiary North Island volcanic succession. Numerous volcanoes associated with the TVZ subsequently erupted high-Mg andesites; these include White Island (Cole et al., 2000), Hauhungatahi (Graham and Hackett, 1987), Titiraupenga (Froude and Cole, 1985), Pureora (Cole and Teoh, 1975), Karangahape, and Ohakune (Houghton and Hackett, 1984). Apart from White Island, these volcanoes occur near the southern tip of the TVZ and along its western boundary (Fig. 5.11). Recent analyses of the high-Mg andesites of White Island (Heyworth et al., 2007) and Hauhungatahi (Cameron et al., 2010) show that they have comparable major element compositions to the Kiwitahi high-Mg andesites, characterized by low Al_2O_3 and TiO_2 , and high MgO, at given SiO_2 , compared to regular andesites. White Island is a large andesitic stratovolcano near the oceanic end of the TVZ that predominantly erupted a calc-alkaline andesite-dacite suite, but has additionally erupted high-Mg andesites since the 1970's. White Island high-Mg andesites have a comparable trace element distribution to regular calc-alkaline North Island andesites that is unlike that of the Kiwitahi high-Mg andesites (Fig. 5.12), and we do not view them as directly analogous to Kiwitahi high-Mg andesites. In contrast, the relatively small Hauhungatahi volcano is nearly entirely composed of high-Mg andesite. It is located at the southern tip of the TVZ, where its development preceded that of nearby Ruapehu volcano by 500-600 kyr (Cameron et al., 2010). Both Kiwitahi and Hauhungatahi high-Mg andesites have subdued incompatible element and Pb enrichments, and a marked positive Sr spike, relative to regular North Island andesites, and so have a comparable geochemistry (Fig. 5.12). This is matched by a similar pyroxene-dominated mineralogy (Cameron et al., 2010). Several older, comparable high-Mg centers line the western boundary of the TVZ (e.g. Titiraupenga, 1.85 Ma (Stipp, 1968)). The young, high-Mg andesite Ohakune center is located several km south of Ruapehu, arguably at the present tip of the TVZ-Kermadec-Tonga arc system. Cameron et al. (2010) suggested that the 940 ka Hauhungatahi high-Mg andesites represented a 'priming' phase that preceded regular andesitic volcanism, i.e. the post-300 ka development of Ruapehu volcano. If this is the case, the string of high-Mg andesite centers that line the western edge of the TVZ can be interpreted as the trace of the tip of the volcanic arc as it propagated into the New Zealand continent. We suggest that the Kiwitahi high-Mg andesites represent

the earliest manifestation of this trace (discussed below).

It is not immediately clear what the low initial $^{207}\text{Pb}/^{204}\text{Pb}$ value in the Ruru sample indicates (Fig. 5.10C). As noted above, it may represent the absence of a crust-derived radiogenic Pb component in the Pb flux from the subducted slab. It is possible that this relates to a change in the configuration of the subduction system, i.e. the subduction of young oceanic crust, as opposed to old Pacific crust prior to 6.2 Ma, could result in the transfer to the mantle wedge of Pb with a non-radiogenic composition. However, old Pacific crust is being subducted at present and also gives rise to the eruption of volcanic rocks with non-radiogenic Pb isotope compositions (Graham et al., 1992). A simpler explanation is that a change occurred in the amount of sediment that was subducted with the continuously subducting Pacific plate. Assuming a convergence rate of approximately 53 mm yr^{-1} (DeMets et al., 1994; Wysoczanski et al., 2010), and a slab dip angle of 50° (Reyners, 1980), it takes 1.7-2.4 My for a slab segment to reach the global average depth of $112 \pm 19 \text{ km}$ underneath the volcanic front (Tatsumi, 1986). Assuming instantaneous eruption of magma formed in the mantle wedge, this interval may be taken as the delay faced by a geochemical signal between subduction and eruption. Thus a decrease in the amount of subducted sediment may have occurred sometime between c. 9.1 and 7.9 Ma. This timeframe overlaps with the first appearance of basaltic volcanism and large silicic eruptions in the mainland CVZ (Adams et al., 1994; Carter et al., 2003). It is tentatively possible that a correlation exists with the collision of thickened oceanic crust of the Hikurangi Plateau with New Zealand, which Rowan and Roberts (2008) proposed to have occurred between 10 and 7 Ma. Further Pb isotope analyses of primitive rocks erupted between 7 and 6 Ma in the Kiwitahi chain and the CVZ could help to confirm the reality, and better constrain the timing, of the change in the Pb isotope signal.

5.2.6.3. *What Does the Kiwitahi Chain Represent?*

High-Mg andesite eruption at the southern end of the Kiwitahi chain marked a break with the pre-6.7 Ma regime, in which the Kiwitahi chain volcanic rocks were not pyroxene-dominated high-Mg andesites, but plagioclase- or amphibole-dominated andesites comparable to those erupted in the CVZ. As discussed above, we view the pre-6.7 Ma Kiwitahi centers as having erupted over the edge of a magmatic system, the main part of which underlay the CVZ where it gave rise to more vigorous and diverse volcanism. In this model the pre-6.7 Ma Kiwitahi centers are a part of the same arc as the CVZ.

Although post-10 Ma volcanism in the CVZ is commonly viewed as part of the greater Colville Arc system (e.g. Brathwaite and Christie, 1996; Ballance et al., 1999), the tectonic configuration prior to 10

Ma is debated. The principal question is whether CVZ (and, by inference, Kiwitahi) volcanism was the expression of a different subduction system to that which produced the predecessor Northland Arc. The Northland Arc strikes NW in Northland and along the Reinga Ridge (Fig. 5.1), and formed between 25 and 16 Ma (Smith et al., 1989; Herzer, 1995; Hayward et al., 2001; Mortimer et al., 2010). Hayward et al. (2001) included the pre-10 Ma volcanism in the CVZ and Kiwitahi chain as part of this Northland Arc. Although the CVZ and Kiwitahi chain strike NNW and are visually continuous with the Northland Arc, that NNW orientation reflects basement structure (Skinner, 1986) and not necessarily the strike of the arc at the time. The strike of the Colville Arc, and its presently active descendant the Kermadec Arc, was NNE. Some workers propose a migration of a single subduction/arc system from a NW- to a NNE-striking configuration (e.g. Nicholson et al., 2004); others propose that the NNE-striking Colville Arc system propagated into New Zealand, along-strike of the arc i.e. in SSW direction, and that this marked the end of the NW-striking Northland Arc system (Ballance et al., 1999). Colville Arc volcanism was likely associated with W-dipping subduction of the Pacific plate (e.g. Crawford et al., 2003; Mortimer et al., 2007; Herzer et al., 2009), whereas Northland Arc volcanism has variously been ascribed to W-dipping Pacific plate subduction (Mortimer et al., 2007), SW-dipping Pacific plate subduction (e.g. Herzer et al., 2009) and SW-dipping South Fiji Basin plate subduction (Herzer, 1995; Whattam et al., 2006).

The Kiwitahi chain forms a small but significant part of the volcanic succession that documents the transition from the early Northland Arc configuration to the current TVZ configuration, because they 1) formed at the edge of a magmatic system, and 2) display an unequivocal age progression that is continuous with younger eruptions along the western edge of the TVZ. The key implication of this is that the main magmatic system associated with the Kiwitahi chain was not located towards the NW, otherwise its migration, trailing the Kiwitahi chain, would have obliterated the older Kiwitahi centers; hence, as discussed above, we identify the CVZ, towards the E and NE, as the main magmatic system. The Kiwitahi chain eruptions therefore mark the maximum extent into the New Zealand continent of the CVZ magmatic system, which was otherwise located closer to the continental edge. The unequivocal age progression of the centers along the Kiwitahi chain, which persisted over the course of 10 My, makes it implausible that they formed behind the main part of a magmatic system that was part of the NW-striking Northland Arc: in that case, a more random pattern of eruptions would be expected. Instead, we propose that a single arc configuration gave rise to volcanism along the Kiwitahi chain and its TVZ extension, and that the Kiwitahi chain and the CVZ erupted as the continental tip of the Colville Arc. In essence this is the same configuration as that which exists at present, where the TVZ occurs as the continental tip of

the largely oceanic Kermadec Arc. The oldest Kiwitahi center, Waiheke Island, erupted c. 15 Ma (Black et al., 1992), suggesting that the current configuration, where a NNE-striking arc impinges on New Zealand, has persisted at least since 15 Ma.

5.2.7. Conclusions

The Kiwitahi volcanic chain records c. 10 million years of volcanism that is part of the volcanism of the Coromandel Volcanic Zone. The 15-10 Ma centers (Waiheke Island, Ness Valley, Miranda and Pukekamaka) erupted plagioclase- and amphibole-dominant basaltic andesites and andesites, which were geochemically similar to coeval andesites that erupted in the Coromandel Volcanic Zone. Compared to CVZ andesites, however, the Waiheke-Pukekamaka rocks show trace element and isotopic evidence for relatively limited crustal interaction. This is consistent with an origin at the cool edge of a magmatic system, the center of which probably underlay the CVZ. The 6.7 Ma Tahuna center erupted plagioclase-dominant andesites without hornblende that were again geochemically similar to coeval andesites of the CVZ. Between 6.2 and 5.5 Ma, a suite of clinopyroxene-dominated basaltic andesites with minor plagioclase erupted at the southern end of the Kiwitahi chain. These rocks show isotopic evidence for minimal crustal interaction, and have major and trace element compositions that are comparable to those of high-Mg andesites globally.

The Kiwitahi high-Mg andesites are the earliest known manifestation of high-Mg andesitic volcanism in the North Island. The Kiwitahi chain is contiguous with a string of high-Mg andesite volcanoes that line the western boundary of the TVZ down to its southern termination. We propose that together, these volcanoes preserve a 15 million year record of evolving volcanism at the tip of the Colville and Kermadec arcs.

Chapter 6. Application to Geochemical Exploration

6.1. Summary

One of the principal aims of this research project has been to test the potential for whole-rock, major element-based geochemical exploration in the Hauraki goldfield. This chapter presents the results of this partial project in the form of a paper that has been accepted for publication in *Economic Geology*. The paper describes the systematic major and trace element concentration trends in Coromandel Group andesites and presents a method to estimate the major element composition of an unaltered Coromandel Group rock based on the relative concentration of the high field strength elements Zr and Ti. This method is applied to hydrothermally altered Coromandel Group rocks collected from exploration drill core from the Waitekauri Area alteration zone. The altered rock set spans a 3 km wide section, from strongly adularia-altered rocks in the central Waitekauri area to comparatively weakly altered rocks at the periphery of the alteration zone, however adularia-bearing rocks occur throughout the section. The high field strength elements, including Zr and Ti, show evidence for near-complete immobility in the altered rocks, meaning their relative concentrations in altered rocks correlate with the original, pre-alteration major element composition of the altered rocks. This allows a quantitative estimate of the loss and gain of mobile elements. In the Waitekauri area, maximum and average K_2O mass gains in adularia-bearing rocks increase from the periphery of the system to the centre. This trend is consistent with trends in clay mineralogy and fluid inclusion homogenisation temperature, and shows that quantitative geochemical data can support qualitative mineralogical data.

This chapter concludes with a section presenting an examination of the applicability of the above technique to Whitianga Group rhyolites. Whitianga Group rhyolites have a low prospectivity because nearly all gold has been produced from deposits hosted in Coromandel Group andesites. Nevertheless, gold mining is ongoing at the rhyolite-hosted Broken Hills deposit. Additionally, the alteration aureoles of andesite-hosted deposits may extend into intercalated or overlying rhyolites, and altered rhyolite dykes can occur in altered andesitic wall rocks. As such, it is relevant to assess whether consistent correlations exist between rhyolite major element composition, and the relative concentrations of immobile high field strength elements. The correlations derived for the Coromandel Group andesitic suite using Zr and Ti concentrations do not apply, however in Whitianga Group rhyolites several other immobile element ratios appear to be viable alternatives that show good correlation with major element composition.

6.2. Quantifying Metasomatism in Epithermal Au-Ag Deposits: a Case Study from the Wait- ekauri Area, New Zealand.

Mathijs A. Booden, Jeffrey L. Mauk, Mark P. Simpson

Published in ECONOMIC GEOLOGY, vol. 106 (6)

6.2.0.0. *Abstract*

Major element geochemical exploration for epithermal deposits can extend the range of traditional pathfinder elements to a 1-10 km scale, and with knowledge of protolith composition, mass changes associated with hydrothermal alteration can be quantified. In the Hauraki Goldfield of New Zealand, altered andesites and dacites host epithermal Au-Ag deposits and prospects. The major element compositions of equivalent unaltered rocks correlate with whole-rock Zr/TiO_2 , an immobile element ratio that is preserved during K metasomatism. We used this feature to estimate the initial composition and calculate a mass balance for veinless altered rocks in the Waitekauri area along a 3-km-wide section that extends from the central Waitekauri Fault to the periphery of the alteration zone. The total transferred mass is equal to approximately 11% of rock mass in illite-dominated altered rocks, and 24% of rock mass in adularia-dominated altered rocks. On average mass losses exceed gains. Potassium was gained in most altered rocks, which contain illite and/or adularia as K-bearing hydrothermal minerals. Silica was gained in adularia-quartz-rich rocks close to the Waitekauri Fault. Other major elements are preferentially lost (Ca, Na, Fe, Mg) or effectively immobile (Al, Ti). The greatest K and Si gains occur in adularia-rich rocks that surround Au deposits along the Waitekauri Fault, whereas K gains are progressively lower and Si gains are mostly insignificant in deposits and prospects farther east where illite or interstratified illite-smectite is the dominant K-bearing mineral. In contrast, Na and Ca losses do not increase significantly from the periphery to the core of the Waitekauri area, because losses are commonly complete, and therefore limited by the initial concentration. However, the K and Si gains correlate with other measures of K metasomatism including K/Sr and Rb/Sr values and molar $K/(K+Na+2Ca)$ values, and together these parameters vector from the barren periphery to the orebody-hosting centre of the Waitekauri area. In contrast to major element trends, the pathfinder elements As, Sb and Hg define more local hydrothermal alteration cells within the larger Waitekauri area, some of which surround Au deposits.

6.2.1. Introduction

Epithermal deposits are surrounded by altered host rocks that have exchanged elements with hydro-

thermal fluids. The magnitude of gains and losses is generally greatest close to epithermal veins, so a regional gradient in the magnitude of gains and losses can point to epithermal mineralization. Many studies have successfully used trace pathfinder elements, such as As, Sb, Hg, Tl and base metals, for vectoring towards mineralization over distances in the order of tens to hundreds of meters (e.g., White and Hedenquist, 1995; Carlile et al., 1998; Hedenquist et al., 2000). However, because pathfinder elements are mainly confined to veins and adjacent wall rocks, major element mass changes in altered host rocks away from veins have the potential to significantly extend the range of geochemical exploration techniques up to several km (Clarke and Govett, 1990; Madeisky, 1996; Sherlock, 1996; Warren et al., 2007). Nonetheless, major element mass change is difficult to quantify on concentration data alone because 1) major element concentration must sum to 100%, which attenuates gains and losses, and 2) compared to pathfinder elements, major element mass changes are small relative to the initial concentration. A mass balance approach is required to accurately assess major element mass gain and loss, which in turn requires the composition of the protolith to be accurately known. Determining the protolith chemistry of altered rocks has been a hurdle in major element-based exploration techniques, because 1) host rocks typically show incipient to intense alteration in the vicinity of orebodies, which changes their geochemistry, and 2) they also show variable geochemistry away from orebodies; this simply reflects the heterogeneity of all rock units in the Earth's crust, but makes it difficult to select a single unaltered host rock geochemical composition for use in mass balance calculations (Madeisky, 1996; Sherlock, 1996; Shikazono et al., 2002; John et al., 2003; Leavitt and Arehart, 2005; Gemmell, 2007; Mauk and Simpson, 2007; Warren et al., 2007). MacLean (1990) presented a method to estimate the composition of heterogeneous protoliths to altered rocks on a sample-by-sample basis based on the bulk-rock Zr/TiO_2 ratio, which allows for mass balance calculations of individual samples without the oversimplifying assumption of a single 'representative' unaltered protolith. In this paper we use a variation on MacLean's (1990) approach to assess mass changes in altered volcanic rocks that host gold mineralization in New Zealand.

Epithermal Au-Ag deposits in the Hauraki Goldfield, New Zealand, are predominantly hosted in calc-alkaline andesite and dacite of the Coromandel Group. The major element composition of unaltered Coromandel Group rocks correlates with SiO_2 concentration, and the SiO_2 concentration in turn correlates strongly with the ratio Zr/TiO_2 . The value of Zr/TiO_2 has been used to characterize protoliths in a range of settings, including altered volcanic rocks in submarine-exhalative (Finlow-Bates and Stumpfl, 1981), altered plutonic rocks in a high-sulfidation Cu-Au deposit (Chambefort et al., 2007), metamorphosed sedimentary rocks (Hickmott and Spear, 1992) and igneous rock type in weathered rocks (Hallberg, 1984;

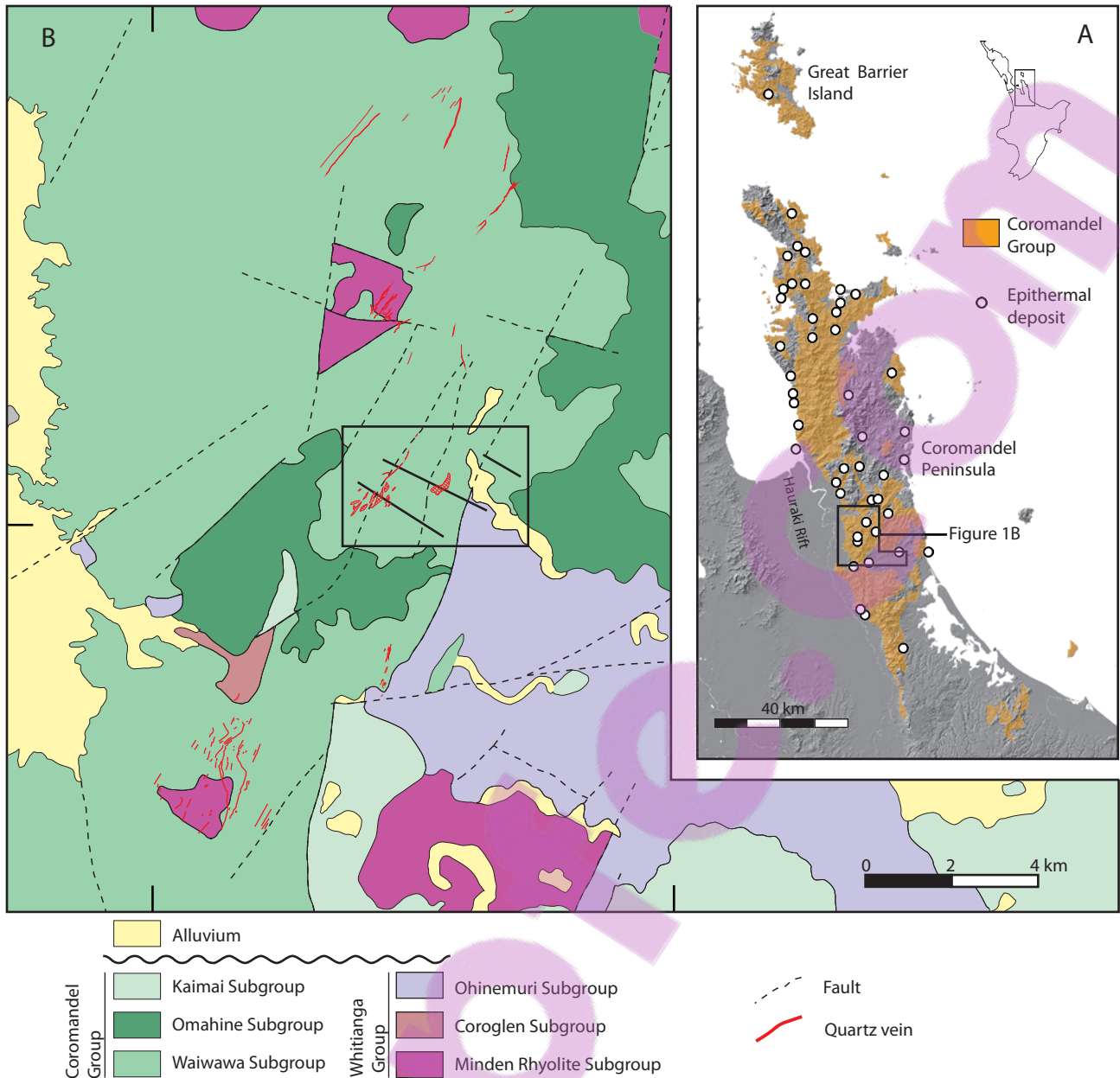


Fig. 6.1 A. Map of the Hauraki Goldfield, showing the distribution of the Coromandel Group and the location of known mineralization occurrences. Modified after Edbrooke (2001). B. Geological map of the southern Coromandel Peninsula modified after Brathwaite and Christie (1996). The box indicates the position of Figure 6.1C. C (next page). Geological map of the Waitekauri area showing the position of the Jasper Creek, Jubilee-Scotia, and Sovereign-Scimitar-Teutonic cross sections and the locations of drill holes. D (next page). Geological cross sections. Several drill holes protrude above the cross section topographic surface due to having been projected up to 100m onto the section. Map and sections based on unpublished mapping by Newmont Mining Corporation, after Simpson and Mauk (in press).

Murphy and Stanley, 2007). Zirconium, Ti and the other high field strength elements (HFSE), which have ionic potential values (ionic charge/radius (\AA); Cartledge, 1928) between 3 and 12, are commonly found to be the most immobile elements during open system alteration in many settings. The HFSE readily hy-

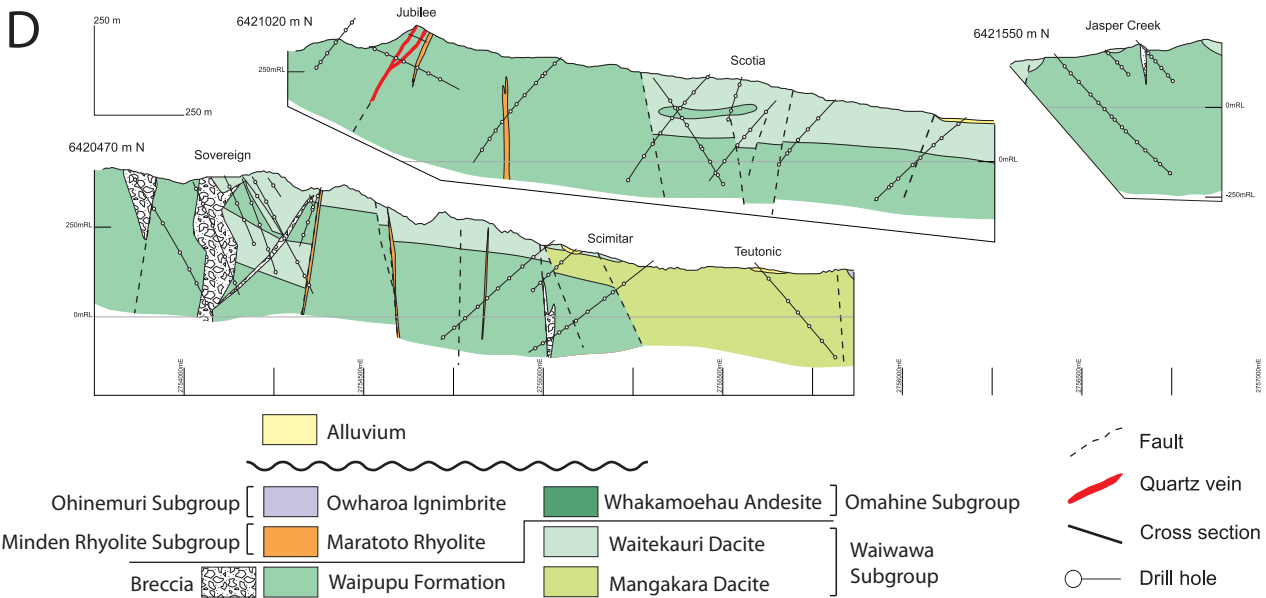
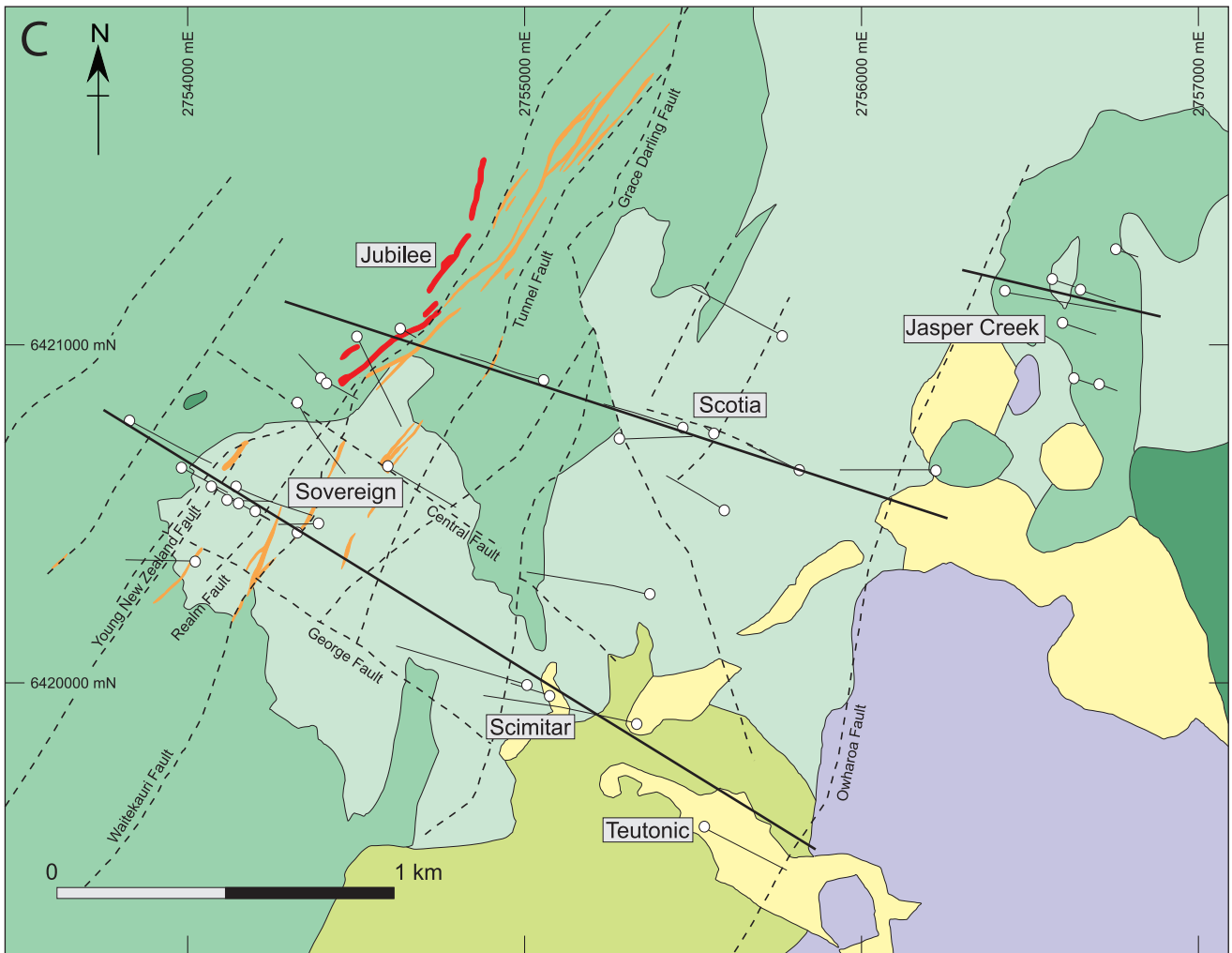


Fig. 6.1 (continued)

dolyse in solution, and form hydroxides and oxides that are sparingly soluble (Baalen, 1993). Although many studies have found some mobility even of the HFSE during hydrothermal alteration, particularly at very high temperatures or at pH < 2.5 (Jiang et al., 2005, and references therein), the HFSE generally represent the best approximation to an immobile element suite. Based on a reference dataset of 98 fresh,

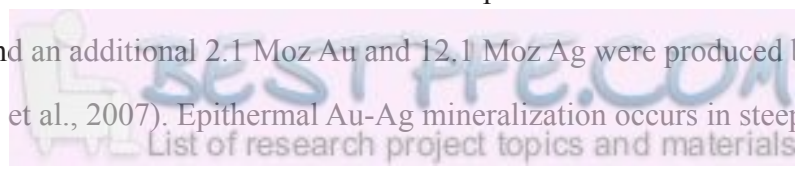
unaltered Coromandel Group rocks, we establish linear regression equations that relate major element concentrations to Zr/TiO_2 . The protolith composition of individual altered Coromandel Group rocks can be estimated based on Zr/TiO_2 , because this ratio is relatively unaffected by metasomatic gains and losses of mobile elements. A mass balance can then be calculated for each rock sample. We test our approach on a suite of altered volcanic rocks that have been drilled along a 3-km-wide section, to a depth of several hundred meters; the suite includes rocks that vary from non- to intensely metasomatized. Large sample sets of this type are rare, and the current data provide an outstanding opportunity to critically assess the potential of major element-based whole-rock geochemical exploration.

6.2.2. The Hauraki Goldfield and Hauraki Volcanic Region

The Hauraki Volcanic Region (HVR) was the main locus of subduction-related volcanism in northern New Zealand between 18 and 1.95 Ma, and records the eruption of basalts, andesites, dacites and rhyolites (Skinner, 1986; Adams et al., 1994; Briggs et al., 2005). The volcanic succession erupted onto Mesozoic Waipapa Terrane basement that is exposed in the northern Coromandel Peninsula, but progressively down-faulted to the south, where the Neogene volcanic succession completely covers the basement rocks. Regional fault sets strike NNE-NE and NW and have similar orientations to epithermal veins (Spörli et al., 2006).

Contained within the HVR is the Hauraki Goldfield, a 100 by 40 km metallogenic province that contains approximately 50 epithermal adularia-sericite Au-Ag deposits and several porphyry Cu-Au-Mo occurrences. Although epithermal deposits occur in andesites, rhyolites and basement rocks, over 97% of gold has been recovered from deposits hosted by altered andesites of the Coromandel Group (Christie et al., 2007). The Coromandel Group erupted between 18 and 2.5 Ma (Stipp, 1968; Adams et al., 1994) and comprises porphyritic basaltic andesites, andesites and dacites with a phenocryst association of plagioclase \pm augite \pm hypersthene with minor magnetite, with olivine in some basaltic andesites, and commonly including hornblende (Skinner, 1986). Analogous to modern counterparts in the central North Island (Price et al., 2005), Coromandel Group rocks are mixtures of a relatively silicic (dacitic to rhyolitic) melt, represented by the groundmass, and a gabbroic crystal cargo, which commonly occurs as complexly zoned crystals, angular crystal fragments and glomerocrysts.

Mining in the Hauraki Goldfield between 1852 and 1952 produced over 8 million ounces (Moz) of Au and 35.3 Moz Ag, and an additional 2.1 Moz Au and 12.1 Moz Ag were produced between 1987 and 2005 inclusive (Christie et al., 2007). Epithermal Au-Ag mineralization occurs in steeply dipping quartz



veins that generally fill normal faults opened by dip-slip movement in an extensional regime (Spörli et al., 2006, and references therein). Veins formed prior to 10 Ma variably strike NW to NE, whereas younger veins generally strike NE (Christie et al., 2007). The deposits occur in the central part of alteration aureoles that are 10 to 50 km² in size, in which volcanic rocks are intensely altered to an association of quartz, chlorite, illite and pyrite, with or without adularia, albite and calcite (Christie et al., 2007, and references therein).

6.2.3. Geology of the Waitekauri Area

In the southern Hauraki Goldfield, a ~20 km² magnetic quiet zone envelops epithermal deposits and prospects in the Waitekauri-Maratoto area and defines an area where magnetite has been destroyed by alteration. A ~24 km² zone of rocks with elevated K/Th overlaps with the magnetic quiet zone and represents the extent of rocks that experienced K metasomatism (Morrell et al., in press). This geophysically defined alteration zone corresponds closely to a geologically defined alteration zone mapped by Brathwaite and Christie (1996). The deposits within the alteration zone have non-overlapping ⁴⁰Ar/³⁹Ar ages (Golden Cross: 6.98 ± 0.11 Ma, Sovereign: 6.81 ± 0.06 to 6.56 ± 0.08 Ma, Maratoto: 6.41 ± 0.04 Ma, Komata: 6.06 ± 0.06 Ma), indicating that the altered zone includes separate hydrothermal alteration aureoles that overlap spatially to produce a large contiguous alteration zone (Mauk et al., in press; Morrell et al., in press).

The altered rock sample set on which this paper is based comprises rocks of the Waitekauri area, which forms the southern half (12.7 km²) of the Waitekauri-Maratoto area and contains the historic workings of the Sovereign, Jubilee and Scotia deposits, and the Jasper Creek, Scimitar and Teutonic prospects (Simpson and Mauk, in press). Prior to 1930, the Sovereign, Jubilee and Scotia deposits produced 392 kg Au-Ag bullion, with 78% mined from Jubilee (Downey, 1935). These deposits and prospects occur in altered Coromandel Group rocks of the Waipupu Formation and the Mangakara and Waitekauri dacites (Fig. 6.1C). The Waipupu Formation consists of lava flows and breccias of porphyritic plagioclase + hypersthene + augite andesite and dacite, locally with quartz or resorbed hornblende. Potassium-argon ages range between 7.9 and 6.3 Ma, however, only the older ages are geologically plausible eruption ages (Brathwaite and Christie, 1996). The Waipupu Formation is the main host rock at Sovereign, Jasper Creek and at depth at Scotia. The Mangakara Dacite overlies the Waipupu Formation and comprises porphyritic plagioclase + quartz + pyroxene + hornblende lava flows that host the Teutonic prospect. A single K-Ar date indicates a minimum age of 6.9 ± 0.5 Ma (Brathwaite and Christie, 1996). The Waitekauri Dacite

overlies both the Waipupu Formation and the Mangakara Dacite and is inferred to be similar in age to the latter. It is the main host rock at the Scotia and Jubilee deposits, and comprises plagioclase + hornblende + pyroxene + quartz lava flows. In addition, altered dykes of the Maratoto Rhyolite occur locally in drill core, underground and at the surface, predominantly at Jubilee (Haworth and Briggs, 2006). On the flanks of the Waitekauri Valley, these older formations are overlain by younger, unaltered Whakamoehau Andesite, which has K-Ar dates of 6.7 and 6.6 Ma (Brathwaite and Christie, 1996). Northeast-striking faults dominate the structure and include the major Waitekauri Fault (Figs. 6.1C-D). The Sovereign and Jubilee deposits occur to the east and west of the Waitekauri Fault, respectively, whereas Scimitar, Scotia, Teutonic and Jasper Creek are located progressively farther to the east (Fig. 6.1C).

Simpson and Mauk (in press) provide detailed descriptions of the nature and distribution of the alteration mineralogy; we provide a summary here. Host rocks in the Waitekauri area are typically intensely altered, with 100% of igneous minerals replaced at Sovereign, Jubilee, Scotia and Scimitar. The alteration intensity is more variable on the eastern margin of Scotia and Scimitar, as well as at Teutonic and in the deepest drill hole at Jasper Creek, and is characterized by moderately to weakly altered rocks where 20 to 50% of the igneous minerals have been replaced by hydrothermal minerals. Moderately altered rocks show partial replacement of plagioclase and magnetite, and complete replacement of mafic minerals and groundmass interstitial glass. In weakly altered rocks where less than 20% of igneous minerals are replaced by alteration minerals, augite and some hypersthene are partially preserved, and plagioclase and magnetite are essentially unaltered. The common alteration minerals in host rocks are quartz (SiO_2), adularia (KAlSi_3O_8), illite (e.g. K mica, $\text{KAl}_3\text{Si}_3\text{O}_{10}(\text{OH})_2$), smectite ($(\text{Na,Ca})_{0.33}(\text{Al,Mg})_2\text{Si}_4\text{O}_{10}(\text{OH})_2 \cdot n\text{H}_2\text{O}$), interstratified illite-smectite, chlorite (e.g. $(\text{Mg,Fe}^{2+})_5\text{Al}_2\text{Si}_3\text{O}_{10}(\text{OH})_8$), calcite (CaCO_3) and pyrite (FeS_2), with minor albite ($\text{NaAlSi}_3\text{O}_8$) and rare epidote, hematite, corrensite and chlorite-smectite. Petrographic data indicate that adularia and albite were among the first alteration minerals to form. Illite invariably replaces adularia; calcite commonly occurs as a late replacement mineral that overprints adularia and illite. The dominant clay species in altered host rocks is illite at Jubilee, westernmost Scimitar and Sovereign; interstratified illite-smectite at Scotia and Scimitar; and smectite at Jasper Creek and Teutonic. Quartz is dominant in epithermal veins at Sovereign and Jubilee and also occurs in stockwork veins at Scotia, whereas calcite is more abundant in veins at Scotia, Scimitar and Jasper Creek. Fluid inclusions

Table 6.1 (following pages) Representative geochemical analyses of Waitekauri area altered rocks. Major element and S concentrations are given in wt%, minor and trace element concentrations in ppm. All analyses by XRF except italicized elements by ICPMS, and Au concentrations determined by fire assay.

Table 6.1	AU number	Core-depth (m)	SiO ₂	TiO ₂	Al ₂ O ₃	Fe ₂ O ₃	MnO	MgO	CaO	Na ₂ O	K ₂ O	P ₂ O ₅	Sum oxides
Jubilee	AU59868	WV06-154	63.40	0.54	15.12	6.21	0.49	3.86	2.92	0.00	3.71	0.10	96.3
Jubilee	AU59878	WV06-351	71.47	0.63	15.02	2.63	0.06	4.62	0.36	0.00	3.50	0.11	98.4
Jubilee	AU59845	WV07-050	64.21	0.65	15.80	6.00	0.10	4.28	3.78	0.04	2.54	0.04	97.4
Jubilee	AU59847	WV07-135	67.13	0.43	14.85	4.01	0.08	1.82	3.41	2.98	2.87	0.09	97.7
Jubilee	AU59850	WV08-020	58.60	0.83	20.01	9.49	0.09	2.88	1.17	0.08	4.41	0.15	97.7
Jubilee	AU59858	WV08-246	61.34	0.97	17.31	8.51	0.07	5.35	0.40	0.75	3.96	0.14	98.8
Scotia	AU59882	SC27-082	66.84	0.49	14.51	4.97	0.06	3.70	0.37	0.14	6.89	0.09	98.1
Scotia	AU59895	SC27-356	62.08	0.68	16.55	5.84	0.09	2.26	4.50	2.54	2.94	0.13	97.6
Scotia	AU59915	SC28-048	72.19	0.47	13.57	2.56	0.01	0.66	0.34	0.33	8.09	0.09	98.3
Scotia	AU59919	SC28-175a	64.44	0.57	16.67	5.06	0.10	2.61	3.67	2.14	2.81	0.10	98.2
Scotia	AU59924	SC33-164	64.15	0.57	16.49	5.03	0.07	2.21	3.61	0.53	5.07	0.11	97.8
Scotia	AU59911	SC36-026	65.83	0.53	20.79	0.74	0.00	0.10	0.17	0.40	9.35	0.30	98.2
Scotia	AU59930	WV02-036	68.05	0.58	16.44	4.17	0.03	2.28	1.77	2.00	2.81	0.11	98.2
Scotia	AU59935	WV02-276	67.38	0.48	14.42	3.26	0.05	1.50	5.39	1.43	2.36	0.10	96.4
Scotia	AU59898	WV04-073	72.42	0.56	17.08	2.03	0.03	0.87	0.81	0.00	4.63	0.03	98.5
Scotia	AU59910	WV04-385	57.02	0.74	16.68	7.19	0.15	5.04	6.94	0.79	3.20	0.15	97.9
Jasper Creek	AU59981	JC15-156	64.02	0.58	16.57	5.71	0.10	2.90	5.21	0.49	3.26	0.10	98.9
Jasper Creek	AU59973	JC17-096	65.53	0.56	16.15	4.65	0.07	3.24	4.24	0.06	3.55	0.10	98.2
Jasper Creek	AU59987	JC20-052	73.19	0.57	14.07	4.30	0.03	2.37	0.79	0.03	3.29	0.09	98.7
Jasper Creek	AU59956	WV09-208	63.60	0.52	15.03	5.27	0.12	3.12	6.38	2.51	2.35	0.10	99.0
Jasper Creek	AU59968	WV09-466	68.85	0.51	15.19	4.34	0.10	2.14	4.30	0.93	2.25	0.10	98.7
Sovereign	AU59767	ML01-027	76.93	0.23	13.40	1.53	0.00	0.19	0.01	0.01	6.86	0.02	99.2
Sovereign	AU59751	ML11-147	61.10	0.88	20.13	7.84	0.14	3.78	0.22	0.06	5.03	0.14	99.3
Sovereign	AU59754	ML11-293	66.14	0.72	15.75	6.34	0.10	3.31	0.22	0.02	6.04	0.13	98.8
Sovereign	AU59737	ML12-022	65.34	0.71	15.84	6.28	0.09	2.44	0.06	0.05	8.07	0.06	98.9
Sovereign	AU59745	ML12-315	64.51	0.76	17.76	6.72	0.08	3.47	0.32	0.02	5.09	0.16	98.9
Sovereign	AU59727	ML13-017	50.36	1.08	27.46	9.71	0.07	8.64	0.67	0.19	0.96	0.20	99.3
Sovereign	AU59730	ML13-171	62.54	0.72	16.94	7.31	0.05	2.89	0.69	2.88	4.97	0.11	99.1
Sovereign	AU59765	ML23-017	78.15	0.17	12.46	6.43	-0.00	0.07	0.00	0.00	1.94	0.13	99.4
Sovereign	AU59762	ML06-085	63.28	0.84	17.26	6.71	0.13	1.84	0.12	0.07	8.76	0.09	99.1
Sovereign	AU59746	ML07-036	67.91	0.68	19.93	3.41	0.01	0.78	0.01	0.00	5.66	0.12	98.5
Sovereign	AU59748	ML07-142	70.61	0.62	14.34	4.51	0.05	1.99	0.04	0.01	6.66	0.06	98.9
Sovereign	AU59757	WV01-225	77.88	0.31	10.82	1.89	0.01	0.59	0.12	0.01	7.36	0.09	99.1
Sovereign	AU59760	WV01-382	60.39	0.75	15.07	7.31	0.12	4.44	5.73	1.11	2.25	0.14	97.3
Scimitar	AU59791	WV11-089	79.25	0.22	14.12	0.96	0.01	0.61	0.14	0.07	3.71	0.02	99.1
Scimitar	AU59802	WV11-477	59.45	0.92	19.02	6.24	0.12	2.48	2.87	0.10	5.34	0.16	96.7
Scimitar	AU59805	WV12-086	72.54	0.53	15.59	3.94	0.01	1.06	0.30	0.11	5.64	0.11	99.8
Scimitar	AU59810	WV15-125	63.47	0.73	19.55	6.77	0.09	2.34	2.30	0.51	3.02	0.08	98.9
Scimitar	AU59821	WV15-501	58.04	0.90	19.09	10.29	0.16	3.22	1.69	3.92	2.19	0.17	99.7
Teutonic	AU59833	WV10-067	71.68	0.43	14.37	4.09	0.05	1.15	2.55	2.46	2.89	0.08	99.8
Teutonic	AU59842	WV10-383	73.72	0.43	14.44	2.65	0.04	0.80	3.05	1.72	2.49	0.09	99.4
	AU59824	WV14-141	66.71	0.53	15.71	4.80	0.09	3.01	4.38	2.51	2.19	0.10	100.0

Table 6.1 (ct'd)	Jubilee	Jubilee	Jubilee	Jubilee	Jubilee	Jubilee	Scotia	Scotia	Scotia	Scotia	Scotia
AU number	AU59868	AU59878	AU59845	AU59847	AU59850	AU59858	AU59882	AU59895	AU59915	AU59919	AU59924
Li	48.4	97.7	112.0	44.6	35.2	110.0	91.0	88.4	66.0	95.9	90.0
Be	0.81	1.06	0.87	1.03	0.78	0.96	0.87	1.18	0.94	0.97	0.97
S (%)	2.57	1.34	0.94	0.35	6.48	0.10	1.05	0.71	1.51	0.19	0.53
Sc	18	26	27	14	38	35	21	24	21	20	25
V	130	150	170	77	285	260	134	145	112	133	151
Cr	217	134	114	30	108	86	85	42	82	135	147
Co	22.4	19.8	22.3	18.0	47.8	30.6	21.6	21.2	43.2	17.8	27.3
Ni	20	31	54	10	33	30	19	12	13	17	20
Cu	10	5	19	6	284	28	7	17	10	15	16
Zn	47	22	71	37	47	93	47	59	50	59	61
Ga	16	15	16	13	22	18	15	17	13	16	16
Ge	0.16	0.13	0.15	0.14	0.24	0.18	0.14	0.16	0.11	0.14	0.14
As	31.6	6.2	79.3	2.7	61.6	3.7	151.0	86.6	192.0	13.3	78.9
Se	3	3	3	2	17	3	2	2	2	1	2
Rb	177	165	143	104	283	205	288	106	358	104	220
Sr	24	14	40	152	52	72	103	260	166	261	123
Y	24	22	28	20	34	37	29	26	24	20	25
Zr	144	139	144	133	114	105	118	140	108	127	119
Nb	6	6	5	6	5	5	5	6	5	5	5
Mo	1.19	63.10	5.73	0.87	2.41	0.14	0.12	0.47	0.87	0.09	0.46
Ag	0.34	0.80	0.13	0.06	0.45	0.07	0.46	0.18	0.69	0.07	0.42
Cd	0.05	<0.02	0.05	0.02	0.11	0.05	<0.02	0.03	0.02	0.06	0.05
In	0.040	0.027	0.038	0.025	0.321	0.043	0.026	0.034	0.023	0.036	0.037
Sn	1.3	7.4	1.3	1.1	2.1	1.0	0.6	1.3	0.7	1.2	1.0
Sb	5.66	0.48	2.08	0.48	6.61	1.85	3.24	2.30	14.15	1.94	3.42
Te	0.61	0.44	0.05	<0.05	0.72	<0.05	<0.05	<0.05	<0.05	<0.05	<0.05
Cs	9.25	7.05	9.12	6.18	15.80	15.40	6.30	8.43	11.50	5.89	14.05
Ba	676	254	369	810	441	347	765	778	504	588	827
La	13	9	11	15	9	17	14	12	9	14	13
Ce	24	28	29	29	27	32	37	34	32	28	30
Hf	0.9	1.3	3.5	1.7	1.3	2.5	1.0	3.0	0.9	2.0	1.6
Ta	0.46	0.38	0.42	0.52	0.28	0.35	0.41	0.48	0.45	0.45	0.43
Re	<0.002	1.375	<0.002	<0.002	0.194	<0.002	<0.002	<0.002	0.003	<0.002	<0.002
Au	<0.005	0.009	0.065	<0.005	<0.005	<0.005	0.146	0.018	0.031	<0.005	0.018
Hg	0.01	<0.01	0.01	0.01	0.05	0.01	0.01	0.01	0.71	0.06	0.25
Tl	1.73	1.78	1.44	0.80	2.55	1.78	4.21	1.20	5.85	1.00	2.91
Pb	10	6	3	9	16	7	7	9	6	10	6
Bi	0.01	0.54	0.69	0.02	3.01	0.02	0.01	0.00	0.00	0.08	0.04
Th	7.1	4.8	6.8	8.9	5.6	4.3	6.4	5.0	5.9	8.3	6.5
U	2.2	0.3	2.0	2.9	0.0	0.7	0.6	1.9	0.0	1.9	0.8
molar K/Al	0.27	0.25	0.17	0.21	0.24	0.25	0.51	0.19	0.65	0.18	0.33
molar (K+Na+2Ca)/Al	0.62	0.30	0.61	0.96	0.35	0.36	0.58	0.94	0.73	0.79	0.78
molar K/(K+Na+2Ca)	0.43	0.85	0.28	0.22	0.68	0.69	0.89	0.20	0.88	0.23	0.42
100/Zr/TiO ₂	2.67	2.21	2.22	3.08	1.38	1.08	2.40	2.05	2.29	2.22	2.09
Easting (m)	2754951	2754833	2754390	2754341	2754516	2754671	2755335	2755494	2755564	2755490	2755712
Northing (m)	6420933	6420974	6420910	6420934	6421018	6420876	6420727	6420732	6420533	6420578	6420684
Elevation (m asl)	183	30	362	297	315	230	169	-54	135	42	56

Table 6.1 (ct'd)	Scotia	Scotia	Scotia	Scotia	Scotia	Jasper Creek	Sovereign				
AU number	AU59911	AU59930	AU59935	AU59898	AU59910	AU59981	AU59973	AU59987	AU59956	AU59968	AU59767
Li	25.4	102.0	97.3	67.6	74.5	89.0	155.5	110.0	27.2	29.5	11.4
Be	0.92	1.04	1.03	1.20	0.96	0.93	0.87	1.07	0.80	0.86	0.90
S (%)	1.03	0.59	0.04	0.52	1.40	<0.01	0.55	1.17	<0.01	0.33	0.01
Sc	21	22	22	19	27	21	21	21	21	15	6
V	125	133	108	162	172	42	135	76	96	94	22
Cr	61	147	92	96	86	41	66	18	78	84	5
Co	8.0	18.4	15.0	23.0	24.0	19.5	18.4	14.8	20.5	14.3	19.9
Ni	37	16	14	17	26	13	16	6	16	10	2
Cu	9	12	7	9	25	13	15	2	17	8	3
Zn	9	40	32	49	77	45	46	52	49	36	7
Ga	16	16	14	18	16	15	16	14	14	14	13
Ge	0.15	0.12	0.16	0.13	0.16	0.16	0.12	0.11	0.14	0.14	0.07
As	364.0	30.6	3.9	128.0	6.9	1.9	66.7	232.0	2.4	75.8	176.0
Se	2	2	2	2	2	2	1	2	2	3	2
Rb	354	145	106	230	150	120	129	181	66	74	297
Sr	381	214	150	51	92	182	149	52	199	95	55
Y	37	18	20	21	21	20	21	23	19	18	27
Zr	142	122	112	119	115	114	109	109	95	110	124
Nb	7	5	5	6	5	5	5	6	4	4	7
Mo	0.38	0.16	0.19	0.30	0.67	<0.05	0.38	0.19	0.24	0.78	1.24
Ag	0.63	0.11	0.03	0.03	0.41	0.03	0.83	0.11	0.03	0.03	0.60
Cd	<0.02	<0.02	<0.02	0.15	0.02	0.04	0.04	0.05	0.13	0.02	0.02
In	0.026	0.032	0.025	0.035	0.034	0.028	0.033	0.023	0.037	0.019	0.020
Sn	1.0	1.0	0.7	1.1	1.1	0.9	1.2	1.0	1.6	1.0	1.5
Sb	12.25	3.91	1.34	26.90	1.34	6.74	8.83	13.45	0.33	6.42	7.40
Te	<0.05	<0.05	<0.05	<0.05	0.10	<0.05	<0.05	<0.05	<0.05	<0.05	0.05
Cs	6.78	16.00	10.85	24.20	7.36	37.50	16.20	16.70	1.88	5.30	5.32
Ba	1244	180	388	925	341	761	429	453	598	530	558
La	17	11	14	13	12	14	10	15	9	13	16
Ce	40	32	23	38	30	23	31	36	28	35	35
Hf	1.5	2.1	0.8	1.6	2.0	2.1	1.9	2.0	2.5	1.3	1.8
Ta	0.54	0.39	0.47	0.48	0.36	0.41	0.36	0.39	0.35	0.42	0.63
Re	<0.002	<0.002	<0.002	<0.002	<0.002	<0.002	<0.002	<0.002	<0.002	<0.002	0.003
Au	0.063	0.006	<0.005	<0.005	<0.005	0.008	0.055	0.015	<0.005	<0.005	0.230
Hg	0.48	0.04	0.01	1.12	0.09	0.04	0.33	0.09	<0.01	0.23	0.07
Tl	5.53	0.94	0.60	6.45	1.58	0.57	2.09	1.50	0.34	0.31	4.92
Pb	9	7	5	10	8	7	6	8	8	8	6
Bi	0.03	0.02	0.01	0.02	0.03	0.03	0.19	0.02	0.00	0.01	0.01
Th	8.1	6.5	7.0	8.1	3.5	6.7	6.4	5.3	6.0	7.3	12.7
U	0.0	2.6	1.8	1.9	1.3	2.2	2.1	1.2	2.7	3.6	1.4
molar K/Al	0.49	0.19	0.18	0.29	0.21	0.21	0.24	0.25	0.17	0.16	0.55
molar (K+Na+2Ca)/Al	0.53	0.58	1.02	0.38	1.04	0.83	0.72	0.36	1.22	0.78	0.56
molar K/(K+Na+2Ca)	0.91	0.32	0.17	0.77	0.20	0.26	0.33	0.71	0.14	0.21	0.99
100/Zr/TiO ₂	2.68	2.10	2.34	2.13	1.55	1.97	1.95	1.92	1.83	2.15	5.47
Easting (m)	2755555	2756191	2756005	2755421	2755236	2756753	2756630	2756665	2756561	2756745	2754379
Northing (m)	6420747	6420630	6420633	6420774	6420830	6421126	6421172	6420888	6421126	6421098	6420481
Elevation (m asl)	211	102	-51	190	-55	74	93	94	-5	-182	336

Table 6.1 (ct'd)	Sovereign										
AU number	AU59751	AU59754	AU59737	AU59745	AU59727	AU59730	AU59765	AU59762	AU59746	AU59748	AU59757
Li	77.8	65.8	56.3	49.9	243.0	59.1	19.4	41.2	9.0	44.8	28.7
Be	1.20	1.19	0.60	0.98	1.44	0.80	0.44	0.76	0.83	0.99	0.57
S (%)	0.17	2.13	2.31	3.63	0.05	3.83	0.02	0.51	1.93	1.70	1.03
Sc	31	30	27	27	37	29	2	35	30	24	12
V	223	216	201	181	178	175	16	277	194	198	84
Cr	168	94	60	79	58	167	7	87	315	139	34
Co	25.9	24.7	24.3	25.0	24.1	35.8	24.4	29.4	52.1	24.5	51.9
Ni	27	17	28	26	32	66	4	25	97	23	9
Cu	14	9	17	17	15	37	17	20	30	33	8
Zn	137	58	93	58	131	78	13	84	46	56	30
Ga	19	16	17	18	22	15	7	17	16	14	9
Ge	0.09	0.11	0.09	0.1	0.1	0.11	0.1	0.11	0.16	0.13	0.11
As	27.6	44.6	127.0	20.1	1.2	13.2	364.0	48.7	93.2	273.0	181.5
Se	2	2	2	2	2	1	1	1	4	2	2
Rb	243	278	325	226	42	190	80	353	303	273	292
Sr	35	68	55	32	33	180	22	93	76	66	70
Y	30	26	24	23	81	22	8	25	154	32	22
Zr	149	98	108	118	192	111	88	101	134	88	71
Nb	7	6	5	6	8	5	5	6	7	5	5
Mo	0.58	0.92	0.95	0.69	0.06	1.59	1.17	0.26	0.48	2.25	5.07
Ag	0.07	0.89	1.04	0.89	0.07	1.77	0.37	0.77	1.46	0.96	1.46
Cd	0.09	0.03	0.05	0.02	0.07	0.11	0.02	0.06	0.12	0.17	0.11
In	0.050	0.047	0.050	0.043	0.058	0.045	0.020	0.048	0.040	0.035	0.020
Sn	1.3	1.1	1.0	1.1	1.9	1.1	0.7	1.3	1.3	1.2	1.3
Sb	4.67	3.64	2.93	2.98	0.50	3.11	18.05	3.16	3.28	6.38	15.65
Te	0.05	0.23	0.05	0.62	0.05	0.11	1.59	0.05	0.06	0.11	0.05
Cs	17.15	12.40	6.73	8.69	5.20	4.42	1.83	7.67	12.95	7.49	7.00
Ba	248	804	536	526	129	463	144	412	676	723	683
La	14	11	7	11	33	7	21	11	30	18	14
Ce	40	23	22	21	74	21	56	24	71	41	31
Hf	2.6	1.5	1.2	1.3	4.9	1.3	1.2	1.8	1.4	1.3	1.6
Ta	0.43	0.38	0.25	0.36	0.51	0.31	0.50	0.45	0.34	0.42	0.47
Re	0.002	0.002	0.002	0.002	0.002	0.006	0.002	0.002	0.004	0.002	0.004
Au	0.005	0.008	0.059	0.009	0.005	0.012	0.401	0.020	0.023	0.131	0.131
Hg	0.06	0.08	0.08	0.03	0.04	0.17	0.16	0.09	0.07	0.05	0.33
Tl	2.43	3.40	5.86	2.09	0.43	2.39	1.41	4.70	3.45	3.27	4.92
Pb	6	11	5	18	3	15	46	8	14	9	13
Bi	0.03	0.08	0.08	0.51	0.01	0.07	0.01	0.04	0.48	0.02	0.15
Th	6.9	6.3	3.4	3.9	6.9	4.2	9.9	7.6	4.5	5.8	8.9
U	0.3	0.0	0.0	0.5	3.8	0.7	3.5	1.3	0.0	1.4	1.8
molar K/Al	0.27	0.42	0.55	0.31	0.04	0.32	0.17	0.55	0.31	0.50	0.74
molar (K+Na+2Ca)/Al	0.29	0.44	0.56	0.34	0.09	0.67	0.17	0.57	0.31	0.51	0.76
molar K/(K+Na+2Ca)	0.92	0.94	0.98	0.90	0.40	0.47	1.00	0.97	1.00	0.99	0.97
100/Zr/TiO ₂	1.70	1.35	1.51	1.55	1.78	1.53	5.08	1.20	1.97	1.41	2.26
Easting (m)	2754194	2754267	2753996	2754123	2753843	2753928	2754334	2754197	2754091	2754137	2754037
Northing (m)	6420548	6420544	6420643	6420570	6420783	6420734	6420452	6420519	6420583	6420556	6420659
Elevation (m asl)	256	124	356	95	382	261	324	321	263	269	219

Table 6.1 (ct'd)	Sovereign	Scimitar	Scimitar	Scimitar	Scimitar	Scimitar	Teutonic	Teutonic	
AU number	AU59760	AU59791	AU59802	AU59805	AU59810	AU59821	AU59833	AU59842	AU59824
Li	100.5	31.6	39.0	25.7	51.3	43.4	39.7	58.6	24.8
Be	0.71	0.81	1.15	1.18	1.16	0.82	1.34	0.81	1.10
S (%)	1.01	0.50	3.51	2.92	0.51	2.34	<0.01	0.70	<0.01
Sc	28	5	21	17	20	21	12	12	16
V	210	19	170	126	140	181	70	73	105
Cr	92	3	38	73	49	36	20	15	48
Co	31.0	9.2	20.2	36.1	26.2	23.7	16.9	28.2	23.1
Ni	26	0	21	19	14	17	9	4	17
Cu	10	6	33	11	17	29	10	12	17
Zn	63	27	66	37	139	99	55	38	55
Ga	16	14	17	16	19	16	12	11	16
Ge	0.13	0.12	0.18	0.16	0.15	0.18	0.11	0.13	0.15
As	25.3	230.0	62.5	171.0	122.0	123.5	2.1	176.0	2.9
Se	2	2	2	2	2	2	1	1	2
Rb	108	173	265	303	175	104	148	98	78
Sr	56	17	41	36	38	294	251	174	245
Y	20	18	27	21	25	25	26	20	18
Zr	105	132	127	136	176	124	156	134	134
Nb	5	6	6	6	8	6	6	5	6
Mo	0.75	2.47	0.63	1.09	0.33	0.62	0.62	1.86	0.54
Ag	0.74	0.18	0.23	1.61	0.14	0.26	0.03	0.36	0.02
Cd	0.02	0.04	0.07	0.04	0.04	0.07	0.05	0.04	0.05
In	0.045	0.023	0.050	0.029	0.039	0.044	0.026	0.013	0.036
Sn	1.3	2.0	1.2	1.3	1.8	1.2	1.5	0.8	1.3
Sb	2.08	5.95	1.77	11.25	4.72	2.54	1.15	8.37	0.44
Te	0.05	<0.05	0.18	<0.05	<0.05	0.39	<0.05	<0.05	<0.05
Cs	5.27	8.97	17.25	13.35	24.90	6.40	7.53	17.65	3.13
Ba	274	198	410	647	386	220	972	493	486
La	10	19	11	20	23	12	23	16	21
Ce	28	51	35	31	33	33	47	40	35
Hf	1.7	3.4	1.8	2.2	3.2	1.4	2.1	2.3	2.6
Ta	0.37	0.69	0.39	0.46	0.53	0.40	0.54	0.50	0.50
Re	0.002	<0.002	<0.002	0.002	0.002	<0.002	0.002	<0.002	0.002
Au	0.005	0.115	0.035	0.040	0.034	0.049	0.026	0.081	0.008
Hg	0.05	0.07	<0.01	0.24	0.03	0.01	<0.01	0.37	<0.01
Tl	0.94	1.93	2.61	3.94	0.98	0.89	0.39	0.39	0.31
Pb	7	17	11	10	11	10	19	9	12
Bi	0.14	0.18	0.05	0.06	0.05	0.03	0.03	0.01	0.08
Th	3.4	11.0	8.0	5.0	10.0	5.0	11.0	9.0	9.0
U	2.0	3.0	0.6	1.6	1.5	0.6	1.6	1.4	1.8
molar K/Al	0.16	0.28	0.30	0.39	0.17	0.12	0.22	0.19	0.15
molar (K+Na+2Ca)/Al	0.97	0.31	0.59	0.44	0.42	0.62	0.82	0.77	0.92
molar K/(K+Na+2Ca)	0.17	0.92	0.52	0.89	0.39	0.20	0.26	0.24	0.16
100/Zr/TiO ₂	1.39	6.00	1.38	2.57	2.41	1.38	3.63	3.12	2.53
Easting (m)	2753954	2754934	2754628	2755007	2755226	2754902	2755573	2755774	2755258
Northing (m)	6420698	6420012	6420101	6419980	6419900	6419954	6419541	6419437	6420279
Elevation (m asl)	88	166	-58	138	92	-88	105	-115	99

trapped in quartz and calcite yield homogenization temperatures of ca. 240°C at Sovereign, Jubilee and Scimitar, 204°C at Scotia and ca. 165°C at Teutonic and Jasper Creek (Simpson and Mauk, in press).

6.2.4. Sample Selection and Analytical Methods

The altered rock sample set on which this paper is based comprises 127 altered rocks that were chemically analyzed, selected from a suite of 225 rocks whose alteration mineralogy was studied in detail. The samples are spaced at approximately 50 to 100 m intervals in drill cores obtained by Newmont Mining Corporation along WNW-striking transects that stretch from the Waitekauri Fault to the eastern edge of the Waitekauri area alteration zone. This study only determined the geochemistry of altered host rocks, and we avoided inclusion of veins, which typically host Au-Ag mineralization and pathfinder elements such as As, Sb and Hg. This approach differs from standard industry practice, which determines total grade over a specified interval including veins, and makes it possible to directly compare the geochemistry of altered host rocks to that of unaltered equivalent rocks.

Unaltered Coromandel Group volcanic rocks (N=98) were selected from collections at the University of Auckland and at GNS Science. These were originally collected and petrographically described for mapping and research. All samples are lavas because these are the freshest, best-preserved rocks, and represent massive flows, breccias, dykes, and massive boulders in reworked deposits. For all rocks, 100-150 g was pulverized in a tungsten-carbide ring mill. Major element concentrations were determined on fused glass beads at the University of Auckland. For major elements the analytical precision error is negligible compared to the reproducibility of the sample splitting process, which is better than 1% based on repeat analyses of three internal standard reference powders. Trace element ICP-MS analyses were performed by ALS Chemex in Vancouver, Canada. The concentrations of trace elements other than Hg and Au were determined in solution by ICP-MS following near-total digestion by hydrochloric, nitric, perchloric and hydrofluoric acids of powdered sample aliquots. Hg concentration was determined by cold vapor atomic absorption spectrometry following aqua regia digestion, and Au concentration by atomic absorption spectrometry following fire assaying. Reproducibility, including sample splitting, is better than 10% for most trace elements. Following standard practice we report major elements (Na, Mg, Al, Si, P, K, Ca, Ti, Mn, Fe) as their respective oxides (Na_2O , MgO , Al_2O_3 , SiO_2 , P_2O_5 , K_2O , CaO , TiO_2 , MnO , Fe_2O_3). Fe_2O_3 represents total iron oxide because the analyses were performed on oxidized material. Major element oxide concentration totals were greater than 97% except in some samples with a high S concentration. The mineralogy of the altered rocks was qualitatively determined using X-ray diffraction

Table 6.2

A. Unaltered Coromandel Group rocks.

N=98	SiO ₂	TiO ₂	Al ₂ O ₃	Fe ₂ O ₃	MgO	CaO	Na ₂ O	K ₂ O	Cu	As	Rb	Sr	Zr	Ag	Sb	Ba	Hg	Tl	K#
TiO ₂	-0.69																		
Al ₂ O ₃	-0.50	0.65																	
Fe ₂ O ₃	-0.92	0.75	0.42																
MgO	-0.70	0.08	-0.15	0.56															
CaO	-0.89	0.41	0.22	0.74	0.82														
Na ₂ O	0.30	0.23	0.35	-0.25	-0.70	-0.55													
K ₂ O	0.81	-0.49	-0.41	-0.69	-0.66	-0.81	0.22												
Cu	-0.39	0.03	-0.00	0.33	0.47	0.44	-0.30	-0.37											
As	0.06	0.06	-0.07	-0.01	-0.09	-0.04	-0.09	0.15	-0.01										
Rb	0.77	-0.48	-0.40	-0.68	-0.59	-0.79	0.24	0.94	-0.33	0.16									
Sr	-0.24	0.23	0.11	0.26	0.06	0.31	-0.29	-0.11	-0.03	0.24	-0.19								
Zr	0.24	0.35	0.18	-0.11	-0.59	-0.44	0.54	0.38	-0.39	0.17	0.41	0.03							
Ag	-0.12	0.09	0.13	0.12	0.01	0.07	-0.04	0.03	0.15	0.09	-0.00	0.23	0.10						
Sb	0.08	-0.03	-0.08	-0.04	-0.02	-0.02	-0.25	0.07	0.02	0.60	0.10	0.20	0.08	0.00					
Ba	0.77	-0.48	-0.48	-0.66	-0.55	-0.67	0.07	0.81	-0.34	0.28	0.77	0.02	0.39	-0.00	0.22				
Hg	-0.13	0.21	0.06	0.18	0.04	0.07	-0.01	-0.06	-0.06	-0.04	-0.05	-0.02	0.15	0.04	-0.10	-0.19			
Tl	0.36	-0.17	-0.14	-0.34	-0.29	-0.34	0.05	0.44	-0.25	0.25	0.55	-0.05	0.28	-0.06	0.26	0.42	-0.03		
K#	0.87	-0.51	-0.43	-0.73	-0.69	-0.87	0.24	0.99	-0.39	0.13	0.93	-0.14	0.36	-0.01	0.09	0.81	-0.07	0.44	
Zr/TiO ₂	0.88	-0.71	-0.52	-0.83	-0.56	-0.75	0.21	0.78	-0.34	0.03	0.78	-0.24	0.38	-0.05	0.06	0.77	-0.11	0.38	0.79

B. Altered rocks with molar K/(K+Na+2Ca) less than 0.50.

N=71	SiO ₂	TiO ₂	Al ₂ O ₃	Fe ₂ O ₃	MgO	CaO	Na ₂ O	K ₂ O	Cu	As	Rb	Sr	Zr	Ag	Sb	Ba	Hg	Tl	K#
TiO ₂	-0.78																		
Al ₂ O ₃	-0.73	0.83																	
Fe ₂ O ₃	-0.73	0.85	0.70																
MgO	-0.68	0.56	0.59	0.67															
CaO	-0.51	0.08	-0.02	0.00	0.16														
Na ₂ O	0.09	-0.15	-0.14	-0.11	-0.31	-0.07													
K ₂ O	0.07	-0.09	-0.13	-0.19	-0.34	-0.13	-0.29												
Cu	-0.48	0.57	0.36	0.57	0.43	0.08	0.06	0.05											
As	-0.03	0.08	0.19	0.08	-0.11	-0.16	-0.21	0.21	-0.01										
Rb	-0.05	0.07	0.02	-0.03	-0.20	-0.12	-0.44	0.91	0.07	0.31									
Sr	0.06	-0.11	-0.04	-0.14	-0.22	0.02	0.71	-0.25	0.11	-0.04	-0.38								
Zr	-0.01	0.16	0.41	0.06	-0.04	-0.31	0.00	0.05	-0.20	0.19	0.14	-0.05							
Ag	-0.14	0.21	0.05	0.28	0.19	-0.11	-0.24	0.30	0.27	0.19	0.29	-0.17	-0.26						
Sb	0.23	-0.07	-0.04	-0.13	-0.17	-0.27	-0.30	0.27	-0.19	0.44	0.24	-0.15	0.00	0.25					
Ba	0.43	-0.48	-0.39	-0.56	-0.46	-0.09	0.20	0.30	-0.26	-0.17	0.09	0.29	0.18	-0.20	0.05				
Hg	0.31	-0.22	-0.12	-0.31	-0.25	-0.17	-0.08	0.19	-0.15	0.24	0.06	0.04	0.03	0.21	0.66	0.29			
Tl	-0.21	0.24	0.15	0.15	0.00	-0.13	-0.39	0.82	0.21	0.33	0.85	-0.28	-0.01	0.47	0.27	0.01	0.17		
K#	0.24	0.02	0.11	-0.02	-0.13	-0.67	-0.42	0.69	-0.02	0.28	0.69	-0.42	0.28	0.30	0.37	0.09	0.17	0.64	
Zr/TiO ₂	0.67	-0.74	-0.46	-0.69	-0.53	-0.27	0.17	0.11	-0.59	0.02	0.02	0.07	0.51	-0.33	0.04	0.54	0.26	-0.25	0.14

Table 6.2 Correlation coefficient matrices for 18 elements' concentrations, molar K/(K+Na+2Ca) (noted as K#) and Zr/TiO₂.

A. Unaltered Coromandel Group rocks (N=98). B. Waitekauri area altered rocks with molar K/(K+Na+2Ca) < 1/2 (N=71). C.

Waitekauri area altered rocks with molar K/(K+Na+2Ca) ≥ 1/2 (N=57). Correlation coefficients equal to or greater than 0.50

or -0.50 are printed in bold.

C. Altered rocks with molar K/(K+Na+2Ca) equal to or greater than 0.50.

N=57	SiO ₂	TiO ₂	Al ₂ O ₃	Fe ₂ O ₃	MgO	CaO	Na ₂ O	K ₂ O	Cu	As	Rb	Sr	Zr	Ag	Sb	Ba	Hg	Tl	K#
TiO ₂	-0.76																		
Al ₂ O ₃	-0.66	0.73																	
Fe ₂ O ₃	-0.68	0.53	0.20																
MgO	-0.59	0.44	0.15	0.67															
CaO	-0.48	0.26	0.28	0.33	0.26														
Na ₂ O	-0.42	0.20	0.24	0.19	0.40	0.20													
K ₂ O	0.10	-0.12	-0.23	-0.32	-0.39	-0.30	-0.14												
Cu	-0.26	0.26	0.24	0.27	0.07	0.17	-0.00	-0.10											
As	0.42	-0.34	-0.39	-0.16	-0.46	-0.21	-0.16	0.24	-0.06										
Rb	0.01	-0.05	-0.14	-0.27	-0.35	-0.17	-0.12	0.93	0.00	0.18									
Sr	-0.14	-0.02	0.14	-0.27	-0.21	-0.07	0.42	0.52	-0.07	0.29	0.44								
Zr	-0.33	0.26	0.60	-0.09	0.10	0.20	0.22	-0.14	-0.07	-0.39	-0.05	0.06							
Ag	0.17	-0.03	-0.31	0.02	-0.18	-0.24	-0.22	0.30	0.10	0.33	0.27	-0.05	-0.31						
Sb	0.39	-0.31	-0.32	-0.10	-0.44	-0.06	-0.17	0.02	-0.07	0.65	0.01	0.08	-0.31	0.14					
Ba	-0.04	-0.07	0.05	-0.34	-0.23	-0.09	0.02	0.61	-0.07	0.08	0.56	0.58	0.10	-0.08	-0.06				
Hg	0.21	-0.21	-0.16	-0.21	-0.27	0.15	0.04	0.11	-0.09	0.31	0.10	0.26	-0.13	0.32	0.58	0.12			
Tl	0.27	-0.21	-0.30	-0.38	-0.50	-0.27	-0.18	0.85	-0.10	0.39	0.80	0.40	-0.26	0.42	0.38	0.45	0.45		
K#	0.56	-0.30	-0.33	-0.43	-0.48	-0.86	-0.51	0.53	-0.15	0.32	0.40	0.05	-0.25	0.34	0.11	0.19	-0.06	0.48	
Zr/TiO ₂	0.60	-0.76	-0.31	-0.53	-0.38	-0.16	-0.06	-0.15	-0.24	0.15	-0.17	-0.04	0.21	-0.19	0.14	-0.08	0.02	-0.06	0.15

Table 6.2 (continued).

for which procedures and results are described in Simpson and Mauk (in press). Representative chemical analyses of altered rocks from the Waitekauri area are listed in Table 6.1. The full dataset is available on request. The unaltered rock dataset forms the basis of an upcoming paper on the volcanic development of the Hauraki Volcanic Region.

6.2.5. Geochemistry of Unaltered Coromandel Group Rocks

Unaltered Coromandel Group rocks have 53-63% SiO₂ and are basaltic andesite, andesite and dacite

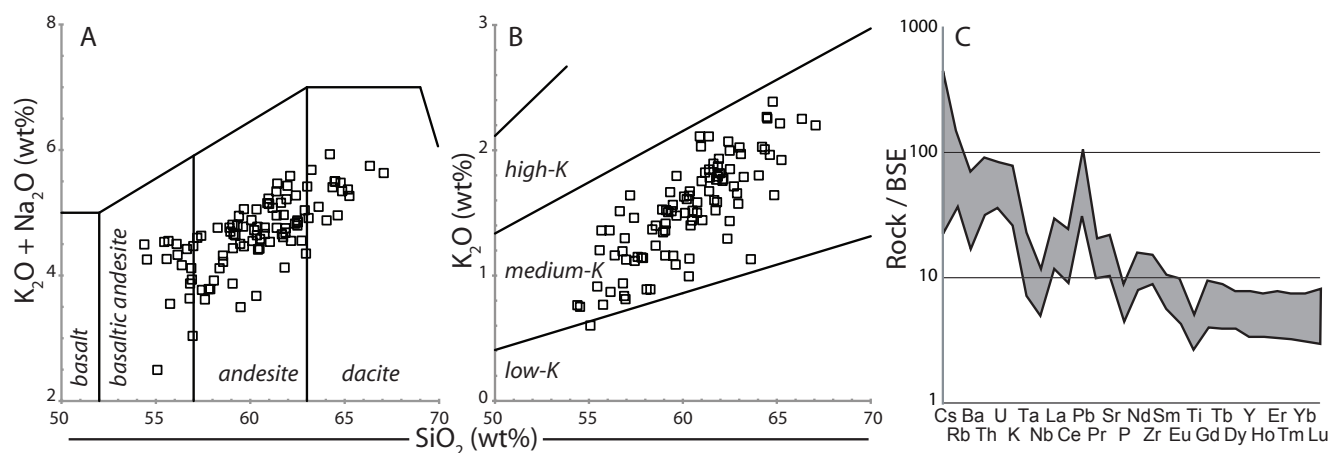


Fig. 6.2 Geochemistry of unaltered Coromandel Group rocks (N=98). A. Total alkali-silica classification following Le Bas et al. (1986). B. Potassium-silica classification diagram following Gill (1981). C. Bulk Silicate Earth (BSE) normalized minor and trace element distribution diagram using the model BSE composition of Sun and McDonough (1989).

following the IUGS total alkali classification (Le Bas et al., 1986; Fig. 6.2A) of medium-K composition (classification of Gill 1981; Fig. 6.2B). Normalized trace element distributions show distinct negative anomalies for the high field strength elements Nb, Ta and Ti, which is typical of subduction-related volcanic rocks (Fig. 6.2C). The samples form an array in terms of major element composition, where SiO_2 concentration correlates with the concentrations of many other elements. K_2O , Rb and Ba correlate positively with SiO_2 ; Na_2O , Zr and Tl correlate weakly positively with SiO_2 ; and TiO_2 , Al_2O_3 , Fe_2O_3 , MgO, CaO, Sr and Cu correlate negatively with SiO_2 (Table 6.2A). Although Na_2O and SiO_2 do not correlate strongly, Na_2O correlates strongly with MgO and Zr. The traditional ‘epithermal suite’ pathfinder elements (e.g., As, Sb, Hg) occur at concentrations of 1 ppm or less, and Ag concentrations are about 0.1 ppm. We did not measure gold concentration in the unaltered volcanic rocks and assume it to be equal to or less than 5 ppb, which is the detection limit for Au in our altered rock analyses.

The SiO_2 -dominated compositional range in Coromandel Group rocks is typical of andesites worldwide (Gill, 1981). With increasing SiO_2 concentration, rocks become more enriched in incompatible elements, which preferentially enter or partition into the melt phase of a magma, and more depleted in compatible elements, which partition into or form the rock-forming minerals. The strong correlation of many of the major elements with each other means that the whole-rock composition of any Coromandel Group rock can be estimated with some precision if the SiO_2 concentration is known. In the next section we assess how a ratio of generally immobile elements, Zr/TiO_2 , correlates with SiO_2 concentration in unaltered Coromandel Group rocks.

6.2.5.1. *Zr and TiO_2 Concentrations in Unaltered Coromandel Group Rocks*

Zirconium and TiO_2 concentrations show contrasting behavior with increasing magmatic differentiation: zirconium is generally incompatible, whereas TiO_2 is compatible. TiO_2 is particularly compatible in magnetite, with partition coefficients in representative magma compositions of 4-8 (Shimizu and Kushiro, 1975) to 16.5 (Sisson, 1991). It is also compatible in amphibole, with partition coefficients of 2 to 4 listed by Brenan et al. (1995) and Sisson (1994). Amphibole phenocrysts are only common in rocks of pre-10 Ma formations of the Coromandel Group, but partially resorbed amphibole crystals occur in younger formations. Amphibole is likely to have been present to some extent at depth in andesitic magmas that contributed to form Coromandel Group rocks, as it is stable in hydrated magma under mid-crustal conditions (Carmichael, 2002; Davidson et al., 2007). Fractionation of relatively TiO_2 -rich magnetite and amphibole deplete the remaining melt in TiO_2 , which is sequestered into amphibole-rich

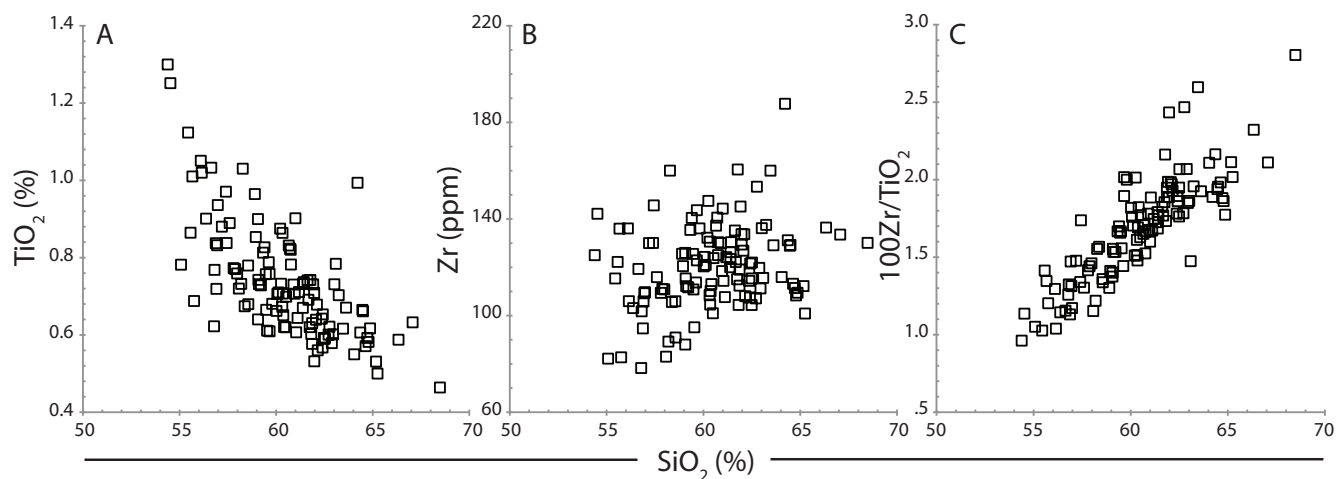


Fig. 6.3 Geochemistry of unaltered Coromandel Group rocks (N=98). A. TiO_2 - SiO_2 . B. Zr - SiO_2 . C. Zr/TiO_2 - SiO_2 .

cumulates in the deep and middle crust. Titanium is not compatible in the dominant phenocryst minerals plagioclase, hypersthene and augite (e.g., Okamoto, 1979; Johnson and Kinzler, 1989), so fractionation of those minerals increases the TiO_2 content of the melt. However, current understanding of arc volcanic systems indicates that such crystals may not control magmatic evolution and are generally not crystallization products of the associated melt (e.g. Charlier et al., 2005; Price et al., 2005). Accordingly, TiO_2 behaves as a compatible element and correlates negatively with SiO_2 in unaltered Coromandel Group rocks (Table 6.2 and Fig. 6.3A).

Table 6.3

A				r	Avg. mass change	2σ
SiO_2	=	8.19X	+ 46.83	0.88	1.0	g/100g 16.8
K_2O	=	1.03X	- 0.16	0.77	0.0	g/100g 0.6
CaO	=	- 2.71X	+ 11.07	-0.75	0.1	g/100g 2.7
Fe_{203}	=	- 2.89X	+ 11.52	-0.82	0.1	g/100g 1.8
Rb	=	43.09X	- 18.01	0.77	0.5	g/t 23.5
Ba	=	187.67X	- 19.67	0.77	3.6	g/t 113.5
TiO_2	=	- 0.35X	+ 1.33	-0.71	N/A	N/A
B. Na_2O mass change				r	Avg. mass change	2σ
Waipupu Fm.	=	1.14X	+ 0.75	0.90	0.5	g/100g 1.0
Whiritoa Andesite Fm.	=	1.18X	+ 0.74	0.86	0.5	g/100g 1.0
C. MgO mass change				r	Avg. mass change	2σ
Waipupu Fm.	=	-3.37X	+ 9.60	-0.86	-1.1	g/100g 2.9
Whiritoa Andesite Fm.	=	-4.39X	+ 11.87	-0.87	-0.5	g/100g 2.7

$$X = 100\text{Zr}/\text{TiO}_2$$

Table 6.3 Linear regression equations relating element concentrations to Zr/TiO_2 in unaltered Coromandel Group rocks. A. Equations based on the whole Coromandel Group dataset (N=98). B-C. Equations for Na_2O (B) and MgO (C) based on sample sets for Waipupu Formation (N=10) and Whiritoa Andesite Formation (N=7). The value r represents the correlation coefficient. 'Avg. mass change' represents the average mass change in unaltered Coromandel Group rocks with double standard deviation 2σ .

Zirconium is moderately incompatible in pyroxene, amphibole and magnetite, with partition coefficients in the range 0.1-0.9 (Ewart and Griffin, 1994). Therefore any fractionation of pyroxene, amphibole or magnetite would enrich the melt mildly in Zr. Assimilation of a crustal partial melt might likewise only moderately enrich Zr concentration. Zirconium is more strongly incompatible in plagioclase but, as noted above, plagioclase fractionation is not a driving force for magmatic differentiation of Coromandel Group rocks. The solubility of zircon decreases in a silicate melt with decreasing temperature; the Zr concentration at which a melt of given major element composition becomes saturated in zircon can be calculated using the method of Watson and Harrison (1983). The Coromandel Group magmas, typically with 100-150 ppm Zr, were undersaturated in zircon even at a theoretical eruption temperature as low as 750°. Actual eruption temperatures were probably higher than this. Consequently, Zr acted incompatibly and correlates weakly with SiO₂ in unaltered Coromandel Group rocks (Table 6.2 and Fig. 6.3B).

The contrasting behavior of Zr and TiO₂ during magmatic differentiation indicates that the ratio Zr/TiO₂ must increase progressively with magmatic differentiation in arc volcanic rocks (Table 6.1 and Fig. 6.3C). Because Zr is present at the 100 ppm level and TiO₂ at the percent level, we multiply all Zr/TiO₂ values by a factor 100 to avoid long decimal numbers. Values of Zr/TiO₂ are 0.9-1.4 for basaltic andesite, 1.1-2.1 for andesite, and 1.8 or higher for dacites (Fig. 6.3C). There are no consistent differences in the value of Zr/TiO₂ at a given SiO₂ concentration between unaltered rocks of different Coromandel Group formations, which means the relation between SiO₂ concentration and Zr/TiO₂ values is the same in all Coromandel Group rocks, even though they erupted over the course of 15.5 My. Therefore, the value of Zr/TiO₂ is a proxy for SiO₂ concentration in unaltered Coromandel Group rocks. Consequently, the Zr/TiO₂ value in altered Coromandel Group rocks can be used to estimate their initial igneous composition.

6.2.6. Estimation of Initial Rock Composition

Table 6.2A lists correlation coefficients for 18 elements and oxides with Zr/TiO₂ values in unaltered Coromandel Group rocks. Silica, TiO₂, K₂O, CaO, Fe₂O₃, Rb and Ba concentrations correlate with Zr/TiO₂ with absolute coefficients greater than 0.7, and can therefore be estimated with some measure of precision based on a rock's Zr/TiO₂ value. Linear regression line equations for these elements versus Zr/TiO₂ can then be used to back-calculate unaltered rock compositions (Table 6.3A). This approach is conceptually equivalent to the approach of MacLean (1990). The method of MacLean (1990) relies on determining the intersection, in a Zr vs. TiO₂ diagram, of a line through the origin with slope equal to a

particular rock's Zr/TiO₂ ratio, and a line that defines the covariation of Zr and TiO₂. The Zr or TiO₂ concentration at the intersection point can then be used to estimate protolith composition. A key difference with our approach is that we rely directly on the ratio Zr/TiO₂, rather than the absolute abundances of Zr or TiO₂, to infer protolith composition. As demonstrated in Figure 6.3 and Table 6.2A, the correlation between Zr/TiO₂ and SiO₂ (r = 0.88) is considerably stronger than that between SiO₂ and Zr (r = 0.24) or TiO₂ (r = -0.69) individually.

The amount of mass transferred for each element (DX) can then be calculated using the mass balance equation of Gresens (1967). Although Gresens' (1967) formula required density data in addition to a chemical analysis, density data ultimately cancel out, and the formula was rewritten based solely on chemical data in the following form by Warren et al. (2007).

$$DX = [(X_{Ai}/X_{Bi}) \times X_B] - X_A \quad (6.1)$$

Where X_A and X_B are the concentrations of an element in fresh and equivalent altered rock, respectively, and X_{Ai}/X_{Bi} is the ratio of the concentrations of an immobile constituent in unaltered and equivalent altered rock. Here we report results in g/100g (%) for major elements and in g/t (ppm) for trace elements. We use TiO₂ as the immobile element to calculate X_{Ai}/X_{Bi}: X_{Ai}, in this case, is the calculated TiO₂ concentration in the protolith, based on values of Zr/TiO₂ in the altered rock and using the equation in Table 6.3, whereas X_{Bi} is the measured concentration in the altered rock. TiO₂ has the advantage over Zr that its concentration in protoliths correlates more strongly with Zr/TiO₂ values (Table 6.2A).

6.2.6.1. *Effect of Metasomatic TiO₂ Loss*

Some intensely altered rocks in our dataset have experienced TiO₂ loss and consequently have anomalously large Zr/TiO₂ ratios. On this basis we have excluded 8 altered rocks with Zr/TiO₂ values of 3 and greater from inclusion in the mass balance approach. Some minor, cryptic loss of TiO₂ may have occurred in other altered rock samples and this would potentially have two effects: (1) loss of TiO₂ raises the values of Zr/TiO₂, which leads to greater estimates for K₂O, Rb, Ba, Na₂O and SiO₂ protolith concentrations, and lesser estimates for protolith concentrations of CaO, Fe₂O₃, MgO and TiO₂ itself; and (2) loss of TiO₂ raises the values of X_{Ai}/X_{Bi}, leading to the apparent addition of mass to a rock. We modeled the result of these competing effects on calculated K₂O mass change for four different hypothetical altered rock compositions (Fig. 6.4). At a Zr/TiO₂ ratio of 1, typical of basaltic andesite, a loss of TiO₂ initially leads to a small apparent K₂O gain, and then to apparent K₂O loss as values of Zr/TiO₂ become very large. At a Zr/TiO₂ ratio of 1.6, typical for andesite, any loss of TiO₂ leads to an immediate decrease in estimated

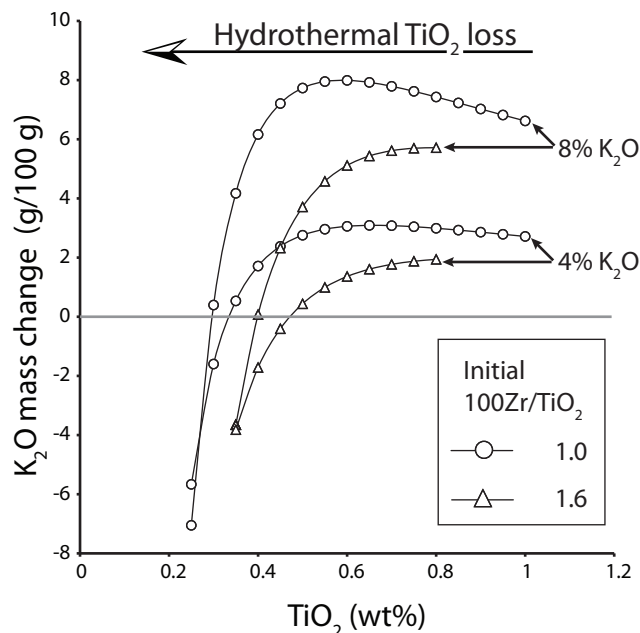


Fig. 6.4 Modelled outcomes of a K_2O mass balance calculation for hypothetical altered rocks at increasing levels of TiO_2 loss, for two different measured K_2O concentrations and two different initial Zr/TiO_2 values. All altered rocks in this study have $Zr/TiO_2 > 1$.

K_2O gain. We conclude that metasomatic TiO_2 loss will attenuate real K_2O gains for most rocks in this study, which are andesitic or dacitic in composition, and therefore this approach is robust because K_2O gains are not overestimated in rocks that have lost some TiO_2 . The same trends apply for other element and oxide gains or losses.

6.2.6.2. Apparent Mass Change Due to Natural Variation

Because concentrations do not correlate perfectly with Zr/TiO_2 values, apparent mass change can occur even in rocks that have not been altered. To assess the magnitude of this error, we used the equations in Table 6.3A and Equation 1 to estimate mass change in the unaltered Coromandel Group rocks on which the equations are based. We use twice the standard deviation (2σ) of the apparent mass change in unaltered Coromandel Group rocks as a cut-off value to determine whether an altered rock shows significant mass change for an element: a significant loss or gain is where the mass change exceeds the 2σ value. Some elements may be initially lost and then gained during later alteration. The mass balance calculation only yields the difference between the measured and initial amounts of mass, therefore all gains and losses reported here are net gains and losses.

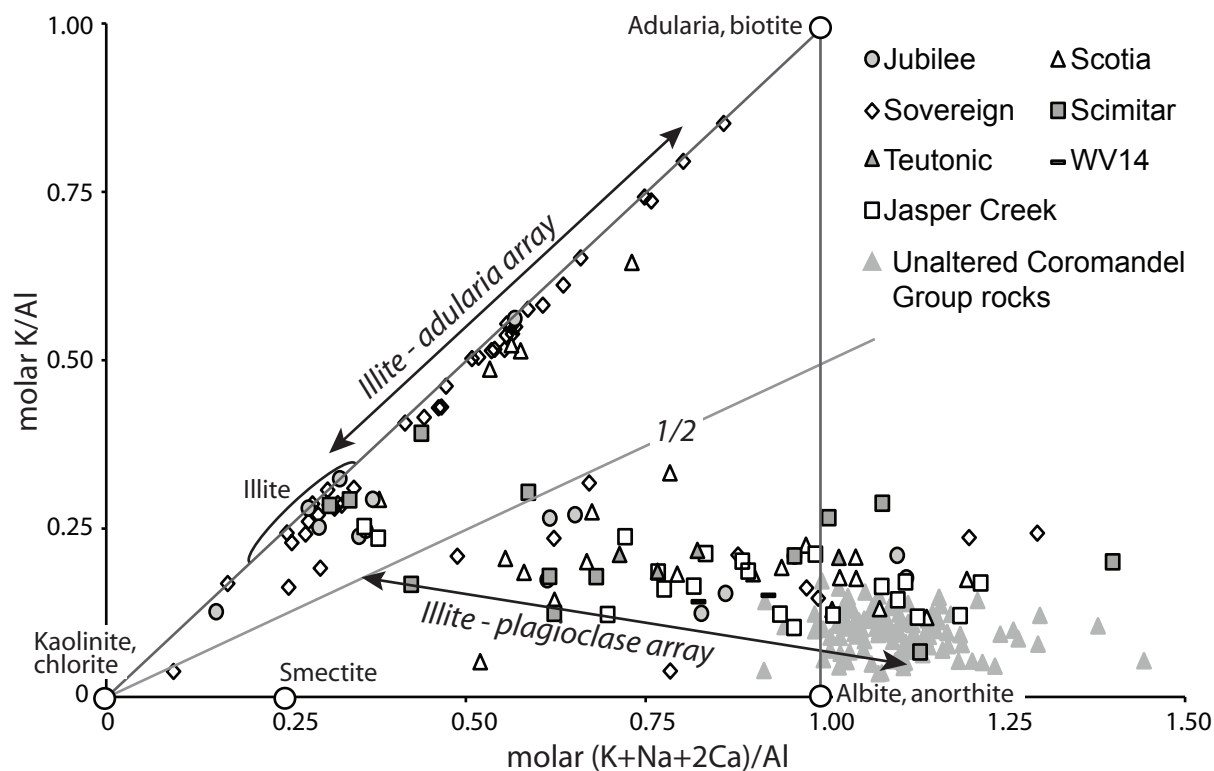


Fig. 6.5 Bivariate diagram of molar $(K+Na+2Ca)/Al$ against molar K/Al . After Madeisky (1996). Circles indicate the position of ideal mineral compositions. A line of molar $K/(K+Na+2Ca) = 1/2$ separates the altered rock sample sets used in the construction of Tables 6.2B and 6.2C.

6.2.6.3. Sodium and Magnesium Concentrations in Individual Formations

Although Na_2O and MgO concentrations do not reliably correlate with SiO_2 in the Coromandel Group dataset as a whole, they do in the Whiritoa Andesite ($N=7$) and the Waipupu Formation ($N=10$), which crop out widely in the southern Hauraki Goldfield (Table 6.3). The linear regression equations for Na_2O and MgO vs. Zr/TiO_2 value are very similar in both formations (Table 6.3B). However, using these equations to calculate mass change in all Coromandel Group rocks shows a considerable bias of at least -0.5 g/100g for MgO and 0.5 g/100g for Na_2O , with large 2σ errors of 1 g/100 g for Na_2O and ca. 2.8 g/100 g for MgO . Therefore, the Na_2O and MgO regression equations are of limited use for most Coromandel Group rocks. However, in this study we use, with caution, the equations derived for the Waipupu Formation, because altered rocks of this formation occur in much of the Waitekauri area.

6.2.7. Geochemistry of Altered Rocks

The gain of K and the loss of Na and Ca account for much of the mass transferred in shallow hydrothermal systems (Giggenbach, 1984, 1988). We evaluate K metasomatism on a diagram that plots molar K/Al against molar $(K+Na+2Ca)/Al$ (Fig. 6.5; Madeisky, 1996). In Figure 6.5, The slope of a line through the origin corresponds to the molar ratio $K/(K+Na+2Ca)$ and ranges between 0 and 1. Increasing molar

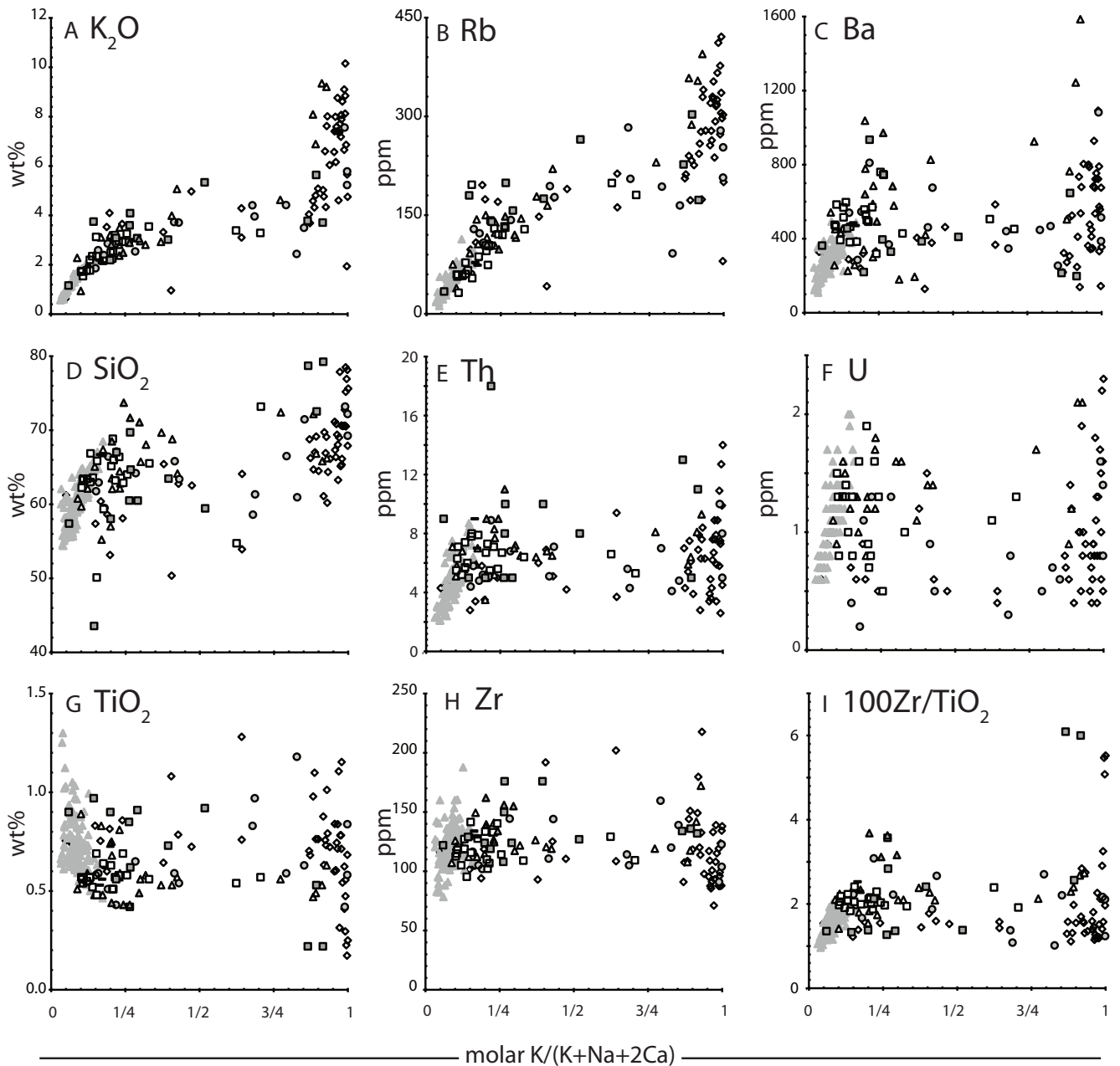


Fig. 6.6 Geochemical parameters plotted against molar $K/(K+Na+2Ca)$. A-H. Major and trace element concentrations. I. Zr/TiO_2 . J-O (next page). Major and trace element concentrations plotted against molar $K/(K+Na+2Ca)$. Key in all diagrams as in Figure 6.5.

$K/(K+Na+2Ca)$ in altered rocks indicates Ca and/or Na loss relative to K. A rock that has lost all Na+Ca has a molar $K/(K+Na+2Ca)$ value of 1. Unaltered Coromandel Group rocks plot to the right of and around the plagioclase-adularia tie line, at K/Al values less than 0.25. Basaltic andesites have the greatest molar $(K+Na+2Ca)/Al$ values, which are progressively lower in andesites and dacites.

6.2.7.1. Major Element Trends in Altered Rocks

The altered rocks of the Waitakauri area form two arrays in Figure 6.5. The illite-plagioclase array trends between unaltered Coromandel Group rocks, which have a plagioclase-dominated composition,

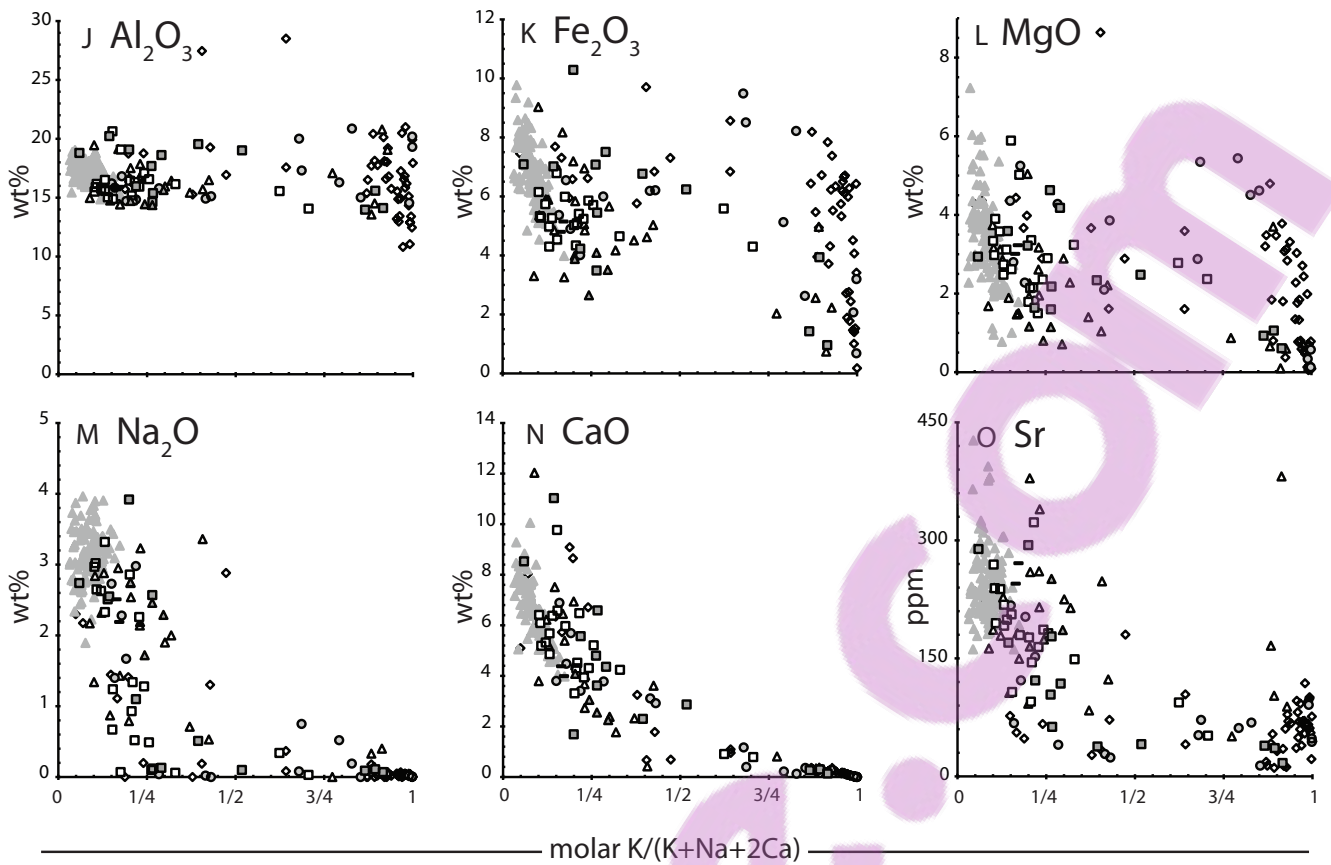


Fig. 6.6 (continued)

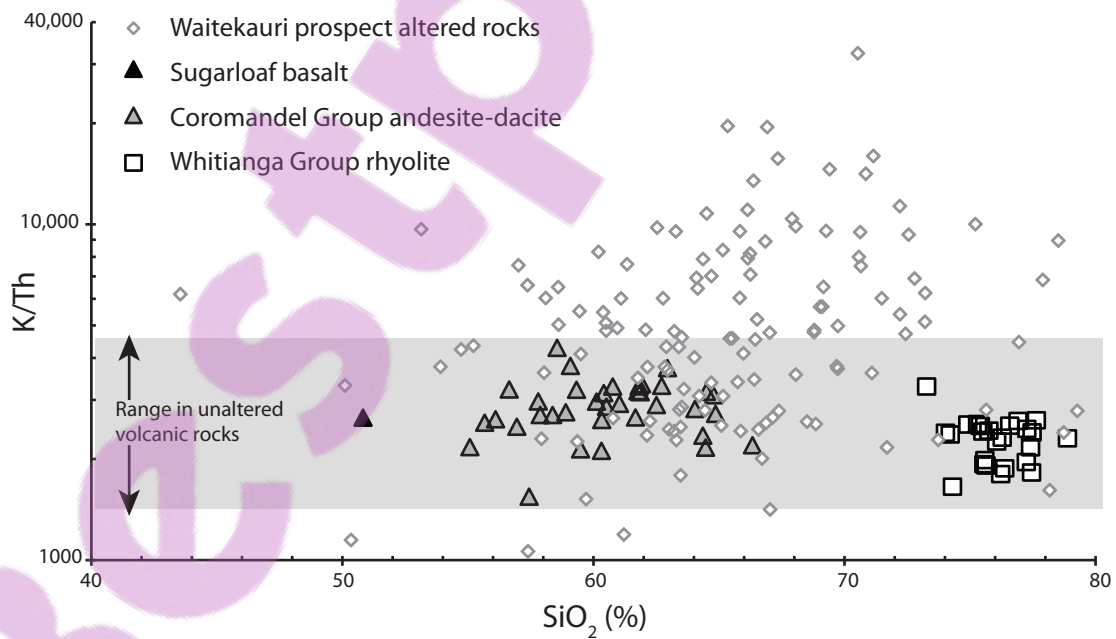


Fig. 6.7 Bivariate diagram of K/Th plotted against SiO_2 . Sugarloaf basalt, Coromandel Group andesites and dacites, and Whitianga Group rhyolites represent unaltered arc volcanic rocks and represent the known range in volcanic rock composition in the Coromandel Volcanic Zone. Altered rocks are from the Waitekauri area.

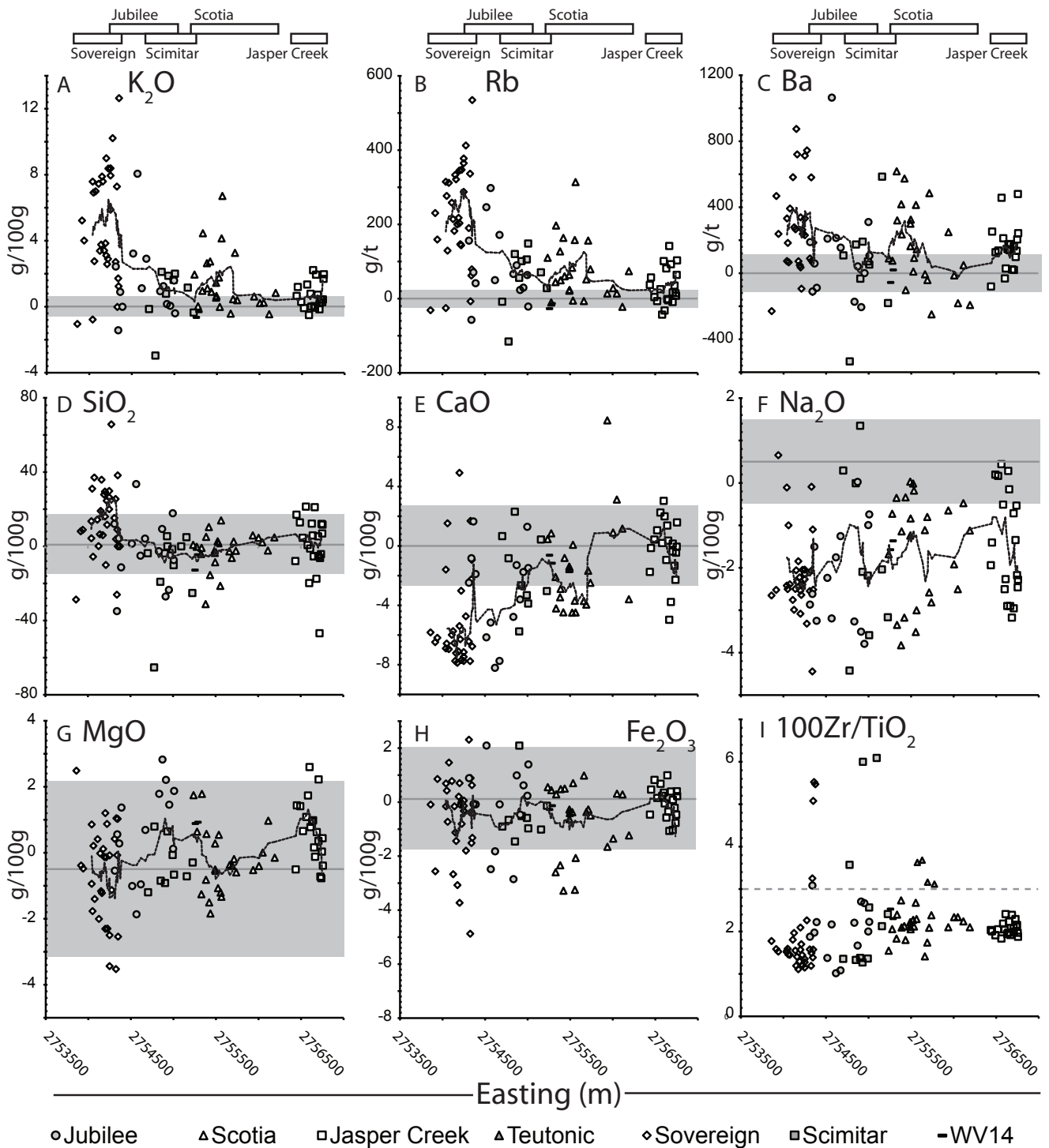


Fig. 6.8 A-H. Mass change in g/100g against samples' easting coordinates in meters in reference to the New Zealand Map Grid. Dark gray lines indicate zero mass change, gray shading indicates the 2σ range of the apparent mass change in unaltered Coromandel Group rocks (Table 6.3). The bias and 2σ values for Na₂O and MgO are based on the application of Waipupu Formation regression equations. Black dotted line indicates the average value calculated over each data point and the four data points to either side. I. Zr/TiO₂ plotted against samples' easting coordinates in meters in reference to the New Zealand Map Grid. Gray dashed line indicates the maximum Zr/TiO₂ for inclusion in the mass balance calculation. Key in all diagrams as in Figure 6.5.

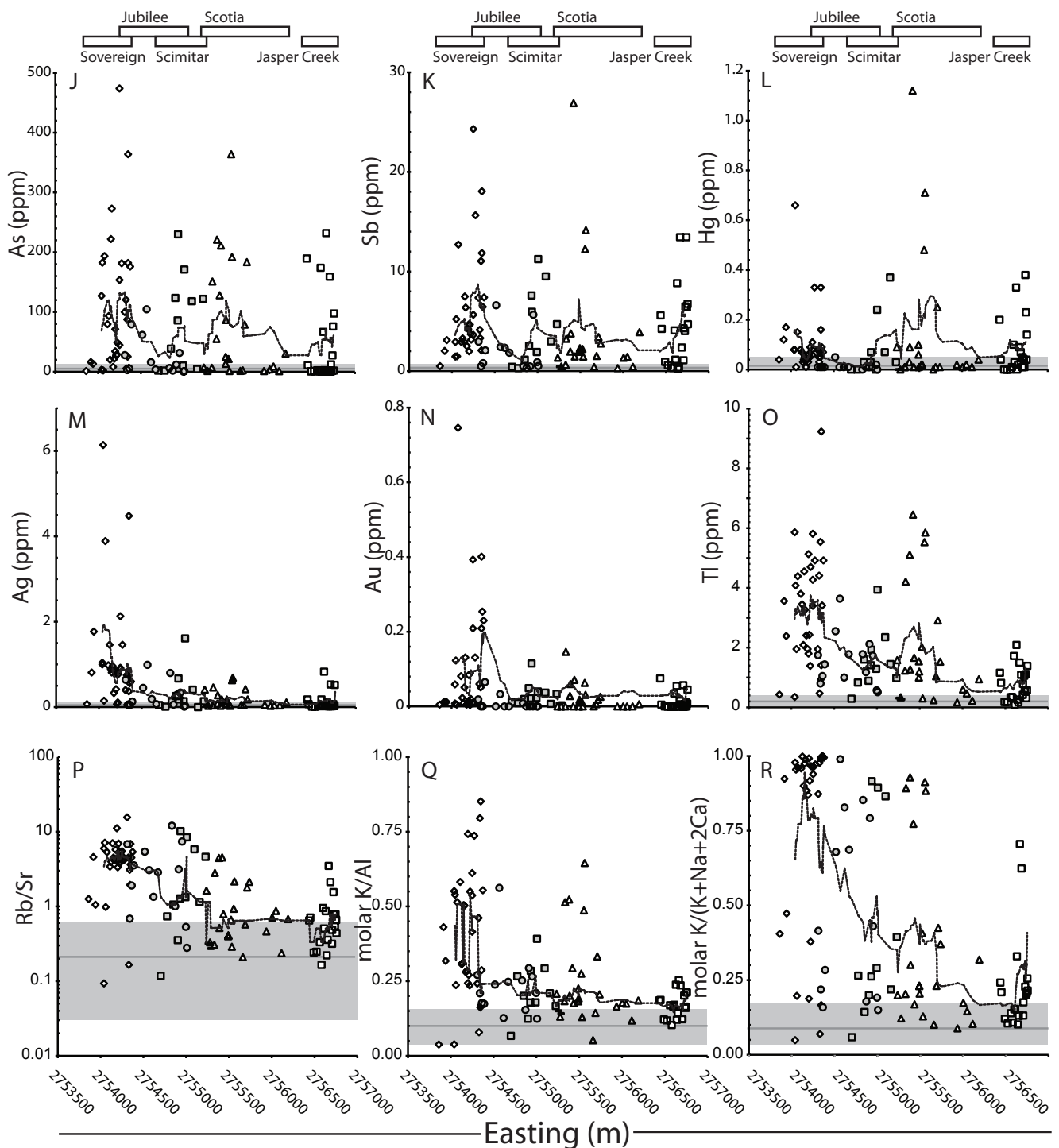


Fig. 6.8 (continued) J-O. Trace element concentrations in ppm plotted against samples' easting coordinates in meters in reference to the New Zealand Map Grid. Dark gray lines indicate the average concentration, gray shaded areas indicate the 2σ range in unaltered Coromandel Group rocks. Black dotted line indicates the average value calculated over each data point and the four data points to either side. P-R. Rb/Sr, molar K/Al and molar K/(K+Na+2Ca) values plotted against samples' easting coordinates in meters in reference to the New Zealand Map Grid. Dark gray lines and gray shading indicate the average values and 2σ range in unaltered Coromandel Group rocks. Black dotted line indicates the average value calculated over each data point and the four data points to either side. In P and Q the average is calculated as the median. Key in all diagrams as in Figure 6.5.

and the clay mineral, illite. This array reflects loss of Ca and Na, coupled with limited gain of K, which causes rocks to change from a plagioclase-dominant igneous composition to an illite-dominant altered composition. The second array, which we refer to as the illite-adularia array, comprises rocks with molar $K/(K+Na+2Ca)$ values close to 1 that plot along the illite-adularia tie line. A rock's location along this array mainly reflects variable replacement of adularia by illite. Altered rocks that form the illite-plagioclase array have up to 5% K_2O (Fig. 6.6A), which is less than the ca. 7.6% K_2O in illite – there are no altered rocks consisting entirely of illite. Altered rocks that plot on the illite-adularia array have much greater K_2O concentrations that range up to 10.4%, less than the 16.9% K_2O in adularia.

6.2.7.2. *Element Behavior During Metasomatism*

We evaluate the behavior of individual elements with increasing metasomatism in the Waitekauri area by plotting raw concentration data against molar $K/(K+Na+2Ca)$ values (Fig. 6.6). K_2O and Rb concentrations consistently increase with molar $K/(K+Na+2Ca)$, as expected (Figs. 6.6A-B). Thallium (not shown) is the only other element that shows this, presumably because it substitutes for K in adularia and/or illite (Gemmell, 2007). Barium concentrations do not increase consistently with molar $K/(K+Na+2Ca)$ values, but are commonly greater in altered rocks than in unaltered Coromandel Group rocks (Fig. 6.6C). SiO_2 concentration is greatest in altered rocks with large molar $K/(K+Na+2Ca)$ values, but some altered rocks with small molar $K/(K+Na+2Ca)$ values have lower SiO_2 concentration than any unaltered Coromandel Group rocks (Fig. 6.6D). The concentrations of Al_2O_3 , TiO_2 , Zr, Th and U, and the ratio Zr/TiO_2 do not change consistently with molar $K/(K+Na+2Ca)$ values, therefore they were generally not significantly mobilized during metasomatism (Figs. 6.6E-J). Their concentrations show more scatter at greater molar $K/(K+Na+2Ca)$, which likely reflects passive dilution or enrichment through the gain or loss of more mobile elements. However, Zr/TiO_2 values are anomalously large in some rocks with molar $K/(K+Na+2Ca)$ values close to 1, which reflects metasomatic removal of TiO_2 . As noted above, rocks with Zr/TiO_2 ratios greater than 3 are excluded from the mass balance calculation. The concentrations of MgO and Fe_2O_3 vary little as molar $K/(K+Na+2Ca)$ values increase up to 0.75, and show a gradual decrease in minimum and maximum concentrations at greater molar $K/(K+Na+2Ca)$ (Figs. 6.6K-L). We infer that Mg and Fe were relatively immobile during metasomatism, because they partition into chlorite and pyrite, respectively, but Fe and especially Mg concentrations can decrease significantly in the cores of hydrothermal alteration zones where chlorite may be less abundant. The concentrations of Na_2O , CaO and Sr consistently decrease with increasing molar $K/(K+Na+2Ca)$ values (Figs. 6.6M-O), which reflects

their removal from altered rocks during K-metasomatism.

6.2.7.3. *Immobility of Th*

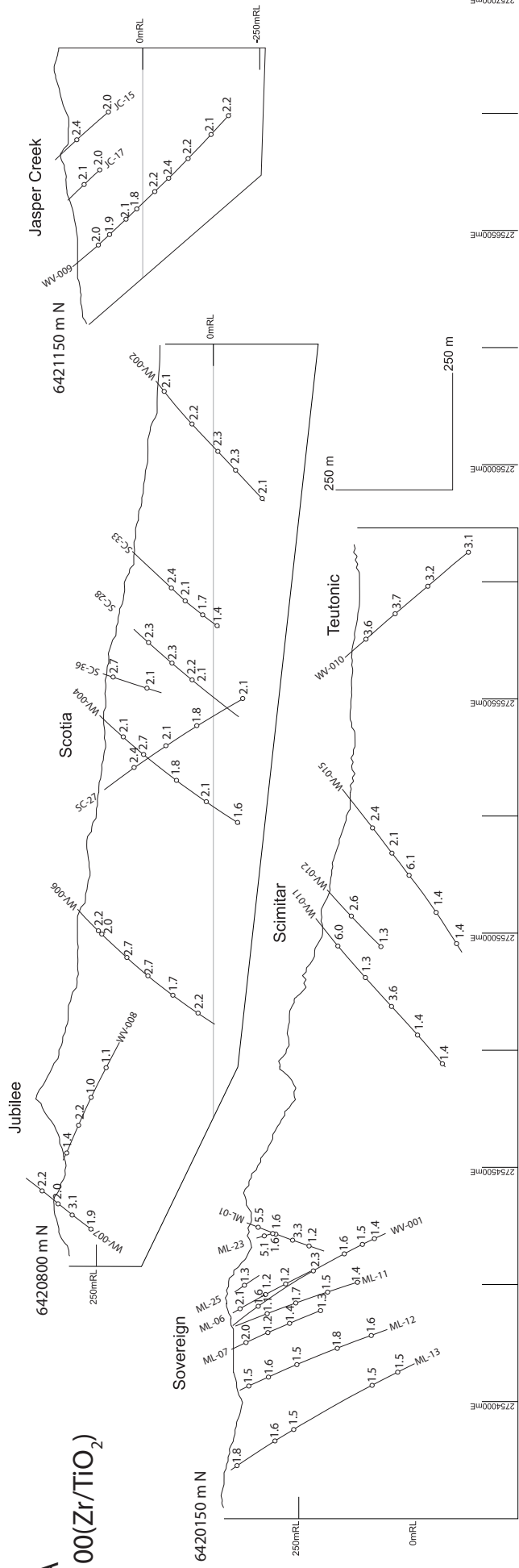
The K_2O concentration in altered rocks, even at low molar $K/(K+Na+2Ca)$ values, is typically greater than in unaltered rocks (Fig. 6.6A). As noted above, Th is relatively immobile during K metasomatism. The implication for geophysical exploration using radiometric K/Th data (e.g. Morrell et al., in press) is that even mild K metasomatism will increase the K/Th value of the altered rocks. The K/Th ratio in unaltered Coromandel Group andesites and dacites ranges between 1500 and 5000, and unaltered basalts and rhyolites from the Hauraki Goldfield have similar K/Th ratios (Fig. 6.7). In contrast, K/Th values in Waitekauri area altered rocks range up to 35,000; therefore any volcanic rocks in the Hauraki Goldfield with K/Th values greater than 5,000 must have experienced K metasomatism.

6.2.8. **Geochemical Zonation in the Waitekauri Area**

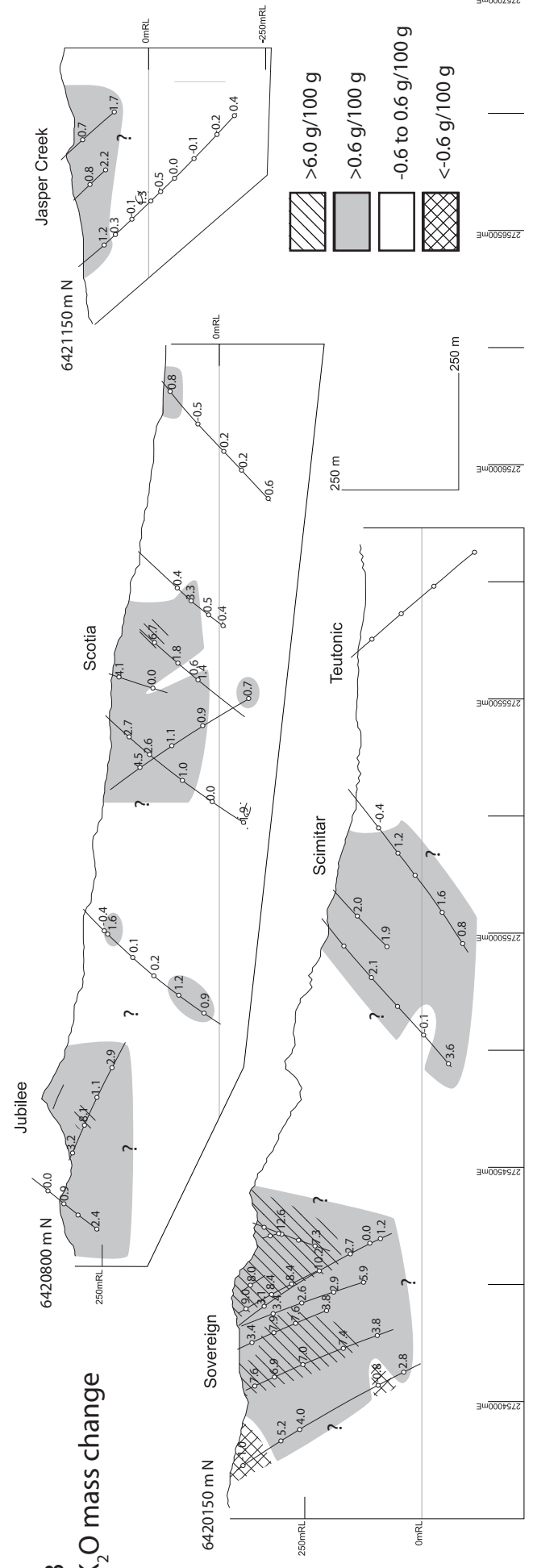
We use two plots to illustrate spatial trends in the geochemistry of altered rocks in the Waitekauri area: diagrams that plot mass change values versus the host rock's easting coordinates (Fig. 6.8A-H), and mass change values for individual rock samples, projected onto three sections through the Waitekauri prospect (Fig. 6.9). We do not plot rock samples from the Teutonic prospect that are hosted in the Mangakara Dacite because of their unusually large Zr/TiO_2 values, although these rocks show only low-rank alteration as indicated by the presence of smectite and vein zeolites (Simpson and Mauk, in press). In Figure 6.8, easting coordinates, in meters, are in reference to the New Zealand Map Grid. A dark gray line indicates zero mass change in each diagram and gray shading indicates the 2σ range as calculated in Table 6.3. Altered rocks that plot within this range have not experienced significant mass change for a given element. At any given point along the section, there are at least some rocks that have not experienced significant mass change. This underscores the necessity of acquiring a sufficiently large database to ensure that geochemical trends are well-represented. In the following discussion, we focus on maximum mass gains and losses, because for some elements and oxides these change laterally across the width of the Waitekauri

Fig. 6.9 (following pages) Geochemical parameters for each sample, projected onto the sections shown in Figure 6.1D. A. Zr/TiO_2 . B. K_2O mass change. C. Ba mass change. D. SiO_2 mass change. E. CaO mass change. F. Na_2O mass change. G. As concentration. H. Sb concentration. I. Au concentration. J. Ag concentration. In sections B-J white indicates rocks with no significant gain or loss. K-N. Distribution of alteration minerals, after Simpson and Mauk (in press). Sections are located as shown in Figure 6.1C.

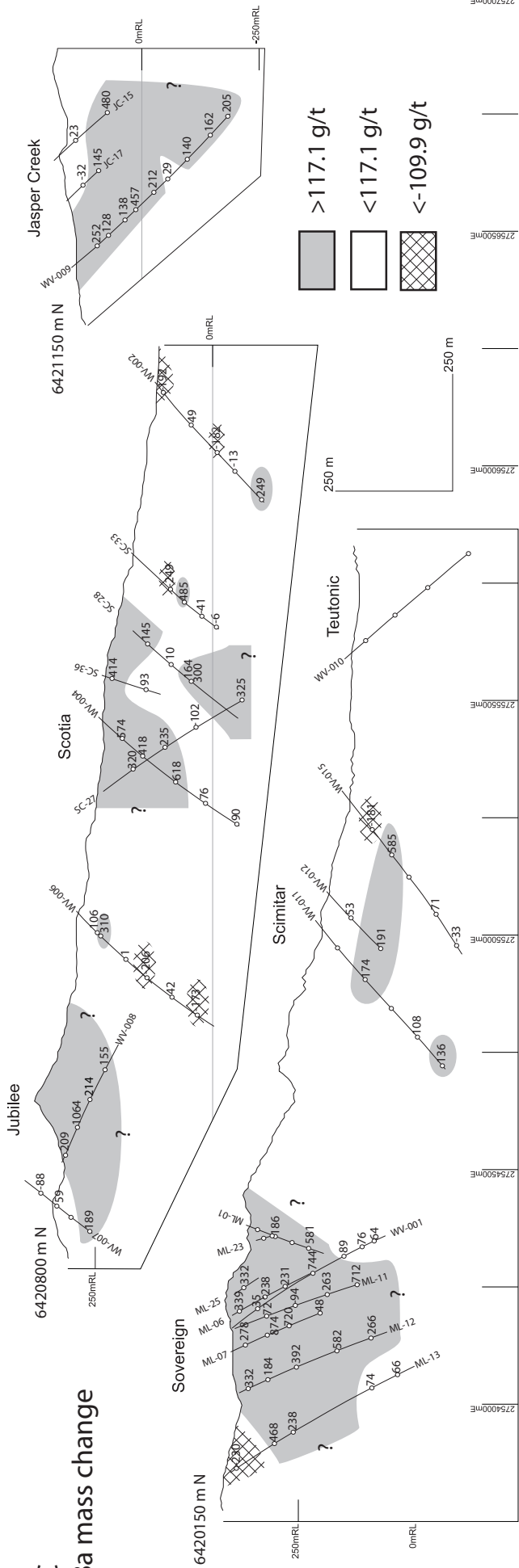
A
100(Zr/TiO₂)



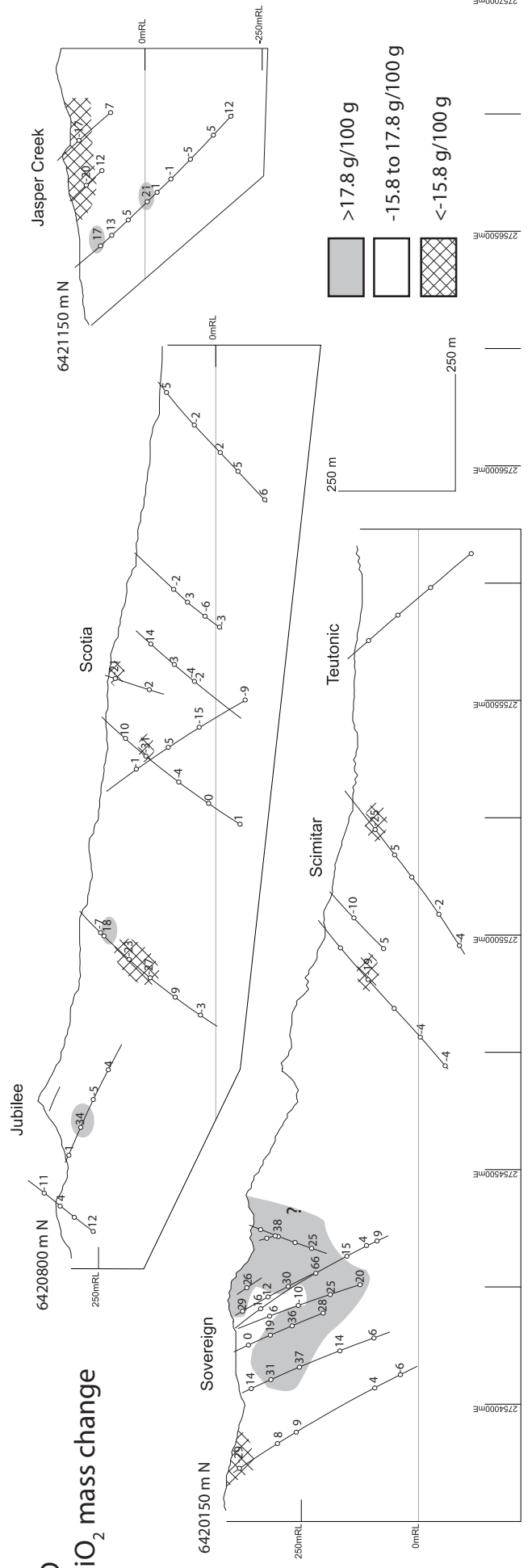
B
K₂O mass change



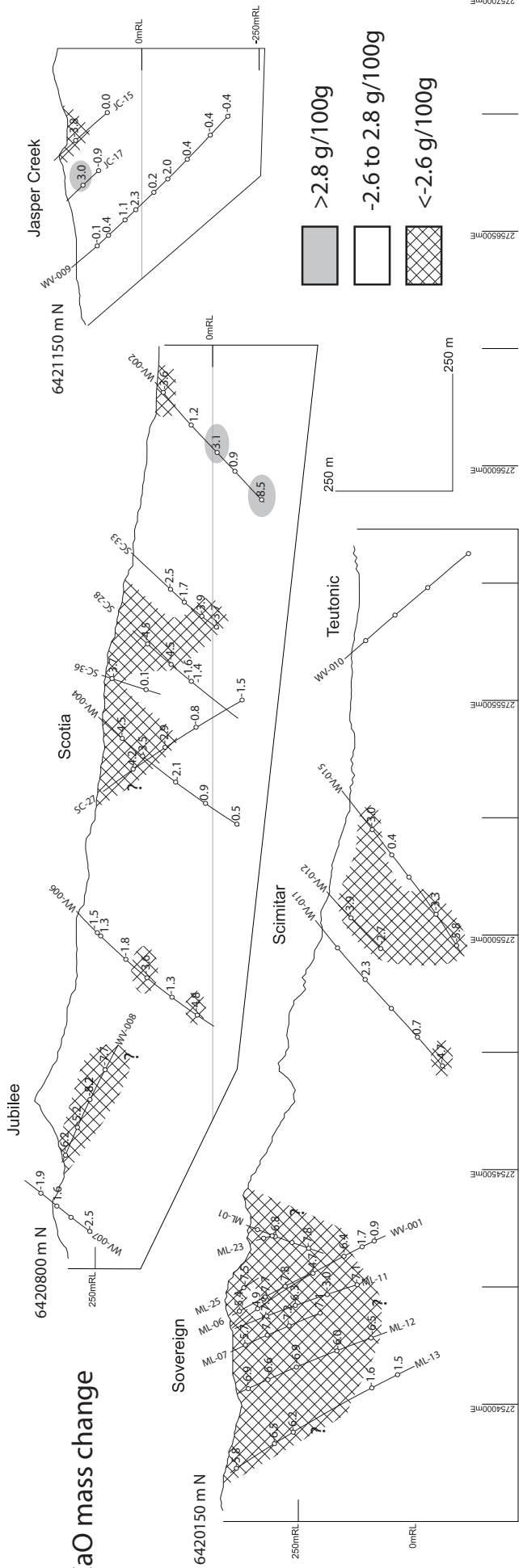
C Ba mass change



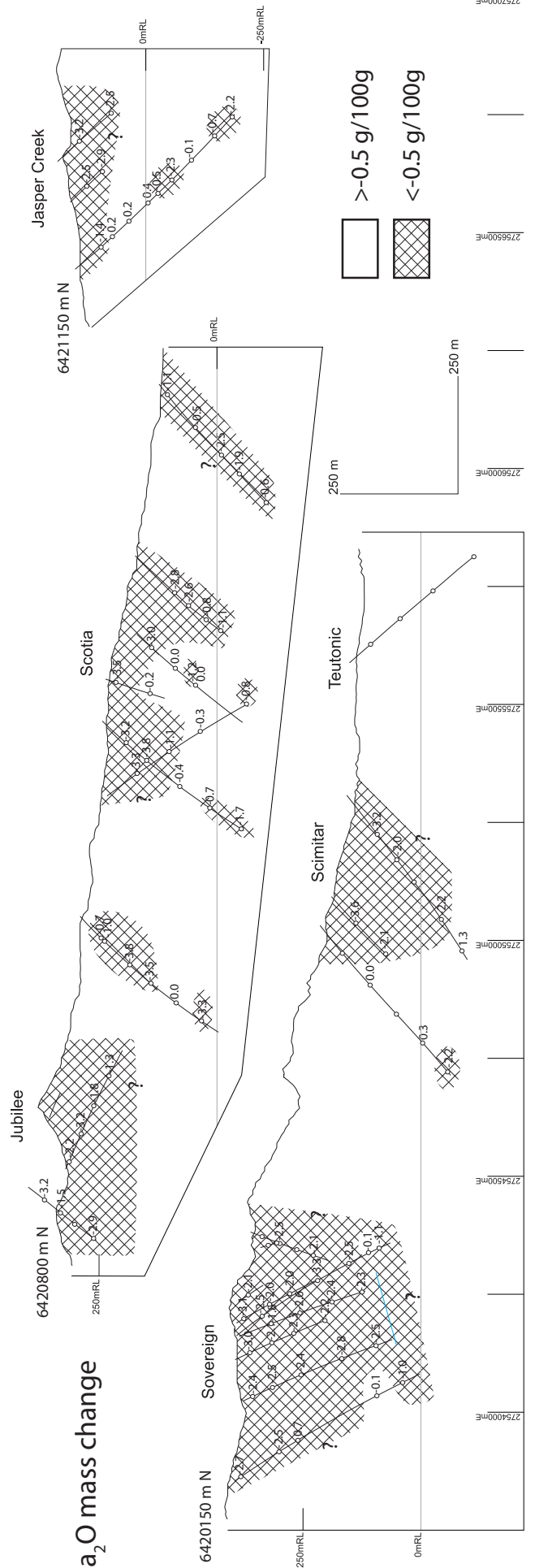
D SiO₂ mass change



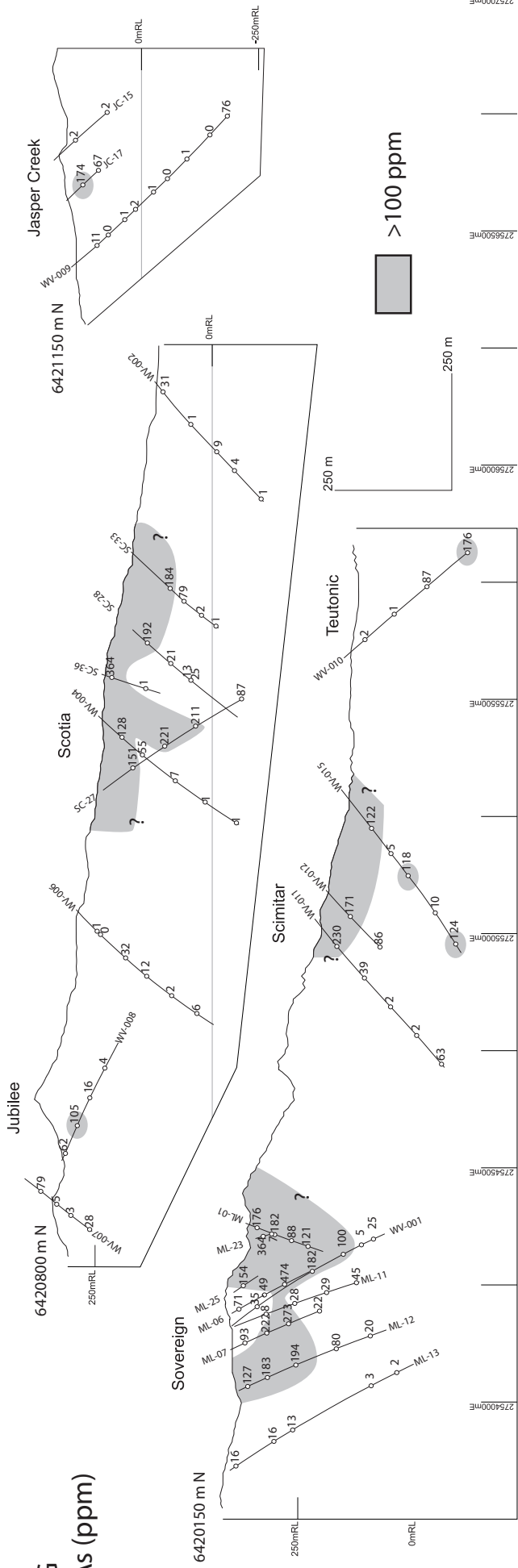
E CaO mass change



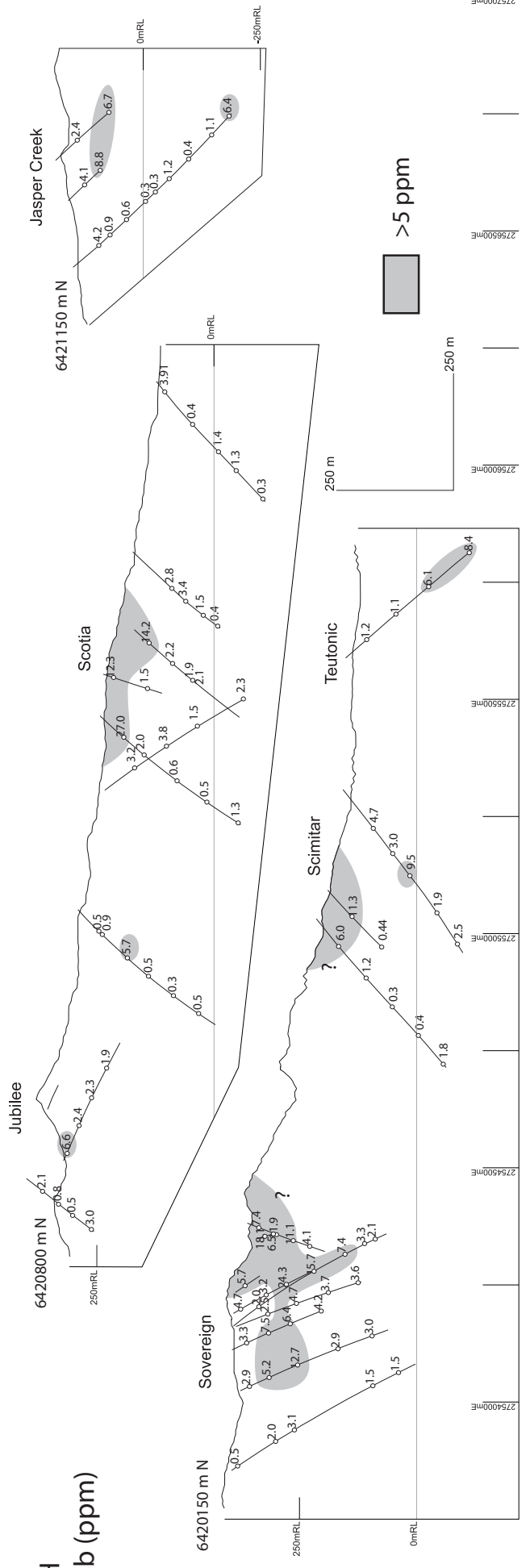
F Na₂O mass change



G
As (ppm)



H
Sb (ppm)



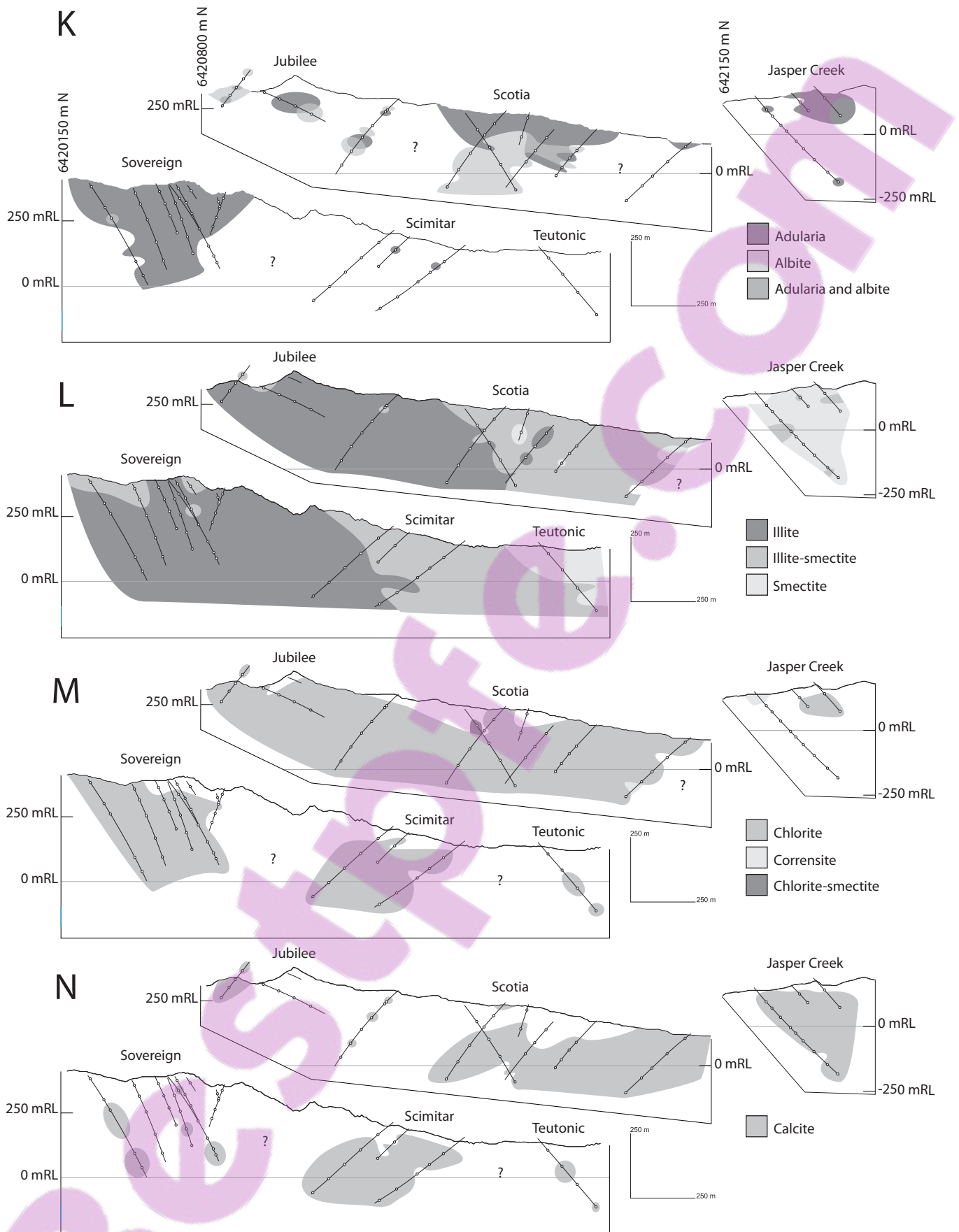


Fig. 6.9 (continued) K-N. Distribution of alteration minerals, after Simpson and Mauk (in press). Sections are located as shown in Figure 6.1C.

area (e.g., K_2O , Fig. 6.8A; CaO , Fig. 6.8E). In addition, a dotted line indicates the moving average value calculated over each datapoint and the four points to either side.

For reference, we also plot values of Zr/TiO_2 against easting (Figs. 6.8I, 6.9A). Rocks from Sovereign, parts of Jubilee and the western part of Scimitar have Zr/TiO_2 values mostly between 1 and 1.6, whereas rocks from eastern Scimitar, Scotia, Teutonic and Jasper Creek have Zr/TiO_2 values around 2. This indicates that host rocks are more differentiated in the eastern deposits and prospects, consistent with the distribution of the Waitekauri Dacite and the andesitic Waipupu Formation (Fig. 6.1C).

6.2.8.1. *Potassium and Rubidium*

Rubidium and K_2O correlate strongly in altered and unaltered Coromandel Group rocks (Table 6.2) and show identical spatial trends in maximum mass change (Figs. 6.8A-B). Maximum K_2O gains increase in a westward direction: from 2 g/100g in rocks at Jasper Creek, to 7 g/100g at Scotia, to 8 g/100g at Jubilee, to 12.5 g/100g at Sovereign. Average gains also increase westward to a maximum of 5 g/100g at Sovereign. Maximum concentrations of K_2O in the altered host rocks at the Scotia and Sovereign deposits are comparable at 9.4% and 10.2%, respectively, but the maximum gains for K_2O at these deposits are 7 g/100g and 12.5 g/100g, respectively, showing that rocks at Sovereign have experienced much greater K-metasomatism (Fig. 6.10).

The westward increase in maximum and average K_2O gain correlates with the increasing proportion of adularia (Fig. 6.9K; Simpson and Mauk, in press) and with the increasing dominance of illite over smectite (Fig. 6.9L). Illite is the dominant K-bearing mineral at Scimitar, and it occurs with adularia in most of the sampled rocks at Sovereign, Jubilee and Scotia (Simpson and Mauk, in press). Adularia occurs in some shallow rocks at Jasper Creek, at Scotia in a shallow carapace, locally at Jubilee and extensively at Sovereign. At the Sovereign, Jubilee and Scotia deposits, the presence of adularia correlates with substantial K_2O gain; as indicated above, the greatest K-metasomatism is at the Sovereign deposit, which has the most widespread adularia alteration (Fig. 6.9K).

6.2.8.2. *Barium*

Barium concentration correlates with K_2O and Rb concentrations in unaltered Coromandel Group volcanic rocks but less strongly in altered rocks (Table 6.2); nevertheless maximum Ba gains show a relatively clear gradient across the Waitekauri area (Fig. 6.8C). Most samples at the Jasper Creek prospect show Ba gains of up to 200 g/t with two outliers up to 500 g/t. Maximum Ba gains at Scimitar and Scotia

are approximately 600 g/t and 900 g/t at the Sovereign deposit. Maximum Ba gains therefore parallel the regional trend in maximum and average K_2O and Rb gains, where the greatest Ba gains occur in adularia-rich rocks (Figs. 6.9C, K).

6.2.8.3. *Silicon*

Most altered rocks in the Waitekauri area show no significant SiO_2 loss or gain (Fig. 6.8D). Greater SiO_2 gains and losses mostly occur at shallow levels (Fig. 6.9D), corresponding to areas of greater K_2O gains in the upper levels of Scotia and Scimitar (Fig. 6.9B), and to the distribution of adularia and albite at Scotia (Fig. 6.9K). Silica gains are generally greatest in the most strongly altered rocks, which have the greatest concentration of hydrothermal quartz (Simpson and Mauk, in press). Our sampling excluded all veins and veinlets in the host rocks; if these had been included, more samples would show SiO_2 gains. Maximum SiO_2 gains are greatest in rocks at the Sovereign deposit, whereas most host rocks from the Jasper Creek, Teutonic and Scimitar prospects show no significant SiO_2 gain (Fig. 6.8D). A limited number of host rock samples, from throughout the Waitekauri area, show significant SiO_2 losses. These rocks do not have a specific mineralogical composition that contrasts with other altered rocks, therefore their low SiO_2 content might reflect a high proportion of clay minerals and/or chlorite relative to feldspar and quartz.

6.2.8.4. *Sodium and Calcium*

All deposits and prospects, except the peripheral Jasper Creek and Teutonic prospects, have some rocks with $<0.2\%$ CaO – it has almost entirely been removed by hydrothermal alteration. Maximum CaO loss is greatest in rocks at Sovereign and Jubilee, lower at Scimitar and lower again at Scotia and Jasper Creek (Fig. 6.8E). However, this trend is an artefact of rock type: the andesitic host rocks at Sovereign, Jubilee and western Scimitar had greater initial CaO concentrations, and therefore could lose more CaO during alteration, than the dacitic rocks at Scotia and Jasper Creek.

Maximum Na_2O losses exceed 3 g/100 g at each deposit and prospect (Fig. 6.8F), although as noted above, Na_2O protolith concentration estimates are probably inaccurate if host rocks are not part of the Waipupu Formation. Losses are generally greater in rocks at Scimitar and Scotia than in rocks at Sovereign. This reflects the greater initial Na_2O concentration in unaltered dacite relative to unaltered andesite, and therefore maximum Na_2O loss trends are an artefact of rock type.

All altered rocks that show Na_2O loss also show CaO loss, and areas of significant Na_2O loss extend

farther than those of significant CaO loss at each deposit and prospect (Figs. 6.9E-F). Calcium gains occur in rocks containing calcite at Teutonic and eastern Scotia, but most rocks that contain calcite also show limited CaO loss (Fig. 6.9N). This reflects the typically late-stage nature of calcite precipitation (Simpson and Mauk, in press), which occurred in rocks that had lost some or all CaO during main-stage alteration. Hydrothermal albite at the Scotia and Jubilee deposits typically occurs in altered rocks that show limited Na₂O loss (Fig. 6.9K).

6.2.8.5. *Iron and Magnesium*

Chlorite is the principal alteration mineral that hosts Mg and Fe²⁺; it is abundant in most rocks in the Waitekauri area (Fig. 6.9M). Pyrite is also ubiquitous, even in the most iron-poor rocks, and indicates the addition of S to the altered rocks (Simpson and Mauk, in press). The greatest Fe₂O₃ and MgO losses occur in adularia-bearing rocks at the Sovereign and Jubilee deposits in the west (Figs. 6.8G-H). This trend partly reflects greater initial concentrations in the andesitic host rocks in the western deposits, and partly the lower abundance of chlorite in intensely metasomatized rocks. Host rocks at the Jubilee deposit and the Jasper Creek prospect show preferential MgO gain instead of loss. There is no clear correlation between MgO gain and the presence or absence of any of the alteration minerals considered in this study.

6.2.8.6. *Precious Metal and Pathfinder Element Concentrations*

Although precious metals and pathfinder elements mainly occur in vein minerals, they also show a wide range in concentrations in altered rocks of the Waitekauri area. These elements occur in trace amounts in unaltered Coromandel Group rocks (Table 6.2A), and they can be enriched by two orders of magnitude in altered rocks (Table 6.1). Therefore, rather than calculating mass change, we simply use raw whole-rock concentrations to assess whether they reflect proximity to mineralization, or regional or local gradients in alteration intensity.

The traditional epithermal pathfinder elements, As, Sb and Hg, are anomalous in the altered rocks of the Waitekauri area, and they show similar distributions, but they do not show a clear gradient on the scale of this section (Figs. 6.8J-L). The greatest concentrations occur at the Sovereign and Scotia deposits but, except for four outliers, the maximum concentrations of As, Sb and Hg are similar in altered rocks at Sovereign, Scimitar, Scotia and Jasper Creek, and are somewhat lower at the Jubilee deposit. Concentrations of pathfinder elements are highly variable on a local scale, changing by an order of magnitude or more over 100-m-scale distances (Figs. 6.9G-H). In contrast, the maximum concentrations of Au and Ag

are similar in altered rocks at Jasper Creek, Scotia, Scimitar and Jubilee, but substantially greater at the Sovereign deposit (Figs. 6.9I-J) where they correlate with K and Si gains (Figs. 6.9B, 6.9D). At the Sovereign deposit, Au and Ag occur in silicified and fractured breccia zones and in narrow veins, in contrast to other areas where Au occurs in veins in lava flows, and it is possible that the elevated Au contents in Sovereign rocks relates to micro-brecciation and/or silica flooding (Simpson and Mauk, in press). Maximum Tl concentrations increase from Jasper Creek to Scotia to Sovereign, although, with the exception of one outlier, similar maximum concentrations occur at the Sovereign and Scotia deposits, with considerably lower maximum concentrations at Jubilee and Scimitar (Fig. 6.8O).

We conclude that precious metal concentrations closely correlate with quartz-adularia-rich rocks that surround Au deposits along the Waitekauri Fault. Pathfinder element concentrations, in contrast, are anomalously high in specific alteration cells throughout the Waitekauri area, but their concentrations do not define a gradient from the central Waitekauri Fault to the peripheral Jasper Creek prospect.

6.2.8.7. *Other Geochemical Parameters*

Apart from a mass balance calculation, the intensity of K metasomatism can be expressed by geochemical parameters, including K/Sr, Rb/Sr, molar K/Al and molar K/(K+Na+2Ca) ratios (Madeisky, 1996; Mauk and Simpson, 2007; Warren et al., 2007). Average and maximum values for these parameters show clear westward trends in the Waitekauri area. K/Sr and Rb/Sr values have identical distributions (we only show Rb/Sr: Fig. 6.8P) with a marked increase in median value westward, although maximum values are similar at Sovereign, Jubilee and Scimitar. Both median and maximum molar K/Al values also increase westward and maximum values are distinctly greater at Sovereign than at Scotia (Fig. 6.8Q). Molar K/(K+Na+2Ca) shows the most distinct increase in average value westward, directly comparable to the trends in maximum and average K₂O and Rb gain (Fig. 6.8R). It is striking that molar K/(K+Na+2Ca) correlates so closely with the distribution of adularia, given that illite and adularia both have molar K/(K+Na+2Ca) values of 1. This likely reflects the more complete leaching of Na and Ca from, and the lack of late-stage calcite in, adularia-rich rocks.

6.2.8.8. *Summary of Alteration Geochemical Trends*

The principal mass change parameters that define a regional gradient towards Au-Ag deposits along the Waitekauri Fault are maximum and average K₂O, SiO₂, Rb and to a lesser extent Ba gains, which increase from east to west in the Waitekauri area along a 3-km-wide section (Figs. 6.8A-D). Mass gains

for K_2O , SiO_2 , Rb and Ba are greatest in adularia-rich rocks at the Sovereign deposit. The increase in K metasomatism is obscured by variation in protolith composition, which leads to similar maximum K_2O concentrations in altered rocks of 10.2% at Sovereign and 9.4%, although we note that average K_2O concentrations show a similar trend to K_2O gains (Fig. 6.10). Other major elements are lost during metasomatism or remain immobile. Elements that are lost can theoretically yield a vector towards the core of an alteration zone, however in the Waitekauri area such elements do not yield clear trends in maximum or average loss. Calcium and Na are commonly completely lost during alteration, therefore the trends in average and maximum CaO and Na_2O losses do not reflect the increasing alteration intensity and metasomatism towards the west, but rather protolith heterogeneity: a greater initial concentration of mobile elements means that more mass can be lost (Figs. 6.8E-F). The maximum losses of MgO and Fe_2O_3 increase westward, but the average losses do not show a distinct trend (Figs. 6.8G-H), which reflects the relative stability under K metasomatism of chlorite and pyrite, the main alteration minerals that host Mg and Fe (Figs. 6.6K-L).

Several geochemical parameters that do not require a mass balance calculation correlate with K_2O mass gain: maximum and average K/Sr, Rb/Sr, molar K/Al and particularly molar $K/(K+Na+2Ca)$ values all increase from east to west in the Waitekauri area (Figs. 6.8P-R). In contrast, the maximum and average concentrations of the pathfinder elements As, Sb and Hg are similar at Jasper Creek, Scotia, Jubilee and Sovereign, and therefore pathfinder elements do not show distinct trends across the Waitekauri area. Taken together, we suggest that pathfinder elements can identify smaller cells of hydrothermal mineralization, which may or may not be economic. In contrast, K and Si mass gains, K/Sr, Rb/Sr and molar $K/(K+Na+2Ca)$ values suggest that the main locus of hydrothermal fluid flow was in the western deposits of the Waitekauri area, where it was focused by the Waitekauri Fault (Simpson and Mauk, in press).

6.2.9. Discussion

6.2.9.1. *Vectors Towards Orebodies*

From an exploration point of view, metasomatism would ideally increase gradually towards the core of an alteration zone. This is unlikely in reality as faults, fractures and heterogeneous host rock lithology and permeability constrain hydrothermal fluid flow on a range of scales in any setting (e.g., Cox et al., 2001; Person et al., 2008; Rosenberg et al., 2009). In the Waitekauri area, the overall westward trend in K and Si gains and $K/(K+Na+2Ca)$ values is superimposed on considerable local variation: strong vertical

gradients in K_2O gain and CaO loss exist at Scotia and Jasper Creek and correlate with the presence of adularia in shallow rocks; K_2O gains at Sovereign are greatest in shallow rocks, even though adularia occurs to depth (Figs. 6.9B, 6.9E, 6.9K). The deposits and prospects of the Waitekauri area, which are defined by the altered rocks at the surface, are also separated by areas with less-altered rocks (Fig. 6.9B; Morrell et al., in press). This kind of variation is to be expected in an alteration zone developed in a complex volcanic stratigraphy comprising massive and autobrecciated lava flows, tuffs and tuff breccias, intruded by dykes and cut by normal faults (Brathwaite and Christie, 1996; Haworth and Briggs, 2006; Simpson and Mauk, in press). Nevertheless, clear regional trends exist in the Waitekauri area in maximum and average K and Si mass gains, Rb/Sr values and molar $K/(K+Na+2Ca)$ values. The geochemical trends persist across a 3-km-wide section, correlate with trends in fluid inclusion homogenization temperature, alteration mineralogy and radiometric K/Th data, and vector towards $Au-Ag$ deposits hosted in adularia-rich rocks at the core of the alteration zone (Morrell et al., in press; Simpson and Mauk, in press).

The west-directed mass change gradient reaches a maximum at the Sovereign deposit, and we speculate that this may either be the result of strong hydrothermal fluid upwelling along the Waitekauri Fault and related faults, or may reflect an ongoing gradient of increasing mass change to areas farther to the

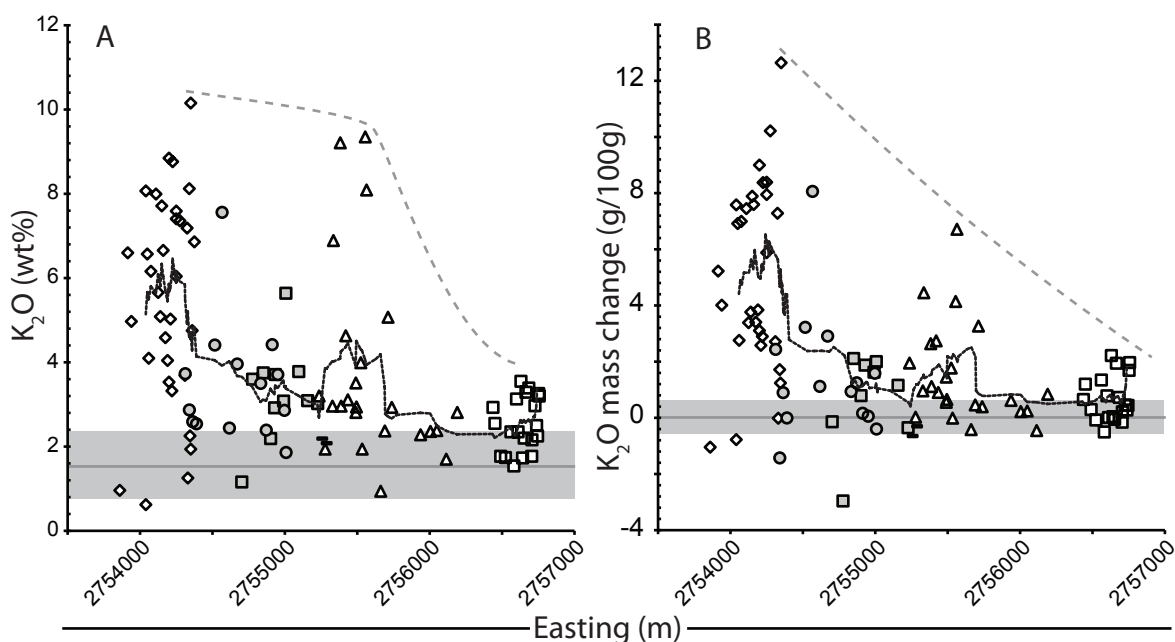


Fig. 6.10 A. Raw K_2O concentrations plotted against samples' easting coordinates in meters in reference to the New Zealand Map Grid. Dark gray line and gray shaded area indicate average and 2σ range in unaltered Coromandel Group rocks. B. K_2O mass change plotted against samples' easting coordinates in meters in reference to the New Zealand Map Grid. Dark gray line indicates zero mass change, gray shaded area indicates the 2σ range of the apparent mass change in unaltered Coromandel Group rocks (Table 6.3). Dotted lines indicate the average value calculated over each data point and the four data points to either side, and dashed lines indicate the maximum value trend. Key in both diagrams as in Figure 6.5.

west and northwest. The area west of Sovereign has not been thoroughly explored because post-mineral Whakamoehau Andesite Formation at the surface covers the Waipupu Formation (Fig. 6.1B), which is the likely host of any orebodies there, and therefore exploration would have to take place through post-mineral cover. Nonetheless, whole-rock geochemical data from the area west of Sovereign could determine whether K metasomatism is stronger or weaker on the western side of the Waitekauri Fault and whether that area is prospective for mineralization.

6.2.9.2. *Mass Transfer in the Waitekauri-Maratoto Area*

The mass balance calculations presented here, coupled with new data on the extent of altered rocks in the Waitekauri area (Morrell et al., in press), provide the opportunity to estimate the total amount of mass transferred in the Waitekauri-Maratoto area. Airborne radiometric surveys reveal a ~24 km² area where K/Th is increased from unaltered volcanic values, within which occur anomalies of very high K/Th. The larger high-K/Th zone overlaps with the magnetic quiet zone (Morrell et al., in press). The very high-K/Th anomalies occur along the Waitekauri Fault and elsewhere in the Waitekauri-Maratoto area and collectively comprise 9.3% of the larger altered zone. The larger high-K/Th zone reflects the overall extent of K metasomatism whereas the localized, very high-K/Th anomalies reflect intense, localized K metasomatism (c.f., Fig. 6.6A). We assume here for simplicity that rocks with illite (including interstratified illite-smectite), but without adularia, cause the generally elevated K/Th values in the larger Waitekauri-Maratoto area, and that the very high-K/Th anomalies within this larger area are associated with adularia-bearing rocks such as those at Sovereign. The illite-bearing rocks in the Waitekauri area on average gained K and lost Si, Na, Ca, Mg and Fe. Assuming immobility of Al and Ti, and disregarding P, the total major element oxide mass transferred (i.e., gained as well as lost) in illitic alteration is ca. 11% of the rock mass. The adularia-bearing rocks at Sovereign on average gained K and Si, and lost Na, Ca, Mg and Fe, with a total major element oxide mass transfer equal to 24% of the rock mass. K₂O accounts for 71% of the gained mass in altered rocks and SiO₂ for the remainder, where significant SiO₂ gains are confined to adularia-rich rocks that surround epithermal deposits along the Waitekauri Fault.

If 9.3% of the 24 km² Waitekauri-Maratoto altered zone consists of very high-K/Th, adularia-bearing rocks like those at Sovereign, and the rest consists of illite-bearing rocks, and if alteration extends downward 1 km with the same distribution of altered rock types, and if the average density of the altered rocks is 2.65 g/cm³, then the total mass of rocks in the Waitekauri-Maratoto area is 6.4·10¹⁰ t, and the total mass transferred is approximately 7.5·10⁹ t, equal to 12% of the rock mass. However, the actual mass

transferred is likely to be greater than this because the mass balance calculation only returns a net mass change estimate. Mass losses exceed mass gains in adularia-, as well as in illite-dominated altered rocks. We only analyzed veinless altered rocks; it is possible that some of the mass that was lost from altered rocks, especially Si and Ca, was redeposited as vein-filling minerals.

6.2.9.3. *Relationship Between Geochemistry and Alteration Mineralogy*

During hydrothermal alteration, host rocks in the Waitekauri area lost Na and Ca and gained K, producing end-member altered rocks with molar $K/(K+Na+2Ca)$ values close to 1 (Fig. 6.5). Potassium is contained in illite and/or adularia. Illite (K mica) contains approximately 7.6% K_2O and adularia contains 16.9% K_2O . Therefore, 7.6% is the maximum K_2O concentration for altered rocks without adularia, whereas 16.9% is the theoretical maximum concentration of K_2O in altered rocks, as no other rock-forming alteration mineral in epithermal deposits has a greater K_2O content than adularia. All rocks in the Waitekauri area with more than 7.6% K_2O have molar $K/(K+Na+2Ca)$ values close to 1 and therefore contain no significant Ca and Na. Coupled with the lack of data points outside the illite-plagioclase and illite-adularia arrays, this suggests that the adularia-bearing altered rocks on the illite-adularia array only formed from illite-dominated altered rocks (Fig. 6.5). This is consistent with the expected succession of mineral precipitation during the dissolution of increasing amounts of rock by a hydrothermal fluid (Giggenbach, 1984).

Petrographic relationships indicate that adularia, where present, is variably replaced by illite (Simpson and Mauk, in press). This is plausibly the result of waning of the hydrothermal system. Alternatively, it is possible that some volcanic rocks were directly altered to an adularia-dominated composition, from which adularia-rich rocks were subsequently altered towards an illite-dominated composition. A possible corresponding set of dual reaction pathways has been inferred at the Broadlands-Ohaaki geothermal system in the central North Island. There, boiling of chloride-rich water in central upflow zones forms adularia and illite, whereas peripheral mixing of chloride-rich water with CO_2 -rich water produces only illite as a K-bearing phase in host rocks (Simmons and Browne, 2000). However, in the molar K/Al vs. $(K+Na+2Ca)/Al$ diagram from the Waitekauri area, there is a gap with no samples that lies between unaltered rocks and adularia (Fig. 6.11A). If the adularia-bearing rocks on the illite-adularia array in the Waitekauri area are derived from adularia-dominated rocks, rather than illite-dominated rocks, the alteration reaction from plagioclase- to adularia-dominated must therefore have run to completion in every adularia-rich rock that we studied in the area (Fig. 6.11A). Although this seems unlikely, we offer this

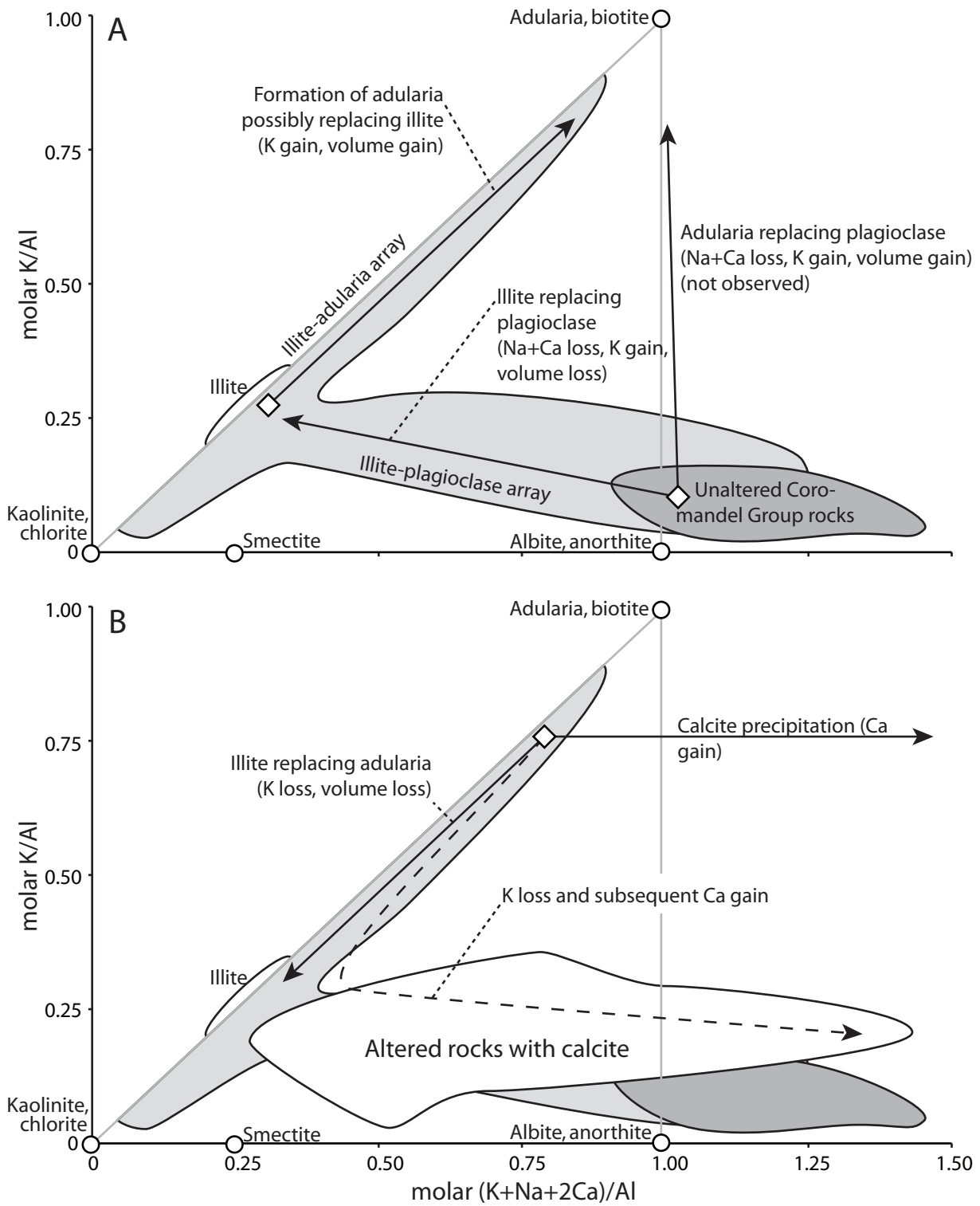


Fig. 6.11 Bivariate diagrams of molar $(K+Na+2Ca)/Al$ against molar K/Al . Circles indicate ideal mineral compositions. A. Schematic of main-stage hydrothermal alteration. Fields represent unaltered Coromandel Group rocks and altered rocks of the Waitekauri prospect excluding those with calcite. B. Schematic of late-stage alteration. White field represents all altered rocks that contain calcite.

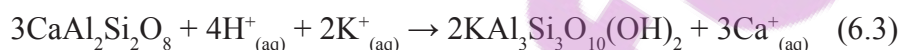
interpretation, in addition to the interpretation that adularia only forms in illite-dominated rocks, because it is more consistent with petrographic data. Our geochemical data could support either option.

6.2.9.4. Volume Change Associated with Alteration

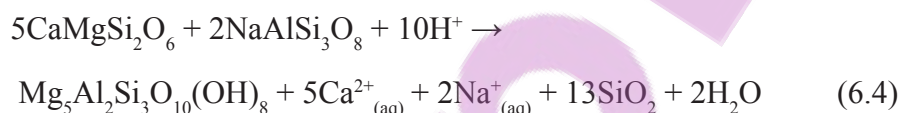
The volume change of hydrothermal reactions can be calculated based on the reaction coefficients and molar volumes of the solid phases, given that the liquid and dissolved phases are lost in an open system (Stanley et al., in press). We use molar volume data of Holland and Powell (1998) for minerals under metamorphic conditions. The minerals have approximately the same relative molar volumes regardless of P, so the same data can be applied to minerals in a shallow epithermal deposit (Berman, 1988). We identify sets of alteration reactions for the illite-plagioclase and the illite-adularia arrays. These sets are not exhaustive but summarize the hydrothermal alteration processes along the arrays, on the assumption that Al is conserved, for a plagioclase + clinopyroxene andesitic source rock. For the illite-plagioclase array:



Albite Illite Quartz



Anorthite Illite



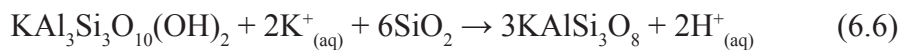
Clinopyroxene Albite Chlorite Quartz



Clinopyroxene Anorthite Chlorite Quartz

The alteration of anorthite and albite to illite and quartz (Reactions 6.2 and 6.3) constitute volume decreases of ca. -8%. The alteration of diopsidic clinopyroxene and plagioclase to chlorite and quartz also results in volume decreases of -8% (Reaction 6.4) and -4% (Reaction 6.5). Progressive alteration of rocks along the illite-plagioclase array therefore leads to a net volume decrease of the altered rock body. Despite the volume decrease, the density of the rocks also decreases because massive, intermediate igneous rock (density >2.7 g/cm³) is altered to rock with a density in the range 2.2-2.7 g/cm³ (at the Golden Cross epithermal deposit; Simpson and Mauk, 2000). Volume and density can both decrease during the alteration process because on average the altered rocks lose soluble elements to the hydrothermal fluid resulting in a net mass loss, as noted above.

For the illite-plagioclase array, the principal reaction is the replacement of illite by adularia or vice versa:



K-mica Quartz Adularia

The alteration of illite to adularia and quartz leads to a 15% volume increase; the reverse reaction, replacement of adularia by illite, which is commonly observed (Simpson and Mauk, in press), leads to a concomitant volume decrease. Late-stage calcite precipitation may be facilitated by that volume decrease, consistent with the observation that calcite does not occur in adularia-rich (high-K/Al) rocks (Fig. 6.11B).

The negative volume change that accompanies illite-chlorite replacement of an igneous plagioclase-pyroxene assemblage can help to explain why illite-altered rocks in the Waitekauri area extend to kilometers away from the central upwelling zone along the Waitekauri Fault. The reactions in Equations 6.2-6.5 create space, through which a hydrothermal fluid can permeate. This in turn promotes further hydrothermal alteration of the rock body and allows the alteration zone to expand outward from a central upwelling zone. In contrast, replacement of illite by adularia as the dominant K-bearing alteration mineral has an associated volume increase, and makes the rock body less permeable as fluid pathways become sealed. This inhibits further hydrothermal fluid interaction. Widespread adularia alteration can therefore only occur when fluid pathways are continually opened by tectonic activity, to offset the self-sealing character of the reaction. In the Waitekauri area, abundant adularia precipitated mostly at Sovereign around the central Waitekauri Fault. The more outlying alteration cell at Scotia developed a smaller adularia-rich rock volume, and rocks there experienced lesser K gains. As a result, maximum and average K₂O and SiO₂ mass gains and K/Sr, Rb/Sr and molar K/(K+Na+2Ca) values in altered rocks vector from the periphery of the Waitekauri area towards the centre of the alteration zone.

6.2.9.5. *Size of the Dataset and Application to Other Districts*

This paper is based on an extensive dataset of samples from numerous drill holes along a 3-km-wide section. Typical exploration datasets may be less exhaustive and the obtained geochemical vectors less conclusive. Nevertheless, the present approach to mass change calculation can be valuable in smaller datasets, if its principal use is the identification the maximum mass change experienced by rocks in a particular altered area. An exploration geologist can distinguish areas where significant alteration to adularia occurred and within each such area, rocks with adularia and without calcite are the most likely to have

preserved large K enrichments from the peak phase of hydrothermal alteration. Selective obtainment and analysis of such rocks can provide a dataset that documents the maximum magnitude of K enrichment. Comparison of the maximum K enrichments across an alteration zone can then determine whether a regional trend exists. In such a selective dataset, both the average and maximum K gain values would show the same trend. In the Waitekauri area dataset, the trend in average K gain values reflects the trend in maximum K gain values but is less pronounced because we analyzed a spectrum of rocks instead of only the most strongly K metasomatized rocks.

The regression equations presented in Table 6.3 are based on a cross-section of the Coromandel Group volcanic succession. They are consequently applicable to all typical Coromandel Group rocks, which are the most likely host for new discoveries in the Hauraki Goldfield. Application in other districts where medium-potassic, calc-alkaline andesites and dacites host mineralization is possible as a way of obtaining an estimate of mass changes. However, at given SiO_2 concentration, K_2O concentrations vary considerably between suites of arc volcanic rocks (Gill, 1981). Calibration to local unaltered or least-altered baseline rock compositions therefore remains a necessary precondition for a precise estimate of K_2O gains. Nonetheless, several other parameters, including K/Sr, Rb/Sr and molar $\text{K}/(\text{K}+\text{Na}+2\text{Ca})$ values can quantify relative K gains.

6.2.10. Conclusions

We used an extensive geochemical dataset to map the compositions of unaltered rocks throughout the volcanic stratigraphy of andesites and dacites in the Hauraki Goldfield. These rocks show a consistent relationship between major element composition and values of the immobile element ratio Zr/TiO_2 , and we used this feature to back-calculate the initial composition of equivalent, veinless altered rocks in the Waitekauri area. The total transferred mass is equal to ca. 11% of rock mass in illite-dominated rocks, whereas in intensely metasomatized adularia-bearing rocks it is ca. 24% of rock mass. On average, altered rocks throughout the Waitekauri area lost mass. Maximum and average K_2O , SiO_2 and Rb gains are insignificant or low in weakly to moderately altered rocks at outlying prospect areas, and reach maxima in adularia-rich rocks that surround Au deposits along the Waitekauri Fault, showing that K metasomatism increases across a 3-km-wide section from the periphery to the centre of the Waitekauri area. Average and maximum K/Sr, Rb/Sr, and molar $\text{K}/(\text{K}+\text{Na}+2\text{Ca})$ and K/Al values correlate with K_2O and SiO_2 mass gain, and together these parameters vector towards adularia-rich rocks that host epithermal Au deposits at the centre of the Waitekauri altered area.



6.3. Determination of Protolith Composition in Whitianga Group Rhyolites

6.3.1. Introduction

Whitianga Group rhyolites host a small fraction of the gold endowment in the Hauraki goldfield, even though they represent c. 40% of the volcanic rocks at the surface (Christie et al., 2007). Nevertheless, Whitianga Group rhyolites can show intense and widespread hydrothermal alteration in the vicinity of epithermal deposits (Moore, 1979; Brathwaite and Christie, 1996). Therefore, determination of the protolith composition of altered rhyolite could be useful for exploration for rhyolite-hosted epithermal orebodies. Some geochemical properties of Whitianga Group rhyolites are examined in Chapter 4. For the purpose of this section, the relevant properties are:

1) Rhyolite compositions commonly form an array in variation diagrams, where pyroxene-phyric rhyolites generally plot on one end of the array and sanidine-phyric rhyolites plot on the opposite end. Rhyolites with hornblende and biotite generally have intermediate compositions between these end members.

2) Major element variation along the rhyolite array is essentially controlled by feldspar fractionation or accumulation. Albite, anorthite and K-feldspar are all involved. Principally, K_2O concentration increases along the array whereas Na_2O and CaO decrease. Alumina concentration decreases along the array, and SiO_2 increases weakly, consistent with the relative concentrations of these oxides in feldspar and Whitianga Group rhyolites.

The purpose of this section is to determine to what extent immobile element ratios in rhyolites cor-

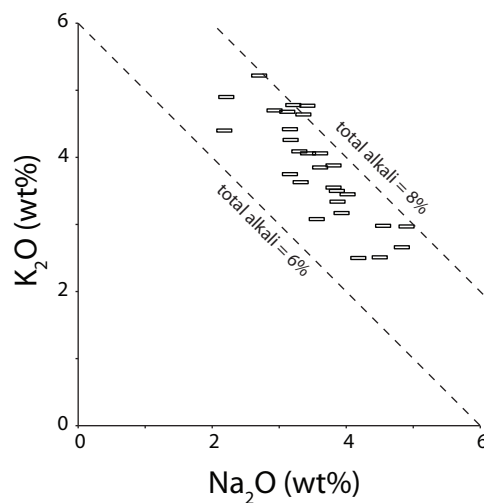


Fig. 6.12 Alkali major element concentrations in Whitianga Group rhyolites. Dashed lines connect points of equal total alkali concentration.

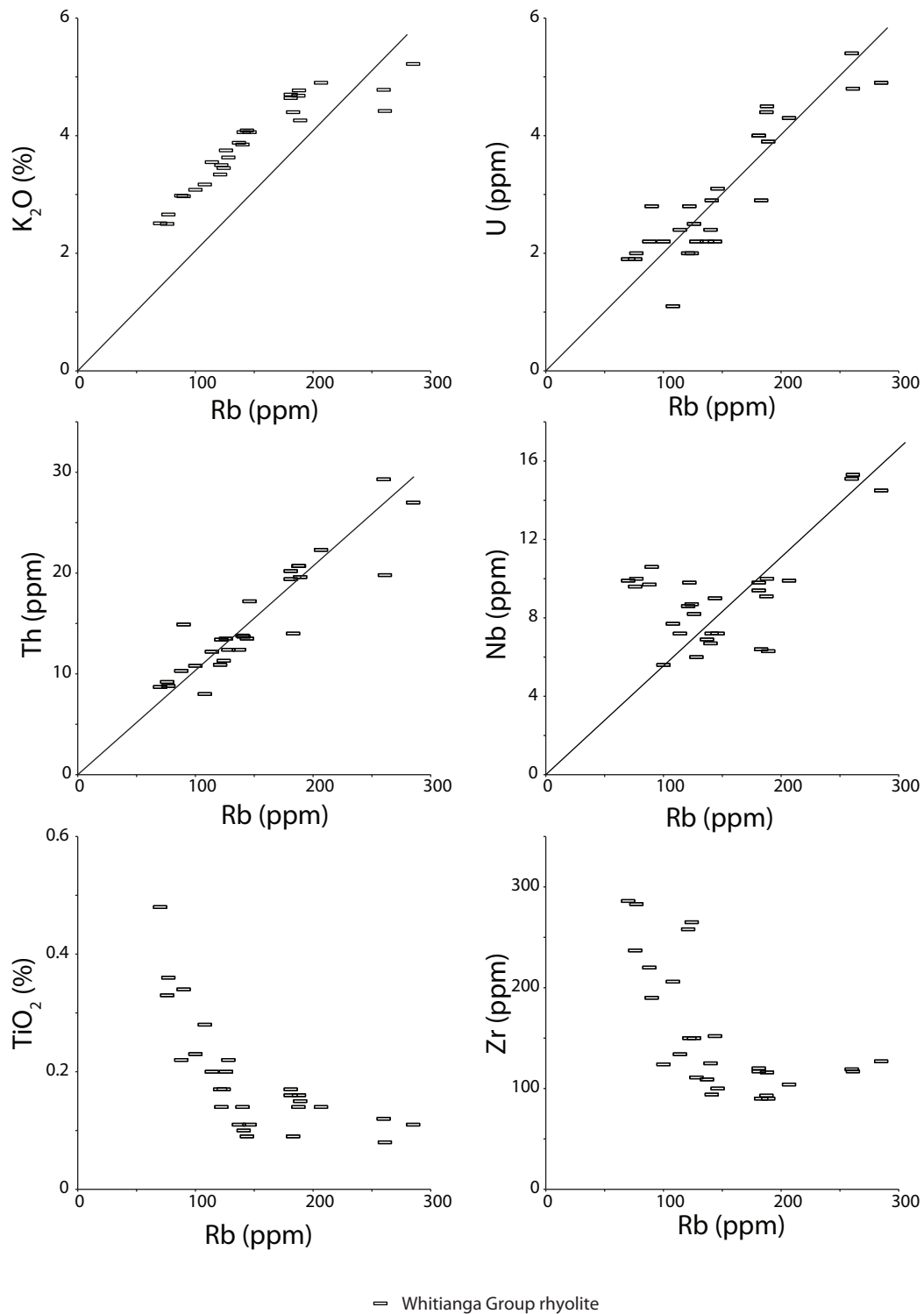


Fig. 6.13 Bivariate diagrams of major and trace element concentrations vs. Rb concentrations in Whitianga Group rhyolites. Lines through the origin were fitted visually for reference and do not represent a statistical model.

relate with rhyolite major element composition. The focus is on the commonly immobile elements Zr, Ti, Nb and Th, because these elements' concentrations are routinely measured. Other commonly immobile elements that substitute for these (e.g. Hf for Zr, Ta for Nb) show identical behaviour and are not separately discussed.

6.3.2. Major Element Variation in Rhyolites

In Coromandel Group andesites, major element composition correlates with the bulk rock Zr/Ti ratio. This reflects the contrasting behaviour of incompatible Zr and compatible Ti during magmatic differentiation, as indicated principally by SiO₂ concentration. In Whitianga Group rhyolites, magmatic differentiation is not well described by SiO₂ variation because differentiation is driven by feldspar fractionation and both albite and K-feldspar have SiO₂ concentrations close to those in Whitianga Group rhyolites (SiO₂-poor anorthite is a subordinate component in the fractionation process given the low CaO concentration in even the least-differentiated Whitianga Group rhyolites). As a consequence, protolith SiO₂ concentration may be difficult to estimate based on the geochemical properties that do vary along the rhyolite array. The concentrations of K₂O and Na₂O in a protolith are of primary interest in geochemical exploration, and in contrast to SiO₂, K₂O and Na₂O concentration correlate inversely with each other (Fig. 6.12) and with other geochemical parameters along the rhyolite array. Concentrations of K₂O in the analysed rhyolites range from 2.5 to 5.2 wt%.

Potassium is the only major element that appears to behave incompatibly during rhyolite differentiation, whereas other major elements behave compatibly like TiO₂ (Fig. 6.13), or do not correlate strongly with either incompatible or compatible elements, such as SiO₂ (not shown). However, some trace element concentrations may be more appropriate differentiation indices than K₂O concentration. In particular, the concentrations of Rb, Th and U in rhyolites, when plotted against one another, define arrays that extend through the diagram origin (Fig. 6.13). This indicates that these elements partition into the fractionating mineral assemblage at constant ratios. Given the contrasting nature of the alkali Rb and the actinides Th and U, it is plausible that the special case applies where the alkali, Rb, and the actinides, Th and U, are all excluded from the fractionating assemblage. Instead, they entirely partition either into the melt or into minerals that form in, but do not fractionate from the magma. For example, Rb is compatible in biotite, which is a common mineral in Whitianga Group rhyolites (Skinner, 1995; Krippner, 2000), but major element trends show no indication for significant biotite fractionation (Chapter 4).

6.3.3. Trace Elements

The concentrations of Rb, Th and U increase linearly as crystals fractionate from rhyolite magma. Figure 6.12 shows that K₂O concentration generally correlates with Rb (and Th and U), however the array does not extend through the origin but passes through the K₂O axis, indicating that K₂O does not act purely as an incompatible element. Furthermore, K₂O concentrations do not increase significantly at Rb

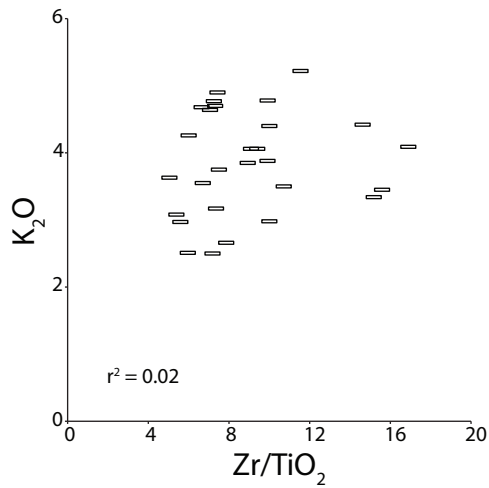


Fig. 6.14 K_2O vs $100Zr/TiO_2$ in Whitianga Group rhyolites.

concentrations greater than c. 200 ppm (Fig. 6.13), and this is also observed at high U and Th concentrations (not shown). Thus, in the most differentiated Whitianga Group rhyolites, K_2O has a partition coefficient close to 1. This correlates with the presence of sanidine in such rhyolites (e.g. Ahu Ahu Rhyolite; Skinner, 1976). Additionally, Nb concentrations are greatest in the most differentiated rhyolites (Fig. 6.13). However, Nb concentrations in less differentiated rhyolites do not correlate appreciably with Rb

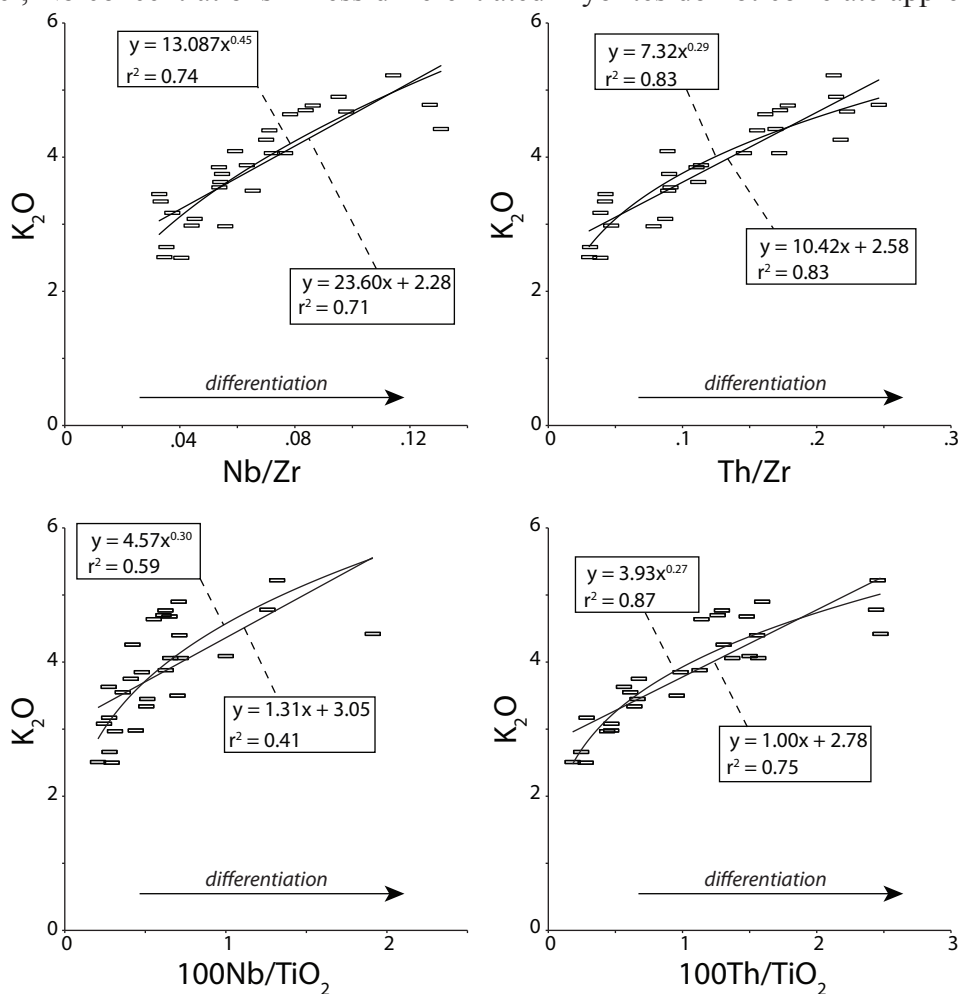


Fig. 6.15 K_2O vs. immobile trace element concentrations in Whitianga Group rhyolites. Linear and curvilinear lines represent linear and power law regression equations derived using Microsoft Excel 2008.

or Th concentrations.

6.3.4. Immobile Element Ratios and Bulk K₂O Concentration

Whereas Th acts incompatibly during rhyolite differentiation, Zr and Ti act as compatible elements (Fig. 6.13). In the case of Zr, this contrasts with its incompatible behaviour in Coromandel Group andesites. Zirconium concentrations in rhyolites are sufficiently high that the magmas were saturated in zircon (following the method of Watson and Harrison, 1983). The compatible behaviour of both Zr and Ti suggests that their relative concentration, as expressed by the ratio Zr/TiO₂, may not correlate well with bulk rock composition. This is illustrated in Figure 6.14. Based on the above, bulk rock composition can be expected to correlate with ratios between the incompatible elements Th and Nb, and the compatible elements Zr and Ti: Zr/Nb, Zr/Th, Nb/TiO₂ and Th/TiO₂. These immobile element ratios correlate marginally to significantly with bulk rock K₂O concentration (Fig. 6.15). Ratios featuring Th show better correlation with bulk rock K₂O concentration than ratios featuring Nb, consistent with the relatively poor correlation between Nb and the most incompatible elements. Linear regression equations between Zr/Th and Th/TiO₂ have correlation coefficients (r) of 0.91 and 0.87, respectively. Power law regression yields comparable correlation coefficients. The power law regression curves account somewhat better for the relatively minor increase in K₂O in the most differentiated rhyolites. Nevertheless, these results show that a linear regression equation has the potential to predict rhyolite bulk K₂O concentration based on bulk rock immobile element ratios. Table 6.8 lists the linear regression equations derived for the four immobile element ratios listed above. These equations can be used to calculate the expected K₂O in the respective rhyolite samples, which can be compared to the measured values. The double standard deviation values (2σ) of this test (Table 6.8) indicate the extent to which natural variation leads to apparent mass change. The 2σ value is lowest, at 0.64 wt% K₂O, for the Th/Zr-based linear regression equation, considerably smaller than the 2.7 wt% range of K₂O concentrations in the analysed rhyolite sample suite.

Although the method for Whitianga Group rhyolite protolith determination presented here is analo-

Table 6.4					r	Average	2σ	
K ₂ O	=	23.60	Nb/Zr	+	2.28	0.84	0.00	0.83
K ₂ O	=	10.42	Th/Zr	+	2.58	0.91	0.00	0.64
K ₂ O	=	1.31	100Nb/Ti	+	3.05	0.64	0.00	1.18
K ₂ O	=	1.00	100Th/Ti	+	2.78	0.87	0.00	0.77

Table 6.4 Linear regression equations derived for the relationship between K₂O concentration and immobile ratios in Whitianga Group rhyolites. Value of 2σ denotes the double standard deviation of the estimate.

gous to that presented for Coromandel group andesites, the rhyolite case requires more expensive data collection. This is because the method for andesites relies on Zr and TiO_2 concentrations, which are routinely measured by XRF with low uncertainty. In contrast, the equations for rhyolites derived here require Nb and Th data. These elements occur in the ~4-30 ppm range in Whitianga Group rhyolites. They are not measured with precision by XRF, and the dataset on which this study is based uses wet-chemistry ICP-MS Nb and Th concentration measurements.

6.3.5. Other Elements

Work on altered Coromandel Group andesites (Section 6.2.9.1) shows that K mass gains are the principal indicator of K metasomatism. Although K gain is coupled with Ca and Na loss, the loss of those elements is commonly complete in altered andesites throughout the Waitekauri area and therefore maximum losses do not show a trend in space. In contrast, elemental gains have no mathematical ceiling. The only major element to show mass gain in altered andesites, besides K, is Si. In Whitianga Group rhyolites, however, Si is not a suitable element for mass change calculation, because: 1) SiO_2 concentration does not correlate strongly with differentiation indices, and can therefore not be reliably estimated based on an immobile element ratio; 2) SiO_2 concentrations are high (73-79%) even in unaltered rocks. Other elements than those listed above only occur as a subordinate component in Whitianga Group rhyolites. As such, based on these considerations, K appears to be the only major element of which, in Whitianga Group rhyolites, the mass gain in altered rocks could yield a regional vector towards the core of an altered area.

6.3.6. Concluding Remarks

The regression equations obtained in this exercise provide a potential means of determining the protolith concentration of K_2O in altered rhyolites. No altered rhyolite sample suite is available, comparable to the Waitekauri area altered andesite suite, to use as a test case. Avenues for future study include 1) testing the immobility of Zr, Nb, Th and Ti in altered Whitianga Group rhyolites; 2) testing the potential of K mass gains in rhyolites to provide a spatial vector towards mineralisation. Furthermore, it must be noted that this study is based on a selection rhyolite lavas representing domes. Substantial volumes of rhyolite in the Hauraki goldfield occur as ignimbrites that, due to the more violent eruption processes involved, have greater potential for the incorporation of extraneous components. This potentially complicates the relatively straightforward correlation derived for the lava samples. However, the present method is a po-

tentially useful tool applied to altered rhyolite domes, or to altered rhyolite dikes.

Chapter 7. Synthesis

7.1. Evolving Volcanic Style

The volcanostratigraphic succession in northern New Zealand preserves a record of subduction-related volcanism from 25.5 Ma, the Late Oligocene, to the Present. Volcanism was more or less continuous from the first activity in the Northland Arc, yet the volcanic style and the nature of the erupted rocks changed markedly over time. These changes in some way reflect the interplay of factors including tectonic processes, variations in thickness and composition of the crust, and variations in mantle source and subducted slab composition.

Based on the petrologic and geochemical properties of lavas that represent a section through the succession, at least the following volcanic rock associations can be distinguished: (1) amphibole-absent, plagioclase + pyroxene-phyric basalts to andesites; (2) andesites with garnet xenocrysts or antecrysts, as well as comparable dacites that show REE evidence for garnet fractionation; (3) anomalous OIB-like basalts. These three volcanic rock types are associated with Northland Arc volcanism; they do not occur in the CVZ-TVZ parts of the succession. (4) Calc-alkaline, medium-K, plagioclase + pyroxene ± hornblende-phyric basaltic andesites, andesites and dacites. Calc-alkaline andesites occur throughout the arc volcanic succession. Hornblende-phyric andesites are mainly associated with the Northland Arc eastern belt and the pre-10 Ma CVZ, although some hornblende-phyric andesites erupted post-10 Ma, e.g. the Uretara Formation in the southern CVZ (Brathwaite and Christie, 1996). Hornblende-absent andesites are mainly associated with the post-10 Ma CVZ and the TVZ, although some andesites with no hornblende erupted prior to 10 Ma, e.g. the Whangapoua Andesite in the northern CVZ (Skinner, 1993). Where hornblende is absent, calc-alkaline andesites may nonetheless contain relict hornblende crystals. (6) Peraluminous to weakly metaluminous, relatively crystal-poor rhyolites containing plagioclase and quartz as well as variably orthopyroxene, hornblende, biotite and sanidine; (7) basalts and basaltic andesites, with or without olivine, with an affinity for high-alumina basalt (HAB) compositions, that erupted in the main arc (e.g. Mercury Basalts) as well as behind the arc (e.g. at Stony Batter and at Ti Point; Smith et al., 1993; Smith et al., 1995; Huang et al., 1997). Rhyolites and HABs appeared in the CVZ succession from 12 Ma. (8) Clinopyroxene-dominated high-magnesium andesites (HMA; Chapter 5), which appeared in the CVZ succession from 6.2 Ma. (9) Relatively low-K dacites, which are an apparently subordinate part of the succession specifically associated with the Little Barrier Island, Hikurangi and

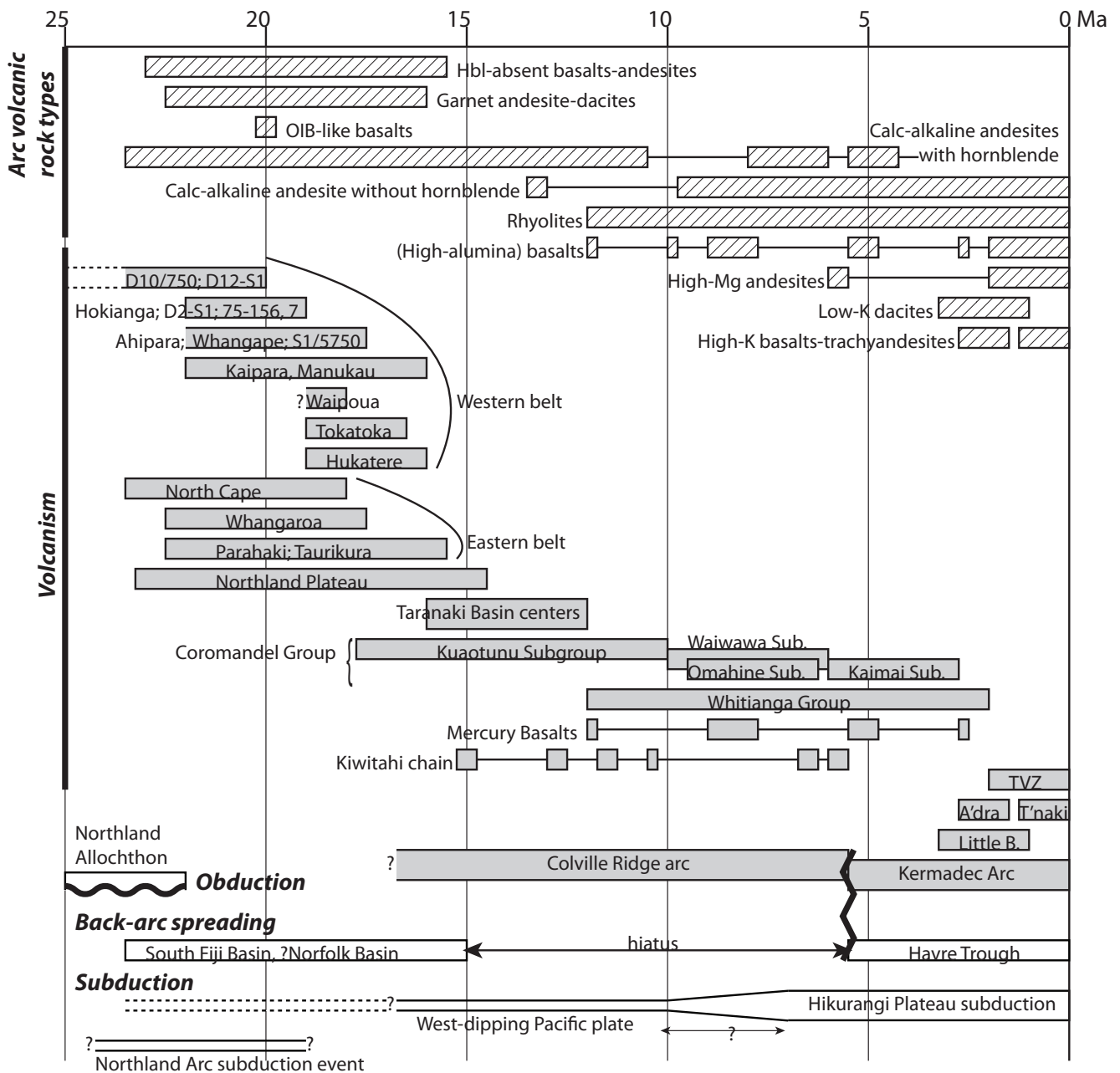


Fig. 7.1 Timing of volcanic and tectonic events in the North Island and southwest Pacific region. Based on data in Black et al. (1992), Adams et al. (1994), Herzer (1995), Nicholson et al. (2004), Briggs et al. (2005), Herzer et al. (2009), Mortimer et al. (2010).

Parakiore behind-arc centres and erupted from 3 Ma; (10) hornblende-phyric, relatively high-K basalts to trachyandesites of the behind-arc convergent margin series that erupted in the Taranaki centres and the Alexandra Volcanics. The timing of the eruption of the petrologic groups that form the North Island arc volcanic succession is summarised in Figure 7.1. This broad classification includes the major volcanic occurrences in the North Island, however it excludes several subordinate volcanic occurrences in the Northland, Auckland and Waikato regions. Volcanism there with an intraplate or transitional convergent margin character occurred in a number of volcanic fields or centres (e.g. Ngatutura, Auckland volcanic

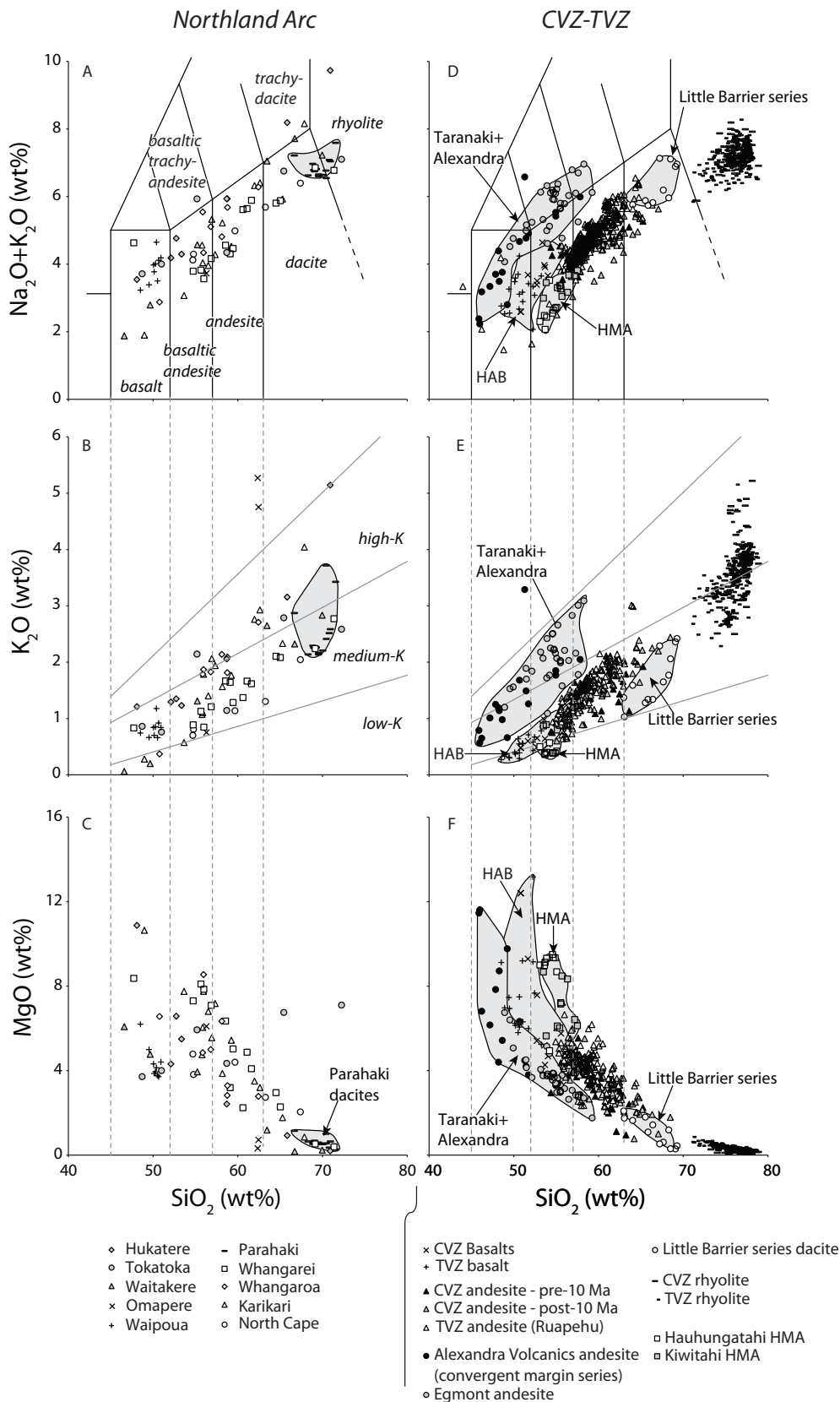


Fig. 7.2 Comparison of the major element geochemistry of major components representing the North Island arc volcanic succession. HAB: high-alumina basalt; HMA: high-magnesium andesite. Northland Arc and CVZ data from this study. Additional data from Graham and Hackett (1987, Ruapehu), Briggs and McDonough (1990, Alexandra convergent margin series), Gamble et al. (1993, TVZ basalts), Lindsay et al. (1999, Little Barrier series), Price et al. (1999, Taranaki), compilation of Deering et al. (2008, TVZ rhyolites) and Cameron et al. (2009, Hauhungatahi).

field). The classification also excludes the Holocene peralkaline rhyolites of Mayor Island in the Bay of Plenty (Houghton et al., 1992).

7.1.1. Northland Arc Subduction System

The Northland Arc and the subsequently formed Coromandel and Taupo volcanic zones erupted markedly different rock types (Fig. 7.1). Although the Northland Arc erupted calc-alkaline andesites that appear to be geochemically comparable to the calc-alkaline andesites of the CVZ and TVZ successions, the Northland Arc also erupted distinct garnetiferous andesites as well as hornblende-absent mafic rocks for which no equivalents exist in the younger parts of the succession. Further, the Northland Arc comprises twin volcanic belts that have no equivalent in the morphology of the Coromandel and Taupo volcanic zones. On the other hand, the Northland Arc did not erupt the rhyolites, high-alumina basalts and high-magnesium andesites that characterise younger parts of the North Island volcanic succession. Why was the Northland Arc different from the younger volcanic zones, whereas the younger CVZ and the TVZ erupted a comparable suite of rock types?

7.1.2. Northland Arc to Colville Ridge Arc Transition

The Northland Arc was a NW-striking arc, whereas the modern TVZ-Kermadec-Tonga arc strikes NNE, nearly perpendicular to the Northland Arc subduction system. As discussed in Chapter 3, the geochemistry of the Northland Arc volcanic rocks suggests an origin from subduction-modified mantle, with no indication for the subduction of particularly young oceanic crust. Additionally, the near-simultaneity

Fig. 7.3 (Next page) Sketch maps showing the possible evolution of the arc system(s) in the Coromandel Volcanic Zone. Shaded fields denote the inferred extent of active arc volcanism during each interval. Dark grey areas: volcanic rocks formed in each interval; light grey areas: volcanic rocks formed prior to interval; horizontal dashes: silicic rocks (rhyolites). Panels I.i and I.ii depict possible configurations for the earliest, ~18 ma CVZ volcanism, which could be an expression of the contemporaneous Northland Arc system (I.i) or alternatively an expression of the earliest activity of the Colville Ridge system in New Zealand. Panels II.i and II.ii depict possible end member configurations for the subsequent arc volcanism recorded by the Kuaotunu Subgroup, where volcanism could either be a late expression of Northland Arc volcanism, or an expression of the Colville Ridge system in New Zealand. It is possible that both arc systems overlapped in the CVZ during the time frames of Panels I and/or II. Panel III depicts a possible configuration subsequent to 10 Ma, where a migration of the locus of volcanic activity to the south and east records a trenchward retreat of the Colville Ridge system. As an alternative (not shown), it is possible that some volcanism occurred as a late manifestation of Northland Arc activity during this time interval.

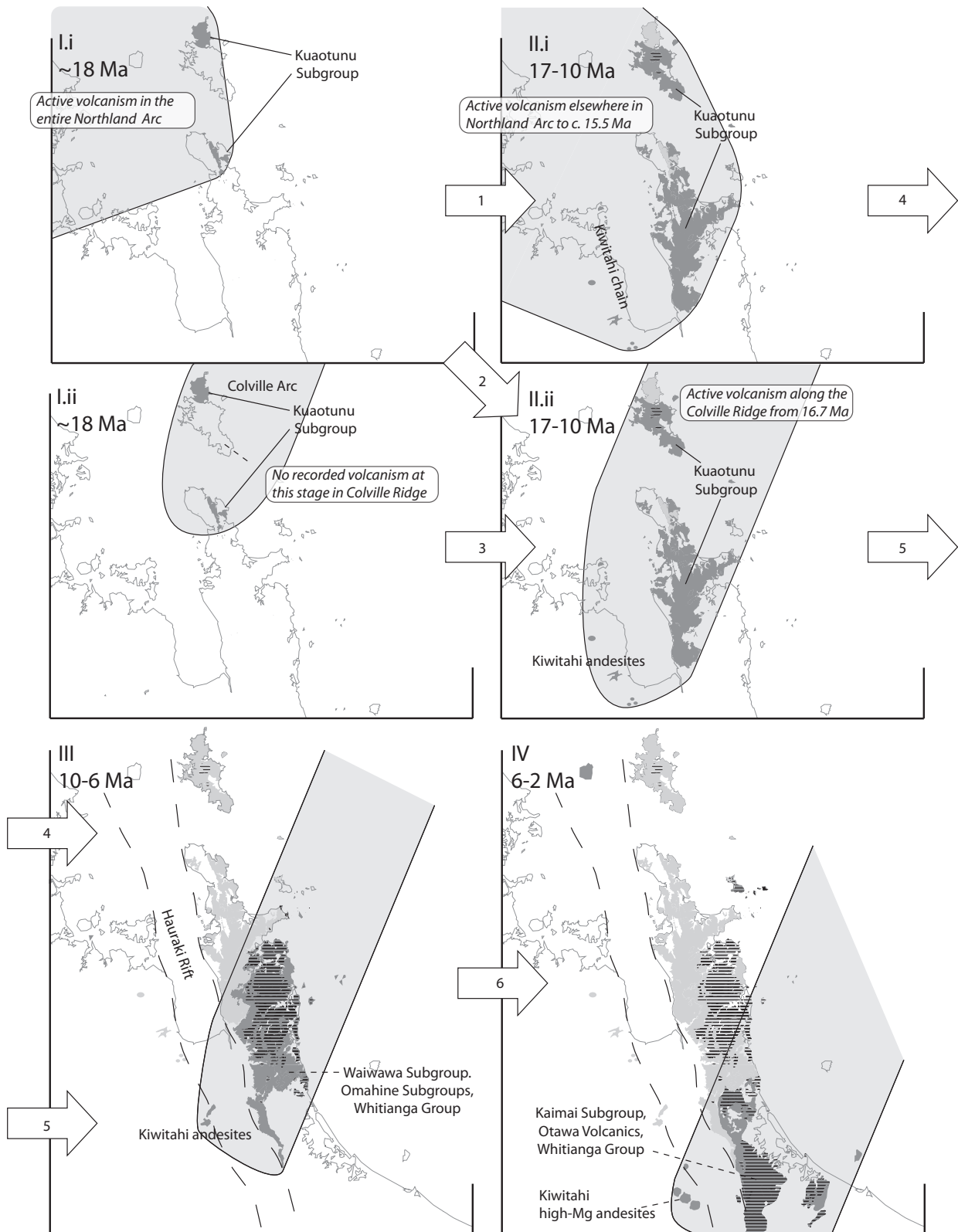


Fig. 7.3 (continued). Panel IV depicts the final stages of CVZ volcanic activity. The beginning of this time interval is marked by the eruption of high-magnesium andesites in the Kiiwitihi chain between 6.2 and 5.5 Ma, the inception of rifting of the Colville Ridge arc to form the Havre Trough at 5.5 Ma, and the eruption of a pulse of basalts in the Mercury Islands. The locus of volcanism has migrated to the south and east relative to earlier periods. Basalts, andesites and rhyolites all erupted during the final 1 Myr of CVZ activity. The end of this interval coincides with the migration of volcanism to the Taupo Volcanic Zone to the southeast.

of volcanism at points 500 km apart in the Northland Arc (Mortimer et al., 2010) suggests that the arc formed over a parallel subduction system. The principal alternative is that it formed over an oblique, north-trending subduction system that retreated towards the east (Mortimer et al., 2007). However, if this were the case, an age progression would be expected in the Northland Arc centres where volcanism occurred at later dates in the more southeastern centres, i.e. with centres towards the southeast recording later inception and cessation of volcanism. Such a progression is not unequivocally observed (Hayward et al., 2001).

The present TVZ-Kermadec-Tonga subduction system trends north, like the associated arc. The Northland Arc and the modern arc therefore appear to have formed in response to differently orientated subduction systems. Nevertheless, the volcanic succession from Northland Arc eastern belt, to Coromandel Volcanic Zone, to Taupo Volcanic Zone, is characterised by essentially continuous andesitic, subduction-related volcanism with comparable geochemical properties (Fig. 7.2).

It is relevant to consider what properties of the North Island volcanic succession could constrain the timing of the transition from the Northland Arc configuration to the modern configuration. The following events are possibly significant: (1) Activity in the western belt of the Northland Arc peaked at 22 Ma, waned from 19 Ma and was extinct by 16 Ma (Herzer, 1995); (2) OIB-like basalts erupted marking the inferred southeastern terminus of the Northland Arc at 20 Ma (Shane et al., 2010); (3) the Colville Ridge, along the extension of which occurs the CVZ, was an active arc along some of its length at least as early as 16.7 Ma (Mortimer et al., 2010); (4) explosive rhyolitic eruptions first occurred on Great Barrier Island and surrounding islands at 12 Ma (Carter et al., 2003; Nicholson et al., 2004); (5) high-alumina basalts first appeared at 12 Ma near Great Barrier Island, after which they erupted sporadically in small volumes in the CVZ and TVZ (Nicholson et al., 2004); (6) high-magnesium andesites first erupted at 6.2 Ma as part of the CVZ, after which they erupted sporadically in the western TVZ (Chapter 5); (7) rifting of the then-active Colville Ridge to form the Havre Trough backarc basin and the Kermadec Arc started at 5.5 Ma (Wyszczanski et al., 2010).

Colville Ridge rifting at 5.5 Ma separated the Kermadec Arc from the newly-extinct eastern half of the north-trending Colville Ridge arc. As such, 5.5 Ma Colville Ridge rifting provides a minimum date for the establishment of the modern tectonic configuration.

Subduction-related volcanism in the Northland Arc western belt waned to extinction between 19 and 16 Ma (Herzer, 1995). This suggests that subduction of oceanic crust at the Northland Arc subduction system slowed or stopped some time around or prior to 19 Ma. Volcanism in the eastern belt centres also

generally ceased by or prior to 15.5 Ma (Hayward et al., 2001).

The 16.7 Ma date for the Colville Ridge dredge sample (Mortimer et al., 2010) provides a minimum age for the inception of activity in the southern segment of the Colville-Lau arc, but does not necessarily imply that onland volcanism occurred in response to west-dipping Pacific plate subduction. Mortimer et al. (2010) recently determined that backarc spreading ceased in the SW Pacific region from 15 Ma onward. Prior to the availability of radiometric dates for much of the arc volcanic succession, Ballance et al. (1982) tentatively placed the transition from Northland Arc to Colville Ridge arc activity in New Zealand around 15 Ma. The waning and extinction of western belt volcanism between 19 and 16 Ma (Herzer, 1995) is in general agreement with these dates.

If this is correct and volcanism related to the Northland Arc subduction system was extinct by 16 Ma, then the post-16 Ma volcanism in the CVZ was presumably driven by west-dipping subduction of the Pacific plate. Ballance et al. (1999) raised the possibility that propagation of the Colville Ridge arc into New Zealand, in a direction parallel to the arc axis, was causally related to the cessation of the Northland Arc subduction regime.

Nevertheless, it is entirely possible that eastern belt volcanism in response to the Northland Arc subduction event continued for some time after 15.5 Ma. The products of such volcanism could form part of the Kuaotunu Subgroup in the CVZ, as well as of the submerged volcanic stack of the Northland Plateau (Herzer et al., 2009). It is relevant to consider what could be an absolute lower age for involvement of the Northland Arc subduction system. A possible date is given by the 5.5 Ma rifting of the Colville Ridge arc to form the extinct Colville Ridge, the Havre Trough backarc basin and the active Kermadec Arc. Rifting of the Colville Ridge arc seems to imply the previous existence of a well-established north-trending arc system. Consequently, it seems appropriate to place the transition from Northland Arc to Colville Ridge arc-related volcanism at some point between 15.5 Ma and 5.5 Ma. Additionally, it is possible that the transition occurred over an interval of time, between 15.5 Ma and 5.5 Ma, during which volcanism occurred in response to two distinct, but overlapping subduction systems.

Ultimately, the geochemical and isotope data collected for this study do not unequivocally resolve the problem of dating the transition from the ancient to the modern arc configuration. In particular, the major and trace element geochemical properties of the andesites in the Northland Arc eastern belt are entirely comparable to those of the andesites of the CVZ and TVZ successions (Fig. 7.2). Also, Pb isotope compositions of least differentiated rocks in the CVZ do not point to involvement of a different slab, other than Pacific plate, in the oldest CVZ volcanism. It is possible that collection of additional Pb isotope data

on least differentiated rocks of the Northland Arc belts could provide evidence for involvement of South Fiji Basin lithosphere. In the absence of additional Pb data, or in the case that additional Pb data fail to provide evidence for involvement of South Fiji Basin lithosphere, a number of other features of the succession could potentially have implications for the timing of the transition (discussed below).

7.1.3. Evolving Tectonic Setting of the CVZ-TVZ Succession

7.1.3.1. Hikurangi Plateau Collision

In the modern tectonic setting, the Pacific plate that is subducted at the Hikurangi Trench, and which drives the arc volcanism in the TVZ and the southernmost Kermadec Arc, consists of anomalously thick (c. 15-17 km) crust of the Hikurangi Plateau. Farther to the north, oceanic crust of normal, c. 10 km thickness is subducted. The Hikurangi Plateau and adjacent normal oceanic crust both have Cretaceous ages (Davy and Wood, 1994; Mortimer and Parkinson, 1996).

The timing of collision of the Hikurangi Plateau and the continental margin is uncertain and has been tentatively placed at variable times by different workers, e.g. 105 Ma (Collot et al., 2009) and 25 Ma (Whattam et al., 2008). The strongest evidence for the timing of collision, however, comes from the extent of thickened slab, which extends underneath the North Island to c. 65 km depth (Reyners et al., 2006). Based on the present-day convergence rate of 42 mm yr⁻¹ (DeMets et al., 1994), Reyners et al. (2006) estimate this to represent subduction of the Hikurangi Plateau since approximately 7 Ma.

The subducted slab beyond 65 km depth is relatively thinner (Reyners et al., 2006), suggesting that, prior to the arrival of the Hikurangi Plateau at the trench, the subducted component comprised Pacific oceanic crust of normal thickness. The normal-thickness part of the slab extends to approximately twice the distance from the Hikurangi Trench as the edge of the subducted Hikurangi Plateau (Reyners et al., 2006).

The relatively recent inferred age of the arrival of the Hikurangi Plateau at the plate boundary, following the earlier subduction of a substantial amount of regular Pacific plate lithosphere, suggests that Hikurangi Plateau collision may not have been related to the cessation of volcanism in the Northland Arc. On the other hand, the substantial length of Pacific plate slab that was apparently subducted even prior to the arrival of the Hikurangi Plateau at the subduction zone appears to suggest that the modern subduction configuration, where Pacific plate is subducted in westward direction underneath the North Island, was well established

7.1.3.2. *Hikurangi Margin Rotation*

A key process in the Miocene to Present tectonic development of the North Island is vertical axis rotation of the Hikurangi margin, which comprises the North Island east of the Taupo Volcanic Zone, relative to the Australian plate (Fig. 7.3). An early indication for this process was the recognition of volcanoclastic sediments and tephras along the Hikurangi margin with ages as old as Early Miocene (Pettinga, 1982). On the basis that these rocks are much older than the adjacent Taupo Volcanic Zone, Ballance et al. (1982) interpreted them to represent the forearc accretionary province to the Miocene arc(s) in Northland and the Coromandel, implying substantial migration of the Hikurangi margin away from the those areas. Recent studies show that the Hikurangi margin comprises a series of tectonic blocks that rotate clockwise at rates between 0.5 and 3.8° Myr⁻¹, possibly in response to the increasingly strong coupling, towards the south, between the subducting Hikurangi Plateau and the overriding Australian plate (Wallace et al., 2004). The poles to the tectonic block rotations cluster at a location about 100-150 km west of Taranaki. Clockwise rotation displaces the northern Hikurangi margin away from the stationary parts of the North Island to the west. This is accommodated by extension west of the Hikurangi margin. The area of maximum extension, since 5 Ma, includes the aerial extent of Taupo Volcanic Zone. In contrast, the southernmost Hikurangi Margin is translated parallel to or towards the stationary Australian plate, leading to a compressional regime in the southern North Island and northern South Island. The transition from extensional to compressional tectonics is located in the central North Island, coinciding with the location of andesitic volcanism at the southern end of the TVZ (Stern et al., 2006). Paleomagnetic studies indicate that the rotational regime was probably established by 7 Ma, but not earlier than 10 Ma (Nicol et al., 2007; Rowan and Roberts, 2008). Provided that rotation of the margin is an effect of the uneven coupling between the Hikurangi Plateau and the Australian plate, this age is consistent with the estimated 7 Ma onset of Plateau subduction (Reyners et al., 2006).

7.1.3.3. *Age Trends in the CVZ*

In the Coromandel Volcanic Zone, volcanic rock ages show decreasing minimum ages towards the SSE (Adams et al., 1994). At least in part, this reflects general downfaulting of blocks of the Coromandel Peninsula horst along SE-dipping normal faults (Skinner, 1986). The greatest uplift has occurred in the northern Colville peninsula, where basement graywacke and the 16 Ma Paritu pluton form the 892 m Moehau Range. It is possible that the apparent SSE younging is solely an effect of the burial of older rocks in the south and the erosion of younger rocks in the north. However, three features suggest that

an actual migration of the volcanic front occurred: (1) no post-10 Ma intrusive rocks have been found in pre-10 Ma rocks of the Kuaotunu Subgroup (Adams et al., 1994); (2) no post-10 Ma mineral deposits are developed in pre-10 Ma of the Kuaotunu Subgroup (Mauk et al., in press); (3) the centres of the Kivitahi volcanic chain, which occur in isolation, consistently young towards the SSE in parallel with the development in the Coromandel peninsula (Black et al., 1992). It therefore appears plausible that the SSE-directed younging trend is a component of an actual volcanic front migration. Herzer (1995) noted a similar trend in the ages of the Taranaki Basin centres.

7.1.3.4. *Inception of Rhyolitic Volcanism*

Early CVZ volcanism was characterised by the eruption of calc-alkaline andesites. During the Middle Miocene to Present migration of arc volcanism from the northern CVZ to the central North Island, the spectrum of erupted rock types expanded to include first rhyolites and high-alumina basalts, and then high-magnesium andesites. The eruption of each of each these rock types can be tentatively interpreted to reflect extension imposed on the arc crust (Chapters 4-5). While basaltic magmas are relatively common in an oceanic arc setting (e.g. the Izu-Bonin arc; Tamura and Tatsumi, 2002), their relatively high density generally causes them to pond at or near the Moho in a continental arc setting, where they can cause the formation of a lower crustal hot zone (LCHZ; Annen et al., 2006).

The compositions of rhyolites in the CVZ are consistent with a derivation by up to 30% dehydration melting of hornblende gabbros, which have comparable compositions to Mercury Basalts (Chapter 4). As such, it is possible that CVZ rhyolites formed principally from stalled basaltic andesitic hornblende gabbro plutons in the lower and middle crust, in response to increasing temperature, or decreasing pressure, in the LCHZ.

It is possible that incremental heating of the LCHZ by ongoing magmatism led to the transition to rhyolitic volcanism. However, a relatively long, more than 13 Myr, delay occurred between the onset of andesitic and of substantial rhyolitic volcanism in the North Island succession, given that the Northland Arc was characterised by an absence of rhyolite eruptions. This argues against a gradual transition to a rhyolite-erupting magmatic system as a result of ongoing magmatism, because delay times between the onsets of andesitic and rhyolitic volcanism elsewhere are commonly considerably shorter than 13 Myr. For example, felsic eruptions at Raoul volcano, in the oceanic Kermadec Arc setting, follow initial andesitic volcanism by c. 1 Myr (Smith et al., 2006b). In the southern Rocky Mountains volcanic field, USA, delays between andesitic precursor volcanism, and subsequent rhyolitic volcanism, are maximally 5 Myr,

and generally less than 1 Myr (Lipman, 2007). Consequently, a model is preferable in which the transition from an andesitic volcanic system (Northland Arc and early Coromandel Volcanic Zone) to a system erupting rhyolites (post-12 Ma CVZ) relates to either an increase in the rate of heating of the LCHZ or a lowering of pressure. Either possibility could occur under the influence of changing tectonic or magmatic constraints on the arc system. As discussed in Chapter 4, it is possible that increased extension imposed on the arc crust was a factor, either by lowering pressure on the LCHZ, or by allowing increased intrusion of mantle-derived magma in the lower crust. In the present tectonic setting, the most intense rhyolitic volcanism, in the TVZ, is strongly linked spatially to extensional tectonics.

The inception of rhyolitic volcanism in the North Island succession, at c. 12 Ma, postdates that of andesitic volcanism in New Zealand by more than 13 Myr. It postdates the earliest known Colville Ridge arc activity, at 16.7 Ma (Mortimer et al., 2010), by more than 4.5 Myr. On the other hand, Hikurangi Plateau collision likely occurred, and initiated rotation of the Hikurangi Margin, no earlier than 10 Ma and possibly as late as 7 Ma (Reyners et al., 2006; Rowan and Roberts, 2008). Why, then, did rhyolitic volcanism start when it did?

As discussed in Chapter 4, it is possible that a change in Pacific plate behaviour affected the Pacific-Australasian plate boundary in such way that it led to the transition. Atwater and Stock (1998) identified perturbations in Pacific plate motion that coincide with key instants in the development of rhyolitic volcanism in New Zealand. At 12 Ma, coinciding with the first basaltic and rhyolitic eruptions in the CVZ, an increase occurred in the rate of displacement of the Pacific plate. At 8 Ma, coinciding with the first phase of major caldera formation on Great Barrier Island and the Coromandel Peninsula, a change occurred in the azimuth of Pacific plate displacement (Atwater and Stock, 1998). The coincidence in timing suggests a connection, even though the causal relationships between these events, if any, are unclear. As one possibility, it could be that the alterations in Pacific plate behaviour had an effect on the rate of slab rollback and that this in turn affected the rate of extension of the arc crust.

An alternative possibility is that the inception of rhyolitic volcanism was tied to the transition from the Northland Arc to CVZ subduction systems. Northland Arc western belt activity effectively ceased around 16 Ma (Herzer, 1995). It is possible that eastern belt volcanism continued for longer, however, and that for some time after 16 Ma, volcanism in the CVZ partly or wholly occurred in response to the final stages of the Northland Arc subduction event. Establishment of the modern, west-dipping Pacific plate subduction system configuration at some time between 16 and 12 Ma would result in a much shorter delay, not exceeding 2-3 Myr, between the onset of andesitic and rhyolitic volcanism in response to this

particular subduction event. This shorter delay time is comparable to that in other settings and might not require a specific tectonic event to trigger a transition to rhyolitic volcanism, rather this transition would have occurred in response to ongoing magmatism in a distinct arc system. This hypothesis still invites the question of why the tectonic setting of the new arc system was more favourable to the production of voluminous silicic magmas than the abandoned Northland Arc system.

7.1.3.5. *Inception of Correlated Basaltic and Rhyolitic Volcanism*

Basalts appear in the northern CVZ from c. 12 Ma, with the first recorded eruptions occurring near Great Barrier Island in close spatial association with the apparently near-simultaneous first eruption of rhyolites in the CVZ (Nicholson et al., 2004). Subsequent basalt eruptions occurred from 9.1 Ma, in a pulse that ended at 7.4 Ma, overlapping in time with intense caldera-forming rhyolitic volcanism between 8 and 7 Ma (Adams et al., 1994; Carter et al., 2003). These early eruptions were followed by subsequent, sporadic basalt eruptions in the CVZ and TVZ.

Basaltic magmas were logically present at depth in all arc magmatic systems in New Zealand. Their eruption therefore may not mark a specific change in the nature of the magmatic system. However, it seems plausible that the appearance of basalts from 12 Ma reflects a change in the tectonic constraints on the arc crust, which was previously apparently impermeable to basaltic magmas. The correlation with rhyolitic volcanism, which also occurred from c. 12 Ma, suggests that the onset of basaltic eruptions reflects greater extension imposed on the arc crust than previously.

A new pulse of basaltic eruptions occurred in the northern CVZ between 5.5 and 4.7 Ma (Adams et al., 1994). This pulse occurred coincidentally with the earliest opening of the Havre Trough backarc basin at c. 5.5 Ma, by rifting of the Colville Ridge arc to form the active Kermadec Arc and the extinct Colville Ridge (Wysoczanski et al., 2009).

7.1.3.6. *Inception of High-Magnesium Andesite Volcanism*

High-magnesium andesites erupted at the southern end of the Kiritahi chain between 6.2 and 5.5 Ma (Black et al., 1992). Eruption of this suite closely preceded the 5.5-4.7 Ma basaltic pulse in the northern CVZ. Despite major compositional differences, both basalts and high-magnesium andesites represent comparatively primitive magmas that show very limited evidence for crustal-level differentiation processes such as assimilation of basement rocks or fractionation of amphibole (Chapters 4, 5). Globally, high-magnesium andesites are generally associated with extensional arc-related settings, e.g. erupting

during Late Miocene opening of the Sea of Japan (Mashima, 2009). In northern New Zealand, high-Mg andesites primarily erupted from volcanoes along the western margin of the TVZ, forming an apparently continuous progression with the Kiwitahi high-Mg andesites, which are in turn possibly contiguous with the pre-6.7 Ma calc-alkaline andesites in the Kiwitahi chain (Chapter 5). As discussed in Chapter 5, a possible interpretation is that this chain of centres records the migration of the continental tip of the largely oceanic NNE-trending arc system: initially, the Colville Ridge arc; after c. 5.5 Ma, the arc rifted to form the Kermadec Arc, coincident with the earliest eruption of high-magnesium andesite.

7.2. Volcanism and Mineralisation

A genetic link has long been established between magmatism and the formation of many classes of hydrothermal ore deposits, indicated by the association of porphyry deposits and intrusive bodies, of active geothermal systems with areas of active volcanism, and by the signature of magmatic stable isotope compositions in some hydrothermal fluids (Hedenquist and Lowenstern, 1994). In northern New Zealand, c. 50 epithermal gold-silver deposits of the Hauraki goldfield formed in the Middle and Late Miocene in close association with evolving arc volcanism in the Coromandel Volcanic Zone (Skinner, 1986; Adams et al., 1994). Recent studies have significantly extended and refined the geochronology of mineralisation (Mauk and Hall, 2004; Mauk et al., in press). A key outcome of the new age data is that the bulk of economic mineralisation occurred following the Middle Miocene inception of rhyolitic volcanism alongside ongoing andesitic volcanism (Carter et al., 2003; Nicholson et al., 2004). In contrast, the earlier, Late Oligocene to Early Miocene subaerial andesitic volcanism in the Northland Arc and early CVZ is not associated with any known ore deposits (Christie and Barker, 2007; Christie et al., 2007).

7.2.1. Co-evolution of Volcanism and Mineralisation

Mineralisation in the Hauraki goldfield overlapped in time with ongoing arc volcanism. Volcanism and mineralisation were apparently correlated in a number of ways.

7.2.1.1. Andesitic Host Rocks

In the CVZ, andesites only form 61% of volcanic rocks at the surface (Christie et al., 2007). Nonetheless, c. 97% of the Hauraki goldfield gold production has been from andesite-hosted deposits. The affinity of economic mineralisation with andesitic host rocks could reflect more favourable lithologic properties relative to rhyolites. For example, epithermal veins in rhyolites are typically narrower, but more clus-

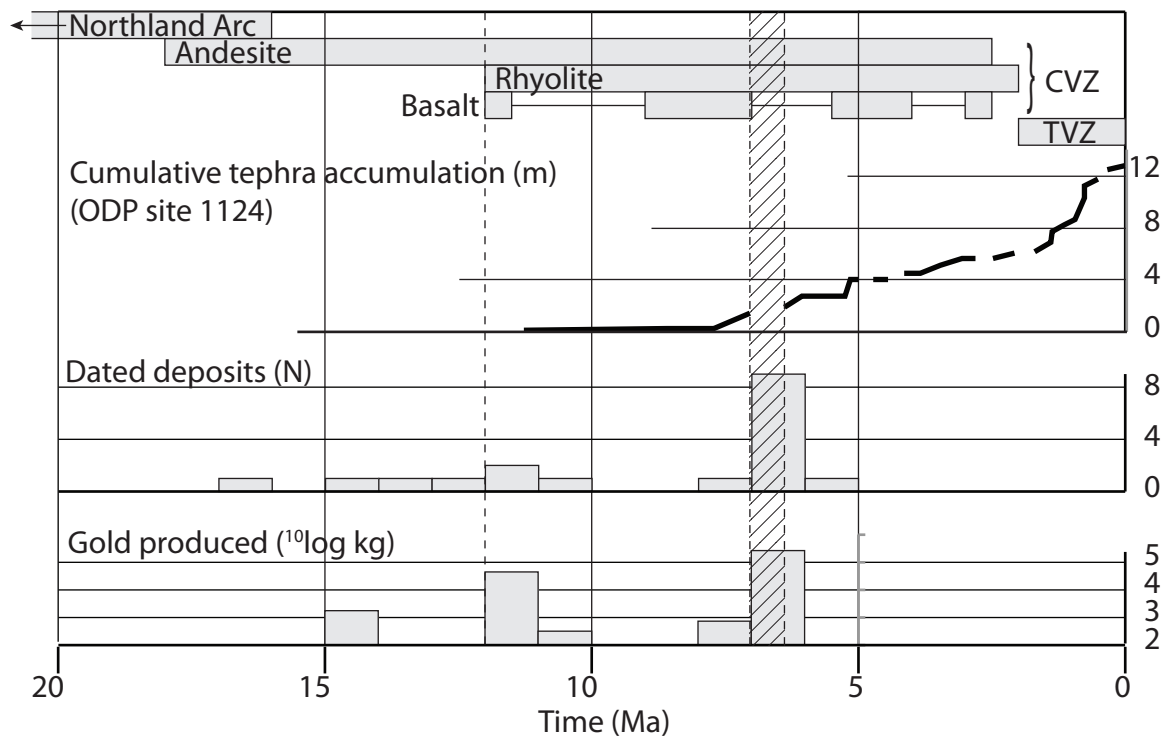


Fig. 7.4 Timing of volcanic development and mineralization events. Compiled from Adams et al. (1994), Briggs et al. (2005), Carter et al. (2003), Christie et al. (2007), Mauk et al. (in press). Dashed area marks 700 kyr hiatus in recorded rhyolitic eruptions.

tered, than veins in andesites (Brathwaite et al., 2001b). Stockwork mineralisation may have resulted in uneconomically low grades at some rhyolite-hosted prospects even though the amount of gold precipitated could be comparable to that in andesite-hosted deposits. In any case, the existence of low-grade stockwork veins in rhyolites implies that gold-bearing fluids did percolate through rhyolitic rocks.

The hydrothermal fluids in active, rhyolite-hosted geothermal systems in the Taupo Volcanic Zone precipitate Au-rich scales on back-pressure plates in geothermal power stations (Brown, 1986). Simmons and Brown (2000) determined that the measured gold flux in some TVZ geothermal systems would, in principle, be sufficient to create a world-class deposit within c. 50 kyr. Although this estimate is based on an ideal scenario where 100% of the transported gold is precipitated in an economic fashion, the 50 kyr time span is short relative to the lifetime of the TVZ, which has been active since 2 Ma. Even if precipitation was much less than 100%, some economic mineralisation might be expected, yet has not been discovered in the rhyolitic host rocks that dominate the TVZ. Simmons and Brown (2007) inferred that the absence of gold deposits in the TVZ could reflect insufficient focusing of fluid flow and metal precipitation, i.e. due to the unfavourable lithologic properties of the rhyolitic host rocks.

Epithermal quartz veins developed in andesitic host rocks in the CVZ tend to be wider, with greater extension, relative to veins in rhyolitic host rocks (Christie et al., 2007). This is especially true where the

andesites are massive lavas as opposed to pyroclastic rocks (Wodzicki and Weissberg, 1970). Alternatively, andesite host rocks could form a chemical trap for ore-bearing fluids, e.g. due to their greater capacity, relative to silicic rocks, to precipitate sulfides and thereby deplete the fluid of S-dependent ligands. The presence of andesitic host rocks may thus be a prerequisite for the formation of large high-grade deposits in the northern New Zealand tectonic setting.

7.2.1.2. *Rhyolitic Volcanism*

The advent of explosive rhyolitic volcanism and the advent of gold mineralisation in northern New Zealand broadly coincide in time (Fig. 7.4). The earliest recorded explosive rhyolitic eruptions in northern New Zealand occurred around 12 Ma (Carter et al., 2003; Nicholson et al., 2004). It is possible that some slightly older Late Miocene rhyolitic eruptions occurred, but if so the associated tephrae are altered and cannot be dated (Carter et al., 2003).

The oldest dated mineral deposit is the 16.3 Ma Paritu Cu porphyry deposit (Mauk et al., in press). The oldest dated epithermal gold deposits in northern New Zealand are the 14.1 Ma Kuaotunu and the 13.2 Ma Opitonui deposits, which together yielded 2284 kg Au (Christie et al., 2007; Mauk et al., in press). Therefore, the oldest known deposits predate the oldest recorded rhyolitic eruptions by c. 2 Myr. Consequently, there is no unequivocal correlation between the first recorded occurrence of economic gold mineralisation and rhyolitic volcanism. On the other hand, andesitic eruptions occurred in the Northland Arc from at least the latest Late Oligocene (25.5 Ma; Hayward et al., 2001), predating the earliest gold mineralisation by over 11 Myr (Christie and Barker, 2007). The Kuaotunu and Opitonui deposits therefore fairly closely predate the first rhyolitic eruptions. Additionally, they comprise a subordinate fraction of the total gold production of the Hauraki goldfield, whereas virtually all gold was produced from deposits that formed subsequent to the inception of rhyolitic volcanism.

7.2.1.3. *Peak Mineralisation During Rhyolitic Quiescence*

Virtually all of the economic gold mineralisation in the Hauraki goldfield post-dated the earliest rhyolitic eruptions; nevertheless, several of the most productive gold deposits were formed during an interval that overlapped with the longest recorded break in explosive rhyolitic eruptions (Fig. 7.2). Following intense, caldera-forming activity in the central CVZ between 7.7-7.0 Ma, a quiet period occurred between 7.0 and 6.3 Ma. Another phase of intense rhyolitic eruptions started thereafter (Carter et al., 2003). The Neavesville, Wharekirauponga, Golden Cross, Maratoto, Sovereign, Jubilee and Karangahake deposits

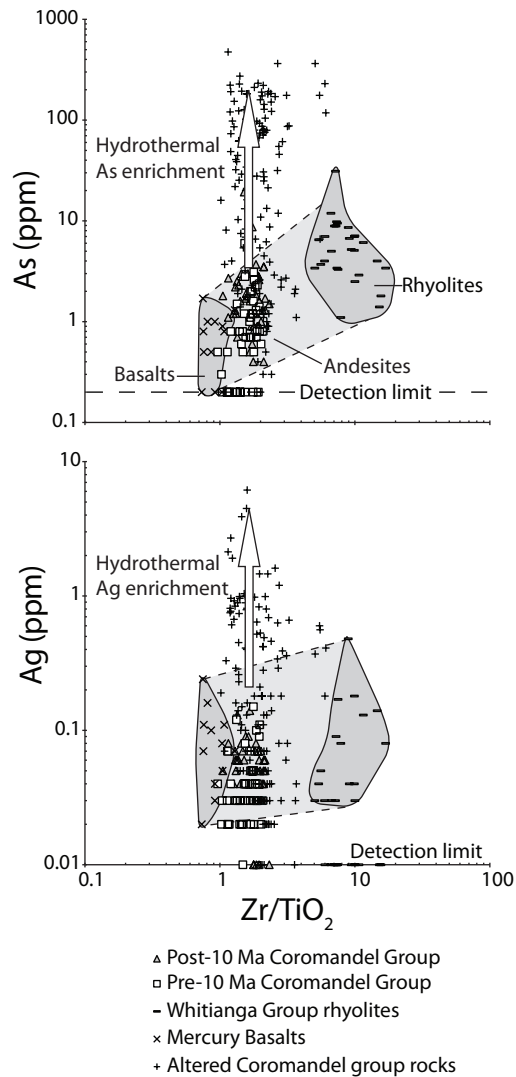


Fig. 7.5 Behaviour of two epithermal suite elements in fresh unaltered and altered volcanic rocks of the CVZ. Data from the datasets presented in Chapters 4 and 6.

formed during the lull in rhyolitic eruptions. The Broken Hills deposit predates it by 100 kyr, whereas the Martha, Favona and Komata deposits formed between 6.16-6.05 Ma (Mauk et al., in press), just post-dating the renewed explosive silicic volcanism. The predominant host rocks of the deposits that formed during this interval is the andesitic 8-7 Ma Waipupu Formation (Brathwaite and Christie, 1996).

7.2.2. Discussion

The onset of mineralisation in the Hauraki goldfield appears to correlate in time with a transition from an andesite-erupting magmatic system to a system that erupted a broad suite of basaltic, andesitic and rhyolitic magmas. In the TVZ, rhyolitic volcanism is coupled to basaltic and andesitic magmatism at depth; this is indicated e.g. by the existence of a dense lower crust (Harrison and White, 2006), by the comparable isotopic compositions of rhyolites and less-differentiated rocks (Price et al., 2005) and by the

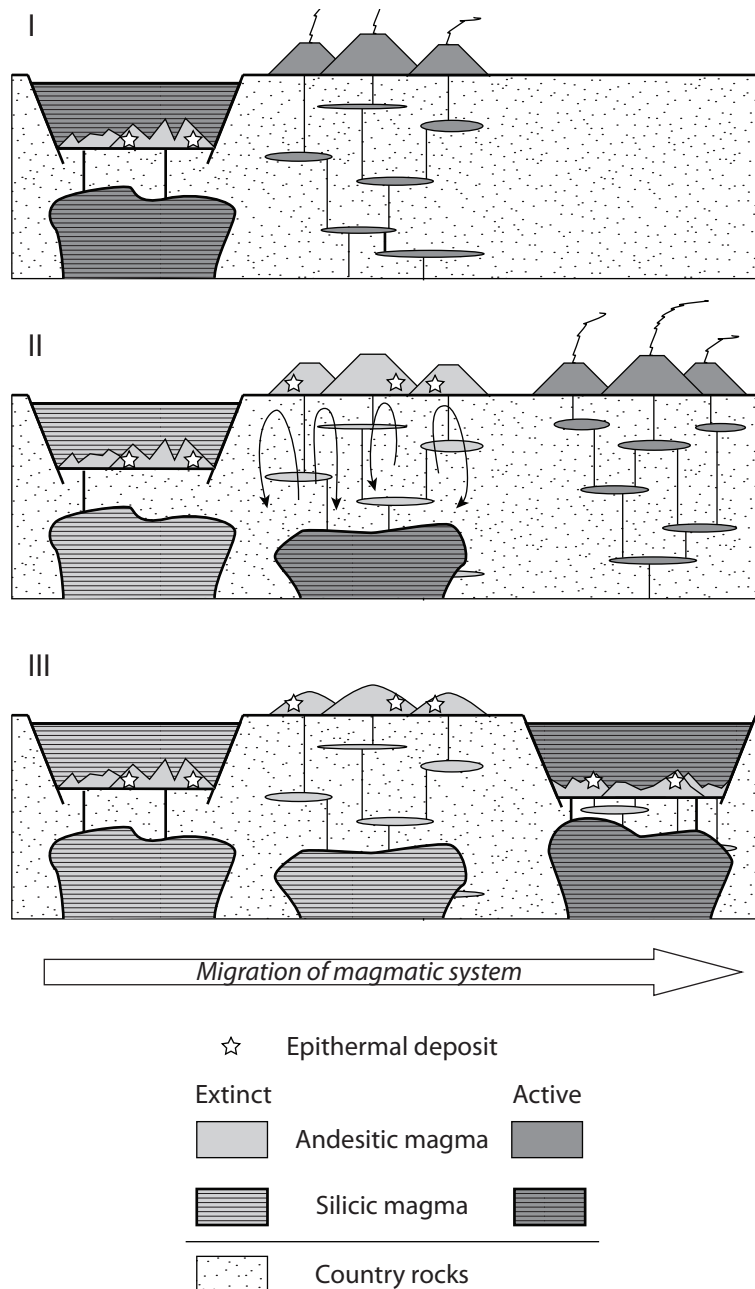


Fig. 7.6 Cartoon crustal sections depicting three consecutive stages of the possible co-development of magmatic systems and epithermal deposits in the Hauraki goldfield. Panel I depicts andesitic magmatism on the system periphery, bordering more mature silicic magmatism in the system centre. Explosive silicic volcanism has buried or destroyed pre-existing, andesite-hosted epithermal deposits. Panel II depicts a subsequent stage where magmatism has migrated. A silicic magmatic system now underlies the previously formed andesite volcanoes and promotes the formation of high-grade epithermal deposits in the andesite host rocks. New andesite volcanoes form on the border of the magmatic system. At this stage, silicic magmatism does not proceed to an explosive eruptive phase, allowing the andesite-hosted epithermal deposits to survive to Panel III. Panel III depicts a final stage where magmatism has further migrated. Silicic magmatism has promoted the formation of new epithermal deposits in andesite host rocks, however explosive silicic volcanism has resumed and destroyed or buried these newly formed deposits. Deposits formed in Panel II are fortuitously preserved in eroded volcanic edifices.

triggering of silicic ignimbrite eruptions by basaltic intrusion (Shane et al., 2007).

Basaltic eruptions in the CVZ, which occurred from c. 12 Ma onward, suggest that the crust became more permeable to dense mafic magmas from 12 Ma. Is it possible that the bimodal, basaltic-rhyolitic magmatic system more efficiently transported epithermal suite elements (Au, Ag, Se, As, Sb, Hg, Tl) to shallow depth than the precursor andesitic system?

7.2.2.1. *Basaltic Gold Sources*

On Lihir Island, New Guinea, and in the northern Great Basin, US, native gold crystals contain alloyed Pb with a mantle-like isotope signature (Kamenov et al., 2005; Kamenov et al., 2007). In contrast, gangue materials in these deposits have isotopic properties that more closely resemble those of wall rocks. As a possible explanation, Saunders et al. (2008) proposed that, in the case of the Great Basin deposits, exsolved fluids from deep-seated mafic intrusions transported gold and silver particles to the epithermal level. The alloyed Pb in these particles reflects the isotopic composition of the mantle-like source of the metals; in contrast, the raw material for the gangue minerals was apparently derived from proximal sources, e.g. by leaching of host rocks. Derivation of gold from deep sources could help to explain why some superficially similar deposits, i.e. with comparable alteration mineral assemblages, have strongly variable grades.

If a similar process operated in the Hauraki Goldfield, then one possible reason why high-grade deposits only formed around and after 14 Ma may be that volatile-exsolving basalts did not previously intrude at a sufficient rate. Additionally, it could be that the fluids that transported any gold particles from the presumed deep-seated intrusions could not properly ascend the crust prior to 14 Ma. Increased extensional stress exposed on the arc crust could have facilitated both processes, and be tied to the advent of silicic volcanism as discussed in Chapter 4.

7.2.2.2. *Silicic Gold Sources*

As an alternative to derivation from basaltic sources, it could be that the epithermal suite elements in Hauraki goldfield deposits were derived from rhyolitic sources. In this case, the appearance of high-grade gold deposits from c. 14 Ma could be directly linked to the presence of silicic magma bodies at shallow depth, underlying mostly andesite-hosted geothermal systems. Magmatic differentiation generally enriches the epithermal suite elements, therefore unaltered silicic rocks tend to contain greater concentrations of these elements than unaltered mafic rocks (Hedenquist and Lowenstern, 1994). Figure

7.5 illustrates the behaviour of two epithermal suite elements (As and Ag) in fresh unaltered and altered volcanic rocks of the CVZ. In the case of As, concentrations in unaltered rhyolites are approximately an order of magnitude greater in rhyolites than in unaltered basalts; in the case of Ag, concentrations in unaltered rhyolites and basalts largely overlapped, although rhyolites on average have somewhat greater Ag concentrations. In both cases, unaltered andesites have compositional ranges that are intermediate between those of basalts and rhyolites. This is consistent with the inference that CVZ andesites appear to be mixtures of a basalt-like and a silicic component (Chapter 4). Consequently, magmatic differentiation can produce some enrichment in the epithermal suite elements.

On the other hand, Hedenquist and Lowenstern (1994) also noted that hydrothermal enrichment is a more efficient enrichment process. For example, gold occurs in volcanic vapor and aerosol emissions (e.g. Larocque et al., 2008); further, magma to vapor Au enrichment factors at Vulcano, Italy, are in the order of $1 \cdot 10^6$ (Toutain et al., 2003). In the Hauraki goldfield, hydrothermally altered volcanic rocks have epithermal suite element concentrations that are up to two orders of magnitude greater than those in equivalent unaltered volcanic rocks (Fig. 7.5). Nevertheless, although hydrothermal enrichment is apparently much more efficient than enrichment through magmatic differentiation, mineralisation is in some cases preferentially associated with felsic members of a magmatic suite (Creasey, 1977). One possible reason for this is that magma composition can indirectly control the solubility of volatile elements, e.g. Cl (Webster, 2004). In turn, the solubility of metals in a hydrothermal fluid correlates positively with Cl content (Bai and Koster van Groos, 1999). Webster (2004) determined that the solubility of Cl decreases from diorite to quartz-monzonite, i.e. with increasing degree of magmatic differentiation. Consequently, a silicic magma could more efficiently exsolve a Cl-rich, and therefore potentially metal-rich hydrothermal fluid, compared to a less differentiated (basaltic or andesitic) magma. Where the exsolving silicic magma resided under amenable host rocks, the exsolved metals could then be trapped in an epithermal deposit.

It appears from the above that basaltic as well as rhyolitic magmas were potentially sources of metal-rich hydrothermal fluids. It is possible that basalts as well as rhyolites contributed gold to the epithermal deposits in the Hauraki goldfield. Evidently, it cannot be excluded that andesitic magmas contributed precious metals, however the processes described above show how the involvement of basaltic and/or silicic magmas might enhance the transport of precious metals to the epithermal level, compared to purely andesitic magmas. One avenue for further study is to determine the isotopic composition of alloyed Pb in gold-silver particles and gangue minerals in the Hauraki goldfield, to assess whether a contrast exists

between the sources of Pb in gold and in gangue minerals.

Alternatively, it is possible that the gold in the Hauraki goldfield epithermal deposits is not derived from magma but was scavenged from basement rocks. In the TVZ, hydrothermal fluids in some hydrothermal systems are undersaturated in gold and would therefore leach gold from any basement rocks they pass through (Simmons and Brown, 2007). In this case, it could be argued that enhanced gold mineralisation correlates with basaltic-silicic magmatism simply because a magmatic system capable of maintaining large intrusive bodies in partially molten state in the shallow crust should produce more sustained and widespread hydrothermal circulation, enhancing metal transport to the epithermal level.

Provided that a magmatic system that erupts basalts, andesites and rhyolites is apparently more inclined to induce the formation of gold deposits than a system that merely produces andesites, it is relevant to consider why the most productive pulse of mineralisation coincided with the longest recorded hiatus in explosive silicic eruptions. One possible factor may be the affinity of high-grade gold deposits with andesitic host rocks. Explosive rhyolitic eruptions have the potential to obliterate or bury the remnants of precursor andesitic volcanoes. This has happened in the TVZ where a number of buried andesitic centres have been recognised underneath silicic cover rocks (Wilson et al., 1995). Any high-grade gold deposits that might have occurred in such andesites, are lost either because they are destroyed in a cataclysmic eruption, or because they are buried to depth where extraction is not economical (Fig. 7.6). The rhyolitic cover rocks that then replace any precursor andesites at the surface may host geothermal systems, as is a common occurrence in the modern TVZ. However, because veins in rhyolite host rocks are generally thinner and more clustered, these rhyolite-hosted geothermal systems would have been less amenable to the formation of high-grade gold-silver deposits than the destroyed andesite-hosted geothermal systems. Consequently, one possible scenario is that the disproportional number of high-grade deposits that remain from the 7-6 Ma interval exist because explosive rhyolitic volcanism ceased during that time. When explosive rhyolitic volcanism resumed, a disproportionate number of high-grade andesite-hosted deposits fortuitously survived, possibly because the locus of volcanism had migrated towards the south and east. If correct, this chain of events represents a best-case scenario that apparently has not subsequently occurred in northern New Zealand.

7.3. Avenues for Future Research

The results of this study present a number of avenues for future research.

7.3.1. Northland Arc Slab Provenance

Part of the motivation to obtain Pb isotope data on least differentiated volcanic rocks of the CVZ (e.g. Mercury Basalts, Port Charles Andesite) was to determine whether any observed shift in Pb isotope compositions over time could be indicative of the provenance (young vs. old oceanic lithosphere) of the subducted slab. The limited results obtained in this study suggest that $^{207}\text{Pb}/^{204}\text{Pb}$ values in the least differentiated rocks decreased rather than increased during the development of the CVZ-TVZ succession, and therefore do not specifically support involvement of young subducted lithosphere (i.e. South Fiji Basin lithosphere) during any stage of CVZ magmatism. Nevertheless, the oldest rocks on which Pb isotope compositions have been determined in this study are the c. 17.7 Ma Port Charles Andesite, which erupted when Northland Arc activity was waning, and 1 Myr prior to the first recorded activity in the Colville Ridge arc. If subducted South Fiji Basin lithosphere was involved in the Northland Arc subduction system, it is possible that some mafic Northland Arc volcanic rocks could retain particularly small initial $^{207}\text{Pb}/^{204}\text{Pb}$ values, compared to the mafic rocks of the Coromandel Volcanic Zone.

7.3.2. Andesite Petrogenesis

Porphyritic Coromandel Group andesites arguably are mixtures of a crystal cargo and one or more melt phases, of which all components are not all necessarily genetically related (Chapter 4). The geochemical bulk compositions of such andesites can in many respects be described as mixtures between a Mercury Basalts-like mafic component, and a silicic component. The silicic component appears to have been similar to, but distinct from Whitianga Group rhyolites. In particular, the silicic component in Coromandel group rocks appears to have been less silicic and less alkaline than the bulk composition of the least differentiated Whitianga Group rhyolites.

Some major element analyses on andesite groundmasses have been obtained for this study with the aim of constraining the composition of the silicic component. The results show that andesite groundmasses are invariably more silicic than the bulk rock, consistent with hypothesis that the groundmass to a large extent represents the silicic component. Nevertheless, Coromandel Group andesite groundmasses are generally devitrified and also commonly contain seriate crystal fragments, so it is probable that the groundmass analyses do not represent true melt compositions. True melt compositions are only likely to be preserved in melt inclusions in andesite-hosted minerals.

A critical step towards a more complete understanding of the petrogenetic processes that formed Coromandel Group andesites is therefore to obtain accurate compositional data on melt inclusions in mafic and

felsic minerals hosted in Coromandel Group andesites. Inclusions in olivine, plagioclase and amphibole are of particular interest. Olivine occurs in some least-differentiated Coromandel Group rocks (Skinner, 1976; Skinner, 1993; Skinner, 1995), and globally hosts the on average most primitive melt inclusions in andesites (Reubi and Blundy, 2009). Compositional analyses on olivine melt inclusions can therefore help to constrain the composition of the mafic component in Coromandel Group, and show whether it has a similar composition to bulk Mercury Basalts or basaltic andesites of the Port Charles and Taurahuehue Andesites (Chapter 4).

Plagioclase and hornblende are common constituents of Coromandel Group andesites and, of the rock-forming silicate minerals in arc volcanic rocks, generally host the most differentiated melt inclusions (Reubi and Blundy, 2009). Plagioclase- and hornblende-hosted melt inclusions can therefore help constrain the composition of the silicic component in Coromandel Group andesites, and show how it compares to the compositional spectrum of Whitianga Group rhyolites as well as to the compositions of andesite groundmasses.

7.3.3. Mantle vs. Slab Isotope Signature

Mafic magmas are a priori the most likely to preserve a radiogenic isotope signature that is representative of the presumed mantle source. Such a signature can reflect the actual mantle source rocks, as well as any input by slab-derived fluids. In this study, Sr, Nd and Pb isotope compositions were determined. Of these, Pb isotope compositions should be the most sensitive to overprinting by slab-flux, as trace element properties show that mafic rocks of the CVZ contain about 90% slab-derived Pb. In the CVZ, mafic volcanic rocks principally occur as the Mercury Basalts and the Kiwitahi high-Mg andesites. A key outcome of the limited Pb isotope dataset obtained for this study is that, compared to the Quaternary basalts of the TVZ, Mercury Basalts have relatively radiogenic Pb isotope compositions, i.e. characterised by high values for $^{207}\text{Pb}/^{204}\text{Pb}$. The high $^{207}\text{Pb}/^{204}\text{Pb}$ values obtained here for Mercury Basalts are consistent with the high values obtained by (Huang et al., 2000). The Pb isotope compositions of Mercury Basalts overlap with the range in Coromandel Group andesites and Whitianga Group rhyolites, and are intermediate between Pb isotope compositions of metasediments of the Waipapa and Torlesse terranes. In Chapter 4 the Pb isotope signature of the Mercury Basalts is tentatively interpreted to reflect the presence of subducted sediment, which comprised a mixture of material derived from the major North Island basement terranes. Although the Mercury Basalts samples analysed in this study only represent the older 9.1-7.4 Ma group (Adams et al., 1994), the four samples analysed by Huang et al. (2000) include two that represent the

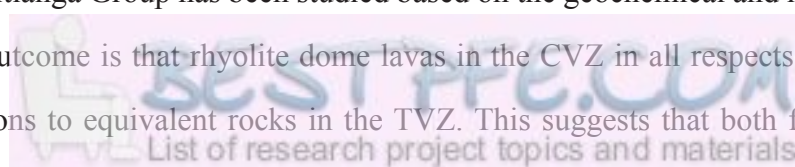
younger 5.5-4.7 Ma group (Adams et al., 1994). In contrast to the high $^{207}\text{Pb}/^{204}\text{Pb}$ values in Mercury Basalts, one high-Mg andesite sample of the Ruru centre in the Kiwitahi chain has a comparatively low $^{207}\text{Pb}/^{204}\text{Pb}$ value that is comparable to that in the TVZ basalts with the least radiogenic Pb isotope compositions (e.g. Kakuki Basalt; Gamble et al., 1993).

The Kiwitahi high-Mg andesites erupted between 6.2 and 5.5 Ma, predating the younger Mercury Basalts pulse of eruptions. The current small dataset therefore shows no particular trend with time to lower $^{207}\text{Pb}/^{204}\text{Pb}$ values in mafic rocks in the CVZ as a whole. Within the North Island succession, however, it appears that lower $^{207}\text{Pb}/^{204}\text{Pb}$ values are generally associated with younger mafic volcanic rocks. In Chapters 4 and 5, this observation is tentatively interpreted to relate to a decrease in the fraction of subducted sediment during the development of the CVZ-TVZ arc system. In the current setting, the subducted slab comprises anomalously thick oceanic crust of the Hikurangi Plateau, which is arguably conducive to the more efficient removal of sediment of prior to subduction. Consequently, it is possible that Hikurangi Plateau subduction, during ongoing subduction of the Pacific plate, relates to the trend to lower $^{207}\text{Pb}/^{204}\text{Pb}$ values in mafic rocks. Alternatively, it is possible that the trend relates to the tectonic re-configuration associated with the transition from Northland Arc to CVZ-related subduction system. It is also possible that the small number of datapoints presently available are not representative of any larger trend. Expanding the current Pb isotope dataset of the mafic volcanic rocks of the CVZ is a first step in resolving between the above options.

7.3.4. Rhyolite Magma Chamber Development

The CVZ volcanic succession records the repeated inception, in a number of localities, of rhyolitic volcanism following initial andesitic activity. Although the oldest rhyolitic tephras date back to c. 12 My (Carter et al., 2003), caldera-forming rhyolitic volcanism is known from c. 8 Ma (Adams et al., 1994; Nicholson et al., 2004). Between 12 and 8 Ma, the rate of tephra accumulation was slower than in the subsequent period of CVZ activity between 8 and 1.95 Ma. The rate of tephra accumulation increased further after c. 2 Ma and the shift of volcanism from the CVZ to the TVZ (Carter et al., 2003). The difference in tephra accumulation rates during CVZ and TVZ activity correlates with the greater rate of caldera formation, and the greater size of calderas, in the TVZ relative to the CVZ (see Chapter 2).

In this study, the Whitianga Group has been studied based on the geochemical and isotopic properties of dome lavas. A key outcome is that rhyolite dome lavas in the CVZ in all respects have comparable geochemical compositions to equivalent rocks in the TVZ. This suggests that both formed by similar



processes. Nevertheless, the apparent increases in the rates of caldera formation and tephra accumulation over time suggest that the rates of processes in silicic magmatic systems in the North Island may also have increased over time. i.e. greater quantities of magma accumulated and erupted more violently and/or in greater eruption volumes. Rhyolitic ignimbrites and fall deposits, rather than lavas, can preserve a record of the structure of magma chambers prior to an eruption. In the TVZ, rhyolitic ignimbrites are typically crystal-poor, like the associated lavas, and relatively homogeneous within eruptive units (Wilson et al., 2006; Wilson, 2008). It is possible that this reflects efficient convective stirring of the silicic magma chamber, possibly enabled by the energetic TVZ setting (Bachmann and Bergantz, 2008). In the CVZ, the ignimbrite and fall deposit record is comparatively poorly preserved. Preserved fall deposits within the CVZ appear to be relatively rare, however ignimbrites are relatively widespread. These ignimbrites have been analysed for geologic mapping purposes (Skinner, 1995; Brathwaite and Christie, 1996), however the existing datasets are small compared to those available for more intensely studied ignimbrites and fall deposits in younger parts of the North Island volcanic succession. Nevertheless, it is possible that some CVZ ignimbrites contain a preserved geochemical compositional zonation indicative of a stratified magma source. If more stratified, less vigorously mixed silicic magma chambers predominated in the earlier parts of the succession, this could be interpreted as evidence for less intense magmatism (smaller volumes of silicic magma, lesser rate of heating by mafic intrusion) and be related to the general increase in the rates of silicic tephra deposition and caldera formation between 12 Ma and the present.

7.4. Conclusions

New data on the volcanic rocks of the Northland Arc indicate that eastern and western belt rocks have distinct geochemical and isotopic properties, which correlate with petrographic properties. Western belt rocks, which are generally basalts and basaltic andesites, are more mafic than eastern belt rocks and have relatively unfractionated rare earth element contents even in more differentiated samples. This characteristic correlates with the absence of amphibole in the same rocks, which suggests that amphibole fractionation did not play a significant role in the differentiation of western belt rocks. Additionally, Northland Arc western belt rocks have relatively low $^{87}\text{Sr}/^{86}\text{Sr}$ values, and high $^{144}\text{Nd}/^{143}\text{Nd}$ values, compared to the least differentiated eastern belt rocks and to the least differentiated rocks (e.g. Mercury Basalts, Port Charles Andesites) of the CVZ volcanic succession. This suggests that these western belt rocks contain a relatively small fraction of crust-derived component.

Northland Arc eastern belt rocks are predominantly andesites and dacites. Compared to western belt

rocks, they have fractionated REE contents in the more differentiated rocks relative to the least differentiated rocks. Rocks that contain amphibole generally show enrichment in the middle REE, consistent with amphibole fractionation. However, the Parahaki dacites and some Whangarei Heads andesites show preferential enrichment in the light REE. This feature indicates a role for garnet fractionation in the magmatic differentiation processes that formed these magmas, or at least a silicic component in these magmas where the bulk rocks represent a mixture. Eastern belt rocks have $^{87}\text{Sr}/^{86}\text{Sr}$ and $^{144}\text{Nd}/^{143}\text{Nd}$ values comparable to, or more radiogenic than, those in comparable rocks of the CVZ succession, suggesting some or substantial crustal involvement.

Despite the geochemical, isotopic and mineralogical differences that contrast eastern and western belt rocks, they have comparable arc-type trace element distributions, indicating that all Northland Arc volcanic rocks analysed in this study ultimately originated from a mantle source that had been metasomatised by a slab-derived fluid. This contrasts with a more intraplate-type trace element signature found in volcanic rocks of comparable age preserved in Waitemata Basin sediments, which may have erupted at the southeastern terminus of the arc (Shane et al., 2010). The contrasting geochemical signatures of the two belts may be attributable to variation, across the Northland Peninsula, in crustal thickness, if such variation led to magmatic differentiation at relatively shallow depth underneath the western belt centres, and, at least in part, at greater depth underneath the eastern belt.

In the CVZ, the basaltic andesites, andesites and dacites that form the Coromandel Group have comparable bulk major and trace element compositions and radiogenic isotope values throughout the CVZ succession. A key result of this study is that there are no appreciable geochemical differences between hornblende-bearing and hornblende-absent rocks. Further, Coromandel Group rocks are also geochemically comparable to the andesites of the Northland Arc eastern belt, with the exception that no rocks in the CVZ show any trace element evidence for garnet fractionation.

The chemical properties of the constituent crystals in Coromandel Group andesites correlate weakly, or not at all, with bulk rock compositions. In contrast, groundmass compositions correlate strongly with bulk rock composition. Further, the groundmass in analysed Coromandel Group andesites invariably has a more differentiated composition than the bulk rock. Coromandel Group andesites appear to be mixtures of a mafic component, principally represented by the crystal cargo, and a silicic component, principally represented by the groundmass. Based on major element differentiation trends, the mafic component in Coromandel Group andesites appears to have a composition comparable to that of Mercury Basalts. The silicic component appears to have a composition comparable in many respects to that of Whitianga

Group rhyolites; however, simple binary mixing between a range of Mercury Basalts and Whitianga Group rhyolite compositions does not reproduce bulk andesite compositions in all geochemical respects. It appears that the silicic component in Coromandel Group andesites was less silicic and less alkaline, compared to the erupted rhyolites.

Hornblende is variably present or absent in the andesitic formations of the Northland Arc eastern belt and the CVZ. Nevertheless, andesites of these formations show consistent compositional trends in all parts of the volcanic succession. Rare earth element behaviour, specifically enrichment in the middle REE relative to LREE and HREE in more differentiated rocks, indicates that amphibole fractionation, or its residual presence during partial melting, was a significant driver of magmatic differentiation. In the context of the mixed nature of the andesites, this property implies that it was the silicic component in the andesites that formed by amphibole fractionation from a more mafic, less fractionated parental material.

Mercury Basalts, which are geochemically basalts or basaltic andesites *sensu stricto*, represent the most mafic rock type erupted in the CVZ. They have no known equivalent in the Northland Arc; however, they have compositions comparable to those of equivalent rocks of the Taupo Volcanic Zone. Compared to Coromandel Group andesites, Mercury Basalts have relatively high Na₂O and TiO₂ contents at a given SiO₂ concentration. Mercury Basalts are further characterised by relatively low ⁸⁷Sr/⁸⁶Sr values, and high ¹⁴⁴Nd/¹⁴³Nd values, compared to other CVZ volcanic rocks, indicating relatively little crustal interaction.

Like the Mercury Basalts, the basaltic andesites of the Coromandel Group formations Port Charles Andesite and Taurahuehue Andesite are characterised by distinctly high Na₂O and TiO₂ concentrations that set them apart from other Coromandel Group rocks, and can be considered additional parts of the Mercury Basalts suite on this basis. Significantly, the Port Charles Andesite and the Taurahuehue Andesite occur at the base of the Kuaotunu Subgroup and the Waiwawa Subgroup, respectively, whereas rocks of overlying formations in these subgroups have more differentiated compositions. It is possible that these basalt-like volcanic rocks represent a nascent phase of an eventually andesite-producing magmatic system.

Whitianga Group rhyolites are peraluminous to weakly metaluminous silicic rocks that represent the most differentiated rocks that erupted in the CVZ. Like the Mercury Basalts, Whitianga Group rhyolites have no known equivalent in the predecessor Northland Arc, but they are in all respects geochemically comparable to the rhyolite lavas of the Taupo Volcanic Zone. Major element compositional variation in the Whitianga Group suite can be attributed to combined plagioclase and alkali feldspar fractionation. All

CVZ rhyolites have an arc-type trace element signature comparable to the distribution in less differentiated rocks, but additionally modified by negative anomalies for certain elements, such as Ti, Sr and Y, that presumably reflect retention of those elements in residual or fractionated phases during rhyolite formation. The least differentiated rhyolites, which have approximately 73% SiO₂, have comparable major element compositions to experimental partial melts derived from hornblende gabbro source materials (Sisson et al., 2005) that were geochemically similar to Mercury Basalts, indicating that the least differentiated rhyolites could have been derived from the plutonic equivalents to Mercury Basalts or the least-differentiated Coromandel Group andesites.

The basaltic andesites and andesites of the Kīwītahi volcanic chain form two distinct groups. Andesites, erupted between c. 15 Ma and 6.7 Ma in the northern and central centres, have comparable major element compositions to Coromandel Group andesites of the CVZ. However, they are distinguished from CVZ andesites by relatively low enrichment in the highly incompatible elements, such as Cs and Rb. The basaltic andesites that erupted between 6.2 and 5.5 Ma in the southernmost centres are compositionally distinct from any rocks that erupted in the CVZ and can be classified as high-Mg andesites. They have comparable major and trace element compositions to Quaternary high-Mg andesites that erupted along the western boundary of the Taupo Volcanic Zone.

Consistent relationships exist between major element composition and other geochemical parameters in Coromandel Group andesites throughout the volcanic succession. Such relationships also apply to some ratios of elements that are not significantly mobile during hydrothermal alteration, which makes it possible to use such ratios in altered Coromandel Group rocks to estimate their initial, pre-alteration composition. The ratio of Zr to TiO₂ is applicable to this end and is based on two elements whose concentrations are routinely and precisely measured by XRF. Other combinations of high field strength elements can also be applied, provided that one behaves incompatibly and the other compatibly during magmatic differentiation. In Whitianga Group rhyolites, the ratio Th/Zr shows an analogous correlation with major element composition.

The difference between an altered rock's measured composition, and its estimated pre-alteration composition, can be used to estimate the mass changes that affected each element's concentration in the rock. In illite-bearing altered Coromandel Group andesites of the Waitekauri area, which surround Late Miocene gold-silver deposits, mass changes amount to c. 11% of total rock mass, whereas in the most intensely altered andesites, which contain abundant adularia, mass changes can amount to 24% of rock mass. The mobile elements in such altered andesites show mass changes that range from 100% loss to

significant gains. The maximum and average mass gains of some elements, principally K and Rb, increase from the periphery of the Waitekauri area to its centre. As well, Si is significantly gained in altered rocks at the centre of the Waitekauri area, but not in peripheral rocks. The maximum and average mass losses of elements that are lost during K metasomatism, principally Na and Ca, do not define a trend because such elements are commonly completely lost during hydrothermal alteration. In the Waitekauri area, quantification of the mass gains of K and Rb yields a distinct vector towards known gold mineralisation. This technique is a potentially significant addition to classic pathfinder element-based geochemical exploration programmes in the Hauraki goldfield.

Chapter 8. References

- Adams, C.J., Graham, I.J., Seward, D. and Skinner, D.N.B., 1994. Geochronological and geochemical evolution of late Cenozoic volcanism in the Coromandel Peninsula, New Zealand. *N. Z. J. Geol. Geophys.* 37: 359-378.
- Adams, C.J. and Maas, R., 2004. Age/isotopic characterisation of the Waipapa Group in Northland and Auckland, New Zealand, and implications for the status of the Waipapa Terrane. *N. Z. J. Geol. Geophys.* 47: 173-187.
- Adams, C.J., Mortimer, N., Campbell, H.J. and Griffin, W.L., 2009. Age and isotopic characterisation of metasedimentary rocks from the Torlesse Supergroup and Waipapa Group in the central North Island, New Zealand. *N. Z. J. Geol. Geophys.* 52: 149-170.
- Adams, C.J., Skinner, D.N.B. and Moore, P.R., 1994. K-Ar ages of some late Cenozoic volcanic rocks on Great Barrier Island. *N. Z. J. Geol. Geophys.* 37: 379-379.
- Annen, C., Blundy, J.D. and Sparks, R.S.J., 2006. The genesis of intermediate and silicic magmas in deep crustal hot zones. *J. Petrol.* 47: 505-539.
- Atwater, T. and Stock, J., 1998. Pacific-North America plate tectonics of the Neogene Southwestern United States: An update. *International Geology Review* 40: 375-402.
- Baalen, M.R., 1993. Titanium mobility in metamorphic systems: a review. *Chem. Geol.* 110: 233-249.
- Bachmann, O. and Bergantz, G.W., 2008. The magma reservoirs that feed supereruptions. *Elements* 4: 17-21.
- Bai, T.B. and Koster van Groos, A.E., 1999. The distribution of Na, K, Rb, Sr, Al, Ge, Cu, W, Mo, La and Ce between granitic melts and coexisting aqueous fluids. *Geochim. Cosmochim. Acta* 63: 1117-1131.
- Ballance, P.F., 1976. Evolution of the upper Cenozoic magmatic arc and plate boundary in northern New Zealand. *Earth Planet. Sci. Lett.* 28: 356-370.
- Ballance, P.F., Ablaev, A.G., Pushchin, I.K., Pletnev, S.P., Biryulina, M.G., Itaya, T., Follas, H.A. and Gibson, G.W., 1999. Morphology and history of the Kermadec trench-arc-backarc basin-remnant arc system at 30 to 32°S: geophysical profile, microfossil and K-Ar data. *Mar. Geol.* 159: 35-42.
- Ballance, P.F. and Campbell, J.D., 1993. The Murihiku arc-related basin of New Zealand (Triassic-Jurassic). In: P.F. Ballance (Editor), *South Pacific Sedimentary Basins. Sedimentary Basins of the World*. Elsevier, Amsterdam, pp. 21-33.
- Ballance, P.F., Pettinga, J.R. and Webb, C., 1982. A model of the Cenozoic evolution of northern New Zealand and adjacent areas of the southwest Pacific. *Tectonophysics* 87: 37-48.
- Ballance, P.F. and Spörl, K.B., 1979. Northland Allochthon. *Royal Society of New Zealand Journal* 9: 259-275.
- Beard, J.S. and Lofgren, G.E., 1991. Dehydration melting and water-saturated melting of basaltic and andesitic greenstones and amphibolites at 1, 3, and 6.9 kbar. *J. Petrol.* 32: 365-401.
- Berman, R.G., 1988. Internally consistent thermodynamic data for minerals in the system: Na₂O-K₂O-CaO-MgO-FeO-Fe₂O₃-Al₂O₃-SiO₂-TiO₂-H₂O-CO₂. *J. Petrol.* 29: 455-522.
- Black, P.M., 1967. Petrology of the Cuvier and Paritu plutons and their metamorphic aureoles. Thesis (PhD Thesis, [s.n.] Geology)--University of Auckland, 1967., Auckland, 354 l. pp.
- Black, P.M., 1994. The "Waipapa Terrane", North Island, New Zealand: subdivision and correlation. *Geoscience Reports of Shizuoka University* 20: 55-62.
- Black, P.M., Briggs, R.M., Itaya, T., Dewies, E.R., Dunbar, H.M., Kawasaki, K., Kuschel, E. and Smith, I.E.M., 1992. K-Ar age data and geochemistry of the Kiritahi Volcanics, western Hauraki Rift, North Island, New Zealand. *N. Z. J. Geol. Geophys.* 35: 403-413.
- Blattner, P., Rui-Zhong, H., Graham, I.J. and Houston-Elefteriadis, C., 1996. Temperatures and isotopic evolution of silicic magmas, Taupo Volcanic Zone and Coromandel, New Zealand. *N. Z. J. Geol. Geophys.* 39: 353-362.
- Booden, M.A., Mauk, J.L. and Simpson, M.P., in press. Quantifying metasomatism in epithermal Au-Ag deposits: a case study from the Waitekauri area, New Zealand. *Econ. Geol.*
- Booden, M.A., Smith, I.E.M., Black, P.M. and Mauk, J.L., in press. Geochemistry of the Early Miocene volcanic succession of Northland, New Zealand, and implications for the evolution of subduction in the Southwest Pacific. *J. Volcanol. Geotherm. Res.*
- Booden, M.A., Smith, I.E.M. and Mauk, J.L., 2009. Petrogenesis of basalts, andesites and dacites in the Coromandel Volcanic Zone – Implications for the genesis of epithermal Au mineralisation, AusIMM New Zealand Branch Annual Conference.

AusIMM, Queenstown.

- Booden, M.A., Smith, I.E.M., Mauk, J.L. and Black, P.M., 2010. Evolving volcanism at the tip of a propagating arc: the earliest high-Mg andesites in northern New Zealand. *J. Volcanol. Geotherm. Res.* 195: 83-96.
- Bottazzi, P., Tiepoli, M., Vanucci, R., Zanetti, A., Brumm, R., Foley, S.F. and Oberti, R., 1999. Distinct site preferences for heavy and light REE in amphibole and the prediction of Amph/LDREE. *Contrib. Mineral. Petrol.* 137.
- Brathwaite, R.L. and Christie, A.B., 1996. Geology of the Waihi area, Sheet T13BD & part U13, Scale 1:50 000. Geological Map, 21. Institute of Geological and Nuclear Sciences, Ltd., Wellington, N.Z.
- Brathwaite, R.L. and Skinner, D.N.B., 1997. The Coromandel epithermal gold-silver province: a result of collision of the Northland and Colville arcs in northern New Zealand, New Zealand Minerals and Mining Conference. Publicity Unit, Crown Minerals, Ministry of Commerce, pp. 111-117.
- Brenan, J.M., Shaw, H.F., Ryerson, F.J. and Phinney, D.L., 1995. Experimental determination of trace element partitioning between pargasite and a synthetic andesitic melt. *Earth Planet. Sci. Lett.* 135: 1-11.
- Briggs, R.M., 1986. Petrology and geochemistry of Maungatautari, a medium-K andesite-dacite volcano. *N. Z. J. Geol. Geophys.* 29: 273-289.
- Briggs, R.M. and Fulton, B.W.J., 1990. Volcanism, structure, and petrology of the Whiritoa-Whangamata coastal section, Coromandel Volcanic Zone, New Zealand - facies model evidence for the Tunaiti Caldera. *N. Z. J. Geol. Geophys.* 33: 623-633.
- Briggs, R.M., Hall, G.J., Harmsworth, G.R., Hollis, A.G., Houghton, B.F., Hughes, G.R., Morgan, M.D. and Whitbread-Edwards, A.R., 1996. Geology of the Tauranga area, sheet U14 1:50 000. Occasional report, 22. Department of Earth Sciences, University of Waikato, Hamilton, New Zealand.
- Briggs, R.M., Houghton, B.F., McWilliams, M. and Wilson, C.J.N., 2005. $^{40}\text{Ar}/^{39}\text{Ar}$ ages of silicic volcanic rocks in the Tauranga-Kaimai area, New Zealand: dating the transition between volcanism in the Coromandel Arc and the Taupo Volcanic Zone. *N. Z. J. Geol. Geophys.* 48: 459-469.
- Briggs, R.M. and McDonough, W.F., 1990. Contemporaneous convergent margin and intraplate magmatism, North Island, New Zealand. *J. Petrol.* 31: 813-851.
- Brown, K.L., 1986. Gold deposition from geothermal discharges in New Zealand. *Econ. Geol.* 81: 979-983.
- Browne, P.R.L., Coulter, G.W., Grant, M.A., Grindley, G.W., Lawless, J.V., Lyon, G.L., MacDonald, W.J.P., Robinson, R., Sheppard, D.S. and Skinner, D.N.B., 1981. The Ngawha Geothermal Area. Department of Scientific and Industrial Research geothermal report, 7.
- Buchanan, L.J., 1981. Precious metal deposits associated with volcanic environments in the southwest. In: W.R. Dickinson and W.D. Payne (Editors), Relations of tectonics to ore deposits in the Southern Cordillera. Arizona Geological Society Digest, pp. 237-262.
- Cameron, E., Gamble, J., Price, R., Smith, I., McIntosh, W.C. and Gardner, M., 2010. The petrology, geochronology and geochemistry of Hauhungatahi Volcano, S.W. Taupo Volcanic Zone. *J. Volcanol. Geotherm. Res.* 190: 179-191.
- Carlile, J.C., Davey, G.R., Kadir, I., Langmead, R.P. and Rafferty, W.J., 1998. Discovery and exploration of the Gosowong epithermal gold deposit, Halmahera, Indonesia. *Journal of Geochemical Exploration* 60: 207-227.
- Carter, L., Shane, P., Alloway, B., Hall, I.R., Harris, S.E. and Westgate, J.A., 2003. Demise of one volcanic zone and birth of another - A 12 m.y. marine record of rhyolitic eruptions from New Zealand. *Geology* 31: 493-496.
- Cartledge, G.H., 1928. Studies on the periodic system, I. The ionic potential as a periodic function. *Journal of the American Chemical Society* 50: 2856-2872.
- Castillo, P.R., Lonsdale, P.F., Moran, C.L. and Hawkins, J.W., 2009. Geochemistry of Mid-Cretaceous Pacific crust being subducted along the Tonga-Kermadec Trench: implications for the generation of arc lavas. *Lithos* 112: 87-102.
- Chambefort, I., Moritz, R. and von Quadt, A., 2007. Petrology, geochemistry and U-Pb geochronology of magmatic rocks from the high-sulfidation epithermal Au-Cu Chelopech deposit, Srenogorie zone, Bulgaria. *Mineral. Depos.* 42: 665-690.
- Charlier, B.L.A., Wilson, C.J.N., Lowenstern, J.B., Blake, S., van Calsteren, P.W. and Davidson, J.P., 2005. Magma generation at a large, hyperactive silicic volcano (Taupo, New Zealand) revealed by U-Th and U-Pb systematics in zircons. *J. Petrol.* 46: 3-32.
- Charlier, B.L.A., Wilson, C.J.N. and Mortimer, N., 2010. Evidence from zircon U-Pb age spectra for crustal structure and felsic magma genesis at Taupo volcano, New Zealand. *Geology* 38: 915-918.
- Christie, A.B. and Barker, R.G., 2007. Mineral resource assessment of the Northland Region, New Zealand.

- Christie, A.B., Simpson, M.P., Brathwaite, R.L., Mauk, J.L. and Simmons, S.F., 2007. Epithermal Au-Ag and related deposits of the Hauraki goldfield, Coromandel volcanic zone, New Zealand. *Econ. Geol.* 102: 785-816.
- Clarke, D.S. and Govett, G.J.S., 1990. Southwest Pacific epithermal gold: a rock geochemistry prospective. *Journal of Geochemical Exploration* 35: 225-240.
- Cloos, M., 1993. Lithospheric buoyancy and collisional orogenesis: subduction of oceanic plateaus, continental margins, island arcs, spreading ridges and seamounts. *Geol. Soc. Am. Bull.* 105: 715-737.
- Close, D.I., Watts, A.B. and Stagg, H.M.J., 2009. A marine geophysical study of the Wilkes Land rifted continental margin, Antarctica. *Geophys. J. Int.* 177: 430-450.
- Cole, J.W., 1978. Andesites of the Tongariro Volcanic Centre, North Island, New Zealand. *J. Volcanol. Geotherm. Res.* 3: 121-153.
- Cole, J.W. and Teoh, L.H., 1975. Petrography, mineralogy and chemistry of Pureora andesite volcano, North Island, New Zealand. *N. Z. J. Geol. Geophys.* 18: 259-272.
- Cole, J.W., Thordarson, T. and Burt, R.M., 2000. Magma origin and evolution of White Island (Whakaari) volcano, Bay of Plenty, New Zealand. *J. Petrol.* 41: 867-895.
- Collot, J., Herzer, R., Lafoy, Y. and Géli, L., 2009. Mesozoic history of the Fairway-Aotea Basin: implications for the early stages of Gondwana fragmentation. *Geochem. Geophys. Geosyst.* 10.
- Cox, S.F., Knackstedt, M.A. and Braun, J., 2001. Principles of structural control on permeability and fluid flow in hydrothermal systems. *Reviews in Economic Geology* 14: 1-24.
- Crawford, A.J., Falloon, T.J. and Eggins, S., 1987. The origin of island-arc high-alumina basalts. *Contrib. Mineral. Petrol.* 97: 417-430.
- Crawford, A.J., Meffre, S. and Symonds, P.A., 2003. 120-0 Ma tectonic evolution of the southwest Pacific and analogous geological evolution of the 600-220 Ma Tasman Fold Belt System. *Geol. Soc. Aus. Spec. Pub.* 22: 377-397.
- Creasey, S.C., 1977. Intrusives associated with porphyry copper deposits. *Bulletin of the Geological Society of Malaysia* 9: 51-66.
- Crisp, J.A., 1984. Rates of magma emplacement and volcanic output. *J. Volcanol. Geotherm. Res.* 20: 177-211.
- Darby, D.J., Hodgkinson, K.M. and Blick, G.H., 2000. Geodetic measurement of deformation in the Taupo Volcanic Zone, New Zealand: the north Taupo network revisited. *N. Z. J. Geol. Geophys.* 43: 157-170.
- Davey, F., 1982. The structure of the South Fiji basin. *Tectonophysics* 87: 185-196.
- Davey, F.J., 2010. Crustal seismic reflection measurements across the northern extension of the Taupo Volcanic Zone, North Island, New Zealand. *J. Volcanol. Geotherm. Res.* 190: 75-81.
- Davidson, J.P., Turner, S., Handley, H., Macpherson, C. and Dosseto, A., 2007. Amphibole "sponge" in arc crust? *Geology* 35: 787-790.
- Davy, B. and Wood, R., 1994. Gravity and magnetic modelling of the Hikurangi Plateau. *Mar. Geol.* 118: 139-151.
- Day, R.A., Green, T.H. and Smith, I.E.M., 1992. The origin and significance of garnet phenocrysts and garnet-bearing xenoliths in Miocene calcalkaline volcanics from Northland, New Zealand. *J. Petrol.* 33: 125-161.
- de Lange, W.P. and Lowe, D.J., 1990. History of vertical displacement of Kerepehi Fault at Kopouatai bog, Hauraki Lowlands, New Zealand, since c. 10 700 years ago. *N. Z. J. Geol. Geophys.* 33: 277-283.
- Deering, C.D., Cole, J.W. and Vogel, T.A., 2008. A rhyolite compositional spectrum continuum governed by lower crustal source conditions in the Taupo Volcanic Zone, New Zealand. *J. Petrol.* 49: 2245-2276.
- Deering, C.D., Gravley, D.M., Vogel, T.A., Cole, J.W. and Leonard, G.S., 2010. Origins of cold-wet-oxidizing to hot-dry-reducing rhyolite magma cycles and distribution in the Taupo Volcanic Zone, New Zealand. *Contrib. Mineral. Petrol.*
- Defant, M.J. and Drummond, M.S., 1990. Derivation of some modern arc magmas by melting of young subducted lithosphere. *Nature* 347: 662-665.
- DeMets, C., Gordon, R.G., Argus, D.F. and Stein, S., 1994. Effect of revisions to the geomagnetic reversal time scale on estimates of current plate motions. *Geophys. Res. Lett.* 21: 2191-2194.
- DiCaprio, L., Müller, R.D., Gurnis, M. and Goncharov, A., 2009. Linking active margin dynamics to overriding plate deformation: Synthesizing geophysical images with geological data from the Norfolk basin. *Geochem. Geophys. Geosyst.* 10: Q01004.
- Downey, J.F., 1935. Gold mines of the Hauraki district. Government Printer, Wellington, New Zealand, 315 pp.
- Edbrooke, S.W. (Editor), 2001. Geology of the Auckland area. 1:250,000 Geological Map, 3. Institute of Geological and

Nuclear Sciences.

- Eggins, S.M., Rudnick, R.L. and McDonough, W.F., 1998. The composition of peridotites and their minerals: a laser ablation-ICP-MS study. *Earth Planet. Sci. Lett.* 154: 53-71.
- Elburg, M., Vroon, P., van der Wagt, B. and Tchalikian, A., 2005. Sr and Pb isotopic composition of five USGS glasses (BHVO-2G, BIR-1G, BCR-2G, TB-1G, NKT-1G). *Chem. Geol.* 223: 196-207.
- Ewart, A. and Griffin, W.L., 1994. Application of proton-microprobe data to trace element partitioning in volcanic rocks. *Chem. Geol.* 117: 251-284.
- Ewart, A. and Stipp, J.J., 1968. Petrogenesis of volcanic rocks of the central North Island, New Zealand, as indicated by a study of $\text{Sr}^{87}/\text{Sr}^{86}$ ratios and Sr, Rb, K, U and TH abundances. *Geochim. Cosmochim. Acta* 32: 699-736.
- Finlow-Bates, T. and Stumpfl, E.F., 1981. The behavior of so-called immobile elements in hydrothermally altered rocks associated with volcanogenic submarine-exhalative deposits. *Mineral. Depos.* 16: 319-328.
- Froude, D.O. and Cole, J.W., 1985. Petrography, mineralogy and chemistry of Titiraupenga volcano, North Island, New Zealand. *N. Z. J. Geol. Geophys.* 28: 487-496.
- Gaina, C., Müller, D., Royer, J.-Y., Stock, J., Hardebeck, J. and Symonds, P., 1998. The tectonic history of the Tasman Sea: A puzzle with 13 pieces. *J. Geophys. Res.* 103: 12413-12433.
- Gamble, J.A., Smith, I.E.M., Graham, I.J., Kokelaar, B.P., Cole, J.W., Houghton, B.F. and Wilson, C.J.N., 1990. The petrology, phase-relations and tectonic setting of basalts from the Taupo Volcanic Zone, New Zealand and the Kermadec Island Arc - Havre Trough, SW Pacific. *J. Volcanol. Geotherm. Res.* 43: 253-270.
- Gamble, J.A., Smith, I.E.M., McCulloch, M.T., Graham, I.J. and Kokelaar, B.P., 1993. The geochemistry and petrogenesis of basalts from the Taupo Volcanic Zone and Kermadec island arc, SW Pacific. *J. Volcanol. Geotherm. Res.* 54: 265-290.
- Gemmell, J.B., 2007. Hydrothermal alteration associated with the Gosowong epithermal Au-Ag deposit, Halmahera, Indonesia: mineralogy, geochemistry and exploration implications. *Econ. Geol.* 102: 893-922.
- Giggenbach, W.F., 1984. Mass transfer in hydrothermal alteration systems - a conceptual approach. *Geochim. Cosmochim. Acta* 45: 393-410.
- Giggenbach, W.F., 1988. Geothermal solute equilibria: derivation of Na-K-Mg-Ca geothermometers. *Geochim. Cosmochim. Acta* 52: 2749-2765.
- Gill, J.B., 1981. *Orogenic andesites and plate tectonics*. Springer-Verlag, Berlin-Heidelberg.
- Glodny, J., Echtler, H., Figueroa, O., Franz, G., Gräfe, K., Kemnitz, H., Kramer, W., Krawczyk, C., Lohrmann, J., Lucasen, F., Melnick, D., Rosenau, M. and Selfert, W., 2006. Long-term geological evolution and mass-flow balance of the South-Central Andes. In: O. Oncken et al. (Editors), *The Andes: Active Subduction Orogeny*. *Frontiers in Earth Sciences*. Springer-Verlag Berlin Heidelberg, Würzburg, Germany, pp. 401-428.
- Graham, I.J., Cole, J.W., Briggs, R.M., Gamble, J.A. and Smith, I.E.M., 1995. Petrology and petrogenesis of volcanic rocks from the Taupo Volcanic Zone: a review. *J. Volcanol. Geotherm. Res.* 68: 59-87.
- Graham, I.J., Gulson, B.L., Hedenquist, J.W. and Mizon, K., 1992. Petrogenesis of Late Cenozoic volcanic rocks from the Taupo Volcanic Zone, New Zealand, in the light of new lead isotope data. *Geochim. Cosmochim. Acta* 56: 2797-2819.
- Graham, I.J. and Hackett, W.R., 1987. Petrology of calc-alkaline lavas from Ruapehu volcano and related vents, Taupo Volcanic Zone, New Zealand. *J. Petrol.* 28: 531-567.
- Green, N., 2006. Influence of slab thermal structure on basalt source regions and melting conditions: REE and HFSE constraints from the Garibaldi volcanic belt, northern Cascadia subduction system. *Lithos* 87: 23-49.
- Gresens, R.L., 1967. Composition-volume relationships of metasomatism. *Chem. Geol.* 2: 47-65.
- Grodzicki, K.R., Rowland, J.V. and Mauk, J.L., in press. Structural controls on epithermal mineralization, Sovereign-Jubilee Mine, Hauraki Goldfield, New Zealand. *Econ. Geol.*
- Gruender, K., Stewart, R.B. and Foley, S.F., 2010. Xenoliths from the sub-volcanic lithosphere of Mt Taranaki, New Zealand. *J. Volcanol. Geotherm. Res.* 190: 192-202.
- Hallberg, J.A., 1984. A geochemical aid to igneous rock type identification in deeply-weathered terrain. *Journal of Geochemical Exploration* 20: 1-8.
- Harrison, A. and White, R.S., 2006. Lithospheric structure of an active backarc basin: the Taupo Volcanic Zone, New Zealand. *Geophys. J. Int.* 167: 968-990.
- Haworth, A.V. and Briggs, R.M., 2006. Epithermal Au-Ag mineralisation in the Lower Waitakauri Valley, Hauraki Goldfield. In: A.B. Christie and R.L. Brathwaite (Editors), *Geology and exploration of New Zealand mineral deposits*. *Australasian*

- Institute of Mining and Metallurgy Monograph, pp. 157-162.
- Hawthorn, B.M., 1996. Volcanic geology of the Opito Bay region, northern Coromandel Peninsula, University of Waikato, Hamilton.
- Hayward, B.W., 1993. The tempestuous 10 million year life of a double arc and intra-arc basin - New Zealand's Northland Basin in the early Miocene. In: P.F. Ballance (Editor), *South Pacific Sedimentary Basins. Sedimentary Basins of the World*. Elsevier, Amsterdam, pp. 113-142.
- Hayward, B.W., Black, P.M., Smith, I.E.M., Ballance, P.F., Itaya, T., Doi, M., Takagi, M., Bergman, S., Adams, C.J., Herzer, R.H. and Robertson, D.J., 2001. K-Ar ages of early Miocene arc-type volcanoes in northern New Zealand. *N. Z. J. Geol. Geophys.* 44: 285-311.
- Hayward, B.W., Grenfell, H.R., Mauk, J.L. and Moore, P.R., 2006. The west-flowing Pliocene "Clevedon River", Auckland. *Geol. Soc. N. Z. Newsletter* 141: 24-29.
- Healy, J., 1962. Structure and volcanism in the Taupo Volcanic Zone, New Zealand. *Geophysical Monograph* 6: 151-157.
- Hedenquist, J.W., Arribas, A. and Gonzales-Urien, E., 2000. Exploration for epithermal gold deposits. *Reviews in Economic Geology* 13: 245-277.
- Hedenquist, J.W. and Lowenstern, J.B., 1994. The role of magmas in the formation of hydrothermal ore deposits. *Nature* 370: 519-527.
- Herzer, R.H., 1995. Seismic stratigraphy of a buried volcanic arc, Northland, New Zealand and implications for Neogene subduction. *Mar. Petrol. Geol.* 12: 511-531.
- Herzer, R.H., Davy, B.W., Mortimer, N., Quilty, P.G., Chaproniere, G.C.H., Jones, C.M., Crawford, A.J. and Hollis, C.J., 2009. Seismic stratigraphy and structure of the Northland Plateau and the development of the Vening Meinesz transform margin, SW Pacific Ocean. *Mar. Geophys. Res.* 30: 21-60.
- Herzer, R.H., Mascle, J., Davy, B.W., Ruellan, E., Mortimer, N., Laporte, C. and Duxfield, A., 2000. New constraints on the New Zealand-South Fiji Basin continent-back-arc margin. *C. R. Acad. Sci. II A.* 330: 701-708.
- Herzer, R.H. and Mortimer, N., 1998. Miocene spreading in the South Fiji Basin? *Geol. Soc. N. Z. Newsletter* 117: 10-16.
- Heumann, A. and Davies, G.R., 2002. A combined U-Th, Sr-Nd-Pb-O isotope study of the Navaisha comendite complex; implications for petrogenesis and magma chamber residence. *J. Petrol.* 43: 557-577.
- Heyworth, Z., Turner, S., Schaefer, B., Wood, B., George, R., Berlo, K., Cunningham, H., Price, R., Cook, C. and Gamble, J., 2007. ^{238}U - ^{230}Th - ^{226}Ra - ^{210}Pb constraints on the genesis of high-Mg andesites at White Island, New Zealand. *Chem. Geol.* 243: 105-121.
- Hickmott, D. and Spear, F.S., 1992. Major and trace element zoning in garnets from calcareous pelites in the NW Shelbourne Falls quadrangle, Massachusetts: garnet growth histories in retrograde rocks. *J. Petrol.* 33: 965-1005.
- Hochstein, M.P., 1995. Crustal heat transfer in the Taupo Volcanic Zone (New Zealand): Comparison with other volcanic arcs and explanatory heat source models. *J. Volcanol. Geotherm. Res.* 68: 117-151.
- Hochstein, M.P. and Ballance, P.F., 1993. Hauraki Rift: a young, active intra-continental rift in a back-arc setting. In: P.F. Ballance (Editor), *South Pacific Sedimentary Basins*. Elsevier, Amsterdam, pp. 293-305.
- Hochstein, M.P., Tearney, K., Rawson, K., Davey, F.J., Davidge, S., Henrys, S. and Backshall, D., 1986. Structure of the Hauraki Rift (New Zealand). *Bull. R. Soc. N. Z.* 24: 333-348.
- Hoernle, K., Abt, D.L., Fischer, K.M., Nichols, H., Hauff, F., Abers, G.A., Van den Bogaard, P., Heydolph, K., Alvarado, G., Protti, M. and Strauch, W., 2008. Arc-parallel flow in the mantle wedge beneath Costa Rica and Nicaragua. *Nature*.
- Hofmann, A.W., 1988. Chemical differentiation of the Earth: the relationship between mantle, continental crust, and oceanic crust. *Earth Planet. Sci. Lett.* 90: 297-314.
- Holland, T.J.B. and Powell, R., 1998. An internally consistent thermodynamic data set for phases of petrological interest. *Journal of Metamorphic Geology* 16: 309-343.
- Hollis, A.G., 1995. Volcanic geology of the central Tauranga Basin, New Zealand. MSc Thesis, University of Waikato, Hamilton, New Zealand.
- Hora, J.M., Singer, B.S., Wörner, G., Beard, B.L., Jicha, B.R. and Johnson, C.M., 2009. Shallow and deep crustal control on differentiation of calc-alkaline and tholeiitic magma. *Earth Planet. Sci. Lett.*
- Horspool, N.A., Savage, M.K. and Bannister, S., 2006. Implications for intraplate volcanism and back-arc deformation in northwestern New Zealand, from joint inversion of receiver functions and surface waves. *Geophys. J. Int.* 166: 1466-1483.

- Houghton, B.F. and Cuthbertson, A.S., 1988. Geological Map of New Zealand, Sheet T14 BD-Kaimai, scale 1:50 000. Department of Scientific and Industrial Research, Wellington.
- Houghton, B.F. and Hackett, W.R., 1984. Strombolian and phreatomagmatic deposits of Ohakune Craters, Ruapehu, New Zealand. A complex interaction between external water and rising basaltic magma. *J. Volcanol. Geotherm. Res.* 21: 207-231.
- Houghton, B.F., Weaver, S.D., Wilson, C.J.N. and Lanphere, M.A., 1992. Evolution of a Quaternary peralkaline volcano: Mayor Island, New Zealand. *J. Volcanol. Geotherm. Res.* 51: 217-236.
- Houghton, B.F. and Wilson, C.J.N., 1995. Volcanic and structural evolution of central Taupo Volcanic Zone, New Zealand. *Australasian Institute of Mining and Metallurgy* 9: 291-296.
- Huang, Y., Hawkesworth, C., van Calsteren, P., Smith, I. and Black, P., 1997. Melt generation models for the Auckland volcanic field, New Zealand: constraints from U-Th isotopes. *Earth Planet. Sci. Lett.* 149: 67-84.
- Huang, Y.M., Hawkesworth, C., Smith, I., van Calsteren, P. and Black, P., 2000. Geochemistry of late Cenozoic basaltic volcanism in Northland and Coromandel, New Zealand: implications for mantle enrichment processes. *Chem. Geol.* 164: 219-238.
- Huppert, H.E. and Sparks, R.S.J., 1988. The generation of granitic magmas by intrusion of basalt into continental crust. *J. Petrol.* 29: 599-624.
- Isaac, M.J., Brook, F.J. and Hayward, B.W., 1988. The Cretaceous sequence at Whatuwhiwhi, Northland, New Zealand, and its paleogeographic significance. *N. Z. Geol. S. Rec.* 26.
- Jaffey, A.H., Flynn, K.F., Glendenin, L.E., Bentley, W.C. and Essling, A.M., 1971. Precision measurement of the half-lives and specific activities of U235 and U238. *Physical Review C* 4.
- Jagoutz, O.E., Burg, J.-P., Hussain, S., Dawood, H., Pettke, T., Iizuka, T. and Maruyama, S., 2009. Construction of the granitoid crust of an island arc part I: geochronological and geochemical constraints from the plutonic Kohistan (NW Pakistan). *Contrib. Mineral. Petrol.* 158: 739-755.
- Jiang, S., Wang, R., Xu, X. and Zhao, K., 2005. Mobility of high-field strength elements (HFSE) in magmatic- metamorphic-, and submarine-hydrothermal systems. *Physics and chemistry of the Earth* 30: 1020-1029.
- John, D.A., Hofstra, A.H., Fleck, R.J., Brummer, J.E. and Saderholm, E.C., 2003. Geologic setting and genesis of the Mule Canyon low-sulfidation epithermal Au-Ag deposit, north-central Nevada. *Econ. Geol.* 98: 425-463.
- Johnson, K.T.M., 1994. Experimental cpx/ and garnet/melt partitioning of REE and other trace elements at high pressures: petrogenetic implications. *Mineralogical Magazine* 58: 454-455.
- Johnson, K.T.M. and Kinzler, R.J., 1989. Partitioning of REE, Ti, Zr, Hf, and Nb between clinopyroxene and basaltic liquid: an ion microprobe study. *EOS* 70: 1388.
- Kamenov, G.D., Perfit, M.R., Jonasson, I.R. and Mueller, P.A., 2005. High-precision Pb isotope measurements reveal magma recharge as a mechanism for ore deposit formation: examples from Lihir Island and Conical seamount, Papua New Guinea. *Chem. Geol.* 219: 131-148.
- Kamenov, G.D., Saunders, J.A., Hames, W.E. and Unger, D.L., 2007. Mafic magmas as sources for gold in Middle Miocene epithermal deposits of the northern Great Basin, United States: evidence from Pb isotope compositions of native gold. *Econ. Geol.* 102: 1191-1195.
- Kear, D., 1994. A "least complex" dynamic model for late Cenozoic volcanism in the North Island, New Zealand. *N. Z. J. Geol. Geophys.* 37: 223-236.
- Kear, D. and Mortimer, N., 2003. Waipa Supergroup, New Zealand: a proposal. *J. R. Soc. N.Z.* 33: 149-163.
- Kelemen, P.B., 1995. Genesis of high Mg# andesites and the continental crust. *Contrib. Mineral. Petrol.* 120: 1-19.
- King, P.R., 2000. Tectonic reconstructions of New Zealand: 40 Ma to the Present. *N. Z. J. Geol. Geophys.* 43: 611-638.
- Krippner, S.J.P., 2000. Volcanic geology, geochemistry and geochronology of the Kapowai Caldera, Coromandel Volcanic Zone, New Zealand. PhD Thesis, University of Waikato, Hamilton, New Zealand.
- Kuschel, E., 1988. A petrological study of the Kivitahi Volcanics. Unpublished BSc (Hons) Thesis, University of Auckland, Auckland, N.Z.
- Kuschel, E. and Smith, I.E.M., 1992. Rare earth mobility in young arc-type volcanic rocks from northern New Zealand. *Geochim. Cosmochim. Acta* 56: 3951-3955.
- Laird, M.G. and Bradshaw, J.D., 2003. The break-up of a long-term relationship: the Cretaceous separation of New Zealand from Gondwana. *Gondwana Res.* 7: 273-286.

- Larocque, J. and Canil, D., 2010. The role of amphibole in the evolution of arc magmas and crust: the case from the Jurassic Bonanza arc section, Vancouver Island, Canada. *Contrib. Mineral. Petrol.* 159: 475-492.
- Le Bas, M.J., Le Maitre, R.W., Streckeisen, A. and Zanettin, B., 1986. A chemical classification of volcanic rocks based on the total alkali silica diagram. *J. Petrol.* 27: 745-750.
- Leavitt, E.D. and Arehart, G.B., 2005. Alteration, geochemistry and paragenesis of the Midas epithermal gold-silver deposit, Elko County, Nevada, Geological Society of Nevada Symposium. Proceedings, Reno, Nevada, pp. 563-627.
- Leonard, G.S., Cole, J.W., Nairn, I.A. and Self, S., 2002. Basalt triggering of the c. AD 1305 Kaharoa rhyolite eruption, Tarawera Volcanic Complex, New Zealand. *J. Volcanol. Geotherm. Res.* 115: 461-486.
- Lin, F.-C., Ritzwoller, M.H., Townend, J., Bannister, S. and Savage, M.K., 2007. Ambient noise Rayleigh wave tomography of New Zealand. *Geophys. J. Int.* 170: 649-666.
- Lindsay, J.M., Worthington, T.J., Smith, I.E.M. and Black, P.M., 1999. Geology, petrology, and petrogenesis of Little Barrier Island, Hauraki Gulf, New Zealand. *N. Z. J. Geol. Geophys.* 42: 155-168.
- Lipman, P.W., 2000. Calderas. In: H. Sigurdsson (Editor), *Encyclopedia of Volcanoes*. Academic Press, San Diego, pp. 643-662.
- Lipman, P.W., 2007. Incremental assembly and prolonged consolidation of Cordilleran magma chambers: Evidence from the Southern Rocky Mountain volcanic field. *Geosphere* 3: 42-70.
- Lonsdale, P., 1997. An incomplete geologic history of the southwest Pacific basin. *Geol. Soc. Am. Abstract with Programs* 29: 4574.
- Lugmair, G.W. and Marti, K., 1978. Lunar initial $^{143}\text{Nd}/^{144}\text{Nd}$: differential evolution of the lunar crust and mantle. *Earth Planet. Sci. Lett.* 39: 349-357.
- Luyendyk, B.P., 1995. Hypothesis for Cretaceous rifting of East Gondwana caused by subducted slab capture. *Geology* 23: 373-376.
- MacLean, W.H., 1990. Mass changes calculations in altered rock series. *Mineral. Depos.* 25: 44-49.
- Madeisky, H.E., 1996. A litho-geochemical and radiometric study of hydrothermal alteration and metal zoning at the Cinola epithermal gold deposit, Queen Charlotte Islands, British Columbia. In: A.R. Coyner and P.L. Fahey (Editors), *Geology and ore deposits of the American Cordillera*, pp. 1153-1185.
- Malahoff, A., Feden, R.H. and Fleming, H.S., 1982. Magnetic anomalies and tectonic fabric of marginal basins north of New Zealand. *J. Geophys. Res.* 87: 4109-4125.
- Malengreau, B., Skinner, D., Bromley, C. and Black, P., 2000. Geophysical characterisation of large silicic volcanic structures in the Coromandel Peninsula, New Zealand. *N. Z. J. Geol. Geophys.* 43: 171-186.
- Malpas, J., Spörl, K.B., Black, P.M. and Smith, I.E.M., 1992. Northland ophiolite, New Zealand, and implications for plate tectonic evolution of the Southwest Pacific. *Geology* 20: 149-152.
- Martin, H., Smithies, R.H., Rapp, R., Moyen, J.-F. and Champion, D., 2005. An overview of adakite, tonalite-trondhjemite-granodiorite (TTG), and sanukitoid: relationships and some implications for crustal evolution. *Lithos* 79: 1-24.
- Mashima, H., 2009. The basalt-high magnesium andesite association formed by multi-stage partial melting of a heterogeneous source mantle: evidence from Hirado-Seto, Northwest Kyushu, Southwest Japan. *Lithos* 112: 351-366.
- Mauk, J.L. and Hall, C.M., 2004. $^{40}\text{Ar}/^{39}\text{Ar}$ ages of adularia from the Golden Cross, Neavesville and Komata epithermal deposits, Hauraki Goldfield, New Zealand. *N. Z. J. Geol. Geophys.* 47: 227-231.
- Mauk, J.L., Hall, C.M., Barra, F. and Chesley, J.T., in press. Punctuated evolution of a large epithermal province: the Hauraki Goldfield, New Zealand. *Econ. Geol.*
- Mauk, J.L. and Simpson, M.P., 2007. Geochemistry and stable isotope composition of altered rocks at the Golden Cross epithermal Au-Ag deposit, New Zealand. *Econ. Geol.* 102: 841-871.
- McCulloch, M.T. and Bennett, V.C., 1994. Progressive growth of the Earth's continental crust and depleted mantle - geochemical constraints. *Geochim. Cosmochim. Acta* 58: 4717-4738.
- McCulloch, M.T., Kyser, T.K., Woodhead, J.D. and Kinsley, L., 1994. Pb-Sr-Nd-O isotopic constraints on the origin of rhyolites from the Taupo Volcanic Zone of New-Zealand - Evidence for assimilation followed by fractionation from basalt. *Contrib. Mineral. Petrol.* 115: 303-312.
- McDonough, W.F. and Sun, S.S., 1988. A primitive mantle composition from xenoliths. *Chem. Geol.* 70: 12-12.
- McDonough, W.F. and Sun, S.S., 1995. The composition of the Earth. *Chem. Geol.* 120: 223-253.
- Middlemost, E.A.K., 1989. Iron oxidation ratios, norms and the classification of volcanic rocks. *Chem. Geol.* 77: 19-26.

- Moore, C.R., 1979. Geology and mineralization of the former Broken Hills gold mine, Hikuai, Coromandel Peninsula, New Zealand. *N. Z. J. Geol. Geophys.* 22: 339-351.
- Morrell, A.E., Locke, C.A., Cassidy, J. and Mauk, J.L., in press. Geophysical characteristics of adularia-sericite epithermal gold-silver deposits in the Waihi-Waitekauri region, New Zealand. *Econ. Geol.*
- Mortimer, N., 2004. New Zealand's geological foundations. *Gondwana Res.* 7: 261-272.
- Mortimer, N., Gans, P.B., Palin, J.M., Meffre, S., Herzer, R. and Skinner, D.N.B., 2010. Location and migration of Miocene-Quaternary volcanic arcs in the SW Pacific region. *J. Volcanol. Geotherm. Res.* 190: 1-10.
- Mortimer, N., Herzer, R.H., Gans, P.B., Laporte-Magoni, C., Calvert, A.T. and Bosch, D., 2007. Oligocene-Miocene tectonic evolution of the South Fiji Basin and Northland Plateau, SW Pacific Ocean: Evidence from petrology and dating of dredged rocks. *Mar. Geol.* 237: 1-24.
- Mortimer, N., Herzer, R.H., Gans, P.B., Parkinson, D.L. and Seward, D., 1998. Basement geology from Three Kings Ridge to West Norfolk Ridge, southwest Pacific Ocean: evidence from petrology, geochemistry and isotopic dating of dredge samples. *Mar. Geol.* 148: 135-162.
- Mortimer, N. and Parkinson, D., 1996. Hikurangi Plateau: A Cretaceous large igneous province in the southwest Pacific Ocean. *Journal of Geophysical Research-Solid Earth* 101: 687-696.
- Murphy, D.M.K. and Stanley, C.R., 2007. Litho-geochemical constraints on the host rock, hydrothermal alteration and weathering of the Groundrush gold deposit. *Geochemistry: Exploration, Environment, Analysis* 7: 363-375.
- Naito, K., Matsuhisa, Y., Izawa, E. and Takaoko, H., 1993. Oxygen isotope zonation of hydrothermally altered rocks in the Hishikari gold deposit, southern Kyushu, Japan: its implication for mineral prospecting. *Resource Geology Special Issue* 14: 71-84.
- Nebel, O., Mezger, K., Scherer, E.E. and Davies, G.R., 2006. Determination of the rubidium decay constant by age comparison against the U-Pb system, American Geophysical Union Fall Meeting. *Eos Trans. AGU*, pp. Abstract V21A-0558.
- Nicholson, K.N. and Black, P.M., 2004. Cretaceous to early Tertiary basaltic volcanism in the Far North of New Zealand: geochemical associations and their tectonic significance. *N. Z. J. Geol. Geophys.* 47: 437-446.
- Nicholson, K.N., Black, P.M., Hoskin, P.W.O. and Smith, I.E.M., 2004. Silicic volcanism and back-arc extension related to migration of the Late Cainozoic Australian-Pacific plate boundary. *J. Volcanol. Geotherm. Res.* 131: 295-306.
- Nicol, A., Mazengarb, C., Chanier, F., Rait, G., Uruski, C. and Wallace, L., 2007. Tectonic evolution of the active Hikurangi subduction margin, New Zealand, since the Oligocene. *Tectonics* 26: 1-24.
- Okamoto, K., 1979. Geochemical study on magmatic differentiation of Asama Volcano, central Japan. *Journal of the Geological Society Japan* 85: 525-535.
- Ovens, S.A., 1976. Geology of the Tairua-Hot Water Beach area. Unpublished MSc Thesis, University of Auckland, Auckland, New Zealand.
- Pearce, J.A., 1982. Trace element characteristics of lavas from destructive plate boundaries. In: R.S. Thorpe (Editor), *Andesites: Orogenic Andesites and Related Rocks*. John Wiley, Chichester, pp. 525-548.
- Pearce, J.A., 1983. Role of the sub-continental lithosphere in magma genesis at active continental margins. In: C.J. Hawkesworth and M.J. Norry (Editors), *Continental Basalts and Mantle Xenoliths*. Shiva, Nantwich, pp. 230-249.
- Pearce, J.A., Baker, P.E., Harvey, P.K. and Luff, I.W., 1995. Geochemical evidence for subduction fluxes, mantle melting and fractional crystallisation beneath the South Sandwich island arc. *J. Petrol.* 36: 1073-1109.
- Pearce, J.A. and Parkinson, I.J., 1993. Trace element models for mantle melting: application to volcanic arc petrogenesis. In: H.M. Prichard, T. Alabaster, N.B.W. Harris and C.R. Neary (Editors), *Magmatic processes and Plate Tectonics*. Special Publication. Geological Society, pp. 373-403.
- Pearce, T.H., 1968. A contribution to the theory of variation diagrams. *Contrib. Mineral. Petrol.* 19: 142-157.
- Person, M., Banerjee, A., Hofstra, A., Sweetkind, D. and Gao, Y., 2008. Hydrologic models of modern and fossil geothermal systems in the Great Basin: Genetic implications for epithermal Au-Ag and Carlin-type gold deposits. *Geosphere* 4: 888-917.
- Pettinga, J.R., 1982. Upper Cenozoic structural history, coastal Southern Hawkes Bay, New Zealand. *N. Z. J. Geol. Geophys.* 25: 149-191.
- Price, R.C., Gamble, J.A., Smith, I.E.M., Stewart, R.B., Eggins, S. and Wright, I.C., 2005. An integrated model for the temporal evolution of andesites and rhyolites and crustal development in New Zealand's North Island. *J. Volcanol. Geotherm. Res.* 140: 1-24.

- Price, R.C., Stewart, R.B., Woodhead, J.D. and Smith, I.E.M., 1999. Petrogenesis of high-K arc magmas: Evidence from Egmont Volcano, North Island, New Zealand. *J. Petrol.* 40: 167-197.
- Reid, F., 1983. Origin of the rhyolitic rocks of the Taupo Volcanic Zone, New Zealand. *J. Volcanol. Geotherm. Res.* 15: 315-338.
- Reubi, O. and Blundy, J., 2009. A dearth of intermediate melts at subduction zone volcanoes and the petrogenesis of arc andesites. *Nature* 461: 1269-1273.
- Reubi, O. and Nicholls, I.A., 2005. Structure and dynamics of a silicic magmatic system associated with caldera-forming eruptions at Batur volcanic field, Bali, Indonesia. *J. Petrol.* 46: 1367-1391.
- Reyners, M., 1980. A microearthquake study of the plate boundary, North Island, New Zealand. *Geophysical Journal of the Royal Astronomical Society* 63: 1-22.
- Reyners, M., Eberhart-Phillips, D., Stuart, G. and Nishimura, Y., 2006. Imaging subduction from the trench to 300 km depth beneath the central North Island, New Zealand, with Vp and Vp/Vs. *Geophys. J. Int.* 165: 565-583.
- Richards, J.R., Cooper, J.A. and Black, P.M., 1966. Potassium-argon age of plutonic intrusives on Cape Colville Peninsula and Uvieu Island, New Zealand. *Nature* 211: 725-726.
- Rosenberg, M.D., Bignall, G. and Rae, A.J., 2009. The geologic framework of the Wairakei-Tauhara Geothermal System, New Zealand. *Geothermics* 38: 72-84.
- Rowan, C.J. and Roberts, A.P., 2008. Widespread remagnetizations and a new view of Neogene tectonic rotations within the Australia-Pacific plate boundary zone, New Zealand. *J. Geophys. Res.* 113: B03103.
- Rutherford, M.J. and Hill, P.M., 1993. Magma ascent rates from amphibole breakdown: an experimental study applied to the 1980-1986 Mount St. Helens eruptions. *J. Geophys. Res.* 98: 19,667-19,685.
- Saunders, J.A., Unger, D.L., Kamenov, G.D., Fayek, M., Hames, W.E. and Utterback, W.C., 2008. Genesis of Middle Miocene Yellowstone hotspot-related bonanza epithermal Au-Ag deposits, Northern Great Basin, USA. *Mineral. Depos.* 43: 715-734.
- Schellart, W.P., 2007. North-eastward subduction followed by slab detachment to explain ophiolite obduction and Early Miocene volcanism in Northland, New Zealand. *Terra Nova* 19: 211-218.
- Schellart, W.P., Lister, G.S. and Toy, V.G., 2006. A Late Cretaceous and Cenozoic reconstruction of the Southwest Pacific region: Tectonics controlled by subduction and slab rollback processes. *Earth-Sci. Rev.* 76: 191-233.
- Schuth, S., Munker, C., König, S., Qopoto, C., Basi, S., Garbe-Schönberg, D. and Ballhaus, C., 2009. Petrogenesis of lavas along the Solomon Island Arc, SW Pacific: coupling of compositional variations and subduction zone geometry. *J. Petrol.* 50: 781-811.
- Shane, P., Martin, S.B., Smith, V.C., Beggs, K.F., Darragh, M.B., Cole, J.W. and Nairn, I.A., 2007. Multiple rhyolite magmas and basalt injection in the 17.7 ka Rerewhakaaitu eruption episode from Tarawera volcanic complex, New Zealand. *J. Volcanol. Geotherm. Res.* 164: 1-26.
- Shane, P., Strachan, L.J. and Smith, I.E.M., 2010. Redefining the Waitemata Basin, New Zealand: a new tectonic, magmatic, and basin evolution model at a subduction terminus in the SW Pacific. *Geochem. Geophys. Geosyst.*
- Sharp, B.M., Locke, C.A. and Cassidy, J.A., 1989. Gravity investigations of the Maungataniwha and Ahipara ophiolite massifs, Northland, New Zealand. *Bull. R. Soc. N. Z.* 26: 175-181.
- Sherlock, R.L., 1996. Hydrothermal alteration of volcanic rocks at the McLaughlin gold deposit, northern California. *Canadian Journal of Earth Sciences* 33: 493-508.
- Shibata, T., Makishima, A. and Nakamura, E., 1989. Trace neodymium isotope analysis and its application to geological problems, Annual Meeting of the Geochemical Society of Japan, Tokyo.
- Shikazono, N., Yonekawa, N. and Karakizawa, T., 2002. Mass transfer, oxygen isotopic variation and gold precipitation in an epithermal system: a case study of the Hishikari deposit, southern Kyushu, Japan. *Resource Geology* 52: 211-222.
- Shimizu, N. and Kushiro, I., 1975. Partitioning of rare-earth elements between garnet and liquid at high pressures - preliminary experiments. *Geophys. Res. Lett.* 2: 413-416.
- Simmons, S.F. and Brown, K.L., 2007. The flux of gold through a volcanic arc, Taupo Volcanic Zone, New Zealand. *Geology* 35: 1099-1102.
- Simmons, S.F. and Browne, P.R.L., 2000. Hydrothermal minerals and precious metals in the Broadlands-Ohaaki geothermal system: Implications for understanding low-sulfidation epithermal environments. *Econ. Geol.* 95: 971-999.
- Simpson, M.P. and Mauk, J.L., 2000. Geochemistry of wall rock alteration at the Golden Cross deposit, New Zealand. *New*

- Zealand Minerals & Mining Conference, Wellington, New Zealand, pp. 197-208.
- Simpson, M.P. and Mauk, J.L., 2004. Epithermal deposits and analogous geothermal systems: A physical size comparison and implications for exploration, Proceedings Australasian Institute of Mining and Metallurgy New Zealand Branch 37th Annual Conference, pp. 229-240.
- Simpson, M.P. and Mauk, J.L., in press. Hydrothermal alteration and hydrologic reconstruction of the Waitekauri epithermal Au-Ag prospect, Hauraki Goldfield, New Zealand. *Econ. Geol.*
- Sisson, T.W., 1991. Pyroxene-high silica rhyolite trace element partition coefficients measured by ion microprobe. *Geochim. Cosmochim. Acta* 55: 1575-1585.
- Sisson, T.W., 1994. Hornblende-melt trace element partitioning measured by ion microprobe. *Chem. Geol.* 117: 331-344.
- Sisson, T.W., Ratajeski, K., Hankins, W.B. and Glazner, A.F., 2005. Voluminous granitic magmas from common basaltic sources. *Contrib. Mineral. Petrol.* 148: 635-661.
- Sivell, W. and McCulloch, M.T., 2000. Reassessment of the origin of the Dun Mountain Ophiolite, New Zealand: Nd-isotopic and geochemical evolution of magma suites. *N. Z. J. Geol. Geophys.* 43: 133-146.
- Skinner, D.N.B., 1972. Subdivision and petrology of the Mesozoic rocks of Coromandel (Manaia Hill Group). *N. Z. J. Geol. Geophys.* 15: 203-227.
- Skinner, D.N.B., 1976. Northern Coromandel. Scale 1:63 360. New Zealand Geological Survey Geological Map of New Zealand, sheet N40 and parts N35, N36 and N39. New Zealand Geological Survey.
- Skinner, D.N.B., 1986. Neogene Volcanism of the Hauraki Volcanic Region. *Bull. R. Soc. N. Z.*: 21-47.
- Skinner, D.N.B., 1993. Geology of the Coromandel Harbour area, Scale 1:50 000. Geological Map, 4. Institute of Geological and Nuclear Sciences, Ltd.
- Skinner, D.N.B., 1995. Geology of the Mercury Bay area, Scale 1:50 000. Geological Map, 17. Institute of Geological and Nuclear Sciences Ltd.
- Smith, I.E.M., Black, P.M. and Itaya, T., 1995. Inception and evolution of Cenozoic arc-type volcanism in northern New Zealand. In: J.L. Mauk and J.D. StGeorge (Editors), 1995 PACRIM Congress on Exploring the RIM, Auckland, New Zealand, pp. 563-567.
- Smith, I.E.M., Okada, T., Itaya, T. and Black, P.M., 1993. Age relationships and tectonic implications of late Cenozoic basaltic volcanism in Northland, New Zealand. *N. Z. J. Geol. Geophys.* 36: 385-393.
- Smith, I.E.M., Price, R.C., Stewart, R.B. and Worthington, T.J., 2009. An assessment of the mantle and slab components in the magmas of an oceanic arc volcano: Raoul Volcano, Kermadec arc. *J. Volcanol. Geotherm. Res.* 184: 437-450.
- Smith, I.E.M., Ruddock, R.S. and Day, R.A., 1989. Miocene arc-type volcanic/plutonic complexes of the Northland Peninsula, New Zealand. *Bull. R. Soc. N. Z.* 26: 205-213.
- Smith, I.E.M., Stewart, R.B. and Price, R.C., 2003. The petrology of a large intra-oceanic silicic eruption: the Sandy Bay Tephra, Kermadec Arc, Southwest Pacific. *J. Volcanol. Geotherm. Res.* 124: 173-194.
- Smith, I.E.M., Worthington, T.J., Price, R.C., Stewart, R.B. and Maas, R., 2006b. Petrogenesis of dacite in an oceanic subduction environment: Raoul Island, Kermadec arc. *J. Volcanol. Geotherm. Res.* 156: 252-265.
- Smith, N., Cassidy, J., Locke, C.A., Mauk, J.L. and Christie, A.B., 2006a. The role of regional-scale faults in controlling a trapdoor caldera, Coromandel Peninsula, New Zealand. *J. Volcanol. Geotherm. Res.* 149: 312-328.
- Spell, T.R., McDougall, I. and Tulloch, A.J., 2000. Thermochronological constraints on the breakup of the Pacific Gondwana margin: the Paparoa metamorphic core complex, South Island, New Zealand. *Tectonics* 19: 433-451.
- Spörli, K.B., Begbie, M.J., Irwin, M.R. and Rowland, J.V., 2006. Structural processes and tectonic controls on the epithermal Au-Ag deposits of the Hauraki Goldfield. In: A.B. Christie and R.L. Brathwaite (Editors), *Geology and exploration of New Zealand mineral deposits*. Australasian Institute of Mining and Metallurgy Monograph, pp. 85-94.
- Stanley, C.R., Baker, T., Mustard, R., Radford, N. and Butler, I., in press. Litho-geochemistry of hydrothermally altered host rocks at the Pajingo low sulfidation gold deposit, Queensland, Australia: The geochemical anatomy of an epithermal alteration zone. *Gechemistry: Exploration, Environment, Analysis*.
- Stern, T., Smith, E.G.C., Davey, F.J. and Muirhead, K.J., 1987. Crustal and upper mantle structure of the northwestern North Island, New Zealand, from seismic refraction data. *Geophysical Journal of the Royal Astronomical Society* 91: 913-936.
- Stern, T., Stratford, W.R., Seward, D., Henderson, D., Savage, M., Smith, E., Benson, A., Greve, S. and Salmon, M., 2010. Crust-mantle structure of the central North Island, New Zealand, based on seismological observations. *J. Volcanol. Geotherm. Res.* 190: 58-74.

- Stern, T.A., Stratford, W.R. and Salmon, M.L., 2006. Subduction evolution and mantle dynamics at a continental margin: Central North Island, New Zealand. *Reviews of Geophysics* 44.
- Stipp, J.J., 1968. The geochronology and petrogenesis of the Cenozoic volcanics of North Island, New Zealand. Unpublished PhD Thesis, Australian National University, Canberra, Australia.
- Stock, J.M. and Cagle, S.C., 2002. Tectonic history of Antarctic seafloor in the Australia-New Zealand-South Pacific sector: implications for Antarctic continental tectonics. *Bull. R. Soc. N. Z.* 35: 251-259.
- Straub, S.M., LaGatta, A.B., Pozzo, A.L.M.D. and Langmuir, C.H., 2008. Evidence from high-Ni olivines for a hybridized peridotite/pyroxenite source for orogenic andesites from the central Mexican Volcanic Belt. *Geochem. Geophys. Geosyst.* 9: Q03007.
- Sun, S.S. and McDonough, W.F., 1989. Chemical and isotopic systematics of oceanic basalts: implications for mantle composition and processes. *Geological Society of London Special Publication* 42: 313-345.
- Sutherland, R., 1999. Basement geology and tectonic development of the greater New Zealand region: an interpretation from regional magnetic data. *Tectonophysics* 308: 341-362.
- Sutton, A.N., Blake, S. and Wilson, C.J.N., 1995. An outline geochemistry of rhyolite eruptives from Taupo volcanic centre, New Zealand. *J. Volcanol. Geotherm. Res.* 68: 153-175.
- Tamura, Y. and Tatsumi, Y., 2002. Remelting of an andesitic crust as a possible origin for rhyolitic magma in oceanic arcs: an example from the Izu-Bonin arc. *J. Petrol.* 43: 1029-1047.
- Tatsumi, Y., 1986. Formation of volcanic front in subduction zones. *Geophys. Res. Lett.* 13: 717-720.
- Tatsumi, Y., 1989. Migration of fluid phases and genesis of basalt magmas in subduction zones. *J. Geophys. Res.* 94: 4697-4707.
- Thompson, B.N., 1965. Introduction: broad distribution of volcanic rocks in North Island, New Zealand. Department of Scientific and Industrial Research information series, 49.
- Toutain, J.P., Sortino, F., Reynier, B., Dupre, B., Munoz, M., Nonell, A., Polve, M. and Chancha Do Vale, S., 2003. A new collector for sampling volcanic aerosols. *J. Volcanol. Geotherm. Res.* 123: 95-103.
- Turner, S., George, R., Jerram, D.A., Carpenter, N. and Hawkesworth, C.J., 2003. Case studies of plagioclase growth and residence times in island arc lavas from Tonga and the Lesser Antilles, and a model to reconcile discordant age information. *Earth Planet. Sci. Lett.* 214: 279-294.
- Urqueta, E., Kyser, T.K., Clark, A.H., Stanley, C.R. and Oates, C.J., 2009. Lithogeochemistry of the Collahuasi porphyry Cu-Mo and epithermal Cu-Ag (-Au) cluster, northern Chile: Pearce element ratio vectors to ore. *Gechemistry: Exploration, Environment, Analysis* 9: 9-17.
- Uruski, C.I., Cook, R.A., Herzer, R.H. and Isaac, M.J., 2004. Petroleum geology of the Northland sector of the greater Taranaki Basin, New Zealand Petroleum Conference proceedings. Crown Minerals, Ministry of Economic Development, Wellington, pp. 10.
- Wallace, L.M., J., B., McCaffrey, R. and Darby, D., 2004. Subduction zone coupling and tectonic block rotations in the North Island, New Zealand. *J. Geophys. Res.* 109.
- Warren, I., Simmons, S.F. and Mauk, J.L., 2007. Whole-rock geochemical techniques for evaluating hydrothermal alteration, mass changes, and compositional gradients associated with epithermal Au-Ag mineralization. *Econ. Geol.* 102: 923-948.
- Watson, E.B. and Harrison, T.M., 1983. Zircon saturation revisited: temperature and composition effects in a variety of crustal magma types. *Earth Planet. Sci. Lett.* 64: 295-304.
- Watts, A.B., Weisell, J.K., Duncan, R.A. and Duncan, R.L., 1988. Origin of the Louisville Ridge and its relationship to the Eltanin Fracture Zone system. *J. Geophys. Res.* 95: 3051-3077.
- Webster, J.D., 2004. The exsolution of magmatic hydrosaline chloride liquids. *Chem. Geol.* 210: 33-48.
- Whattam, S.A., Malpas, J., Ali, J.R. and Smith, I.E.M., 2008. New SW Pacific tectonic model: Cyclical intraoceanic magmatic arc construction and near-coeval emplacement along the Australia-Pacific margin in the Cenozoic. *Geochem. Geophys. Geosyst.* 9: Q03021.
- Whattam, S.A., Malpas, J., Smith, I.E.M. and Ali, J.R., 2006. Link between SSZ ophiolite formation, emplacement and arc inception, Northland, New Zealand: U-Pb SHRIMP constraints; Cenozoic SW Pacific tectonic implications. *Earth Planet. Sci. Lett.* 250: 606-632.
- Whattam, S.A., Malpas, J.G., Ali, J.R., Smith, I.E.M. and Lo, C.H., 2004. Origin of the Northland Ophiolite, northern New Zealand: discussion of new data and reassessment of the model. *N. Z. J. Geol. Geophys.* 47: 383-389.

- Whelan, P.M., Gill, J.B., Kollman, E., Duncan, R.A. and Drake, R.E., 1985. Radiometric dating of magmatic stages in Fiji. In: D.W. Scholl and T.L. Vallier (Editors), *Geology and offshore resources of Pacific island arcs: Tonga region*. Circum-Pacific Council for Energy and Mineral Resources, Houston, Texas, pp. 415-440.
- White, N.C. and Hedenquist, J.W., 1995. Epithermal gold deposits: styles, characteristics and exploration. *Society of Economic Geology Newsletter* 23: 1-13.
- Willner, A.P., Glodny, J., Gerya, T.V., Godoy, E. and Massone, H.-J., 2004. A counterclockwise P-T-t-path of high pressure-low temperature rocks from the Coastal Cordillera accretionary complex of South Central Chile: constraints for the earliest stage of subduction mass flow. *Lithos* 75.
- Wilson, C.J.N., 1993. Stratigraphy, chronology, styles and dynamics of Late Quaternary eruptions from Taupo Volcano, New Zealand. *Philosophical Transactions: Physical Sciences and Engineering* 343: 205-306.
- Wilson, C.J.N., 2008. Supereruptions and supervolcanoes: processes and products. *Elements* 4: 29-34.
- Wilson, C.J.N., Blake, S., Charlier, B.L.A. and Sutton, A.N., 2006. The 26.5 ka Oruanui eruption, Taupo Volcano, New Zealand: development, characteristics and evacuation of a large rhyolitic magma body. *J. Petrol.* 47: 35-69.
- Wilson, C.J.N. and Charlier, B.L.A., 2009. Rapid rates of magma generation at contemporaneous magma systems, Taupo Volcano, New Zealand: Insights from U-Th model-age spectra in zircons. *J. Petrol.* 50: 875-907.
- Wilson, C.J.N., Gravley, D.M., Leonard, G.S. and Rowland, J.V., 2009. *Volcanism in the central Taupo Volcanic Zone, New Zealand*, Geological Society of London Special Publication: *Studies in Volcanology: The Legacy of George Walker*.
- Wilson, C.J.N., Houghton, B.F., McWilliams, M.O., Lanphere, M.A., Weaver, S.D. and Briggs, R.M., 1995. Volcanic and structural evolution of Taupo Volcanic Zone, New Zealand: a review. *J. Volcanol. Geotherm. Res.* 68: 1-28.
- Wilson, C.J.N., Rogan, A.M., Smith, I.E.M., Northey, D.J., Nairn, I.A. and Houghton, B.F., 1984. Caldera volcanoes of the Taupo Volcanic Zone, New Zealand. *J. Geophys. Res.* 89: 8463-8484.
- Wodzicki, A. and Weissberg, B.G., 1970. Structural control of base metal mineralization at the Tui mine, Te Aroha, New Zealand. *N. Z. J. Geol. Geophys.* 13: 610-630.
- Wolf, M.B. and Wyllie, P.J., 1994. Dehydration-melting of an amphibolite at 10 kbar: the effects of temperature and time. *Contrib. Mineral. Petrol.* 115: 369-383.
- Wood, B.J. and Turner, S.P., 2009. Origin of primitive high-Mg andesite: constraints from natural examples and experiments. *Earth Planet. Sci. Lett.* 283: 59-66.
- Wright, I.C., Parson, L.M. and Gamble, J.A., 1996. Evolution and interaction of migrating cross-arc volcanism and backarc rifting: an example from the southern Havre Trough (35°20'-37°S). *J. Geophys. Res.* 101: 22,071-22,086.
- Wysoczanski, R.J., Todd, E., Wright, I.C., Leybourne, M.I., Hergt, J.M., Adam, C. and Mackay, K., 2010. Backarc rifting, constructional volcanism and nascent disorganised spreading in the southern Havre Trough backarc rifts (SW Pacific). *J. Volcanol. Geotherm. Res.* 190: 39-57.
- Yoshikawa, M. and Nakamura, E., 1993. Precise isotopic determination of trace amounts of Sr in magnesium-rich samples. *J. Jpn. Mineral. Petrol. Econ.* 88: 548-561.
- Zindler, A. and Hart, S., 1986. Chemical Geodynamics. *Ann. Rev. Earth Pl. Sc.* 14: 493-571.

Appendices

Appendix A. Supplementary Dataset to Chapter 3

Appendix A. Supplementary dataset to Chapter 3 “Geochemistry of the Early Miocene volcanic succession of Northland, New Zealand, and implications for the evolution of subduction in the Southwest Pacific”. See Chapter 3, Section 3.2.4 for analytical methods.

Bestpfe.com

Table 8.1	33095	33129	33169	33170	33168	33162	33005	33006	33004	33131	33162
Locality	Parahaki										
Rock type	dacite	rhyolite									
SiO ₂	66.7	68.3	68.8	68.9	69.1	69.3	69.5	69.5	70.0	70.4	70.4
TiO ₂	0.6	0.3	0.3	0.3	0.3	0.3	0.3	0.3	0.3	0.4	0.3
Al ₂ O ₃	17.6	17.3	17.3	17.4	17.3	17.2	17.4	17.2	17.3	15.6	17.0
FeO	2.38	2.00	1.85	1.91	1.77	1.62	1.73	1.71	1.50	1.64	1.42
Fe ₂ O ₃	0.95	0.80	0.74	0.76	0.71	0.65	0.69	0.68	0.75	0.82	0.71
MnO	0.0	0.0	0.0	0.0	0.0	0.0	0.0	0.0	0.0	0.1	0.0
MgO	1.2	0.6	0.5	0.5	0.7	0.5	0.6	0.6	0.5	1.0	0.6
CaO	3.3	3.8	3.3	3.1	3.3	3.5	3.0	3.2	2.8	3.3	2.9
Na ₂ O	4.3	4.5	4.7	4.5	4.5	4.6	4.5	4.5	4.4	3.1	4.1
K ₂ O	2.9	2.1	2.3	2.3	2.2	2.3	2.1	2.2	2.2	3.7	2.4
P ₂ O ₅	0.1	0.1	0.1	0.1	0.1	0.1	0.1	0.1	0.1	0.1	0.1
LOI	1.09	0.76	0.94	1.29	0.96	0.68	1.10	0.88	1.10	1.52	1.42
Sc	6.58	3.35	3.17	3.15	35.08	2.97	3.11	3.00	3.07	4.92	2.73
V	55.65	40.81	41.79	38.86	260.87	40.43	40.61	40.60	40.61	51.37	38.87
Cr	18.84	6.76	7.48	7.02	185.42	6.87	7.25	7.05	6.93	29.81	6.67
Co	22.88	26.01	18.84	15.73	34.28	27.49	19.49	18.71	19.21	23.17	12.46
Ni	15.00	4.16	4.53	4.05	29.02	4.09	4.07	4.13	4.02	9.35	4.06
Cu	12.06	10.21	7.49	15.10	31.68	8.13	9.00	9.39	9.08	4.31	11.83
Zn	53.17	53.42	51.68	51.96	79.78	50.37	53.24	63.26	40.10	48.13	35.16
Ga	18.37	18.58	19.33	18.71	23.73	19.15	19.34	19.21	19.16	18.19	19.20
Rb	97.00	78.43	81.63	77.29	63.42	82.86	76.68	77.23	78.91	151.13	87.49
Sr	266.10	290.39	264.32	245.78	481.06	271.52	268.86	286.06	278.35	200.88	248.04
Y	11.24	4.93	4.01	3.76	28.13	3.70	4.08	4.03	4.07	4.10	2.79
Zr	142.36	183.76	182.35	181.83	178.37	179.19	179.08	179.35	178.32	147.09	170.05
Nb	7.38	8.86	8.94	9.02	7.78	8.80	8.96	8.87	8.89	7.98	8.76
Cs	1.83	3.64	4.36	3.00	1.11	2.12	4.01	3.33	4.24	4.64	3.91
Ba	563.10	495.48	495.30	486.85	569.61	503.64	510.25	518.30	498.64	645.92	549.91
La	21.91	28.78	28.59	28.09	23.09	28.49	29.65	28.56	31.01	23.79	28.95
Ce	47.04	59.03	57.47	55.72	51.25	58.14	57.50	57.55	57.66	50.79	57.51
Pr	5.25	6.21	6.01	5.88	6.87	6.04	5.98	5.99	5.96	5.50	5.92
Nd	21.04	23.08	22.27	21.58	23.72	22.15	22.38	21.92	22.08	21.42	21.73
Sm	4.24	3.83	3.62	3.50	6.01	3.56	3.77	3.83	3.66	4.02	3.41
Eu	1.02	0.95	0.91	0.86	1.51	0.90	0.92	0.93	0.95	0.85	0.82
Gd	3.69	2.45	2.25	2.23	5.66	2.28	2.36	2.18	2.31	2.57	1.96
Tb	0.46	0.27	0.23	0.22	0.53	0.22	0.24	0.21	0.24	0.23	0.18
Dy	2.47	1.24	1.01	0.91	4.68	0.89	1.06	0.99	1.01	1.02	0.74
Ho	0.39	0.16	0.14	0.13	1.19	0.12	0.14	0.13	0.15	0.15	0.09
Er	1.03	0.42	0.34	0.31	3.69	0.32	0.31	0.32	0.32	0.36	0.20
Tm	0.13	0.07	0.06	0.05	0.00	0.05	0.05	0.05	0.05	0.06	0.04
Yb	0.73	0.38	0.34	0.26	3.39	0.25	0.30	0.26	0.30	0.32	0.17
Lu	0.12	0.05	0.04	0.04	0.00	0.03	0.04	0.04	0.04	0.05	0.02
Hf	4.08	4.74	4.86	4.84	4.59	4.76	4.95	4.71	4.78	4.40	4.63
Ta	0.73	0.72	0.74	0.73	0.00	0.71	1.03	0.92	1.00	0.74	0.67
Pb	17.54	16.74	17.11	17.26	11.53	16.81	17.20	17.74	16.21	18.59	17.81
Th	9.07	13.06	13.12	13.06	7.13	13.17	12.93	12.87	12.89	10.69	13.11
U	2.84	2.63	2.59	2.44	1.98	2.77	2.65	2.66	2.71	2.68	2.67

Table 8.1	32985	33155	37624	41244	38601	41120	41137	41384	41386	41339	41382
Locality	Parahaki	Parahaki	Parahaki	Karikari	Karikari	Karikari	Karikari	Karikari	Karikari	Karikari	Karikari
Rock type	rhyolite	rhyolite	rhyolite	basalt	basaltic andesite	basaltic andesite	basaltic andesite	dyke bas. andesite	basaltic andesite	dyke bas. andesite	dyke bas. and.
SiO ₂	70.8	70.9	71.5	49.0	53.7	55.8	55.9	56.0	56.5	56.9	57.3
TiO ₂	0.2	0.2	0.4	1.4	0.6	0.9	0.8	0.8	0.7	0.9	0.8
Al ₂ O ₃	16.7	16.6	15.2	13.2	16.3	18.3	16.8	14.2	15.7	16.8	14.7
FeO	1.13	1.14	1.94	11.95	7.00	5.75	6.21	6.71	7.24	5.76	6.66
Fe ₂ O ₃	0.57	0.57	0.97	2.39	2.10	1.73	1.86	2.01	2.17	1.73	2.33
MnO	0.0	0.0	0.0	0.2	0.2	0.1	0.1	0.2	0.2	0.2	0.2
MgO	0.4	0.6	0.3	10.6	7.7	4.8	6.0	7.8	6.8	5.6	7.2
CaO	3.0	2.8	1.9	9.3	9.2	7.8	8.2	8.4	6.6	6.7	6.4
Na ₂ O	4.6	4.5	4.2	1.6	2.5	3.5	2.9	2.0	2.6	3.3	2.3
K ₂ O	2.5	2.6	3.4	0.3	0.6	1.1	1.1	1.8	1.4	2.1	1.9
P ₂ O ₅	0.1	0.1	0.1	0.1	0.1	0.2	0.1	0.2	0.1	0.2	0.2
LOI	0.72	0.85	0.97	0.17	0.38	0.96	0.94	2.59	2.71	1.82	2.51
Sc	2.33	2.34	6.93	49.78	34.26	23.38	29.35	32.35	28.91	24.62	29.10
V	39.79	39.25	65.84	507.73	212.88	191.76	218.29	230.97	193.45	178.68	215.28
Cr	6.49	6.75	10.73	289.79	297.14	188.29	234.47	433.05	388.50	232.15	376.96
Co	18.73	15.19	15.67	53.31	37.37	30.53	34.19	41.10	33.95	26.47	34.54
Ni	3.91	4.22	7.89	60.91	59.36	40.29	46.01	47.19	96.70	31.85	47.96
Cu	7.54	10.79	11.95	30.00	29.17	44.77	35.89	14.39	74.20	6.46	6.86
Zn	56.14	47.93	40.57	93.41	60.84	53.11	52.63	138.91	77.19	102.83	106.57
Ga	19.09	19.54	17.14	13.10	14.44	16.49	15.11	14.66	14.19	15.58	14.72
Rb	90.62	91.01	131.74	8.20	18.99	35.39	33.54	71.62	39.39	35.34	63.64
Sr	262.70	254.37	155.11	204.24	257.08	276.12	238.77	329.85	210.97	251.14	315.07
Y	2.23	1.72	24.88	10.82	12.43	16.75	15.14	19.07	16.81	18.75	19.28
Zr	151.88	139.83	158.86	24.97	48.50	79.81	78.01	113.85	84.36	125.44	123.80
Nb	8.50	8.73	10.79	1.49	2.39	5.46	4.17	4.99	3.76	7.36	5.40
Cs	3.32	2.65	10.52	0.43	2.12	3.20	1.96	0.86	4.76	1.56	0.95
Ba	558.62	567.29	308.19	82.94	160.57	220.42	270.80	379.72	260.56	600.35	506.55
La	26.17	21.97	23.25	3.39	6.64	11.90	9.36	14.64	10.59	14.95	15.38
Ce	51.03	45.00	43.08	7.91	14.34	25.64	19.52	31.17	23.89	32.20	32.98
Pr	5.34	4.63	5.54	1.09	1.75	3.06	2.31	3.95	2.98	3.76	4.02
Nd	19.51	16.96	21.72	5.44	8.08	13.30	10.17	16.57	13.39	16.14	17.48
Sm	3.18	2.85	4.62	1.61	2.01	3.14	2.35	3.91	3.32	3.61	3.91
Eu	0.85	0.77	0.74	0.64	0.77	1.05	0.87	1.03	0.85	1.00	1.06
Gd	1.75	1.60	4.24	1.88	2.21	3.04	2.71	3.75	3.47	3.48	3.81
Tb	0.16	0.15	0.68	0.31	0.35	0.47	0.42	0.56	0.51	0.55	0.59
Dy	0.60	0.45	4.53	2.18	2.38	3.16	2.88	3.77	3.41	3.53	3.67
Ho	0.09	0.06	0.89	0.44	0.50	0.65	0.58	0.75	0.67	0.73	0.72
Er	0.18	0.13	2.63	1.33	1.48	1.85	1.72	2.13	1.93	2.16	2.20
Tm	0.03	0.03	0.41	0.20	0.22	0.28	0.29	0.32	0.30	0.32	0.30
Yb	0.12	0.07	2.80	1.30	1.59	1.94	1.93	2.13	2.12	2.18	2.25
Lu	0.01	0.01	0.39	0.20	0.24	0.29	0.27	0.31	0.30	0.32	0.32
Hf	4.49	4.07	4.50	0.82	1.45	2.27	2.16	3.13	2.45	3.34	3.42
Ta	0.77	0.69	1.52	0.30	0.46	0.59	0.55	0.50	0.39	0.60	0.52
Pb	18.80	18.69	14.46	2.69	5.24	5.62	5.85	3.11	5.02	3.88	7.34
Th	12.00	10.59	11.82	0.94	2.02	3.71	3.58	4.95	3.71	5.48	5.71
U	2.71	2.33	4.35	0.26	0.55	0.92	0.88	1.18	1.14	1.16	1.34

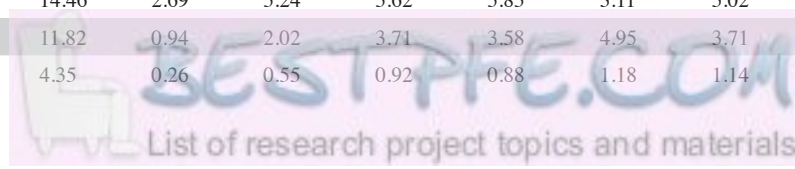


Table 8.1	41119	41335	41278	41292	28223	41294	38650	37987	38649	38651	38635
Locality	Karikari	Karikari	Karikari	Karikari	Karikari	Karikari	North Cape	North Cape	North Cape	North Cape	North Cape
Rock type	andesite	andesite	andesite	andesite	andesite	trachy-dacite	dacite	basaltic andesite	basaltic andesite	andesite	Dacite
SiO ₂	58.2	59.2	62.0	62.6	65.3	67.9	63.3	54.7	54.8	59.7	67.4
TiO ₂	0.8	0.6	0.7	0.7	0.6	0.4	0.6	1.0	1.2	0.7	0.5
Al ₂ O ₃	17.8	15.5	16.1	16.1	17.0	16.6	17.5	18.3	14.8	17.1	16.7
FeO	5.30	5.29	4.34	4.15	3.10	1.85	3.38	6.06	9.60	4.55	2.01
Fe ₂ O ₃	1.86	1.85	1.52	1.45	1.24	0.74	1.35	1.82	2.88	1.59	0.81
MnO	0.1	0.1	0.1	0.1	0.1	0.0	0.1	0.2	0.2	0.1	0.0
MgO	3.9	5.4	3.5	3.2	1.8	0.9	2.7	4.8	3.8	4.4	2.0
CaO	6.7	7.3	5.3	5.1	4.9	3.4	5.3	8.9	8.3	6.8	4.0
Na ₂ O	3.7	2.8	3.6	3.5	3.6	4.1	4.4	3.4	3.5	3.8	4.4
K ₂ O	1.6	1.8	2.8	2.9	2.3	4.0	1.3	0.7	0.8	1.1	2.0
P ₂ O ₅	0.2	0.1	0.2	0.2	0.1	0.1	0.1	0.1	0.2	0.2	0.1
LOI	1.05	0.54	0.95	0.54	1.13	0.36	1.35	0.48	1.03	1.17	1.39
Sc	21.31	22.70	18.99	18.79	16.09	9.04	11.59	35.03	39.38	22.83	6.95
V	160.55	148.09	146.66	140.65	103.16	72.47	92.28	238.54	444.14	152.01	65.45
Cr	135.36	421.63	123.81	122.34	62.46	18.55	62.40	111.74	18.62	174.36	56.42
Co	31.29	21.44	36.22	26.57	210.58	38.28	30.69	36.99	57.34	37.34	23.45
Ni	30.40	56.87	23.59	23.16	13.30	6.68	21.86	23.61	14.49	35.60	18.34
Cu	55.57	13.92	44.13	25.25	14.42	10.99	24.06	23.19	165.83	31.64	33.07
Zn	61.57	36.62	45.72	48.83	54.82	18.04	53.25	67.73	89.20	52.28	58.96
Ga	16.24	17.02	16.78	16.70	17.57	17.04	17.47	19.90	16.38	16.99	19.61
Rb	49.85	76.10	90.95	99.09	73.43	111.40	66.20	29.89	16.73	64.36	60.38
Sr	248.00	317.23	287.09	280.51	262.65	242.79	322.15	293.48	261.34	295.41	361.43
Y	16.12	15.34	42.05	20.93	13.23	23.48	12.21	19.61	27.05	14.01	4.68
Zr	81.94	121.33	209.85	175.93	147.76	233.67	126.33	81.60	84.84	105.28	138.64
Nb	5.79	5.92	7.36	7.50	6.83	7.66	5.78	4.13	2.58	5.16	7.20
Cs	3.99	4.34	1.82	7.62	3.76	1.48	4.31	3.08	2.36	5.01	3.43
Ba	380.79	239.04	537.12	620.94	621.64	652.57	569.65	252.01	345.22	423.15	833.19
La	13.19	15.01	24.26	22.40	18.86	25.62	14.63	9.00	11.33	13.65	18.07
Ce	27.43	32.20	48.62	45.50	36.96	52.91	30.09	21.32	25.24	29.57	36.78
Pr	3.15	3.70	5.65	5.20	4.03	5.86	3.27	2.59	3.35	3.37	3.84
Nd	13.42	15.00	23.07	21.14	16.70	23.44	13.28	13.65	15.82	14.33	14.13
Sm	2.91	3.37	5.01	4.49	3.23	4.69	2.65	3.51	4.20	2.95	2.38
Eu	0.98	0.91	1.24	1.07	0.91	0.94	0.74	1.54	1.32	0.92	0.66
Gd	3.10	3.23	5.23	4.28	2.93	4.34	2.38	4.14	4.61	2.77	1.75
Tb	0.44	0.46	0.91	0.62	0.43	0.65	0.33	0.63	0.72	0.43	0.19
Dy	2.95	2.99	7.03	3.88	2.54	4.37	2.12	3.84	5.05	2.78	1.01
Ho	0.62	0.61	1.57	0.78	0.53	0.87	0.41	0.76	1.06	0.55	0.18
Er	1.90	1.68	4.71	2.29	1.46	2.56	1.24	2.65	3.25	1.61	0.45
Tm	0.29	0.27	0.82	0.35	0.22	0.38	0.19	0.00	0.48	0.25	0.08
Yb	1.93	1.73	4.63	2.38	1.41	2.65	1.22	2.29	3.25	1.65	0.45
Lu	0.28	0.27	0.66	0.35	0.22	0.40	0.18	0.00	0.48	0.24	0.07
Hf	2.46	3.38	4.60	4.77	4.04	6.46	3.74	0.00	2.71	3.04	4.25
Ta	0.71	0.75	1.12	0.89	1.76	1.53	0.90	0.00	0.38	0.97	0.70
Pb	6.29	4.14	8.68	9.51	14.18	5.45	13.97	17.15	7.05	13.48	17.98
Th	5.14	7.57	10.49	10.22	7.34	14.00	6.03	1.81	3.55	5.97	7.99
U	1.26	1.77	2.76	1.98	1.88	3.19	1.54	0.00	0.89	1.64	1.87

Table 8.1	5715	5716b	5716a	3840	33142	33115	32975	33059	33054	19901	33161
Locality	Omapere	Omapere	Omapere	Whangarei	Whangarei	Whangarei	Whangarei	Whangarei	Whangarei	Whangarei	Whangarei
Rock type	basaltic andesite	andesite	andesite	basalt	andesite	basaltic andesite	basaltic andesite	basaltic andesite	basaltic andesite	andesite	andesite
SiO ₂	56.3	62.3	62.4	47.7	54.7	55.6	56.0	56.9	58.6	59.1	59.4
TiO ₂	0.7	0.3	0.2	2.9	0.9	0.7	0.7	0.7	0.7	1.0	0.6
Al ₂ O ₃	17.0	21.0	20.8	12.6	16.7	16.0	16.1	16.2	16.0	17.8	17.2
FeO	5.90	1.39	1.30	9.32	6.16	5.86	5.91	5.67	5.09	5.52	4.81
Fe ₂ O ₃	1.77	0.49	0.45	1.86	1.85	1.76	1.77	1.70	1.78	1.93	1.69
MnO	0.1	0.0	0.0	0.3	0.1	0.1	0.1	0.1	0.1	0.2	0.1
MgO	6.1	0.3	0.7	8.4	7.3	8.1	7.9	7.1	6.3	3.2	5.0
CaO	8.2	3.2	3.3	11.9	8.3	7.9	7.9	7.5	6.7	6.7	6.6
Na ₂ O	3.0	5.7	5.9	3.8	2.9	2.7	2.7	3.0	2.9	2.7	3.2
K ₂ O	0.8	5.3	4.8	0.8	0.9	1.1	0.8	1.2	1.7	1.6	1.3
P ₂ O ₅	0.1	0.1	0.1	0.5	0.1	0.1	0.1	0.1	0.1	0.2	0.1
LOI	1.17	0.33	0.19	1.62	1.15	0.85	0.96	0.56	0.96	2.29	2.43
Sc	28.60	2.68	2.40	39.00	31.26	29.50	27.64	28.81	25.24	25.75	23.77
V	197.70	42.30	57.35	283.81	222.66	177.52	167.09	180.15	153.27	165.35	128.92
Cr	248.39	6.66	6.55	504.52	419.95	598.71	515.08	444.44	481.90	16.51	352.50
Co	31.95	8.96	5.15	43.64	38.54	40.92	44.56	38.75	52.67	91.03	36.31
Ni	49.45	3.94	6.88	77.84	121.09	140.64	126.53	111.19	97.14	7.06	58.40
Cu	29.40	9.52	18.51	61.55	43.36	44.35	43.31	47.60	27.50	29.79	36.63
Zn	54.54	60.12	65.34	90.44	56.66	52.82	52.09	50.37	53.00	672.75	52.54
Ga	15.63	20.16	21.62	18.27	14.98	14.13	14.16	14.79	15.16	16.54	15.80
Rb	34.90	129.44	136.29	15.24	28.63	38.95	39.40	45.08	62.15	48.81	111.56
Sr	243.45	365.45	333.15	373.41	178.83	177.85	211.30	162.85	195.82	272.41	234.91
Y	16.43	1.79	1.38	25.14	18.95	18.28	16.04	16.90	18.01	22.16	15.94
Zr	101.75	135.02	106.35	188.74	80.60	79.33	83.95	71.03	110.61	82.03	103.15
Nb	4.58	5.51	3.18	45.61	2.95	3.74	3.92	3.04	4.87	6.43	4.99
Cs	2.38	1.49	2.79	0.46	1.18	1.55	4.27	3.24	4.50	0.54	7.41
Ba	313.04	1527.90	1113.94	295.69	184.79	225.40	264.24	228.90	335.94	255.10	480.03
La	11.33	10.76	6.47	28.08	7.68	10.11	10.36	8.98	13.94	24.97	13.80
Ce	24.91	21.25	13.32	56.79	17.42	21.42	22.34	19.09	27.86	31.92	27.92
Pr	3.04	2.13	1.49	7.12	2.20	2.68	2.69	2.39	3.37	3.75	3.44
Nd	12.87	7.80	5.96	31.75	10.25	11.53	11.41	10.76	14.34	15.88	14.09
Sm	2.90	1.34	1.14	7.12	2.66	2.65	2.63	2.78	3.23	3.77	3.13
Eu	0.93	0.39	0.39	2.24	0.88	0.83	0.78	0.79	0.89	0.98	0.84
Gd	3.02	0.90	0.78	6.96	3.12	2.85	2.96	2.90	3.38	4.05	3.09
Tb	0.48	0.10	0.09	0.98	0.52	0.48	0.45	0.49	0.57	0.65	0.46
Dy	3.15	0.47	0.28	5.85	3.56	3.18	3.03	3.14	3.50	4.35	2.98
Ho	0.67	0.08	0.05	1.01	0.75	0.68	0.62	0.66	0.69	0.86	0.62
Er	1.86	0.19	0.13	2.55	2.25	2.07	1.79	1.89	2.04	2.51	1.69
Tm	0.29	0.04	0.03	0.34	0.33	0.33	0.29	0.31	0.30	0.37	0.29
Yb	2.02	0.19	0.08	2.06	2.18	2.03	1.81	1.96	2.05	2.38	1.89
Lu	0.30	0.02	0.02	0.28	0.33	0.34	0.29	0.31	0.31	0.34	0.27
Hf	2.81	4.09	3.74	5.03	2.31	2.19	2.46	2.07	3.05	2.74	2.89
Ta	0.63	0.68	0.33	2.97	0.26	0.31	0.35	0.50	1.12	0.97	0.43
Pb	9.06	23.22	23.34	2.38	6.38	8.90	9.45	9.53	12.09	34.52	12.56
Th	4.63	4.08	2.81	3.35	2.73	4.11	4.38	3.46	5.90	9.78	6.10
U	1.24	0.96	1.57	0.96	0.81	1.09	1.18	1.28	1.61	2.36	1.48

Table 8.1	32942	33070	32993	29387	28224	33166	32953	39823	39832	34917	34924
Locality	Whanga-rei	Wairakau	Wairakau	Wairakau	Wairakau						
Rock type	andesite	andesite	andesite	dacite	dacite	rhyolite	rhyolite	basalt	basalt	basaltic andesite	basaltic andesite
SiO ₂	60.6	61.1	61.6	64.5	65.0	69.1	71.4	50.8	55.9	56.0	56.8
TiO ₂	0.9	0.6	0.6	0.5	0.6	0.3	0.2	1.9	1.0	0.8	1.2
Al ₂ O ₃	18.6	16.3	16.9	16.6	17.1	17.2	17.2	14.8	16.1	13.9	16.6
FeO	4.31	4.12	4.09	3.32	2.66	1.65	1.20	10.22	6.31	6.43	5.59
Fe ₂ O ₃	1.51	1.44	1.43	1.33	1.06	0.66	0.60	2.04	1.89	1.93	1.68
MnO	0.1	0.1	0.1	0.1	0.0	0.0	0.0	0.2	0.2	0.1	0.1
MgO	2.2	4.9	4.1	3.0	2.3	0.5	0.4	6.6	4.8	8.5	5.0
CaO	6.0	5.8	5.2	4.8	5.3	3.6	2.2	10.5	8.0	7.8	7.6
Na ₂ O	4.2	4.0	4.3	3.7	3.8	4.6	4.0	2.5	3.8	2.5	3.3
K ₂ O	1.4	1.7	1.6	2.1	2.1	2.2	2.8	0.4	1.8	1.9	1.8
P ₂ O ₅	0.2	0.1	0.1	0.1	0.1	0.1	0.1	0.2	0.2	0.2	0.3
LOI	1.15	0.59	1.25	0.89	0.92	0.49	1.74	0.93	2.57	0.92	0.06
Sc	8.75	20.71	17.53	15.72	14.69	2.98	2.57	44.88	28.35	28.80	29.16
V	71.00	130.37	118.37	101.36	96.77	40.20	39.72	366.27	210.66	211.11	238.91
Cr	21.74	296.27	210.21	150.52	96.11	6.93	5.67	224.81	149.70	505.86	149.78
Co	20.59	44.83	28.60	47.98	72.66	17.50	7.00	45.87	27.69	45.15	51.39
Ni	11.87	75.33	52.79	33.31	28.74	4.20	3.76	63.61	23.49	114.29	28.78
Cu	17.71	30.16	29.73	20.43	28.90	7.47	10.45	55.24	25.56	48.29	39.35
Zn	53.07	46.85	46.67	45.16	49.30	28.59	48.92	74.97	64.82	54.46	63.41
Ga	19.09	15.15	15.56	15.17	16.01	19.53	19.03	17.98	19.31	14.37	16.79
Rb	43.02	65.10	61.63	76.96	72.81	82.29	107.39	17.92	51.10	50.78	50.67
Sr	323.14	202.15	216.59	373.11	246.31	285.92	225.78	142.64	388.77	337.71	424.48
Y	12.75	15.63	15.88	57.86	14.22	3.83	1.65	39.86	22.69	17.77	23.95
Zr	265.70	102.61	108.20	112.04	123.64	181.10	143.21	125.60	144.47	112.76	131.56
Nb	7.87	5.20	4.66	5.56	6.45	8.97	8.83	3.17	6.32	4.56	6.96
Cs	3.88	4.14	1.53	5.58	2.05	4.11	4.35	1.15	0.91	2.51	0.82
Ba	300.00	390.22	356.88	597.78	512.23	524.48	582.97	47.37	460.01	356.05	404.62
La	42.58	13.57	12.92	29.60	18.44	28.89	20.00	5.29	18.62	15.79	17.97
Ce	88.84	27.87	26.17	37.05	36.19	59.00	39.18	15.78	41.40	33.30	39.04
Pr	9.91	3.11	3.03	5.30	4.13	6.16	4.03	2.30	5.54	4.06	4.90
Nd	39.23	12.66	12.42	22.20	16.16	22.69	14.73	14.78	19.38	17.42	21.71
Sm	7.04	2.86	2.82	4.92	3.33	3.66	2.43	4.23	4.76	3.85	5.07
Eu	1.67	0.85	0.79	1.67	0.89	0.90	0.60	1.63	1.26	1.06	1.33
Gd	5.37	2.87	2.85	6.90	3.02	2.32	1.36	5.92	4.70	3.62	4.98
Tb	0.64	0.41	0.44	1.12	0.43	0.23	0.13	0.93	0.00	0.52	0.74
Dy	3.13	2.90	2.85	8.27	2.63	0.93	0.44	9.02	3.92	3.50	4.64
Ho	0.46	0.58	0.56	1.85	0.52	0.14	0.05	1.36	0.97	0.68	0.94
Er	1.14	1.74	1.61	5.77	1.44	0.29	0.11	4.22	3.00	1.93	2.58
Tm	0.15	0.26	0.25	0.85	0.21	0.05	0.03	0.82	0.00	0.30	0.37
Yb	1.00	1.71	1.67	5.89	1.36	0.26	0.08	4.30	2.75	1.96	2.45
Lu	0.13	0.27	0.24	0.97	0.20	0.03	0.01	0.67	0.00	0.28	0.37
Hf	6.41	2.89	2.96	3.16	3.43	4.82	4.29	2.73	3.62	3.17	3.70
Ta	0.80	0.46	0.47	0.87	1.59	0.73	0.69			0.69	0.85
Pb	10.18	12.80	16.05	15.26	15.20	16.95	17.56		9.25	7.87	8.69
Th	17.86	5.87	5.52	6.49	7.01	13.42	10.45		5.79	6.11	5.84
U	2.51	1.73	1.85	1.83	1.73	2.79	2.68		1.59	1.41	1.32

Table 8.1	34930	34918	34929	39762	36210	38494	38510	38504	38515	38496	37979
Locality	Wairakau	Wairakau	Wairakau	Wairakau	Hukatere						
Rock type	andesite	andesite	andesite	andesite	basalt	basalt	basalt	basalt	andesite	dacite	rhyolite
SiO ₂	58.1	58.8	58.8	62.4	48.1	52.1	52.7	53.4	58.7	65.8	70.9
TiO ₂	0.8	0.9	1.0	0.8	1.0	1.1	1.1	1.1	0.9	0.7	0.3
Al ₂ O ₃	14.7	18.4	16.7	17.5	15.3	17.7	16.5	16.9	18.1	16.0	15.0
FeO	5.48	4.81	5.50	3.45	9.03	8.00	7.15	7.48	5.48	3.70	1.58
Fe ₂ O ₃	1.92	1.68	1.93	1.21	1.81	2.40	2.15	2.25	1.92	1.48	0.79
MnO	0.1	0.1	0.2	0.1	0.2	0.3	0.2	0.2	0.2	0.1	0.1
MgO	6.3	2.8	3.3	2.8	10.9	4.3	6.6	5.5	2.4	0.9	0.2
CaO	7.5	6.4	6.7	5.3	10.0	9.8	8.6	8.8	6.1	2.9	1.4
Na ₂ O	2.7	4.1	3.6	3.6	2.3	2.9	3.4	3.1	3.9	5.0	4.6
K ₂ O	2.1	1.8	2.1	2.7	1.2	1.3	1.3	1.2	2.1	3.2	5.1
P ₂ O ₅	0.2	0.2	0.2	0.2	0.2	0.2	0.2	0.2	0.2	0.2	0.1
LOI	1.06	0.49	-1.00	1.44	1.34	0.50	-0.03	0.68	0.27	1.45	1.68
Sc	27.28	16.41	24.12	18.63	38.05	32.64	26.23	30.72	21.53	13.57	6.60
V	202.78	155.17	196.60	156.39	282.40	316.53	206.01	247.74	169.90	66.36	44.39
Cr	328.17	35.01	70.79	113.01	667.29	19.98	258.17	164.36	11.34	6.62	7.29
Co	38.43	21.75	38.91	26.47	46.83	40.81	57.00	38.15	33.56	23.94	87.53
Ni	61.65	11.36	16.07	29.40	199.12	11.49	141.88	36.38	10.45	6.11	4.53
Cu	41.75	21.01	20.41	38.69	63.26	16.10	73.34	36.54	16.18	27.16	16.94
Zn	53.73	55.35	59.53	53.32	58.18	70.96	64.73	67.65	175.66	99.20	39.14
Ga	15.21	18.16	17.25	18.51	14.17	16.63	16.48	16.39	19.45	17.51	18.04
Rb	58.00	51.50	57.86	90.16	34.22	34.18	42.47	47.72	56.71	98.18	170.62
Sr	348.36	367.11	393.74	357.21	293.53	266.44	255.70	273.50	280.79	145.68	72.67
Y	18.18	25.15	21.86	19.62	18.74	29.43	20.65	21.03	57.54	44.14	89.92
Zr	123.33	164.08	147.82	168.19	82.44	108.00	144.10	106.48	153.06	280.78	356.22
Nb	5.19	6.73	7.16	6.94	4.78	5.45	11.33	5.84	7.67	14.62	15.00
Cs	2.91	1.31	1.66	6.18	1.55	1.03	2.26	1.64	2.74	5.72	10.15
Ba	412.38	388.88	506.31	483.28	325.03	326.94	291.61	255.71	425.44	765.69	860.75
La	17.11	17.42	19.91	20.78	12.66	13.18	15.58	12.87	57.87	32.11	72.88
Ce	35.47	38.50	42.37	43.49	27.19	27.70	31.10	27.50	109.50	66.38	161.79
Pr	4.36	4.73	5.11	5.13	3.47	3.56	3.79	3.47	12.85	7.98	20.54
Nd	18.18	20.58	21.47	21.38	15.50	15.93	16.68	15.76	56.90	34.15	93.66
Sm	3.99	4.90	4.66	4.61	3.72	3.99	3.92	3.85	12.30	7.52	21.04
Eu	1.09	1.40	1.29	1.17	1.17	1.17	1.12	1.09	3.51	1.72	4.92
Gd	3.83	4.78	4.51	4.20	3.70	4.40	4.10	3.99	13.92	7.97	21.93
Tb	0.53	0.73	0.66	0.59	0.59	0.69	0.60	0.59	2.08	1.26	3.24
Dy	3.47	4.82	4.29	3.77	3.68	4.58	3.77	4.10	13.15	8.26	19.83
Ho	0.69	0.96	0.80	0.73	0.73	0.98	0.79	0.82	2.55	1.66	3.73
Er	2.02	2.80	2.34	2.14	2.03	2.99	2.19	2.38	6.99	4.96	10.55
Tm	0.31	0.43	0.34	0.33	0.31	0.43	0.34	0.36	1.03	0.74	1.58
Yb	1.97	2.81	2.36	2.19	2.01	3.07	2.17	2.37	7.05	5.05	10.88
Lu	0.28	0.42	0.35	0.30	0.31	0.46	0.32	0.35	0.97	0.73	1.53
Hf	3.46	4.37	3.98	4.52	2.31	2.99	3.79	3.03	4.10	7.66	9.41
Ta	0.92	0.66	0.79	0.85	0.39	0.52	0.95	0.56	0.87	1.35	2.89
Pb	9.04	7.22	9.09	12.06	6.02	8.04	5.82	7.25	11.47	20.91	29.55
Th	6.77	5.98	6.94	9.25	3.75	4.92	8.05	4.47	7.08	13.34	21.29
U	1.57	1.36	1.43	2.27	0.82	1.13	1.61	1.01	1.63	3.31	5.21

Table 8.1	7841	6754	7831	7305	7815	7306	26720	26412	23223	26723	26724
Locality	Tokatoka	Tokatoka	Tokatoka	Tokatoka	Tokatoka	Tokatoka	Waipoua	Waipoua	Waipoua	Waipoua	Waipoua
Rock type	basalt	basalt	basaltic andesite	andesite	dacite	rhyolite	basalt flow	basalt flow	basal dyke	basalt flow	basalt flow
SiO ₂	48.7	51.0	55.2	58.7	65.4	72.2	48.5	49.5	50.1	50.1	50.3
TiO ₂	1.1	0.9	1.1	0.6	0.4	0.3	1.0	1.0	1.2	1.1	1.3
Al ₂ O ₃	16.5	17.0	15.6	16.5	17.5	16.9	17.7	18.2	17.9	19.1	18.0
FeO	9.24	6.84	8.31	4.71	2.85	0.37	8.69	9.23	9.65	8.87	9.71
Fe ₂ O ₃	1.85	1.37	2.49	1.65	1.14	0.19	1.74	1.85	1.93	1.77	1.94
MnO	0.2	0.1	0.2	0.1	0.1	0.0	0.2	0.2	0.2	0.2	0.2
MgO	7.5	9.0	2.7	6.3	1.2	0.1	6.2	5.0	4.3	3.9	3.9
CaO	11.2	9.6	8.1	7.0	4.5	2.8	12.5	11.4	10.6	11.1	10.4
Na ₂ O	2.9	3.2	3.8	3.2	4.0	4.5	2.5	2.7	3.1	3.1	3.2
K ₂ O	0.9	0.8	2.1	1.1	2.8	2.6	0.7	0.7	0.8	0.7	0.9
P ₂ O ₅	0.1	0.2	0.4	0.1	0.2	0.1	0.2	0.2	0.2	0.2	0.3
LOI	2.67	0.03	0.66	0.60	0.86	0.89	0.48	0.63	-0.06	0.26	0.35
Sc	54.42	31.96	31.50	24.08	5.86	3.48	36.54	35.97	32.70	31.67	30.60
V	408.54	243.45	168.98	164.86	80.34	44.20	306.67	357.85	370.22	344.96	364.81
Cr	183.73	368.67	16.15	358.16	12.22	6.54	136.70	71.13	32.03	39.77	24.92
Co	41.90	36.11	31.55	31.39	56.43	6.62	38.92	42.96	37.99	32.39	36.25
Ni	42.31	128.44	10.12	97.11	5.10	4.33	56.05	35.36	23.23	27.47	20.68
Cu	61.20	62.40	107.01	48.57	21.24	11.31	148.39	99.26	114.97	359.13	125.51
Zn	56.68	45.12	68.51	62.83	39.32	29.95	53.80	62.39	69.00	72.14	71.15
Ga	15.88	14.23	20.41	16.02	17.20	18.29	15.54	16.76	17.53	17.11	18.14
Rb	20.02	16.69	50.28	40.11	71.67	104.51	15.73	12.12	14.46	11.37	13.83
Sr	291.63	377.86	340.14	204.77	375.94	293.54	396.95	324.94	330.12	338.70	371.26
Y	17.50	18.91	40.65	65.58	16.24	13.57	17.30	19.82	22.85	20.51	23.62
Zr	69.96	90.12	156.80	91.19	187.48	195.54	65.14	66.05	84.48	70.78	92.33
Nb	2.53	3.11	5.75	3.03	8.60	9.94	4.93	3.73	4.57	3.38	5.06
Cs	0.90	0.19	0.46	2.73	1.43	3.02	0.24	0.20	0.53	0.60	1.38
Ba	319.53	261.18	943.82	293.03	1459.82	1348.92	249.30	242.99	322.49	248.60	424.41
La	9.28	11.29	23.39	36.01	31.35	30.36	10.33	8.75	11.68	8.96	14.04
Ce	20.65	24.01	52.61	69.91	56.47	58.66	21.78	19.10	25.00	19.56	29.86
Pr	2.87	2.99	7.05	9.47	5.95	5.87	2.84	2.61	3.34	2.69	3.84
Nd	13.69	13.08	32.69	44.98	21.59	20.67	13.49	12.31	16.24	12.72	17.89
Sm	3.47	3.02	7.98	10.90	3.90	3.24	3.32	3.17	3.93	3.36	4.41
Eu	1.08	1.07	2.05	2.96	1.08	0.97	1.04	1.13	1.31	1.14	1.39
Gd	3.72	3.28	8.25	12.71	3.38	2.72	3.32	3.44	4.25	3.77	4.46
Tb	0.54	0.55	1.24	1.78	0.46	0.37	0.51	0.56	0.69	0.59	0.72
Dy	3.57	3.66	8.02	11.67	2.98	2.31	3.44	3.85	4.43	3.93	4.59
Ho	0.69	0.75	1.59	2.43	0.59	0.48	0.70	0.78	0.89	0.81	0.94
Er	2.05	2.17	4.59	6.99	1.83	1.42	1.93	2.27	2.55	2.37	2.66
Tm	0.31	0.32	0.67	0.97	0.27	0.24	0.29	0.35	0.41	0.34	0.39
Yb	1.86	2.24	4.59	6.75	2.19	1.84	1.90	2.24	2.69	2.37	2.63
Lu	0.26	0.33	0.67	1.02	0.36	0.31	0.27	0.33	0.40	0.36	0.40
Hf	2.79	2.55	4.70	2.54	4.59	4.87	1.87	1.88	2.47	1.99	2.56
Ta	0.33	0.39	0.92	0.55	0.81	0.98	0.34	0.49	0.33	0.25	0.34
Pb	3.49	4.54	3.88	10.08	11.43	19.99	4.80	3.07	6.32	3.24	7.00
Th	3.06	3.28	6.67	3.98	12.67	13.36	2.39	2.14	3.08	2.21	4.07
U	0.61	0.51	1.58	1.19	3.25	3.71	0.62	0.53	0.76	0.54	0.93

Table 8.1	26408	26406	26407	23222	24275	24154	33489	24175	38485	24126
Locality	Waipoua	Waipoua	Waipoua	Waipoua	Manukau	Manukau	Manukau	Manukau	Manukau	Manukau
Rock type	basalt flow	basalt flow	basalt flow	basalt flow	basalt	basalt	basaltic andesite	andesite flow	dacite	rhyolite
SiO ₂	50.4	50.5	50.7	50.9	46.6	49.6	55.2	63.4	66.7	70.0
TiO ₂	1.5	1.0	1.2	1.4	0.9	0.9	0.9	0.9	0.9	0.5
Al ₂ O ₃	17.0	20.1	18.6	15.3	20.7	19.0	17.6	16.0	16.6	16.6
FeO	9.95	7.87	9.22	11.86	9.18	8.69	7.02	4.87	2.90	2.25
Fe ₂ O ₃	1.99	1.57	1.84	2.37	1.84	1.74	2.11	1.95	1.16	0.90
MnO	0.2	0.2	0.2	0.2	0.2	0.2	0.2	0.1	0.0	0.0
MgO	4.1	3.8	3.7	4.4	6.1	4.8	3.9	1.2	0.2	0.2
CaO	9.9	11.4	10.2	9.2	12.7	12.1	8.2	4.2	3.5	2.2
Na ₂ O	3.5	2.8	3.2	3.3	1.8	2.6	3.3	4.4	5.4	4.4
K ₂ O	1.2	0.7	0.9	0.8	0.1	0.2	1.3	2.6	2.3	2.8
P ₂ O ₅	0.3	0.2	0.2	0.2	0.0	0.1	0.2	0.3	0.3	0.0
LOI	0.15	-0.01	0.48	-0.26	-0.24	0.34	0.18	0.27	0.22	1.26
Sc	31.44	31.45	29.99	39.06	37.16	43.10	32.29	22.25	19.62	12.57
V	403.82	313.86	366.66	457.23	423.30	337.16	275.39	66.02	59.94	86.05
Cr	15.24	39.59	16.71	7.61	29.52	53.65	19.14	6.92	6.30	7.27
Co	38.36	32.19	37.84	47.82	46.80	35.34	34.57	20.30	11.67	25.87
Ni	21.19	22.83	18.39	15.05	14.56	25.11	11.12	4.41	4.07	4.40
Cu	123.33	80.77	111.35	138.46	36.88	233.26	36.43	16.98	181.59	13.47
Zn	76.32	55.03	64.08	89.66	56.73	63.13	64.05	73.13	81.58	39.04
Ga	18.58	16.64	17.91	17.07	15.81	15.86	16.34	17.75	19.60	16.16
Rb	22.06	10.76	16.60	14.05	0.78	1.77	32.77	78.50	48.67	72.46
Sr	380.94	332.54	358.65	292.62	291.73	244.45	257.60	198.72	188.30	118.67
Y	26.22	21.00	23.40	26.85	6.59	20.11	24.15	41.93	47.85	26.97
Zr	107.58	58.89	84.62	84.81	9.06	48.27	107.59	239.31	188.56	235.74
Nb	6.98	3.02	5.08	3.90	0.33	1.64	3.78	7.23	4.62	5.62
Cs	0.35	0.25	0.29	0.17	0.05	0.07	1.65	3.23	1.28	1.47
Ba	529.73	219.05	318.70	304.59	35.27	28.21	260.75	442.46	450.10	449.86
La	19.09	7.56	12.42	10.48	1.85	3.30	11.90	24.17	24.96	11.56
Ce	39.67	16.04	26.22	22.89	3.94	8.39	26.11	53.48	44.51	23.11
Pr	5.12	2.22	3.46	3.20	0.58	1.37	3.46	6.76	7.97	2.98
Nd	22.88	11.09	16.10	15.12	2.91	7.28	15.38	30.12	37.33	12.74
Sm	5.22	2.78	4.08	4.19	0.85	2.30	3.54	7.04	9.06	3.31
Eu	1.62	1.00	1.36	1.35	0.64	0.91	1.05	1.64	2.38	1.01
Gd	5.39	3.35	4.33	4.70	1.11	3.11	4.01	7.25	9.85	3.42
Tb	0.81	0.51	0.67	0.72	0.18	0.51	0.64	1.13	1.50	0.62
Dy	5.05	3.70	4.44	5.07	1.29	3.62	4.37	7.59	9.89	4.51
Ho	1.02	0.76	0.91	1.05	0.28	0.76	0.89	1.62	1.94	1.02
Er	2.94	2.30	2.67	3.14	0.80	2.30	2.78	4.64	5.46	3.26
Tm	0.44	0.36	0.40	0.48	0.12	0.34	0.40	0.72	0.81	0.54
Yb	2.79	2.32	2.70	3.14	0.86	2.32	2.80	4.89	5.13	3.94
Lu	0.42	0.36	0.38	0.45	0.13	0.33	0.41	0.72	0.73	0.60
Hf	2.97	1.69	2.44	2.54	0.32	1.53	3.23	6.57	5.54	6.85
Ta	0.47	0.21	0.39	0.31	0.57	0.37	0.83	0.62	0.69	0.51
Pb	9.83	3.45	3.23	8.99	1.25	1.31	7.10	11.61	7.11	8.68
Th	5.16	1.74	3.19	2.56	0.11	0.34	4.42	10.04	6.88	8.80
U	1.22	0.45	0.80	0.68	0.04	0.12	1.18	2.20	8.79	2.14

Appendix B. Appendix B. Supplementary bulk rock geochemistry dataset to Chapter 4

Appendix B. Supplementary bulk rock geochemistry dataset to Chapter 4 “The transition from intermediate to silicic volcanism in the North Island of New Zealand”. See Chapter 4, Section 4.2.3 for analytical methods.

Table 8.2	Locality	Rock type	SiO ₂	TiO ₂	Al ₂ O ₃	FeO	Fe ₂ O ₃	MnO	MgO	CaO	Na ₂ O	K ₂ O	P ₂ O ₅
AH197	Matakana (Mercury Basalts)	Plag basalt	53.4	1.1	19.1	6.2	1.9	0.1	4.0	9.5	3.7	0.9	0.2
SP124	Moturoa (Mercury Basalts)		55.6	1.3	15.9	7.1	2.1	0.2	5.8	7.5	3.1	1.2	0.2
SP099	Moturoa (Mercury Basalts)		56.1	1.0	16.8	6.7	2.0	0.2	4.9	7.7	3.2	1.3	0.2
BH33	Opito (Mercury Basalts)	Aphyric (plag) basalt	53.7	1.4	16.8	8.5	2.6	0.2	4.3	8.6	3.3	0.6	0.2
BH35	Opito (Mercury Basalts)	Aphyric (plag) basalt	54.0	1.1	17.3	7.8	2.3	0.2	4.7	8.7	3.1	0.5	0.1
BH28	RedBay (Mercury Basalts)	Low-phyric ol+plag basalt	55.8	1.3	17.0	8.1	2.4	0.2	3.3	7.5	3.5	0.8	0.2
MC45	Sugar Loaf (Mercury Basalts)	Ol+cpx basalt	50.8	0.7	14.1	7.8	1.6	0.2	12.4	9.8	2.1	0.5	0.1
AU60071	Sugar Loaf (Mercury Basalts)	Ol+cpx basalt	50.8	0.7	14.1	7.8	1.6	0.2	12.4	9.8	2.1	0.5	0.1
BH21	Tahanga (Mercury Basalts)	Low-phyric plag+cpx+mag ±(res. hbl) basalt	52.7	1.1	17.4	7.8	2.3	0.2	5.4	9.6	2.9	0.5	0.1
BH1	Tahanga (Mercury Basalts)	Low-phyric plag+cpx+mag ±(res. hbl) basalt	53.6	1.2	17.2	7.6	2.3	0.2	5.2	8.7	3.0	1.0	0.2
BH76	Tokarahu (Mercury Basalts)	Ol+cpx+opx ±plag basalt	51.7	1.1	15.7	7.4	1.5	0.2	9.3	9.4	3.1	0.6	0.2
BH75	Tokarahu (Mercury Basalts)	Ol+cpx+opx ±plag basalt	52.8	1.1	16.3	6.8	2.0	0.1	7.6	9.6	2.9	0.7	0.2
SP084	Ahuahu (Whitianga Group)	Bi+hbl+san rhyolite	77.3	0.1	12.5	0.5	1.1	0.0	0.1	0.3	3.2	4.8	0.1
SP101	Ahuahu (Whitianga Group)	Bi+hbl+san rhyolite	77.5	0.1	13.2	0.4	0.8	0.0	0.1	0.3	3.2	4.4	0.0
SP079	Ahuahu (Whitianga Group)	Bi+hbl+san rhyolite	78.2	0.1	12.3	0.4	0.8	0.0	0.1	0.2	2.7	5.2	0.0
NM1229	Boom (Whitianga Group)	Plag+bi rhyolite	76.2	0.2	13.1	0.5	1.0	0.0	0.4	1.2	3.2	4.3	0.0
SK743	Bulls (Whitianga Group)	Plag rhyolite	76.1	0.3	12.9	0.7	1.4	0.1	0.2	1.5	4.2	2.5	0.1
JR1	CooksB (Whitianga Group)	Plag±san rhyolite	76.6	0.1	13.7			0.0	0.1	0.8	3.3	4.1	0.0
JR11	HaheiD (Whitianga Group)	Plag+bi±hbl rhyolite	77.5	0.1	13.3			0.0	0.2	0.5	2.2	4.9	0.0
JR14	LillieD (Whitianga Group)	Plag+bi±hbl rhyolite	76.4	0.1	13.3	0.4	0.8	0.0	0.2	0.9	3.1	4.7	0.0
Min36	Minden (Whitianga Group)	Plag+bi±hbl ±opx rhyolite	75.5	0.2	13.6	0.5	1.1	0.0	0.2	1.5	3.8	3.6	0.0
GH20	MtMaunga (Whitianga Group)	Plag+bi±hbl ±opx rhyolite	76.9	0.1	12.9	0.4	0.8	0.0	0.1	1.0	3.8	3.9	0.0
GH37	MtMaunga (Whitianga Group)	Plag+bi±hbl ±opx rhyolite	77.3	0.1	13.1	0.4	0.7	0.0	0.1	0.8	3.4	4.1	0.0
SA1279	Onemana (Whitianga Group)	Plag+bi rhyolite	77.6	0.1	13.1	0.4	0.8	0.0	0.3	1.1	2.2	4.4	0.0
WT46	PauaRy (Whitianga Group)	Plag rhyolite	74.3	0.3	14.1	0.8	1.6	0.1	0.4	1.9	4.9	3.0	0.1
SK995	Pinnacles (Whitianga Group)	Plag+opx rhyolite	74.0	0.5	14.0	1.0	2.0	0.0	0.1	1.4	4.5	2.5	0.0
CG47	Pukekotare (Whitianga Group)	Plag+opx+hbl rhyolite	73.3	0.3	14.1	0.9	1.7	0.0	0.3	2.2	3.9	3.2	0.1
NM1228	Puketui (Whitianga Group)	Plag+hbl+bi ±opx rhyolite	74.2	0.2	14.8	0.6	1.1	0.0	0.4	2.1	3.6	3.1	0.0
JR18	Purangi (Whitianga Group)	Plag±san rhyolite	77.4	0.1	13.2	0.3	0.6	0.0	0.1	0.8	3.9	3.5	0.0
SK600	Rangihau (Whitianga Group)	Plag+opx rhyolite	75.4	0.4	13.9	0.4	0.9	0.0	0.1	1.4	4.8	2.7	0.0
SK1005	Ruahine (Whitianga Group)	Plag+bi±hbl rhyolite	75.8	0.2	13.6	0.6	1.3	0.0	0.1	1.4	3.3	3.6	0.0
WT61	Staircase (Whitianga Group)	Plag rhyolite	77.2	0.1	13.1	0.4	0.8	0.0	0.1	0.7	3.6	4.1	0.0

Table 8.2	Locality	Rock type	SiO ₂	TiO ₂	Al ₂ O ₃	FeO	Fe ₂ O ₃	MnO	MgO	CaO	Na ₂ O	K ₂ O	P ₂ O ₅
SK865	T'nikau (Whitianga Group)	Plag rhyolite	77.5	0.2	12.7	0.4	0.9	0.0	0.1	0.7	4.6	3.0	0.0
BF67	Tunaiti (Whitianga Group)	Plag rhyolite	76.3	0.1	13.0	0.5	1.1	0.0	0.2	1.0	3.6	3.9	0.0
SK807	Welcome Jack (Whitianga Group)	Plag+bi rhyolite	78.9	0.2	11.8	0.4	0.8	0.0	0.2	0.8	3.2	3.8	0.0
JA126	WhenRy (Whitianga Group)	Plag+bi rhyolite	75.3	0.2	14.6	0.4	0.7	0.0	0.1	1.5	3.9	3.3	0.0
JA127	WhenRy (Whitianga Group)	Plag+bi rhyolite	74.9	0.2	14.7	0.4	0.8	0.0	0.1	1.5	4.0	3.5	0.0
JA114	Wigmore Dome (Whitianga Group)	Plag+bi±hbl rhyolite	75.6	0.2	13.5	0.5	1.0	0.2	0.3	0.8	3.4	4.6	0.0
JA118	Wigmore Dome (Whitianga Group)	Plag+bi±hbl rhyolite	75.6	0.2	14.0	0.5	1.0	0.0	0.3	0.7	2.9	4.7	0.0
JA110	Wigmore Dome (Whitianga Group)	Plag+bi±hbl rhyolite	75.6	0.2	13.2	0.5	1.0	3.0	0.3	0.9	3.4	4.8	0.0
AU18153	Undifferentiated Omahine Subgroup	Pyroxene andesite	56.8	0.6	16.5	5.7	1.7	0.1	5.9	8.8	2.4	1.2	0.1
AU18152	Undifferentiated Omahine Subgroup	Pyroxene andesite	61.9	0.6	16.4	4.6	1.6	0.1	3.4	6.2	2.9	1.9	0.1
R17881	Whakamoehau Andesite (Omahine)	Pyroxene andesite	62.5	0.6	15.9	4.4	1.5	0.1	3.5	6.5	2.8	2.0	0.1
R17878	Whakamoehau Andesite (Omahine)	Pyroxene andesite	64.6	0.6	16.0	3.6	1.5	0.1	2.8	5.7	3.0	2.0	0.1
R17868	Whakamoehau Andesite (Omahine)	Pyroxene andesite	68.5	0.5	15.3	2.8	1.1	0.1	1.8	4.0	3.3	2.4	0.1
R12413	Taurauikau Andesite (Omahine)	Pyroxene andesite	59.7	0.6	16.1	4.9	1.7	0.1	4.6	7.6	3.0	1.5	0.1
R17847	Ananui Andesite (Kaimai)	Pyroxene andesite	58.6	0.7	18.3	4.8	1.7	0.1	3.8	7.6	2.8	1.4	0.1
R17827	Ananui Andesite (Kaimai)	Pyroxene andesite	59.1	0.6	16.8	5.2	1.8	0.1	4.8	7.4	2.7	1.2	0.1
R17828	Ananui Andesite (Kaimai)	Pyroxene andesite	61.0	0.9	18.2	5.2	1.8	0.1	2.1	5.3	3.4	1.8	0.2
R19794	Matangia Andesite (Kaimai)	Pyroxene dacite	64.2	1.0	16.7	4.3	1.7	0.1	0.8	4.8	3.9	2.0	0.4
R17870	Uretara Formation (Kaimai)	Pyroxene andesite	58.1	0.7	18.3	4.9	1.7	0.1	4.1	7.9	3.0	0.9	0.1
R17860	Uretara Formation (Kaimai)	Pyroxene andesite	60.5	0.6	16.3	5.0	1.8	0.1	4.1	6.9	3.0	1.4	0.1
R17833	Uretara Formation (Kaimai)	Hornblende andesite	62.2	0.6	15.6	4.9	1.7	0.1	3.6	6.5	2.8	1.8	0.1
R17845	Uretara Formation (Kaimai)	Hornblende dacite	63.0	0.7	17.0	4.2	1.7	0.1	2.1	5.5	3.4	2.0	0.1
R17829	Uretara Formation (Kaimai)	Pyroxene dacite	63.1	0.8	17.3	4.3	1.7	0.1	2.0	5.5	2.9	2.0	0.1
R17825	Uretara Formation (Kaimai)	Hornblende dacite	65.2	0.5	16.0	3.8	1.5	0.1	2.2	5.3	3.2	2.2	0.1
R17871	Uretara Formation (Kaimai)	Pyroxene andesite	67.1	0.6	16.8	3.2	1.3	0.0	1.0	4.0	3.4	2.2	0.1
R12382	Tapuaetahi Andesite (Waiwawa)	Pyroxene andesite	60.1	0.7	17.0	5.1	1.8	0.1	3.7	6.6	3.1	1.5	0.1
AU45371	Tapuaetahi Andesite (Waiwawa)	Pyroxene andesite	60.5	0.7	16.9	5.0	1.8	0.1	3.7	6.5	3.1	1.5	0.1
AU25796	Tapuaetahi Andesite (Waiwawa)	Pyroxene andesite	60.8	0.8	17.2	4.9	1.7	0.1	3.1	6.5	3.2	1.6	0.1
R12383	Tapuaetahi Andesite (Waiwawa)	Pyroxene andesite	61.7	0.7	16.9	4.8	1.7	0.1	2.9	6.4	3.1	1.6	0.1
R12414	Tapuaetahi Andesite (Waiwawa)	Pyroxene andesite	61.8	0.7	16.7	4.7	1.7	0.1	3.2	5.8	3.2	1.8	0.1
R12769	Taurahuehue Andesite (Waiwawa)	Pyroxene basaltic andesite	55.7	1.0	18.2	7.1	2.1	0.3	3.3	7.5	3.2	1.4	0.2

Table 8.2	Locality	Rock type	SiO ₂	TiO ₂	Al ₂ O ₃	FeO	Fe ₂ O ₃	MnO	MgO	CaO	Na ₂ O	K ₂ O	P ₂ O ₅
R12767	Taurahuehue Andesite (Waiwawa)	Pyroxene basaltic andesite	56.1	1.1	18.0	6.5	2.0	0.2	3.7	7.7	3.1	1.4	0.2
R10404	Taurahuehue Andesite (Waiwawa)	Pyroxene basaltic andesite	56.6	1.0	17.9	6.4	1.9	0.2	3.5	7.7	2.9	1.5	0.2
R17862	Kapukapu Andesite (Waiwawa)	Pyroxene andesite	57.9	0.8	17.8	5.4	1.9	0.1	3.8	8.3	2.6	1.1	0.1
R17869	Kapukapu Andesite (Waiwawa)	Pyroxene andesite	58.6	0.8	17.3	5.7	2.0	0.1	3.9	7.1	3.1	1.2	0.1
R17831	Kapukapu Andesite (Waiwawa)	Pyroxene andesite	58.9	1.0	17.8	5.8	2.0	0.1	2.7	6.7	3.2	1.5	0.2
R17879	Kapukapu Andesite (Waiwawa)	Pyroxene andesite	59.1	0.7	17.0	5.3	1.8	0.1	4.1	7.1	3.0	1.4	0.1
R17872	Kapukapu Andesite (Waiwawa)	Pyroxene andesite	59.3	0.8	17.6	5.2	1.8	0.1	3.6	6.5	3.1	1.7	0.2
R17864	Kapukapu Andesite (Waiwawa)	Pyroxene andesite	60.4	0.6	16.4	4.9	1.7	0.1	4.0	7.1	3.0	1.4	0.1
AU45402	Kapukapu Andesite (Waiwawa)	Pyroxene andesite	61.0	0.6	17.0	4.6	1.6	0.1	3.3	6.9	3.1	1.4	0.1
R17873	Kapukapu Andesite (Waiwawa)	Pyroxene andesite	61.9	0.7	17.7	4.3	1.5	0.1	2.4	5.8	3.3	1.9	0.2
R17876	Waipupu Formation (Waiwawa)	Pyroxene andesite	55.1	0.8	16.6	6.6	2.0	0.1	6.0	10.1	1.9	0.6	0.1
R17867	Waipupu Formation (Waiwawa)	Pyroxene andesite	56.9	0.8	17.3	6.0	1.8	0.1	5.3	8.4	2.2	0.8	0.1
AU45404	Waipupu Formation (Waiwawa)	Pyroxene andesite	57.4	0.8	18.1	5.7	2.0	0.1	4.3	7.5	2.7	1.1	0.2
R17861	Waipupu Formation (Waiwawa)	Pyroxene andesite	57.8	0.8	17.8	5.4	1.9	0.1	3.8	8.3	2.6	1.1	0.1
R17836	Waipupu Formation (Waiwawa)	Pyroxene andesite	59.5	0.7	16.1	5.0	1.8	0.1	5.1	8.0	2.3	1.2	0.1
R17863	Waipupu Formation (Waiwawa)	Pyroxene andesite	60.3	0.9	16.8	5.4	1.9	0.1	2.8	6.6	3.4	1.6	0.2
AU43430	Waipupu Formation (Waiwawa)	Pyroxene andesite	62.7	0.6	16.1	4.7	1.7	0.1	3.6	5.7	2.8	1.7	0.1
R17858	Waipupu Formation (Waiwawa)	Pyroxene andesite	62.9	0.6	16.2	4.3	1.5	0.1	3.6	6.1	2.8	1.6	0.1
R17880	Waipupu Formation (Waiwawa)	Pyroxene dacite	64.0	0.5	16.1	3.8	1.5	0.1	2.4	6.4	3.1	1.8	0.1
R17857	Waipupu Formation (Waiwawa)	Pyroxene dacite	64.5	0.7	16.5	3.9	1.6	0.1	2.0	5.0	3.2	2.3	0.1
P33345	Waiwawa Subgroup (undiff) (Waiwawa)	Pyroxene andesite	60.3	0.7	17.1	4.8	1.7	0.1	3.6	7.7	2.7	1.0	0.1
AU18189	Waiwawa Subgroup (undiff) (Waiwawa)	Px+qtz+bi dacite	64.8	0.6	16.0	3.8	1.5	0.1	2.7	4.7	3.1	2.4	0.1
AU45416	Waiwawa Subgroup (undiff) (Waiwawa)	Pyroxene dacite	64.9	0.6	16.7	3.7	1.5	0.1	1.9	5.1	3.7	1.6	0.1
R17866	Whiritoa Andesite (Waiwawa)	Pyroxene andesite	58.4	0.7	15.9	5.5	1.9	0.1	5.5	7.6	2.7	1.4	0.1
R17877	Whiritoa Andesite (Waiwawa)	Pyroxene andesite	61.8	0.6	16.3	4.8	1.7	0.1	4.2	6.1	2.5	1.6	0.1
AU45394	Whiritoa Andesite (Waiwawa)	Pyroxene andesite	61.9	0.6	16.5	4.6	1.6	0.1	3.3	6.6	2.9	1.8	0.1
R17874	Whiritoa Andesite (Waiwawa)	Pyroxene andesite	62.5	0.6	16.1	4.4	1.6	0.1	3.3	6.3	3.0	1.8	0.1
R17865	Whiritoa Andesite (Waiwawa)	Pyroxene dacite	64.4	0.6	15.9	4.0	1.6	0.1	2.5	5.3	3.4	2.0	0.1
R17856	Whiritoa Andesite (Waiwawa)	Pyroxene dacite	64.5	0.7	16.5	3.9	1.6	0.1	2.0	5.1	3.2	2.3	0.1
AU45405	Whiritoa Andesite (Waiwawa)	Pyroxene dacite	66.3	0.6	15.6	3.5	1.4	0.1	1.9	4.6	3.5	2.3	0.1

Table 8.2	Locality	Rock type	SiO ₂	TiO ₂	Al ₂ O ₃	FeO	Fe ₂ O ₃	MnO	MgO	CaO	Na ₂ O	K ₂ O	P ₂ O ₅
AU45378	“Pauporoa Basaltic Andesite” (Kuaotunu)	Pyroxene andesite	57.2	0.9	18.0	5.3	1.9	0.1	4.0	7.8	3.0	1.6	0.2
AU45377	“Pauporoa Basaltic Andesite” (Kuaotunu)	Hornblende andesite	62.0	0.7	17.4	4.3	1.5	0.1	2.7	5.7	3.6	1.8	0.1
AU45368	Beeson’s Island Volcanics (Kuaotunu)	Pyroxene basaltic andesite	55.6	0.9	18.1	6.7	2.0	0.2	4.4	7.7	3.1	1.2	0.2
AU45386	Beeson’s Island Volcanics (Kuaotunu)	Pyroxene basaltic andesite	55.8	0.7	15.4	5.9	1.8	0.2	7.2	9.3	2.8	0.8	0.1
AU46749	Beeson’s Island Volcanics (Kuaotunu)	Pyroxene basaltic andesite	56.9	0.8	18.6	6.1	1.8	0.2	3.9	7.4	3.3	0.8	0.1
AU45324	Beeson’s Island Volcanics (Kuaotunu)	Pyroxene andesite	57.0	0.9	17.9	6.1	1.8	0.1	4.0	7.4	3.3	1.1	0.1
R12404	Beeson’s Island Volcanics (Kuaotunu)	Hornblende andesite	57.4	1.0	17.6	5.9	2.1	0.2	3.7	7.3	3.2	1.5	0.2
AU45383	Beeson’s Island Volcanics (Kuaotunu)	Hornblende andesite	59.4	0.8	18.1	5.1	1.8	0.1	3.1	6.4	3.4	1.5	0.2
AU46752	Beeson’s Island Volcanics (Kuaotunu)	Px+qtz andesite	59.5	0.8	17.4	5.3	1.9	0.1	3.7	6.7	2.9	1.6	0.1
AU45362	Beeson’s Island Volcanics (Kuaotunu)	Pyroxene andesite	59.6	0.8	18.2	5.4	1.9	0.1	2.8	6.2	3.7	1.1	0.1
AU45355	Beeson’s Island Volcanics (Kuaotunu)	Pyroxene andesite	59.7	0.8	17.0	5.1	1.8	0.1	3.6	6.6	3.3	1.8	0.2
AU46744	Beeson’s Island Volcanics (Kuaotunu)	Pyroxene andesite	60.2	0.9	17.7	5.2	1.8	0.1	3.2	5.8	3.1	1.6	0.1
AU45361	Beeson’s Island Volcanics (Kuaotunu)	Hornblende andesite	60.3	0.7	16.9	5.0	1.8	0.1	3.8	6.5	3.5	1.1	0.1
R12397	Beeson’s Island Volcanics (Kuaotunu)	Hornblende andesite	60.8	0.8	17.1	5.0	1.8	0.2	3.0	6.5	3.2	1.5	0.1
AU45382	Beeson’s Island Volcanics (Kuaotunu)	Hornblende andesite	61.4	0.7	17.1	4.7	1.7	0.1	2.6	5.8	3.7	1.8	0.2
AU45360	Beeson’s Island Volcanics (Kuaotunu)	Hornblende andesite	62.1	0.7	18.5	4.1	1.4	0.1	1.1	6.0	3.8	1.8	0.2
R12403	Beeson’s Island Volcanics (Kuaotunu)	Hornblende andesite	62.4	0.6	16.8	4.5	1.6	0.1	3.2	5.8	3.5	1.3	0.1
AU19788	Beeson’s Island Volcanics (Kuaotunu)	Hbl+qtz andesite	62.4	0.7	16.9	4.7	1.7	0.1	2.7	5.4	3.2	2.1	0.1
AU19812	Beeson’s Island Volcanics (Kuaotunu)	Hornblende andesite	62.5	0.6	17.5	4.1	1.4	0.1	3.0	5.7	3.4	1.4	0.1
R12405	Beeson’s Island Volcanics (Kuaotunu)	Hbl+qtz+bi andesite	63.2	0.7	18.9	3.2	1.3	0.1	1.0	5.7	3.9	1.8	0.2
AU45359	Beeson’s Island Volcanics (Kuaotunu)	Hornblende dacite	63.6	0.7	17.6	3.5	1.4	0.1	2.4	5.5	4.0	1.1	0.1
AU45327	Kokumata Dacite (Kuaotunu)	Hornblende andesite	57.6	0.9	16.3	6.0	2.1	0.1	5.5	7.6	2.5	1.1	0.1
AU45352	Mahinapua Andesite (Kuaotunu)	Hornblende andesite	61.0	0.7	17.0	5.1	1.8	0.1	2.9	5.9	3.2	2.0	0.1
AU45343	Mahinapua Andesite (Kuaotunu)	Hornblende andesite	61.4	0.7	16.5	5.0	1.8	0.1	3.1	5.9	3.2	2.1	0.1
R12389	Matarangi Andesite (Kuaotunu)	Hornblende andesite	60.4	0.7	16.8	4.8	1.7	0.1	4.0	6.6	3.1	1.7	0.1
AU45385	Matarangi Andesite (Kuaotunu)	Hornblende andesite	62.9	0.6	16.9	4.3	1.5	0.1	2.8	5.6	3.4	1.7	0.1
R12401	Matarangi Andesite (Kuaotunu)	Hornblende dacite	65.2	0.5	16.9	3.5	1.4	0.1	2.3	4.6	3.3	1.9	0.1
R12416	Maupaupaki Formation (Kuaotunu)	Hornblende andesite	60.9	0.7	17.5	4.7	1.6	0.1	2.8	6.2	3.0	2.1	0.1
R12415	Maupaupaki Formation (Kuaotunu)	Hornblende andesite	61.2	0.7	17.3	5.3	1.8	0.1	2.0	6.2	3.3	1.8	0.1
R12417	Maupaupaki Formation (Kuaotunu)	Hornblende andesite	61.4	0.7	16.6	5.8	2.0	0.1	2.2	5.9	3.1	1.8	0.2

Table 8.2	Locality	Rock type	SiO ₂	TiO ₂	Al ₂ O ₃	FeO	Fe ₂ O ₃	MnO	MgO	CaO	Na ₂ O	K ₂ O	P ₂ O ₅
R10403	Maupaupaki Formation (Kuaotunu)	Hornblende andesite	61.6	0.7	17.7	4.7	1.7	0.0	2.2	5.9	3.3	1.9	0.1
R12388	Maupaupaki Formation (Kuaotunu)	Hornblende andesite	61.7	0.6	17.1	4.3	1.5	0.1	3.1	6.6	3.1	1.5	0.1
AU45333	Port Charles Andesite (Kuaotunu)	Pyroxene basaltic andesite	54.4	1.3	18.9	7.5	2.3	0.2	2.9	7.7	3.7	0.8	0.2
R12395	Port Charles Andesite (Kuaotunu)	Pyroxene basaltic andesite	54.5	1.3	17.8	7.2	2.2	0.2	3.9	8.5	3.5	0.8	0.2
R12391	Port Charles Andesite (Kuaotunu)	Pyroxene basaltic andesite	55.4	1.1	19.0	6.3	1.9	0.1	3.4	7.8	3.6	0.9	0.2
R12392	Port Charles Andesite (Kuaotunu)	Pyroxene basaltic andesite	56.1	1.0	17.7	6.2	1.9	0.1	4.3	8.1	3.5	0.9	0.1
R12393	Port Charles Andesite (Kuaotunu)	Hornblende basaltic andesite	58.3	1.0	18.0	5.9	2.1	0.2	2.7	6.8	3.9	0.9	0.2
R12390	Te Tutu Andesite (Kuaotunu)	Pyroxene basaltic andesite	56.9	0.7	16.3	5.8	1.7	0.2	6.0	8.2	2.6	1.3	0.1
AU45326	Tuataewa Andesite (Kuaotunu)	Hornblende andesite	58.9	0.9	17.0	5.1	1.8	0.1	4.3	6.8	3.4	1.3	0.1
R12396	Tuataewa Andesite (Kuaotunu)	Hornblende andesite	59.1	0.9	17.9	4.6	1.6	0.1	3.7	7.1	3.4	1.4	0.2
R12399	Whangapoua Andesite (Kuaotunu)	Pyroxene basaltic andesite	56.4	0.9	18.4	6.4	1.9	0.1	3.8	7.7	3.0	1.2	0.1
AU45339	Whangapoua Andesite (Kuaotunu)	Pyroxene basaltic andesite	56.8	0.8	18.3	6.4	1.9	0.1	4.8	6.8	2.9	0.9	0.1
R10432	Whangapoua Andesite (Kuaotunu)	Pyroxene andesite	59.1	0.7	17.6	5.3	1.9	0.1	3.7	6.7	3.1	1.5	0.1
AU45341	Whangapoua Andesite (Kuaotunu)	Pyroxene andesite	59.2	0.7	17.4	5.3	1.9	0.1	3.6	6.8	3.1	1.5	0.1
AU45384	Whangapoua Andesite (Kuaotunu)	Pyroxene andesite	60.1	0.7	17.5	5.1	1.8	0.1	3.4	6.2	3.3	1.6	0.1
R10433	Whangapoua Andesite (Kuaotunu)	Pyroxene andesite	61.4	0.7	16.4	4.9	1.7	0.1	3.5	6.2	3.1	1.7	0.1

Table 8.2	AH197	SP124	SP099	BH33	BH35	BH28	MC45	AU60071	BH21	BH1	BH76	BH75	SP084	SP101
Sc	28.7	31.3	27.8	33.4	35	34.3	36.2	35.8	39.9	37.1	31.7	31.5	2.4	2.4
V	256	233	192	276	317	348	227	235	317	360	227	226	2	2
Cr	39.0	202.0	167.0	11.0	16.0	9.0	906.0	906.0	24.0	12.0	462.0	376.0	4.0	5.0
Co	33.7	58.5	41.2	28.3	31.8	32.4	53.5	58.2	40.0	47.8	44.4	40.8	10.8	10.4
Ni	21.6	100.0	98.2	2.5	3.5	1.1	273.0	264.0	6.3	3.5	192.5	136.5	2.9	0.5
Cu	33.4	43.7	40.9	51.9	32.7	13.7	63.4	63.5	32.9	28.4	31.3	26.1	4.0	2.7
Zn	96.0	101.0	80.0	91.0	102.0	118.0	74.0	75.0	106.0	113.0	82.0	88.0	36.0	42.0
Ga	21.0	272.0	20.0	19.0	19.0	19.0	15.0	15.0	19.0	18.0	17.0	18.0	22.0	23.0
Rb	26.0	50.0	48.0	15.0	15.0	22.0	5.0	5.0	13.0	19.0	16.0	18.0	260.0	261.0
Sr	407.0	305.0	272.0	318.0	303.0	316.0	301.0	307.0	316.0	318.0	294.0	290.0	10.7	10.2
Y	23.2	28.5	24.6	23.9	25.4	39.2	19.4	19.0	92.4	28.3	26.3	46.2	28.2	25.3
Zr	80.0	142.0	134.0	99.0	86.0	112.0	67.0	67.0	82.0	98.0	110.0	114.0	119.0	117.0
Nb	4.8	7.0	5.2	4.4	3.9	5.1	2.2	2.2	3.8	4.5	4.8	4.8	15.1	15.3
Cs	1.4	5.7	9.9	0.5	0.9	0.7	0.3	0.4	0.6	0.9	0.7	0.7	10.2	10.4
Ba	485.0	272.0	254.0	234.0	219.0	287.0	132.0	132.0	211.0	244.0	207.0	218.0	116.0	147.0
La	11.4	14.2	12.6	10.7	8.8	19.6	7.4	6.9	52.4	10.9	13.2	19.2	24.9	10.7
Ce	26.1	33.1	28.7	25.5	21.9	45.7	19.1	18.6	22.8	26.4	31.0	32.1	49.5	21.1
Pr	3.5	4.5	3.8	3.5	3.1	8.7	2.5	2.4	18.6	3.6	4.2	5.6	6.9	2.3
Nd	14.6	19.9	16.6	13.9	12.9	38.5	10.2	9.9	78.1	15.7	16.9	22.4	25.6	8.7
Sm	3.4	4.8	4.0	3.4	3.4	10.3	2.5	2.5	21.3	4.0	4.0	5.3	5.8	2.3
Eu	1.3	1.6	1.2	1.3	1.3	3.0	1.0	0.9	6.2	1.4	1.4	2.0	0.2	0.2
Gd	3.8	5.3	4.3	3.9	4.0	9.5	3.0	2.9	21.6	4.6	4.4	7.0	5.4	2.8
Tb	0.6	0.9	0.7	0.7	0.7	1.7	0.5	0.5	3.7	0.8	0.8	1.2	1.0	0.6
Dy	3.7	5.2	4.4	3.9	4.1	9.3	3.0	2.9	20.6	5.0	4.1	6.9	5.7	4.3
Ho	0.8	1.1	1.0	0.9	1.0	1.8	0.7	0.7	4.1	1.1	0.9	1.7	1.2	1.0
Er	2.5	3.2	2.7	2.4	2.6	5.2	1.9	1.9	12.1	3.3	2.6	4.5	3.6	3.3
Tm	0.3	0.5	0.4	0.4	0.4	0.8	0.3	0.3	1.7	0.5	0.4	0.7	0.6	0.5
Yb	2.1	3.0	2.5	2.3	2.4	4.9	1.8	1.8	10.8	3.0	2.3	3.9	3.7	3.7
Lu	0.4	0.5	0.4	0.4	0.4	0.8	0.3	0.3	1.7	0.5	0.4	0.7	0.5	0.6
Hf	2.4	4.2	3.3	2.4	2.2	3.2	1.8	1.8	2.5	2.9	2.7	2.7	4.4	4.4
Ta	0.4	0.6	0.4	0.3	0.3	0.4	0.2	0.2	0.3	0.4	0.3	0.4	1.6	1.7
Pb	6.3	7.6	8.0	2.8	3.0	5.2	2.9	2.7	5.9	5.4	4.7	4.5	25.0	21.3
Th	3.5	4.7	4.1	1.9	1.2	2.8	1.6	1.5	1.7	2.2	2.3	2.3	29.3	19.8
U	0.7	1.2	1.1	0.2	0.1	0.7	0.3	0.2	0.4	0.5	0.3	0.3	5.4	4.8

Table 8.2	SP079	NM1229	SK743	JR1	JR11	JR14	Min36	GH20	GH37	SA1279	WT46	SK995	CG47
Sc	1.9	2.8	12.4	4	3.7	3.4	4.1	3.5	2.7	4.9	9.1	12.4	9.2
V	1	14	8	1	8	9	15	4	2	1	4	14	21
Cr	5.0	7.0	9.0	1.9	3.4	2.5	2.0	1.0	1.0	2.0	2.0	3.0	25.0
Co	9.7	36.3	8.9	4.7	7.1	8.9	26.9	18.1	12.6	28.6	10.2	9.2	9.6
Ni	0.4	3.3	0.3	0.3	1.0	0.8	0.8	0.4	0.3	0.7	0.4	0.2	2.7
Cu	1.0	3.8	2.1	1.1	1.7	1.7	2.1	1.5	1.1	0.9	4.9	2.4	2.5
Zn	38.0	33.0	67.0	42.0	23.0	22.0	32.0	22.0	24.0	33.0	38.0	63.0	39.0
Ga	22.0	11.0	14.0	17.3	15.1	14.7	796.0	15.0	12.0	15.0	15.0	16.0	14.0
Rb	285.0	189.0	76.0	143.8	206.7	187.5	114.0	137.0	141.0	183.0	90.0	70.0	108.0
Sr	10.8	105.0	128.5	76.4	38.1	57.8	123.0	85.0	71.1	112.5	72.8	107.5	142.5
Y	24.9	20.6	38.0	21.1	53.9	17.8	15.9	12.2	14.9	33.2	26.0	28.9	32.2
Zr	127.0	90.0	237.0	152.0	104.0	93.0	134.0	109.0	94.0	90.0	190.0	286.0	206.0
Nb	14.5	6.3	9.6	9.0	9.9	9.1	7.2	6.9	7.2	6.4	10.6	9.9	7.7
Cs	9.8	46.6	4.7	3.4	10.2	10.0	5.7	6.0	6.3	27.9	3.4	1.5	3.2
Ba	133.0	995.0	640.0	741.0	590.2	600.0		851.0	845.0	761.0	646.0	652.0	664.0
La	20.2	36.6	30.5	26.8	47.7	28.6	22.9	23.5	24.1	36.4	16.9	59.8	26.3
Ce	39.2	53.9	58.6	51.6	44.9	53.0	47.2	48.3	46.4	58.4	32.8	54.8	50.0
Pr	5.8	6.1	7.3	6.8	9.7	6.0	5.4	5.2	5.3	8.4	3.8	7.1	7.1
Nd	19.1	17.2	30.5	22.5	29.3	18.0	17.0	16.1	16.3	27.7	15.0	28.8	23.7
Sm	4.3	2.6	6.8	4.3	6.2	3.1	3.1	2.8	2.8	5.5	3.1	6.1	5.1
Eu	0.3	0.8	1.6	1.0	1.2	0.6	0.8	0.7	0.7	0.8	0.6	1.7	1.7
Gd	4.4	3.2	6.7	4.4	7.8	3.3	3.1	2.8	2.9	6.1	3.8	6.3	5.7
Tb	0.8	0.5	1.0	0.7	1.4	0.5	0.5	0.4	0.4	1.0	0.6	0.9	1.1
Dy	4.7	2.5	6.7	3.3	7.9	2.6	2.5	2.0	2.3	5.3	4.1	6.1	5.7
Ho	1.1	0.6	1.5	0.8	1.9	0.6	0.5	0.4	0.5	1.2	0.9	1.2	1.3
Er	3.2	1.9	4.5	2.1	5.4	1.6	1.6	1.1	1.4	3.2	2.8	4.0	3.4
Tm	0.5	0.3	0.7	0.3	0.9	0.2	0.2	0.2	0.2	0.5	0.4	0.6	0.5
Yb	3.4	2.0	4.5	2.0	5.5	1.6	1.6	1.0	1.4	2.8	3.0	4.0	3.0
Lu	0.6	0.4	0.7	0.3	1.0	0.3	0.3	0.2	0.2	0.5	0.4	0.6	0.5
Hf	4.5	2.1	6.8	3.3	2.7	2.4	2.3	2.0	2.7	2.9	4.6	7.6	1.4
Ta	1.7	0.9	0.7	0.8	1.3	1.1	0.8	0.7	0.8	0.8	0.9	0.7	0.7
Pb	21.5	19.9	16.7	22.6	18.8	19.7	17.2	18.1	20.0	15.1	15.3	13.2	12.3
Th	27.0	19.6	9.2	13.5	22.3	20.7	12.2	12.4	13.7	14.0	14.9	8.7	8.0
U	4.9	3.9	1.9	2.2	4.3	4.4	2.4	2.2	2.9	2.9	2.8	1.9	1.1

Table 8.2	NM1228	JR18	SK600	SK1005	WT61	SK865	BF67	SK807	JA126	JA127	JA114	JA118	JA110
Sc	3.9	6.1	11.9	3.1	3.2	10.4	5.5	4.4	11.4	12.2	3.6	3.4	4.1
V	20	2	7	20	1	2	8	7	1	1	11	10	11
Cr	9.0	1.8	3.0	3.0	1.0	3.0	0.1	8.0	2.0		2.0	2.0	2.0
Co	28.5	3.1	14.5	8.3	11.9	22.9	39.5	12.1	18.4	16.9	16.9	20.6	15.6
Ni	3.3	0.4	0.2	0.7	0.2	0.2	0.8	0.5	0.3	0.2	0.8	1.0	0.9
Cu	5.6	1.0	0.9	1.1	1.2	0.9	13.3	1.7	1.9	2.0	1.9	2.2	2.6
Zn	30.0	31.0	36.0	28.0	32.0	46.0	48.0	28.0	51.0	47.0	27.0	27.0	23.0
Ga	14.0	15.6	16.0	12.0	13.0	13.0	13.0	12.0	19.0	17.0	15.0	15.0	13.0
Rb	100.0	122.0	77.0	128.0	146.0	88.0	140.0	126.0	121.0	124.0	181.0	181.0	188.0
Sr	129.0	74.2	109.5	74.7	74.5	62.3	80.6	28.4	115.0	116.5	59.8	56.7	63.4
Y	74.2	32.7	39.8	6.3	26.3	37.5	44.8	21.3	44.4	42.3	26.1	21.6	28.3
Zr	124.0	150.0	283.0	111.0	100.0	220.0	125.0	150.0	258.0	265.0	120.0	117.0	116.0
Nb	5.6	9.8	10.0	6.0	7.2	9.7	6.7	8.2	8.6	8.7	9.4	9.8	10.0
Cs	5.7	4.1	0.9	3.5	6.1	2.1	8.1	4.4	2.5	2.7	6.9	8.2	9.3
Ba	702.0	641.8	674.0	814.0	852.0	724.0	676.0	791.0	663.0	672.0	711.0	685.0	705.0
La	103.0	37.4	30.4	20.5	33.8	23.7	33.8	23.3	30.6	28.8	31.2	41.6	32.2
Ce	77.5	67.0	62.4	32.1	46.1	49.4	52.8	42.3	51.4	50.2	54.3	52.1	58.2
Pr	20.9	9.0	7.7	3.3	6.7	6.0	7.9	4.7	8.9	7.7	7.5	7.5	6.9
Nd	63.5	29.8	31.4	10.7	24.5	23.9	28.7	17.2	31.1	26.6	23.6	21.7	24.7
Sm	11.2	6.1	6.9	1.7	4.4	5.4	5.8	3.5	6.7	5.7	4.4	3.9	4.7
Eu	3.6	1.2	1.6	0.4	0.9	1.2	1.2	0.5	1.4	1.4	0.7	0.6	0.5
Gd	13.2	6.5	7.0	1.7	5.0	6.4	7.4	3.5	7.5	6.4	4.7	4.0	4.5
Tb	2.1	1.0	1.1	0.2	0.7	1.0	1.3	0.5	1.3	1.1	0.8	0.6	0.6
Dy	11.3	5.4	7.2	1.3	4.3	6.9	7.7	3.3	7.0	6.2	4.1	3.2	4.1
Ho	2.6	1.2	1.5	0.3	0.8	1.5	1.7	0.7	1.6	1.5	0.9	0.7	0.8
Er	7.1	3.4	4.5	0.9	2.6	4.4	5.3	2.5	4.5	4.1	2.7	2.1	2.6
Tm	1.1	0.5	0.7	0.1	0.4	0.7	0.8	0.4	0.7	0.7	0.4	0.3	0.4
Yb	6.3	3.3	4.4	1.0	2.6	4.5	4.1	2.7	4.1	4.0	2.8	2.1	2.8
Lu	1.1	0.5	0.7	0.1	0.4	0.7	0.7	0.4	0.7	0.7	0.5	0.3	0.4
Hf	2.3	3.5	7.6	2.0	3.1	5.1	2.1	3.2	4.2	4.8	2.6	2.8	3.4
Ta	0.7	0.9	0.8	0.7	0.8	0.8	0.8	0.8	0.7	0.8	1.1	1.2	1.1
Pb	16.2	18.8	13.9	11.3	16.8	14.5	22.4	15.9	16.6	16.8	18.4	21.4	19.5
Th	10.8	13.4	8.8	12.4	17.2	10.3	13.8	13.5	10.9	11.3	19.4	20.2	20.7
U	2.2	2.8	2.0	2.2	3.1	2.2	2.4	2.5	2.0	2.0	4.0	4.0	4.5

Table 8.2	AU18153	AU18152	R17881	R17878	R17868	R12413	R17847	R17827	R17828	R19794	R17870	R17860
Sc	29.6	20.9	19	17.7	11	23.6	20.5	22.5	15.4	21.7	19.8	20.8
V	175	146	119	112	75	144	144	147	127	42	152	135
Cr	177.7	25.0	68.2	84.1	25	123.9	30.0	238.0	1.0	0.0	57.0	147.0
Co	28.0	19.1	27.4	16.3	15.3	32.9	30.6	25.7	17.1	22.9	35.2	28.0
Ni	30.7	6.8	13.5	13.8	10.1	40.5	12.1	55.6	1.8	0.4	27.9	42.0
Cu	32.6	9.3	18.9	15.0	11	30.8	18.0	54.3	7.9	5.2	37.3	23.6
Zn	59.0	70.0	60.0	60.0	52	56.0	69.0	76.0	81.0	123.0	66.0	67.0
Ga	21.1	22.0	21.1	20.0	20	20.0	21.0	20.0	23.0	27.1	22.0	19.0
Rb	35.1	62.1	77.3	68.1	86	43.0	39.0	43.0	64.1	77.3	26.0	55.0
Sr	315.0	277.0	258.0	235.0	192.5	285.0	275.0	240.0	246.0	304.0	290.0	245.0
Y	15.7	18.8	15.3	14.3	15	26.0	17.2	15.9	22.4	36.4	15.9	16.1
Zr	78.3	119.1	115.4	113.2	130	122.9	90.9	88.0	144.3	187.7	83.0	101.0
Nb	2.8	4.5	4.7	4.7	5.5	4.4	4.8	4.4	6.4	7.3	3.8	4.2
Cs	1.3	2.0	2.8	2.0	2.2	1.5	3.0	2.7	2.1	4.0	0.9	3.3
Ba	241.9	338.3	327.1	355.6	487	277.7	228.8	228.0	372.8	411.6	182.0	294.9
La	12.7	15.2	14.6	15.6	17.5	19.0	10.8	10.7	18.6	23.9	9.5	11.0
Ce	22.3	29.7	28.7	28.5	33.9	39.6	20.9	20.1	39.1	52.2	19.0	22.8
Pr	2.9	3.4	3.4	3.4	3.8	4.8	2.9	2.6	4.7	7.0	2.7	2.9
Nd	12.3	14.0	13.0	12.8	14	19.5	12.1	11.0	19.8	29.6	11.7	11.8
Sm	2.7	2.9	2.7	2.6	2.7	4.2	2.8	2.5	4.4	6.7	2.5	2.6
Eu	0.9	0.8	0.7	0.6	0.6	1.1	0.7	0.8	1.2	1.5	0.7	0.6
Gd	3.1	3.3	2.3	2.4	2.3	4.6	2.7	2.7	4.5	5.9	2.4	2.4
Tb	0.5	0.6	0.4	0.4	0.4	0.8	0.5	0.5	0.7	1.1	0.4	0.4
Dy	3.0	3.3	2.9	2.7	2.8	4.4	3.3	2.9	4.2	7.2	3.0	3.0
Ho	0.6	0.7	0.6	0.5	0.5	0.9	0.6	0.6	0.9	1.4	0.6	0.6
Er	1.8	2.1	1.8	1.7	1.7	2.8	2.0	1.8	2.6	4.2	1.9	1.9
Tm	0.2	0.3	0.3	0.2	0.3	0.3	0.3	0.2	0.3	0.6	0.2	0.2
Yb	1.7	1.9	1.7	1.7	1.9	2.5	1.9	1.8	2.4	3.8	1.7	1.9
Lu	0.3	0.3	0.2	0.2	0.2	0.3	0.3	0.2	0.3	0.5	0.2	0.2
Hf	2.4	2.7	2.5	2.2	2.1	3.5	2.8	2.5	4.0	5.6	2.4	2.8
Ta	0.2	0.4	0.4	0.4	0.5	0.6	0.4	0.3	0.5	0.5	0.3	0.3
Pb	5.2	10.9	8.1	7.0	9	9.8	6.9	7.7	10.1	13.0	4.5	6.0
Th	4.4	5.1	4.7	4.9	7.3	5.2	3.0	3.1	4.7	5.0	2.1	4.2
U	1.0	1.3	1.1	1.1	1.6	1.2	0.8	0.9	1.2	1.2	0.6	1.0

Table 8.2	R17833	R17845	R17829	R17825	R17871	R12382	AU45371	AU25796	R12383	R12414	R12769	R12767
Sc	25.1	16.5	17.9	16.1	13.5	24.4	23.9	21.4	21.6	18.3	29.4	27.2
V	144	110	127	116	73	176	167	168	151	133	206	216
Cr	90.0	1.0	6.0	19.0	8.0	50.0	48.9	15.0	20.0	63.2	20.0	7.0
Co	28.2	15.0	19.7	23.3	15.7	44.5	33.8	24.4	26.6	25.1	43.1	75.2
Ni	18.0	2.4	6.7	7.7	4.6	16.9	15.8	4.8	5.2	27.8	6.9	3.3
Cu	31.4	6.4	20.3	17.3	12.0	24.5	23.9	11.0	11.2	15.9	21.2	13.0
Zn	67.0	63.0	66.0	56.0	66.0	66.0	64.0	66.0	63.0	60.0	82.0	78.0
Ga	19.0	22.0	21.1	19.0	21.1	21.0	21.0	23.1	22.0	23.1	25.0	23.0
Rb	63.0	78.1	61.3	78.2	75.3	51.0	52.9	52.2	57.1	61.2	42.0	43.0
Sr	243.0	222.0	274.0	209.0	240.0	215.0	209.0	231.0	223.0	205.0	316.0	310.0
Y	24.7	17.8	25.3	33.7	30.6	33.3	16.0	21.0	24.4	24.3	24.2	25.2
Zr	108.0	136.2	115.6	112.2	133.5	121.0	123.8	130.4	122.2	160.5	136.0	136.1
Nb	4.6	5.7	5.3	4.9	6.1	4.3	4.5	5.4	5.1	6.4	5.9	8.2
Cs	4.3	3.1	5.7	5.2	5.8	1.9	1.9	1.4	1.4	2.1	1.6	1.4
Ba	390.2	367.6	312.6	439.9	423.7	287.0	264.6	273.8	290.4	288.9	253.0	263.2
La	22.2	16.1	17.1	22.5	18.4	15.5	8.7	13.3	15.9	18.4	14.6	16.3
Ce	31.7	33.7	33.6	37.1	30.6	30.6	19.8	28.2	31.2	38.6	35.8	37.1
Pr	5.1	4.2	4.1	4.4	4.7	4.1	2.4	3.2	3.6	4.7	4.4	4.6
Nd	20.3	16.4	17.0	17.2	19.0	16.9	9.6	13.7	14.7	18.7	18.2	18.9
Sm	4.3	3.4	3.9	3.7	4.1	4.2	2.3	3.1	3.4	4.3	4.2	4.3
Eu	1.2	0.8	1.1	1.1	0.8	1.1	0.7	0.9	0.9	1.0	1.3	1.4
Gd	4.4	2.9	4.2	4.3	4.0	4.4	2.5	3.7	3.6	4.5	4.6	4.9
Tb	0.7	0.5	0.7	0.7	0.7	0.9	0.4	0.7	0.7	0.8	0.7	0.8
Dy	4.2	3.6	4.0	4.7	4.9	5.1	2.7	3.8	3.8	4.4	4.5	4.6
Ho	0.9	0.7	0.9	1.0	1.0	1.1	0.6	0.9	0.9	0.9	0.8	0.9
Er	2.6	2.0	2.6	3.3	3.2	3.4	1.7	2.5	2.5	2.7	2.7	2.8
Tm	0.3	0.3	0.3	0.5	0.4	0.5	0.3	0.3	0.4	0.3	0.3	0.3
Yb	2.6	2.1	2.6	3.5	3.0	3.3	1.6	2.4	2.5	2.5	2.5	2.6
Lu	0.3	0.2	0.3	0.6	0.4	0.6	0.3	0.4	0.4	0.3	0.3	0.3
Hf	2.6	3.4	3.6	3.0	4.4	3.0	3.3	3.3	3.1	4.3	3.9	3.8
Ta	0.4	0.4	0.4	0.5	0.5	0.9	0.4	0.5	0.8	0.7	1.0	1.4
Pb	7.3	9.3	8.8	11.1	11.5	5.7	6.2	7.0	6.0	9.9	10.0	6.2
Th	5.6	5.6	5.2	8.1	7.2	4.2	4.4	4.0	5.0	4.6	4.4	4.3
U	1.2	1.4	1.3	2.0	1.7	1.0	1.1	1.0	1.2	1.2	0.9	1.0

Table 8.2	R10404	R17862	R17869	R17831	R17879	R17872	R17864	AU45402	R17873	R17876	R17867	AU45404
Sc	26.3	27.7	22.2	22.7	21.6	19.2	21	23.5	17.1	32.3	24.9	24.2
V	207	190	157	205	155	149	140	138	123	214	185	163
Cr	20.1	42.0	39.0	1.0	53.2	22.1	167.1	154.2	19.0	135.3	108.3	64.8
Co	38.2	51.0	27.5	29.0	26.1	22.0	31.2	30.0	20.7	28.3	27.5	32.1
Ni	6.2	76.5	15.7	2.7	19.5	13.2	43.5	35.5	11.4	25.4	32.3	23.7
Cu	19.1	39.0	45.1	20.9	45.8	23.4	43.9	37.9	20.7	45.5	23.9	26.9
Zn	85.0	94.0	78.0	83.0	72.0	70.0	69.0	67.0	79.0	73.0	77.0	94.0
Ga	23.1	23.0	22.0	24.1	23.1	22.1	21.0	20.9	25.0	23.1	23.1	24.9
Rb	54.1	28.0	41.0	41.2	47.2	58.2	49.0	47.7	73.1	12.0	22.1	59.9
Sr	288.0	271.0	265.0	394.0	236.0	262.0	219.0	224.0	256.0	365.0	264.0	296.0
Y	26.4	19.9	20.8	23.1	21.6	18.9	19.9	18.2	20.3	16.2	19.0	21.3
Zr	119.3	111.1	105.9	125.6	115.4	135.5	113.1	114.4	145.2	82.2	109.3	145.6
Nb	7.2	4.2	4.4	5.6	4.5	6.2	4.4	4.5	6.8	3.1	4.8	5.8
Cs	2.9	4.2	1.6	0.9	1.4	1.2	1.2	1.1	2.3	1.6	2.7	156.5
Ba	239.6	293.1	234.9	326.5	299.0	326.2	332.2	313.3	355.4	140.3	239.6	387.0
La	14.8	11.4	12.8	15.1	13.4	18.4	14.1	12.1	15.7	10.6	10.6	13.2
Ce	33.1	23.9	23.9	30.9	26.8	31.6	24.1	22.6	32.7	21.4	23.9	30.1
Pr	3.9	3.1	3.7	3.7	3.6	4.0	3.1	2.7	4.3	2.9	3.1	3.5
Nd	17.6	13.2	15.2	16.0	14.8	16.5	12.7	10.5	17.2	12.0	13.2	13.8
Sm	4.2	3.1	3.5	3.7	3.2	3.7	3.0	2.5	3.7	2.7	3.1	3.2
Eu	1.2	0.8	1.0	1.2	0.7	0.8	0.7	0.8	0.8	0.7	0.8	0.9
Gd	4.5	2.9	3.2	4.0	3.1	3.2	2.8	2.7	3.2	2.5	2.9	3.4
Tb	0.8	0.5	0.7	0.7	0.5	0.6	0.5	0.5	0.6	0.4	0.5	0.6
Dy	4.7	3.7	4.1	4.0	3.7	4.0	3.6	2.8	3.8	3.2	3.7	3.5
Ho	1.0	0.7	0.9	0.8	0.8	0.8	0.7	0.6	0.8	0.6	0.7	0.8
Er	2.9	2.3	2.6	2.6	2.4	2.3	2.4	1.8	2.4	2.0	2.3	2.2
Tm	0.4	0.3	0.4	0.4	0.3	0.3	0.3	0.3	0.3	0.3	0.3	0.3
Yb	2.7	2.2	2.4	2.5	2.3	2.3	2.3	1.7	2.2	1.8	2.2	2.1
Lu	0.4	0.3	0.4	0.3	0.3	0.3	0.3	0.3	0.3	0.2	0.3	0.3
Hf	3.8	3.3	3.1	4.0	3.2	4.0	3.5	3.0	4.2	1.7	3.1	3.8
Ta	0.6	0.3	0.3	0.4	0.3	0.4	0.4	0.4	0.5	0.2	0.3	0.5
Pb	8.4	6.6	5.7	7.3	8.0	7.6	5.7	5.8	7.7	6.7	6.6	8.4
Th	3.9	3.5	2.4	4.6	3.1	4.3	3.7	4.1	4.8	2.3	2.7	6.0
U	1.1	0.8	0.7	1.0	0.8	1.1	1.0	1.0	1.2	0.6	0.7	1.4

Table 8.2	R17861	R17836	R17863	AU43430	R17858	R17880	R17857	P33345	AU18189	AU45416	R17866	R17877
Sc	22.3	23.1	20.8	22	19.5	20.2	20.5	20.4	17.8	16.3	25.2	20.2
V	182	143	152	133	146	117	136	141	115	117	164	136
Cr	38.1	339.5	40.2	104.1	118.3	43.0	12.0	64.3	32.1	2.0	194.2	52.2
Co	23.1	25.6	23.1	34.5	23.7	28.2	24.3	22.7	19.0	19.7	33.3	19.0
Ni	12.8	89.3	13.8	17.2	24.0	16.5	14.2	30.0	10.4	3.9	51.7	20.4
Cu	23.3	26.4	21.3	23.4	34.5	25.9	15.5	15.8	17.0	27.0	27.1	30.2
Zn	78.0	69.0	84.0	61.0	69.0	50.0	61.0	65.0	49.0	60.0	70.0	59.0
Ga	21.1	20.2	22.1	21.0	20.0	21.0	22.0	22.1	20.1	19.9	21.1	18.1
Rb	28.1	37.3	50.2	57.1	52.1	62.0	78.1	22.1	95.3	58.7	48.3	54.2
Sr	325.0	252.0	274.0	233.0	251.0	221.0	244.0	276.0	161.5	227.0	232.0	207.0
Y	17.2	17.7	21.3	14.5	14.7	18.0	18.5	20.0	19.5	38.9	17.2	14.2
Zr	109.4	110.8	130.6	107.1	111.2	116.0	129.2	108.4	108.4	109.5	105.7	104.4
Nb	5.1	4.6	6.3	5.0	5.8	4.1	5.6	4.1	5.3	4.5	4.7	3.8
Cs	3.1	1.1	4.1	1.9	3.7	1.6	1.4	1.6	7.8	3.4	2.0	1.3
Ba	272.0	339.5	349.7	370.4	358.8	399.9	455.8	258.1	377.2	384.1	277.7	313.3
La	12.7	13.0	14.4	14.4	10.5	15.4	15.3	15.3	15.1	19.3	11.7	12.1
Ce	27.0	27.5	31.4	27.2	22.5	31.2	30.1	30.4	29.3	25.0	24.6	24.5
Pr	3.4	3.0	4.0	2.9	2.9	3.5	3.6	3.5	3.3	4.6	3.0	2.9
Nd	14.1	12.8	16.1	11.8	11.5	13.5	14.1	14.8	13.5	19.3	12.2	11.3
Sm	3.1	2.8	3.6	2.4	2.5	3.0	2.9	3.2	2.8	5.0	2.8	2.3
Eu	0.7	0.8	0.9	0.8	0.6	0.8	0.7	1.0	0.7	1.9	0.7	0.6
Gd	2.8	3.1	3.3	2.9	2.2	3.2	2.8	3.4	3.4	6.0	2.6	2.2
Tb	0.5	0.5	0.6	0.5	0.4	0.5	0.5	0.6	0.6	1.1	0.4	0.4
Dy	3.4	3.1	4.2	2.7	2.8	3.0	3.2	3.5	3.5	6.3	3.2	2.7
Ho	0.7	0.6	0.8	0.6	0.6	0.6	0.7	0.7	0.8	1.4	0.6	0.5
Er	2.1	2.0	2.6	1.7	1.8	1.9	2.1	2.2	2.2	4.0	2.0	1.7
Tm	0.3	0.3	0.4	0.2	0.2	0.2	0.3	0.3	0.3	0.6	0.3	0.2
Yb	2.0	2.0	2.4	1.7	1.7	1.8	2.1	2.2	2.1	4.2	2.0	1.7
Lu	0.3	0.3	0.3	0.3	0.2	0.2	0.3	0.3	0.3	0.7	0.2	0.2
Hf	3.0	2.5	4.0	2.2	3.0	2.6	2.9	2.5	2.9	2.8	3.0	2.4
Ta	0.3	0.4	0.5	0.5	0.4	0.4	0.5	0.3	0.5	0.4	0.4	0.3
Pb	6.5	6.3	5.4	6.6	7.3	7.4	8.6	7.1	7.2	7.4	6.3	5.2
Th	3.2	4.5	5.2	4.3	3.5	5.3	5.9	3.9	6.4	5.0	4.2	4.0
U	0.7	1.0	1.2	1.1	0.9	1.1	1.4	0.9	1.6	1.3	1.0	1.0

Table 8.2	AU45394	R17874	R17865	R17856	AU45405	AU45378	AU45377	AU45368	AU45386	AU46749	AU45324
Sc	16.8	20	23	16.1	17.9		14.6	20.9	36.2	22.6	26.1
V	140	122	119	129	102		125	193	202	193	196
Cr	54.7	53.0	54.7	10.1	20.9	47.0	9.0	33.8	364.8	17.9	35.2
Co	21.3	18.7	38.4	23.1	24.4		24.2	30.4	41.5	34.8	29.6
Ni	8.8	10.5	15.9	6.5	9.9		4.8	12.1	116.5	11.0	18.6
Cu	10.8	12.1	16.7	15.4	7.5		15.4	20.5	48.5	22.7	21.2
Zn	58.0	61.0	54.0	60.0	58.0		63.0	81.0	64.0	124.0	79.0
Ga	18.9	19.0	19.9	21.2	20.9	24.0	23.0	23.8	20.9	20.9	24.2
Rb	63.7	66.0	71.6	77.6	79.7	60.0	64.9	35.8	32.9	26.9	35.2
Sr	227.0	215.0	208.0	284.0	223.0		192.5	298.0	232.0	187.5	207.0
Y	21.2	28.5	18.3	21.1	20.7		18.0	29.9	14.3	28.5	19.1
Zr	112.4	122.0	131.2	128.9	136.5	130.0	133.8	122.2	82.7	94.7	109.7
Nb	3.1	4.6	4.6	5.5	5.6		6.4	5.3	3.2	2.8	4.0
Cs	1.9	2.0	2.2	3.5	3.0		2.2	0.5	2.8	0.8	0.9
Ba	346.2	369.9	372.7	454.3	435.3	242.0	285.5	219.6	143.5	108.7	203.3
La	12.7	18.3	15.0	18.6	15.3		16.7	15.1	7.9	9.5	10.4
Ce	24.2	29.2	31.1	30.9	29.7		31.7	35.5	17.6	21.4	22.0
Pr	3.0	4.3	3.8	4.4	3.5		3.5	4.2	2.1	2.8	2.6
Nd	11.3	17.0	14.6	17.2	12.9		13.3	17.6	8.6	12.0	11.4
Sm	2.6	3.7	3.4	3.5	2.8		2.9	4.2	2.1	3.3	2.7
Eu	0.8	0.9	0.9	0.9	0.8		0.9	1.2	0.7	1.2	1.0
Gd	3.0	3.6	3.5	3.2	3.2		3.1	4.3	2.3	4.1	3.5
Tb	0.5	0.6	0.6	0.5	0.6		0.5	0.8	0.4	0.8	0.6
Dy	3.1	4.4	3.2	3.8	3.1		2.9	4.5	2.4	4.7	3.7
Ho	0.7	0.9	0.6	0.7	0.7		0.6	1.0	0.5	1.0	0.8
Er	2.0	2.9	2.0	2.4	2.0		1.9	2.9	1.5	3.0	2.2
Tm	0.3	0.4	0.2	0.3	0.3		0.3	0.5	0.2	0.5	0.3
Yb	1.9	2.7	1.9	2.5	2.0		1.9	3.0	1.4	3.1	2.2
Lu	0.3	0.4	0.2	0.3	0.3		0.3	0.5	0.2	0.5	0.3
Hf	2.0	2.8	3.5	3.9	3.6		2.3	3.0	2.2	2.2	2.8
Ta	0.3	0.4	0.5	0.5	0.5		0.5	0.4	0.3	0.2	0.3
Pb	4.8	7.0	8.6	9.7	9.3		9.1	6.0	5.4	4.7	7.1
Th	4.7	5.3	7.1	8.7	8.5		4.7	2.5	3.1	2.1	3.0
U	1.1	1.3	1.6	1.9	2.0		1.3	0.6	0.8	0.6	0.8

Table 8.2	R12404	AU45383	AU46752	AU45362	AU45355	AU46744	AU45361	R12397	AU45382	AU45360	R12403	AU19788
Sc	24.6	19.9	23.1	17.5	22.3	27.2	21.7	26.7	16.9	9.5	17.3	17.7
V	184	107	127	144	164	153	154	184	132	84	117	141
Cr	23.0	17.9	45.8	15.0	34.9	66.6	88.6	19.0	13.9	0.0	68.2	14.1
Co	34.6	37.0	24.2	33.8	62.1	26.8	47.5	28.3	37.0	29.7	23.3	63.0
Ni	13.1	12.4	8.1	11.2	8.7	13.5	25.7	6.8	11.3	1.4	22.5	5.8
Cu	54.0	22.2	21.1	28.1	38.0	17.3	18.1	27.4	29.6	11.6	18.8	15.2
Zn	79.0	77.0	73.0	73.0	72.0	87.0	82.0	75.0	68.0	64.0	58.0	74.0
Ga	23.0	22.9	22.9	22.9	24.9	22.9	23.9	23.0	24.9	21.9	21.1	22.1
Rb	48.0	60.8	57.8	32.9	79.8	59.7	35.9	72.0	63.7	63.8	57.2	74.4
Sr	219.0	264.0	183.0	218.0	252.0	207.0	213.0	300.0	229.0	235.0	223.0	305.0
Y	27.0	19.0	23.0	53.6	22.3	27.3	25.8	23.1	18.8	25.8	18.2	19.2
Zr	130.1	140.5	125.5	113.7	143.6	132.2	104.6	125.1	130.4	133.7	114.4	121.6
Nb	5.3	6.2	5.7	3.8	6.2	6.0	4.1	6.1	6.1	5.2	4.7	5.9
Cs	2.4	2.8	1.6	1.0	3.6	6.6	2.0	3.9	3.2	2.1	3.6	1.6
Ba	276.2	304.8	268.0	186.6	286.3	345.0	270.9	263.1	301.6	293.3	257.9	329.6
La	14.3	15.2	14.6	13.8	17.5	17.5	14.6	17.6	15.8	17.8	15.2	15.2
Ce	31.6	33.1	30.3	24.9	37.5	34.9	29.6	35.7	29.5	38.9	32.1	29.3
Pr	4.0	3.8	3.5	4.2	4.2	4.9	3.4	4.2	3.3	4.6	3.6	3.2
Nd	16.9	14.5	13.9	18.7	16.2	19.3	13.6	16.3	12.8	18.1	14.0	12.8
Sm	4.0	3.2	3.3	5.2	3.6	4.7	3.2	3.7	2.8	4.1	3.0	2.7
Eu	1.2	0.9	1.0	1.4	1.0	1.4	0.9	1.2	0.9	1.1	1.0	0.8
Gd	4.5	3.4	3.7	6.1	3.7	5.1	3.5	4.2	3.0	4.1	3.5	3.4
Tb	0.8	0.6	0.7	1.3	0.7	0.9	0.7	0.7	0.6	0.8	0.6	0.6
Dy	4.8	3.2	3.8	7.7	3.6	4.9	3.8	4.1	3.0	4.0	3.3	3.4
Ho	1.0	0.7	0.8	1.8	0.8	1.0	0.9	0.8	0.7	1.0	0.6	0.8
Er	3.0	2.0	2.4	5.1	2.3	2.9	2.6	2.5	2.0	2.6	2.0	2.2
Tm	0.4	0.3	0.4	0.8	0.3	0.4	0.4	0.3	0.3	0.5	0.2	0.3
Yb	2.9	1.9	2.2	4.8	2.1	2.5	2.5	2.4	1.9	2.6	2.0	2.3
Lu	0.4	0.3	0.4	0.9	0.3	0.4	0.5	0.3	0.3	0.5	0.2	0.4
Hf	3.3	4.0	3.1	2.8	3.9	3.5	2.3	3.1	3.6	3.3	2.0	2.3
Ta	0.8	0.5	0.4	0.3	0.5	0.5	0.4	0.6	0.6	0.5	0.5	0.6
Pb	7.2	10.0	7.7	5.4	11.4	8.4	7.1	9.6	10.6	12.8	9.0	10.4
Th	4.1	6.6	4.5	2.7	5.8	5.6	4.8	5.6	7.0	3.9	6.4	6.0
U	1.0	1.2	1.1	0.8	1.4	1.4	1.2	1.6	1.7	1.1	1.4	1.5

Table 8.2	AU19812	R12405	AU45359	AU45327	AU45352	AU45343	R12389	AU45385	R12401	R12416	R12415	R12417
Sc	17.7	11	14.2	28.9	21	22.1	25	19.1	15.6	17.4	21.5	20.6
V	133	81	94	202	162	166	157	123	112	148	156	97
Cr	55.2	4.0	14.0	124.9	7.0	17.0	65.1	25.9	12.9	6.0	26.0	10.0
Co	18.4	23.0	20.5	39.5	24.5	26.1	26.7	27.4	19.9	24.8	21.4	20.9
Ni	16.2	2.1	9.2	23.1	3.6	3.2	24.9	10.0	6.0	4.0	6.3	4.6
Cu	27.7	15.8	9.8	38.6	12.2	12.3	27.5	21.5	15.6	14.5	25.8	17.5
Zn	77.0	63.0	61.0	95.0	79.0	64.0	62.0	62.0	60.0	66.0	59.0	56.0
Ga	21.1	25.1	23.0	22.0	21.9	21.0	23.0	21.0	18.1	23.0	21.0	22.1
Rb	55.2	67.3	40.0	33.0	68.7	74.0	57.1	58.9	64.7	73.0	61.1	59.2
Sr	189.0	232.0	252.0	267.0	252.0	259.0	224.0	222.0	239.0	266.0	266.0	271.0
Y	20.3	23.6	23.1	18.1	18.7	18.0	14.5	10.8	19.6	16.5	20.7	22.6
Zr	104.4	137.6	129.1	115.9	118.4	120.0	110.2	119.8	100.9	130.1	124.2	123.4
Nb	3.4	6.1	5.1	6.1	5.6	5.4	5.0	4.9	5.0	5.6	5.6	5.8
Cs	2.4	2.9	2.4	4.1	1.9	1.7	2.4	1.8	2.5	3.4	2.0	1.6
Ba	209.8	323.3	299.3	207.9	323.5	336.1	263.4	278.4	225.0	329.2	298.4	291.0
La	10.7	18.5	18.5	15.0	18.7	16.2	11.7	9.2	19.7	13.1	16.5	18.0
Ce	21.2	39.2	38.1	30.6	37.9	34.5	25.2	18.1	37.2	27.9	35.2	40.0
Pr	2.5	4.6	4.7	3.4	4.2	3.7	2.8	2.0	4.5	3.2	4.1	4.5
Nd	10.6	18.0	17.6	14.6	15.5	14.0	11.4	7.5	17.1	12.7	15.8	17.9
Sm	2.5	4.0	3.8	3.1	3.4	2.9	2.4	1.6	3.5	2.7	3.4	4.0
Eu	0.8	1.1	1.2	0.9	0.9	0.9	0.7	0.5	1.0	0.8	1.1	1.1
Gd	3.2	4.2	4.1	3.8	3.4	3.2	2.6	1.8	3.7	3.1	3.8	4.3
Tb	0.6	0.7	0.9	0.6	0.6	0.5	0.4	0.3	0.6	0.5	0.6	0.7
Dy	3.6	4.0	3.9	3.5	3.2	3.0	2.5	1.7	3.2	2.8	3.6	3.8
Ho	0.8	0.8	1.0	0.7	0.7	0.6	0.5	0.4	0.6	0.6	0.7	0.7
Er	2.4	2.6	2.5	2.1	2.0	1.9	1.6	1.1	2.1	1.8	2.3	2.4
Tm	0.4	0.3	0.5	0.3	0.3	0.3	0.2	0.2	0.3	0.2	0.3	0.3
Yb	2.7	2.5	2.4	1.9	2.0	1.8	1.5	1.1	2.0	1.7	2.1	2.3
Lu	0.4	0.4	0.6	0.3	0.3	0.3	0.2	0.2	0.3	0.2	0.3	0.3
Hf	2.7	3.9	2.4	0.9	2.7	2.3	2.5	2.2	1.7	3.0	2.4	1.4
Ta	0.3	1.0	0.4	0.5	0.5	0.5	0.6	0.4	0.6	0.9	0.6	0.5
Pb	8.9	13.3	8.8	7.5	8.5	8.6	8.5	7.9	10.6	9.4	7.4	7.7
Th	4.4	5.6	6.7	3.9	6.9	6.9	6.5	6.0	7.3	6.1	6.4	6.4
U	1.3	1.4	1.7	0.8	1.7	1.6	1.5	1.4	1.7	1.4	1.4	1.0

Table 8.2	R10403	R12388	AU45333	R12395	R12391	R12392	R12393	R12390	AU45326	R12396	R12399	AU45339
Sc	20.9	23	26.7	26.6	24.3	32.5	17.4	29	21.6	24.2	29.4	27.3
V	151	129	231	222	217	244	143	186	167	171	220	161
Cr	13.0	54.0	9.9	10.0	19.1	57.0	2.0	279.7	79.3	56.0	50.1	70.9
Co	18.8	59.9	46.0	29.1	37.4	55.9	26.7	54.0	27.0	37.8	27.1	57.7
Ni	4.5	6.6	5.2	7.4	8.0	14.1	3.3	90.8	28.9	24.9	10.9	33.1
Cu	20.6	13.9	29.9	36.7	27.3	19.7	17.4	36.7	44.6	39.6	19.1	32.5
Zn	52.0	62.0	100.0	93.0	83.0	85.0	93.0	71.0	72.0	77.0	70.0	72.0
Ga	20.0	23.0	24.8	25.0	24.1	23.0	24.0	23.0	23.1	23.0	22.0	22.0
Rb	57.1	54.0	21.8	19.0	26.1	23.0	26.0	52.9	46.2	46.0	38.0	33.9
Sr	272.0	257.0	241.0	236.0	233.0	211.0	222.0	230.0	204.0	240.0	266.0	178.5
Y	20.0	14.1	27.0	35.8	22.7	22.6	35.2	15.7	19.4	23.1	28.0	16.2
Zr	135.2	115.0	125.0	142.2	115.4	106.0	160.0	105.9	120.5	126.0	103.1	101.8
Nb	5.7	5.1	4.1	5.1	4.0	3.8	5.6	5.7	4.8	5.5	5.1	4.0
Cs	1.7	2.7	1.1	0.4	0.9	0.6	0.4	4.0	0.8	1.0	3.6	1.9
Ba	313.5	341.1	145.9	186.2	169.6	135.0	157.0	238.7	239.0	232.0	196.2	164.7
La	19.3	13.6	9.0	12.5	9.1	10.8	13.5	10.4	12.5	16.0	14.5	9.0
Ce	36.9	29.6	21.3	29.1	21.3	24.1	31.4	23.0	25.8	33.5	29.0	21.4
Pr	4.1	3.1	2.8	4.0	2.7	3.0	4.2	2.7	2.9	4.1	3.7	2.5
Nd	17.1	11.7	12.2	18.1	12.1	13.0	18.4	11.2	12.6	16.8	15.7	10.0
Sm	3.5	2.5	3.5	4.8	3.2	3.3	4.6	2.6	2.9	3.9	3.7	2.4
Eu	1.0	0.8	1.2	1.7	1.1	1.1	1.6	0.8	0.9	1.2	1.2	0.8
Gd	3.8	2.6	3.8	5.6	3.5	3.8	5.5	2.8	3.6	4.3	4.3	2.6
Tb	0.6	0.4	0.7	1.0	0.6	0.7	1.0	0.5	0.6	0.7	0.7	0.5
Dy	3.5	2.5	4.4	6.4	4.0	4.0	6.1	2.8	3.6	4.1	4.4	2.8
Ho	0.7	0.5	1.0	1.2	0.8	0.8	1.2	0.5	0.8	0.8	0.9	0.6
Er	2.2	1.5	2.8	3.9	2.5	2.5	3.9	1.7	2.2	2.5	2.7	1.8
Tm	0.3	0.2	0.4	0.5	0.3	0.3	0.5	0.2	0.3	0.3	0.3	0.3
Yb	2.2	1.5	2.7	3.7	2.3	2.2	3.7	1.6	2.1	2.3	2.5	1.7
Lu	0.3	0.2	0.4	0.5	0.3	0.3	0.5	0.2	0.3	0.3	0.3	0.3
Hf	3.5	2.5	3.3	4.1	3.0	2.8	4.4	2.9	2.9	3.3	2.7	2.6
Ta	0.4	0.8	0.3	0.5	0.7	0.8	0.6	1.0	0.4	0.7	0.6	0.4
Pb	8.0	8.8	5.1	5.3	4.1	4.0	5.9	7.1	6.0	6.1	7.8	6.4
Th	6.2	7.5	2.3	3.0	2.9	3.0	3.0	4.2	3.2	4.6	3.5	3.4
U	1.4	1.5	0.6	0.7	0.7	0.8	0.8	1.0	0.8	1.1	0.8	0.7

Table 8.2	AU45341	AU45384	R10433	R10432	AU45341	AU45384	R10433
Sc	21.8	20.7	23.4	24.5	21.8	20.7	23.4
V	167	131	159	164	167	131	159
Cr	51.9	51.7	44.1	51.1	51.9	51.7	44.1
Co	59.5	27.4	21.6	31.2	59.5	27.4	21.6
Ni	12.9	14.8	10.0	14.3	12.9	14.8	10.0
Cu	28.7	24.8	25.1	31.2	28.7	24.8	25.1
Zn	76.0	80.0	71.0	79.0	76.0	80.0	71.0
Ga	22.9	21.9	22.0	23.0	22.9	21.9	22.0
Rb	51.9	58.7	58.1	53.1	51.9	58.7	58.1
Sr	181.0	214.0	238.0	194.5	181.0	214.0	238.0
Y	17.8	20.5	21.2	22.9	17.8	20.5	21.2
Zr	111.7	124.3	126.3	112.2	111.7	124.3	126.3
Nb	4.7	6.1	5.2	5.4	4.7	6.1	5.2
Cs	1.5	2.4	1.6	1.6	1.5	2.4	1.6
Ba	268.4	289.4	265.6	269.5	268.4	289.4	265.6
La	9.6	14.2	15.9	16.9	9.6	14.2	15.9
Ce	21.2	30.3	33.1	32.6	21.2	30.3	33.1
Pr	2.4	3.5	3.8	3.7	2.4	3.5	3.8
Nd	9.4	13.5	15.9	15.7	9.4	13.5	15.9
Sm	2.1	3.0	3.6	3.6	2.1	3.0	3.6
Eu	0.7	0.9	1.0	1.0	0.7	0.9	1.0
Gd	2.6	3.3	3.8	3.8	2.6	3.3	3.8
Tb	0.5	0.6	0.6	0.6	0.5	0.6	0.6
Dy	2.8	3.3	3.8	3.9	2.8	3.3	3.8
Ho	0.6	0.7	0.8	0.8	0.6	0.7	0.8
Er	1.7	2.1	2.3	2.6	1.7	2.1	2.3
Tm	0.3	0.3	0.3	0.4	0.3	0.3	0.3
Yb	1.7	2.1	2.3	2.6	1.7	2.1	2.3
Lu	0.3	0.3	0.3	0.3	0.3	0.3	0.3
Hf	2.8	3.6	3.5	3.6	2.8	3.6	3.5
Ta	0.5	0.5	0.4	0.4	0.5	0.5	0.4
Pb	7.0	9.9	7.8	16.0	7.0	9.9	7.8
Th	4.2	5.3	5.8	5.1	4.2	5.3	5.8
U	1.0	1.2	1.4	1.2	1.0	1.2	1.4

Appendix C. Supplementary crystal and groundmass geochemistry dataset to Chapter 4

Appendix C. Supplementary crystal and groundmass geochemistry dataset to Chapter 4 “The transition from intermediate to silicic volcanism in the North Island of New Zealand”. See Chapter 4, Section 4.2.3 for analytical methods. Following sections: rock descriptions.

C.1. AU45386 - Beesons’s Island Volcanics, Kuaotunu Subgroup

Fresh two-pyroxene andesitic lava with seriate porphyritic texture. Approximately 60% crystal content comprising plagioclase, orthopyroxene, subordinate clinopyroxene and Fe-Ti oxide. Plagioclase and orthopyroxene occur as euhedral and subhedral, angular crystals up to 1 mm across, and as smaller angular crystals or crystal fragments. Clinopyroxene occurs as smaller crystals or fragments. Plagioclase and orthopyroxene crystals additionally occur in glomeroporphyritic aggregates up to 3 mm across. Groundmass is very fine-grained devitrified comprising plagioclase, orthopyroxene Fe-Ti oxide.

C.2. AU45360 - Beeson’s Island Volcanics, Kuaotunu Subgroup

Fresh andesite lava with seriate porphyritic texture. Approximately 30% crystal content comprising plagioclase, less orthopyroxene, subordinate hornblende. Plagioclase and pyroxene occur as euhedral and subhedral, angular and subangular crystals up to 1 mm across, and as smaller angular crystal fragments. Hornblende as rare sub-mm anhedral rounded crystal fragments with reacted rims. Groundmass very fine-grained devitrified comprising plagioclase, orthopyroxene Fe-Ti oxide.

C.3. R17872 - Kapukapu Andesite, Waiwawa Subgroup

Porphyritic two-pyroxene andesite lava with approximately 30% crystal content comprising predominantly plagioclase and orthopyroxene with minor clinopyroxene and Fe-Ti oxides. Plagioclase occurs as subhedral, subangular crystals up to c. 0.5 to 1 mm across, and as smaller angular crystal fragments. Pyroxene as mm and smaller eu- to subhedral crystals. Groundmass is fine-grained devitrified, mainly plagioclase and pyroxene.

C.4. R17869 - Kapukapu Andesite, Waiwawa Subgroup

Fresh pyroxene andesite lava with seriate porphyritic texture comprising c. 40% crystal content, principally plagioclase and orthopyroxene and subordinate clinopyroxene and Fe-Ti oxides. Plagioclase occurs as angular eu- to subhedral crystals or crystal fragments up to 1 mm across, as well as sub-rounded to rounded crystals typically with a turbid outer rim. Some plagioclase crystals show internal optical zonation.

tion parallel to crystal boundaries. Pyroxene as sub-mm angular eu- to subhedral crystals. Plagioclase and orthopyroxene additionally occur in glomeroporphyritic aggregates where they look identical to single crystals in the groundmass. Groundmass is very-fine grained, devitrified comprising plagioclase and Fe-Ti oxides.

C.5. R17831 - Kapukapu Andesite, Waiwawa Subgroup

Porphyritic pyroxene andesite with < 10% crystal content. Plagioclase occurs principally as c. 0.1 mm laths that define a flow banded texture. Clinopyroxene occurs as mm-sized, angular to subangular euhedral crystals. Some clinopyroxene crystals have reacted rims. Groundmass is fine-grained crystalline and comprises minor Fe-Ti oxides in addition to plagioclase laths.

C.6. R17861 - Waipupu Formation, Waiwawa Subgroup

Seriate porphyritic pyroxene andesite lava with c. 50% crystal content. Plagioclase occurs as up to 1 mm across euhedral to subhedral, angular crystals. Some mm-size plagioclase crystals show internal optical zonation parallel to crystal boundaries. Plagioclase crystals of all sizes in some cases show patchy alteration of crystal core to clay. Subordinate orthopyroxene occurs as <1 mm angular euhedral crystals. Fe-Ti oxides occur as <0.1 mm crystals. Groundmass is fine-grained, probably devitrified, effectively also comprises small crystal fragments seriate with larger crystals.

C.7. R17880 - Waipupu Formation, Waiwawa Subgroup

Porphyritic pyroxene andesite lava with c. 40% crystal content, predominantly plagioclase with subordinate pyroxene and Fe-Ti oxides as well as xenocrystic quartz. Plagioclase occurs as up to 3 mm angular euhedral, in cases fragmented, crystals with internal optical zonation and glassy patches along fractures. Some larger plagioclase crystals are instead subrounded with a reacted rim. Smaller, up to 1 mm plagioclase crystals are eu- to subhedral, subangular, or angular crystal fragments. Some plagioclase crystal cores have patchy alteration to clay. Pyroxene and Fe-Ti oxides occur as <0.5 mm crystals, and also occur with plagioclase in the fine-grained devitrified groundmass.

C.8. AU45340 - Whangapoua Andesite, Kuaotunu Subgroup

Seriate porphyritic two-pyroxene andesite lava with plagioclase, ortho- and clinopyroxene and minor Fe-Ti oxides. Plagioclase occurs as angular to subangular, euhedral to subhedral crystals. Some plagioclase crystals show internal optical zonation, and some plagioclase crystals show patchy alteration to clay of crystal cores and/or rims. Ortho- and clinopyroxene occur as <1 mm angular to subangular euhedral

crystals. Plagioclase and pyroxene additionally occur in glomeroporphyritic crystal aggregates up to 3-4 mm across. Groundmass is very fine-grained to aphanitic.

C.9. R17874 - Whiritoa Andesite, Waiwawa Subgroup

Porphyritic pyroxene andesite lava with c. 10-20% crystal content. Plagioclase occurs as angular to subangular, euhedral crystals up to 1 mm across. Some plagioclase crystals have a turbid outer rim overgrown by a clear outermost rim. Equant orthopyroxene occurs as up to 2 mm across angular euhedral or subhedral crystals. Pyroxene also occurs in glomeroporphyritic crystal aggregates up to 2-3 mm across. Groundmass is fine-grained, crystalline with plagioclase, pyroxene and Fe-Ti oxides.

C.10. R17866 - Whiritoa Andesite, Waiwawa Subgroup

Seriate porphyritic two-pyroxene andesite lava with c. 50% crystal content, comprising plagioclase, clinopyroxene and orthopyroxene in a fine-grained, crystalline groundmass. Plagioclase occurs as angular, eu- to subhedral crystals up to 2 mm across. Some plagioclase crystals form glomeroporphyritic aggregates, and some plagioclase crystals show internal optical zonation. Plagioclase laths occur in the groundmass. Clinopyroxene occurs as mm-sized subhedral rounded crystals that are partially altered to ?chlorite. Subordinate orthopyroxene occurs as sub-mm equant crystals, some of which form crystal aggregates up to 2 mm across. Groundmass is fine-grained, crystalline comprising plagioclase laths, orthopyroxene and Fe-Ti oxides. Some groundmass crystals may be fragments of larger crystals.

C.11. R17856 - Whiritoa Andesite, Waiwawa Subgroup

Porphyritic pyroxene andesite with predominantly plagioclase and orthopyroxene, minor Fe-Ti oxides, c. 30% crystal content. Plagioclase occurs as angular, euhedral 0.5-1.5 mm crystals, some with internal optical zonation, Orthopyroxene occurs as up to 2 mm angular euhedral crystals. Plagioclase and orthopyroxene occur together in glomeroporphyritic aggregates maximally several mm across. Groundmass is very fine-grained.

C.12. AU60071 - Sugarloaf Basalt, Mercury Basalts

Fresh porphyritic olivine basalt lava with subordinate clino- and orthopyroxene, Fe-Ti oxides. Approximately 20% crystal content. Olivine occurs as < 1 mm across, subhedral, subangular to subrounded crystals or crystal fragments in a fine-grained groundmass. Pyroxene and Fe-Ti oxides occur as small, angular sub- to anhedral crystals. Groundmass is fine-grained and includes tabular <0.1 mm plagioclase laths, as well as <0.1 mm equant pyroxene and oxide crystals.

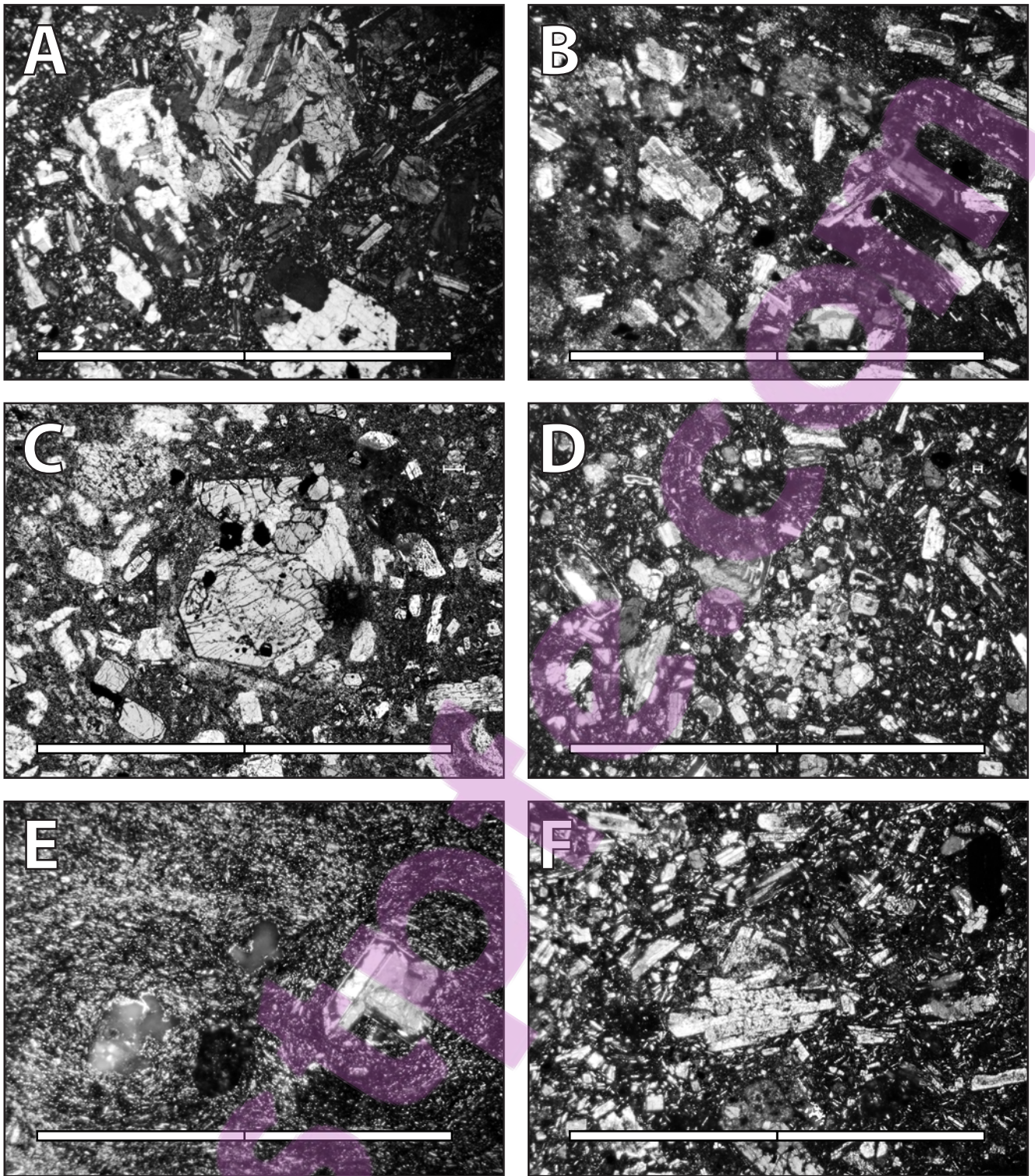


Fig. A Thin section photomicrographs of samples used for electron microprobe analyses. Each scale bar increment denotes 1 mm length. A. AU45386. Pyroxene andesite, Beeson's Island Volcanics. B. AU45360. Pyroxene andesite with minor hornblende, Beeson's Island Volcanics. C. R17872. Pyroxene andesite, Kapukapu Andesite. D. R17869. Pyroxene andesite, Kapukapu Andesite. E. R17831. Pyroxene andesite, Kapukapu Andesite. F. R17861. Pyroxene andesite, Waipupu Formation.

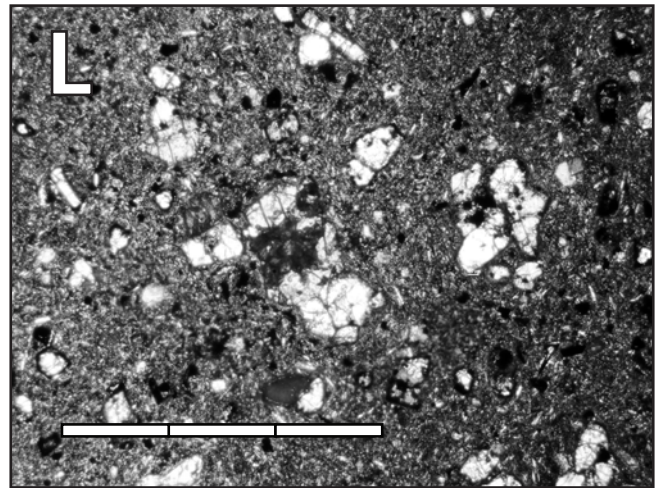
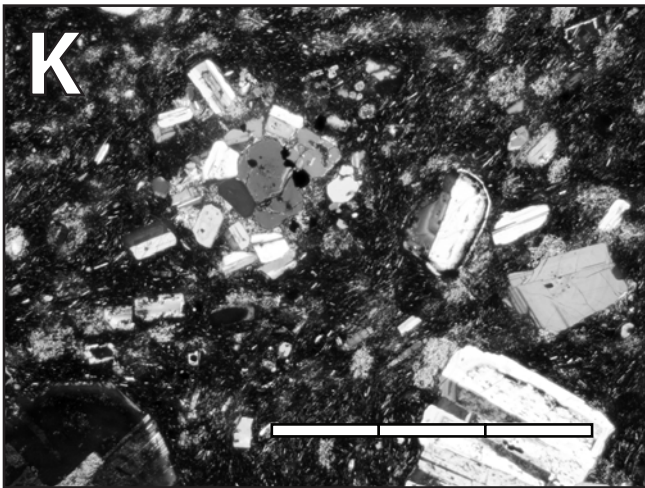
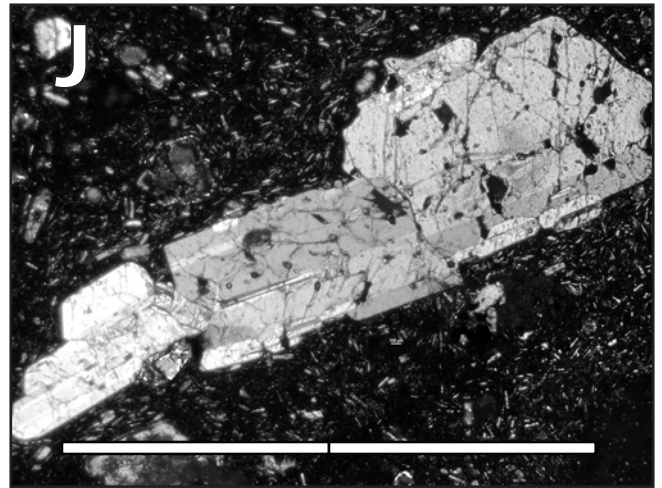
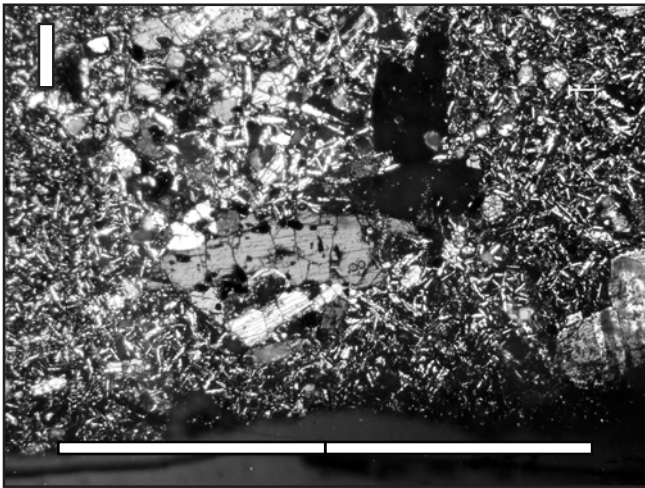
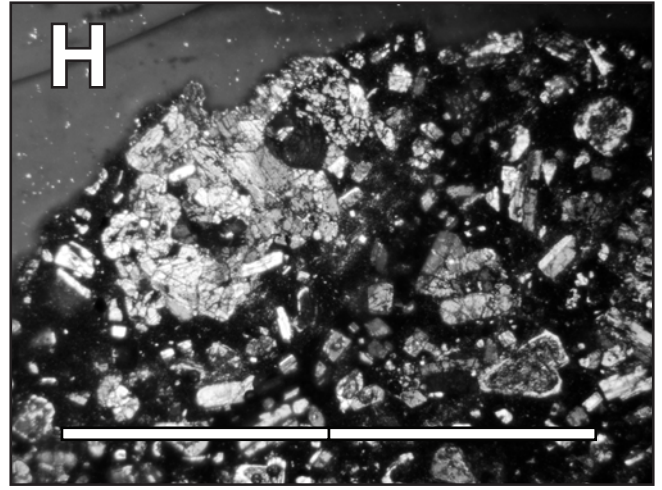
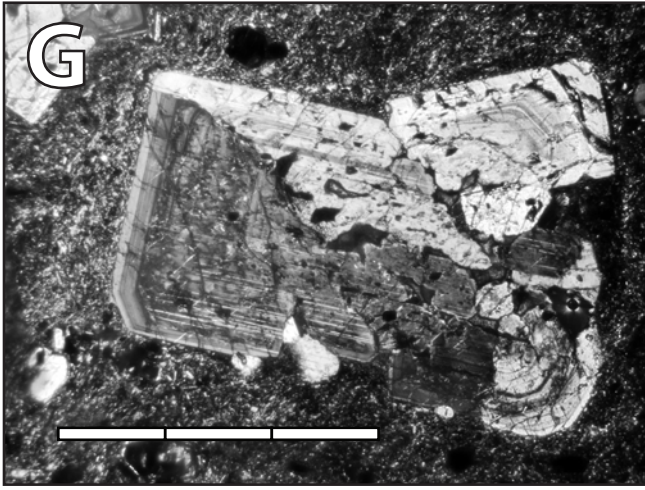


Fig. A (continued) G. R17880. Pyroxene andesite, Waipupu Formation. H. AU45340. Pyroxene andesite, Whangapoua Andesite. I. R17874. Pyroxene andesite, Whiritoa Andesite. J. R17866. Pyroxene andesite, Whiritoa Andesite. K. R17856. Pyroxene andesite, Whiritoa Andesite. L. AU60071. Olivine basalt, Sugarloaf Basalt.

Table 8.3	SiO ₂	TiO ₂	Al ₂ O ₃	FeO	MnO	MgO	CaO	Na ₂ O	K ₂ O	P ₂ O ₅	SO ₃	Cl	Cr ₂ O ₃	NiO	TOTAL
AU45386 - Beeson's Island Volcanics - Kuaotunu Subgroup															
Groundmass	61.07	0.81	13.84	7.25	0.16	3.56	4.03	3.77	2.28	0.22	0.11	0.05	0	0.02	97.16
Groundmass	63.03	0.41	19.62	1.47	0.1	0.28	5.59	4.85	2.08	0.09	0.01	0	0.05	0.2	97.78
Opx in glomerocryst	53.19	0.37	1.03	20.07	0.44	23.14	1.88	0	0.06	0.17	0.06	0.01	0	0.17	100.58
Opx adjacent to glomerocryst	53.24	0.43	2.32	19.53	0.47	23.29	1.6	0	0.09	0.08	0	0	0.07	0	101.1
Opx in glomerocryst	53.31	0.37	1.54	18.75	0.53	23.96	1.46	0	0.06	0	0.01	0.05	0	0	100.04
Opx adjacent to glomerocryst	53.56	0.34	1.55	19.76	0.44	23.56	1.6	0	0.05	0	0	0	0.03	0.02	100.91
Opx adjacent to glomerocryst	53.01	0.4	2.33	19.21	0.54	23.64	1.67	0	0.04	0	0	0	0.06	0	100.91
Plag in glomerox; clear rim	48.92	0.1	31.75	0.67	0.07	0.1	15.41	2.55	0.21	0	0	0.01	0.1	0	99.87
Plag in glomerox; turbid zone	49.43	0.12	30.98	0.67	0.03	0.01	14.91	2.86	0.24	0.07	0.01	0.01	0.13	0	99.46
Plag adjacent to glomerocryst	51.38	0.08	29.76	0.61	0.05	0.04	13.58	3.47	0.33	0.04	0.02	0	0.01	0	99.37
Zoned plag; core	50.21	0.05	30.71	0.6	0	0.05	14.49	3.04	0.16	0.05	0	0.02	0	0.02	99.41
Zoned plag; clear zone	48.85	0	31.68	0.58	0.07	0.02	15.65	2.55	0.25	0	0	0	0.09	0.1	99.83
Zoned plag; turbid zone	48.34	0	31.84	0.51	0.01	0	15.44	2.44	0.23	0	0.15	0.02	0.04	0	99.01
Turbid plag in glomerocryst; clear zone	49.34	0.04	31.84	0.58	0.08	0.17	15.61	2.64	0.21	0	0.01	0.01	0.1	0.03	100.65
Turbid plag in glomerocryst; core	49.37	0.08	31.38	0.54	0	0	15.19	2.57	0.2	0.01	0.02	0.03	0.07	0.1	99.55
AU45360 - Beeson's Island Volcanics, Kuaotunu Subgroup															
Mottled plag; core	47.29	-0.08	32.95	0.55	0.1	-0.04	16.72	1.74	0.17	-0.13	-0.05	-0.05	0.11	0.2	99.48
Opx; no zonation	52.95	0.28	0.82	21.8	0.57	21.75	2	-0.09	0.12	0.11	0.1	0.05	0	0.08	100.52
Opx; no zonation	52.63	0.15	0.51	24.87	0.83	19.82	1.18	-0.15	0.1	0.06	0.09	0.01	-0.1	-0.03	99.98
Opx; no zonation	53.11	0.21	0.84	21.22	0.56	22.16	1.67	-0.03	0.1	0.09	0.04	0.02	-0.03	0.03	100.01
Plag; no zonation	45.94	0.02	33.64	0.68	0	-0.04	17.56	1.49	0.17	0.08	0.01	0.02	0.05	0.14	99.75
Groundmass	70.83	0.39	15.1	1.65	0	0.25	3.12	4.43	2.54	0.24	-0.06	0	0.07	0.06	98.62
Groundmass	67.18	0.64	13.35	3.94	0.09	1.15	2.83	3.93	2.66	0.42	-0.01	0.02	0	0.04	96.25
R17872 - Kapukapu Andesite, Waiwawa Subgroup															
Cpx; core	50.76	0.50	2.31	11.37	0.33	13.84	19.00	0.06	0.06	0.07	-0.03	0.00	0.11	0.16	98.55
Cpx; rim	51.99	0.56	1.52	11.13	0.33	14.10	19.89	0.19	-0.01	0.25	0.00	0.05	0.16	0.14	100.30
Opx; core	52.69	0.24	1.01	22.75	0.45	20.87	1.41	-0.13	0.04	-0.01	-0.11	-0.03	0.08	-0.03	99.23
Opx; rim	52.91	0.18	1.28	20.57	0.44	23.00	1.45	-0.09	0.14	0.08	0.13	0.07	0.01	0.11	100.29
Opx; no zonation	52.94	0.18	0.70	22.46	0.66	21.02	1.67	-0.04	0.03	-0.09	0.00	0.05	-0.04	0.17	99.72
Opx; no zonation	51.47	0.17	1.54	23.59	0.60	20.43	1.50	-0.09	0.01	-0.07	0.05	0.00	0.01	0.17	99.38
Plag; core	46.15	0.04	32.77	0.50	0.10	-0.05	17.18	1.52	0.15	-0.07	0.02	0.00	0.11	0.01	98.42
Plag; between core-rim	48.81	0.05	31.78	0.50	0.15	-0.02	15.47	2.55	0.19	-0.09	0.09	0.00	0.01	-0.07	99.44
Plag; between core-rim	54.72	0.01	26.84	0.77	0.07	-0.01	10.68	4.97	0.50	-0.02	0.10	0.05	0.03	-0.07	98.64
Plag; core	49.41	-0.03	31.38	0.43	-0.02	-0.08	15.32	2.76	0.25	-0.11	0.00	-0.01	-0.04	0.06	99.30
Plag; rim	50.66	0.12	30.32	0.71	-0.03	0.05	14.30	3.27	0.29	-0.04	-0.06	0.06	0.04	0.09	99.80
Plag; core	48.93	0.02	31.44	0.42	-0.03	-0.03	15.13	2.72	0.24	-0.03	0.07	-0.01	0.07	0.06	99.00
Plag; rim	51.92	0.03	29.68	0.58	0.09	-0.06	13.27	3.77	0.25	0.14	0.10	0.01	-0.01	0.06	99.83
Plag; core	52.16	0.02	29.65	0.50	0.12	-0.01	13.29	3.86	0.36	0.18	-0.02	-0.01	0.00	0.04	100.14
Plag; rim	50.91	-0.02	30.36	0.54	-0.01	-0.05	13.96	3.27	0.26	-0.04	0.04	0.05	-0.03	-0.02	99.20
Plag; core	49.17	0.04	31.77	0.55	0.00	-0.06	15.15	2.73	0.17	0.01	0.10	0.05	0.02	-0.17	99.53
Plag; rim	49.14	0.07	31.01	0.37	0.05	0.07	14.82	2.93	0.22	-0.04	0.00	0.03	0.14	-0.05	98.76
Plag; core	54.45	0.06	27.25	0.44	-0.09	-0.04	10.65	3.29	3.01	-0.04	0.04	0.05	0.06	0.02	99.17
Plag; rim	47.60	-0.03	32.45	0.49	-0.10	-0.05	16.37	2.21	0.13	-0.14	-0.06	0.01	0.20	0.04	99.11
Plag; rim	47.76	-0.02	32.44	0.38	0.03	-0.03	16.32	1.98	0.16	0.06	-0.05	0.04	0.14	-0.12	99.09
R17869 - Kapukapu Andesite, Waiwawa Subgroup															
Cpx; no zonation	54	0.2	1.43	4.66	0.19	19.43	19.28	0.06	0.07	-0.02	-0.04	0.08	0.66	-0.09	99.9
Opx; no zonation	52.51	0.15	1.31	22.55	0.71	21.65	1.2	-0.02	0.06	-0.08	0.06	-0.02	0	0.18	100.25
Opx adjacent to glomerocryst	52.45	0.19	1.26	22.23	0.73	21.89	1.23	-0.09	0.01	-0.07	-0.08	0.05	-0.04	0.05	99.8
Plag, resorbed w/ turbid rim; rim	55.01	0.04	27.45	0.23	0.02	0.07	10.57	5.21	0.4	-0.07	-0.01	0	0.04	0.22	99.18
Plag, resorbed w/ turbid rim; core	52.86	0.04	28.76	0.24	0.07	-0.11	12.14	4.37	0.3	-0.12	-0.07	0.02	0.04	0.05	98.59
Plag in glomerocryst	51.68	0.05	29.68	0.37	0.13	-0.08	13.17	3.69	0.22	-0.05	0.07	-0.03	0.06	0.11	99.08

Table 8.3	SiO ₂	TiO ₂	Al ₂ O ₃	FeO	MnO	MgO	CaO	Na ₂ O	K ₂ O	P ₂ O ₅	SO ₃	Cl	Cr ₂ O ₃	NiO	TOTAL
Plag; no zonation	52.33	0.06	29.67	0.48	0.04	0	13.08	4.14	0.3	-0.03	0.01	0.05	0.05	0.06	100.24
R17831 - Kapukapu Andesite, Waiwawa Subgroup															
Groundmass	60.45	0.22	20.11	2.61	0.04	0.78	6.68	3.54	2.42	0.02	-0.05	0	0.08	-0.01	96.89
Groundmass	61.53	0.36	18.72	2.94	0.15	1.05	6.47	3.7	2.33	0.19	0.01	0.07	-0.02	0.03	97.55
Clay after plag	46.16	0.14	37.1	1.19	0.09	0.08	0.21	-0.02	0.28	-0.06	0.18	0.08	0.04	0.1	85.58
Opx in glomerocryst	53.25	0.26	1.54	16.37	0.44	25.67	1.23	0.12	0.04	-0.13	0.05	0.05	0.06	-0.11	98.86
Opx; rim	53.25	0.3	1.91	16.85	0.44	25.72	1.39	0.06	0.08	-0.09	0.07	0.06	0.03	-0.16	99.93
Plag; core	46.02	0.01	32.43	0.57	0.12	0.05	16.62	1.7	0.11	-0.19	0.07	0.04	0.14	0.11	97.78
Plag; rim	46.4	0.01	32.79	0.48	-0.1	0.1	16.55	1.7	0.08	-0.12	0.02	0.01	0.09	0.05	98.06
Plag; core	46.67	-0.04	32.89	0.32	0.04	0.16	17.04	1.61	0.14	-0.14	-0.02	0.02	0.12	-0.1	98.71
Plag; rim	45.73	0.11	33.68	0.53	-0.01	0.19	17.56	1.28	0.09	-0.05	0.1	-0.04	-0.01	0.15	99.32
Clay after plag	43.31	-0.01	37.39	0.89	-0.01	0.03	0.15	0.11	0.39	-0.03	0.04	0.2	-0.02	0.02	82.45
R17861 - Waipupu Formation, Waiwawa Subgroup															
Cpx; no zonation	51.38	0.72	2.17	10.34	0.32	14.78	19.66	0.17	0.05	-0.01	-0.05	0.04	0.2	-0.02	99.74
Cpx; no zonation	49.39	0.47	3.82	6.74	0.19	15.63	19.28	0.05	0.07	-0.01	0.06	0.03	0.12	0.01	95.85
Plag; core	46.54	0.07	32.93	0.54	0.07	-0.07	17.11	1.55	0.13	-0.14	-0.14	0.05	0.03	-0.01	98.66
Plag; inner rim	46.31	0.03	33.36	0.43	-0.09	0.03	17.22	1.4	0.12	-0.09	-0.06	0.01	0.06	-0.05	98.67
Plag; outer rim	50.16	0	30.68	0.86	-0.07	0.01	14.85	2.98	0.27	0.02	-0.02	-0.05	0.25	0	99.94
Plag w/ turbid core; core	54.13	-0.02	28.21	0.74	-0.1	-0.03	11.57	4.73	0.35	-0.03	0	0.03	0.04	-0.11	99.52
Plag w/ turbid core; rim	53.22	0.01	28.67	0.55	-0.01	0.03	12.14	4.38	0.22	-0.02	-0.01	-0.01	0.13	-0.06	99.25
Plag; core	52.93	-0.01	28.1	0.49	0.03	0.05	11.36	4.58	0.29	-0.04	-0.07	0	0.07	-0.07	97.7
Plag; rim	53.22	0	28.07	0.48	-0.03	-0.02	11.76	4.54	0.35	-0.03	0.01	0.03	0.13	0.1	98.61
R17880 - Waipupu Formation, Waiwawa Subgroup															
Plag; core	57.76	0.09	25.63	0.32	-0.02	0.06	8.33	6.38	0.62	-0.17	0.02	0.03	0.05	-0.12	98.99
Plag; rim	56.88	0.08	26.36	0.23	-0.02	0.03	8.82	6.02	0.6	-0.17	0.09	0.02	0.03	-0.13	98.85
Plag; outer rim	56.69	0	26.22	0.25	-0.02	-0.01	8.97	6.14	0.48	-0.17	-0.1	0.04	-0.07	-0.05	98.36
Plag w/ turbid core; core	53.75	0.08	28.34	0.34	0.08	-0.07	11.37	4.9	0.3	-0.1	-0.07	-0.04	0.14	0.15	99.18
Plag w/ turbid core; rim	58.79	-0.03	24.94	0.16	0.07	-0.07	7.69	6.54	0.81	-0.03	0.07	0	0.02	-0.24	98.74
Plag; core	54.27	0.02	28.26	0.2	0.05	-0.03	11.33	4.97	0.36	0.14	0.08	-0.02	0.17	0.01	99.8
Quartz; partially resorbed	97.91	-0.02	-0.01	-0.03	0.16	-0.04	0.05	0	-0.05	-0.03	0.17	0.02	-0.04	0.14	98.24
AU45340 - Whangapoua Andesite, Kuaotunu Subgroup															
Cpx in glomerocryst	52.52	0.35	2.68	5.89	0.07	17.21	20.19	0.14	0.06	0.12	0.04	0	0.47	0.03	99.79
Cpx in glomerocryst	53.81	0.06	1.29	4.65	0.24	18.21	20.17	0.09	0.07	0	0	0	0.74	0	99.32
Cpx in glomerocryst	53.71	0.21	1.63	5	0.24	18.35	19.72	0.28	0.02	0.07	0.15	0.04	1.01	0	100.42
Cpx in glomerocryst	51.9	0.36	1.68	11.66	0.21	13.79	19.48	0.1	0.04	0.01	0.07	0.02	0.06	0	99.37
Cpx in glomerocryst	52.56	0.44	2.88	6.01	0.02	16.82	20.45	0	0.14	0.15	0	0.03	0.32	0.08	99.92
Cpx in glomerocryst	52.56	0.44	2.88	6.01	0.02	16.82	20.45	0	0.14	0.15	0	0.03	0.32	0.08	99.92
Groundmass	61.48	1.29	18.11	4.49	0	1.19	5.37	4.26	1.98	0.13	0	0.02	0.05	0.09	98.46
Opx in glomerocryst	54.07	0.14	2.44	14.72	0.22	26.95	1.32	0	0.08	0	0	0	0.22	0	100.15
Opx in glomerocryst	52.7	0.25	1.27	21.53	0.59	21.98	1.45	0	0.04	0	0	0	0	0	99.8
Plag w/ turbid core; core	46.74	0	33.24	0.47	0.01	0	17.19	1.36	0.15	0.07	0.07	0	0	0.03	99.32
Plag w/ turbid core; rim	50.07	0	30.51	0.67	0	0	14.37	3.05	0.26	0.02	0	0.02	0.05	0	99.02
Plag; outer rim	50.96	0.08	29.85	0.35	0	0	13.41	3.51	0.22	0	0.01	0.01	0.06	0.07	98.52
Plag; core	49.54	0.1	31.76	0.37	0	0	15.29	2.52	0.18	0	0	0	0	0.19	99.95
Plag; core	48.29	0.07	32.72	0.14	0.03	0.04	16.12	2.12	0.15	0	0.02	0.04	0.08	0.03	99.85
Plag; core	52.76	0.02	29.27	0.4	0	0	12.54	4.26	0.33	0	0	0	0.03	0.09	99.69
Plag; rim	49.74	0.07	31.07	0.37	0.07	0	14.73	3.05	0.24	0	0	0.03	0.05	0	99.43
R17874 - Whiritoa Andesite, Waiwawa Subgroup															
Groundmass	65.76	0.04	16.25	1.46	0.14	0.27	6.85	2.20	0.42	0.22	-0.02	0.03	-0.05	0.02	93.58
Groundmass	67.71	0.24	14.40	1.42	0.09	0.68	2.64	3.18	4.92	0.19	0.01	0.07	-0.04	0.10	95.60
Groundmass	66.14	0.39	17.43	1.92	0.05	0.4	4.85	3.86	2.9	0.29	0.02	-0.01	-0.06	0.06	98.25
Opx in glomerocryst; rim	52.89	0.09	0.65	23.68	0.71	21.04	1.02	-0.14	-0.02	-0.04	0.10	0.04	-0.02	-0.07	99.93
Opx; core	40.16	0.06	0.24	11.5	0.21	46.5	0.14	-0.07	0.01	0.05	0	0	0.08	0.04	98.93
Opx in glomerocryst	53.42	0.02	0.46	23.22	0.81	21.48	0.9	-0.03	0.01	-0.06	-0.05	-0.03	0	-0.02	100.12
Opx; core	53.49	0.14	0.51	22.76	0.73	21.64	0.95	-0.09	0.08	-0.04	0.1	0.09	-0.07	-0.07	100.22
Opx in glomerocryst; core	52.84	0.21	0.59	24.05	0.63	20.9	1.1	-0.11	0.07	0.14	-0.05	0.05	0.07	0.01	100.48
Opx in glomerocryst	52.9	0.18	0.62	23.73	0.87	20.71	1	-0.05	0.07	0.08	-0.03	0.04	-0.03	0.05	100.13
Opx; no zonation	54.93	0.2	0.95	14.81	0.44	27.56	1.29	-0.06	0.04	-0.06	0.06	-0.02	0.07	0.11	100.32

Table 8.3	SiO ₂	TiO ₂	Al ₂ O ₃	FeO	MnO	MgO	CaO	Na ₂ O	K ₂ O	P ₂ O ₅	SO ₃	Cl	Cr ₂ O ₃	NiO	TOTAL
Opx; no zonation	52.92	0.16	0.54	22.62	0.71	22	0.84	-0.09	0	-0.06	-0.02	0	-0.06	0	99.56
Plag; core	56.31	-0.06	27.27	0.37	-0.08	-0.10	10.21	5.63	0.52	0.16	0.02	0.04	0.08	0.06	100.44
Plag; rim	55.87	0.02	26.98	0.33	-0.06	-0.08	9.81	5.57	0.47	-0.06	0.12	0.00	-0.03	-0.08	98.86
Plag; outer rim	49.86	-0.01	31.65	0.70	-0.12	0.01	15.51	2.75	0.26	-0.01	0.00	0.00	0.03	0.02	100.65
Plag; turbid inner rim	47.74	-0.03	32.55	0.69	0.01	-0.02	16.62	2.04	0.10	-0.01	-0.05	0.00	0.11	0.01	99.74
Plag; turbid inner rim	53.35	0.10	28.94	0.44	0.10	0.00	12.27	4.37	0.53	-0.01	-0.03	0.06	0.06	0.06	100.24
Plag; turbid inner rim	54.78	0.12	27.72	0.25	-0.06	-0.01	10.92	5.10	0.41	-0.03	-0.05	-0.01	0.07	0.07	99.29
Plag; between core-rim	56.31	0.03	26.55	0.28	-0.06	0.00	9.85	5.70	0.45	-0.07	0.04	0.02	0.12	-0.05	99.18
Plag; core	56.81	0.01	26.91	0.37	0.05	-0.05	9.82	5.80	0.35	0.00	-0.05	0.01	0.16	0.09	100.29
Plag; core	52.99	0.07	28.95	0.36	-0.02	-0.08	12.24	4.32	0.30	0.05	0.04	0.02	0.03	0.01	99.28
Plag; rim	55.56	0.07	27.24	0.26	0.02	0.01	10.18	5.51	0.42	0.05	-0.02	0.00	0.01	0.13	99.43
Plag; core	56.76	-0.10	26.74	0.35	-0.01	0.12	9.72	5.59	0.38	-0.05	-0.05	0.08	-0.02	0.00	99.52
Plag; outer rim	55.90	0.09	27.01	0.29	0.04	0.04	10.04	5.60	0.56	0.12	-0.02	0.00	0.00	0.16	99.81
Plag; inner rim	54.81	0.05	27.60	0.23	-0.02	0.05	10.88	5.08	0.35	0.01	-0.02	0.00	0.04	0.03	99.09
R17866 - Whiritoa Andesite, Waiwawa Subgroup															
Plag; no zonation	55.49	0.01	27.22	0.31	0.05	0.03	10.5	5.13	0.38	0.07	0	0	0.1	-0.02	99.26
Plag; inner rim	54.76	-0.01	28.11	0.31	-0.02	0.06	10.99	5	0.32	0.11	0.02	0	0.09	-0.09	99.64
Plag; outer rim	53.32	0.05	29.05	0.43	0.1	-0.02	12.22	4.42	0.34	0	0.02	0.02	-0.03	0.03	99.97
Plag; core	58.35	0.02	25.29	0.17	-0.02	0.04	8.1	6.51	0.64	0.06	-0.12	-0.07	-0.04	-0.03	98.9
Plag; core	54.4	-0.05	26.49	0.32	0.03	0.01	10.04	5.1	0.41	0.04	0.02	-0.03	0	-0.01	96.76
Plag; core	56.83	0.01	26.07	0.29	-0.02	0.02	9.13	5.84	0.52	0.07	-0.02	-0.01	0.04	-0.02	98.75
Plag; rim	50.04	-0.02	30.26	0.12	-0.01	-0.05	13.74	3.29	0.28	0.02	-0.01	-0.01	-0.01	0.14	97.78
Plag in glomerocryst; core	56.23	-0.09	27.14	0.29	-0.02	0.07	10.03	5.55	0.37	0.01	0.04	0	0.02	-0.05	99.59
Plag; no zonation	47.02	0.06	33.14	0.61	-0.03	-0.02	17.18	1.66	0.13	0.2	0.12	-0.01	0.11	0.17	100.34
Plag; no zonation	55.08	0.04	27.73	0.34	0.1	-0.05	10.5	5.46	0.41	-0.01	-0.02	0.05	0.03	0.24	99.88
R17856 - Whiritoa Andesite, Waiwawa Subgroup															
Plag; rim	56.22	0.07	26.47	0.27	-0.01	-0.01	9.14	5.83	0.61	-0.05	0.04	0.05	0.1	0.13	98.86
Plag in glomerocryst	54.89	0.04	27.9	0.33	0.02	-0.02	10.79	5.32	0.48	0	0.11	0.01	0.18	0.21	100.27
Plag in glomerocryst; core	55.55	0.02	27.45	0.24	-0.04	-0.07	10.24	5.33	0.47	-0.05	0.1	0.01	0.14	0.05	99.46
Plag in glomerocryst; rim	55.85	-0.03	26.88	0.13	-0.02	-0.06	9.77	5.57	0.49	0.1	0.04	0	0.06	0.02	98.8
Plag in glomerocryst; core	53.86	0.04	28.03	0.24	-0.05	-0.08	11.35	4.76	0.33	0.01	-0.02	0.05	-0.1	-0.11	98.3
Plag in glomerocryst; rim	55.79	0.11	26.66	0.25	0.01	-0.01	9.55	5.74	0.58	0.13	-0.02	-0.04	0.09	0.17	99
Plag; core	56.77	-0.04	26.73	0.46	-0.01	-0.05	9.64	5.79	0.39	0.01	0.02	-0.03	0.03	0.02	99.73
Plag; rim	56.3	-0.01	26.83	0.35	0.02	-0.06	9.68	5.4	0.58	-0.03	-0.01	-0.03	0.07	0.03	99.13
Plag; no zonation	55.01	-0.04	27.85	0.3	0.03	0.03	10.69	5.12	0.45	-0.06	-0.07	-0.02	0.09	0.02	99.42
Plag; core	56.4	0.05	26.75	0.25	0.03	0.01	9.85	5.47	0.52	0.19	0.01	0	0.01	0	99.54
AU60071 - Sugarloaf Basalt, Mercury Basalts															
Cpx; no zonation	49.98	0.91	5.03	6.46	0.08	15.69	20.43	0.12	0.13	0.23	0.16	-0.01	0.16	-0.02	99.35
Groundmass	52.24	0.45	10.32	12.28	0.33	17.95	4.79	1.42	0.19	0.19	0.06	0.07	0.03	0.06	100.36
Groundmass	51.92	0.71	18.02	6.84	0.19	8.1	9.46	2.79	0.34	0.1	0.05	0.12	-0.04	0.04	98.64
Olivine; no zonation	40.31	-0.06	0.09	15.54	0.28	43.73	0.17	-0.18	0.04	-0.13	0.16	0.04	0.02	0.06	100.06
Olivine; no zonation	40.28	0.09	0.08	14.88	0.2	44.73	0.1	-0.02	0.04	-0.13	-0.05	0.07	0.05	0.5	100.81
Olivine; no zonation	40.67	0.04	-0.01	13.1	0.18	45.61	0.2	-0.25	0.05	0.04	0.12	0	0.01	0.22	99.96
Olivine; no zonation	41.39	0.05	-0.03	12.28	0.18	47.01	0.1	-0.06	0.03	-0.07	-0.01	-0.01	-0.02	0.57	101.41
Olivine; no zonation	40.25	0.06	0	15.87	0.19	43.99	0.12	-0.11	0.03	0.09	0.07	0.02	0.01	0.2	100.78
Olivine; no zonation	40.87	-0.05	0	13.39	0.25	45.53	0.13	-0.11	0.06	0.02	0	0.01	-0.08	0.1	100.13
Opx; no zonation	46.29	1.57	0.93	23.29	0.45	23.34	1.69	-0.07	0.04	-0.1	0.27	0.06	0.39	-0.03	98.12
Opx; no zonation	55.67	0.56	1.09	11.31	0.29	29.55	1.54	0.01	0.08	0.13	0.04	0.11	0.02	0.01	100.4
Opx; no zonation	51.83	0.66	1.39	16.16	0.35	27.75	1.35	-0.11	0.09	0.05	0.1	0.03	0.06	0.13	99.84
Opx; no zonation	40.6	0.19	1.73	23.43	0.19	22.63	0.93	0	-0.03	0.1	0.06	0.06	3.37	-0.01	93.25

Appendix D. Supplementary Dataset to Chapter 6

Appendix D. Supplementary Dataset to Chapter 6 “Quantifying metasomatism in epithermal Au-Ag deposits: a case study from the Waitekauri area, New Zealand”. See Chapter 6, Section 6.7.4 for analytical methods.

Table 8.4		Jasper Creek											
AU#		59975	59981	59971	59973	59991	59992	59994	59986	59987	59988	none	59949
Sample		jc15-050	jc15-156	jc17-049	jc17-096	jc19-032	JC19-050	jc19-078	jc20-017	jc20-052	jc20-116	jc28-270	wv9-044
SiO ₂ (wt%)	XRF	54.74	64.02	50.12	65.53	66.40	65.16	63.22	62.25	73.19	59.36	62.90	65.97
TiO ₂ (wt%)	XRF	0.54	0.58	0.69	0.56	0.58	0.63	0.57	0.57	0.57	0.64	0.69	0.51
Al ₂ O ₃ (wt%)	XRF	15.56	16.57	20.64	16.15	15.94	16.44	16.33	15.51	14.07	19.09	17.09	14.77
Fe ₂ O ₃ (wt%)	XRF	5.59	5.71	6.79	4.65	5.24	5.03	5.41	6.15	4.30	5.99	5.86	5.09
MnO (wt%)	XRF	0.05	0.10	0.16	0.07	0.07	0.09	0.13	0.10	0.03	0.06	0.09	0.09
MgO (wt%)	XRF	2.78	2.90	5.89	3.24	1.50	1.79	2.16	3.34	2.37	5.02	2.36	3.36
CaO (wt%)	XRF	0.91	5.21	9.77	4.24	3.94	3.31	6.48	6.41	0.79	5.97	4.31	4.52
Na ₂ O (wt%)	XRF	0.34	0.49	0.67	0.06	2.26	2.86	0.52	2.97	0.03	0.07	1.28	1.34
K ₂ O (wt%)	XRF	3.39	3.26	3.13	3.55	2.97	2.50	3.20	1.73	3.29	2.16	2.93	2.55
P ₂ O ₅ (wt%)	XRF	0.09	0.10	0.12	0.10	0.10	0.12	0.10	0.11	0.09	0.12	0.13	0.09
Total		83.99	98.94	97.98	98.15	99.00	97.93	98.12	99.14	98.73	98.48	97.64	98.29
Li	ICP-MS	50.8	89	100.5	155.5	78.4	71.6	96.1	21.1	110	129	93.2	144
Be	ICP-MS	1.02	0.93	1.09	0.87	1.23	1.36	0.94	1.15	1.07	1.1	1.16	0.8
S (wt%)	ICP-MS	0.07	<0.01	1.22	0.55	<0.01	0.49	1.33	<0.01	1.17	0.8	0.94	0.08
Sc	XRF	21	21	29	21	20	21	20	24	21	23	26	19
V	XRF	78	42	188	135	111	135	92	148	76	144	166	77
Cr	XRF	42	41	53	66	22	18	48	107	18	36	51	49
Co	ICP-MS	14.2	19.5	20.3	18.4	23.5	21.2	21.9	40.7	14.8	20	20.7	26
Ni	XRF	22	13	17	16	9	8	8	19	6	12	11	15
Cu	XRF	8	13	17	15	7	5	15	23	2	17	14	14
Zn	XRF	79	45	63	46	66	54	43	64	52	58	62	44
Ga	XRF	16	15	19	16	16	17	14	16	14	18	17	14
Ge	ICP-MS	0.08	0.16	0.15	0.12	0.16	0.16	0.14	0.16	0.11	0.15	0.15	0.15
As	ICP-MS	1.5	1.9	174	66.7	0.9	27.4	97.5	2.6	232	159	189.5	10.9
Se	ICP-MS	1	2	2	1	2	2	2	2	2	2	2	2
Rb	XRF	199	120	196	129	130	96	142	60	181	87	121	103
Sr	XRF	94	182	206	149	165	177	323	269	52	180	187	145
Y	XRF	27	20	25	21	24	21	20	26	23	21	26	18
Zr	XRF	129	114	142	109	133	134	107	113	109	128	140	102
Nb	XRF	5	5	6	5	6	6	5	5	6	5	6	4
Mo	ICP-MS	0.08	<0.05	0.19	0.38	0.47	0.91	<0.05	0.76	0.19	0.08	0.9	0.08
Ag	ICP-MS	0.02	0.03	0.18	0.83	0.02	0.07	0.52	0.04	0.11	0.53	0.18	0.07
Cd	ICP-MS	<0.02	0.04	0.07	0.04	0.02	0.05	0.06	0.15	0.05	0.21	0.07	0.04
In	ICP-MS	0.017	0.028	0.029	0.033	0.02	0.037	0.036	0.038	0.023	0.027	0.043	0.033
Sn	ICP-MS	0.5	0.9	1.1	1.2	1.2	1.3	1.1	1.2	1	0.9	1.7	1.1
Sb	ICP-MS	2.37	6.74	4.09	8.83	6.49	13.45	4.71	0.2	13.45	4.3	5.6	4.24
Te	ICP-MS	<0.05	<0.05	<0.05	<0.05	<0.05	<0.05	<0.05	<0.05	<0.05	<0.05	<0.05	<0.05
Cs	ICP-MS	10.75	37.5	26.4	16.2	15.15	8.4	28.2	4.24	16.7	29.2	12.95	9.61
Ba	XRF	506	761	382	429	570	558	492	475	453	384	319	500
La	XRF	18	14	15	10	17	16	12	19	15	11	14	12
Ce	XRF	39	23	42	31	34	34	30	38	36	35	35	26
Hf	ICP-MS	1.6	2.1	2.4	1.9	2.3	2.6	2	2	2	2.5	3	1.9
Ta	ICP-MS	0.31	0.41	0.48	0.36	0.5	0.53	0.39	0.47	0.39	0.48	0.43	0.37
W	ICP-MS	11.2	36.9	6.3	29.4	77.9	68.4	19.5	145.5	45.3	10.6	31.9	34.1
Re	ICP-MS	<0.002	<0.002	<0.002	<0.002	<0.002	<0.002	<0.002	0.002	<0.002	<0.002	<0.002	<0.002
Au	fire assay	0.006	0.008	0.035	0.055	<0.005	0.012	0.045	<0.005	0.015	0.057	0.075	0.005
Hg	ICP-MS	0.07	0.04	0.1	0.33	0.01	0.38	0.14	<0.01	0.09	0.05	0.2	0.04
Tl	ME-MS61	1.09	0.57	1.72	2.09	0.54	1.11	1.39	0.26	1.5	0.79	1.16	0.82
Pb	XRF	9	7	9	6	10	9	8	11	8	6	9	6
Bi	ME-MS61	0.03	0.03	0.1	0.19	0.01	0.03	0.02	0.03	0.02	0.04	0.02	0.02
Th	XRF	6.6	6.7	7.8	6.4	7.1	6.7	5.5	5.5	5.3	7.9	5.6	5.1
U	ME-MS61	1.1	0.5	1.3	1	1.6	1.9	0.8	1.5	1.3	1.6	1.3	0.7

Table 8.4	Jasper Creek	Jubilee	Jubilee	Jubilee	Jubilee	Jubilee								
AU#	59952?	59953	59956	59957	59959	59962	59966	59968	59860	59862	59864	59865	59868	
Sample	wv9-107	wv9-152	wv9-208	wv9-238	wv9-279	wv9-339	wv9-410	wv9-466	J 3_005.5	J 3_075.4	wv6-069	wv6-079	wv6-154	
SiO ₂ (wt%)	63.42	63.30	63.60	63.47	65.86	63.01	66.87	68.85	72.20	69.26	61.77	66.44	63.40	
TiO ₂ (wt%)	0.55	0.56	0.52	0.54	0.48	0.57	0.57	0.51	0.58	0.84	0.58	0.51	0.54	
Al ₂ O ₃ (wt%)	15.75	15.89	15.03	16.17	14.89	16.51	15.57	15.19	20.19	19.32	16.21	14.72	15.12	
Fe ₂ O ₃ (wt%)	5.74	5.33	5.27	5.28	4.54	4.98	4.30	4.34	0.68	3.20	6.94	4.90	6.21	
MnO (wt%)	0.08	0.09	0.12	0.09	0.13	0.10	0.08	0.10	0.00	0.01	0.27	0.12	0.49	
MgO (wt%)	3.58	2.98	3.12	3.90	2.62	2.48	2.74	2.14	0.13	0.58	4.36	2.28	3.86	
CaO (wt%)	5.32	6.09	6.38	5.19	6.58	5.68	4.86	4.30	0.00	0.00	3.80	5.69	2.92	
Na ₂ O (wt%)	2.63	3.02	2.51	2.65	1.24	3.32	2.33	0.93	0.01	0.00	2.73	1.67	0.00	
K ₂ O (wt%)	1.77	1.74	2.35	1.54	2.35	2.20	1.77	2.25	5.23	5.78	1.86	2.86	3.71	
P ₂ O ₅ (wt%)	0.10	0.10	0.10	0.09	0.09	0.11	0.08	0.10	0.03	0.03	0.10	0.09	0.10	
Total	98.94	99.10	99.00	98.92	98.78	98.96	99.17	98.71	99.05	99.01	98.62	99.28	96.35	
Li	32	14.3	27.2	35.4	25.5	19	35.8	29.5	9.0	15.6	77.8	66.6	48.4	
Be	0.88	0.89	0.8	0.97	0.91	1.03	1.14	0.86	0.46	0.44	0.89	0.84	0.81	
S (wt%)	<0.01	<0.01	<0.01	<0.01	<0.01	<0.01	<0.01	0.33	0.01	2.12	0.31	0.02	2.57	
Sc	25	21	21	19	13	21	22	15	27	35	22	20	18	
V	129	132	96	88	69	121	128	94	114	259	140	113	130	
Cr	76	56	78	95	61	90	114	84	105	109	121	121	217	
Co	24	22.3	20.5	19.6	13	19.9	19.2	14.3	15.7	41.8	33.6	18.3	22.4	
Ni	16	17	16	20	14	18	14	10	15	15	34	19	20	
Cu	26	24	17	13	8	22	14	8	6	187	27	23	10	
Zn	44	45	49	51	39	52	46	36	5	10	66	47	47	
Ga	15	16	14	16	13	16	15	14	15	20	16	14	16	
Ge	0.16	0.15	0.14	0.15	0.13	0.14	0.14	0.14	0.11	0.09	0.15	0.13	0.16	
As	0.4	1.3	2.4	0.5	0.3	0.8	0.3	75.8	81.1	97.9	1	0.2	31.6	
Se	2	2	2	2	2	2	2	3	2	2	2	2	3	
Rb	58	59	66	32	54	78	61	74	207	253	61	108	177	
Sr	238	239	199	195	107	218	192	95	48	44	217	203	24	
Y	17	18	19	17	18	20	16	18	41	20	22	17	24	
Zr	105	115	95	118	116	127	119	110	123	104	129	102	144	
Nb	5	4	4	4	5	5	5	4	6	6	5	4	6	
Mo	0.38	0.4	0.24	0.16	0.06	0.48	0.13	0.78	0.84	0.98	0.65	0.35	1.19	
Ag	0.01	0.01	0.03	0.02	0.04	0.02	0.02	0.03	0.05	1.91	0.03	0.01	0.34	
Cd	0.04	<0.02	0.13	0.06	0.04	0.02	0.03	0.02	0.02	0.02	0.07	0.06	0.05	
In	0.03	0.027	0.037	0.041	0.025	0.023	0.033	0.019	0.037	0.049	0.042	0.027	0.04	
Sn	1.1	1	1.6	2	0.8	1.2	1.4	1	1.3	1	1.2	0.9	1.3	
Sb	0.93	0.6	0.33	0.32	1.15	0.35	1.09	6.42	2.11	4.12	0.51	0.9	5.66	
Te	<0.05	<0.05	<0.05	<0.05	<0.05	<0.05	<0.05	<0.05	0.08	0.05	0.11	<0.05	0.61	
Cs	6.14	2.04	1.88	2.76	5.53	2.47	4.17	5.3	2.86	4.41	5.75	9.77	9.25	
Ba	393	467	598	585	465	569	516	530	387	515	541	546	676	
La	11	15	9	15	11	16	14	13	18	12	11	11	13	
Ce	29	31	28	30	28	30	32	35	41	29	30	24	24	
Hf	2.7	2.9	2.5	2.6	2	2.5	3	1.3	2.6	1.6	0.8	2.4	0.9	
Ta	0.38	0.41	0.35	0.43	0.46	0.47	0.48	0.42	0.47	0.34	0.41	0.37	0.46	
W	36.9	67.6	34.9	19.4	10.8	52.4	54.7	22.5	84.2	47.9	94.9	46.5	76.6	
Re	<0.002	<0.002	<0.002	<0.002	<0.002	<0.002	<0.002	<0.002	0.002	0.002	<0.002	<0.002	<0.002	
Au	<0.005	<0.005	<0.005	<0.005	<0.005	<0.005	<0.005	<0.005	0.155	0.042	<0.005	<0.005	<0.005	
Hg	<0.01	<0.01	<0.01	0.01	0.03	0.02	0.01	0.23	0.04	0.07	<0.01	0.02	0.01	
Tl	0.18	0.18	0.34	0.34	0.09	0.17	0.42	0.31	3.08	3.38	0.51	0.57	1.73	
Pb	10	9	8	16	8	10	10	8	13	10	6	6	10	
Bi	0.02	0.01	0	0.01	0.01	0	0.04	0.01	0.02	0.09	0.06	0.03	0.01	
Th	5.2	6.3	6.0	7.1	8.0	7.4	5.7	7.3	8.0	5.0	4.4	5.2	7.1	
U	1.3	1.3	1	0.8	0.8	1.3	1.4	0.9	1.4	0.8	0.4	1.1	0.5	

Table 8.4	Scimitar	Scotia	Scotia											
AU#	59797	59800	59802	59805	59809	59810	59813	59814	59817	59821	59783	59882	59886	
Sample	WV11-288	WV11-384	WV11-477	WV12-086	WV12-190	WV15-125	WV15-207	WV15-279	WV15-400	WV15-501	WV16-175	sc27-082	sc27-170	
SiO ₂ (wt%)	69.72	57.40	59.45	72.54	60.51	63.47	67.03	78.71	60.50	58.04	64.69	66.84	65.74	
TiO ₂ (wt%)	0.42	0.90	0.92	0.53	0.85	0.73	0.56	0.22	0.91	0.90	0.62	0.49	0.56	
Al ₂ O ₃ (wt%)	14.64	18.80	19.02	15.59	17.69	19.55	15.97	13.98	18.62	19.09	15.39	14.51	15.95	
Fe ₂ O ₃ (wt%)	3.49	7.09	6.24	3.94	7.08	6.77	4.23	1.43	7.51	10.29	5.45	4.97	5.66	
MnO (wt%)	0.07	0.12	0.12	0.01	0.11	0.09	0.19	0.01	0.11	0.16	0.11	0.06	0.09	
MgO (wt%)	1.60	2.94	2.48	1.06	4.63	2.34	1.64	0.93	4.18	3.22	2.18	3.70	2.89	
CaO (wt%)	3.62	8.53	2.87	0.30	4.80	2.30	5.57	0.27	4.36	1.69	6.59	0.37	2.38	
Na ₂ O (wt%)	2.57	2.74	0.10	0.11	0.10	0.51	1.10	0.09	0.13	3.92	0.12	0.14	1.90	
K ₂ O (wt%)	3.60	1.16	5.34	5.64	2.92	3.02	3.09	3.78	3.08	2.19	4.09	6.89	2.96	
P ₂ O ₅ (wt%)	0.09	0.16	0.16	0.11	0.13	0.08	0.11	0.05	0.14	0.17	0.13	0.09	0.10	
Total	99.81	99.83	96.70	99.83	98.82	98.86	99.49	99.47	99.54	99.66	99.36	98.06	98.23	
Li	35.3	31.8	39	25.7	44.3	51.3	76.7	33.2	54.3	43.4	32.1	91	100.5	
Be	0.95	0.98	1.15	1.18	0.71	1.16	0.9	1.3	1.05	0.82	0.84	0.87	1.17	
S (wt%)	0.09	0.08	3.51	2.92	0.53	0.51	0.36	0.85	0.06	2.34	0.06	1.05	0.81	
Sc	12	20	21	17	27	20	20	6	28	21	17	21	26	
V	74	180	170	126	196	140	120	19	182	181	103	134	152	
Cr	19	45	38	73	64	49	82	3	44	36	44	85	104	
Co	23.5	32.7	20.2	36.1	28.8	26.2	17.7	6.4	23.4	23.7	24.3	21.6	23.4	
Ni	5	19	21	19	26	14	14	0	20	17	18	19	18	
Cu	8	29	33	11	36	17	15	2	33	29	18	7	20	
Zn	41	76	66	37	86	139	52	28	93	99	62	47	54	
Ga	13	16	17	16	17	19	15	14	19	16	15	15	16	
Ge	0.15	0.15	0.18	0.16	0.17	0.15	0.13	0.11	0.17	0.18	0.17	0.14	0.14	
As	1.9	1.9	62.5	171	85.9	122	4.5	118	10.3	123.5	2.2	151	221	
Se	1	1	2	2	1	2	2	2	2	2	1	2	2	
Rb	131	34	265	303	133	175	140	227	157	104	199	288	116	
Sr	178	289	41	36	104	38	122	39	118	294	63	103	225	
Y	20	24	27	21	23	25	21	23	30	25	30	29	20	
Zr	150	122	127	136	108	176	119	134	124	124	176	118	117	
Nb	7	6	6	6	6	8	5	8	6	6	7	5	5	
Mo	0.99	0.54	0.63	1.09	1.05	0.33	0.6	3.6	0.13	0.62	0.43	0.12	0.53	
Ag	0.01	0.05	0.23	1.61	0.67	0.14	0	0.41	0.14	0.26	0.03	0.46	0.28	
Cd	0.03	0.12	0.07	0.04	0.1	0.04	0.03	0.05	0.06	0.07	0.05	<0.02	0.04	
In	0.029	0.051	0.05	0.029	0.053	0.039	0.024	0.041	0.054	0.044	0.044	0.026	0.035	
Sn	1	1.2	1.2	1.3	1.2	1.8	0.8	2	1.3	1.2	1.2	0.6	1.1	
Sb	0.3	0.43	1.77	11.25	7.6	4.72	2.99	9.51	1.92	2.54	0.69	3.24	3.78	
Te	<0.05	<0.05	0.18	<0.05	<0.05	<0.05	<0.05	<0.05	<0.05	0.39	<0.05	<0.05	<0.05	
Cs	5.32	2.53	17.25	13.35	8.57	24.9	12.1	7.04	10.7	6.4	11.05	6.3	9.15	
Ba	748	363	410	647	396	386	935	215	330	220	745	765	579	
La	16	11	11	20	14	23	16	26	30	12	22	14	12	
Ce	27	22	35	31	26	33	22	36	54	33	39	37	33	
Hf	1.4	2.5	1.8	2.2	2.6	3.2	1.9	3.2	2.9	1.4	1.5	1	1.8	
Ta	0.52	0.42	0.39	0.46	0.35	0.53	0.41	0.67	0.38	0.4	0.52	0.41	0.44	
W	137	89.4	29.1	132.5	48.8	16.2	24.3	38.1	15.5	64.2	147.5	38.3	59.4	
Re	<0.002	0.002	<0.002	0.002	<0.002	0.002	<0.002	<0.002	0.003	<0.002	0.002	<0.002	<0.002	
Au	0.009	0.012	0.035	0.04	0.022	0.034	0.007	0.037	0.023	0.049	0.031	0.146	0.060	
Hg	<0.01	<0.1	<0.01	0.24	0.03	0.03	0.37	0.07	<0.01	0.01	<0.01	0.01	0.09	
Tl	0.83	0.29	2.61	3.94	1.41	0.98	1.45	2.35	1.29	0.89	1.55	4.21	1.27	
Pb	12	8	11	10	11	11	6	13	7	10	9	7	6	
Bi	0.02	0.06	0.05	0.06	0.07	0.05	<0.01	0.22	0.06	0.03	0.02	0.01	0.05	
Th	8.0	9.0	8.0	5.0	5.0	10.0	18.0	13.0	5.0	5.0	10.0	6.4	7.2	

Table 8.4	Scotia	Scotia	Scotia	Scotia	Scotia	Scotia	Scotia	Scotia	Scotia	Scotia	Scotia	Scotia	Scotia
AU#	59892	59895	59915	59916	59919	59919	59923	59924	59926	59929	59911	59913	59930
Sample	sc27-249	sc27-356	sc28-048	sc28-116	sc28-175a	sc28-175b	sc33-123	sc33-164	sc33-202	sc33-253	sc36-026	sc36-104	wv2-036
SiO ₂ (wt%)	55.23	62.08	72.19	68.79	64.44	62.84	69.68	64.15	62.15	59.71	65.83	63.52	68.05
TiO ₂ (wt%)	0.83	0.68	0.47	0.53	0.57	0.59	0.53	0.57	0.81	0.89	0.53	0.56	0.58
Al ₂ O ₃ (wt%)	19.13	16.55	13.57	15.71	16.67	16.86	15.42	16.49	17.86	19.45	20.79	16.18	16.44
Fe ₂ O ₃ (wt%)	8.17	5.84	2.56	4.62	5.06	4.85	4.51	5.03	6.95	9.03	0.74	5.89	4.17
MnO (wt%)	0.19	0.09	0.01	0.04	0.10	0.09	0.08	0.07	0.11	0.12	0.00	0.10	0.03
MgO (wt%)	1.47	2.26	0.66	1.04	2.61	1.95	1.40	2.21	3.17	3.74	0.10	2.86	2.28
CaO (wt%)	6.45	4.50	0.34	0.42	3.67	4.01	2.32	3.61	2.73	3.79	0.17	5.22	1.77
Na ₂ O (wt%)	2.95	2.54	0.33	3.36	2.14	3.23	0.71	0.53	2.19	1.34	0.40	2.88	2.00
K ₂ O (wt%)	3.11	2.94	8.09	3.99	2.81	3.51	2.93	5.07	2.37	0.94	9.35	1.94	2.81
P ₂ O ₅ (wt%)	0.16	0.13	0.09	0.10	0.10	0.11	0.08	0.11	0.14	0.14	0.30	0.10	0.11
Total	97.69	97.61	98.31	98.60	98.17	98.04	97.66	97.84	98.48	99.15	98.21	99.25	98.24
Li	58.5	88.4	66	72.1	95.9	73	90.2	90	103.5	81.9	25.4	47.9	102
Be	1.26	1.18	0.94	1	0.97	0.94	0.99	0.97	1.22	1.16	0.92	1.01	1.04
S (wt%)	1.43	0.71	1.51	0.86	0.19	0.49	1.13	0.53	0.09	<0.01	1.03	0.02	0.59
Sc	33	24	21	21	20	25	20	25	27	36	21	23	22
V	192	145	112	81	133	150	92	151	171	187	125	143	133
Cr	60	42	82	85	135	91	108	147	107	72	61	101	147
Co	23.7	21.2	43.2	31.8	17.8	22.7	14.6	27.3	25	29.7	8	26	18.4
Ni	16	12	13	21	17	19	11	20	16	18	37	23	16
Cu	17	17	10	13	15	16	10	16	22	16	9	14	12
Zn	66	59	50	56	59	64	41	61	82	75	9	49	40
Ga	18	17	13	14	16	15	16	16	17	18	16	16	16
Ge	0.18	0.16	0.11	0.13	0.14	0.15	0.14	0.14	0.17	0.18	0.15	0.15	0.12
As	211	86.6	192	21.3	13.3	24.9	183.5	78.9	2.3	1.4	364	1.2	30.6
Se	2	2	2	2	1	2	2	2	2	2	2	2	2
Rb	143	106	358	165	104	139	178	220	123	39	354	66	145
Sr	182	260	166	248	261	340	84	123	215	186	381	227	214
Y	32	26	24	24	20	18	21	25	25	22	37	19	18
Zr	149	140	108	121	127	125	126	119	141	126	142	119	122
Nb	7	6	5	6	5	5	5	5	6	5	7	4	5
Mo	0.36	0.47	0.87	0.06	0.09	0.14	0.06	0.46	0.15	0.22	0.38	0.32	0.16
Ag	0.18	0.18	0.69	0.05	0.07	0.13	0.18	0.42	0.05	0.05	0.63	0.03	0.11
Cd	0.24	0.03	0.02	0.02	0.06	0.14	<0.02	0.05	0.03	0.04	<0.02	<0.02	<0.02
In	0.045	0.034	0.023	0.025	0.036	0.041	0.042	0.037	0.038	0.067	0.026	0.038	0.032
Sn	1.5	1.3	0.7	0.7	1.2	1.3	1.2	1	1.3	1.4	1	1.1	1
Sb	1.47	2.3	14.15	2.23	1.94	2.11	2.77	3.42	1.52	0.41	12.25	1.46	3.91
Te	<0.05	<0.05	<0.05	<0.05	<0.05	<0.05	<0.05	<0.05	<0.05	<0.05	<0.05	<0.05	<0.05
Cs	14.35	8.43	11.5	4.19	5.89	7.03	8.08	14.05	16.8	8.71	6.78	1.85	16
Ba	259	778	504	421	588	686	194	827	301	257	1244	454	180
La	19	12	9	13	14	14	13	13	14	9	17	13	11
Ce	41	34	32	36	28	34	33	30	38	28	40	26	32
Hf	3.2	3	0.9	1.7	2	2.1	2	1.6	3.1	2.6	1.5	2	2.1
Ta	0.46	0.48	0.45	0.46	0.45	0.47	0.4	0.43	0.45	0.38	0.54	0.44	0.39
W	21.5	66.7	212	112	27.2	64.8	17.7	56.4	14.1	22.8	34.5	90.3	31.9
Re	<0.002	<0.002	0.003	0.002	<0.002	<0.002	<0.002	<0.002	<0.002	<0.002	<0.002	<0.002	<0.002
Au	0.071	0.018	0.031	0.011	<0.005	0.011	0.026	0.018	0.006	<0.005	0.063	<0.005	0.006
Hg	0.01	0.01	0.71	0.02	0.06	0.1	0.01	0.25	0.01	<0.01	0.48	0.02	0.04
Tl	1.66	1.2	5.85	2.02	1	1.54	1.53	2.91	1.04	0.24	5.53	0.3	0.94
Pb	6	9	6	7	10	10	5	6	11	8	9	8	7
Bi	0.03	0	0	0.03	0.08	0.08	0.07	0.04	0.01	0.05	0.03	0.03	0.02
Th	5.9	5.0	5.9	6.8	8.3	7.7	6.4	6.5	5.2	5.1	8.1	5.6	6.5
U	1.3	1.3	0.9	1.4	1.7	1.8	1.1	1.4	1.2	0.9	2.1	1.5	1.6

Table 8.4	Scotia	Sovereign	Sovereign	Sovereign	Sovereign									
AU#	59932	59934	59935	59938	59898	59901	59904	59908	59910	59767	59768	59771	59772	
Sample	wv2-132	wv2-218	wv2-276	wv2-365	wv4-073	wv4-133	wv4-222	wv4-309	wv4-385	ML1-027	ML1-071.2	ML1-111.9	ML1-151.6	
SiO ₂ (wt%)	63.21	65.09	67.38	60.78	72.42	66.23	63.52	62.13	57.02	76.93	70.52	78.50	70.64	
TiO ₂ (wt%)	0.54	0.48	0.48	0.51	0.56	0.63	0.75	0.59	0.74	0.23	0.56	0.30	0.78	
Al ₂ O ₃ (wt%)	15.59	14.76	14.42	14.97	17.08	19.06	17.51	16.02	16.68	13.40	12.91	11.05	16.85	
Fe ₂ O ₃ (wt%)	5.36	4.85	3.26	3.30	2.03	2.23	3.99	5.90	7.19	1.53	4.07	1.01	2.76	
MnO (wt%)	0.09	0.12	0.05	0.15	0.03	0.01	0.09	0.10	0.15	0.00	0.02	0.00	0.01	
MgO (wt%)	3.16	1.89	1.50	1.68	0.87	0.60	1.92	3.12	5.04	0.19	0.71	0.06	0.68	
CaO (wt%)	6.20	7.51	5.39	12.03	0.81	0.36	4.42	6.22	6.94	0.01	0.03	0.02	0.08	
Na ₂ O (wt%)	2.84	0.87	1.43	2.17	0.00	0.07	2.74	2.32	0.79	0.01	0.02	0.02	0.03	
K ₂ O (wt%)	1.70	2.38	2.36	2.28	4.63	9.21	2.96	1.94	3.20	6.86	10.15	8.12	7.19	
P ₂ O ₅ (wt%)	0.10	0.10	0.10	0.10	0.03	0.08	0.14	0.11	0.15	0.02	0.04	0.04	0.03	
Total	98.79	98.05	96.37	97.97	98.46	98.48	98.04	98.45	97.90	99.18	99.01	99.11	99.04	
Li	54.6	89.4	97.3	37.3	67.6	24.4	79.9	40.7	74.5	11.4	27.4	26.1	12.4	
Be	1.01	1.1	1.03	0.9	1.2	1.15	1.38	0.95	0.96	0.9	0.37	0.41	1.16	
S (wt%)	<0.01	0.26	0.04	<0.01	0.52	1.32	0.08	0.6	1.4	0.01	2.07	0.67	1.76	
Sc	22	18	22	23	19	24	27	25	27	6	29	13	31	
V	134	109	108	115	162	132	146	144	172	22	179	58	260	
Cr	105	68	92	69	96	77	66	95	86	5	135	49	69	
Co	29	16.5	15	15.3	23	8.2	23.1	21.2	24	19.9	39.8	32	34.7	
Ni	18	14	14	16	17	8	11	12	26	2	29	8	12	
Cu	19	6	7	10	9	11	17	8	25	3	12	5	20	
Zn	45	45	32	33	49	49	54	52	77	7	71	10	12	
Ga	16	14	14	13	18	17	16	15	16	13	13	7	18	
Ge	0.16	0.15	0.16	0.15	0.13	0.12	0.14	0.15	0.16	0.07	0.09	0.08	0.08	
As	0.9	8.7	3.9	1.1	128	54.8	6.6	1.3	6.9	176	182	87.5	120.5	
Se	2	2	2	1	2	2	2	2	2	2	1	2	2	
Rb	57	92	106	75	230	395	116	59	150	297	421	305	318	
Sr	240	106	150	163	51	89	379	179	92	55	61	99	71	
Y	19	18	20	21	21	44	32	19	21	27	25	22	23	
Zr	121	112	112	107	119	172	138	121	115	124	88	96	93	
Nb	4	5	5	4	6	8	6	4	5	7	5	5	6	
Mo	0.33	0.16	0.19	0.13	0.3	0.36	0.29	0.44	0.67	1.24	15.30	1.54	1.61	
Ag	0.04	0.04	0.03	0.05	0.03	0.08	0.04	0.03	0.41	0.6	4.48	0.66	0.75	
Cd	0.04	0.05	<0.02	0.13	0.15	0.02	0.15	0.05	0.02	0.02	0.27	0.05	0.03	
In	0.036	0.026	0.025	0.048	0.035	0.032	0.043	0.037	0.034	0.02	0.03	0.02	0.05	
Sn	1.1	0.7	0.7	1.8	1.1	1.4	1.5	1.1	1.1	1.5	0.7	1	1.3	
Sb	0.43	1.43	1.34	0.3	26.9	1.96	0.63	0.46	1.34	7.4	11.85	11.05	4.14	
Te	<0.05	<0.05	<0.05	<0.05	<0.05	<0.05	<0.05	<0.05	0.1	0.05	0.05	0.05	0.05	
Cs	1.93	12.2	10.85	4.43	24.2	16.6	12.1	6.08	7.36	5.32	3.82	3.63	16.4	
Ba	452	227	388	542	925	1585	1038	433	341	558	332	790	675	
La	12	11	14	10	13	20	12	11	12	16	5	15	10	
Ce	29	31	23	25	38	43	26	29	30	35	22	35	28	
Hf	2.1	1	0.8	1.3	1.6	2.2	3.1	2.6	2	1.8	1.3	1.9	1.7	
Ta	0.43	0.44	0.47	0.41	0.48	0.62	0.45	0.39	0.36	0.63	0.29	0.48	0.46	
W	111.5	31	49.7	23.9	23.2	34.4	52.1	50.1	27.6	201	169	225	71.2	
Re	<0.002	<0.002	<0.002	<0.002	<0.002	<0.002	<0.002	<0.002	<0.002	0.003	0.004	0.003	0.002	
Au	<0.005	<0.005	<0.005	<0.005	<0.005	0.028	<0.005	<0.005	<0.005	0.230	0.209	0.051	0.060	
Hg	0.01	0.02	0.01	0.02	1.12	0.03	0.01	<0.01	0.09	0.07	0.33	0.07	0.05	
Tl	0.22	0.47	0.6	0.17	6.45	5.11	1.23	0.34	1.58	4.92	9.23	5.54	4.41	
Pb	7	7	5	11	10	7	5	9	8	6	7	10	8	
Bi	0.05	0.01	0.01	0.01	0.02	0.01	0.01	0.02	0.03	0.01	0.02	0.09	0.11	
Th	5.8	7.8	7.0	7.1	8.1	9.3	5.3	6.8	3.5	12.7	2.6	7.5	7.9	
U	1.5	1.2	1	1.1	1.7	2.1	1.2	1.6	0.8	2.2	0.6	1.5	1.3	

Table 8.4	Sovereign	Sovereign	Sovereign	Sovereign									
AU#	59750	59751	59752	59754	59737	59738	59739	59742	59745	59727	59728	59730	59734
Sample	ML11-077.4	ML11-146.6	ML11-222.4	ML11-292.8	ML12-022.4	ML12-070.3	ML12-138.9	ML12-235.2	ML12-315.0	ML13-017.05	ML13-120.6	ML13-170.5	ML13-373.8
SiO ₂ (wt%)	64.70	61.10	65.43	66.14	65.34	71.14	70.84	66.37	64.51	50.36	66.92	62.54	61.21
TiO ₂ (wt%)	0.98	0.88	0.64	0.72	0.71	0.60	0.60	0.60	0.76	1.08	0.76	0.72	0.75
Al ₂ O ₃ (wt%)	17.71	20.13	15.27	15.75	15.84	13.19	12.97	14.87	17.76	27.46	16.59	16.94	17.50
Fe ₂ O ₃ (wt%)	5.47	7.84	5.76	6.34	6.28	5.75	6.51	6.19	6.72	9.71	4.31	7.31	7.45
MnO (wt%)	0.08	0.14	0.10	0.10	0.09	0.05	0.06	0.14	0.08	0.07	0.07	0.05	0.11
MgO (wt%)	4.80	3.78	3.67	3.31	2.44	1.35	1.76	3.03	3.47	8.64	3.08	2.89	4.28
CaO (wt%)	0.20	0.22	3.25	0.22	0.06	0.14	0.14	0.17	0.32	0.67	0.29	0.69	5.10
Na ₂ O (wt%)	0.18	0.06	0.00	0.02	0.05	0.05	0.01	0.04	0.02	0.19	0.04	2.88	2.30
K ₂ O (wt%)	4.59	5.03	3.32	6.04	8.07	6.57	6.16	7.99	5.09	0.96	6.60	4.97	0.62
P ₂ O ₅ (wt%)	0.14	0.14	0.11	0.13	0.06	0.10	0.11	0.11	0.16	0.20	0.15	0.11	0.14
Total	98.84	99.31	97.56	98.78	98.95	98.93	99.17	99.53	98.88	99.34	98.79	99.09	99.47
Li	125.5	77.8	67.1	65.8	56.3	37.8	47.7	60.3	49.9	243.0	52.8	59.1	92.7
Be	0.97	1.2	1.11	1.19	0.6	0.61	0.66	0.5	0.98	1.44	0.75	0.8	1.03
S (wt%)	0.19	0.17	0.23	2.13	2.31	3.41	4.2	2.22	3.63	0.05	1.96	3.83	2.37
Sc	33	31	25	30	27	19	22	22	27	37	27	29	23
V	236	223	177	216	201	157	190	165	181	178	185	175	174
Cr	120	168	73	94	60	57	86	48	79	58	126	167	65
Co	21.1	25.9	19.9	24.7	24.3	35.8	32.3	28.1	25	24.1	18.9	35.8	31.5
Ni	25	27	18	17	28	34	43	10	26	32	10	66	15
Cu	9	14	23	9	17	32	41	10	17	15	5	37	14
Zn	73	137	65	58	93	48	89	54	58	131	43	78	70
Ga	18	19	15	16	17	13	14	14	18	22	16	15	16
Ge	0.1	0.09	0.1	0.11	0.09	0.09	0.11	0.11	0.1	0.1	0.1	0.11	0.12
As	8.1	27.6	29.1	44.6	127	182.5	193.5	79.6	20.1	1.2	16.2	13.2	3.2
Se	2	2	2	2	2	2	3	1	2	2	2	1	2
Rb	240	243	148	278	325	256	264	278	226	42	277	190	22
Sr	42	35	27	68	55	36	49	82	32	33	61	180	235
Y	26	30	21	26	24	20	24	25	23	81	27	22	21
Zr	109	149	93	98	108	96	88	109	118	192	120	111	116
Nb	5	7	6	6	5	4	4	5	6	8	6	5	6
Mo	0.05	0.58	0.96	0.92	0.95	1.78	2.02	1.63	0.69	0.06	0.35	1.59	0.93
Ag	0.33	0.07	0.11	0.89	1.04	6.14	3.89	0.98	0.89	0.07	0.81	1.77	1
Cd	0.03	0.09	0.06	0.03	0.05	0.1	0.24	0.04	0.02	0.07	0.03	0.11	0.04
In	0.038	0.05	0.038	0.047	0.05	0.034	0.034	0.04	0.043	0.058	0.04	0.045	0.038
Sn	0.8	1.3	1.2	1.1	1	0.9	0.8	1.2	1.1	1.9	1	1.1	1.2
Sb	2.51	4.67	3.7	3.64	2.93	5.22	12.7	2.92	2.98	0.5	2.03	3.11	1.46
Te	0.05	0.05	0.05	0.23	0.05	0.31	0.37	0.09	0.62	0.05	0.06	0.11	0.3
Cs	9.95	17.15	8.75	12.4	6.73	10.05	6.67	4.11	8.69	5.2	9.85	4.42	1.73
Ba	273	248	405	804	536	362	477	787	526	129	735	463	329
La	12	14	11	11	7	6	5	10	11	33	9	7	9
Ce	33	40	31	23	22	18	22	26	21	74	22	21	29
Hf	1.9	2.6	1.5	1.5	1.2	1.3	1.2	2.1	1.3	4.9	1.9	1.3	1.5
Ta	0.37	0.43	0.4	0.38	0.25	0.27	0.22	0.37	0.36	0.51	0.36	0.31	0.32
W	26.5	24.3	53.8	66.6	48	87.8	69.8	95.2	36.9	21.2	52.1	59.1	71.9
Re	0.002	0.002	0.004	0.002	0.002	0.002	0.003	0.002	0.002	0.002	0.002	0.006	0.002
Au	0.005	0.005	0.005	0.008	0.059	0.123	0.746	0.081	0.009	0.005	0.013	0.012	0.008
Hg	0.01	0.06	0.05	0.08	0.08	0.66	0.15	0.08	0.03	0.04	0.12	0.17	0.08
Tl	2.41	2.43	1.39	3.4	5.86	4.08	4.39	3.8	2.09	0.43	3.56	2.39	0.35
Pb	5	6	7	11	5	11	20	13	18	3	6	15	17
Bi	0.19	0.03	0.11	0.08	0.08	0.08	0.05	0.04	0.51	0.01	0.02	0.07	0.04
Th	5.4	6.9	6.0	6.3	3.4	3.4	3.6	4.9	3.9	6.9	2.8	4.2	4.3
U	0.6	1	1.2	0.9	0.4	0.5	0.4	0.7	0.4	1.5	0.5	0.5	0.6

Table 8.4	Sovereign	Sovereign	Sovereign	Sovereign	Sovereign	Sovereign	Sovereign	Sovereign	Sovereign	Sovereign	Sovereign	Sovereign	Sovereign
AU#	59736	59784	59785	59786	59787	59788	59789	59790	59879	59880	59765	59766	59764
Sample	ML13-438.2	ML15-029.6	ML15-080.05	ML15-128.9	ML15-180.0	ML15-231.8	ML15-287.1	ML15-343.7	ML18-114.4	ML18-156.5	ML23-017.4	ML23-036.5	ML25-034.8
SiO ₂ (wt%)	53.15	53.92	69.11	69.15	57.38	62.77	58.10	64.10	69.02	66.13	78.15	75.63	68.05
TiO ₂ (wt%)	0.81	1.28	0.73	0.76	0.83	0.79	0.86	0.76	1.11	1.15	0.17	0.25	0.71
Al ₂ O ₃ (wt%)	18.74	28.51	18.03	18.13	16.50	19.27	18.76	17.57	20.49	20.99	12.46	17.94	14.93
Fe ₂ O ₃ (wt%)	6.59	6.84	6.23	4.94	7.69	6.84	6.62	8.56	2.72	1.78	6.43	0.18	6.11
MnO (wt%)	0.24	0.02	0.00	0.01	0.14	0.04	0.10	0.08	0.01	0.01	-0.00	0.00	0.09
MgO (wt%)	3.98	1.61	0.38	0.80	4.36	1.61	2.89	3.59	0.80	0.54	0.07	0.09	1.33
CaO (wt%)	8.65	1.09	0.21	0.35	6.34	1.78	6.71	0.95	0.09	0.06	0.00	0.00	0.12
Na ₂ O (wt%)	1.41	0.37	0.00	0.00	1.45	1.30	0.20	0.08	0.00	0.04	0.00	0.00	0.05
K ₂ O (wt%)	4.10	4.29	4.34	4.81	2.23	3.72	3.65	3.10	4.61	7.89	1.94	4.75	7.41
P ₂ O ₅ (wt%)	0.16	0.23	0.03	0.18	0.14	0.18	0.18	0.14	0.06	0.10	0.13	0.02	0.09
Total	97.83	98.15	99.05	99.14	97.07	98.31	98.07	98.95	98.89	98.70	99.36	98.87	98.89
Li	96.7	32.5	16.9	18.6	122.0	34.7	68.4	98.9	12.7	14.2	19.4	12.4	45.1
Be	1.09	1.33	0.88	0.94	0.78	0.87	1.01	0.77	1.06	1.16	0.44	0.62	0.71
S (wt%)	0.44	4.01	3.84	3.3	0.83	4.21	0.31	0.12	0.01	0.66	0.02	0.01	1.1
Sc	17	31	36	24	32	24	25	30	32	41	2	4	26
V	169	338	195	175	175	165	177	211	235	238	16	25	222
Cr	47	32	203	12	77	77	60	163	71	97	7	4	77
Co	21.2	29.4	61.6	14	31.2	23.5	17.8	29.4	13.6	32.6	24.4	14.6	28.1
Ni	20	13	40	4	37	30	17	35	11	22	4	4	19
Cu	28	6	28	3	33	25	19	15	41	43	17	0	19
Zn	103	75	410	66	69	66	75	65	32	25	13	5	88
Ga	18	30	17	20	16	18	18	17	21	22	7	11	16
Ge	0.11	0.09	0.12	0.11	0.14	0.12	0.12	0.12	0.08	0.2	0.1	0.07	0.13
As	2.1	21	102	74.2	4	93.4	8.3	7.5	191.5	73.3	364	6.6	153.5
Se	2	2	1	2	2	2	2	1	1	3	1	1	2
Rb	174	213	174	233	98	176	170	162	238	366	80	200	327
Sr	178	104	12	11	77	72	67	41	39	118	22	45	60
Y	25	41	30	29	23	24	29	18	28	66	8	27	25
Zr	119	202	114	151	102	125	133	109	133	139	88	138	91
Nb	6	9	5	7	4	6	6	6	6	7	5	7	6
Mo	0.29	4.92	1.25	0.84	0.19	0.63	0.43	0.61	1.06	0.82	1.17	0.14	0.33
Ag	0.15	0.13	0.07	0.21	0.61	0.16	0.1	0.1	2.7	0.96	0.37	0.56	0.92
Cd	0.04	0.09	0.12	0.08	0.06	0.09	0.19	0.28	0.02	0.02	0.02	0.02	0.07
In	0.043	0.082	0.047	0.045	0.046	0.043	0.043	0.056	0.054	0.057	0.02	0.016	0.041
Sn	1.1	2	1.3	1.1	0.7	1	1.3	2.1	1.2	1.2	0.7	1.5	1
Sb	1.49	5.24	23.2	6.45	1.03	3.68	1.04	0.5	4.33	4.49	18.05	6.45	5.66
Te	0.05	0.05	0.05	0.05	0.05	0.13	0.05	0.05	0.12	0.05	1.59	0.05	0.05
Cs	9.68	14.3	11.6	20.7	7.36	11.05	13.5	5.48	15.55	12.85	1.83	3.8	6.92
Ba	320	585	139	306	289	378	332	367	349	722	144	355	449
La	7	190	18	15	8	9	12	5	13	53	21	21	11
Ce	16	36	50	37	24	23	30	17	31	110	56	47	32
Hf	1.3	4.6	2.2	2.1	1.3	1.8	1.4	1	2	2.1	1.2	2.4	1.6
Ta	0.37	0.57	0.36	0.43	0.25	0.34	0.36	0.32	0.41	0.4	0.5	0.68	0.37
W	33.2	9.3	91.2	29.5	26.8	36.8	15.4	26.9	40.3	32.5	148	77.7	94.5
Re	0.002	0.002	0.002	0.002	0.002	0.002	0.002	0.003	0.002	0.002	0.002	0.002	0.002
Au	0.005	0.005	0.044	0.039	0.005	0.068	0.005	0.005	0.081	0.052	0.401	0.254	0.209
Hg	0.01	0.11	0.07	0.06	0.07	0.03	0.03	0.02	0.13	0.03	0.16	0.09	0.06
Tl	1.95	2.58	2.73	2.48	0.82	1.55	1.43	1.33	3.14	4.84	1.41	3.41	4.27
Pb	4	8	10	3	5	10	5	4	24	12	46	21	7
Bi	0.02	0.1	0.11	0.02	0.01	0.01	0.05	0.01	0.03	0.03	0.01	0.04	0.02
Th	3.5	9.4	6.3	6.1	2.8	5.1	5.0	3.7	6.7	5.9	9.9	14.0	6.2
U	0.6	0.4	1.9	1.2	0.7	0.6	0.5	0.5	0.8	0.8	1.6	2.3	0.9

Table 8.4	Sovereign	Sovereign	Sovereign	Sovereign	Sovereign	Sovereign							
AU#	59761	59762	59763	59746	59747	59748	59749	59755	59757	59758	59759	59760	59773
Sample	ML6-018.2	ML6-084.6	ML6-135.7	ML7-036.0	ML7-089.2	ML7-141.9	ML7-215.7	WV001-074.7	WV001-225.3	WV001-305.5	WV001-351.7	WV001-381.8	WV003-020.05
SiO ₂ (wt%)	75.20	63.28	69.40	67.91	65.15	70.61	68.78	58.62	77.88	66.25	57.94	60.39	69.73
TiO ₂ (wt%)	0.47	0.84	0.74	0.68	0.78	0.62	0.70	0.60	0.31	0.68	0.74	0.75	0.63
Al ₂ O ₃ (wt%)	12.90	17.26	13.43	19.93	16.55	14.34	15.37	15.72	10.82	16.51	17.22	15.07	18.10
Fe ₂ O ₃ (wt%)	1.40	6.71	6.66	3.41	5.99	4.51	6.44	5.95	1.89	8.19	7.46	7.31	3.72
MnO (wt%)	0.00	0.13	0.03	0.01	0.09	0.05	0.26	0.21	0.01	0.13	0.13	0.12	0.05
MgO (wt%)	0.13	1.84	0.77	0.78	2.71	1.99	3.20	3.67	0.59	3.48	4.37	4.44	1.80
CaO (wt%)	0.00	0.12	0.16	0.01	0.08	0.04	0.36	9.09	0.12	0.32	8.02	5.73	0.25
Na ₂ O (wt%)	0.04	0.07	0.01	0.00	0.04	0.01	0.00	0.00	0.01	0.00	2.17	1.11	0.00
K ₂ O (wt%)	8.85	8.76	7.59	5.66	7.71	6.66	4.04	3.53	7.36	3.69	1.25	2.25	4.77
P ₂ O ₅ (wt%)	0.03	0.09	0.12	0.12	0.06	0.06	0.13	0.11	0.09	0.14	0.12	0.14	0.11
Total	99.03	99.10	98.92	98.51	99.16	98.89	99.28	97.49	99.07	99.39	99.42	97.32	99.16
Li	18.6	41.2	22.1	9.0	49.1	44.8	69.8	75.0	28.7	86.9	41.3	100.5	48.8
Be	0.4	0.76	0.74	0.83	1.15	0.99	1.14	0.89	0.57	0.9	0.88	0.71	1.28
S (wt%)	1.1	0.51	3.89	1.93	2.8	1.7	1.16	1.21	1.03	1.06	0.01	1.01	0.04
Sc	15	35	34	30	31	24	24	26	12	35	26	28	23
V	87	277	258	194	267	198	201	181	84	212	194	210	178
Cr	47	87	93	315	86	139	57	107	34	103	93	92	105
Co	21.9	29.4	37.5	52.1	30.2	24.5	24.1	29	51.9	30.6	29.9	31	17.4
Ni	10	25	27	97	20	23	14	20	9	20	21	26	30
Cu	17	20	15	30	28	33	16	17	8	5	22	10	16
Zn	16	84	22	46	65	56	50	68	30	67	67	63	97
Ga	9	17	16	16	17	14	16	16	9	19	16	16	19
Ge	0.12	0.11	0.13	0.16	0.16	0.13	0.13	0.14	0.11	0.13	0.14	0.13	0.14
As	71.1	48.7	474	93.2	222	273	21.9	34.2	181.5	99.9	5.4	25.3	2.6
Se	2	1	2	4	2	2	2	2	2	2	2	2	3
Rb	336	353	330	303	316	273	206	196	292	212	36	108	259
Sr	101	93	70	76	70	66	19	48	70	14	217	56	13
Y	22	25	31	154	26	32	21	25	22	24	20	20	34
Zr	99	101	86	134	93	88	91	94	71	108	110	105	180
Nb	5	6	5	7	5	5	5	5	5	5	5	5	7
Mo	0.11	0.26	0.85	0.48	0.86	2.25	1.29	0.16	5.07	0.15	0.58	0.75	0.32
Ag	0.42	0.77	2.13	1.46	0.81	0.96	0.84	0.79	1.46	0.4	0.05	0.74	0.18
Cd	0.05	0.06	0.02	0.12	0.04	0.17	0.02	0.06	0.11	0.06	0.07	0.02	0.02
In	0.038	0.048	0.034	0.04	0.047	0.035	0.042	0.038	0.02	0.049	0.052	0.045	0.05
Sn	1.2	1.3	0.9	1.3	1.5	1.2	1.4	1.2	1.3	1.1	1.3	1.3	2
Sb	4.71	3.16	24.3	3.28	7.49	6.38	4.21	1.99	15.65	7.37	3.31	2.08	1.38
Te	0.05	0.05	0.05	0.06	0.05	0.11	0.24	0.06	0.05	0.05	0.05	0.05	0.05
Cs	4.84	7.67	12.75	12.95	9.06	7.49	12.3	11	7	7.32	3.94	5.27	16.55
Ba	573	412	344	676	929	723	219	240	683	323	310	274	411
La	19	11	11	30	15	18	10	11	14	9	13	10	22
Ce	41	24	33	71	29	41	25	33	31	27	27	28	49
Hf	2	1.8	1.4	1.4	1.6	1.3	1.6	1.6	1.6	1.7	2.8	1.7	2.4
Ta	0.41	0.45	0.33	0.34	0.4	0.42	0.41	0.36	0.47	0.29	0.38	0.37	0.59
W	97.7	46	105	31.3	66.6	71.7	44.8	29.5	176.5	39.2	53.7	37	27.5
Re	0.002	0.002	0.002	0.004	0.002	0.002	0.002	0.003	0.004	0.002	0.002	0.002	0.002
Au	0.084	0.020	0.393	0.023	0.051	0.131	0.008	0.015	0.131	0.009	0.005	0.005	0.005
Hg	0.06	0.09	0.11	0.07	0.04	0.05	0.04	0.03	0.33	0.08	0.03	0.05	0.02
Tl	5.13	4.7	5.81	3.45	4.55	3.27	1.95	1.8	4.92	1.95	0.47	0.94	1.86
Pb	15	8	8	14	8	9	6	7	13	4	9	7	4
Bi	0.02	0.04	0.03	0.48	0.1	0.02	0.23	0.14	0.15	0.01	0.04	0.14	0.03
Th	7.3	7.6	4.3	4.5	7.6	5.8	7.0	5.8	8.9	4.3	4.5	3.4	7.9
U	1	0.9	0.6	0.5	1.1	0.8	0.8	0.9	1.8	0.7	0.9	0.6	1

Table 8.4	Sovereign	Sovereign	Sovereign	Sovereign	Sovereign	Sovereign	Teutonic	Teutonic	Teutonic	Teutonic	Waitekauri area	Waitekauri area
	59775	59776	59778	59779	59780	59782	none	59835	59839	59842	59823	59824
	WV003-166.7	WV003-209.8	WV003-264.4	WV003-309.7	WV003-359.8	WV003-431.9	WV10-062	WV10-157	WV10-258	WV10-383	WV14-102	WV14-141
SiO ₂ (wt%)	60.20	67.34	67.02	70.56	72.78	64.36	71.68	68.50	71.08	73.72	66.57	66.71
TiO ₂ (wt%)	1.01	0.84	1.10	0.54	0.41	0.79	0.43	0.44	0.49	0.43	0.56	0.53
Al ₂ O ₃ (wt%)	19.21	15.53	20.42	16.19	15.11	16.81	14.37	14.72	15.65	14.44	15.92	15.71
Fe ₂ O ₃ (wt%)	7.38	5.33	3.95	2.44	1.47	5.52	4.09	3.88	3.51	2.65	5.15	4.80
MnO (wt%)	0.12	0.06	0.04	0.00	0.00	0.09	0.05	0.12	0.04	0.04	0.15	0.09
MgO (wt%)	3.13	2.28	1.84	0.47	0.13	2.84	1.15	1.16	0.71	0.80	3.23	3.01
CaO (wt%)	0.29	0.17	0.21	0.07	0.02	0.31	2.55	4.08	2.25	3.05	3.99	4.38
Na ₂ O (wt%)	0.07	0.04	0.13	0.03	0.05	0.04	2.46	2.75	2.29	1.72	2.19	2.51
K ₂ O (wt%)	7.62	7.41	4.32	8.61	9.10	8.01	2.89	2.82	3.06	2.49	2.08	2.19
P ₂ O ₅ (wt%)	0.14	0.10	0.06	0.02	0.03	0.17	0.08	0.09	0.10	0.09	0.11	0.10
Total	99.16	99.09	99.09	98.95	99.09	98.95	99.76	98.55	99.18	99.43	99.96	100.03
Li	58.3	47.2	95.1	19.4	14.8	64.8	39.7	27.7	66.4	58.6	28	24.8
Be	0.96	0.9	1.9	0.88	0.58	1.67	1.34	0.96	1.16	0.81	0.97	1.1
S (wt%)	0.42	2.16	0.27	1.54	1.01	1.12	<0.01	<0.01	0.42	0.7	<0.01	<0.01
Sc	34	34	34	30	22	26	12	11	11	12	17	16
V	261	313	266	155	109	176	70	76	84	73	116	105
Cr	86	75	76	106	86	139	20	24	21	15	40	48
Co	31.6	32.8	58.6	36.5	23.9	21.2	16.9	28.3	16.7	28.2	20.4	23.1
Ni	25	22	87	10	7	19	9	8	5	4	15	17
Cu	29	30	32	7	9	21	10	9	11	12	19	17
Zn	99	61	82	12	7	76	55	44	43	38	57	55
Ga	20	18	20	19	15	20	12	16	16	11	16	16
Ge	0.17	0.18	0.14	0.13	0.13	0.15	0.11	0.14	0.11	0.13	0.15	0.15
As	32.2	228	40.6	143	61.1	45.7	2.1	1.1	86.5	176	1.2	2.9
Se	2	4	2	2	2	2	1	1	1	1	1	2
Rb	329	320	173	412	377	340	148	106	120	98	74	78
Sr	79	96	54	65	96	70	251	165	186	174	271	245
Y	35	137	35	25	29	37	26	20	22	20	21	18
Zr	133	117	144	115	119	218	156	162	155	134	129	134
Nb	7	7	7	6	7	9	6	6	7	5	6	6
Mo	0.75	1.46	0.98	3.26	0.92	2.10	0.62	0.66	0.76	1.86	0.66	0.54
Ag	0.29	0.99	0.16	0.49	0.39	1.2	0.03	0.04	0.08	0.36	0.02	0.02
Cd	0.03	8.69	0.34	0.02	0.48	0.09	0.05	0.05	0.03	0.04	0.03	0.05
In	0.061	0.053	0.06	0.062	0.037	0.045	0.026	0.027	0.024	0.013	0.044	0.036
Sn	1.5	1.4	1.8	4.3	1.7	1.4	1.5	1.1	1.2	0.8	1.4	1.3
Sb	3.3	10.05	2.79	5.62	3.17	3.06	1.15	1.12	6.11	8.37	0.22	0.44
Te	0.05	0.05	0.05	0.05	0.05	0.05	<0.05	<0.05	<0.05	<0.05	<0.05	<0.05
Cs	14.2	12.25	13.65	12.85	5.83	10.4	7.53	5.32	9.56	17.65	2.61	3.13
Ba	537	801	509	754	1092	679	972	640	684	493	471	486
La	18	15	19	11	23	16	23	19	23	16	17	21
Ce	38	40	44	25	44	38	47	23	35	40	27	35
Hf	1.8	1.6	2.7	2.1	2.2	2.3	2.1	2.1	3.7	2.3	2.6	2.6
Ta	0.46	0.45	0.55	0.53	0.59	0.51	0.54	0.53	0.57	0.5	0.48	0.5
W	31	67.5	47	101.5	97.8	51.8	62.5	95.4	69.8	143.5	66.5	83.3
Re	0.002	0.003	0.002	0.003	0.002	0.002	0.002	<0.002	<0.002	<0.002	<0.002	0.002
Au	0.005	0.223	0.014	0.073	0.010	0.167	0.026	0.024	0.012	0.081	0.01	0.008
Hg	0.05	0.06	0.02	0.02	0.01	0.04	<0.01	<0.01	0.3	0.37	<0.01	<0.01
Tl	3.61	4.41	2.26	4.72	5.03	3.48	0.39	0.33	0.53	0.39	0.27	0.31
Pb	7	9	11	13	15	13	19	11	12	9	9	12
Bi	0.08	0.07	0.12	0.85	0.05	0.02	0.03	0.04	0.06	0.01	0.12	0.08
Th	7.6	3.9	7.5	8.9	10.9	8.4	11.0	9.0	7.0	9.0	7.0	9.0
U	0.8	0.8	1.4	1.3	1.7	1						